COMPUTATIONAL STUDIES, SYNTHESIS AND CHARACTERIZATION OF RUTHENIUM(II) ANTICANCER COMPLEXES

ADEBAYO AZEEZ ADENIYI

University of Fort Hare
Together in Excellence

COMPUTATIONAL STUDIES, SYNTHESIS AND CHARACTERIZATION OF RUTHENIUM(II) ANTICANCER COMPLEXES

by

ADEBAYO AZEEZ ADENIYI

A thesis submitted in fulfilment of the requirements for the degree of

Philosophical Doctor

in the Faculty of Science and Agriculture at the University of Fort Hare.

January 2014

Supervisor: Prof. P. A. Ajibade

DECLARATION OF THE STUDENT

NAME: ADEBAYO AZEEZ ADEBAYO

STUDENT NUMBER: 201205578

QUALIFICATION: PhD (CHEMISTRY)

TITLE OF THE PROJECT: COMPUTATIONAL STUDIES, SYNTHESIS AND CHARACTERIZATION OF RUTHENIUM(II) ANTICANCER COMPLEXES

DECLARATION:

I hereby declare that the above mentioned thesis is my own work and that it has not previously been submitted for assessment to another University or for another qualification.

Signature:

Date: 08/01/2014

TABLE OF CONTENTS

LIST OF TABLES

DEDICATION

This thesis work is dedicated to the impact of the saving grace and salvation brought to me by my Lord and Saviour Jesus Christ.

In addition to Jesus Christ being my Lord and Saviour since year 1995 when I fully gave my life to him, He is also my helper, my counsellor, my sponsor, my comforter in the time of trouble and He is my friend. Despite the facts that I was not privilege to know who is my biological Father and Mother as a result of their death, yet the power of Jesus Christ made me educated and I am at this time becoming a PhD holder to the glory of His name. By His mercy alone, I started my academic journey in the year 2000 just by the strength of His promise never to leave me nor forsake me. I had neither bank account nor any physical person as my sponsor, but Jesus alone who is very real and visible to me, promised that He will go ahead of me and grant me success. All my academic achievement today is by divine favour that is based on the heavenly account. My Lord has never failed me, He miraculously provided for my needs during the undergraduate; He gave me Federal Government Scholarship in Nigeria which I used to round up my BSc; He favoured me during the NYSC Service; He lead me into MSc in University of Ibadan in 2007; He took me out of the country for international ATOSIM Master program in 2008 and brought me to University of Fort Hare in South Africa in 2012. Lord Jesus, I sincerely dedicate this thesis to the memory of your loving care, tender mercy and your saving grace. You are indeed my Lord and my Saviour forever and ever (amen). Thank you Jesus.

ACKNOWLEDGEMENTS

I am indebted to give all the glory to God who provided the life, the peace, the favour, the knowledge and the opportunity to carry out this PhD work. May His infinite and matchless name be exalted forever and ever in Jesus name (Amen).

My first and outstanding thanks go to my project supervisor, Prof. P. A. Ajibade for his unflinching support, guidance and assistance that makes this thesis a success.

My profound thanks go to my former supervisor Prof. B. B. Adeleke of the University of Ibadan who was not just a supervisor to me but also a father. He is such a selfless supervisor who never considered his own gain but ever desiring the best for me and ready always to support. I also like to acknowledge Dr I. A. Adejoro of the University of Ibadan who was my MSc supervisor and strongly believe in my future and make all effort within his power to assist. I will like to show my gratitude to my friend Bro. Joseph Belo for his financial support and encouragement during my undergraduate, Dr. O. O. Ojebiyi in LAUTECH and his family for their love and care for me, Dr. Adewuyi in UNIUYO and his family for their assistance and love. I will also like to acknowledge Dr Dayo Adewole who is one of the people God used mightily to make my trip to South Africa a reality. My acknowledgement also goes to my younger brother, Mr Ranti Adeniyi who is the only one in my extended family that we understand each other and share common faith.

I will also sincerely and whole heartedly acknowledge my Father in the Lord, Pastor W.F. Kumuyi for the spiritual grace, blessing and the impartation I receive from him daily. God has used him mightily to break every yoke of mediocrity in my life, thank you my Pastor and my father in the Lord. My thanks will never be completed without reference to all my spiritual mentors and pastors like Dr. Eyarefe in UI, Dr. Chrish in UI, Dr Fagbola in UI, Pastor Adesina in UKZN and my beloved brother in the Lord Dr Dayo Adewole for his love and financial support. My thanks go to my fellowship brethren at the University of Fort Hare, Pastor and Mrs Fayemi, Dr and Mrs Ugbenyen, Dr and Mrs Hosu, Dr

and Mrs Unofin, Bro. and Mrs Avose, Bro. Moday, Bro. Andrew, Bro. Yinka, Bro. Peter and all other brethren whose name are not mentioned here.

My unreserved gratitude also goes to ATOSIM Master Organisers who qualify me for the ATOSIM program which serves as foundation of all my knowledge and impact in the field of computational chemistry. I will like to also thank my former supervisor during the ATOSIM program Prof. Paul Lessard-Fleurat at ENS, Lyon for his unquantifiable influence in making me a computational chemist and for his being always there to assist even after many years of our separation from each other. My list for acknowledgement can never be completed without my heartfelt gratitude to my Sweetheart Joy Bathy for her love for me, faith in me and her words of prophecy and encouragement to me.

Finally, I will like to thank GMRD University of Fort Hare for supervisor-linked PhD bursary, the academic and non-academic Staff members in the Department of Chemistry for their token of contribution to my successful program at the University of Fort Hare.

LIST OF PUBLICATIONS

Publication included as part of the thesis

1. Adeniyi, A.A.; Ajibade, P.A. Effects of bidentate coordination on the molecular properties RAPTA-C based complex using theoretical approach. *J. Mol. Model.* **2013**, 19, 1325-1338.

2. Adeniyi, A.A.; Ajibade, P.A. Computational properties of h6-toluene and h6-trifluorotoluene half-sandwich Ru(II) anticancer complexes. *J. Biomol. Struc. Dynamics* **2013**, 1-15, http://dx.doi.org/10.1080/07391102.2013.819299

3. Adeniyi, A.A.; Ajibade, P.A. Insights into the intramolecular properties of h6-arene-Ru based anticancer complexes using quantum calculations. *J. Chem.* **2013**, 1-25.

4. Adeniyi, A.A.; Ajibade, P.A. Theoretical study of the electronic and spectroscopic properties of some Ru(II) anticancer complexes. *Spec. Acta Part A: Mol. Biomol. Spec.* **2013**, 105, 456–465.

5. Adeniyi, A.A.; Ajibade, P.A. Computational studies of the electronic, conductivities, and spectroscopic properties of hydrolysed Ru(II) anticancer complexes. *Spec. Acta Part A: Mol. Biomol. Spec.* **2013**, 115 , 426–436.

6. Adeniyi, A.A.; Ajibade, P.A. Inhibitory activities and possible anticancer targets of Ru(II)-based complexes using computational docking method. *J. Mol. Graph. Model.* **2012**, 38, 60-69.

7. Adeniyi, A.A.; Ajibade, P.A. Comparing the suitability of autodock, gold and glide for the docking and predicting the possible targets of Ru(II)-based complexes as anticancer agents. *Molecules* **2013**, 18, 3760-3778.

8. Adeniyi, A.A.; Ajibade, P.A. An insight into the anticancer activities of Ru(II) based metallocompounds using docking methods. *Molecules* **2013**, 18, 10829-10856.

Oral presentation:

i. **Adeniyi, A.A.** The prediction of organometallic anticaner complexes using computational docking. CHPC National Meeting of 3rd-7th December 2012 at the Durban International Conference Centre, South Africa. Theme: HPC and Data Applications for Increased Impact on Research. http://www.chpcconf.co.za/index.cfm?x = presentations.

ii. **Adeniyi, A.A.,** Ajibade, P.A. Rational design of Ru(II)-based complexes as potential anticancer agents. CHPC National Meeting of 2rd-6th December 2013 at the Cape Town International Conference Centre, South Africa. Theme: Solving Industry Challenges Through HPC and Data Adoption.

iii. **Adeniyi, A.A.**; Ajibade, P.A. Understanding the complexity, stability and possible target of ruthenium-based complexes as anticancer agents using computational methods. 2013 South African Chemical Institute (SACI) Conference, 1st-6th December 2013, at East London, South Africa.

Postal presentation:

i. **Adeniyi, A.A.**; Ajibade, P.A. Computational studies of Ru(II) anticancer complexes. INORG2013 Conference, Hosted by the South African Chemical Institute (SACI), 30 June - 4 July 2013, Held at the Southern Sun Elangeni Hotel, Durban, South Africa.

ii. **Adeniyi, A.A.**; Ajibade, P.A. Computational studies of Ru(II) anticancer complexes. 2013 South African Chemical Institute (SACI) Conference, 1st-6th December 2013, at East London, South Africa.

ABSTRACT

This thesis is centred on the application of Ru-based complexes as a promising alternative to *cis*-platin in cancer chemotherapy. *Cis*-platin is known to be the most prescribed chemotherapy which has more than 70% application in cancer cases especially the testicular cancer. An insight is provided in Chapter One and Two into the literatures reports on the application of Ru(II)-based complexes in cancer chemotherapy. In order to address some of the pressing challenges in rational design of Ru-based anticancer complexes, section 3.3 and 3.4 deal with efforts to elucidate the complication of their chemistry and instability while in section 3.5 efforts are made to find solution to the lack of proper knowledge of their targets using different theoretical approaches as presented in Chapter Three. In addition to the theoretical study, this thesis also comprises of the synthesis of the bis-pyrazole derivatives type of ligands and the derivatives of their Ru(II)-based complexes as provided in Chapter Four and Five respectively. Also the computational methods were used to elucidate the structural and spectroscopic properties of the synthesised ligands and their Ru(II)-based complexes.

The geometrical and electronic properties are studied in relation to the stability and the reported anticancer activities of Ru(II)-based complexes in section 3.3. In subsection 3.3.1, several quantum properties including the natural energy decomposition analysis (NEDA) and quantum theory of atoms in a molecule (QTAIM) are computed on three models of RAPTA-C complexes using DFT with hybrid functional and basis set with ECP and without ECP. The higher stability of *Carbo*-RAPTA-C and *Oxalo*-RAPTA-C over RAPTA-C comes from the lower exchange repulsion and higher polarization contributions to their stability which gives insight into experimental observation. A similar study was carried out in subsection 3.3.2 on half-sandwich Ru(II)-based anticancer complexes with η^6-toluene and η^6-trifluorotoluene. The trifluorotoluene and the hydrated models are characterised with higher charge transfer, polarizability, synergistic effect of ligand fragments, stronger and higher HB interactions that support their reported experimental anticancer activities and the mechanism of their

activation by hydrolysis. Also in the subsection 3.3.3, the factors that determine the stability and the effects of non-covalent interaction on the two models of these half-sandwich η^6-arene ruthenium anticancer complexes and their respective hydrated forms were investigated using DFT method. Lastly in section 3.3, the subsection 3.3.4 deals with the intramolecular properties of five sets of ruthenium based anticancer complexes using DFT method.

The spectroscopic and the non-linear optical properties of selected Ru(II) anticancer complexes are shown in Section 3.4. In subsection 3.2.1, DFT method was applied to study the thermodynamic and spectroscopic properties of three Ru-based complexes in order to give possible reasons for the reported experimental stability of complexes **1** and **2** with bidentate chelating ligands than complex **3**. A further study was carried out in Subsection 3.4.2 where computational method was used to gain insight into the correlation between the chemistry of the hydrolysis and the anticancer activities of selected Ru(II)-based complexes. Lastly in this section, subsection 3.2.3 deals with application of different density functional methods (DFT) to optimize and study the chemistry of five potential anticancer complexes in terms of their electronic, conductive and spectroscopic properties. The carboxylic and pyrazole units are found to significantly enhance the polarizabilities and hyperpolarizabilities of the complexes while the chloride only improves the polarity of the complexes.

The possible targets of Ru(II)-based anticancer complexes are predicted using docking methods as presented in section 3.5 of this thesis. In subsection 3.5.1, the interactions of selected Ru(II)-based complexes with different cancer receptors are carried out using computational docking. The study focuses more on finding alternative protein targets other DNA for some Ru(II)-based complexes using computational docking. A further study on addressing the problem of the improper knowledge of of the targets of Ru-based anticancer complexes was carried out in subsection 3.5.2. Some promising anticancer complexes of Ru(II) such as RAPTA based complexes formulated as [Ru(η^6-p-cymene)L_2(pta)] and those with unusual ligands are docked against receptors using Autodock, Glide and Gold. Lastly in section 3.5, docking packages Molegro and Autodock were applied in subsection

3.5.3 to predict the anticancer activities of selected Ru(II) complexes against twelve anticancer targets. Introducing the quantum calculated atomic charges of the optimized geometries is found to significantly improve the docking predictions of these anticancer metallocompounds.

In section 4.3-4.6, the spectroscopic and the geometric properties of ligands with pyrazole, methylpyrazole, bipyridine and phenanthroline derivatives were studied at both experimental and computational levels. The computational results are perfectly in agreement with the experimental results especially in terms of the spectroscopic properties. The spectroscopic analyses as well as the computed properties were used to establish the successful synthesis of the ligands. Many of the functional groups in these ligands are found to be Raman active which also help in their spectroscopic elucidation.

Lastly in chapter five, the method used for the synthesis of forty Ru(II)-based complexes were presented with their experimental spectroscopic features being elucidated using theoretical methods. A very high correlation was observed between experimental and theoretical characterisation of the complexes which is an indication of successful synthesis of the complexes.

CHAPTER ONE

1 INTRODUCTION

1.1 Introduction

Cancer is known medically as a malignant neoplasm [1-4] which means a progressively worse growth or abnormal proliferation of cells that result in an abnormal mass of tissue. These cells divide and grow uncontrollably, forming malignant tumours, and metastasised by invading other parts of the body. There are more than 200 different types of cancer that are known and vary in nature from one site to another. The causes of many cancers are not completely understood as the origin of many can neither be traced to bacterial nor to viral infection. A primary cancer can be treated by surgery but when it is metastasised into a systemic problem, chemotherapy is the best method of treatment. The most efficient drug recognised for the treatment of more than 70% of cancer cases is *cis*-platin [5, 6]. Many promising potential anticancer drugs of metal-based complexes have been proposed to have better activities than the most commonly used platinum chemotherapy against cancer but their targets remain unknown [5-14]. There are evidences that proteins are the most likely targets for organometallic anticancer complexes other than Deoxyribonucleic acid (DNA) which is an established *cis*-platin target. Ruthenium antitumor agents generally display lower reactivity towards double-stranded DNA and their cellular mechanisms of action are not known [15]. In an effort to address the present problems in cancer therapy like non-selectivities of the cytotoxic cancer drugs, ineffectiveness towards many metastasised cancer cells, drug resistance and toxicity, many researchers are focusing on the design of metal-based anticancer complexes with better selectivity. The motivation behind metal-based anticancer design is due to the recorded success of *cis*-platin above all the available organic anticancer counterparts despite its nonselectivity [13, 16-18]. Dyson and co-researchers designed different

derivatives of Ru-based complexes containing a kinetically favourable 1,3,5-triaza-7-phosphaadamantane (PTA) group with many derivatives of the type [(η^6-arene)RuCl(PTA)$_2$], [(η^6-cymene)RuCl(PTA)$_2$], [CpRuCl(PTA)$_2$] and [Cp*RuCl(PTA)$_2$] which are generally referred to as RAPTA complexes and are characterised by strong *in vivo* but weak *in vitro* activity [5-7, 18, 19]. Another group in this field is Sadler and co-researchers [20-35] who are working on Ru-based complexes called the "piano-stool" [36, 37] that are often characterised with bidentate nitrogen donor atoms (e.g. ethylenediamine) coordinating with the metal. Both group of researchers are exploring the use of cyclic π-ligand with other ligands coordinated to the Ru metal centre as potential anticancer agents. It has been observed that metal in a way has been enhancing and even inducing some pharmacological properties into ligands as some non-cytotoxic ligands in metal complexes lead to compounds with significant anticancer activities [38-40].

Our research effort is directed towards proposing the possible target of anticancer organometallic complexes of ruthenium(II) using docking methods and designing more selective anticancer agents by focusing more on cancer peculiar proteins other than DNA. We are interested in designing complexes that will display higher activity at lower dose because most of the current compounds with potential anticancer are only effective at high dose [19]. The search for the alternative targets for Ru-based complexes is a research challenge as the targets of many of these complexes can not be ascertained [5, 8-11]. There has been some controversy about similarities and differences in the anticancer chemistry of *cis*-platin and Ru(II) complexes with some suggesting that Ru(II) complexes probably function in a different manner from *cis*-platin while other stated that they mimic *cis*-platin [41]. However, organometallic Ru(II) anticancer complexes are reported to be more similar to *cis*-platin than to inorganic Ru(II) compounds [41]. The lack of proper understanding of the targets of Ru-based complexes is hindering their rational design [10] and its the major factor that is hindering the national cancer institute (NCI) approval of Ru-based complexes like indazolium trans-[tetrachloridobis(1H-

indazole)ruthenate(III)] (KP1019), and imidazolium trans-[tetrachlorido(1H-imidazole)(S-dimethyl sulfoxide)ruthenate(III)] (NAMI-A) [7].

There has been a great deal of research directed towards generating novel complexes for anticancer testing but the rational design has been hampered due to lack of understand of their mode of actions [10]. Many of these organometallic complexes have been reported to be unstable and have complicated ligand exchange chemistry [5]. However, some ruthenium organometallics have displayed high water- and air-stability [8, 42]. There have been many experimental reports on the anticancer activities of metal-based complexes without any detail understanding of electronic structural properties in relation to the observed activities and the instability of some complexes [5]. The theoretical methods have been used enough to complement and sometimes even to challenge experimental data in areas like predicting the geometries, vibrational frequencies, bond dissociation energies, and other chemically important properties [43]. In drug design there is need for a clear understanding of the physicochemical properties of the drug candidates [44] which will enhance their rational design.

Another significant part of this project is the experimental synthesis of the proposed complexes from computation and the study of their anticancer activities.

1.2 Methods of cancer treatment and need for alternative metal-based anticancer agents

There are four standard methods of treating cancer which are surgery, chemotherapy, radiation therapy, immunotherapy and biological therapy [45]. Surgery is taken to be the first and the best approach for external tumours and primary cancer that have not been metastasised. Radiation therapy uses high-energy radiation from X-rays, gamma rays, and radioactive particles to shrink tumours and kill cancer cells. Chemotherapy deals with application of drugs which is found to be the best means of

controlling metastasised cancer and also found useful for many primary cancers even before any attempt of surgery. Water-soluble organometallics based on radioactive elements such as 99mTc, 188Re and 186Re are applicable for diagnosing and to potentially treat cancer. The radioactive metal centre will provide the activity while the ligands that are attached to the metal centre will determine the selectivity and efficiency of these compounds to target diseased cells [5]. Also, some drugs like Bexxar combine both the radioactive and chemical properties together. Bexxar is a radioactive tositumomab that is linked covalently with iodine-131. Bexxar binds to CD20 and also directs radioactivity to B-cells. The function of CD20 is not clear but it is known as a B cell-specific surface antigen that plays role in B cell activation and proliferation [46]. Another example is Zevalin (Yttrium-90 ibritumomab tiuxetan) which is a radioactive antibody directed against CD20 on B lymphocytes. It is analogous to iodine-131 tositumomab. Zevalin is a tissue-selective agent against both normal and malignant B cells which induces apoptosis in CD20+ B-cell lines and also send the radiation from Y-90 to induce cellular damage in the target and neighbouring cells [46]. However, the focus of this thesis is on chemotherapy aspect of cancer treatment.

The goal of the National Cancer Institute (NCI) is to eliminate suffering and death due to cancer by year 2015 [47]. The possible means of achieving this aim by using chemotherapy anticancer drugs is suggested to be in the combination of the three classes of chemotherapeutic anticancer drugs which entails:

i. Cancer-specific targets

ii. Universally-vital targets but with selective protection of normal cells and

iii. Tissue-specific targets [47].

Each of these classes of chemotherapeutics for cancer treatment is associated with limitations as the cancer-selective agents are limited to rare Kinase-addictive cancers, semi-selective agents are not effective alone, cytotoxic agents are too toxic alone, and tissue-selective agents are reported to be

accidental [46]. Several efforts have been made in the past 30 years to elucidate the specific targets for cancer therapy and find the mechanisms of their actions. One of the first cancer targets identified is Bcr-Abl Kinase with the inhibitors gleevec and imatinib developed to treat Bcr-Abl-positive-leukemia [47]. Despite the growing rate of research on cancer therapy and the number of drugs as anticancer agents, yet the rate of the survival (65.3 per 100000 people) of cancer infection is far less than the rate of cancer death (181.3 per 100000 people) which is an indication that more efforts are needed to address the issue. Out of the list of more than 100 drugs that have been approved as anticancer agent from the NCI [48], it is only *cis*-platin and its derivatives that are metal-based drugs. The *cis*-platin is known since the history of cancer treatment as the most notable anticancer therapeutic drug [49]. The superior activities of *cis*-platin are traceable to the opportunities that are offered by metal in drug design such as ability to go beyond the coordination number four in carbon atom, act as glue to attach different ligands that may act in a synergistic fashion with each part, exploit endobiotic metal transport pathways to give a degree of tumour cell targeting, redox properties offer tumour cell selectivity and also accord some unique properties like structural diversity, adjustable ligand exchange kinetics, fine-tuned redox activities and distinct spectroscopic signatures [7, 49]. Because of several binding geometries that are possible using metal atom which gives it an improved ability to build many structures, it is referred to be serving as a stable imaginary ‘‘hypervalent carbon’’ [49].

Cis-platin and its derivatives are the only metal-based anticancer drugs that are at present in clinical usage and continue to be used in up to 70% of all cancer patients [5, 6]. They have been used to treat many cancerous cells and organ including ovarian, oropharyngeal, bronchogenic, cervical and bladder carcinomas, lymphoma, osteosarcoma, melanoma, neuroblastoma [18] and testicular cancer which prior to the introduction of these drugs, 90% of patients usually died [7]. Despite their tremendous success, they still suffer some disadvantages like being inefficient against platinum-resistant tumours especially their inactivity against many cancer cell lines and metastasis (secondary)

cancers [6] and are associated with severe side effects such as nephrotoxicity due to their high general toxicity [8]. *Cis*-platin protein interactions are often considered to be random and non-specific, with *cis*-platin being particularly susceptible to interactions with sulfur-containing residues such as cysteine and methionine. They also offer very little possibility for rational improvements to increase its tumour specificity because of its particular structure.

There are three metal-based antineoplastic chemotherapeutics of Pt compounds namely *cis*-platin, *carbo*-platin, and *oxalo*-platin, which are approved for worldwide clinical practice. However, they are frequently accompanied by severe side effects, and their activity is limited in many widespread tumours due to acquired or intrinsic resistance [14]. As a result of the limitations of *cis*-platin, many other metallic and organometallic anticancer drugs have been suggested and some are already passing through the phase II clinical test. There is also the cruel consequence of cancer development after approximately 10 years of *cis*-platin therapy because of *cis*-platin-induced DNA lesions which lead to incentives to develop therapies that do not target DNA [7]. The cancer-induction is believe to be the result of the irreversible binding of *cis*-platin to DNA but metal like ruthenium has been discovered to bind to DNA reversibly. Another disadvantage of DNA target compared to protein targets is that DNA is present in both healthy and cancerous cells including eventual tumours and their metastases while protein targets provide the possibility of obtaining selective drugs as many of the proteins are diseases peculiar [7]. Examples of metallic anticancer drugs are metallocenes. All medicinally important bent metallocenes have a *cis*-dihalide motif which is similar to the *cis*-dichloro motif of the well-established anticancer drug *cis*-platin [8]. Besides platinum, other metals like Fe, Ga, Ti, Ir, Co, Ru, Au, Os and Rh are the most often screened metal-based complexes as anticancer agents but Ru in the oxidation state of +2 and +3 is taking the lead. In the quest for metal compounds to extend the spectrum of activity of metallodrugs, ruthenium complexes have been identified to be the most promising alternatives to Pt complexes [14]. A very important organometallic anticancer drugs of recorded efficiency against cancer

cells are ruthenium-based antitumor drugs. The idea of using ruthenium-containing organometallics as anticancer agents was first developed by Tocher *et al*. [50]. Ruthenium complexes have a stronger affinity for cancer tissues more than normal tissues due to its ability to bind readily to transferrin molecules in plasma where it is transported to the tumour tissues. Then the ruthenium-transferrin complex is internalized into tumour cells through transferrin receptors to accumulate specifically in cancer tissues [51, 52]. Besides KP1019, and NAMI-A which are Ru-based drugs in clinical test, many other promising Ru complexes such as RAPTA (R = Ru, A = ≈6-arene, PTA = 1,3,5-triaza-7-phosphaadamantane) and piano-stool form of complexes have been found to have high inhibitory activities against tumours. These type of cancer therapy can not be classified as cytotoxic and also they are non-toxic to healthy cells because the ruthenium may mimic iron in binding to biological molecules such as serum transferrin and albumin [5], they have been found to inhibit cancer metastasis and have only mild effects on the primary tumour [8]. PTA ligand in RAPTA complexes confers water solubility and is of critical importance for it could facilitate the administration and transportation of the drugs and exhibit the pH-dependent DNA damage [5, 9]. One of the limitations of RAPTA complexes is that they are prone to hydrolysis and would have to be administered in saline to suppress the cleavage of the chloride ligands. One of the suggested means of circumventing this problem is the synthesis of RAPTA with bidentate ligands to replace the labile chloride ligands. Some ruthenium-arene complexes are unstable and have complicated ligand exchange chemistry. Increasing their stability might provide better drug candidates [5].

1.3 Methods of improving anticancer activities of metal-based drugs and proposing their targets

Recent studies on several cytotoxic metallodrugs revealed that their biological and

pharmacological actions are independent of DNA contrary to the initial opinion that the mechanism of their action relies on direct DNA damage [8, 9]. Dyson and Sava [6] in their study observed that the discovery of innovative agents that will address the tumour malignancy lies not simply assuming that DNA is the only relevant target of metal-based drugs but focus must be on how these organometallic cancer drugs could match and pharmacologically interact with protein targets of significant function to cancer existence. Another strategy that is being used in designing organometallic drugs is attaching an organometallic fragment to compounds of known biological function [5, 6]. This alternative approach to the discovery of new metallodrugs involves binding an organic compound of known therapeutic value to a metal-containing fragment which results in the metal-drug synergism in which the metal acts as a carrier and stabilizer for the drug until it reaches its target, while the organic drug fragment carries and protects the metal, preventing side reactions in its transit toward a second target of biological action [53]. This is gaining recognition because of its ability to endow existing drugs with new properties which include overcoming drug resistance. This was reported to be used by Brocard and co-workers to modify the chloroquine series of drugs, to produce a ferrocenyl derivative called ferroquine which has been proven to be effective against chloroquine resistant malaria parasites and is now completing phase II clinical trials [6, 8, 54]. Also in a research, Rajapakse et al [53] found out that the potency of Ru(II) complexes of chloroquine against malarial resistant parasites is consistently higher than that of chloroquine. The compounds also inhibited the growth of colon cancer cells, independently of the p53 status and of liposarcoma tumour cell lines with increased sensitivity. Also, ruthenium complexes were discovered as protein Kinases and HIV-1 reverse transcriptase inhibitors [55]

The activities of any potential pharmaceutical compound as representative of their *in vivo* behaviour can be predicted through the study of their effects on cell culture. The growing of cells *in vitro* is made possible because of the genetic modifications that take place in the diseased cells like cancer cells since the normal cells do not grow in tissue culture [5]. Due to the complexity of

mammalian cells, it is not possible to identify all the *in vivo* interactions of the biomolecules with the drugs using *in vitro* study [5]. The complexity of cancer in human patients can not be completely represented by *in vitro* studies nor entirely modelled by one *in vivo* system but through the combination of appropriate *in vitro* and i*n vivo* models [56]. The metabolism of many diseased cell are altered, which results in a lower oxygen concentration, reduced pH and elevated levels of glutathione in the cancerous tissues. This promotes a reducing environment which helps in the activation of many anticancer drugs [5] especially the Ru-based drugs. Sava *et al* [7] suggested that protein inhibition assays should become the first screening step in metal-based drug development. Although there are many *in vitro* promising metal-based complexes, yet they have a relatively low representation in the clinic because most of the drugs with good *in vitro* properties fail to show any therapeutic effect *in vivo*. This has been reported to be due to pharmacokinetic limitations, cross-reactivity, general toxicity, low initial efficacy and rapid development of drug resistance [7].

Cancer progression is known to start from the primary tumours and migrate to metastasised tumours which become a systemic problem that is very much difficult to treat. The process of metastases was explained to involve tumour cells migration from the primary tumour to enter the circulation (intravasation), detachment of tumour cells from the local primary tumour, invasion of intercellular matrices, penetration of basement membranes of blood vessels, resist anoikis that initiate cells apoptosis when out of their cellular contact, circulation while undergoing homotypic aggregation, extravasation, immune escape, induction of new blood vessels (angiogenesis), proliferate and successfully grow into a clinically relevant metastatic lesion [56, 57]. Access to primary tumour has made it possible to carry out *in vivo* sensitivity testing and to obtain tissue for studying the therapeutic mechanism and molecular changes in response to treatment [58].

1.4 The mechanism of anticancer activities and proposed targets.

There are many proteins that are proposed to play some significant roles in cellular tumour invasion apart from DNA. Some of them are urokinase plasminogen activator receptor (uPAR) [59], cathepsins B [59], topoisomerase I and II (top I & II) [58, 60], HER-2 [58], the tumour suppressor protein p53 and its regulators (including c-Jun NH_2-terminal Kinase (JNK)) [13], hypoxia-scolaroinducible transcription factor-1 (HIF-1) is also another attractive target for enhancing the therapeutic efficacy against many tumour cells especially non-small cell lung cancer (NSCLC) cell lines [61]. Several studies have shown that an elevated level of HIF-1 is associated with radio-resistance and chemo-resistance which leads to a poor prognosis especially in lung cancer that is still the leading cause of cancer deaths worldwide. It is found to be related with more aggressive phenotypes of tumour cells and the therapeutic resistance of tumour cells. HIF-1 is a heterodimer composed of HIF-1 alpha and HIF-1 betal subunits and is one of the most important regulatory molecules that respond to hypoxia for cell survival. Therefore, down-regulation of HIF-1 was associated with proteosomal degradation and decreased Akt phosphorylation [61]. However, it is not easy to find them because HIF-1 is a transcriptional factor, which is not a conventional target of drugs.

The interaction of metallodrugs with plasma proteins is also relevant, as platinum and ruthenium compounds may bind to proteins such as serum transferrin and albumin, which are normally used to deliver iron to the cells [5]. Different methods have been used to improve the effective delivery of anticancer drugs to tumour tissue in order to improve their selectivity and consequently, reduce side effects. This has lead to enhancement of the intracellular concentration of drugs in cancer cells, usually without being blocked by P-glycoprotein, a protein responsible for multidrug resistance [62]. Serum albumin has been exploited as a drug-delivery system as albumin conjugates for the delivery of anticancer agents and albumin nanoparticles for drug encapsulation because of its accumulation in solid

tumours. Albumin conjugates with methotrexate and a doxorubicin derivative and an albumin paclitaxel nanoparticle (nab-paclitaxel; abraxane) have been evaluated in clinical trials. Also albumin conjugates of the platinum(II) anticancer drug *carbo*-platin were shown to be as, or more, effective and even in some cases, were less toxic than *carbo*-platin in reducing the tumour size of nude mice bearing human breast tumours [62]. In another attempt to improve the physicochemical properties and bioavailability of organometallic anticancer, researchers have coupled cyclin-dependent Kinase (Cdk) inhibitors with organometallic moieties [62]. Stepanenko et al [62] have synthesized the complexes of [RuCl(η6-arene)(L)]Cl in which the arene is 4-formylphenoxyacetyl-η6-benzylamide and L is a Cdk inhibitor [3-(1H-benzimidazol-2-yl)-1H-pyrazolo[3,4-b]pyridines and indolo[3,2-d] benzazepines to evaluate the antiproliferative activity and bioavailability. Some of the promising effects of these complexes are increased solubility in physiologically relevant media and synergistic effects from metal and ligand leading to highly cytotoxic species [62]. A report has revealed that conjugation of the ruthenium moiety to modified rHSA was realized via hydrazone bond formation and cleavage of the hydrazone bond under acidic conditions has been exploited for drug release in cancer cells [63].

However, since there are many enzymes or proteins that have been discovered to play some vital role in cancer growth and metastasis, it is not feasible to consider all in a single project. But it is interesting to know that some drugs that are designed against cancer associating prominent enzymes like top II can also significantly hinder the expression of some of the other enzymes. There are reports on inhibition of hypoxia-induced HIF-1 protein accumulation in tumour cells through the administration of individually camtothecins, topotecan and etoposide which are Top II inhibitors [61, 64] and a better effect was even observed when topotecan and etoposide were combined [61]. It has been experimentally shown that the modulation of the HIF-1 expression by Top inhibitors requires the expression of Top [61].

Even though cell apoptosis through drugs that are cytotoxic is the main approach in cancer

treatment yet the use of multi drug therapy is necessary especially to administer cytotoxic with other drugs that have the ability to deactivate the activities of some enzymes that will prevent cell apoptosis. Many common chemotherapeutic drugs and other inducers of DNA apoptosis result in activating NF-κB nuclear translocation and its DNA-binding. Because some of the anthracyclines such as daunorubicin that induce DNA-damage through inhibiting topoisomerase II also undergoes redox cycling to produce oxygen free radicals, it was initially believed that production of oxygen free radicals is responsible for the activation of NF-κB binding to DNA until it was recently disproved [65]. Many proteins or enzymes have been proved to be significant in tumour growth and metastasis. The connection between the level of expression of these enzymes in the tumour cell and the degree of apoptosis has been demonstrated experimentally. In one of the studies, the higher apoptosis level discovered in patients with breast cancer who responded to anthracyclines such as daunorubicin, doxorubicin and aclarubicin [65] treatment showed that top II levels declined in responsive tumours [58]. Some additional ezymes or proteins of interest to us in this project as potential target in cancer therapy are:

i). Ribonucleotide reductases (RNR): The action of this enzyme is responsible for the synthesis of DNA from the corresponding building blocks of RNA. These enzymes convert ribonucleotides (a base and phosphate group linked to a ribose sugar) into deoxyribonucleotides (a base and phosphate linked to deoxyribose sugar) [66].

ii). Histone Deacetylase (HDAC7): Histones are proteins that assist in the packaging of DNA into chromosomes as well as in gene regulation and are effective through acetylation and deacetylation. The inhibition of this becomes the drug target because without its function of removing acetylated groups, the signalling switches will become stuck in one position and loses their effectiveness [66]. Histone deacetylase (HDAC) inhibitors have been shown to be potent inducers of growth arrest, differentiation and apoptotic cell death [67].

iii). Cathepsins B: Cathepsin B has been reported to play significant roles in glioma invasion which is a complex primary brain disease of tumour invasion [59]. Cathepsin B (CatB) is an enzyme that is involved in cellular metabolism and it is implicated to take part in the tumour progression and metastasis processes which makes it a suitable target for the design of anti-metastatic drugs [68]. The use of Cat B inhibitors has been reported to reduce both the *in vitro* tumour cell mobility and invasiveness [9].

iv). Topoisomerase II (Top II): This plays an important role in replication, transcription, recombination and segregation of chromosomal pairs during cell division. Topoisomerase IIa (top IIa) has been reported experimentally as a known molecular target for anthracyclines and it is found to be frequently co-amplified with HER-2 in breast cancer [58]. In the absence of drug, Top1 plays a key role in relaxing supercoiled DNA for replication and transcription [60]. It is also involved in maintaining the structural organization of the mitotic chromosomal scaffold [52].

v). Thioredoxin reductase (TrxR): TrxR system (TrxR reductase, and NADPH) is an ubiquitous flavoenzyme of thiol oxidoreductase system that regulates cellular reduction/oxidation (redox) status [9, 69]. It is a large homodimer with a glutathione reductase-like structure. TrxR is a likely pharmacological target for a range of metallodrugs because its active site selenolate group manifests a large propensity to react with "soft" metal ions after its reduction [9]. Human TrxR has a conserved dithiol active site, Cys32-Gly-Pro-Cys35, and contains three structural cysteine residues (Cys62, Cys69, and Cys73) [70].

vi). Thymidylate synthase (TS): Thymidylate synthase (TS) gene is located on chromosome 18p11.32 and it is a critical enzyme in maintaining a balanced supply of deoxynucleotides required for DNA synthesis and repair [71]. Thymidylate synthase and dihydrofolate reductase are choice targets of chemotherapy to test the vulnerability of cancer cells to the inhibition of TMP synthesis [66].

vii). Recombinant Human albumin (rHA). This has been reported [36] as the most abundant protein

in blood (ca. 0.6 mm) which plays a significant role in the pharmacokinetic availability of a wide range of drugs, including metallodrugs and consequentially determines their bioavailability and toxicology. Serum proteins can play a divergent role either in delivery of metal-based anticancer drugs to their cellular targets or in deactivating them even before reaching the target(s) [38].

viii). DNA gyrase: This is included in this project to know the possibility of anticancer agents also acting as antimalarial agents which can be relevant since bacterial infections are known to be opportunistic infections. DNA gyrase controls the topological state of DNA [72] and uses the free energy of ATP hydrolysis to catalyze the negative supercoiling of double-stranded circular DNA [73]. Since the relaxation of DNA is essential for DNA replication and transcription, therefore the inhibition of DNA gyrase blocks relaxation of supercoiled DNA, which makes gyrase a suitable target for antibacterial agents [72, 73].

ix). BRAF Kinase: Among the RAF isoforms, BRAF Kinase represents an excellent target for anticancer drug development because it differs significantly from CRAF and ARAF as a major activator of MEK1/2 and requires fewer regulatory events for activation [74]. These BRAF mutations are found in a variety of cancers which includes 67% of melanomas, 30-50% of thyroid cancers, 30% of ovarian cancers, 5-20% of colorectal cancers, and 1-3% of other cancer types [74].

x). Histone Protein in Nucleosome core particle (HP-NCP): NCP has been pointed out as a basic repeating element of histone-packaged DNA comprising chromatin. Chromatin has become one of the potential superlative therapeutic targets for metallodrugs and other compounds because of its abundance and primary regulatory function of histone proteins in DNA sites [15].

1.5 Computer-aided drug design application

The major focus of computational science is to transform theories into computer algorithms and

use it to understand the science of its systems. This computational method helps to solve problems whose difficulty or complexity places them beyond analytical approach or human endurance [75].

In the pre-clinical drug discovery, an indispensable computational method that is commonly used is docking of ligands into the target protein binding site in order to understand their mode of interaction, find the correct conformation of a ligand and its receptor and to screen the library of ligands through their binding energy. This is used as one of the important tools of high-throughput virtual screening to generate “hits” and enrich compound libraries. It is also used to optimize “hits” into lead series which includes testing of structure-activity relationship (SAR) hypotheses as well as evaluation of novel scaffolds and core templates [76].

The first step in structural based drug design is to find out the structure and the enzymes or the proteins that are unique to the life-cycle and functions of the responsible pathogens. The most sensitive work of the researcher in this step is to be sure that the enzymes that are identified as significant to the pathogens are not having strong hit with any of the human proteins [77]. Computational chemistry is applicable at the early stage of drug research to reduce the number of possible ligands and also at the end during lead-optimization stages in an effort to reduce experimental costs and times [78]. Though it is possible to get the detail structures of biological macromolecules such as protein experimentally, it is hard to study the change on a short time scales as individual structures of the molecules functions. Also, experiment alone cannot study the molecular mechanisms of fast processes such as chemical reactions in enzymes or ion transport through membranes. These problems are solved through the use of fundamental physics theorems which are used in modelling how proteins and other biomolecules move, fluctuate, interact, react and function. Through simulation, structures can be analysed in atomic detail and experimental data can be interpreted in terms of atomic level interaction to show the mechanisms of biomolecular function rather than providing pretty pictures as in experiment. Also, it reduces the cost and the time of new drug to reach the market. For instance in in less than 2 years from

the start a novel, potent, and selective anti-anxiety, anti-depression 5-HT1A agonist reached the stage for clinical trials with less than 6 months of lead optimization and synthesis of only 31 compounds [79]. The development of more accurate and reliable algorithms in computational chemistry has made it a significant method that is used to exploit the opportunities of potential new drug targets emerging from genomic and proteomic initiatives and to screen the large libraries of small compounds now readily available through combinatorial chemistry [78].

The best known success stories of computer-aided drug design are in HIV and flu drugs. Since the early success in the application of computational modelling, it has become an integral part of drug discovery and almost every recent drug from big pharmaceutical companies to market has involved some sort of collaboration with computational chemistry. Computational modelling plays a salient role in drug discovery mostly because no drug is created solely *in silico* [80]. Though high-throughput screening are now available in both academic laboratories and drug companies, the cost of random screening of very large collections of compounds can be prohibitive. Therefore, where possible *in silico* or virtual screening has become a significant tool in drug discovery to filter down the number of compounds used in real screens to solve the problem of delay and expense in synthesis [81].

Compared to organic compounds, organometallic complexes are rarely studied computationally due to difficulties of optimizing and computing metal complexes [68]. Taking an instance of RAPTA complexes, there are little computational studies of these complexes such as in clarifying the experimental data on pK_a values [82], docking to cancer macromolecules [51], QM/MM study of the interaction of Ru(II)-based complexes to macromolecules [68], DFT study of the interaction of the complexes with residues that characterise the binding sites of cancer macromolecules [41]. Also, there have been several successful applications of molecular docking studies in rational drug design but they have limited application to study metal complexes [9] mostly due to the lack of appropriate force fields to take care of metal atoms [83] and their relativity properties.

CHAPTER TWO

2 LITERATURE REVIEW

2.1 Metal based complexes as promising anticancer agents

Since 1960s when Rosenberg discovered that *cis*-platin inhibits cell division in bacteria, it was subsequently identified as a potent anticancer agent in 1970 and quickly became the most widely used cancer chemotherapeutic drug [16]. *Cis*-platin entered clinical trials in 1971 and, within a relatively short time, became the most widely used anticancer medicine [13]. *Cis*-platin is extremely effective against several cancers like testicular and ovarian cancers [16]. Its application is also accompanied by severe side effects, like nausea, vomiting and hearing loss, and many tumours show intrinsic or acquired resistance against the drug [16]. Its application is also limited by its activity in a few numbers of tumours [17], severe toxicity, and also by drug resistance which may be natural resistance to *cis*-platin or a developed resistance after initial treatment [13]. Other *cis*-platin derivatives that are developed as a result of these limitations are *carbo*-platin and *oxalo*-platin (Table 2.1) which defer from *cis*-platin mainly in terms of their rate of aquation and therefore their overall reactivity [16]. Other drug that have been developed to treat *cis*-platin resistant cancers are complexes of ruthenium, gallium, titanium and gold [17]. These drugs exhibit a different mode of action compared with platinum-based drugs and are found to treat *cis*-platin resistant cancers [17].

Since the last 30 years, many experimentalists together with theoreticians have been partaking in the design and evaluation of the antitumour properties of a wide selection of metal-organic compounds against cancer targets with the aim of getting better potent therapies for cancer cells. The significant impact of metal-based drug (*cis*-platin) in clinical application and the limitations associated with its uses have motivated extensive investigations into alternative metal-based cancer therapies. The

investigations to produce drugs that will be widely used as *cis*-platin and its derivatives have not been successful even though many other drug targets have been identified along the way [13] as well as many potential anticancer agents. This is what call for further research efforts to discover other metal-based drugs that will address the limitations that are associated with the use of *cis*-platin and its derivatives. Besides the *carbo*-platin and *oxalo*-platin derivatives of *cis*-platin that are approved for worldwide usage, there are other platinum-based drugs that have been approved for regional uses. Nedaplatin is approved in Japan, heptaplatin in South Korea, lobaplatin in China (Table 2.1) [84]. Report has shown that the first ever marketed transition organometal drug was ferrocerone that was clinically approved in the USSR as antianeamics [8]. Organometallic complexes offer aspects for medicinal chemistry that are not available with organic drugs, in particular because of their coordination and redox properties [85]. The quest for alternative anticancer drugs, resulted in a variety of cytotoxic organometallics, of which (arene)-ruthenium complexes occupy a prominent position because of their unique combination of lipophilic and hydrophilic properties [51]. Many of the ruthenium potential drugs are characterised by low general toxicity, which is attributed to the ability of ruthenium to accumulate specifically in cancer tissues, possibly via the transferrin pathway [51].

In the field of cancer chemotherapy, the cyclopentadienyl complex, $[Cp_2TiCl_2]$ has been in clinical trials and a ferrocene derivative of tamoxifen is also in clinical trials for breast cancer therapy [37]. Since metal-based drugs tend to undergo activation following administration, they are then being considered as prodrugs that are activated *in vivo* [17]. The mechanism of their action comprises simple hydrolysis/aquation and subsequent reaction with proteins or DNA [17]. Many promising compounds which include derivatives of the clinically tested titanocene dichloride (Table 2.1), ferrocene-modified established drugs, square-planar gold drugs, and ruthenium–arene and osmium–arene complexes appear to have the potential to overcome the limitations of current chemotherapeutics [17]. Among the most prominent potential anticancer candidates today are KP1019 [12, 86], NAMI-A [87-92] and

[dichlorido(η6-toluene)(PTA)ruthenium(II)], where PTA is 1,3,5-triaza-7-phosphaadamantane (RAPTA-T) [16] (Table 2.1). NAMI-A and RAPTA-T seem to be highly effective against metastases, whereas KP1019 shows good activity towards primary tumours. Also, several other Ru-based complexes have been synthesised and characterised as anticancer agents [41, 93-124].

Table 2.1 The metal-based drugs that are already in clinical use, in clinical trial and in research level [84].

Structure/Name/level of application	Structure/Name
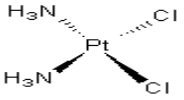 *Cis*-platin The first and the best metal-based anticancer drug in clinical use worldwide	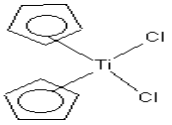 Titanocene This entered clinical trials as an anticancer agent in 1990s
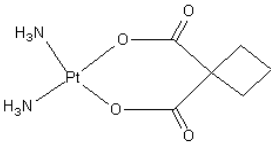 *Carbo*-platin Derivative of *cis*-platin in clinical use worldwide	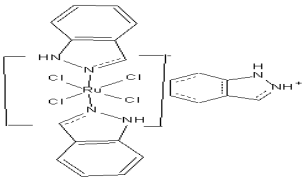 KP1019 In clinical trial
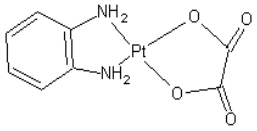 *Oxalo*-platin Derivative of *cis*-platin in clinical use worldwide	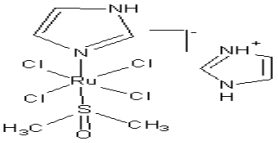 NAMI-A In phase II clinical trial
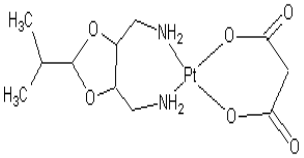 Heptaplatin Heptaplatin is a derivative of *cis*-platin approved in South Korea only	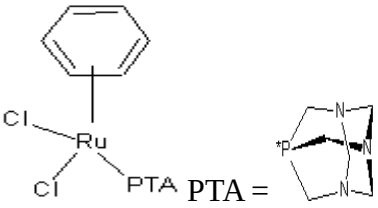 PTA = RAPTA-B Still at laboratory research level

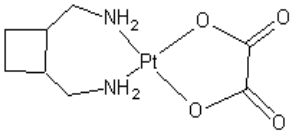 Lopaplatin Lobaplatin derivative of *cis*-platin approved in China only	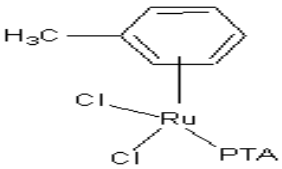 RAPTA-T Still at laboratory research level
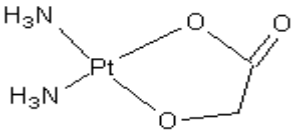 Nedaplatin Nedaplatin is a derivative of *cis*-platin approved in Japan only	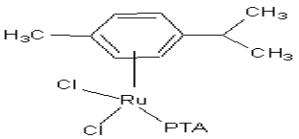 RAPTA -C Potential anticancer drugs from Dyson *et al*.
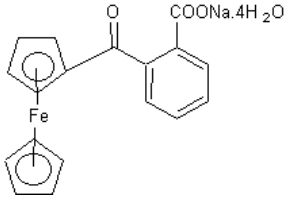 Ferrocerone Ferrocerone (sodium salt of O-carboxybenzonyl ferrocene) is the first ever marketed transition organometal drug that was clinically approved in the USSR to treat iron-defficiency anemia (antianemics).	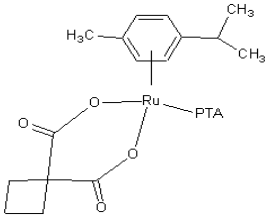 Carbo-RAPTA-C Still at laboratory research level
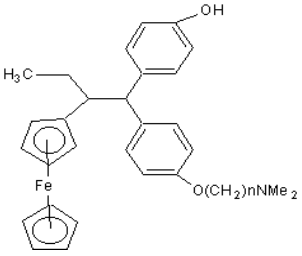 Ferrocifen This is a metal-based derivative of the anticancer drug tamoxifen. It is shown to inhibit proliferation of both hormone-dependent and hormone-independent forms of breast cancer	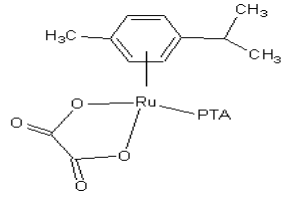 Oxalo-RAPTA-C Still at laboratory research level
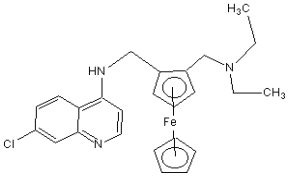 Ferroquine Found to be highly active against chloroquine-resistant strains of the malaria parasite.	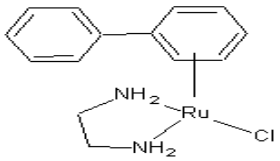 Piano-Stool Ru-Complex Potential Anticancer drugs of Ru(II) arene ethylenediamine derivatives (refers to as “piano stool”) from Sadler et al Lab

It is very important in drug design to make a careful choice of the chemical reactivity of the complexes so as to balance the inertness required for the drug to reach its target site (e.g., DNA) and minimize attack on other sites (side effects) yet allow the activation necessary for binding to the target [37]. Hydrolysis has been seen as an important activation mechanism of reactions of Ru complexes with biomolecules. Therefore, the factors that control the aqueous chemistry of organometallic complexes are proposed as tools that may allow the design of effective anticancer agents. The presence of an arene in Ru(II) complexes has been found to greatly stabilize Ru(II) compared with Ru(III) even though ruthenium has a rich redox chemistry. It has also been reported that the reactions of chloro Ru(II) arene complexes with nucleotides appear to involve initial aquation, and also Ru–OH_2 bonds appearing more reactive than Ru–OH bonds [37]. There is a high chloride concentration in blood plasma (the concentration of chloride in blood plasma or culture medium is ~104 mM and in the cytoplasmic is ~22 mM). The hydrolysis rate decreases in the order Cl ~ Br > I. Hydrolysis of *cis*-platin has been shown to be of rate constants of $7.56x10^{-5}$ and $6.32\ x10^{-5}$ s-1 for the first and second chloride ligands respectively [37].

Among new classes of Ru-based antitumor drugs emerging as alternative to the platinum-based anticancer therapy are: Ru(III) complexes such as trans-Ru(imidazole)$_2Cl_4$ and trans-Ru(dimethyl-sulphoxide)(imidazole)Cl_4 as anti-metastatic agents [68]. Presently, research focus is on the anticancer potency of Ru(II) due to research evidences that the Ru(III) pro-drug will interact with biological reductants in human system to form Ru(II) before it accomplishes its biological activity [68].

2.2 Inherent advantages of Ru-based anticancer complexes

Research interest has focused on organometallic compounds specifically on ruthenium(II)-arene compounds, which show excellent antiproliferative properties both *in vitro* and *in vivo* [125]. Cytotoxic drugs based on ruthenium have shown the greatest potential and remain the subject of extensive drug discovery efforts [51]. Ruthenium coordination compounds have been high lighted as most prominent non-platinum-based anticancer agents, with two representatives namely NAMI-A (Table 2.1) and KP1019 (Table 2.1) completed phase I clinical trials [13,17, 126]. The qualities of Ru metal that makes it the centre of research attraction as a substitute for *cis*-platin are further stressed in terms of the extensively developed chemistry of its coordination particularly with ligands of biological relevance; the preferred octahedral coordination for the common +2 and +3 oxidation states in aqueous solution, the adequate substitution rates, redox potentials for biological interactions and a demonstrated low toxicity [53]. Recently, Ru(II) is gaining more research attention as the mechanism of activation of known Ru(III)-based complexes like K1092 and NAMI-A is believe to be through the process of activation-by-reduction from Ru(III) as pro-drug to Ru(II) before accomplishing their biological activity [68].

There have been several excellent *in vivo* antitumor activities of ruthenium complexes but the *in vitro* activities are approximately 10 times lower than that of *cis*-platin [13]. More specifically, ruthenium complexes containing indazole heterocycles coordinated to the metal centre through nitrogen have been shown to act as cytostatic and cytotoxic drugs in colorectal tumour cells both *in vivo* and *in vitro* [13]. The process of their entering into the cells is suggested to be probably via interactions with transferrin [13]. However, the cellular molecular mechanisms of apoptosis induction the signalling pathways are yet unknown. Another Ru complexes is ruthenium(II)–arene complexes containing a 1,3,5-triaza-7-phosphaadamantane (PTA) ligand. These have been shown to have

moderate anticancer activity in various cell lines and an excellent activity with regard to reducing the number and weight of solid metastases but do not affect the primary tumour [13, 51]. These compounds show high selectivity toward cancer cell lines *in vitro*, and *in vivo*. They are reported to effectively reduce lung metastases in mice without significantly affecting the primary tumour. Out of many derivative of RAPTA that have been identified, synthesized and characterised, [Ru(η6-p-cymene)Cl_2(pta)] (RAPTA-C) (Table 2.1) is the best anticancer compound [13]. Experimentally, it has been shown that there is a reduced likelihood of RAPTA-C developing some types of drug resistance because the anticancer effect of RAPTA-C is mediated via different molecular pathways [13]. RAPTA-C was reported to exhibit effective cell growth inhibition by triggering G2/M phase arrest and apoptosis in cancer cells of Ehrlich ascites carcinoma (EAC) bearing mice [13]. In another study, the platinum compounds were demonstrated to be less reactive and considerably less selective in protein binding than RAPTA-C, which showed a high affinity towards ubiquitin and cytochrome c, but not superoxide dismutase [126].

Many derivatives of [(η6-arene)RuCl$(PTA)_2$], [(η6-cymene)RuCl$(PTA)_2$], [CpRuCl$(PTA)_2$] and [Cp*RuCl$(PTA)_2$] have been synthesized by Dyson *et al.* [127-141]. Many of these compounds have been reported to be similar because they display only weak *in vitro* activity but RAPTA-C shows excellent *in vivo* characteristics comparable to those of NAMI-A, which is only achieved at higher doses [19]. There is still several research efforts in place to derive compounds of π-ligand, PTA and halide ligands, of more cytotoxic at lower doses that will reduce tumour mass *in vivo* [19]. Compound of the type [(Cp′OR)RuCl$(PTA)_2$] are found promising with two orders of magnitude more active than a close model structure and also show excellent activity in a *cis*-platin resistant cancer cell lines [19]. Another cytotoxic RAPTA compounds especially in A2780 human ovarian cancer cells and also significantly more cytotoxic than other simple RAPTA compounds is [Ru(η^6-$C_6H_5CF_3$)(pta)Cl_2], termed RAPTA-CF_3, with the electron-withdrawing a,a,a-trifluorotoluene ligand [17]. This compound

has significantly lower pH, to achieve higher selectivity in the treatment of cancer and it has been found to associate with a more pronounced degree of decomposition of the oligonucleotide compared with RAPTA-C. It is observed that the biomolecule reaction mixtures of RAPTA-CF_3 contained mostly [Ru(pta)]–biomolecule adducts which were not observed in the protein or DNA binding studies of [Ru(pta)(arene)] adducts typical of other RAPTA compounds [17]. Therefore, the facile arene loss is proposed to be responsible for the increased cytotoxicity of RAPTA-CF_3 [17]. This can be another breaking ground for using RAPTA as a conveyor of notable cancer drugs into the cancer sites.

Despite the high volume of the *in vitro*, *in vivo* and theoretical studies on the behaviour of the RAPTA based compounds, their mechanism of action are not well known [68] and thus affect their further development. The poor correlation between the binding of RAPTA compounds to DNA and their cytotoxicity suggested that these compounds act through a mechanism different from the classical platinum anticancer drugs [68]. The mechanisms of action of ruthenium-based anticancer compounds are comparatively yet to be explored. It is predicted that ruthenium compounds might directly interfere with specific proteins involved in signal transduction pathways and/or alter cell adhesion and migration processes [126].

The best studied organometallic compounds are based on the ruthenium–arene scaffold and bear monodentate and bidentate ligands which include halides or dicarboxylates as leaving groups and 1,2-ethylenediamine (en), pta, pyrone, and paullone derivatives, and others as activity-determining moieties [17, 142-153]. It has been shown analytically, that most of the ruthenium-based drug candidates mentioned are capable of binding strongly to biological nucleophiles especially those bearing halides, mostly chloride, proceed via their replacement with soft donor atoms, such as the imidazole of histidine, the thiol of cysteine, or the thioether of methionine in the case of proteins or with N7 of purine bases, predominantly guanine, in the case of DNA. The bonding between Ru and N7 (guanine) is considered the predominant mode of action with DNA for Ru antitumor compounds [154]. It was

earlier established that compounds of RAPTA show a very favourable biological and pharmacological profile and a strong preference for protein binding over DNA [7, 9]. Their mechanism of action is DNA-independent and substantially different from *cis*-platin and related anticancer platinum drugs [9]. Both metallodrugs, *cis*-platin and RAPTA-C have affinities for the same amino acid residues on protein binding [126]. Metallation of specific amino acid residue affects the function of biologically crucial proteins through the formation of strong coordinate covalent bonds. The possibility of the combined ligands competing for the same binding site was revealed through the experimental observation that RAPTA-C competes with *cis*-platin for the same binding sites on three selected proteins, ubiquitin, cytochrome c and superoxide dismutase [126].

The unique function of ruthenium based complexes that distinguished them from *cis*-platin is the proposed function of binding protein targets more preferably than DNA which promotes their apoptosis function in wider tumour cells than *cis*-platin. To substantiate the hypothesis that DNA might not be the primary target for ruthenium-based complex, its adduct formation with DNA has been shown to proceed more slowly compared with *cis*-platin [16]. Triruthenium clusters are reported to be very active compared to ruthenium compounds. The predicted reason behind the higher biological activities of triruthenium clusters is traced to their known ability to form supramolecular interactions with arenes and other functions [125]. Such interactions may possibly be playing important roles in their mode of biological activity. Rhodium and Osmium analogues were evaluated in HT29 colon carcinoma, A549 lung carcinoma and T47D breast carcinoma cell lines *in vitro* and found to display activities that are not too dissimilar from the related ruthenium(II)-arene complexes [125].

Several works have been done on ruthenium-based antiumor, chelated RAPTA compounds [51], RAPTA with labile chloride ions [18], RAPTA chelated with potential Cdk inhibitors [62], the cytotoxic of diruthenium complex $[(p\text{-}MeC_6H_4Pri)_2Ru_2(SC_6H_4\text{-}p\text{-}Me)_3]^+$ which is shown to efficiently catalyze oxidation of the thiols cysteine and glutathione to give the corresponding disulfides [85]. In an

attempt to develop drugs that could resist hydrolysis in aqueous media, research attention has been given to the organometallic arene-capped ruthenium-(II) 1,3,5-triaza-7-phosphatricyclo[3.3.1.1]decane (RAPTA) complexes bearing chelating carboxylate ligands. Some of the new complexes, Ru(η^6-cymene)(PTA)(C_2O_4) (i.e. *Oxalo*-RAPTA-C, Table 2.1) and Ru(η^6-cymene)(PTA)($C_6H_6O_4$) (i.e. *Carbo*-RAPTA-C, Table 2.1), were found to be highly soluble and kinetically more stable than their RAPTA precursor that contains two chloride ligands in place of the carboxylate ligands [51].

The mechanism of Ru-based complexes is understood to be through hydrolysis where one of the chloride ion is replaced with water molecule, but that of the bidentate without any chloride ion is not well known but believe to be through ring-opening reactions [37]. The possibility of bidentate complexes following the same mechanism of hydrolysis for activation was also reported for Ru(II)- and Os(II)-arene complexes with alkoxycarbonylmethyl-3-hydroxy-2-pyridone ligands [38]. The highlight on the possible hydrolysis of these metal-hydroxypyr(id)ones was shown using the ^{1}H-NMR and ESI-MS on the incubated complexes with ***Gly***, ***Ala***, ***His***, ***Met***, and ***Cys*** [38]. There were observed signals that indicate the reaction of respective amino acid replacing the used bidentate hydroxypyridone within which ***Cys*** takes the lead by decomposing the Ru complex within minutes (the reason is suggested to be probably due to strong trans-effect of the thiol functionality) then followed by ***Met*** and ***His*** which also released pyridone ligand within 24 h [38]. The reason for the activity of ***Met*** and ***His*** to release the pyridone ligand is suggested to be due to the ability of both amino acids to act as bidentate or tridentate chelating ligands (with the thioether of ***Met*** and N1 or N3 atoms of the imidazole moiety of ***His*** as third donors in addition to NH_2 and COOH) [38]. Many chelate metal-arene complexes with chloride ion of the type [M(η^6-arene)-(XY)Cl]$^{n+}$ where M = Ru, Os; XY = bidentate of N,N-, N,O-, O,O- or S,O-chelating ligand; n = 0, 1 have shown promising cytotoxicity profiles [38]. Their significant feature for the cytotoxicity of metal complexes is their hydrolysis. Their complexes were found to hydrolyse rapidly upon dissolution in water by exchange of the chlorido ligand with a neutral water molecule and

exist predominantly as the charged monoaqua species of the general formula $[M(cym)\text{-}(XY)(OH_2)]^+$.

The choice of ligands is important because a ligand that binds too strongly could render the drug inactive, while a labile ligand could be easily hydrolysed or replaced. In order to obtain hydrophilic metal-based complexes, ligands with hydrophilic properties are often used as one of the most common approaches. One of those ligands of high solubility in water that is gaining research attention is the cage-like tertiary phosphane 1,3,5-triaza-7-phospha-adamantane (PTA) among water-soluble phosphanes due to extensive participation of its three nitrogen atoms in hydrogen bonding interactions with water molecules [155]. PTA has in recent years become a highly appreciated ligand because of its high water solubility properties and the catalytic applications of its metal complexes [156]. The RAPTA complexes with labile chloride atoms are prone to hydrolysis and would have to be administered in saline to suppress the cleavage of the chloride ligands. The problems that are associated with hydrolysed complexes are that they are often difficult to characterise and would be problematic for pharmacokinetics studies which can consequently affect the clinical trial [51]. The notable ligands that have been used to resist hydrolysis are bidentate carboxylate ligands. These were used to endow *cis*-platin derivatives, namely *carbo*-platin and *oxalo*-platin with high aquatic solubility and resistance to hydrolysis. Though *carbo*-platin is active in the same range of tumours as *cis*-platin, it has been found to be much less toxic than *cis*-platin and may be administered at higher doses. The derivative, *oxalo*-RAPTA-C has been shown to completely resist hydrolysis while *carbo*-RAPTA-C is susceptible to hydrolysis [51].

The hypothetical reasons why ruthenium-based complexes are becoming promising anticancer drugs than *cis*-platin and its derivatives are due to the facts that the cancerous cells have more chemically reducing environment than healthy ones [10]. Thus favouring the reactivity of ruthenium-based anticancer as Ru(II) rather than Ru(III) whereas platinum-based drugs does not follow reduction. In contrast to *cis*-platin, Ru compound (NAMI-A) which was recently launched in the clinic shows

remarkably low general toxicity. Ruthenium complexes have been shown to specifically accumulate in tumour cells and thereby reduce general toxicity of NAMI-A compared to platinum drugs which could be due to ruthenium selectivity [18]. Ruthenium complexes have a stronger affinity for cancer tissues than normal tissues because ruthenium binds readily to transferrin molecules in plasma forming ruthenium-transferrin complex and is transported and internalized into tumour cells through transferrin receptors which are abundantly expressed on the surface of tumour cells [52]. Among the metal atoms used in anticancer metal complexes, ruthenium is most unique [52, 53]. It is a rare noble metal unknown to living systems and has a strong complex-forming ability with numerous ligands [52]. The properties that accord ruthenium drugs all the promising advantages are summarised in the rate of ruthenium ligand exchange, the range of accessible oxidation states of the metal and the ability of ruthenium to mimic iron in binding to certain biological molecules [11]. $RuCl_2(C_6H_6)$(dmso) was reported to completely inhibit DNA relaxation activity of topoisomerase II and form a drug-induced cleavage complex [52].

Also, functional group modification of the ligands can significantly affect the activities of the entire complexes. It has been reported that modifications on the PTA ligands through functionalization of the PTA phosphane like [1-R-PTA](where R = Me,Et, (CH_2)4I, CH2Ph, CH_2py (pymePTA), di-N-methylated, di-N-acylated (DAPTA) or di-N-formylated (DFPTA), N-boranyl adduct 1-BH3-PTA, affect their chemical properties, and many have been found to improve the water-solubility, as well as the DNA binding properties and antimicrobial activity [156]. There have been many functionalized PTA phosphanes but very less research on the chemistry of the metal complexes of these ligands [156]. Many of the complexes of the functionalize PTA with hydridotris(pyrazolyl)borate (Tp) ruthenium(II) complexes were also reported [156].

2.3 Review of some Ru-based complexes

Among the metal atoms used in anticancer metal complexes, ruthenium has been defined to be the most unique [52, 53]. In some complexes of Ru-based, Ru metal has been proved to be significant and suggested to take part in the anticancer activity since substitution with another metal resulted in lower anticancer activity (e.g. NAMI-A, RM175) [157]. The possibility of metal in a complex not directly involve in interaction but acts as an holder for ligands interaction with receptors has been reported in the literature [157] though the metal has significant electronic effect on the ligands interactions and stability. The greatest limitation in effective design of the Ru-based complexes is the absence of convincing data on the fine mechanism of their actions and lack of clear knowledge of their target [157]. Functional group has significant effect on the cytotoxicity of Ru-based complexes as Sadler et al [158] reported the loss of cytotoxic activity of Ru arene organometallics upon oxidation of their amine ligand such as o-phenylenediamine (o-pda) to the corresponding imine ligand o-benzoquinonediimine (o-bqdi). Several derivatives of Ru-based complexes have been screened as potential anticancer agents as shown in Table 2.2.

Table 2.2 Selected mononuclear Ru(0), Ru(II) and Ru(III) complexes that have been screened as anticancer agents except where otherwise stated.

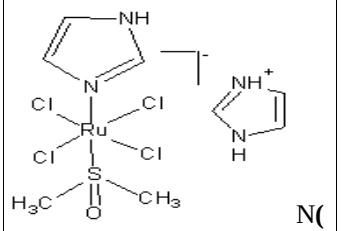 N(**1) N**AMI-A [157]	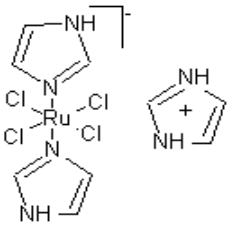 **(2)** KP418 [157]	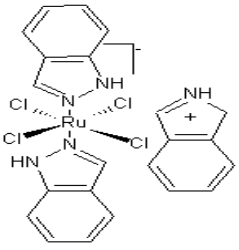 **(3)** KP1019 [157]	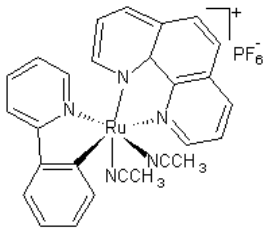 **(4)** RDC11 [157]

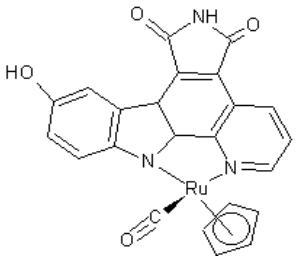 **(5)** DW1 [157, 159]	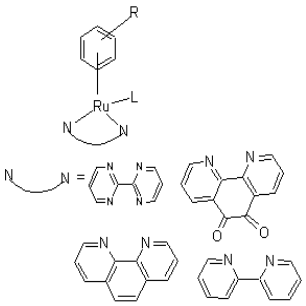 **(6)** (arene)-Ru(II) complexes from Sadler et al [160].	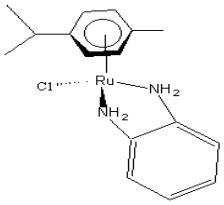 **(7)** Ru-(arene) o-phenylenediamine (o-pda) complex from Sadler et al lab [158]	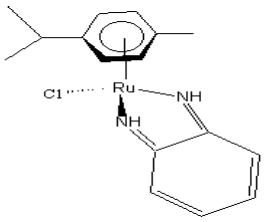 **(8)** Ru-(arene) o-benzoquinonediimine (o-bqdi) complexfrom Sadler et al lab [158]
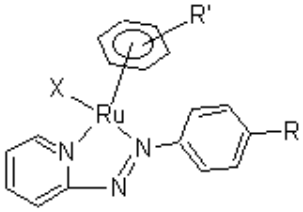 **(9)** Ruthenium(II) Arene Phenylazopyridine Complexes from Sadler lab [161]	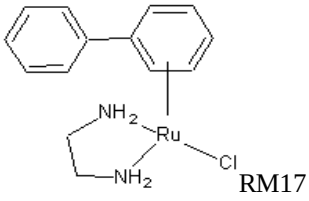 **(10)** (Piano Stool) [157]	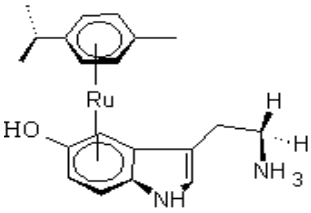 **(11)** [162] Not screened as anticancer agent	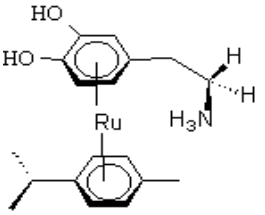 **(12)** [162] Not screened as anticancer agent
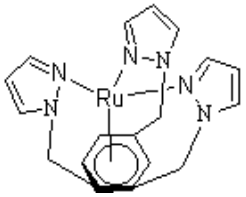 **(13)** [163]	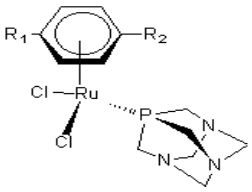 **(14)** RAPTA- [B (R_1 = H, R_2 = H); T (R_1 = H, R_2 = CH3), C (R_1 = CH_3, R_2 = $CH(CH_3)_2$)] [51]	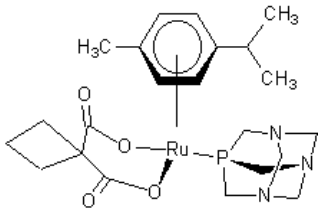 **(15)** Carbo-RAPTA-C [51]	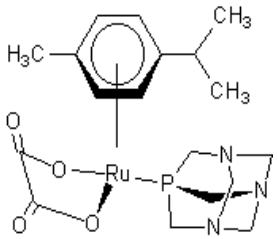 **(16)**Oxalo-RAPTA-C [51]
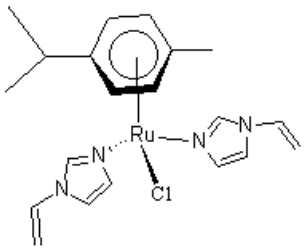 **(17)** RAPTA-NAMI form Dyson et al lab [164].	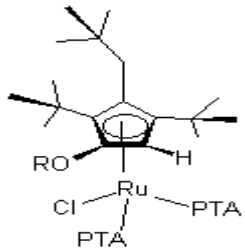 **(18)** Cp-Ru complex from Dyson et al lab [19].	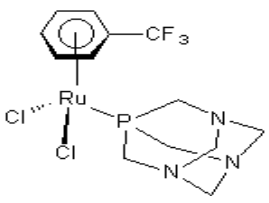 **(19)** [17]	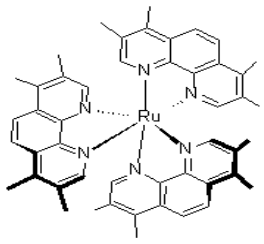 **(20)** Dwyer compound [165]

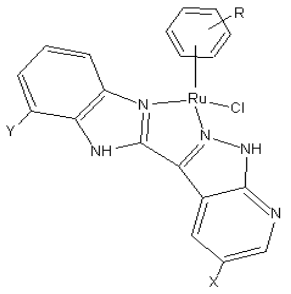 **(21)** (from Dyson Lab) [62]	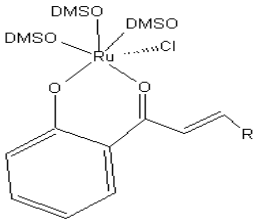 **(22)** Ru(II)−DMSO−Cl−Chalcone Complexes [166]	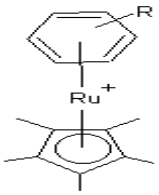 **(23)** Ru(II) Arene Cp Complexes [167]	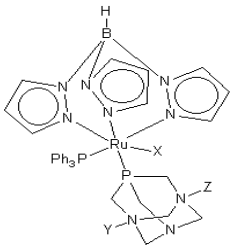 **(24)** [156]
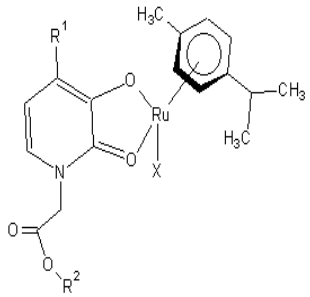 **(25)** [38]	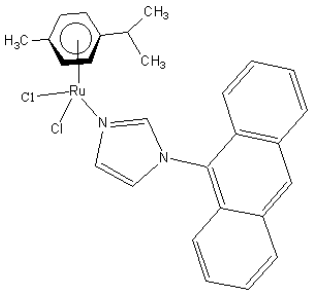 **(26)** Pgb Inhibitor [8]	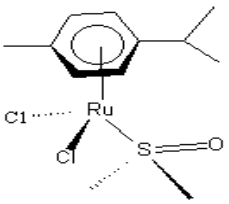 **(27)** [8]	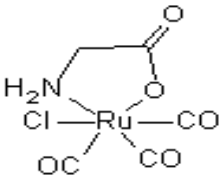 **(28)** CORM-3 for Cardio-protective action [5]
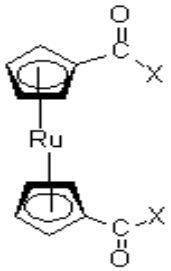 **(29)** [168]	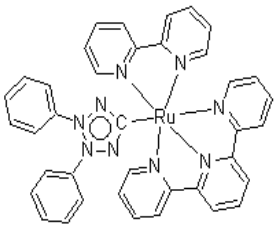 **(30)** There is no anti-cancer screening information on this molecule [169].	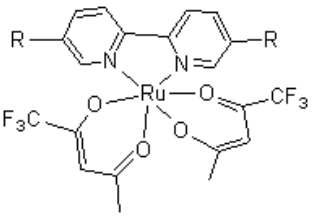 **(31)** This is not screened as anticancer agents. It is only the photoconductive properties that are determine [170].	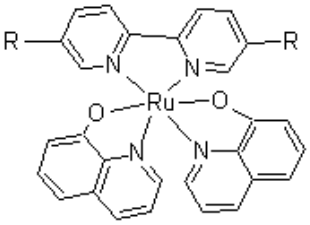 **(32)** This is not screened as anticancer agents. It is only the photoconductive properties that are determine [170].
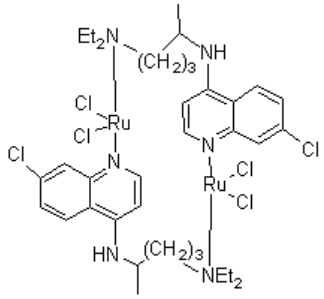 **(33)** [53, 171]	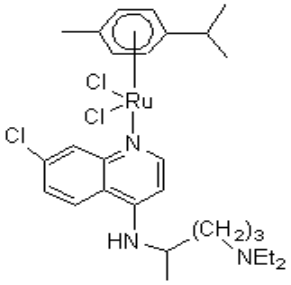 **(34)** [8, 53]	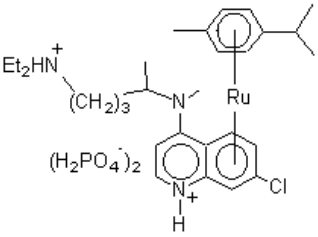 **(35)** [8, 53]	

The key concept in the design of anticancer complexes of metal is summarised as optimization

of chemical reactivity to allow facile attack on the target site like DNA but yet avoid attack on other sites associated with unwanted side effects [37]. Some of the unique properties of interest in the designing of metal complexes as potential anticancer and anti-metastasis are the ability of the metal-based complexes to exhibit water solubility and the capacity to link to nucleobases, DNA fragments, aminoacids, peptides, and proteins [155]. Therefore, besides the modification of functional groups, there is still a wide chemical space in terms of the choice of ligands in complex with the metals.

2.4 Limitations of ruthenium and other organometalic anticancer therapies and the way forward.

Current inorganic drugs such as *cis*-platin have been successfully used in the treatment of many cancers, including testicular, ovarian, oropharyngeal, bronchogenic, cervical and bladder carcinomas, lymphoma, osteosarcoma, melanoma and neuroblastoma [18]. But the inherent limitations with *cis*-platin, primarily its high toxicity, unwanted side effects, low administration dosage [51], and drug resistance [18] have shifted researchers attention towards Ru-based anticancer to address the problems that are associated with metal-based drugs. Currently, the action of ruthenium complexes is still hypothetical with two main theories that ruthenium compounds target DNA or unknown proteins. Till date, there is relatively little rational design or work aimed at elucidating the modes of action of these complexes even though there is a great deal of research which has been directed at generating novel complexes for testing [10]. This is a major limitation in ruthenium drug discovery.

The ruthenium based drugs have shown promising clinical applications showing modest and reversible DNA adduct formation leading to apoptosis activation of the metastasised tumour but not primary tumour and they do not induce significant *in vitro* cytotoxicity [7]. Two of ruthenium drugs in clinical trial are KP1019 and NAMI-A. The targets of KP1019 and of NAMI-A remain unknown after

more than 15 years of their discovery which is posing difficulties to their study and hampers the possibility to explore new analogues of KP1019 or of NAMI-A with superior pharmacological profiles [7]. Numerous studies have been focused on the interaction of KP1019 with serum proteins, and the intracellular fate of KP1019 and KP1339 after uptake into tumour cells is widely unknown [12]. The ultimate targets of many bioorganometallics still remain unclear and controversial but the essential mode of action is considered to be the mono-functional covalent binding accompanied by a hydrogen bond to DNA nucleobases [38].

Three ongoing research approaches to address the ruthenium and other metals therapy limitations have been summarised [10]:

i). The first approach is to generate large numbers of different compounds to screen against different targets and cell lines without a thorough understanding of their biological targets [10]. Many organometallic potential anticancer drugs including Rh(III) and Ir(III) have been reported in the literature targeting different potential biomolecules but their exact mode of cytotoxic action is still unknown even though it was shown that these compounds were indeed targeting the desired biomolecules [8].

ii). The second is directing research attention to elucidate the mode of action and the behaviour in biological media of existing ruthenium which is a progressive step towards rational design of ruthenium anticancer drug [10]. Research effort are now directed toward linking the medicinal properties of inorganic drugs to specific biological properties in an attempt to elucidate their mechanism step by step in order to use the information to design improved drugs with increased potency and reduced side effects. The mechanism of many inorganic drugs are complex and the exact route of activity for many of them remains unknown [11]. The advantage of this rational drug design approach is that there are a number of direct assays that can be performed looking at both specific interactions and drug activity in whole cells, which are not possible if the target is unknown [5].

Because of the possibility to clone topoisomerase II from number of sources and to make it recombinantly, it has provided an easily accessible, pure and homogeneous source for characterization and the effect of the drug on enzyme activity can be probed directly. By using gel electrophoresis ruthenium compounds have been shown to inhibit topoisomerase II [5 and ref there in].

iii). Lastly, the generation of further complexes in which ruthenium is chemically linked to an 'organic directing molecule' (ODM) mostly notable drugs of known biological target [10] or known organic protein binders [49, 172], in which an organic molecule binds to the active site of an enzyme and the attached ruthenium ion binds to a nearby residue of the same protein [10]. The advantages in this aspect are that molecular recognition will be combined with properties that are unique to metal complexes, such as photophysical signatures or catalysis, in order to create compounds with novel and unprecedented properties [49].

Another related ODM is what is called metal-drug synergism as an alternative approach to the discovery of new metallo-drugs which involves binding an organic compound of known therapeutic value to a metal-containing fragment [53]. This results in the metal acting as a carrier and stabilizer for the drug until it reaches its target and also the organic drug carries and protects the metal which prevent side reactions in its transit toward a second target of biological action. The mechanism of action of metal-drug complexes especially that of metal-CQ (where CQ is chloroquine) has been investigated to show the role of the metal fragment as an alteration of the structure, the basicity, and most importantly the lipophilicity of CQ to make it less recognizable to the parasite's defense mechanism [53]. For instance, the activity of organic antimicrobial drugs has been enhanced by binding the organic molecule to a ruthenium centre of which the resulted complex are found overcoming resistance that the parasite has developed to the organic compound alone [11]. Also, Polypyridyl-containing half-sandwich complexes with Ru(II) and Rh(III) central atoms and hexamethylbenzene or pentamethylcyclopentadienyl ligands have been reported to show stable intercalative binding with

DNA and exhibited excellent cytotoxic activities [8 and the ref there in].

Ferrocifen is a derivative of the anticancer drug tamoxifen in which a phenyl group is replaced by a ferrocene moiety. Tamoxifen is the front-line chemotherapeutic agent for patients with hormone-dependent breast cancer whose activity depends on its competitive binding to the estrogen receptor, ERa, thus repressing the estradiol-mediated DNA transcription in the tumour tissue [49]. Therefore ferrocifen is also believed to act in the same manner but recent findings have shown a more effective strength of ferrocifen to act against tumour cells that lack this estrogen receptor although the mode of action is yet unknown. Isostructural ruthenocene derivative also acts as an antiestrogen in hormone-dependent breast cancer cells but lacks the antiproliferative effect of ferrocifen against hormone-independent cells [49].

Many nanomolar and even picomolar ATP-competitive ruthenium-based inhibitors for different protein Kinases have been discovered, some of them by combinatorial chemistry, some by rational design, or a combination of both [49]. New Ru(II) chloroquine complexes [Ru(η^6-arene)(CQ)Cl_2] (CQ) chloroquine; arene) p-cymene, benzene), ([Ru(η6-p-cymene)(CQ)$(H_2O)_2$][BF_4]$_2$, [Ru(η6-p-cymene)(CQ)(en)][PF_6]$_2$(en = ethylenediamine), and [Ru(η6-p-cymene)(η6-CQDP)][BF4]2 (CQDP = chloroquine diphosphate)) have been found to show a consistent higher potency against resistant parasites than that of the standard drug chloroquine diphosphate [53].

2.5 The metal coordinating ligands of interest and their functionalization

2.5.1 Half-sandwich and heterocyclic nitrogen coordinating ligands

The synthesis of both sandwich and half-sandwich complexes were made available through the experimental works of Bennett [173-199]. Ru-arene complexes especially those with cyclopentadienyl,

ruthenocene, benzenoid η^6-electron donor ligands are all experimentally feasible using Bennett's synthetic method [200]. Since then, several Ruthenium half-sandwich complexes have been synthesised [17, 200-202] and found numerous applications as catalysts for organic transformations, in the supramolecular field, solar cell and medicinal chemistry [203-228]. However, the ruthenium half-sandwich complexes seem to be widely screened as anticancer agents [142-153, 229-241]. In the synthesis of anticancer Ru-based complexes, Dyson experimental team members combined the features of half-sandwich and PTA ligands in many of their synthesised anticancer complexes of ruthenium [9, 13, 16, 17, 51, 54, 63, 127-141, 242-257] while Sadler team members are known to combine the half-sandwich with N-N bidentate or tridentate ligands [20-37, 258-272].

In addition to the half-sandwich features, our interest is equally in Ru complexes of heterocyclic nitrogen coordinating ligands to possibly mimic the feature of the best anticancer complex called *cis*-platin which is characterised with two units of NH_2 ligand. In addition to the complexes from Sadler's research group that are most often characterised by heterocyclic nitrogen containing ligands, many other researchers have equally characterised the Ru-based complexes that contained 1,10-phenanthroline [273-280], bipyridine [281-284], terpyridine [285-293], bis(pyrazoly-l-yl) [294-300] for different purposes like electro-chemiluminescence, catalyst, photochemical and anticancer complexes. However, the application of these type of ruthenium complexes as potential anticancer are predominant [259, 301-312].

2.6 Justification of the work

This research is targeted towards addressing some of the existing gaps in cancer chemotherapy. There are over 100 existing anticancer drugs in clinical application but limited to some specific anticancer cells while many remained incurable. The targets of organometallic anticancer agents like ruthenium complexes that have been found to be promising anticancer candidates that are competitively active as *cis*-platin remained unknown even though it is established that other target proteins are the most likely points of interaction for organometallic anticancer agents besides the establish *cis*-platin target called DNA [5, 7-14]. In the clinical trials ruthenium compounds may provide a less toxic and more effective alternative to platinum therapy but there is no enough investigation and understanding of modes of action of different ruthenium compounds. There are many designed promising anticancer metal-based drugs but yet to come to clinical uses except *cis*-platin and its derivatives because of limitation in ascertaining their targets. *Cis*-platin and its derivatives as the only metal-base drugs and the most widely used clinically is also suffering from resistance and ineffectiveness toward metastases cancer cells. Due to problems suggested like pharmacokinetic limitations, cross-reactivity, general toxicity, low initial efficacy and rapid development of drug resistance, many *in vitro* promising metal-based complexes as alternative to *cis*-platin have a relatively low representation in the clinic because many with good *in vitro* properties fail to show any therapeutic effect *in vivo*. [7]. In another way, several Ru-based complexes have shown excellent *in vivo* antitumor activities comparable to *cis*-platin but are found to be approximately 10 times lower than that of *cis*-platin in their *in vitro* activities [13] which is hindering their rational design. Selectivity and cytotoxicity are the unique properties of an ideal cancer drugs, but most of the highly effective cancer drugs are cytotoxic i.e. they mediate their effect principally via genotoxicity (cytotoxicity) and are therefore clinically criticized because of some associated sever side effects [7, 46, 47]. There is yet to

be any single cancer drug that is effective against over 200 types of cancer in existence and all of the cancer drugs in existence have limited and selected cancer cells or tissues they target while many cancer cells are incurable or have developed drug resistant. The investigations to produce drugs that will widely be used as *cis*-platin and its derivatives have not been successful even though many drug targets have been identified along the way [13] and many potential anticancer agents have been synthesised.

Based on our interest in the synthesis of organometallic derivatives of Ru(II)-based anticancer complexes, as well as understanding their biological activities, we are attempting first the theoretical study of Ru(II)-based anticancer complexes utilizing quantum and docking calculations to investigate their possible activities as inhibitors of notable enzymes that are significant in cancer growth and metastases. The project will contribute to addressing these challenges in two different ways which are: studying the interaction of Ru-based organometallic cancer complexes against some possible enzymes of interest to suggest the possible *in vivo* target using mostly computational approach and a little experimental approach and designing new complexes from the scaffold of organometallic Ru-based complexes and studying their binding affinity computationally and experimentally. With this we hope to understand better the mechanism of Ru-based organometallic drugs which will enhance the rational approach of designing better efficient drugs. More over, we hope to discover a better derivative of Ru-based organometallic drugs that are pharmacokinetically and pharmacologically effective against some forms of cancer including the metastasised and *cis*-platin resistant cancer cells.

There are clear evidences on the need for further research on ruthenium-based cancer drugs that will result to an effective delivery of anticancer drugs to tumour tissue, improve their selectivity and consequently reduce drug side effects. Our efforts therefore are toward obtaining more effectively Ru-based anticancer drugs if their targets can be predicted.

2.7 Statement of problem

The grave challenge in cancer therapies is treatment of metastasised cancers [6] since medical surgery is limited to primary cancer. *Cis*-platin and its derivatives are the only metallic anticancer drugs that are already in clinical use but are associated with some side effects and are limited to some cancer cells and metastasised platinum resistant cancer cells. Other promising anticancer drugs is the Ru metallic drugs like KP1019 and NAMI-A [51] that have reached the phase II clinical test [164] but are yet to pass the NCI test [6] because the mode of their actions are yet to be fully understood in order to allow better rational design for improved therapy and selectivity. There is therefore urge for better cancer drugs and researchers have found Ru organometallic drugs as the most promising one. However, the anticancer mechanism of Ru-based organometallic drugs is yet to be understood in terms of what their main targets are, even though they have been found effective *in vitro* and *in vivo*. Therefore some of the questions that this research seeks to answer include: how can the possible targets of Ru(II)-based metal complexes be predicted through computational methods?, how can we find a better Ru-based organometallic anticancer that can address the limitation of the known *cis*-platin drug?, can we design some Ru(II) complexes that are active as the promising RAPTA complexes that are still at research level and also overcome their limitations? Can a more selective Ru(II) complexes be predicted through docking considering proteins as their targets just as it was proposed that RAPTA complexes have a strong preference for protein binding over DNA [7]? Can computational docking better predict the experimental behaviour of Ru-based complexes using some proteins that are peculiar to cancer growth?

The possibility of reducing the toxicity of cancer therapy is to increase their selectivity, but selectivity usually limits the range of the application of the drugs since there will always be cancer cells where the selected targets will not be present, therefore the interest of this research is how toxicity can be reduced and at the same time increase the effectiveness and application? Rational drug design is the

only and the most promising way if the mechanism of the cancer growth and metastases including the mode of action of the available cancer therapy can be fully comprehended.

Another important question we are trying to address is that if addition of metal to chloroquine has been found to improve the effectiveness of the drug notably [53], can the same thing be apply to some of these cytotoxic anticancer drugs that are natural product in order to increase their effectiveness and selectivity?

2.8 Aims

The aims of this work are to computationally predict the most likely possible biological targets of the ruthenium-based anticancer complexes and to synthesize new forms of ruthenium-based antitumor in an attempt to increase their cytotoxicity.

2.9 Objectives

i). Build new forms of ruthenium-based anticancer complexes starting from the existing complexes that have been screened by researchers as anticancer agents. This attempt is to increase the cytotoxicity and effectiveness. This will involve functional group manipulations on the ligands.

ii). The pharmacokinetic studies using ADMET properties and by docking of the complexes to Human serum albumin (HAS) (PDB ID 1BM0) to determine their binding energy. Understanding the metal coordination chemistry of albumin (HSA) become crucial because of its significant role in drug transport and metabolism [36].

iii). Quantum calculation of the kinetics of the organometallic drugs for the change in their free state to the substrate binding [41]. Kinetic study of the hydrolysis of the Ru-Cl bond of the prodrug to generate an active $[(\eta 6\text{-arene})Ru(en)(H_2O)]^{2+}$ [41]. Detailed kinetic studies showed that the Ru-Cl bond hydrolysis can be strongly influenced by the nature of the coligands as well as the nature of the metal ion. We will seek to relate some of the quantum thermodynamic and electronic properties to the anticancer effect of the potential drugs.

iv). The theoretical study of our anticancer agents by utilizing quantum and docking calculations to determine the quantum properties of some existing Ru(II) complexes as anticancer and the new model of the complexes built. The quantum calculation is relevant to comprehend the quantum properties that determine their stability and effectiveness while docking will be used as a tool to predict their possible

targets. Some of the enzymes that will be used in this research are Topoisomerase II (top II), Thioredoxin reductase (TrxR), Cathepsin B (Cat B), Ribonucleotide reductases (RNR), Histone Deacetylase (HDAC7) and Recombinant Human albumin (rHA). Since the target of many anticancer metallodrugs can not be ascertained [8, 9], then we chose many cancer enzymes of significant function to cancer growth to discover the most likely target of these complexes.

v). Synthesize some of the promising complexes which have shown significant anticancer activities against some selected protein targets through docking.

vi). Characterization of the synthesized complexes.

Part of Chapter Three has been reported as:

1. Adeniyi, A.A.; Ajibade, P.A. Effects of bidentate coordination on the molecular properties RAPTA-C based complex using theoretical approach. *J. Mol. Model*. **2013**, 19, 1325-1338.

2. Adeniyi, A.A.; Ajibade, P.A. Computational properties of h6-toluene and h6-trifluorotoluene half-sandwich Ru(II) anticancer complexes. *J. Biomol. Struc. Dynamics* **2013**, 1-15, http://dx.doi.org/10.1080/07391102.2013.819299

3. Adeniyi, A.A.; Ajibade, P.A. Insights into the intramolecular properties of h6-arene-Ru based anticancer complexes using quantum calculations. *J. Chem*. **2013**, 1-25.

4. Adeniyi, A.A.; Ajibade, P.A. Theoretical study of the electronic and spectroscopic properties of some Ru(II) anticancer complexes. *Spec. Acta Part A*: *Mol. Biomol. Spec*. **2013**, 105, 456–465.

5. Adeniyi, A.A.; Ajibade, P.A. Computational studies of the electronic, conductivities, and spectroscopic properties of hydrolysed Ru(II) anticancer complexes. *Spec. Acta Part A*: *Mol. Biomol. Spec*. **2013**, 115, 426–436.

6. Adeniyi, A.A.; Ajibade, P.A. Inhibitory activities and possible anticancer targets of Ru(II)-based complexes using computational docking method. *J. Mol. Graph. Model*. **2012**, 38, 60-69.

7. Adeniyi, A.A.; Ajibade, P.A. Comparing the suitability of autodock, gold and glide for the docking and predicting the possible targets of Ru(II)-based complexes as anticancer agents. *Molecules* **2013**, 18, 3760-3778.

8. Adeniyi, A.A.; Ajibade, P.A. An insight into the anticancer activities of Ru(II) based metallocompounds using docking methods. *Molecules* **2013**, 18, 10829-10856.

CHAPTER THREE

3 COMPUTATIONAL STUDY OF RUTHENIUM(II)-BASED COMPLEXES

3.1 Background of the chapter

This chapter is made up of computational works carried out on ruthenium complexes which have been reported in the literatures and proposed new models. For easy understanding, this chapter is grouped into three sections: Section 3.3 deals with the geometrical and the electronic properties of selected Ru complexes in relation to their stability and available anticancer activities, Section 3.4 deals with the spectroscopic properties and their possible applications as non-linear optical materials and Section 3.5 deals with the computational docking of the selected ruthenium complexes to different receptors that have been reported to play significant roles in cancer invasion, progression and metathesis as mentioned in Section 1.3 of this thesis. This chapter is a combination of all ten manuscripts that have been written on the computational studies of ruthenium complexes of which eight are already published [313-320] and two are under review. However, in order to reduce the volume of this thesis, the details are avoided but can be found in the reference papers cited at the beginning of each subsection.

3.2 Computational methods

3.2.1 Computational methods for geometric and the electronic properties

The methods shown here are the summary of the computational approaches used in this section but does not contain all the variations of the methods used in each of the subsections. The computational simulations were done using FIREFLY 7.1.G [321], Gaussian 03/09 [322, 323] and AIMAll 12.06.03 [324]. Firefly QC package [321], which is partially based on the GAMESS (US) [325] source code, was used for for all the NBO and NEDA analysis. The geometries of the complexes were optimized twice with PBE0 [326] functional and a mixed basis sets SBKJC VDZ that have effective core potential (ESP) [327] approximation and 6-31G* or 6-31+G(d,p) basis set. In the first optimization, the ECP basis set SBKJC VDZ is applied on the Ru and Cl atoms where applicable while other atoms in the complexes are treated with basis set 6-31G* which shall subsequently be referred to as ECP(Ru,Cl)[6-31G*]. In the second optimization, the SBKJC VDZ is limited to only the ruthenium atom while the scaled up basis set 6-31+G(d,p) was applied on other atoms in the complexes which shall subsequently be referred to as ECP(Ru)[6-31+G(d,p)]. Other properties of the complexes are computed at B3LYP hybrid functional [328] level of theories using other higher basis set like DGDVZP applied on Ru atom while others are treated with 6-31G* or 6-31+G(d,p) referred to as DGDVZP(Ru)[6-31G*] or DGDVZP(Ru)[6-31+G(d,p)]. We also considered the accuracy of computing the properties using the minimal basis set 3-21G [329] applied uniformly on all the atoms of the complexes which can be helpful for the treatment of large molecules. External basis set are obtained from EMSL Basis Set Library [330, 331] which were incorporated into the input file in a format that each FIREFLY and Gaussian programs can read. The choice of SBKJC VDZ ECP basis set with PBE0 is as a result of a large number of electrons and configurations to be treated and due to the past records

of their effectiveness in computational study of metal clusters [332, 333] and because it incorporates relativistic corrections for the metal atoms [334].

The Bader's quantum theory of atoms in a molecule (QTAIM) analysis were done mainly using the wavefunction obtained form using B3LYP hybrid functional [328] and basis sets either ECP(Ru)[6-31+G(d,p)] or DGDVZP(Ru)[6-31+G(d,p)] or a minimal all electron basis set 3-21G [329]. A topological analysis was performed in order to calculate the charge density (ρ) and its second Laplacian derivative of charge density ($\nabla^2\rho$) for the bond critical points (BCP). AIMAll 12.06.03 package was used for QTAIM analysis [324] while the NBO 5.0G program [335] as implemented in FIREFLY 08 was used for the natural bond orbital (NBO) analysis [336] and natural energy decomposition analysis (NEDA) [337].

3.2.2 Computational method for the spectroscopic and non-linear optical properties

The ruthenium atom was treated with SBKJC VDZ ECP as described in the previous section. The choice of SBKJC VDZ ECP basis set is necessary for large systems of our type which also contain heavy metal like ruthenium. This functional has been reported to improve the accuracy of excitation energies and charge transfer bands in metal complexes both in gas phase and in solution [338]. Also, the ECP basis set has been pointed out as a viable method for accurate calculations of transition metal polarizabilities [339]. All of the computed properties were done using Becke's three- parameter exchange [328] and Lee-Yang-Parr's correlation non-local functional which is usually denoted by B3LYP, combined with different combination of basis set. The properties of the systems optimize with PBE0/ECP(Ru)|6-31+G(d,p) are computed with the combination of DGDZVP basis for ruthenium atom and 6-31+G(d,p) basis set for other atoms which will be further referred to as DGDZVP(Ru)|6-31+G(d,p). The properties of the same set of the optimized systems are also computed with the same

combinations of basis set as was used for the optimization (ECP(Ru)|6-31+G(d,p)). The properties of all the systems optimized with lower basis sets ECP(Ru,Cl)|6-31G* were computed with the same combination of basis sets as those used for their optimization (ECP(Ru,Cl)|6-31G*) and also computed with minimal all electron basis set 3-21G [329] applied on all atoms. The external SBKJC VDZ ECP was obtained from EMSL Basis Set Library [330, 331] and incorporated into input files in a readable format for Gaussian 09 [323] suite of programs used for the computation. The NMR and one-bond NMR spin-spin coupling constants J(A,B) [340, 341] were computed in Gaussian package using the GIAO method. The wavefunction (WFX) files for the computation of QTAIM properties were obtained at the same level of theory through the fchk generated files using the AIMAll program package [324]. Intra- and inter-atomic properties were computed by the Proaim integration approach, as implemented in the AIMAll suite of programs. The accuracy of the integration process was guaranteed by keeping the atomic integral of the one-electron density Laplacian below the 10^{-4} a.u. within all atomic basins. In addition, the summation of all basin energies was compared with the total electronic energy of the molecule, calculated independently at the above-mentioned computational level, to check that the differences remain below the 1 kcal/mol.

The thermodynamic properties like Zero-point correction (ZPE), Zero-point energy ($E_0 = E_{elec}$ + ZPE), Total energy ($E = E_0 + E_{rot} + E_{tran}$), Enthalpy ($H = E + RT$), Gibb free energy ($G = H - TS$), constant volume molar heat capacity (CV) and entropy (S) are computed for each complex.

Infrared (IR) stretch spectra, i.e. wavenumbers (ν) in cm^{-1} and intensities (I) in km/mol, of complexes were obtained using vibrational frequencies calculated at hybrid functional PBE0. The NMR isotropic shielding (σ) were calculated using the Gauge-Including Atomic Orbitals (GIAO) [342] method and the one-bond NMR spin-spin coupling constants J(A,B) [340, 341] associated with atoms A and B are also determined.

The proton, the carbon and nitrogen chemical shifts of the ligands are computed theoretically

using a direct method and a fitting equation. In a direct method, the isotropic shielding of the proton, carbon and nitrogen are subtracted directly from that of a reference compound (tetramethylsilane (TMS) for ^{1}H and ^{13}C and CH_3NO_2 for ^{15}N [343, 344]) while in the fitting method, the following equations are used as reported in the literature [343]:

$\sigma^{1}H = 31.0 - 0.97 * \sigma^{1}H$

$\sigma^{13}C = 175.7 - 0.963 * \sigma^{13}C$

$\sigma^{15}N = -152.0 - 0.946 * \sigma^{15}N$

where $*\sigma^{1}H$, $*\sigma^{13}C$ and $*\sigma^{15}N$ represent the computed isotropic shielding tensor of proton, carbon and nitrogen respectively.

The different terms in the energy of a molecule that is subjected to a static electric field (F) are computed. This type of energy (E) can be expressed as [338]:

$$E = E^{0} - \mu_i F_i - \frac{1}{2}\alpha_{ij} F_i F_j - \frac{1}{6}\beta_{ijk} F_i F_j F_k - \frac{1}{26}\gamma_{ijkl} F_i F_j F_k F_l - \ldots$$

where E^0 = is the energy of the molecule in the absence of an electronic field

μ_i = the component of the dipole moment vector

α_{ij} = the linear polarizability tensor,

β_{ijk} and γ_{ijkl} are first and second hyperpolarizability tensors where i, j, and k label are the x, y, and z components respectively [338].

All these terms are computed except the second hyperpolarizability tensor (γ_{ijkl}) to understand the polarizability and the hyperpolarizability properties of the ligands.

The dipole was computed using:

$\mu = (\mu^2_x + \mu^2_y + \mu^2_z)^{1/2}$

The anisotropy polarization was calculated using

$<\alpha> = 1/3\ (\alpha_{xx} + \alpha_{yy} + \alpha_{zz})$

$\Delta\alpha_1 = 1/2\ (\alpha_{xx} + \alpha_{yy}) - \alpha_{zz}$

$\Delta\alpha_2 = \{1/2\ [(\alpha_{xx} - \alpha_{yy})^2 + (\alpha_{xx} - \alpha_{zz})^2 - (\alpha_{yy} - \alpha_{zz})^2 + 6\ (\alpha^2_{xy} + \alpha^2_{xz} + \alpha^2_{yz})]\}^{1/2}$

$\Delta\alpha_3 = [(\Delta\alpha_2)^2 - (\Delta\alpha_1)^2]^{1/2}$

In addition to the mean polarizability ($<\alpha>$) and polarizability anisotropies ($\alpha1$, $\alpha2$, $\alpha3$), the polarizability exaltation index (Γ) was also evaluated as:

$\Gamma = \alpha(mol) - \Sigma i<\alpha>i$ where

$\alpha(mol)$ = mean polarizability of a molecule

$\Sigma_i<\alpha>_i$ = summation of the atomic polarizability of the atoms which constitute the molecule.

The values of Γ have been employed to estimate relative aromaticity of furan homologues and stabilities of atomic clusters [345]. A large negative Γ value denotes a very stable structure.

The accurate single values of first static hyperpolarizability (ß) of the ligands were computed using Quasi-Pythagorean equation [346] on the 10 components of the 3 x 3 x 3 matrix as β_{xxx}, β_{xxy}, β_{xyy}, β_{yyy}, β_{xxz}, β_{xyz}, β_{yyz}, β_{xzz}, β_{yzz}, β_{zzz} respectively from G09 output as:

$$\beta_{tot} = (\beta_x^2 + \beta_y^2 + \beta_z^2)^{\frac{1}{2}}$$

where $ß_x = (ß_{xxx} + ß_{xyy} + ß_{xzz})$, $ß_y = (ß_{yyy} + ß_{yxx} + ß_{yzz})$ and $ß_z = (ß_{zxx} + ß_{zyy} + ß_{zzz})$.

The atomic units (a.u.) of ß in G09 were converted into electrostatic units (esu) (1a.u. = 8.6393×10^{-33} esu).

The relative stability and reactivity of series of compounds can be predicted from the molecular property of their hardness (η) [345, 347]. The values of η is given in terms of difference in the ionization energy (IE) and electron affinity (EA), which can be approximated by highest occupied molecular orbital (HOMO) and lowest unoccupied molecular orbital (LUMO) energies (ε), respectively:

$$\eta = \frac{1}{2}(IE - EA) \approx \frac{1}{2}(\varepsilon_{HOMO} - \varepsilon_{LUMO})$$

3.2.3 Computational methods for the docking study

There are limitations in the application of docking to metal-based complexes which results in very few reports in the literatures compared to organic compounds due to lack of appropriate force fields to take care of the metals [83] and their relativities and the difficulty of optimising the initial structures. In this research, the geometries of the Ru-based complexes used were first optimized using Firefly package [321] or Gaussian 03/09. The optimized structures which are the first criteria for any possible successful docking of metal-based complexes were used. Different docking packages that have been used are Autodock 4.2 suit [348], GOLD (Genetic Optimisation for Ligand Docking) 5.1 [349], Molegro [350] and the Glide 5.8 [351] as part of Maestro 9.3 suite of programs. The molecular graphics and other analyses were performed with the UCSF Chimera package [352].

In Autodock, the Lamarckian genetic algorithm is chosen because it as been pointed out to be most efficient, reliable and successful than others like simulated annealing (SA) and a genetic algorithm (GA) methods in autodock [353, 354]. For the Ru atom charge, we applied the native charge of +2 which is general and can be applied to any complex/receptor interaction study though it may not be as accurate as using an optimized charge which is more specific to the type of the system as it was

reported for the docking of the metalloenzymes that contain Zn atom [83]. The active site was defined using AutoGrid version 4 and the grid size was set to 60 × 60 × 60 points with a grid spacing of 0.375 Å centred on the selected residues of the binding site of each receptor. The grid box includes the entire binding site of the enzyme and provides enough space for the ligand translational and rotational walk. Step sizes of 2Å for translation and 50^{o} for rotation were chosen and the maximum number of energy evaluations was set to 1,750, 000. Twenty runs were performed and for each of the 20 independent runs, a maximum number of 27,000 GA operations were generated on a single population of 100 individuals. Default values for the operator weights for crossover (0.80), mutation (0.02) and elitism (1.00) parameters were used.

The obtained trial version of GOLD (Genetic Optimisation for Ligand Docking) 5.1 [349] was used for the docking. The Hermes visualiser in the GOLD Suite was used to further prepare the metal complexes and the receptors for docking. The region of interest used for Gold docking was defined as all the protein residues within the 5 Å of the reference ligands that accompanied the downloaded protein complexes except for the protein complex with no accompanied ligand where the binding site was defined from the list of protein residues reported in literatures to characterised their binding site. Default values of all other parameters were used and the complexes were submitted to 10 genetic algorithm runs using the GOLDScore fitness function.

In Molegro, the docking scoring function of MolDock which make use of piece-wise linear potential (PLP) was used. The maximum interation was set to 2500 against the default 1500 and the population number also increased from default values of 50 to 100. Five maximum posses were selected and a more stringent re-scoring applied on them for a better prediction of the binding activities of the metallocompounds. MolDock scoring considers the hydrogen bonding, inter molecular protein-ligand and intra molecular ligand interactions and has been successfully applyed for molecular docking [355]. Since the Molegro docking package is designed for the ligand-protein interaction, the simple

trick employed to consider the ligand-DNA interaction is to include DNA as a cofactor of the protein. This is achieved by incorporating protein into the DNA pdb file 3LPV (named DNA-1) or using pdb 4DL7 input which contain both DNA and protein (named DNA-2) obtained from protein data base [356].

The trial version of Glide [351, 357] which is part of the Maestro 9.3 suite of programs was also used for docking. The method use in Glide docking is referred to as funnel approach where a series of ligand conformations are initially created by Glide and then removing the unfavourable ones [358]. After this, refinement is performed by energy minimization followed by a restricted Monte Carlo search on the lowest energy conformations to refine the initial structure. The protein structures in mol2 format were prepared using the protein preparation wizard with default values and the incomplete residues of the receptors were corrected using Prime package [359]. Since, Glide ligand preparation package lack the force field to take care of metal-based complex, then protein preparation wizard was manipulated to prepare the metal-based complexes for docking as if the Ru(II) metal is a part of the protein. The Grids for the prepared protein were generated using 25 Å box with the centre of the grid being defined by using the ligand that is on the binding site of the protein and the force field used is OPLσ2005 which recognizes the metal atom. The default parameters in Glide for standard precision (SP) docking mode were used. In both Autodock and Glide dockings, flexibility of the complexes was allowed. The correlation table was derived using the statistical tool R (http://www.R-project.org).

3.3 The geometric and the electronic properties

In the subsection 3.3.1, we studied RAPTA-C and its two derivatives *carbo*- and *oxalo*-RAPTA-C (Figure 3.1) which have been reported as potential anticancer agents [5, 13, 51]. Both *carbo*-and *oxalo*-RAPTA-C are reported to resist hydrolysis [8] and have high anticancer activities similar to the

parent complex RAPTA-C. However, *oxalo*-RAPTA-C is known to completely resist hydrolysis while *carbo*-RAPTA-C can moderately be hydrolysed [51]. Also, *carbo*-RAPTA-C is known to show higher anticancer activity than *oxalo*-RAPTA-C [13, 51]. These two bidentate are reported stable while their native complex RAPTA-C is kinetically unstable [5, 51]. Many of the Ruthenium-arene complexes of these types have been reported to be unstable and have complicated ligand exchange chemistry [5]. In drug design there is a need for a clear understanding of the physicochemical properties of the drug candidates [44] which will enhance their rational design. Therefore, it is of prime importance to us to explore the electronic properties of the *carbo*-RAPTA-C, *oxalo*-RAPTA-C and their parent complex RAPTA-C (Figure 3.1) which have been proposed as anticancer agents [13, 51].

In subsection 3.3.2, we have selected RAPTA-T (complex **1** in Figure 3.4) and a model with electron-withdrawing a,a,a-trifluorotoluene ligand $[Ru(\eta^6\text{-}C_6H_5CF_3)(pta)Cl_2]$ (i.e. RAPTA-CF_3) (complex **3**) [17] to give the feature of the interatomic properties of these complexes, the factors that determine their stability and the properties of their hydrolysed forms (complexes **2** and **4**) respectively (Figure 3.4). The complexes that hydrolyse rapidly have been shown to be active over cancer cells than those that do not aquate easily [37] indicating that the significant feature of these cytotoxic metal complexes is hydrolysis [38]. This section presents the unique features, natures and magnitudes of the electronic properties with the intra-molecular interactions that influence the stability of four Ru-based complexes in relation to their reported anticancer activities. Researches have shown that these type of compounds can be characterised with favourable interactions between electron-rich and π-deficient groups [360]. Complex **3** has been found to be most cytotoxic RAPTA compounds especially in A2780 human ovarian cancer cells and also significantly more active than other simple RAPTA compounds [17]. The biomolecule reaction mixtures of complex **3** has been observed to contain mostly [Ru(pta)]– biomolecule adducts which were not observed in the protein or DNA binding studies of

[Ru(pta)(arene)] adducts typical of other RAPTA complexes [17]. Therefore, this facile arene loss is proposed to be responsible for the increased cytotoxicity of complex **3** [17].

In the subsection 3.3.3, we have selected two of the model compounds (Figure 3.7) which are [Ru(η^6-p-benzene)Cl_2(pta)] (RAPTA-H named as complex **1** and **2**) and [Ru(η^6-p-cymene)Cl_2(pta)] (RAPTA-C named as complex **3** and **4**) reported by Dyson et al as anticancer agents [13]. The hydrated form of these complexes which are [Ru(η^6-p-benzene)Cl(H_2O)(pta)] named complexes **2** and [Ru(η^6-p-cymene)Cl(H_2O)(pta)] named complex **4** (Figure 3.7) are considered since activation of Ru complexes are known to occur through hydration [8, 17, 37, 38]. In order to improve their anticancer activities and obtain better lead compounds, their stability must be improved [5]. In this study, we have used the quantum theory of atom in a molecule (QTAIM) to understand the effects of non-covalent interactions on the stability and hydration of these complexes.

In the subsection 3.3.4, five ruthenium half-sandwich complexes are selected for theoretical studies. These have the feature similar to the type of complexes that have gained researcher attention of the Sadler et al laboratory [20-26] but there are little differences because of the carboxylic and/or pyrazole unit(s) (Figure 3.10) that are introduced into the complexes. Ruthenium based complexes seems to have attracted serious research attentions than any other metal complexes [12, 86-92] as potential anticancer agents. Even though there is yet to be any approved anticancer complexes that match the anticancer activities of cis-platin, many of the promising anticancer ruthenium complexes have been synthesised and analysed [93, 94, 95, 96, 97, 98]. Other notable anticancer complexes still at laboratory level are the RAPTA complexes from Dyson et al [9, 13, 16, 17, 51, 54, 63, 127-129]. These five complexes have been theoretically compared to the RAPTA complexes against many anticancer receptors and are predicted to be promising [318].

3.3.1 The effects of bidentate coordination on the molecular properties of RAPTA-C based complexes using theoretical approach

3.3.1.1 Natural orbital analysis

The hybridization of Ru(II) metal (Table 3.1) for all the three complexes (Figure 3.1) shows that the $4d^7$ orbitals are used preferentially in complex formation compared to the $5s^1$ orbital as the computed occupancy of s-orbital ranges from 0.13 to 0.40 which is far less than one. This further confirms that the 4d orbitals are lower than that of 5s. The natural Lewis structure description in terms of the percentage of the total electron density confirm the stability of the complexes with three complexes having more than 97% Lewis electrons (Table 3.1). Also, valence non-Lewis orbitals (description of antibonds or electron delocalization) play a relatively important role in the stability of the complexes as it is associated with relatively significant percentages compared to the extra-valence orbitals (i.e. Rydberg) in the slight departures from a localized Lewis structure model.

The features of the metal-ligand interaction and bonding (Table 3.2 and 3.3) indicate that there is metal to ligand charge transfer (MLCT) in all the three complexes. This is evidence from the assymetric polarization of the bonding electron in the natural bond orbital (NBO) analysis of Table 3.2 where bonding electrons are directed towards the ligand atoms. Metal complexes are known to posses intense, low energy metal ligand charge transfer (MLCT), ligand metal charge transfer (LMCT), or intraligand charge transfer (ILCT) excitations [346]. The feature of the HOMO and the LUMO in Figure 3.2 also shows that the Ru atom and the bidentate ligands dominate the HOMO while the arene unit which is a π-ligand are predominantly the LUMO which further confirm the electron transfer from metal to arene carbon atoms. Different from what is obtained in the bidentate complexes, the HOMO in monodentate is dominated with the PTA ligand. There is a significant electron transfer from the Ru(II) lone pair into the carbon atoms of arene unit which range from 0.44596e to 0.48942e in the three

complexes considered. In this NPA analysis, the Ru atom interaction with arene C atoms are suggested as adjacent bonded atom (vicinal, "v"), or a more remote ("r") site since each of the three complexes are split into two different units made of of arene unit and all other atoms taking as second unit (Table 3.3).

The strength of these intramolecular interaction obtained using the bond order analysis (Table 3.4) of ligand atoms that are in direct bonding with metal is in good agreement with the result obtained from the QAIM analysis. The bond order of the metal-ligand atoms are in the order of Ru-Cl > Ru-P > Ru-O > Ru-C where the carbon atoms are from the arene ligand. The highest bond order of Ru-Cl up to 0.967 and lower bond order of Ru-P and Ru-C coupled with the topological analysis done with AIMAll (Table 3.5) show that the Ru-Cl is a strong ionic bond while the rest of metal-ligand bond should be dative bond. We observed that the strength of the bond order is not in direct relation with the bond distance for the Ru-Cl in complex **3** which have the highest bond distance also have the highest bond order (Table 3.4).

3.3.1.2 Natural energy decomposition analysis

In the NEDA calculation, charge transfer (CT) is found to make a significant contribution to the Ruthenium-Ligand (Ru-L) interaction for all model studied (Table 3.6). The magnitude of CT is far higher than the electrical interactions which include both the electrostatic (ES) and polarization (POL) contributions. The POL with CT and SE which may make largest individual contributors to strong attractions that are necessary for binding to overcome the strong CORE repulsions at the equilibrium geometry of H-bonding (far inside van der Waals contact) resulting in the final net H-bond stabilization energy (E). The results from NEDA analysis shows that **1** and **2** have higher hydrogen bond stability (Table 3.6) than the precursor complex **3** which is the direct effect of their higher polarizabilty than complex **3**. Interestingly also, the feature of the intramolecular interation of atoms obtained from

AIMALL also shows that complex **1** has higher hydrogen network (Figure 3.3 and Table 3.5) than the other two complexes just as NEDA rated to have the highest hydrogen bond stability (Table 3.6). This is in good agreement with the reported experimental results where **1** and **2** were found to be highly soluble and kinetically more stable than their precursor complex **3** that contains two chloride ligands in place of the carboxylate ligands [51]. The higher solubility of the two bidentate complexes **1** and **2** should also be the direct effect of their higher intramolecular hydrogen bond (HB) interaction which will enhance their interaction with the polar solvent environment. HB has been described to be based on two different effects which are electrostatic field effect and orbital delocalization effect [166].

3.3.1.3 Atoms in molecules analysis using B3LYP/3-21G functionals

The atoms in molecular analysis of complexes using AIMAll confirmed the presence of both strong and weak noncovalent interactions. In interpreting the features of the quantum theory of atoms in molecules (QTAIM) topology, the critical points density ($\nabla\rho$) gives information about the existence of bonds, while the sign of the Laplacian of the density ($\nabla^2\rho$) at that point reflects the kind of interaction which if it is negative is a critical point for covalent interactions (open shells), and if it is positive is a closed shell interactions, such as hydrogen bonds [361] or ionic bond or Van der Waals interaction [362]. The Laplacian features of each complex electron density ($\nabla^2\rho$) are shown using the contour plot along the plane of the P, Ru and Cl or O in the bidentate complexes (Figure 3.3) and many of the atoms of the complexes are found on the chosen plane. All the ligand-ligand bonds are characterised with negative $\nabla^2\rho$ (dash lines) while the metal-ligand bonds are characterised with positive $\nabla^2\rho$ (solid lines) which further confirmed that they are covalent and non-covalent interactions respectively.

The typical nature of covalent bond which is an open shell interaction is high negative value of $\nabla^2\rho(r)$, higher $\rho(r)$ value, low kinetic energy per electron and higher magnitude of the ratio of potential

to kinetic energy (V/G) [363]. The covalent bonds have higher negative values of V, high $\rho(r)$, higher negative values of $\nabla^2\rho(r)$, higher negative value of V/G and lower kinetic G. The $\nabla^2\rho$ values for the BCP of M-L bonds are positive but far higher than that of exiting hydrogen bonds (HB) which are characterised with low +ve value of $\nabla^2\rho$ as shown in (Table 3.5). The high +ve $\nabla^2\rho$ values of BCP for M-L and the corresponding high values of $\rho(r)$ is an indication of strong non-covalent bonds [362]. This gives the reason why the bond order for M-L bonds are relatively low (Table 3.4) except for Ru-Cl of complex **3** that is suggested to be ionic bond. This further highlights the NBO analysis that indicates d-orbitals of the metal as the orbital which carries highest percentage of bonding to ligand atoms. Also, the feature of the Lewis bonding and non-Lewis antibonding in Table 3.2 shows that one of the Ru-O bond is missing for complex **1** and the bond order in Table 3.4 also shows that the Ru-O bonds of complex **1** are associated with longer unequal bond which will further enhance its hydrolysis compared to **2**.

3.3.1.4 The correlation of the computed bond properties

The relationship that exist between the computed bond properties can be comprehended using the correlation Table 3.7 that is constructed over all existing bonds in the three complexes. From this table, a high value of $\rho(r)$ should have a high negative value of $\nabla^2\rho(r)$ except where there is a stronger non-covalent bond as in M-L bonds. The values of $\nabla^2\rho(r)$ appear to be strongly related with the values of V/G which is an indication that a stronger bond should be characterised with stronger potential energy density than Lagrangian form of kinetic energy density. A very flat electron density region that is usually characterised with very low average values for $\rho(r)$ and $\nabla^2\rho(r)$ are usually found to have a relatively high ellipticity [364] which can be interpreted that ellipticity is inversely proportional to $\rho(r)$ and negative values of $\nabla^2\rho(r)$. The correlation of the ellipticity of all the bonds in the three

complexes with $\rho(r)$ and negative $\nabla^2\rho(r)$ shows that it is inversely proportional and averagely high. The correlation values of ellipticity with $\rho(r)$ as shown in Table 3.7 are -0.57,-0.72 and -0.65 while with the negative values of $\nabla^2\rho(r)$ are 0.57, 0.65 and 0.60 for complexes **1**, **2** and **3** respectively. The implication is that a high negative value $\nabla^2\rho(r)$ and high positive values of $\rho(r)$ which is a picture of strong open shell covalent bond are characterised with lower ellipticity while the close shell interaction of low positive $\nabla^2\rho(r)$ as in HB are characterised with higher ellipticity. Therefore the Ru-Ligand bonds (Table 3.5) are characterised with higher ellipticity than covalent bonding within the ligands which is a further indication that the metal-ligand bonds are closed shell interaction. The higher ellipticity values of the ruthenium monodentate bonds in complex **3** and ruthenium bidentate bonds in complexe **1** than complex **2** further supports the reported hydrolysis of complex **1** and **3** while complex **2** completely resist hydrolysis [8, 51]. Also, bonds with relatively high ellipticity are those with higher bond stretching (BPL-GBL_I) with correlation of 0.51, 0.93 and 0.74 in complexes **1**, **2**, and **3** respectively (Table 3.5).

3.3.1.5 The intraatomic properties of the complexes

As expected for all the heavy atoms with largely core electrons, the population of each atom is highly localized (Table 3.8) while electron density of all the H atoms is strongly delocalized and therefore can easily be perturbed by external influences such as an electric field [363]. The properties of some of the selected atoms of interest which are directly bonded to Ru metal are shown in Table 3.8. All the atomic basins have integrated Laplacian values L(A) of approximately equals to zero (Table 3.8), indicating satisfactory numerical integration [363]. As clearly shown in Table 3.8, the arene carbon atoms become more electronegative as a result of MLCT. The complex HB bonds network observed in the complexes as shown in Figure 3.3, are direct consequence of one centre being electronegative than the other as the atoms that are involved in HB are of different atomic charges

(Table 3.8).

Taking a critical look at the molecular sum total of the atomic properties for the complexes **1**, **2**, and **3**, we observed that the total K(A) are 6045.16, 5891.34 and 6432.41 while the total V(A) 3603.91, 3116.36 and 3069.81. It is interesting to point out that the higher total values of K(A) of complexes **3** and **1** over complex **2** is in the order of their reported anticancer activities [13].

3.3.1.6 Atoms in molecules analysis using PBE0/6-31G(SBKJC VDZ ECP) functionals*

When ECP basis set was applied on P, Ru and Cl atoms where applicable, the intramolecular features in QTAIM topology shows that there is Non-Nuclear Attractor (NNA) Critical Point (CP) i.e. (3,-3) CP but this NNA disappeared when all electron basis set was applied on the three complexes. A typical feature for the complex one is shown in Figure 3.3 as **1a** and **1b** when ECP basis set and all electron basis set were used respectively. In making use of the ECP, even though we obtained similar features when all electron basis set was used yet there is a higher number of RCPs because of the introduction of NNA into complex **1a** (pink sphere in Figure 3.3 (1a)). The computed feature of the topology when the ECP was applied on Ru and P atoms shows that there is a common NNA between the Ru-P bond in the three complexes which is very closed to P atom characterised with $\nabla^2\rho$ of 3.22, 3.22 and 3.18 for P-NNA bond and 0.11, 0.12 and 0.11 for NNA-Ru bond in the complexes **1**, **2** and **3** respectively. The higher values of $\nabla^2\rho$ for P-NNA and lower for NNA-Ru is an indication that the electronic configuration of metal atom was well represented with the ECP basis set. Also, the contour plot in Figure 3.3 for complex **1a** shows that the NNA is within the negative contour (dash lines) around P atom which further confirms that the NNA was introduced to compensate for the deficiency of electrons around P due to application of ECP.

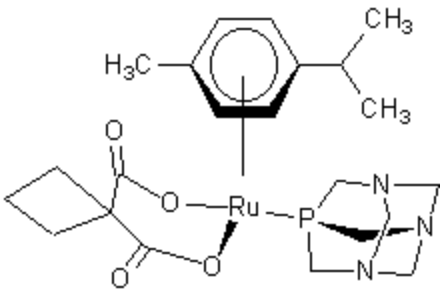

Complex **1** (*carbo*-RAPTA-C)

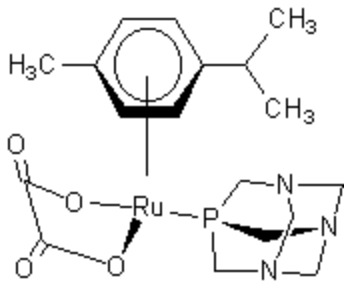

Complex **2** (*oxalo*-RAPTA-C)

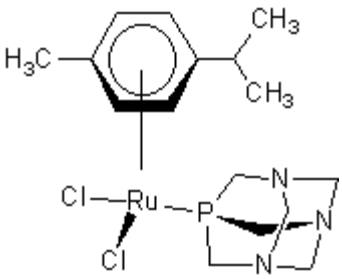

Complex **3** (RAPTA-C)

Figure 3.1: The schematic structures of complexes **1**, **2** and **3**

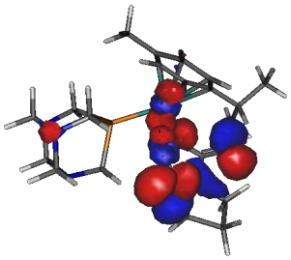

Complex **1** HOMO

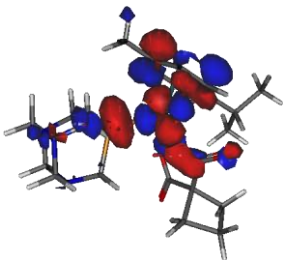

Complex **1** LUMO

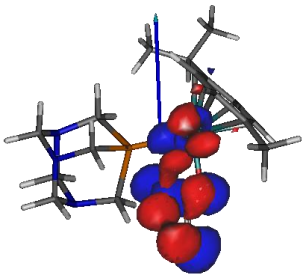

Complex **2** HOMO

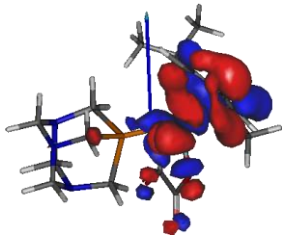

Complex **2** LUMO

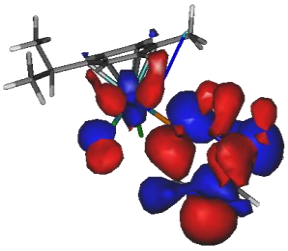

Complex **3** HOMO

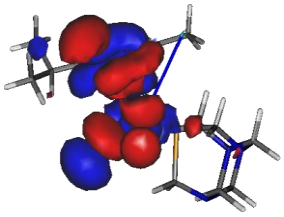

Complex **3** LUMO

Figure 3.2: The HOMO and the LUMO of complexes **1**, **2**, and **3** in a ascending order.

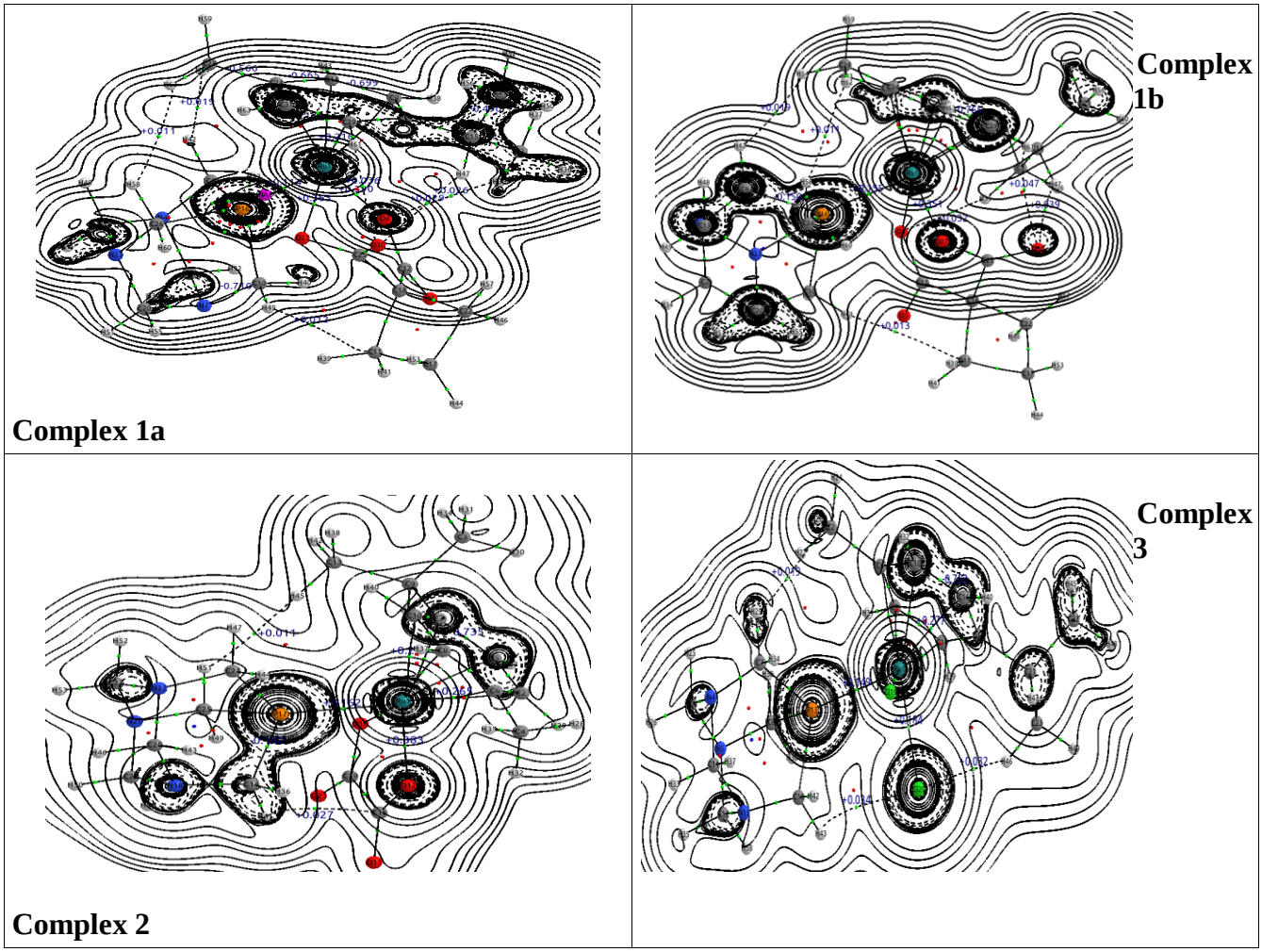

(3,-1) bond critical points (BCPs) are shown as small green spheres, (3,+1) ring critical points (RCPs) as small red spheres, and (3,+3) cage critical points (CCPs) as small blue spheres and the Non-Nuclear Attractor (NNA) in complex **1** as a large pink sphere. **1a** and **1b** stand for when ECP basis was used and when all electron minimal basis was used for complex **1**.

Figure 3.3: Laplacian of the electron density in a plane containing P, Ru and Cl or O nuclei (positive contours as solid and negative contours as dash lines are drawn from 0 to ±800) and bonds (strong bonds in solid and HB in dash lines) for complexes **1**, **2** and **3**.

3.3.2 Computational properties of η^6-toluene and η^6-trifluorotoluene *half-sandwich Ru(II) anticancer complexes*

3.3.2.1 The geometries of the complexes

The geometries of the complexes (Figure 3.4) were optimized to their lowest ground state energy characterised with zero imaginary frequencies. The obtained bond distances and angles are within the experimental ranges [365]. The computed Ru-arene bond distances of complex **3** ranges from 2.197 to 2.257 Å which is very close to the reported experimental range of 2.151-2.169 Å. Comparing the computed geometries of the complexes to the experimental reports (in bracket), the range of bond distances (in Å) for Ru-P is 2.419-2.443 (2.279-2.297), Ru-Cl is 2.481-2.496 (2.410-2.434) while the bond angles (in degree) ranges for Cl-Ru-Cl is 89.73-90.75 (87.25-87.88) and Cl-Ru-P is 79.96-82.75 (82.61-87.86). All the bond distances of the ruthenium-ligand (Ru-L) with their respective bond orders are shown in Table 3.9 (for the systems treated with B3LYP/DGDZVP(Ru)|6-31+G(d,p)). The bond order of the two chloride atoms in each of complex **1** and **3** are relatively the same. This indicates that any one of the two chloride atoms can be a leaving group in their hydrolysis to complexes **2** and **4** respectively (Table 3.9). After the hydrolysis, the possibility of the last chloride atom becoming a leaving group is rare [255] as the bond order of chloride atom increases from the unhydrolyzed complexes (**1** and **3**) to the hydrolysed ones (**2** and **4**) while that of the Ru-P decreases. Therefore for any possible covalent interactions of the central metal atom with biological residue as proposed experimentally [38, 68, 126], the water molecule has to be a leaving group and possibly the PTA ligand. The bond order analysis recognised the existence of the hydrogen bond (HB) that exists within each of the complex. The fluorination in complexes **3** and **4** respectively seems to have very

little effect on the bond order of the complexes with a little improvement in the Ru-P and Ru-Cl bond order.

In all the complexes, the natural bond order (NBO) and NEDA properties computed with ECP (PBE0/ECP(Ru, P, Cl)|6-31G*) (Table 3.14)) and the QTAIM properties computed with minimal basis set 3-21G (Table 3.18, 3.20 and 3.21) are in a close range with those computed with higher basis sets where Ru atom is treated with DGDZVP basis set and other atoms treated with 6-31+G(d,p) basis set (Table 3.6 - 3.11) (referred to as B3LYP/DGDZVP(Ru)|6-31+G(d,p) systems). This is an indication that the properties computed with minimal basis set 3-21G for these type of complexes is reliable enough and can be helpful to treat large system.

3.3.2.2 Natural bond orbital analysis

The $4d^7$ orbitals are used in bond interactions preferentially to 5s orbitals in all the four models (Figure 3.4). The Lewis carries the highest percentage (ranges from 97.68% to 98.11%) which is an indication that the structure is stable. The effect of the non-Lewis orbitals is relatively significant (ranges from 1.71% to 2.16%) as a measure of the backbonding interactions in the complexes. The polarization (c_A) of the bonding atoms and the percentage of the NBO (c_A-squared) on each hybrid (Table 3.10) is in favour of the coordinated ligand atoms as they are associated with higher values. This suggests the possibility of metal to ligand charge transfer (MLCT) transitions. The better feature of the charge transfers is observed when second perturbation energies ($E^{(2)}$) of the delocalized orbitals were computed as shown in Table 3.11. The higher value of $E^{(2)}$ is an indication of higher stability ascribed to contribution due to delocalization. A critical observation of the common charge transfer (CT) from the Ru atom to the arene C=C double bonds shows that the stabilization energy ($E^{(2)}$) of this CT decreases upon the hydrolysis of the complexes and fluorination of the complexes (Table 3.11). However, the values of the $E^{(2)}$ are not the direct measure of the magnitude of charge transfer from the

Ru atom to the arene carbon atoms because higher charge transfer are observed from the Ru atom to the arene carbon atoms (Table 3.12) in the hydrolysed complexes (i.e. complexes **2** and **4**) and fluorinated complexes (i.e. complexes **3** and **4**). It is interesting to point out that both hydrolysis and fluorination significantly leads to the lower energy values of the antibonding orbitals of the complexes which enhances both the MLCT and LMCT properties of the complexes. This should also be responsible for the higher electrical energy (EC) contribution and charge transfer (CT) of the hydrolysed and fluorinated complexes from the NEDA analysis of the complexes (Table 3.13). Also from NEDA analysis, we observed the total charges transferred from the Ru lone pairs to the ligand lone pairs or Ru-L bonds (after all the transferred from the ligand atoms have been subtracted) to be 0.494, 0.472, 0.533 and 0.409 e for complexes **1**, **2**, **3** and **4** respectively which is an indication that hydrolysis decrease the MLCT while fluorination increases it.

The nature of the HOMO and the LUMO of the complexes (Figure 3.5) further confirmed mixed features of the MLCT and LMCT in the complexes. HOMO is predominantly the Ru, Cl and PTA atoms while the arene ligand atoms including also the Cl and Ru atoms dominate the LUMO. The hydrolysis of the complexes results to lower HOMO contribution of Ru atom in the complexes **2** and **4** which is the effect of the significant backbonding of electron from the oxygen atom of the water molecule to the antibonding orbital of the Ru atom (Table 3.12). Fluorination of the arene reduces the HOMO contribution of the chloride atoms in the complexes which result to HOMO being predominantly characterised with only the Ru and the PTA atoms (complexes **3** and **4**) which further confirm the features obtained from NEDA analysis.

3.3.2.3 Natural energy decomposition energy analysis

The results obtained from the NEDA analysis of the complexes are shown in Table 3.13 and Table 3.14. The high values of charge transfer (CT) further shows its significance contribution to the

stability of the complexes. CT is the most significant factor that determines the stabilization of the un-hydrolysed complexes while POL is the most important factor in the hydrolysed complexes (Table 3.15). A significant increase in the value of hydrogen energy (E) from un-hydrolysed complexes to the hydrolysed complexes is an evidence of improved stability which may be responsible for the reported activation of these complexes by hydrolysis [8, 37]. The presence of trifluorotoluene in complexes **3** and **4** lead to increase in the CT and Electrical properties of the complexes but lower overall hydrogen interaction energy (E).

The synergistic effect of fragments in complexes on each other through the decomposition analysis of the complexes can be seen from Table 3.15. Both the synergistic properties of the induced energy and dipole increases as a result of presence of the trifluorotoluene in complexes **3** and **4** which could be responsible for the reported better anticancer activities of these complexes than complexes **1** and **2** [17]. The overall strong synergistic effects of ligand units that are coordinated to metal centre in all the complexes can lead to highly cytotoxic species as it was experimentally suggested [62].

3.3.2.4 The QTAIM analysis of bonds

Further analysis of the electron density wavefunction through the quantum theory of atoms in a molecule (QTAIM) as implemented in AIMAll package give a better features of the interatomic interaction in the complexes. The QTAIM properties obtained from combination of higher basis sets DGDZVP(Ru)|6-31+G(d,f) (Table 3.16, 3.19) is very similar to the properties computed using minimal basis set 3-21G (Table 3.18 and 3.21).

In QTAIM analysis of the complexes, all the inter-atomic bonds within each of the ligand are characterised with covalent bonds which is an open shell interaction with negative value of $\nabla^2\rho(r)$ (Figure 3.6), higher $\rho(r)$ value, low kinetic energy per electron (K) and higher magnitude potential to Lagrangian kinetic energy ratio [363]. A positive $\nabla^2\rho(r)$ characterised all the metal-ligand bonds

(dotted lines in the contour plots of Figure 3.6) and the HB (Tables 3.16 and Table 3.18) which is an indication of a closed shell interactions typical of hydrogen bonds [361] or dative or ionic or van der waals bond [362]. The very high positive $\nabla^2\rho(r)$ is an indication that the metal-ligand bonds in these complexes are dative bond [362] except Ru-Cl bonds that may be suggested to be ionic bond. Also, all the HB bonds have the same properties of M-L bonds but lower values of $\rho(r)$ and $\nabla^2\rho(r)$ [361] and are weaker than the dative bond that exist within the M-L bonds (Table 3.18).

The communication of electron through hydrogen bond (HB) interactions between the arene and PTA units which are remote to each other improved significantly due to fluorination. All the four complexes are associated with intramolecular HB interaction some of which are unusual [366-368]. In complex **1** and **2** there is unusual HB between the C of arene and one H atoms of the PTA which is as a result of the arene unit acting as charge acceptor since it is a π-ligand that is characterised with electron deficiency. In all the complexes, the strongest HB exist in the hydrated complexes between the Cl and the H atoms of water molecule (Figure 3.6) which were also confirmed by the bond order analysis and higher values of $\rho(r)$ and $\nabla^2\rho(r)$ (Tables 3.35). Fluorination in complexes **3** and **4** significantly improved their HB network and can be ascribed to the higher charge transfer and electrical properties but lower overall hydrogen interaction energy observed for these complexes (Table 3.13 and Table 3.14). This may be responsible for the reported higher anticancer activities of the fluorinated complexes as a result of increase in number and strength of HB which can lead to increase in the sensitivity of some of the atoms and stability of complexes.

The correlation table was constructed for all the bond parameters computed during the QTAIM analysis (Table 3.17) over all the existing bonds in each of the four complexes. This is to understand the relative effect of these parameters on the strength of all atomic bond interactions in the complexes. The values of the density ($\rho(r)$) are shown to be highly inversely proportional to the Laplacian values

of the density ($\nabla^2\rho(r)$) which is an indication that a bond with high $\rho(r)$ values will be associated with very high negative values of $\nabla^2\rho(r)$ which is typical of strong covalent bonds except the metal-ligand bonds with high positive $\nabla^2\rho(r)$.

3.3.2.5 The QTAIM analysis of intra- and inter-atomic properties

The properties of selected atoms of interest which participate in the M-L bond, HB and nitrogen atoms of the PTA are presented (Table 3.19, 3.21). All the atoms (except H atoms) in the complexes are more localized with higher %Loc(A) while H atoms are characterised with higher %Deloc(A,A') which is an indication that the H atoms of these complexes can easily be perturbed by external influences such as an electric field [363]. Atoms such as Cl, Ru and P have the highest Vol(A) in a descending order which consequently resulted in lower $\rho(r)$ and $\nabla^2\rho(r)$ bond interactions for the Ru-Cl and Ru-P bonds (Table 3.16 and Table 3.19) that involve the interaction of two atoms of large V(A). The changes in the atomic properties of Ru metal give insight into the hypothesis of the activation of these complexes by hydrolysis. The charge distribution on the arene carbon atoms (Table 3.9 and 3.21) shows that these atoms are charge acceptor centre which further explains the observed MLCT.

In order to understand the chemistry of each atom in the complexes, the correlation of all the computed atomic properties is constructed over all the atoms present in each complex (Table 3.20). The electronic kinetic energy of each atom (K(A)) is significantly affected by the magnitude of the bond dipole moment of each atom ($|\mu_{Bond}(A)|$) and the total dipole of each atom ($|\mu(A)|$). The μ-Bond(A) is the main determinant factor of the total dipole ($|\mu(A)|$) and also have high effect on all the computed atomic properties except its poor correlation with the atomic charge (q(A)).

The sum total of all the intra- and inter-atomic properties computed over all the atoms in each complex is presented in Table 3.22. The sum over of the total dipole (μ) and K(A) of the

trifluorotoluene complexes **3** and **4** is higher than that of complexes **1** and **2** which may contribute to the reported higher anticancer activities of the fluorinated complexes. Comparing the properties of the hydrolysed complexes to the unhydrolysed complexes, there is decrease in the LI(A), K(A) and dipole properties while there is a increase in the DI(A,A')/2.

*3.3.2.6 QTAIM analysis using PBE0/ECP(Ru, Cl, P)|6-31G**

The topological features using the mixed basis set where the SBKJC VDZ ECP basis set is applied on Ru, P and Cl atoms of the complexes as explained in the computational method referred to as PBE0/ECP(Ru, Cl, P)|6-31G*, shows a common Non-Nuclear Attractor (NNA) Critical Point (CP) i.e. (3, -3) between the Ru-P bond which was never observed when all electron higher basis sets DGDZVP(Ru)|6-31+G(d,P) and when minimal basis set 3-21G were used. This is an indication that the presence of NNA in these complexes is just a computational artefact of ECP basis set which could not effectively account for all the electrons density around the atoms.

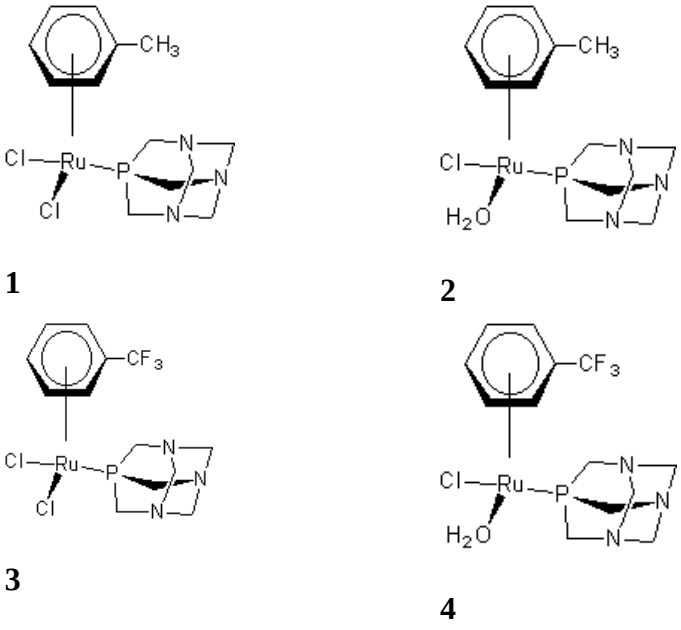

Figure 3.4: The schematic feature of complexes **1**, **2**, **3** and **4**

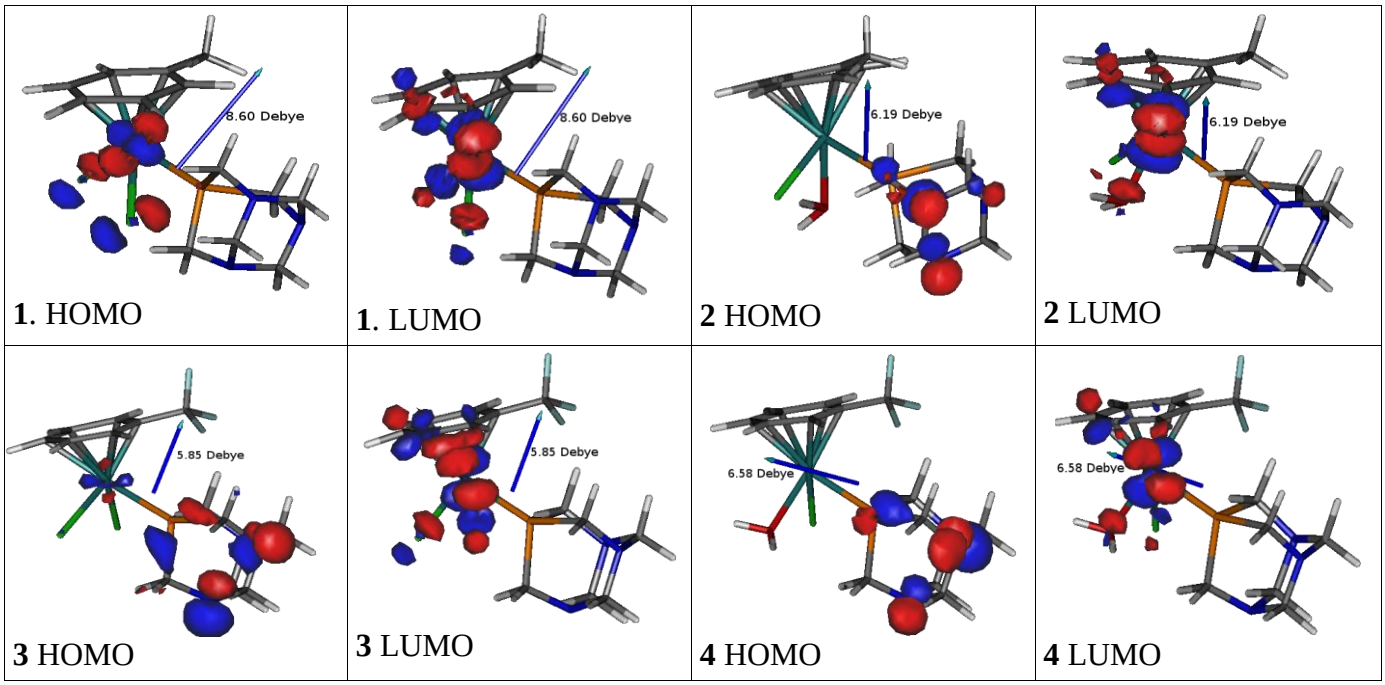

1. HOMO | **1**. LUMO | **2** HOMO | **2** LUMO

3 HOMO | **3** LUMO | **4** HOMO | **4** LUMO

Figure 3.5: The HOMO and the LUMO of complexes **1**, **2**, **3** and **4** with arrow showing the direction of the dipole moment

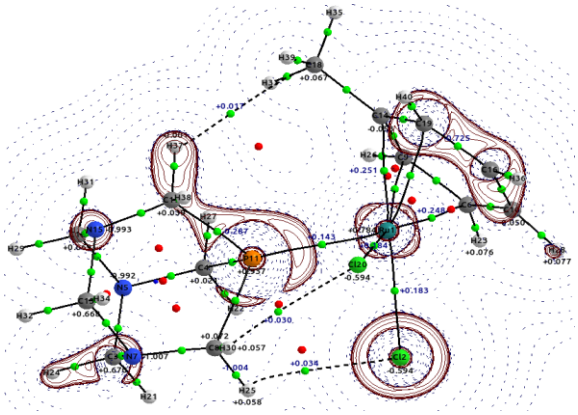

1

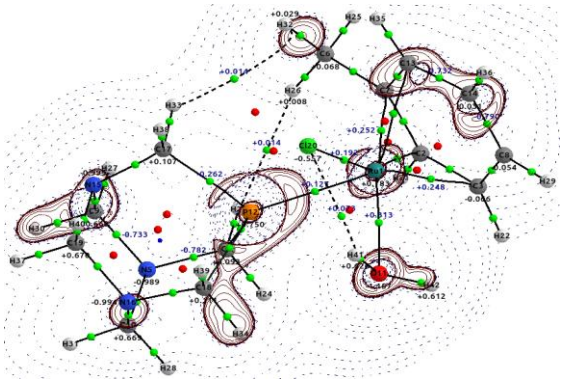

2

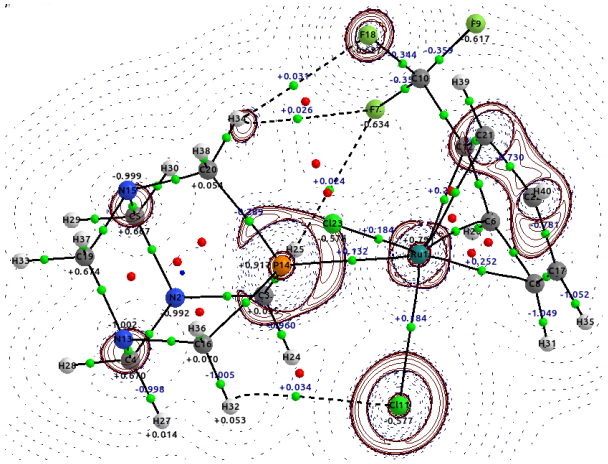

3

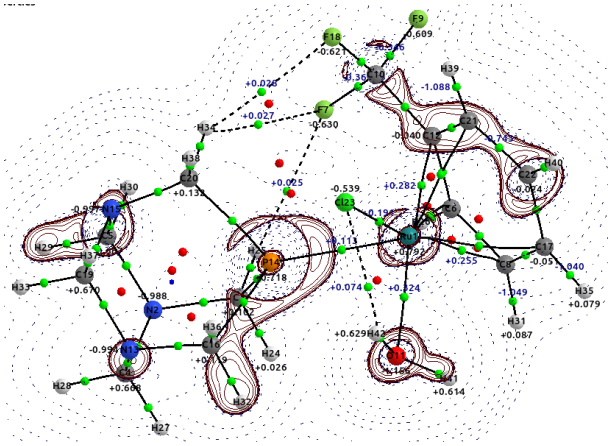

4

(3,-1) bond critical points (BCPs) are shown as small green spheres, (3,+1) ring critical points (RCPs) as small red spheres, and (3,+3) cage critical points (CCPs) as small blue spheres

Figure 3.6: Laplacian of the electron density in a plane containing P, Ru and Cl or O nuclei (positive contours as solid and negative contours as dashes lines are drawn from 0 to ±800 a.u) and bonds (strong bonds in solid and HB in dash lines) for complexes **1**, **2**, **3** and **4**.

3.3.3 Insights into the intramolecular properties of η^6-arene-Ru based anticancer complexes using quantum calculations

Stable stationary geometries were obtained for the four complexes (Figure 3.7) which are characterised by zero imaginary number from the thermodynamic calculation. When the geometries of the complexes were further optimized from PBE0/ECP(Ru,P,Cl)|6-31G* to PBE0/ECP(Ru)|6-31+G(d,p), the highest contraction of bond lengths up to 0.05 Å was observed for Ru-Cl bonds (Table 3.23). There is also a slight change in bond orders up to 0.1 when comparing the two steps of optimization. Applying uniform basis set 3-21G on all atoms of the complexes, there are no significant changes in the total energies from the first optimization (-6307.84, -5925.61, -6464.66 and -6082.04 A.U. respectively) to the second optimization (-6307.84, -5925.61, -6464.26 and -6082.04 a.u.). The bond orders of the Ru-Cl bonds increase in the hydrated complexes **2** and **4** which suggest that the possibility of displacing the second Cl atom with aqua ligand will be difficult [255]. But on the order hand, the Ru-P bond order decreases upon hydration of the complexes. The properties computed using combination of higher basis sets DGDVZP(Ru)|6-31+G(d,p) and those computed using lower basis sets 3-21G follow the same trend which is an indication that lower basis sets can give insight into the trend though it either underestimate or overestimate the computed properties.

3.3.3.1 The natural bond orbitals (NBO) analysis

The polarization features of some visible Ru-L bonding orbitals are shown in Table 3.24, while Table 3.25 shows the nature of the electron delocalization orbitals with their second-order perturbation energy ($E^{(2)}$). The number of the electron transfer into each of the acceptor orbitals in Table 3.25 are shown in Table 3.26 with the values of their energy level. The bonding polarizations of the Ru-L are directed towards the ligand atoms (Table 3.24). The reverse is the case in all the antibonding orbitals

interactions as a result of backbonding of electrons into the antibonding lone pair of ruthenium atom. The features of the charge transfer is clearly seen from the delocalized orbitals that have notable interaction with the Ru atom or bonds and have significant stabilization energy ($E^{(2)}$) equal or greater than 10 kcal/mol as presented in Table 3.25. There are many bond to bond, atoms to bond and atom to atom delocalization of electrons in the complexes. The most significant feature is the presence of metal to ligand charge transfer (MLCT) from the lone pair of Ru to the antibonding lone pair of arene C atoms in all the complexes. There is also an observed MLCT from the lone pair of ruthenium to the bonding lone pair of the same arene C atoms in complex **2** and **3**. From the NEDA analysis, if the total charge transfer from ligand to the lone pair of ruthenium metal (LMCT) is subtracted from that of metal to ligand (MLCT), the overall features shows that complexes **1** and **4** are predominantly characterised by LMCT with respective total charges of -0.56209 and -0.47667 transfer to the lone pair of ruthenium atom from ligand atoms while complexes **2** and **3** are predominately characterised with MLCT of total charges of 0.37489 and 0.45986 transfer from the Ru lone pair to the ligand atoms on bonds. These features are typical nature of π ligand metal complexes with intense intramolecular CT between metal and ligand (MLCT or LMCT) transitions and associated with π back-bonding [369, 370].

The features of the electronic orbitals in Figure 3.8 give an insight observed MLCT and LMCT observed in the complexes. The ruthenium atom is characterised as part of both HOMO and LUMO as a result of bonding electron contribution of metal and the backbonding contribution of the ligands. The PTA ligand dominates the HOMO orbitals of the hydrated complexes **2** and **4** compared to the Ru and Cl atoms which characterise the HOMO of the un-hydrated complexes **1** and **3**. The arene ligand is predominantly the LUMO which confirm the existence of MLCT between the Ru atom and the π-orbital of the arene moiety of the ligand. The HOMO nature of the Ru and the Cl atom in complexes **1** and **3** significantly reduced upon being hydrolysed to complexes **2** and **4** respectively.

3.3.3.2 Natural energy decomposition analysis

The results obtained from the NEDA analysis are shown in Table 3.27. The complexes **1**, **2**, **3** and 4 are fragmented into four, three, two and six units respectively. The respective fragmentations of complexes **1**, **2**, **3** and **4** are shown in Table 3.28 except the last two fragments of complex **4** which are the two hydrogen atoms of the aqua ligand that have negligible zero contribution. The number of the fragmentations in the complexes significantly correlates with their total interaction energy (Table 3.27). The strength of the interaction energy does not correlate with the number of hydrogen bond in the complexes. There are two, one, four and five hydrogen bonds in complexes **1**, **2**, **3** and **4** respectively as shown in Figure 3.9. The result shows that either polarization (POL) (complexes **1**, **2**, and **3**) or charge transfer (CT) (complex **4**) has the greatest contribution to the stability of the complexes. The significant values of the POL and ES result to the electrical energy having the highest contribution to the stability of the complexes (Table 3.27). The hydrated complex **4** has the highest interaction energy as a result of its significant high CT, ES and POL. On the contrary, the hydrated complex **2** has lower interaction energy compared to its unhydrated complex **1**. The high stability of interaction energy of RAPTA-C (i.e. hydrated complex **4**) should significantly contribute to its experimentally reported higher anticancer activity than the other RAPTA complexes [13].

3.3.3.3 The bond critical points analysis

The bond properties from both the B3LYP/DGDVZP(Ru)|6-31+G(d,p) treated systems (Table 3.29) and B3LYP/3-21G (Table 3.30) methods of computation were obtained from the quantum theory of atoms in a molecule (QTAIM) analysis of their respective electron density wavefunction. The $\rho(r)$ and $\nabla^2\rho(r)$ of all the Ru-L bonds are shown in Table 3.29 and 3.30. All the Ru-L bonds of the complexes are characterised by positive but higher $\nabla^2\rho$ (Table 3.29, 3.30 and Figure 3.9) than hydrogen bonds confirming that they are closed shell interactions like dative, hydrogen, ionic and van der waals

bonds [361, 362]. The features of the bonds are shown using the contour plot of the $\nabla^2\rho$ along the plane of the P, Ru and Cl or O atoms where the hydrated complexes are considered (Figure 3.9).

Complex **1**, **2**, **3** and **4** have two, one, four and five hydrogen bonds respectively (Figure 3.9). In literatures, there have been reports of unusual alkyl and halogen H-bonds [371-377] which are also observed in these complexes. There are unusual H-bonds between the alkyl C atoms of the cymene unit of complexes **3** and **4** and also H-bonds between the chloride atoms and H atom of aqua, PTA and arene ligands which contribute significantly to the H-bond networks of complexes **1**, **3** and **4**. The higher HB network in complexes **3** and **4** indicates that many of the atoms in these complexes will be sensitive to macromolecular interactions and should be responsible for their experimental reports of high cytotoxic activities than complexes **1** and **2** [13]. The hydrated form (complexes **2** and **4**) are characterised with extra and stronger HB suggesting that the activation mechanism of these complexes by hydration [8, 17, 37, 38] can possibly be the result of increase in the sensitivity of the atoms as a result of increased networks of HB and electronic interactions. There is a unique HB that exists between Cl and H atoms of the water molecules in the hydrated forms that is stronger than any other existing HB based on a higher value of $\nabla^2\rho(r)$ and $\rho(r)$ (Figure 3.9). The values of the ratio of the magnitude of potential energy (P.E) and the kinetic energy (K.E) of the electrons ($|V|/G$) in Tables 3.29 and 3.30 is relatively low indicating a balance between a stronger bond interactions and high density in the regions [363]. A high value of $|V|/G$ corresponds to higher density and stronger bonds except were the $\nabla^2\rho(r)$ is small (Table 3.29, 3.30 and correlation Table 3.31).

The strength of the two Ru-Cl bonds in terms of the $\nabla^2\rho$ and ε is not equal in complex **3** compared to complex **1** (Table 3.29 and 3.30) which is also observed in their bond order (Table 3.23). The imbalance features of the two Ru-Cl in complex **3** can enhance the aqua substitution of the weaker Ru-Cl to form Ru-OH_2 which may also play significant role in the reported higher anticancer of

RAPTA-C since easy hydration has direct correlate with the higher anticancer activity [37].

The relationships between the computed factors of the bonds are constructed over all the existing bonds in the complexes (Table 3.31). A very high negative value of $\nabla^2\rho(r)$ is an indication of strong covalent bond while a high positive value corresponds to a strong non-covalent bond. The general relation is that high negative values of $\nabla^2\rho(r)$ is directly proportional to high $\rho(r)$, high ∇^2Ven, lower bond stretch (BPL-GBL_I), lower kinetic energy (K), high negative values of potential energy (V), lower ellipticity (ε) and relatively high value of |V|/G. The higher electronic kinetic energy (K) is an indication of lower values of $\nabla^2\rho(r)$, ε and potential energy (V) but a higher value of $\rho(r)$ (Table 3.31). These observed correlations further confirmed the reported nature of a very flat electron density region that is characterised by very low average values for $\rho(r)$, $\nabla^2\rho(r)$ which is usually found to have a relatively high ε [364].

3.3.3.4 The intraatomic properties

The properties of some selected atoms in each of the four complexes are presented in Table 3.32 and Table 3.33. The integrated Lagrangian values L(A) of all the atomic basins are approximately equals to zero, which is an indication of satisfactory numerical integration [363]. The distribution of the atomic charges shows that the arene C atoms have gained charges confirming the existence of MLCT. For all the atoms in the complexes other than H atoms, the values of the percentage localization (%λ(A)) are higher than the percentage delocalization (%δ(A,A')).

The features of the relation within the computed intramolecular properties can be seen from the constructed correlation correlation Table 3.34. Higher K(A) is found to be as a result of higher bonding dipole moment contribution of the atoms ($|\mu_{bond}(A)|$), high number of electron and relatively low Vol(A) that is poorly correlated. The high values of $|\mu_{bond}(A)|$ is an indication of low %δ(A,A'), high

%λ(A) and high Vol(A) of atoms. The atoms that are characterised with bigger volume will be associated with higher negative values of the χ_{zz}. The atomic energy contribution (Ee(A)) to the virial energy of the system depend significantly on the number of the electrons and the number of localized electrons. The out of plane magnetizability (χ_{zz}) is proportional to the number of the atomic localized electrons and inversely proportional to the atomic delocalized number of electrons.

The sum total of the intraatomic properties computed over all existing atoms show the changes in the computed atomic properties from one complex to another (Table 3.35). The decrease in the values of the atomic energy contributions like Ee(A) and K_{Scaled} of the respective hydrated complexes shows the significant contribution of the Cl atom to the total energy of the systems. The average values of the percentage electron delocalization over all the atoms increases in the respective hydrated complexes while the average electron localization decreases which correspond with the theory of activation of this complexes by hydration. Also, the average electron delocalization and the three types of dipole moments in complexes **3** and **4** are higher than complexes **1** and **2** which further distinguishes RAPTA-C complex of reported better anticancer activities.

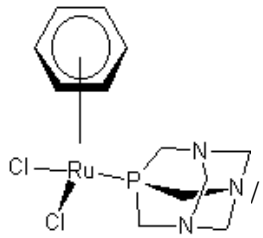

Complex **1**

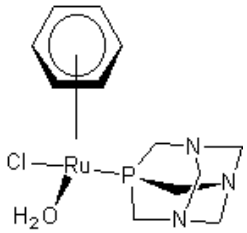

Complex **2**

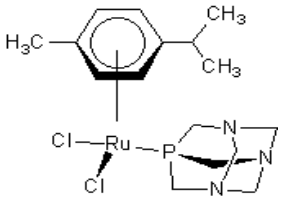

Complex **3**

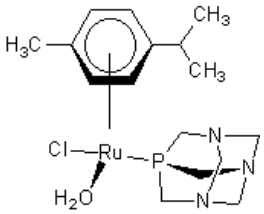

Complex **4**

Figure 3.7: The schematic structures of complexes **1**, **2**, **3** and **4**

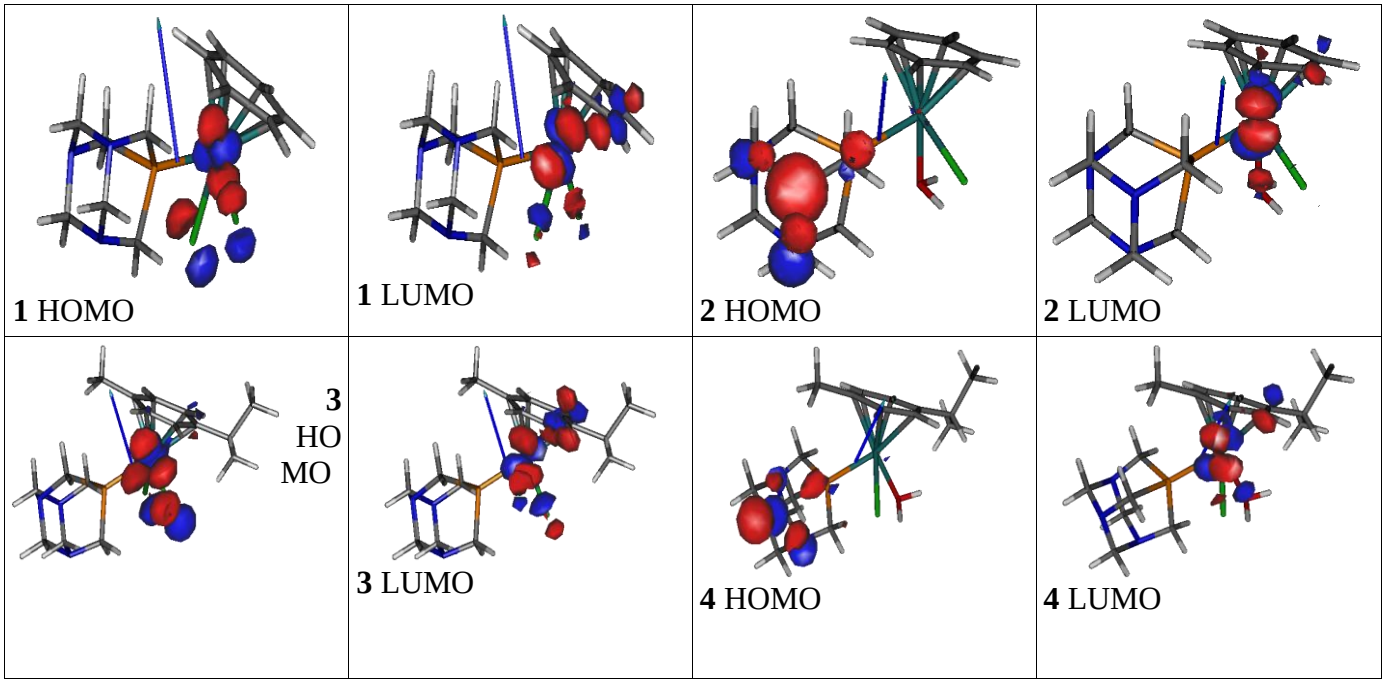

Figure 3.8: The HOMO and the LUMO of complexes **1**, **2**, **3** and **4** in a ascending order.

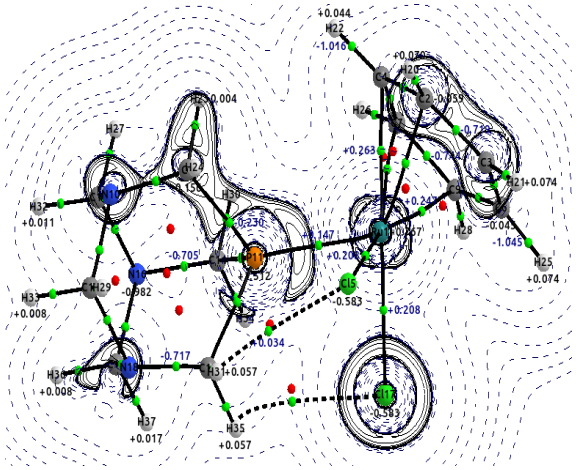

Complex **1**

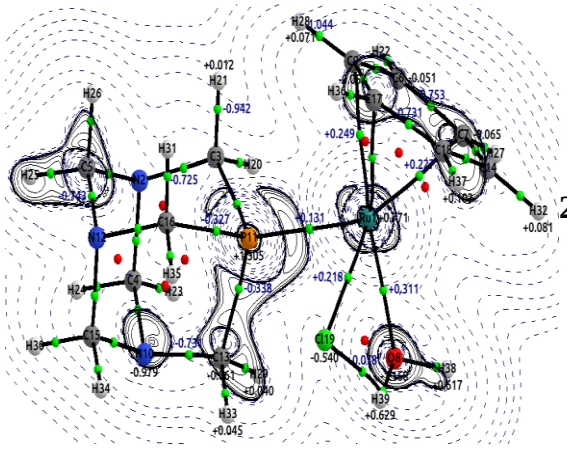

Complex **2**

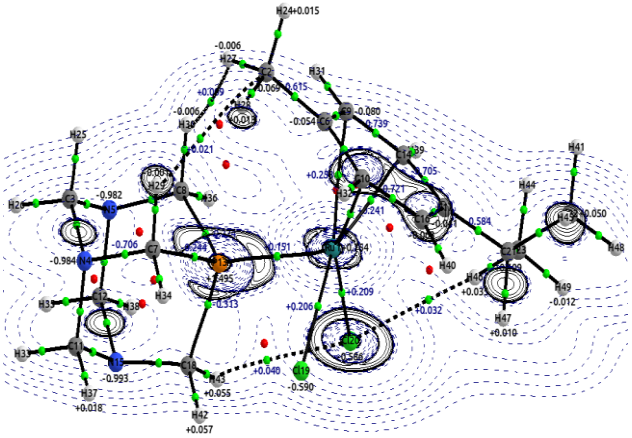

Complex **3**

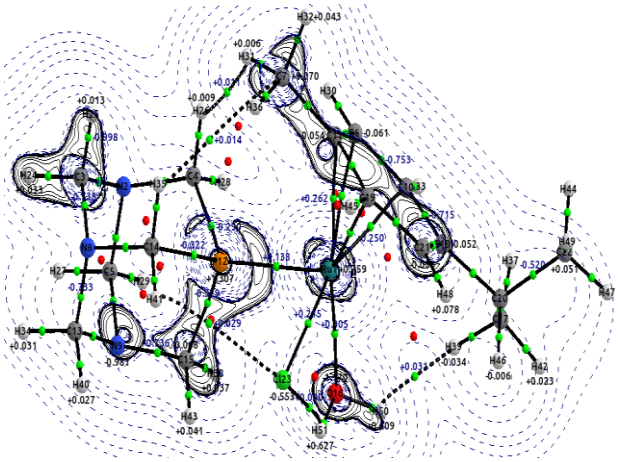

Complex **4**

Figure 3.9: Laplacian of the electron density in a plane contains P, Ru and Cl or O nuclei (positive contours as dash and negative contours as solid lines are drawn from 0 to ±800 and bonds (strong bonds in solid and HB in dash lines).

3.3.4 Interatomic properties of ruthenium half-sandwich anticancer complexes containing Ru-N bonds

The optimization and computation of the properties for these complexes were done twice, first applying ECP SBKJC VDZ basis set on Ru and Cl atoms where applicable and all other atoms treated with 6-31G* basis set while in the second method the ECP is limited to only the ruthenium atom and the other atoms in the systems are treated with 6-31+G(d,p) basis set which will subsequently be referred to as PBE0/ECP(Ru,Cl)[6-31G*] and PBE0/ECP(Ru)[6-31+G(d,p)] respectively. All the stationary geometries of the complexes studied are obtained using the PBE0ECP(Ru,Cl)[6-31G*] and PBE0/ECP(Ru)[6-31+G(d,p)] and the respective thermodynamic properties obtained from these are shown in Table 3.36. Change of the functionals significantly affects the total energy of these complexes than changes in the basis sets (Table 3.37). The functional B3LYP in all the cases over estimate the energy of the system while PBE0 gives values closed to higher perturbation method of MP2 as show in Table 3.37. This further support the literature reports that metal complexes are better optimized using PBE0 with ECP basis sets [332, 333]. However, the NBO, NEDA and QTAIM properties of the complexes were computed using B3LYP functional because it is one of the most used functionals in computational studies and also shown to behave well in computing QTAIM properties [378]. Considering the functional B3LYP only, there is a much closed relationship in the energy values computed by scaling up the basis set to a limit of aug-cc-pVTZ-DK as shown in Table 3.37. The energies are computed following the scaling: 3-21G → ECP(Ru,Cl)[6-31G*] → ECP(Ru)[6-31+G(d,p)] → DGDZVP(Ru)[6-31G*] → DGDZVP(Ru)[6-31+G(d,p)] → aug-cc-pVTZ-DK. The basis set aug-cc-pVTZ-DK and the functional MP2 are prohibitively expensive for computing the properties of these type of metal complexes with atoms ranging from 36-45, therefore the energy values provided for functional MP2 and basis set aug-cc-pVTZ-DK in Table 3.37 are the unconverged values.

The QTAIM properties of the complexes are computed using 3-21G, DGDZVP(Ru)[6-31+G(d,p)] and ECP(Ru)[6-31+G(d,p)] basis sets but the NBO and NEDA analysis a limited to only the higher combination of basis set DGDZVP(Ru)[6-31+G(d,p)]. In line with the literature reports, we observed that all methods can either overestimate or underestimate QTAIM properties (Table 3.45, 3.46 and 3.47) [378].

An interesting aspect of this work is to understand the chemistry of these five Ru(II)-based anticancer complexes based on their intramolecular interactions, strength of the Ru-N bonds and the stability of these complexes in relation to their proposed anticancer behaviours [318].

3.3.4.1 Thermodynamic and the geometry properties

The schematic geometries of the five complexes studied in this work are shown in Figure 3.10. These are half-sandwich complexes with bidentate (complexes **1**, **2**, and **3**) and tridentate (complexes **4** and **5**) ligands. Both complexes **4** and **5** have no chloride atom as ligand and there is no carboxylic unit in complex **4** among all other complexes. The high negative values of the energy, enthalpy and the free energy of the complexes at both level of theories (Table 3.36) shows that they are thermodynamically stable complexes. The values of the thermodynamic properties of the complexes at the two level of theories ECP(Ru,Cl)[6-31G*] and ECP(Ru)[6-31+G(d,p)] as applied for their optimization are shown in Table 3.36.

All the present metal-ligand bonds in the complexes with their bond order obtained through NBO analysis are shown in Table 3.38. The ruthenium-nitrogen (Ru-N) bonds are the shortest bonds in all the complexes ranges from 2.00 to 2.162 while their bond orders ranges from 0.361 to 0.424 which are relatively within the bond order of Ru-C_{arene} bonds. Compared to the available experimental Ru-N bond lengths, the computed Ru-N_{bpyr} bonds in complex **2** (where subscript bpyr indicates ruthenium-bipyridine bonds) are both 2.09 Å while Ru-N_{phn} in complex **3** (where subscript phn indicates

ruthenium-phenanthroline bonds) are both 2.138 Å which are closed to the experimental range of values for Ru-N_{bpyr} (2.040 to 2.056 Å) and for R-N_{phn} (2.073 to 2.087 Å) bonds [379]. In very good agreement with the experimental reports typical of Ru-N_{bpyr} and R-N_{phn}, the Ru-N_{bpyr} bonds in complex **2** is shorter than the R-N_{phn} bonds in complex **3**. The bond order (Table 3.38) with the Laplancian values ($\nabla^2\rho(r)$) of the electron density of the bonds (Table 3.45) also indicate that the Ru-N_{bpyr} is stronger than the R-N_{phn} in perfect agreement with the experimental report [379]. The computed N-Ru-N angle of complex **2** is a little lower than complex **3** which agrees with the experimental order and range of values 78.9 and 79.5 to 80.1 typical of N_{bpyr}-Ru-N_{bpyr} and N_{phn}-Ru-N_{phn} respectively [379]. The Ru-C_{arene} bonds ranges from 2.222 (in complex **1**) to 2.289 Å (in complex **5**) and their bond orders ranges from 0.35 (in complex **2**) to 0.435 (in complex **4**). The Ru-Cl bonds distances range from 2.39 to 2.396 and their bond order ranges from 0.996 to 1.052. Both the computed Ru-C_{arene} and Ru-Cl bonds are within the experimental ranges of 2.197 to 2.257 Å for Ru-C_{arene} and 2.410 to 2.434 for Ru-Cl as reported for RAPTA complexes [365]. The features of bond orders suggest Ru-Cl to be strongest (Table 3.38) but disapproved from the QTAIM analysis (Table 3.45) which shows it is weaker than other bonds and will be a good leaving unit for the activation of these complexes by hydrolysis [8, 17, 38].

The HOMO of the complexes is predominantly the metal atom and the chloride atom where applicable which indicate the electrons being pulled away from metal orbital by the coordinated ligand and also electron being back-bonded into the metal's low lying orbital from the coordinated ligand atoms which are responsible for the metal atom being also part of the LUMO (Figure 3.11).

3.3.4.2 The features of H-bonding and Ru-N bonds

Hydrogen bond is the most widely studied noncovalent interaction in chemical and biological systems because of it is significance important to the stability and biological functions of compounds

[380-383]. It is reported to be undoubtedly the most important weak interaction in nature [382]. To the best of our understanding, this is the first time the intramolecular H-bonding of this type of complexes is reported. All the H-bonding in the complexes are shown in Table 3.39 while the properties of the hydrogen donor mostly C-H with another C-H which are not involved in H-bonding but are in the same chemical environment with those involved in H-bonding are shown in Table 3.40. The classical effect is observed in complex **1** as the C5-H24 and C15-H29 that are involved in H-bonding are weaker with Laplacian ($\nabla^2\rho(r)$) of -1.106 and -1.105 compared to C11-H30 and C21-H35 with $\nabla^2\rho(r)$ of -1.107 and -1.107 respectively which are in the same ligand chemical environment (Figure 3.12 and Table 3.40). The bond length of the two C-H bonds that are involved in H-bonding also are found to increase and consequentially have higher bond extension than the rest of the C-H bonds. The higher H-bonding of the H24···O2 than the H29···O2 is reflected in their receptive C-H as that of the formal is shorter than the later (Table 3.40). The H atoms that are involved in the H-bonding become more electropositive while the C atoms of the C-H bonds become less electropositive compared to carbon in the same chemical environment [Figure 3.12]. The C=O unit of the carboxylic group in complexes **1** and **3** contributes significantly to the H-bonding networks of the complexes and the total hydrogen stability energy of the complexes **1**, **2**, **3** and **5** with carboxylic unit (Table 3.44). There is every possibility that the near contact effect of the two carboxylic unit contribute to the observed H···H hydrogen bond observed in complex **2**. This type of interaction is not completely strange as it was observed in the H_2-HH non-covalent interaction [381, 382]. Interestingly also, these complexes have the highest stabilization energy (Table 3.44) which are in a closed range compared to other complexes.

Considering the strength of the H-bonds formed (the $\nabla^2\rho(r)$ in bracket) in complexes **1** (+0.038 and +0.039), **2** (+.040) and **3** (+0.061 and +0.063), the strongest one is in complex **3** while that of complex **1** is the lowest (Table 3.39). The H···H interaction in complex **2** has greater ellipticity and

bond stretching than other H-bonds in other complexes yet its strength is still a bit higher than H-bonds in complex **1** considering their $\nabla^2\rho(r)$ values (Table 3.39). Other interesting features of the C-H that acts as proton donor in complexes **1** and **2** is that its C atom becomes less electropositive and its electronic volume appreciate while proton becomes more electropositive and its electron volume depreciate when compared to another C-H in the same chemical environment. This further indicates the elongation and weakening of the C-H bonds as a result of the H-bonding (Table 3.40).

In all the complexes, the strength of the Ru-N bonds is higher than the Ru-C bonds and Ru-Cl bonds in the complexes. Considering the mid Ru-N bonds in complexes **4** and **5**, the order of the Ru-N bonds in the five complexes is **5** > **2** > **4** > **3** > **1** which agrees with the experimetal report of stronger Ru-N bonds of the metal-bipyridine than metal-phenanthroline [379].

3.3.4.3 The nature of the charge transfer and stability of the complexes

The lowest percentages of non-Lewis Rydberg and highest percentages of Lewis orbital indicates that there geometries are stable. Also, relatively significant percentages of the Valence non-Lewis orbitals shows the importance of charge transfer which can be metal to ligand (MLCT) or ligand to metal (LMCT) in determination of the stability of the complexes. In Table 3.41, the donor and the acceptors NBO that have the perturbation stabilization energy ($E^{(2)}$) ≥ 10.00 kcal/mol are presented and the amount of the electron (e) transferred into the anti-Lewis orbitals of the acceptors are presented in Table 3.42. The features of the perturbation energy presented in Table 3.41 for the five complexes show that they are dominated by back-bonding of electrons from the lone pair of the ligand atoms to the anti-Lewis lone pair (LP) orbitals of the Ru atom. The amount of electrons that were transferred into all the anti-Lewis orbitals (acceptors) with the energy level of the orbitals is shown in Table 3.42. There is a significantly high amount of electron transfer into the anti-Lewis lone pair orbitals of metal atom. From

the NEDA, it is observed that the features of LMCT overshadowed the presence of MLCT. The lone pairs in the metal atom (both Lewis and non-Lewis) are the main orbitals that are involved in the charge transfer.

The fragmentation of the complexes into different units (Table 3.43) gives the features of the synergistic effect of the metal coordinated fragments on each other. It is observed that the stability of the ligand units of these complexes were strongly enhanced through the synergistic effects where the bidentate unit in complexes **1**, **2** and **3** and tridentate unit of complexes **4** and **5** (fragment unit two in all the complexes) are the most enhanced. The next to this is the arene unit (fragment unit three in complexes **1**, **2**, and **5**, fragment unit four and two in complexes **3** and **4** respectively) which is also characterised with lower energy minimum.

It is obvious from the features of the NEDA analysis (Table 3.44) that polarizability (POL) is the predominant factor that determines the stability of these complexes except in complex **2** where charge transfer (CT) is a little prevalent than POL. Electrostatic energy (ES) also contribute significantly to the stability of the complexes after the effects of the POL and CT. Complexes **2** and **3** are significantly stable than the rest of the complexes and complex **4**. However, the main reason for the lower stability energy of complex **4** can be traced to the low magnitude of CT due to the absence of carboxylic unit in the complex compared to other complexes.

3.3.4.4 The bond properties from QTAIM analysis

The bond properties of the complexes are computed through QTAIM analysis using AIMAll package. For the systems optimized with PBE0/ECP(Ru,Cl)[6-31G*], the properties were computed using functional with all electron minimal basis set B3LYP/3-21G while the properties of the systems that were optimized with PBE0/ECP(Ru)[6-31+G(d,p)] were computed using both the

PBE0/ECP(Ru)[6-31+G(d,p)] and B3LYP/DGDZVP(Ru)[6-31+G(d,p)] functional and basis sets. The bonds properties are presented for the B3LYP/DGDZVP(Ru)[6-31+G(d,p)] in Table 3.45 for B3LYP/3-21G and PBE0/ECP(Ru)[6-31+G(d,p)] in Table 3.46 and 3.47 respectively. The features of Laplacian plots of electron density for all the complexes using B3LYP/DGDZVP(Ru)[6-31+G(d,p)] basis sets is shown in Figure 3.12. Also, the correlation among the computed bonds properties are shown in Table 3.48 (for B3LYP/DGDZVP(Ru)[-31+G(d,p)] only). The first thing that was observed is the disappearance of the NNCP in the topological surface of these complexes when the ECP basis set is limited to only ruthenium atom but appears especially in complexes **1**, **2**, and **3** when the chloride atom was also treated with ECP as explained for the optimization. The change in bond distance in the complexes from the PBE0/ECP(Ru,Cl)[6-31G*] to PBE0/ECP(Ru)[6-31+G(d,p)] optimized systems is less than 0.1 hatree and atomic properties obtained using a higher basis set DGDZVP(Ru)[6-31+G(d,p)] (Table 3.45 and 3.49) and minimal basis set 3-21G (Table 3.46 and 3.50) are in very close proximities which is an indication that there is no serious change in the geometries of the systems when they were optimized with higher basis set (ECP(Ru)[6-31+G(d,p)]) and lower basis set (ECP(Ru,Cl)[6-31G*]) respectively. Another implication is that all electron minimal basis set 3-21G is good enough for the construction of topological features of complexes especially when the system in big. However, the values of the Hamiltonian form of kinetic energy density (K) are under estimated using 3-21G basis set (comparing Table 3.45 with Table 3.45). The bond properties of the complexes obtained when the system was treated with ECP(Ru)[6-31+G(d,p)] (Table 3.47) are very similar to that obtained from all electron basis set DGDZVP(Ru)[6-31+G(d,p)] (Table 3.45) but ECP is found to underestimate the atomic properties (comparing Table 3.49 with Table 3.51) which is an indication that constructing the topological features with ECP may not accurately provide both intra and inter atomic properties of the complexes though it provides the same trends of values.

The bond distances (GBL_I) computed for complex **1** at the two method of optimization (Table

3.45 and Table 3.46) are very similar but there is a significant change in the dihedral angles of the carboxylic unit which resulted to one H-bonding in the system optimized with ECP(Ru,Cl)[6-31G*] but two when optimized with ECP(Ru)[6-31+G(d,p)]. The Laplacian plot of the electron density of complex **2** (Figure 3.12(2)) shows that many of its atoms are on the same plane. In complex **3**, there is also no traceable changes in the geometries and the topologies from both 3-21G (Table 3.46) and DGDZVP(Ru)[6-31+G(d,p)] (Table 3.45) and two H-bonding are recognised in both methods (Figure 3.12(3), Table 3.45 and Table 3.46).

All the ruthenium-ligand (Ru-L) bonds are characterised with positive $\nabla^2\rho(r)$ and a lesser value of $\rho(r)$ (within the range of 0.07 to 0.10) compared to the covalent bonds that exist within the atoms of each coordinated ligands (Table 3.45 and Figure 3.12) which are characterised with negative $\nabla^2\rho(r)$ and higher $\rho(r)$ values (within the range of 0.2 to 0.41).

The features of the metal-chloride bonds in complexes **1**, **2**, and **3** that contain coordinated chloride indicates that the chloride will be a good living group where necessary in their biological interactions which has been suggested to proceed through hydrolysis [8, 17, 37, 38]. The Ru-Cl bonds are characterised with lowest $\rho(r)$ and $\nabla^2\rho(r)$ indicating it is weaker than other Ru-L bonds but associated with lower stretching and lower ellipticity (Table 3.45).

The correlation of the bond properties constructed over all the existing bonds in the complexes (Table 3.48) gives a clear picture of the factors that define a strong bond and their relationship. A strong bond with a high negative values of $\nabla^2\rho(r)$ (i.e. covalent bond) or high positive values of $\nabla^2\rho(r)$ (i.e. non-covalent bond) should also be characterised with high values of $\rho(r)$. These strong bond should also be associated with lower ellipticity, lower bond length and bond stretching. The correlation of potential energy density (V) and the Lagrangian form of kinetic energy density (G) on the strength of bonds greatly become significant when considering their ratio (|V|/G). The values of K is highly

correlated with the electron density ($\rho(r)$) of each atom (0.89, 0.88, 0.90, 0.90 and 0.88 respective complexes) and also have higher effect than G on the values of $\nabla^2\rho(r)$, ellipticity and bond distance (Table 3.48).

3.3.4.5 Intra- and inter-atomic properties

The properties of the atoms in each of the five complexes which are coordinated to metal are presented in the Table 3.49. The integrated Lagrangian values L(A) of all the atomic basins are approximately equals to zero, which is an indication of satisfactory numerical integration [363]. For all the atoms in the complexes other than H atoms, the values of the percentage localization (%Loc(A)) are high while the percentage delocalization (%Deloc(A,A')). The reverse nature of the %Loc(A) and %Deloc(A,A') of the H atoms indicates they can be easily perturbed by an external electric field [363].

The correlation of the computed atomic properties in Table 3.52, gives the summary of the changes in the properties in relation to each other. The atoms that are highly electronegative in the complexes are associated with higher bonding dipole, total dipole and higher volume of atomic density. The high number of electrons or of localized electron significantly favours the bonding dipole, total dipole and volume of electron density of the complexes while high de-localization has reverse effects. The total dipole of each atom is significantly determined by its bonding dipole than the contribution of its intra atomic dipole.

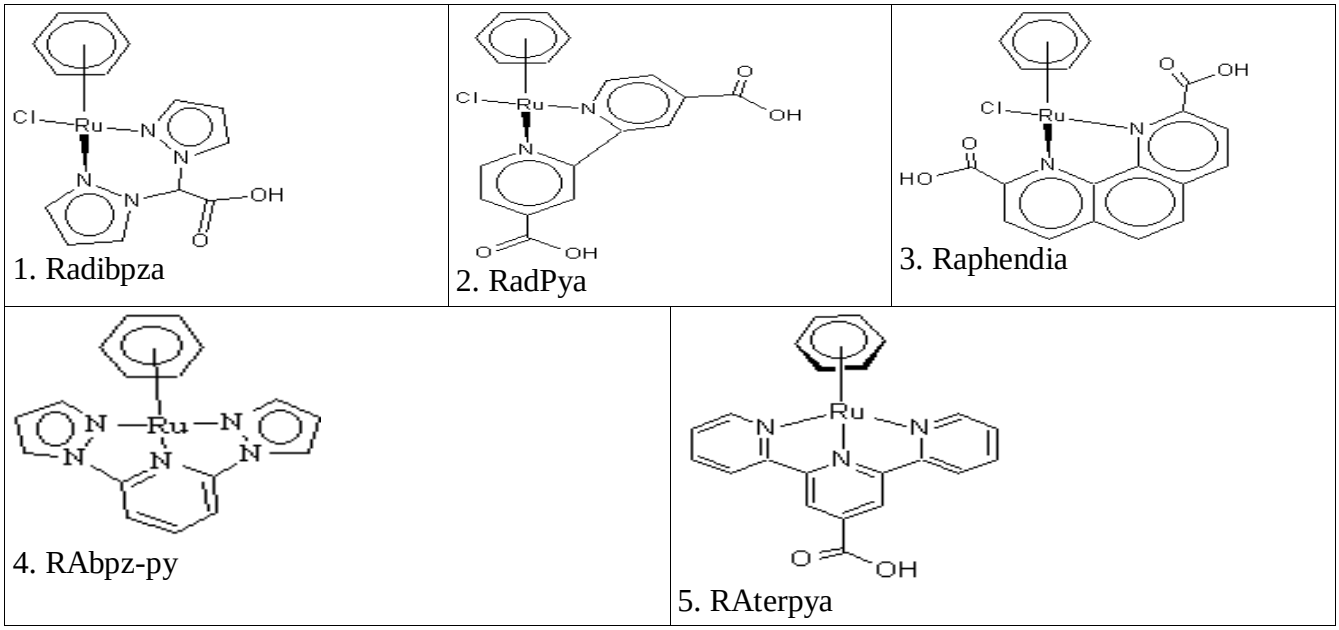

RA = Ruthenium-(η6-arene); phendia = phenanthroline-diacetic; dpya = di(pyridine-acetic) bpza = bis(pyrazol-1-ly)acetic, bpz-py = bis(pyrazol-1-ly)pyridine, terpya = terpyridine-monoacetic

Figure 3.10: The schematic structures of the five complexes

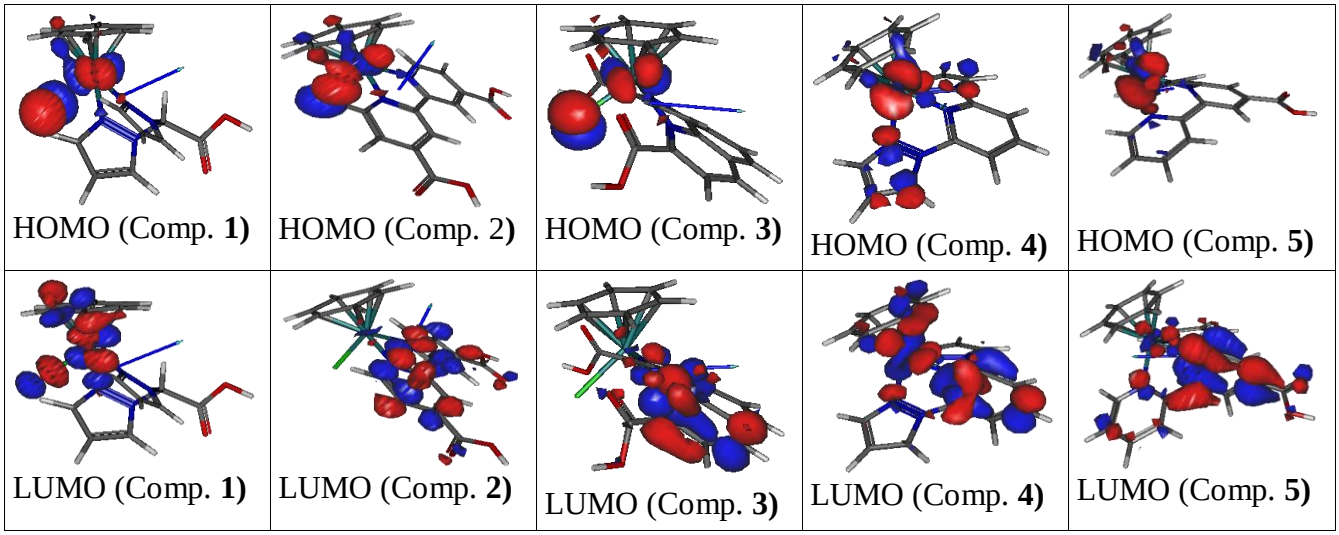

Figure 3.11: The HOMO and the LUMO of the complexes

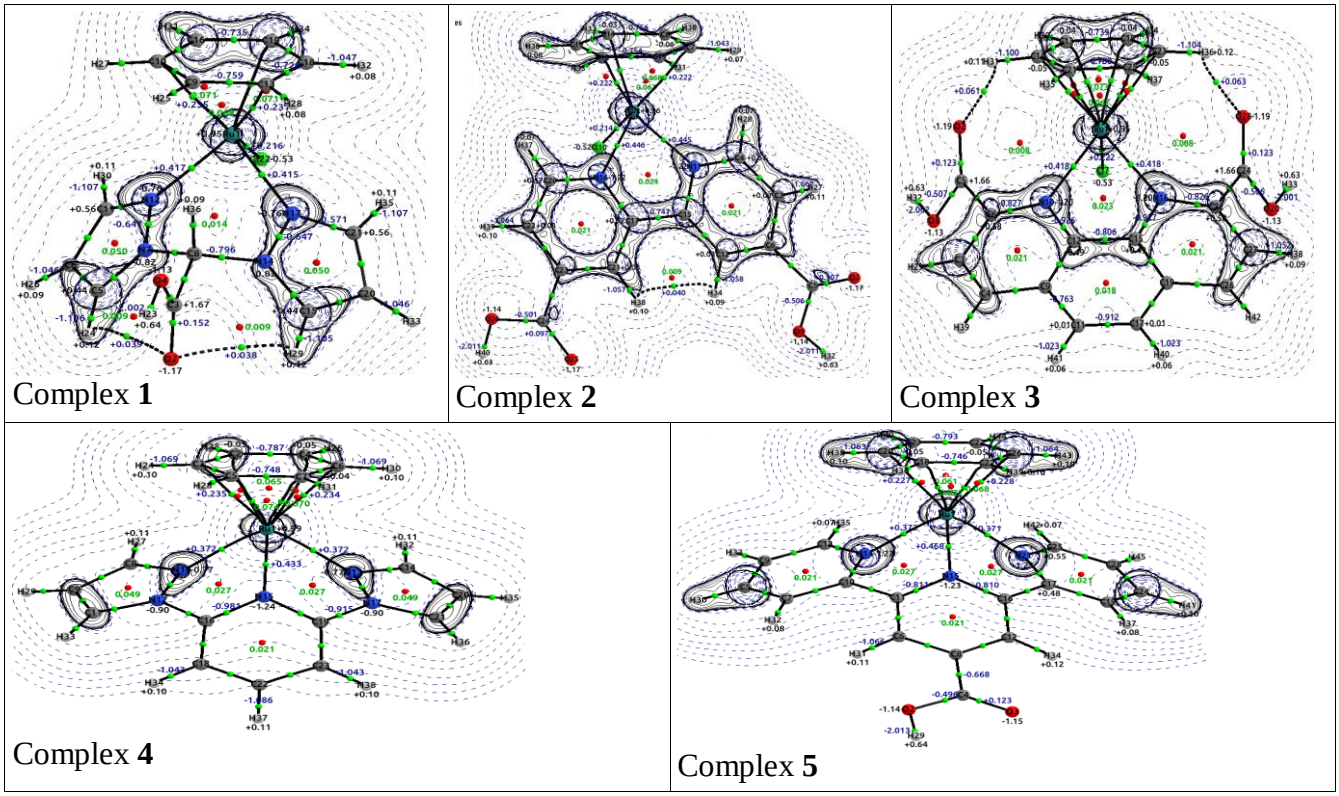

(3,-1) bond critical points (BCPs) are shown as small green spheres, (3,+1) ring critical points (RCPs) as small red spheres, and (3,+3) cage critical points (CCPs) as small blue spheres.

Figure 3.12: Laplacian of the electron density plots in the plane of N, Ru and N nuclei (positive contours as solid and negative contours as dashes lines are drawn from 0 to ±800) showing the features of bonds (strong bonds in solid and HB in dash lines) for five complexes.

3.4 The spectroscopic and non-linear optical properties of some Ru(II)-based complexes

This section is made up of three subsections on the spectroscopic and non-linear optical properties of Ru(II)-based complexes. Two of these subsections have been published in the literatures [316, 317]. Section 3.4.1 illustrates the chemistry of the three model of RAPTA-C (r = Ru, a = η^6-arene, PTA = 1,3,5-triaza-7-phosphaadamantane and C means the ligand unit arene is cymene) which will enhance the experimental means of increasing their stability that is suggested as a means of getting better drug candidates [5]. The models considered in this work are the RAPTA-C and its bidentate forms which are oxalo-RAPTA-C and carbo-RAPTA-C (Figure 3.13). The chelate effect on *oxalo*-RAPTA-C has lead to a structure that completely resists hydrolysis while there is a possible hydrolysis of *carbo*-RAPTA-C [51]. The possible application of Ru(II) complexes as photocatalysts or photoinitiators has been reported [384]. In this work, electric dipole moments, hyperpolarizabilities, isothropic and anisotropi C-NMR properties of these selected Ru(II)-based complexes are calculated. The goal of this work is to investigate the physicochemical nature of the intramolecular non-bonded forces that drive the stability in relation to their anticancer behaviour. For this purpose, in addition to the thermodynamic properties, we have computed the IR, NMR shifts, spin-spin coupling constants and nonlinear optical (NLO) properties like hyperpolarizability.

In Section 3.4.2, computational method was applied to compute the properties of four different forms of organometallic Ru(II) anticancer complexes known as RAPTA-H (complex **1**), RAPTA-C (complex **3**), RAPTA-T (complex **5**) [8] and RAPTA-CF3 (complex **7**) [17] with their respective hydrated complexes **2**, **4**, **6** and **8** to understand the properties that enhance their activation by hydrolysis (Figure 3.16). There are reported kinetic study of the hydrolysis of the Ru-Cl bond of the prodrug to generate active complexes of the form $[(\eta 6\text{-arene})Ru(en)(H_2O)]^{2+}$ [41]. The kinetic studies

showed that the Ru-Cl bond hydrolysis can be strongly influenced by the nature of the coligands as well as the nature of the metal ion. What is of interest to us is the possible changes in the properties of these complexes upon hydrolysis that is responsible for their activation using the electronic and the quantum theory of atoms in a molecule (QTAIM). Based on the knowledge that these type of the complexes should be characterised with an intense intramolecular CT between metal and ligand (MLCT or LMCT) which will definitely lead to a very large value for hyperpolarizability (β) [369] as a consequence of the π back-donation in the complexes [369, 370], the non-linear optical (NLO) properties were also computed to understand their correlation to the anticancer activities and the possibility of using the complexes alternatively as NLO materials. To the best of our knowledge, these type of correlation studies of the electronic and spectroscopic properties of these complexes with their anticancer activities have not been considered in the literatures.

In the section 3.4.3, the complexes of interest (Figure 3.19) have similar structures with the types of half-sandwich ruthenium anticancer complexes designed and studied under Sandler research team [20-29]. The interest of this research work is to compute the chemical properties of these complexes in relation to the unique features of the carboxylic or pyrazole units, total stability, conductivity and reactivity either as anticancer or NLO materials. There is little known information about the hyperpolarizabilities of ruthenium metal complexes but many of the computed properties in this study have not been reported for these types of metal complexes to the best of our knowledge. The complexes used in this work are designed to play a dual role as anticancer and non-linear optical (NLO) materials.

3.4.1 Theoretical study of the electronic and spectroscopic properties of Ru(II)-based complexes of RAPTA-C derivatives

The electronic, electrochemical and structural properties like thermodynamic, nonlinear optical (NLO), NMR and spin-spin coupling constant of complexes **1**, **2** and **3** are computed using DFT method. There have been no previous considerations on the correlation of these properties to the biological activities of the complexes to the best of our knowledge. The conceived interest is to know the possible correlation to the anticancer activities of these complexes since they have been reported to have complex chemistry [5] and to also envisage other alternative applications of these complexes.

3.4.1.1 The geometry, thermodynamic and infra red (IR)

The geometries of the three complexes are presented in Figure 3.13 with their bond distances in atomic unit (au). Ru-P bond distances in angstrom (Å) for complexes **1**, **2** and **3** (experimentally available values in parenthesis) are 2.43, 2.43 (2.31) and 2.42 respectively; Ru-arene carbon bonds ranges from 2.21 to 2.23 in complex **1**, from 2.22 to 2.23 in complex **2** while it ranges from 2.20 to 2.24 in complex **3**. The two Ru-O bond distances for the bidentate complex **1** are 2.10 and 2.12 while complex **2** has approximately the same distance of 2.09 (2.09, 2.10). The two Ru-Cl bonds for complex **3** are ~ 2.50. A closer look at the bond distances of complexes **1**, **2** and **3** with the available experimental values from literature [51] in parenthesis shows strong similarities in the complexes. The common bond angle O-Ru-O for complexes **1** and **2** are 84.56° and 79.47° (78.43°) while the unique bond angle Cl-Ru-Cl for complex **3** is 89.64°(89.16°). According to Ang *et. al* [51], the significantly smaller than 90° for **1** and **2** six-membered and five-membered metallacycles respectively is an indication that they are strained. The close values of our computation to the available experimental values obtained from literature [51] is an indication that the geometries of the complexes are well optimized with DFT functional PBE0 and mixture of basis set 6-31G* and SBKJC VDZ with ECP

which further confirm the efficacies of this PBE0 functional with ECP basis set in computing the structural properties of metal-based complexes according to literatures [332-339].

A critical look at the thermodynamic properties in Table 3.53 shows that the effect of the rotational and translational energy (E_{rot} + E_{tran} = E^0-E) is very low as they are found to be 0.08, 0.08, 0.07 KJ/mol for the three complexes **1**, **2** and **3** respectively. It is not appropriate to compare the thermodynamic properties between the three complexes since each complex contains different number of atom but the individual thermodynamic nature shows that they are characterised with negative Gibbs free energy and have relatively high entropy which indicate they are thermodynamically stable.

The low intensities at 3040-3051 cm^{-1} region as shown in Figure 3.14 are ascribed to υ(C-H) antisymmetric stretches while the high intensity bands at 1242-1303 cm^{-1} regions were characterised as υ(C-H) bend of CH_2 of the ligands. The sharp frequencies at 2975- 2992 cm^{-1} region are assigned to υ(C-H) of the arene alkyl CH_3 side chain. The arene υ(C-H) stretches as a low intensity frequencies at 1427-1450 cm^{-1} which is close to the experimentally assigned for arene υ(C-H) stretches of 1614 cm^{-1} [53]. The high intensity at 1633-1727 cm^{-1} region are ascribed to the υ(OCO) of the carboxylate units of the bidentate complexes as it is absent in the complex **3** without the bidentate as shown in Figure 3.13 which is close to the experimentally reported υ(C=O) 1612-1628 cm^{-1} of the similar complex [154]. The common frequencies within 933-1020 cm^{-1} are assigned to the C-C, C-O and C-N vibrations in three complexes. The lowest frequencies in 480-680 cm^{-1} region are assigned to υ(Ru-P) and Ru-Cl where applicable which is very close to experimental value 424-428 cm^{-1} assigned to υ(Ru-S) [154]. There is significant upper (red) shift of bidentate υ(OCO) vibration from **1** to **2** and significant change in the intensity of the picks are observed in the complexes. The intensity of υ(C-H) bend at 1242-1303 cm^{-1} region is very high in **1** and very low in **3** which further shows the higher number of CH_2 in **1** than the other two complexes.

3.4.1.2 The hyperpolarizability

We observed that there are other important factors like higher isotropic polarizability that can possibly define the higher hyperpolarizability of complex **1** above **2** and **3** despite its contradicting higher band gap and lower dipole moment (Table 3.54). The hyperpolarizability of the complexes **2** and **3** are very close to each other and lower band gap is found to favour complex **3** while higher dipole moment favours complex **2**. The lowest band gap of **3** is an indication that there is a better electron communication within this complex which could also be responsible for its reported activity as the best anticancer among the three [13]. Interestingly, there is high possibility that high conductive properties of these complexes may likewise contribute to their anticancer activities since it can enhance their binding to receptors' residues.

We observed that these complexes that were originally designed as anticancer complexes are found having higher hyperpolarizability than many of the reported complexes that were originally designed as NLO materials. They are found to be better NLO material than reported high hyperpolarizability materials like ruthenium complexes with redox-switching non-innocent ligands (NILs) [338], far better than NLO reported for η^5-monocyclopentadienylnitrilecobalt complexes [370] and very competitively close to some of the high first static hyperpolarizabilty values reported for bimetallic complexes [369] and that of the nitrogen bound low valent (M^0) group six metal carbonyls [346]. The implication is that systems with intense intramolecular CT between metal and ligand (MLCT or LMCT) transitions will lead to a very large value for β [369] which is also the consequence of the π back-donation in the complexes [369, 370].

3.4.2 The Ramsey terms and nuclear spin-spin coupling ($J_{ru\text{-}A}$)

We make use of four Ramsey terms Fermi contact (FC), spin dipole (SD), diamagnetic spin orbit (DSO), paramagnetic spin orbit (PSO)) leading to total nuclear spin-spin coupling (J) [385]. The

result obtained by using all electron basis set, give a better picture of the contribution of different factors to the total nuclear spin-spin coupling J(HZ) (Table 3.55, 3.56). The spin-spin coupling, J(HZ), of Ru-C bonding where the C atoms are from arene ligand is far less deshielded (i.e. highly shielded) than the J(HZ) for Ru-P and Ru-O where the P atom is from PTA ligand and O are the two bonding oxygen of the bidentate ligand. Also, the higher less negative values of J(HZ) Ru-C in complex **3** shows that there is higher shielding of arene ruthenium bonding in complex **3** than in complex **2**. Both Ru-Cl and the Ru-P are highly deshielded in complex **3** which suggest the possibility of both to be labile unit even though only the Cl atom has been experimentally reported to be labile for this complex [5]. The Ru-O bonding in complex **2** is associated with high J(HZ) shielding which further explain the reason why it is experimentally found to completely resist hydrolysis [51]. Also, the reported correlation of the change in each factor with the change in J(HZ) as shown in Table 3.57, further confirm the significant effect of the hyperfine function FC. The results that we obtained from using ECP basis set significant underestimate the FC and PSO effect (Table 3.58). The reason is that the core electrons that were represented with pseudopotential were not properly accounted for during the spin-spin computation, and this consequentially leads to lower FC since the core electrons also play important role in determining FC. Contrary to all electron basis set (Table 3.55, 3.56), all the four parameters using ECP (Table 3.58) are very small with PSO having the highest contribution and correlation follow by SD.

The results of the correlation of isotropic, anisotropic and charges of all atoms are present in complexes **2** and **3** with the four Ramsey terms for atomic coupling properties with Ru atom (Table 3.57). There has been reported change in NMR isotropic shieldings (σ) with change in the electron density of atoms [386]. We observed a low correlation in the distribution of atomic charges and their NMR isotropic shielding (Table 3.57). There are some unique differences and similarities in the properties of complex **2** and **3**. Isotropic is poorly correlated with anisotropic properties in complex **2**

but a very high correlation is observed in complex **3** when both 3-21G and and 3-21G** basis sets were used. There is an average relation between the isotropic properties of atoms in the complexes and their total nuclear spin-spin coupling with ruthenium atom (J_{ru-A}) (Table 3.57). In complex **2** there is a very high correlation of the Isotropic with Ramsey term FC while it is strongly correlated with SD and PSO in complex **3**. The total nuclear spin-spin coupling of Ru atom with all the atoms in the complexes (J_{ru-A}) is significantly characterised with FC and followed by SD term. PSO term has a very negligible effect on the value of J_{ru-A} in complex **2** compared to complex **3**.

3.4.2.1 The analysis of the magnetizabilities and NMR shielding properties using AIMAll

The correlation of all the magnetic properties computed is presented in Table 3.59. The atomic charge q(A) appears to have average effect on the intraatomic magnetizability contribution of each atom ($\chi_{Intra\_Iso}(A)$) which consequentially cause its relatively high correlation with the total magnetizability contribution of each atom ($\chi_{Iso}(A)$). When we consider the correlation of q(A) with intraatomic shielding tensor ($\sigma_{Iso}(A,A)$) and total magnetic shielding tensor of each atom ($\sigma_{Iso}(A)$) as found in a literature [386], there exist an averagely good and inverse correlation in complex **3** but very low correlation in complex **2**. $\sigma_{Iso}(A,A)$ and $\sigma_{Iso}(A)$ are significantly inversely correlated with $\chi_{Intra\_Iso}(A)$ and $\chi_{Iso}(A)$ and are also directly correlated with bonding magnetizability contribution of an atom ($\chi_{Bond\_Iso}(A)$). What determine the total magnetic shielding tensor of each atom ($\sigma_{Iso}(A)$) is the intraatomic $\sigma_{Iso}(A,A)$ which is a function of the intraatomic electrons. The total dipole $\mu(A)$ is found to depend more on the bonding dipole moment contribution ($\mu_{Bond}(A)$) than intraatomic dipole moment contribution $\mu_{Intra}(A)$ while the total magnetic shielding tensor ($\chi_{Iso}(A)$) depends more on the intraatomic $\chi_{Intra\_Iso}(A)$ than bonding $\chi_{Bond\_Iso}(A)$. The $\sigma_{Iso}(A',A)$ is inversely correlated with

$\chi_{Bond\_Iso}(A)$. $\chi_{Bond\_Iso}(A)$ correlated averagely and inversely with $\mu_{Bond}(A)$ and $\mu(A)$.

The charges, dipole, magnetizabilities and NMR shielding of some selected atoms in complexes **2** and **3** are presented in the Table 3.60. In the computed isotropic shielding complex **1** and its atomic charge which are not presented, we observed that the two bonding bidentate oxygen atoms to Ru atom are more electronegative with high shielding tensor than what is observed in complex **2**. Also, there is a very high imbalance in the shielding of these two bonding bidentate oxygen atoms of complex **1** which can possibly enhance the process of ring opening as suggested means of hydrolysis of bidentates [37] and could probably be responsible for the reported better hydrolysis of **1** than **2** [51]. We observed that there is relatively high similarities in the atomic charges, dipole, magnetizabilities and NMR shielding properties of similar atoms like N atoms from PTA and C atoms from arene unit of complexes **2** and **3** (Table 3.61, 3.62). Table 3.60 give the sum over of all the magnetizabilities and the shielding tensor. Just as the correlation indicated, the higher value of the sum over of the total dipole of complex **2** is higher than **3**, then there is corresponding higher negative value of the sum over of $\chi_{Bond\_Iso}(A)$ of **2** than **3**. Also, since the $\sigma_{Iso}(A,A)$ and $\sigma_{Iso}(A)$ of complex **2** is far less than **3** then the negative value of the sum over of $\chi_{Intra\_Iso}(A)$ of **2** is also higher than that of **3**. The implication of these is that the major factor that determines the NMR shielding tensor of each atom is their intraatomic magnetizability contribution rather than ordinary charge. The intraatomic shielding tensor ($\sigma_{Iso}(A,A)$) in complex **3** is far greater than complex **2** which consequentially resulted to higher total magnetic shielding tensor ($\sigma_{Iso}(A)$) of the complex (Table 3.60). A more critical look at the complexes shows that the higher the shielding the more sensitive the atoms as the N atoms of the PTA (223.15, 226.89, 222.53 for complex **2** and 221.04, 220.35, 216.69 for complex **3**) are found to be highly shielded which are reported to be significant in the kinetic of the potential drugs as they act as hydrogen bonding acceptors [9]. The hydrogen bonding of this chloride further gives the reason why complex **3** which as been

experimentally reported to be less kinetically stable is also found to be a transition state structure as given in Table 3.53.

The feature of the contribution of bond between atom A and Atom B ($\chi_{Bond}(A|B)$) to total bonding magnetizability contribution of each atom $\chi_{Bond}(A)$ is shown in Figure 3.15. The atoms that are directly bonded to metal centre have the highest atom-atom magnetizabilities and the total shielding compared to others. In the two complexes we found that the Ru atom is contributing more to $\chi_{Bond}(A|B)$ that exist between it and the electron depleted pi ligand of arene. The analysis of the contribution to bonding magnetizability show that Ru atom contribution ranges from 2.75 to 2.91 and 2.77 to 3.18 in cgs-ppm for complexes **2** and **3** respectively in bonding to arene ligand which is higher than any contribution of the C atoms of the arene ligand. These further suggest that there exist metal to ligand charge transfer (MLCT) between the Ru atom and the electron depleted arene ligand which is commonly reported to metal complexes [346].

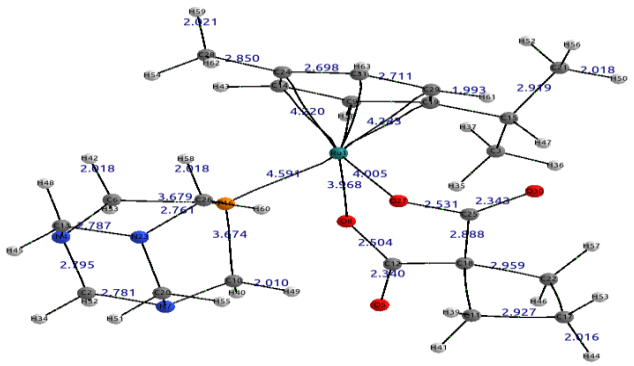

1. Carbo-RAPTA-C

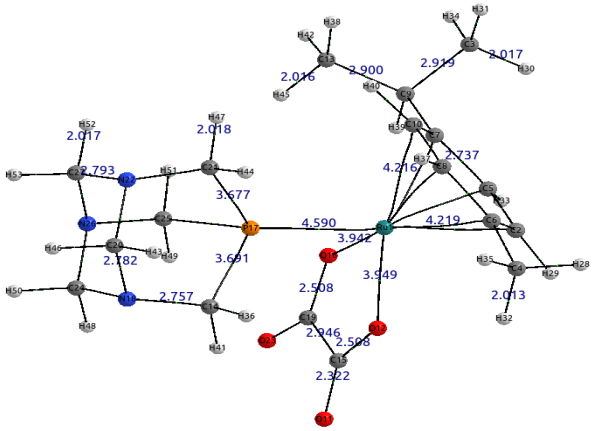

2. Oxalo-RAPTA-C

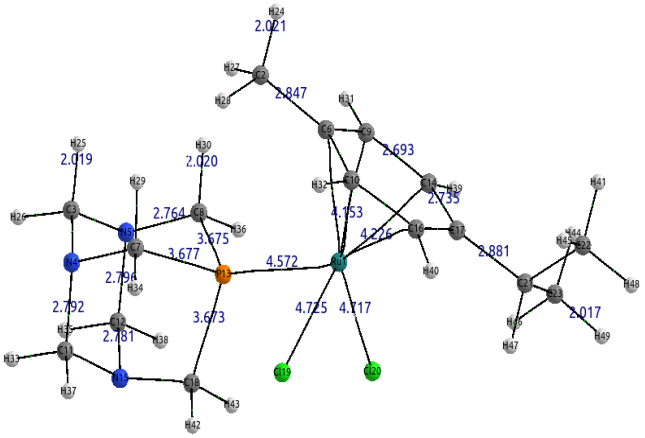

3. RAPTA-C

Figure 3.13: The geometric structures of complexes **1**, **2** and **3** with their bond distances shown in angstrom (Å).

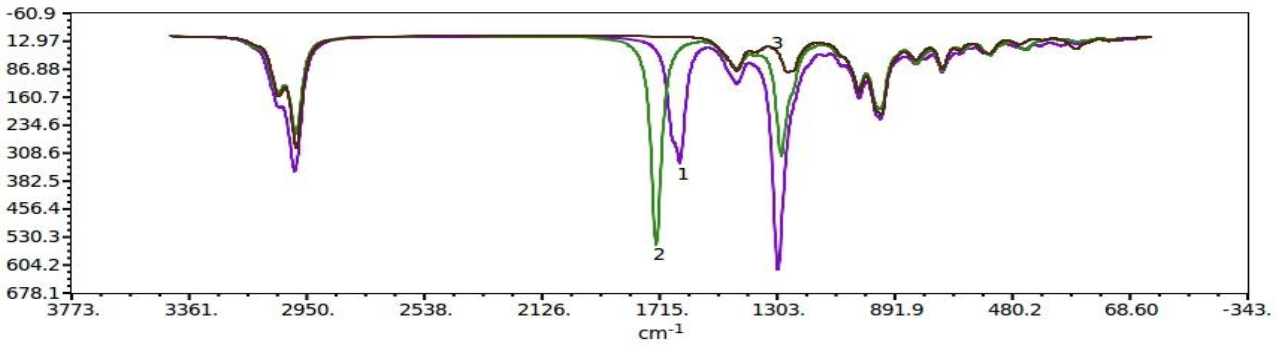

Figure 3.14: The IR spectral of complexes **1** (purple), **2** (green) and **3** (red).

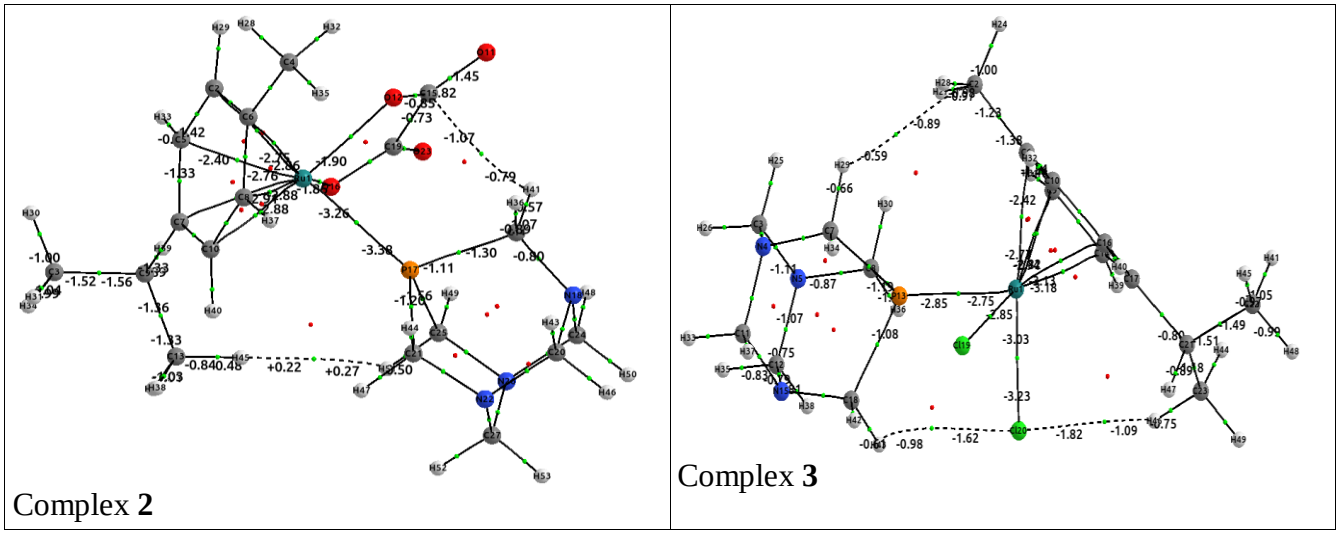

Figure 3.15: The contribution of each atom to the bond magnetizability.

3.4.3 Electronic, conductivities, and spectroscopic properties of hydrolysed Ru(II) anticancer complexes

3.4.3.1 The geometrical and the infra red properties

The optimized geometries of the complexes (Figure 3.16) were obtained using PBE0 hybrid functional and two mixed basis sets that comprises of SBKJC VDZ basis set with ECP that was applied on the Ru, Cl and P atoms and all electron basis set 6-31G* that was applied on the remaining atoms of each complex. All the Ru-Cl bond distances through all the complexes are within the range of 4.67 to 4.73 (a.u.), the Ru-O where the O atom is from water molecule is within the range of 4.21 to 4.25 (a.u.). The bond angle Cl-Ru-Cl in complexes **1**, **3**, **5** and **7** are 90.42^{O}, 89.64^{O}, 90.75^{O} and 89.73^{O} respectively while the bond angle Cl-Ru-O of their respective hydrated complexes **2**, **4**, **6** and **8** are 79.99^{O}, 76.65^{O}, 76.99^{O} and 77.02^{O} respectively.

The features of the infra red (IR) (Figure 3.17) show that complexes share many common bands which indicate that the overall structures of the complexes are not very different. Large spectra differences are observed only when each of the complexes hydrolysed to their respective complexes. A further difference is also observed when the methyl group on the arene units of complexes **5** and **6** are substituted with trifloromethyl group to form complexes **7** and **8**. From the knowledge of the reported experimental IR value for the Ru-O stretching frequency at 580 cm^{-1} [387], we can allocate the computed Ru-O strength in the hydrated complexes **2**, **4**, **6** and **8** to the observed absorption at 645, 636, 626 and 638 cm^{-1} respectively which is not obvious in the unhydrated complexes **1**, **3**, **5** and **7** (Figure 3.17). In the hydrated complexes **2**, **4**, **6** and **8**, there is a peculiar vibration at 1622, 1617, 1617 and 1616 cm^{-1} respectively which can be assigned to the activities of the water molecules that donate at least one hydrogen bond to the complexes in line with a range of 1600-1700 cm^{-1} that have been

experimentally proposed for such kind of water molecule activities [388]. While two other unique stretching vibrations of each hydrated complexes **2** (3635, 3309 cm^{-1}), **4** (3623, 3292 cm^{-1}), **6** (3636, 3304 cm^{-1}) and **7** (3640, 3308 cm^{-1}) can be assigned to O-H from water molecule having two different modes due to the formation of hydrogen bond. In another reported experimental IR information, Ru-P is assigned 280 cm^{-1}, (C-H) or δ(C-H) of the benzene ring 3057-3024 cm^{-1} or 1035-1000 cm^{-1}, the υ(C-H) of the CH_3 is assigned 2932-2874 cm^{-1} [389]. Therefore the Ru-P is assigned to be the prominent lowest frequencies at 274 cm^{-1} in complexes **1** and **2**, 280 cm^{-1} in complexes **3** and **4**, 262 cm^{-1} in complexes **5** and **6** and at 262 cm^{-1} in complexes **7** and **8**. Also a shoulder like stretching vibrations observed at 3045 cm^{-1} for all the complexes of which the unhydrated is higher than the hydrated are assigned to the υ(C-H) of the arene units. The sharp and very prominent bands found at 2987, 2980, 2978, and 2988 cm^{-1} in the unhydrated complexes **1**, **3**, **5** and **7** and in the hydrated complexes **2**, **4**, **6** and **8** at 3002, 3005, 3003 and 3014 cm^{-1} are assigned to υ(C-H) of the CH_3 on the arene units.

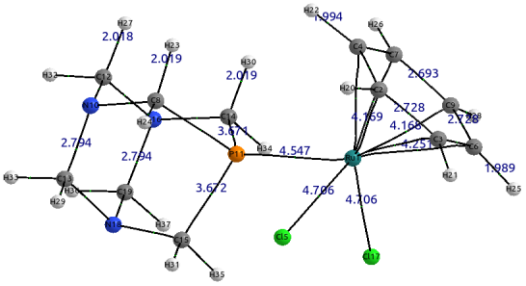

Complex 1

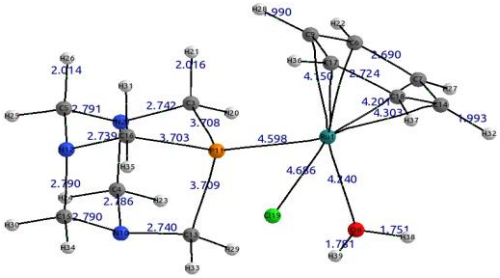

Complex 2

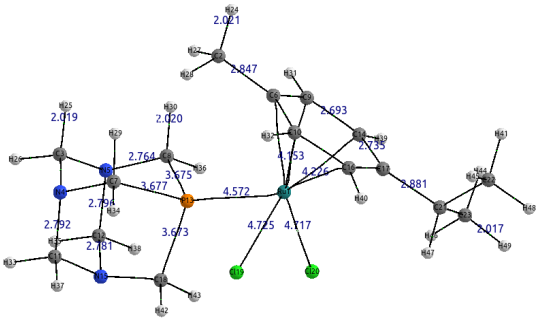

Complex 3

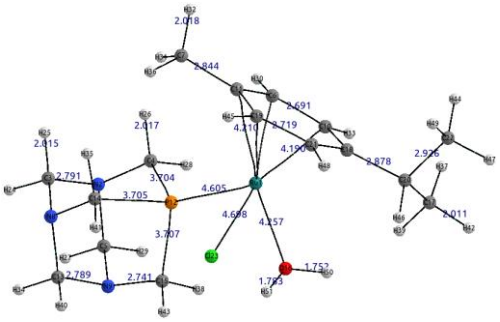

Complex 4

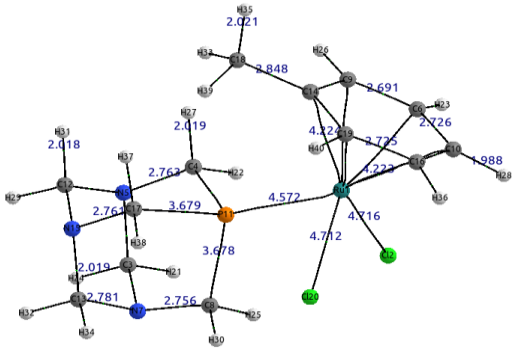

Complex 5

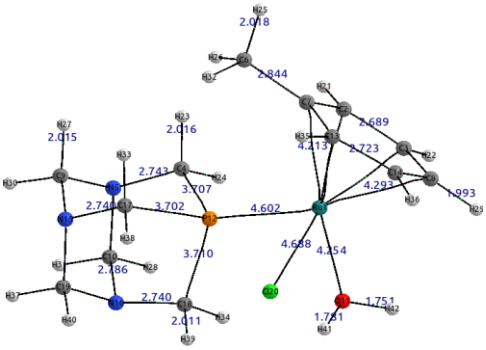

Complex 6

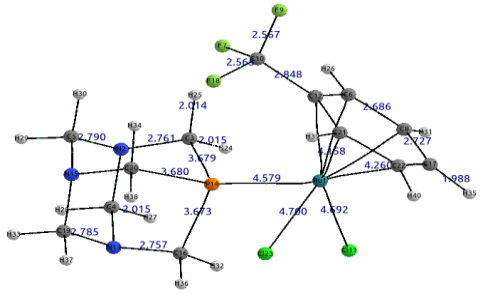

Complex 7

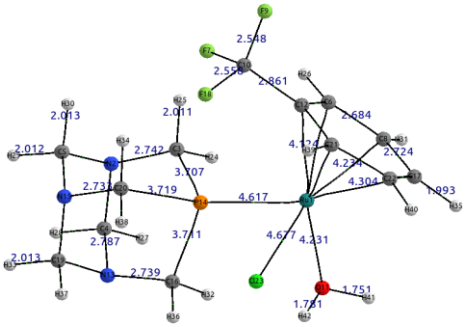

Complex 8

Figure 3.16: The optimized geometries of complexes **1**, **3**, **5**, **7** (left) and their hydrolysed **2**, **4**, **6**, **8** (right) respectively

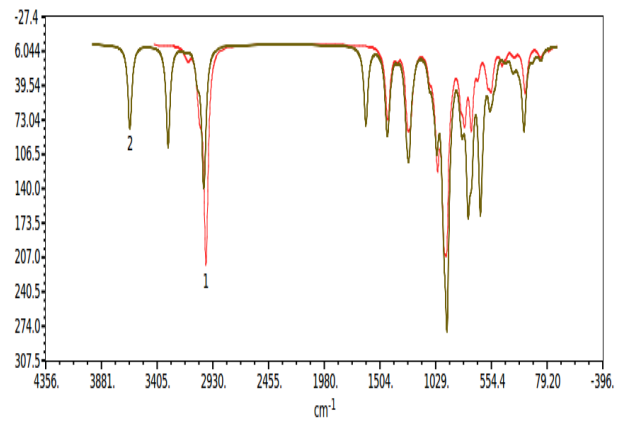

a). IR for complexes **1** (red) and **2** (green) as indicated in the plot

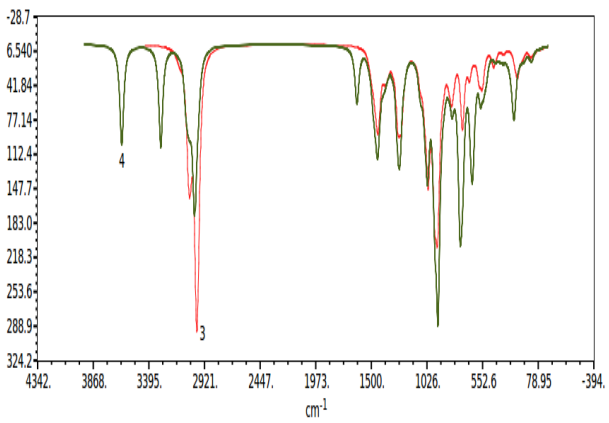

b). IR for complexes **3** (red) and **4** (green) as indicated in the plot

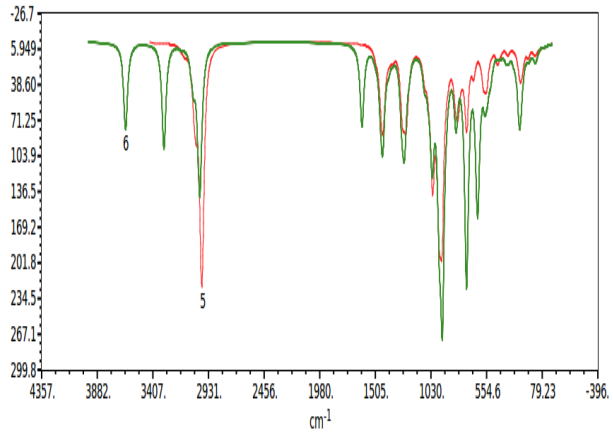

c). IR for complexes **5** (red) and **6** (green) as indicated in the plot

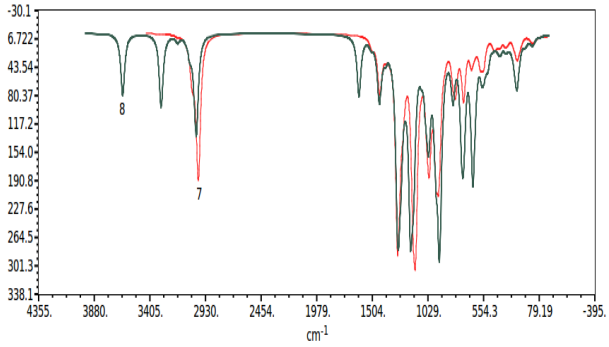

d). IR for complexes **7** (red) and **8** (green) as indicated in the plot

Figure 3.17: IR plot of the complexes as indicated in the figures

3.4.3.2 The thermodynamic properties

The thermodynamic properties of the complexes are shown in Table 3.63 using the functional and mixed basis sets used for the optimization. Many of the complexes are found to be stable minimum geometries except **2**, **3** and **5** that have single imaginary. However, this observation is not strange as there have been reported instability of some of these complexes [5, 51]. A critical look at the thermodynamic properties as shown in Table 3.63 indicates that the effect of the rotational and translational energy ($E_{rot} + E_{tran} = E^0$-E) is very low as their values ranges from 0.048 to 0.066 Kjmol^{-1} through all the complexes. The thermodynamic natures of the complexes show that they are characterised with negative Gibbs free energy (G), negative enthalpy (H) and have relatively high entropy (S) which indicate they are thermodynamically stable.

We consider the change in the thermodynamic properties during the process of hydrolysis of complexes **1**, **3**, **5** and **7** to their respective hydrolysed complexes **2**, **4**, **6** and **8** as shown in Table 3.64. There have been little study on the thermodynamic change for the hydrolysis of Ru(II) complexes of the type [Ru(η^6-arene)(en)Cl]$^+$ but that of the [Ru(η^6-arene)(pta)Cl_2] in relation to the variation of their anticancer activities has not been considered to the best of our knowledge [41]. The simple method used in computing the thermodynamic changes follow from a simple equation:

rec_Cl + H_2O → prod_H_2O + Cl

$\Delta X = X(prod\_H_2O + Cl) - X(rec\_Cl + H_2O)$

where rec_Cl represent complexes **1**, **3**, **5** and **7** which contain the leaving Cl atom and prod_H_2O represent the hydrated complexes **2**, **4**, **6** and **8** with a water molecule.

The results (Table 3.64) shows that the hydration of the complexes are not spontaneous but require some energy like high temperature in the system before the hydrolysis can take place as the ΔH and ΔG are positive. The possibility of the hydration taking place in the blood before reaching the cell

[5] or the possibility of the hydration taking place only in the cell due to high chloride concentration in the blood [8] depend on other reaction activities in the blood or in the cell respectively that will initiate the hydrolysis. The complexes that hydrolyse very slowly have been reported to have very poor anticancer activities [37]. However, the strong anticancer effect of complex **7** above complex **5** despite the unfavoured thermodynamic of its hydrolysis can be traced to the reported formation of [Ru(pta)]–biomolecule adducts (the arene unit being separated) which were not observed in the protein or DNA binding studies of other [Ru(pta)(arene)] adducts of RAPTA compounds [17]. This unique arene separation in complex **7** may enhance its hydrolysis and consequently improve its anticancer properties.

3.4.3.3 Conductive properties

The conductive properties of these complexes in the form of the NLO hyperpolarizability were computed to determine any possible correlation with their anticancer activities and also the possibility of using them as NLO materials. The NLO properties of the complexes are computed as the first static hyperpolarizability (ß) (Table 3.64). The hydrolysed complexes **2**, **4**, **6** and **8** are accompanied with higher hyperpolarizability and consequential lower band-gap than their respective complexes **1**, **3**, **5** and **7** (Table 3.65). This suggests that the mechanism of activation by hydrolysis can be as a result of increase in the conductive strength of the hydrolysed complexes which will enhance easy charge transfer and interaction.

The hyperpolarizability of complex **7** and its hydrated complex **8** are higher with lower band-gap compared to complex **5** and its hydrated complex **6** respectively. This further gives another possible reason why complexes **7** and **8** are better anticancer compared to complexes **5** and **6**. The hyperpolarizability of complex **3** is a little higher than that of complex **1** but reverse is the case when comparing their hydrolysed complexes **4** and **2** respectively. However the isotropic polarizability polarization of complexes **3** and **4** is higher than that of complexes **1** and **2** which further suggest

possible effect of the higher conductive effect of complexes **3** and **4** to their higher anticancer activities.

It is interesting to point out that these complexes that were originally design as anticancer complexes are found to have high first static hyperpolarizability (ß) than many of the reported complexes that were originally designed as NLO materials [338, 346, 369, 370].

3.4.3.4 Ramsey properties of Nuclear magnetic resonance (NMR)

The NMR Ramsey properties of some selected bonds in the complexes and that of their respective hydrolysed complexes are shown in Tables 3.66.

The Ru-Cl bond has the highest PSO and SD values but the lowest values of the DSO and FC than other Ru-L bonds. This bond is also characterised with higher J(HZ) values except for Ru-P bond that is characterised with the highest coupling constant. Upon hydrolysis, the Ramsey parameters of Ru-Cl of the retained Cl atom are lower compared to the Ramsey parameters of Ru-Cl in the unhydrated complexes but the J(HZ) of all the Ru-P and Ru-C bond increases upon hydrolysis. Despite the significant difference in the arene unit of the unhydrated complexes **1**, **3**, **5** and **7**, the Ramsey properties of their Ru-Cl, Ru-P and Ru-C are relatively the same.

In order to understand the most significant factors that determine the J(HZ), we computed the correlation within all the Ramsey factors over all bonds that exist in the complexes (Table 3.67). The FC is found to be the most significant factor as it has the highest correlation with the J(HZ) ranging from 0.88 to 0.96 in all the complexes. The next significant factor is SD which has a correlation range from 0.74 to 0.87, typical in nature of π–systems [166]. The PSO and DSO correlations with the J(HZ) are negligible. We also observed that in all the hydrolysed complexes, high correlation exists between the FC and SD.

3.4.3.5 NMR bond properties using QTAIM analysis

The features of the first-order net current vector obtained using the QTAIM analysis as implemented in the AIMAll shows that the highest part of these induced currents are out of plane (J_ZZ) and the hydrolysed complexes are characterised with the highest values compared to their respective unhydrolysed complexes (Table 3.68). Also, complexes **3** and **4** are characterised with higher values than complexes **1** and **2** and likewise complex **7** is characterised with higher values than complex **5** which correlate with their reported anticancer activities.

The bonding magnetizability between Atom A and Atom B ($\chi_{Bond}(A|B)$) of some selected atoms are shown for the complexes in Figure 3.18. We observed that the $\chi_{Bond}(A|B)$ give some interesting feature to the existing HB interactions in the complexes. All of the HB are significantly characterised by different atomic contribution of $\chi_{Bond}(A|B)$ along their line of HB interaction which is an indication that each atomic $\chi_{Bond}(A|B)$ may play significant role in determining the possibility of HB interaction between two atoms. However, there is no significant difference in the $\chi_{Bond}(A|B)$ of two atoms that formed a real bond which implies that the $\chi_{Bond}(A|B)$ is negligible in determining real bonds.

3.4.3.6 NMR atomic properties using QTAIM analysis

The atomic charges (q(A)), magnetizability contribution ($\chi_{Iso}(A)$), dipole ($\mu(A)$) and magnetic shielding tensor ($\sigma_{Iso}(A)$) were computed using QTAIM analysis as implemented in AIMAll (Table 3.69-3.75). The bonding magnetizability contribution of each atom ($\chi_{Bond\_Iso}(A)$) in cgs-ppm is found to be higher than the intraatomic magnetizability contribution of each atom ($\chi_{Intra\_Iso}(A)$) for the Ru, C, and P atoms but reverse is the case for the Cl, N and O atoms. The H atoms from arene, PTA and water molecule which are involved in HB interaction are included in Table 3.69-3.75. The general observation is that the H atoms from water molecule are characterised with high $\sigma_{Iso}(A,A)$ and

consequently high total magnetic shielding tensor of each atom ($\sigma_{Iso}(A)$) than any other H atoms from arene and PTA units.

Interestingly, we observed that complexes **3** and **4** which are known to be the best anticancer [13] are having the highest magnitude of $\chi_{Intra\_Iso}(A)$ and the lowest $\chi_{Iso}(A)$ compared to the rest of the unhydrated and hydrated complexes respectively. However, complex **7** which is expected to have higher $\chi_{Intra\_Iso}(A)$ and lower $\chi_{Iso}(A)$ than complex **5** because of its reported better anticancer activity [17] does not follow, which is an indication that the experimentally found unique feature of the arene separation in its adduct interaction should be responsible for its higher anticancer activity as we have discussed in the thermodynamic properties (Table 3.63 and 3.64).

The sum total of all the computed properties over all the existing atoms in each complexes (Table 3.76) can only make sense when comparing the hydrated complexes and the unhydrated complexes separately because of the significant differences in the ruthenium-ligand (Ru-L) bonds. We can then state that high values of $\chi_{Intra\_Iso}(A)$ are directly related to their anticancer activities as the value for the unhydrated complex **3** is having the highest value and also complex **7** as expected is at this point correlate with its anticancer activity as it is characterised with higher $\chi_{Intra\_Iso}(A)$ than complex **5**. Also, as expected, the hydrated complex **4** is having the highest value of $\chi_{Intra\_Iso}(A)$ compared to all other hydrated complexes.

3.4.3.7 Correlation of the NMR atomic properties

The possible correlations within the computed properties are also considered (Table 3.77). The atomic charge (q(A)) is averagely correlated with the $\chi_{Intra\_Iso}(A)$ which happen to be its best recorded correlation. The $\chi_{Intra\_Iso}(A)$ is also found to be the most significant factor that determined the values of $\chi_{Iso}(A)$ than the contribution from the $\chi_{Bond\_Iso}(A)$. The $\chi_{Bond\_Iso}(A)$ is found to be most significantly

correlated with the anisotropy of the atoms. The $\chi_{Intra\_Iso}(A)$ has better inverse correlations with $\sigma_{Iso}(A,A)$ and $\sigma_{Iso}(A)$ while the $\chi_{Bond\_Iso}(A)$ has better inverse correlations with the $\sigma_{Iso}(A,A')$. The $\chi_{Iso}(A)$ is found to have the best correlation with the $\mu_{Bond}(A)$ and $\mu(A)$ than any other computed properties. The values of $\sigma_{Iso}(A)$ is significantly determined by the values of $\sigma_{Iso}(A,A)$ and are both strongly correlated with the anisotropy though inversely.

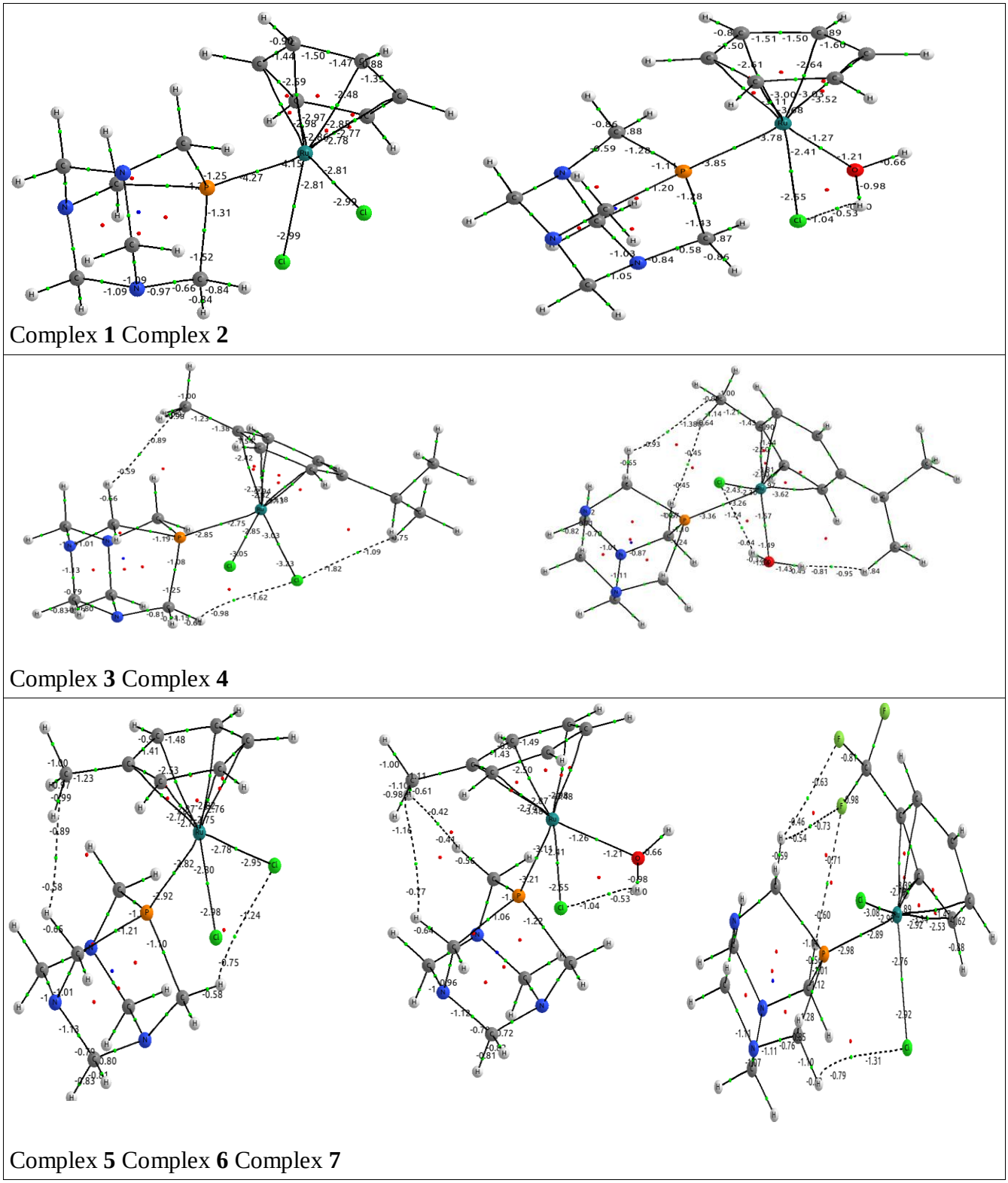

Figure 3.18: The Contribution of each atom to the bonding magnetizability between Atom A and Atom B ($\chi_{Bond}(A|B)$)

3.4.4 The spectroscopic and conductive properties of Ru(II)-based complexes as potential anticancer

3.4.4.1 The geometry and the IR spectroscopic

The geometry of the complexes (Figure 3.19) are optimized twice using the combined basis set ECP(Ru,Cl)|6-31G* for the first optimization and ECP(Ru)|6-31+G(d,p) for the second optimization. The zero imaginary obtained for the five complexes during the two methods of optimization is an indication that both methods detect the minimum geometry of the complexes except for complex **4** that was predicted during ECP(Ru,Cl)|6-31G* as transition with single imaginary frequency. There is no significant changes in the bond lengths (>>0.01 Å), angles (>> 2.0^{O}) and the conformations (>> 0.1) of the complexes when optimized with ECP(Ru,Cl)|6-31G* and with higher basis set ECP(Ru)|6-31+G(d,p) (Table 3.78). The little significant change observed is in the conformational change of the carboxylic units of complex **1** which is responsible in having the highest recorded RMSD of 0.068 (Table 3.78) when the geometries from the two optimizations are matched.

Differences in the complexes and their respective IR spectra were used to suggest the corresponding bond vibrations. The Ru-Nitrogen (Ru-N) bonds are assigned to indicate the differences in the vibration of ruthenium bonded to pyrazole or pyridine or phenanthroline units. The peculiarity of weak vibrations around 700 cm^{-1} for the complexes **1**, **2** and **3** with chloride ligands which are not obvious in other complexes without chloride is an indication of Ru-Cl vibration around this region. The Ru-Carbon (Ru-C) bonds are assigned to vibration at 797 cm^{-1} which is common to all the complexes. The assigned Ru-C vibrations are within the possible Metal-C vibrations (548-829 cm^{-1}) reported for carbonyl metal bonds [390] and of that which was specifically reported for the Ru-C vibration (838 cm^{-1}) [391]. The common vibrations around 1419 cm^{-1} that is peculiar to complex **4** and that at 1477 cm^{-1} for other complexes are assigned to the possible C-C, C-N vibrations and can be equally suggested to

be as a result of Ru-ligand (Ru-L) charge transfer [392]. All the vibrations at 3600-3625, 1758-1784, 1050-1150 and 735-745 cm^{-1} are all peculiar to the complexes with carboxylic unit and are assigned to different modes of vibrations as indicated in Table 3.79.

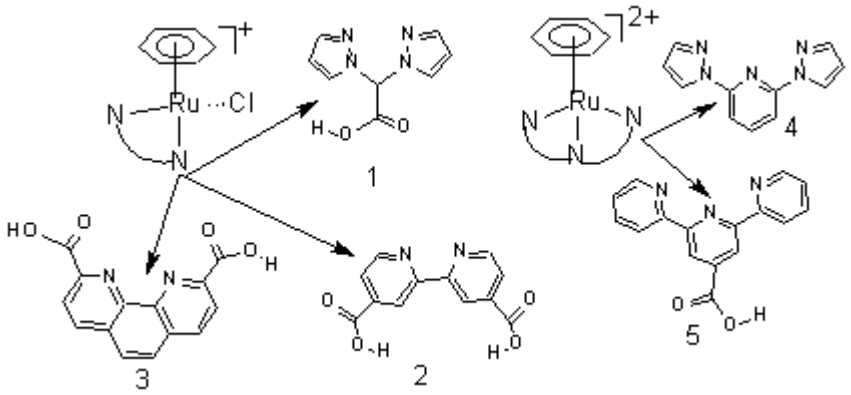

Figure 3.19: The schematic features showing all the bidentate ligands of complexes **1**, **2**, **3** and tridentate ligands of complexes **4** and **5**.

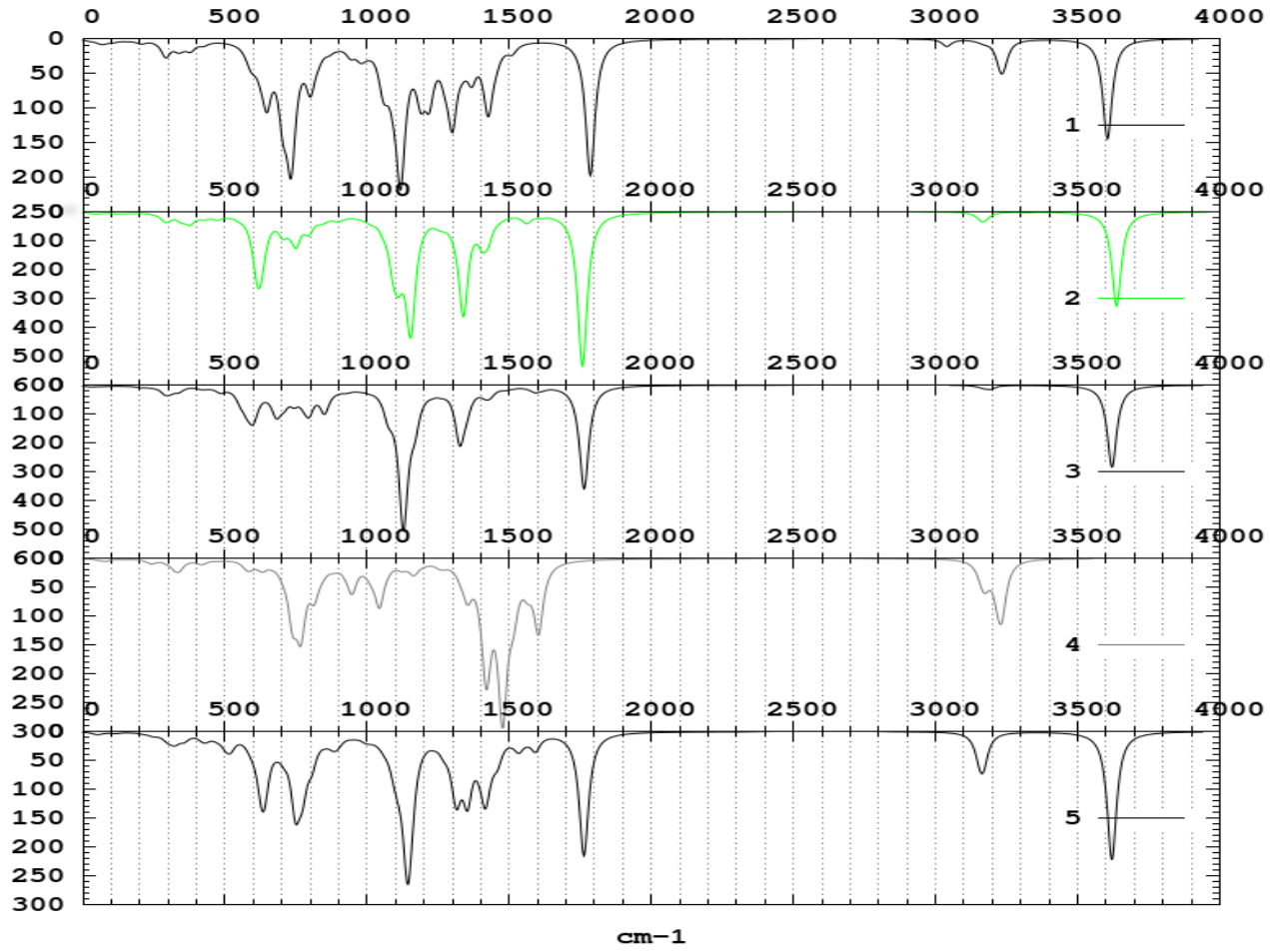

Figure 3.20: The IR spectra of the indicated complexes showing the variation in their vibrational modes

3.4.4.2 Spin Spin Coupling (J(HZ)) of Ru-Ligand bonds

The Ramsey Terms are computed with different combinations of basis sets. The properties computed with DGDZVP(Ru)|6-21+G(d,p) and 3-21G are shown in Table 3.80 while those computed with ECP(Ru)|6-21+G(d,p) and ECP(Ru,Cl)|6-21G* are shown in the Table 3.81. The FC and SD represent the spin polarization densities while DSO and PSO represent orbital current densities [385].

The Ramsey terms computed with only minimal basis set 3-21G are in a close relationship with

the one computed with higher basis set DGDZVP(Ru)|6-21+G(d,p) but it underestimates the values of the FC, SD and consequentially the values of the total spin spin coupling constant (J(HZ)) (Table 3.80) while the magnitude of PSO and DMO remains virtually the same. However, the same trends of values obtained with 3-21G and DGDZVP(Ru)|6-21+G(d,p) (R-square = 0.9864, P-value = 2.20E-016, F-statistic = 3192) is a clear indication that the minimal basis set can equally reproduce a good feature of the Ramsey terms of these complexes. All the Ramsey properties computed with basis sets either when only the Ru atom is treated with ECP (ECP(Ru)|6-21+G(d,p)) or when Ru and Cl atoms are treated with ECP (ECP(Ru,Cl)|6-21G*) significantly underestimate the Ramsey terms except the DSO which appears to be unaffected with core electron approximation with ECP (Table 3.81). The trend and the values of the total spin spin coupling constant (J(HZ)) of the ECP(Ru)|6-21+G(d,p) systems improved (R-square = 0.7781, P-value = 7.28E-016, F-statistic = 155.3) compared to the ECP(Ru,Cl)|6-2G* systems (R-square = -0.007818, P-value = 0.4215, F-statistic = 0.6587).

The Ramsey term which has the greatest magnitude is the FC term followed by the PSO while the DSO is the smallest. The least magnitude of DSO further support the report that DSO is the least interesting and also the least investigated mechanism [166].

The chloride atoms in complexes **1**, **2** and **3** have the lowest magnitude of the FC and DSO but highest SD and PSO which consequentially lead to the highest magnitude of the J(HZ) compared to other coordinated atoms of the ligands. The relatively the same values of the spin spin coupling of the chloride atoms in complexes **1**, **2** and **3** is an indication that there is no serious effect on the coupling strength of the chloride to the ruthenium metal atom due to changes in their chemical environment (Table 3.80).

In complexes **1**, **2** and **3** where there is chloride atom, a very high correlation of the SD with the PSO (0.93, 0.89 and 0.98 respectively) are observed but no such high correlation is observed for complexes **4** (0.32) and **5** (0.08) without the chloride atoms. The effect of SD on the total spin-spin

coupling (J(HZ)) was also high on the three complexes with chloride (Table 3.82) while the effect of the FC on the spin spin coupling constant significantly improved in complexes **4** and **5** without the chloride atoms. Generally, the Ramsey terms which have the highest effects on the total spin spin coupling constants are FC and PSO while SD and DSO are average and depend on the type of the complexes (Table 3.82). Even though the magnitude of DSO is the least in all the complexes (Table 3.80), yet it has a significant effect in complexes **4** and **5** (Table 3.82) which have no chloride ligand.

3.4.4.3 NMR properties of the complexes

The computed NMR properties using the combined basis set DGDZVP(Ru)|6-31+G(d,p) (Table 3.83) and a single minimal basis set 3-21G are in a close range (Table 3.85) but when the ECP(Ru)|6-31+G(d,p) basis was used, the isotropic NMR shielding tensor of Ru atom was underestimated which equally affect the values obtained for other atoms (Table 3.86). The magnitude of the magnetizabilities, isotropic NMR shielding and many other atomic properties computed with the minimal basis set 3-21G and DGDZVP(Ru)|6-31+G(d,p) are relatively close. This observation further supports the view that the isotropic magnetizability is generally insensitive to electron correlation corrections and vibrational corrections [393].

The hydrogen atoms that are involved in HB are characterised by higher magnetizability bond contribution ($\chi_{Bond}(A)$), lower intra atomic magnetizability and lower shielding tensor than any other hydrogen atoms in the complex (Figure 3.21). The QTAIM properties obtained from the highest combination of basis set DGDZVP(6-31+G(d,p)) (Table 3.83) will be considered for further discussion. The magnitude of the total bonding magnetizability ($\chi_{Bond\_Iso}(A)$) of Ru atom is higher than other atoms in the complexes but it is not the case for its total bonding isotropiC-NMR shielding ($\sigma_{Iso}(A',A)$) contribution. The highest among each of the bonding magnetizability contribution ($\chi_{Bond}(A|B)$) of Ru to all the coordinated atoms is to arene carbon atoms (Ru-C bonding) except in complex **3** where the

highest contribution is towards the Ru-Cl bonding. The lowest values obtained for the Cl atom interatomic magnetizability ($\chi_{Bond\_Iso}(A)$) (Table 3.83) is an indication that it could be ionic bond. It has been demonstrated that inter-atomic magnetizability (bond magnetizability) is able to verify the exact nature of aromaticity/antiaromaticity among different molecules and also distinguish the correct aromaticity order among the sets of aromatic/antiaromatic molecules [394].

The selected correlation of the computed QTAIM NMR atomic properties with the isotropic magnetizabilities and NMR shielding are shown in Table 3.84. Besides those shown in Table 3.84, the values of Anisotropy is highly correlated with intra-atomic magnetizabilities ($\chi_{Intra\_Iso}(A)$) with the correlation values of 0.69, 0.62, 0.68, 0.96, 0.89 for the respective complexes while it is inverse correlation with inter-atomic magnetizabilities ($\chi_{Bond\_Iso}(A)$) with correlation values of -0.80, -0.79, -0.83, -0.86 and -0.80 for the respective complexes. It is interesting to point out that, there is a very strong correlation of atomic charges with the intra-atomic magnetizabilities as was previously observed in the literature [394] but low with inter-atomic magnetizabilities (Table 3.84). Also, the correlation of the atomic charges with the intra-atomic isotropic shielding is very low.

The high correlation obtained from the computed atomic properties makes us to proposed a model for easy computation of NMR properties of molecules.

The proposed model equation is:

$$\sigma_{Iso(A)} = C_0 + C_1*ABS(X_1) + C_2*X_2 + C_3(X_3^2) + C_4*X_4 + C_5*X_5$$

Where X_1 = q(A), X_2 = K(A), X_3 = K_Scaled(A), X_4 = LI(A) and X_5 = DI(A,A')/2

The Ci values, the level of the correlation and the significance of the QTAIM properties (X_i) used to model the NMR isotropic shielding are shown in Table 3.87. From the values of the R^2, there is a clear indication that a very high correlation of the NMR shielding with the computed electronic kinetic energy of atoms (K(A)), number of electrons localized in atoms (Loc(A)), approximation to

virial-based total energy of atoms (K_Scaled(A)) and number of electron delocalization from atoms (Deloc(A,A')). However, despite the high correlation, wide residual ranges are observed for complexes **1**, **2**, **3** and **5** with carboxylic units. The carboxylic group is responsible for a wide margin as the oxygen and the hydroxyl units are very poorly fitted among all the atoms in each of the complexes.

3.4.4.4 Polarizability and hyperpolarizabilities of the complexes

In addition to the hyperpolarizability, mean polarizability (<α>), polarizability anisotropies (α1, α2, α3), we evaluated the polarizability exaltation index (Γ), which is determined as Γ = α(mol) - Σi<α>i, where α(mol) is the mean polarizability of a molecule and $\Sigma_i<\alpha>_i$ is the summation of the atomic polarizability of the atoms which constitute the molecule. According to literature [345], calculated Γ values have been employed to estimate relative aromaticity of furan homologues and stabilities of atomic clusters. A large negative Γ value denotes a very stable structure.

The calculated hardness (η) values are included in Table 3.88 with all other conductive properties of the complexes. In agreement with the relative energies, the most stable isomer is predicted to be the hardest one [345]. However, the molecules having a small energy gap are known as soft and having a large energy gap are known as hard molecules [347].

In both cases of ECP basis sets ECP(Ru,Cl)|6-31G* and ECP(Ru)|6-31+G(d,p), the computed conductive properties are overestimated beside the dipole (μ), polarizability exaltation index (Γ), Band gap and hardness (η) that were underestimated. However, ECP(Ru)|6-31+G(d,p) give better results that follows the same trend with the basis set DGDZVP(Ru)|6-31+G(d,p). The trend of the results obtained from 3-21G are very similar to the best result obtained from DGDZVP(Ru)|6-31+G(d,p) basis sets but there is a little overestimation of the values of Γ and underestimation of other properties. Complex **2** have the highest value of the first hyperpolarizabilities (β) while complex **5** have the least. The trend of

the magnitude of computed conductivity properties of the complexes for Dipole, $<\alpha>$, $\Delta\alpha_1$, $\Delta\alpha_2$, $\Delta\alpha_3$, Γ, β, and Band gap (or η) are **3** < **1** = **2** < **5** < **4**; **5** < **3** < **2** < **4** < **1**; **2** < **5** < **3** < **4** < **1**; **5** < **2** < **3** < **4** < **1**; **4** << **5** < **1** < **3** < **2**; **2** < **3** < **5** < **4** < **1**; **2** << **3** < **1** < **4** < **5** and **1** < **4** < **5** < **2** < **3** respectively. The computed values of $\Delta\alpha_3$ using different basis sets do not follow the same trend which is an indication that the values of $\Delta\alpha_3$ are very sensitive to the type of the basis sets. Since the values of Γ can be used to predict the stability of the complexes [345], therefore complexes **2** and **3** may probably be the most stable and coupled with their lowest band gap (very soft) will make them very reactive [395] which may eventually help in their anticancer activities. Also, complex **2** and **3** having the highest values of β is an indication that they are the best NLO materials which may eventually help in their anticancer activities.

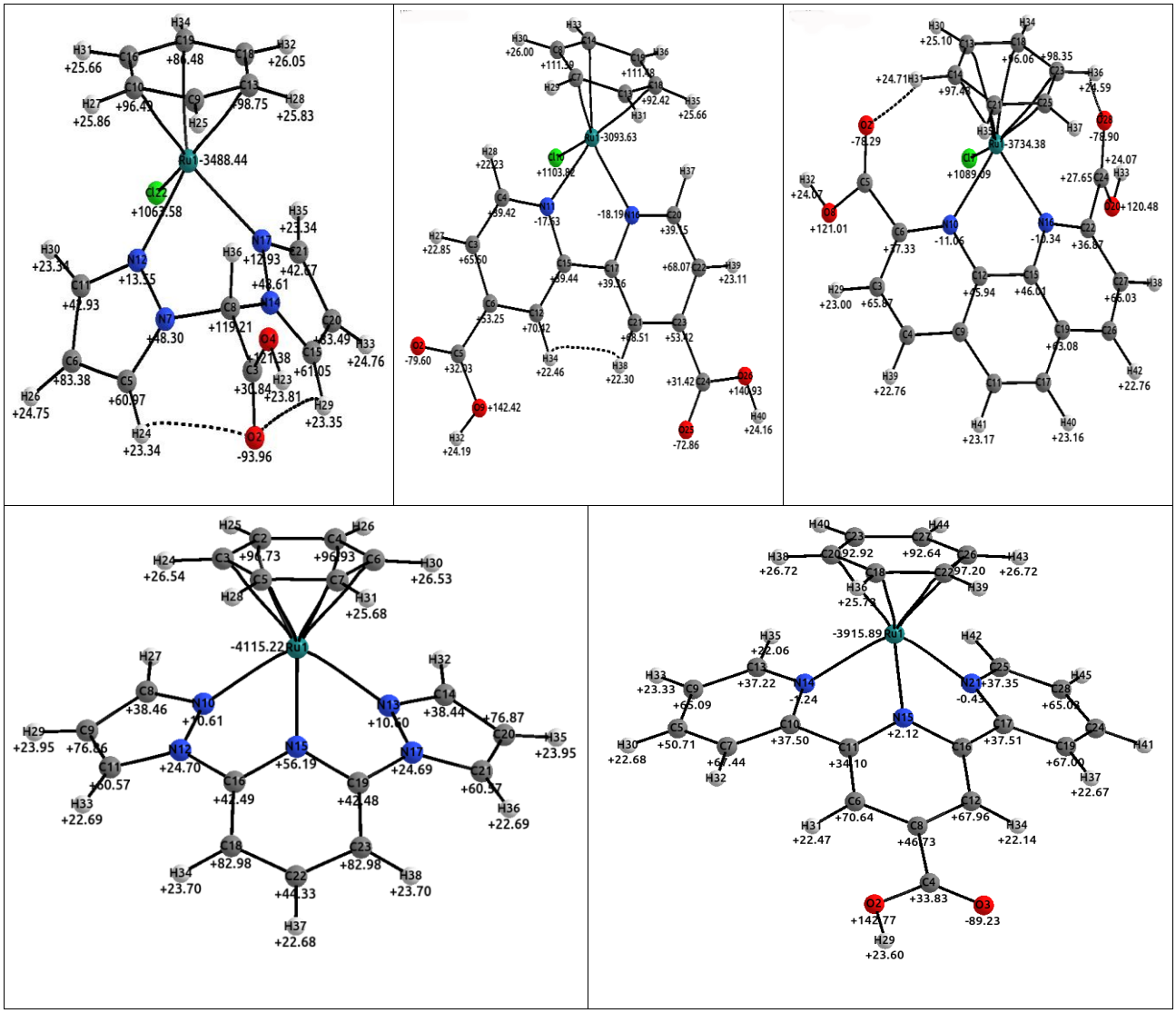

Figure 3.21: The optimized geometries of the complexes showing the isotropiC-NMR shielding of selected atoms computed with DGDZVP(Ru)|6-31+G(d,p)

3.5 Computational docking of the selected ruthenium complexes

In this section, three different sets of docking results from Ru(II)-based complexes are reported and all the results of this section have been published respectively as three different articles [318-320]. In subsection 3.5.1, our effort is directed towards proposing better selective anticancer agents by focusing more on cancer peculiar proteins other than DNA and also predicts complexes that display higher activity at lower dose because most of current potential anticancer complexes are only effective at high dose [19]. The search for the alternative targets for Ru-based complexes is a research challenge as the targets of many of these complexes can not be ascertained [5, 8, 9, 11, 396]. The lack of proper understanding of the targets of Ru-based complexes is hindering their rational design [396] and it is the major factor that is hindering the NCI approval of Ru-based complexes like Indazolium trans-[tetrachloridobis(1H-indazole)ruthenate(III)] (KP1019), and imidazolium trans-[tetrachlorido(1H-imidazole)(S-dimethyl sulfoxide)ruthenate(III)] (NAMI-A) [7]. In our attempt to predict the possible target and the mechanism of the anticancer activities of Ru(11)-based complexes (Figure 3.22), ten different receptors of various relevance in cancer chemotherapy targets are considered. The receptors used are Recombinant Human albumin (rHA), Thymidylate synthase (TS), Ribonucleotide reductases (RNR)**,** Histone Deacetylase (HDAC7), Cathepsin B (CatB), Topoisomerase 11 (Top 11), Thioredoxin reductase (TrxR), BRAF Kinase and Histone Protein in Nucleosome core particle (NCP) and DNA-gyrase was included to study the possibility of anticancer complexes also acting as antimalarial agents. Their respective pdb files 1BM0, 2G8D, 4R1R, 3C0Z, 1CSB, 1QZR, 1H6V, 3Q4C, 3MNN and 1AJ6 were obtained from protein data base (pdb) [356].

In subsection 3.5.2, some of the different models of RAPTA complexes that have been reported in the literatures [13, 17, 51] are used with other proposed structures especially the unusual metal-based complexes (Figure 3.24). In order to predict the possible targets and reasons for some of the traceable

ineffectiveness of these metal-based complexes, ten protein targets are used as potential targets of the Ru(II)-based complexes. Also, DNA gyrase was included to study the possibility of anticancer complexes also acting as antimalarial agents.

In the section 3.5.3, another docking package called Molegro which sufficiently recognise the ruthenium atom as metal centre than Glide, Gold and Autodock was used. Unlike the organic counterparts, there is a very serious limitation in making use of docking tools for metal complexes mainly due to lack of proper force fields to take care of the metal centre [83]. Also, we have enhance the prediction of our docking results by introducing the atomic charges of each metallocompound obtained from their optimized structures in quantum calculation (Figure 3.26). In addition to the number of receptors considered in our previous works [318, 319], we have also included DNA as part of targets to see the possibility of some of these metallocompounds having favourable interaction properties like that of *cis*-platin.

3.5.1 The inhibitory activities and possible anticancer targets of Ru(II)-based complexes using computational docking method

In this subsection, we focus our interest on predicting the best targets for some of the Ru(II)-based complexes as anticancer agents which as being a great research challenge [5-9, 11-14, 396] and also try to compare the newly predicted hypothetical anticancer complexes with the known RAPTA complexes. The structure of the complexes that were docked into the binding sites of the proposed ten targets using Autodock and Glide docking are shown in Figure 3.22.

The analysis of the results obtained from Glide docking (Table 3.89) gives the picture of the predicted inhibitory strength of the Ru(II)-based complexes used. According to the results obtained

through Glide docking, many of the complex-receptor binding activities preferentially predicted our newly proposed structures especially **9** and **10** to bind more favourably compared to the RAPTA type of complexes. The strongest bindings among all the complex-receptor interactions are the inhibitory interaction of **9** and **10** with RNR. Also, these two complexes happens to be the best predicted inhibitors of RNR and also the best two inhibitors of TrXR in a reverse order. Combination of same **10** with **7** is predicted as the best inhibitors of Kinases above every other complex considered. The complex **9** with **8** or **11** are predicted as the best for HP-NCP or DNA-Gyrase respectively. The same **9** followed by **6** are predicted as the best inhibitors of Cat B. For HDAC7, **10** and **6** are also predicted as the best inhibitors. The complex **3** is taking to be the best inhibitor of Top11 followed by **9**, **6** and **5**. The complex **11** followed by **6** or by **3** are predicted the best for rHA or TS respectively. The best targeted receptors of the complexes with the highest activities are RNR (because of strong interaction of **9** and **10** only), Kinase (due to strong interaction of **10**, **7**, **2**, **11**, **8** and **1** in a decreasing order), Top11 (predicted as good target of most of the complexes except **1** and **2** where no activity is recorded) and Cat B (mainly **9**, **11**, **6**, **3** and **5**), followed by HP-NCP, TS (but is a poor target of **1** and **4**), DNA-Gyrase and TrXR are average targets while HDAC7 and rHA are predicted to be relatively poor targets. The general features of the Glide docking shows that **9** and **10** followed by **6** are predicted as the best inhibitors of most of the receptors considered using Glide. The feature of the interaction of the complexes with Cat B shows that besides our proposed **9**, **11**, and **6** the best of the RAPTA complexes are predicted to be **3**, **5** and **4** but **1** predicted poor.

The suggested targets as most favourable of the complexes from the Autodock docking (Table 3.90) are Cat B, HP-NCP, HDAC7 (except **9**, **10**, **11**), Kinase and DNA-Gyrase. Those suggested as average targets are TS (still one of the best targets for **1** and **2**), TrXR (the best target for **10**) and rHA (the best target for **11**) while RNR (part of the best target for **10** and **11**) and Top11 (but still a good target for **10**) are suggested as poor targets for most of the complexes. In line with the reported

experimental results, Cat B is still the best predicted target of the RAPTA complexes in the order of **1**, **2** and **4** which is an indication that prediction of Autodock agree better with the experimental finding than Glide as **4** is experimentally proposed as having the best anticancer activity and interaction with Cat B than many other RAPTA's complexes [9, 13]. This shows **1** and **2** as derivative of **4** can resist hydrolysis [5] interact more competitively with Cat B than the parent complexes. However, **8** among our complexes is predicted a better inhibitor of Cat B than RAPTA complexes. Also, a critical look at the best predicted activities of the complexes across the best targets shows that complex **8** is predicted best inhibitor for Cat B, HP-NCP, HDAC7 while **1** and **2** are predicted better inhibitors than **8** for DNA-Gyrase which is a suggestion that RAPTA complexes can equally act as antimalarial [72, 73]. Therefore, in most cases the order of activities of the complexes follows as **8**, **1**, **2** and **4** as the best inhibitors.

There is good agreement between the predicted behaviour of the receptors toward the complexes as predicted by the Autodock and Glide packages. Both predicted Cat B and Kinases as good targets of most of the complexes and TS as average target. While DNA-Gyrase, TrXR, HP-NCP are either predicted as an average or one of the best by each of the two methods. These are in good agreement with the experimental findings as Cat B [9], HP-NCP [15] and Kinase [74] have been suggested as possible targets of Ru(II)-based complexes. Also, the prediction of TrXR as less preferred target compared to Cat B by both Glide and Autodock docking agree well with experimental report especially for RAPTA's complexes [9]. The correlation of ranking order of the complexes from Autodock and Glide in Table 3.91 further gave a clear picture of the disparity in their ranking as most of the correlation determined for each receptor are highly negative which is an indication that the ranking of the complex activities by the two method are nearly reverse of each other. However, the comparison between the activities of the complexes predicted by the two methods of docking are not of interest, but the interest is to understand and to predict the optimal orientation and conformation of the

complexes embedded in a proteins which is the primary objective of all the research efforts in the area of protein-ligand interactions, development of many different techniques and the associated software tools [354].

In order to gain better insight into the binding site interaction and orientation of the complexes, a more critical look is presented in Table 3.92 for the best two inhibitors of each receptor in terms of hydrogen bond (HB) and Metal-Receptor (MR) possible interactions with residues within the range of 4.5Å. The result from Glide docking shows that, the orientation of the best two inhibitors of Cat B are alike with the carboxylic unit forming hydrogen bond with carboxylic unit of the GLU 122E. A likewise orientation also occur in the binding of the best two predicted inhibitors of DNA-Gyrase as the two inhibitors have common hydrogen bond interaction with ASP 73. The complex predicted as first of this two has no residue within the 4.5 Å of the metal radius that would possibly suggest any MR relationship. In HP-NCP the two complexes are characterised with single HB and MR with one oxygen unit of the COO group of **8** interacting with the NH unit of the imidazole group of HIS 106 H. In interaction of complexes with Kinase, complex **7** that is ranked second is found to penetrate further into receptor and characterised with many possible MR interactions (some are presented in the Table 3.92) than **10** that was ranked first. The binding sites located on rHA by the two best ranked (**11** and **6**) are very widely separated from each other. The relative importance of MR interactions and other possible interactions with HB interaction is shown in the interaction of **6** with rHA where there is only single HB with higher MR compared with **11** (Table 3.92) where there is higher HB and yet their interacting energy is very close as shown in Table 3.89.

Also, the observations from Autodock further give insight into the binding site interaction of the complexes. A critical look at the interacting feature of the complexes with HDAC7 in relation to Cat B (Table 3.92) indicates that though the inhibitory activities of their best two inhibitors are very close (Table 3.90) yet the HDAC7 inhibitors are characterised with very few HB and MR which is an

indication that there are other factors that are playing significant role on the inhibitory activities of complexes. In HP-NCP there is the possibility of a very strong MR interaction as the side group of ASP 65A (i.e. CH_2COO) is having a closed and free space interaction with the Ru(II) metal. The sites of binding of the best two inhibitors of Top II are widely separated from each other suggesting two possible binding sites. The high inhibitory activities of the best two inhibitors of DNA-Grase and HDAC7 despite very few numbers of HB and MR interaction coupled with the best for TS where there is no recorded HB and MR shows the significant effects of other types of possible interactions.

There is further similarity between Autodock and Glide in the best two inhibitors that are predicted for some of the receptors as **8** is commonly predicted for receptor HP-NCP, **11** for rHA, **10** for RNR and **10** for TrXR (Table 3.92 and Figure 3.23). A more critical look at these four receptors with the same complexes predicted among the best two, the binding site located by Autodock for the complexes are different form Glide predicted binding site in HP-NCP, rHA and TrXR but the same in RNR as shown in Figure 3.23a, b, d, & c respectively. The orientation of **10** on the binding site of RNR as predicted by Autodock and Glide is very similar with the carboxylic units contributing to the stability by forming HB as shown in Figure 3.23(c). As shown in Figure 3.23, all the four interactions of complexes with receptors are characterised with multiple HB (represented by orange and cyan cylinder shape). The different binding sites suggested by Autodock and Glide for the interaction of some complexes with some receptor give the possibility of having more than one binding site as it is even observed within the same package when Glide suggested different site for the best two inhibitors of rHA and Autodock suggest widely separated binding sites for the best two inhibitors of Top II. This is not far from the experimental report of multiple binding sites for Ru-(II)-based complexes with HP-NCP [15] and Kinase [74]. However, the possible reason for the observed disparities in the ranking of the Glide to that of Autodock methods was suggested in another part of our work to possibility result from the bias of the Glide docking of the metal complexes toward the steric hindrance.

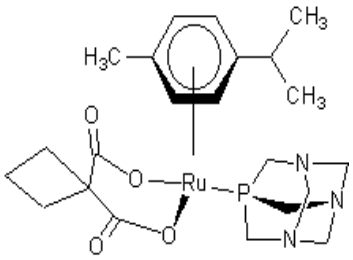

1). CRAPTA-C

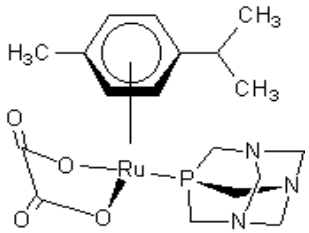

2). ORAPTA-C

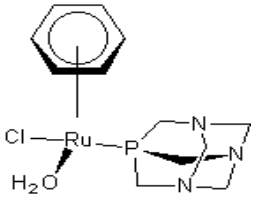

3). RAPTAB-H_2O

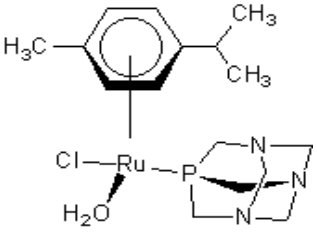

4). RAPTA-C-H_2O

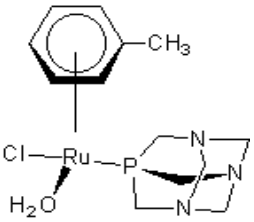

5). RAPTAT-H_2O

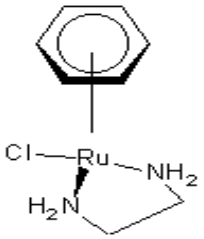

6). piano

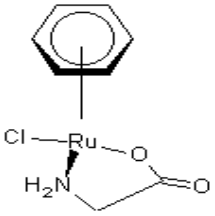

7). ragly

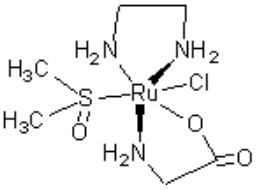

8). etdiaglydmso

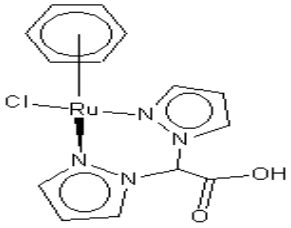

9). radipyrazoic

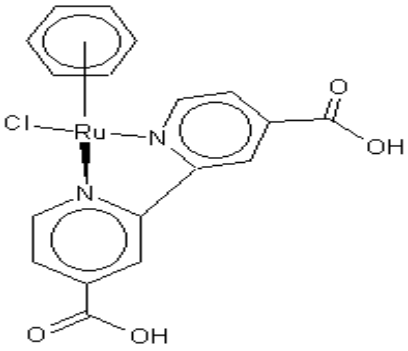

10). radipyrdioic

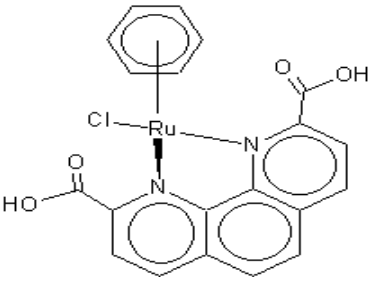

11) raphendioic

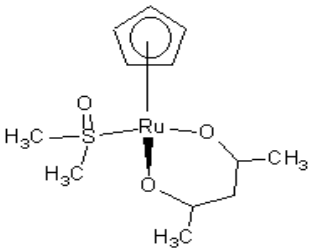

12). rCpbkdmso

[where ra = Ruthenium-(η6-arene); etdia = ethylenediamine, phen = phenanthroline; pyr = pyridine; pyraz = pyrazole, PTA = 1,3,5-triaza-7-phosphaadamantane; Cp = cyclopentadienyl, bk = β-diketone, piano = model of piano-stool]

Figure 3.22: The structures of the Ru(II)-based complexes as anticancer agents

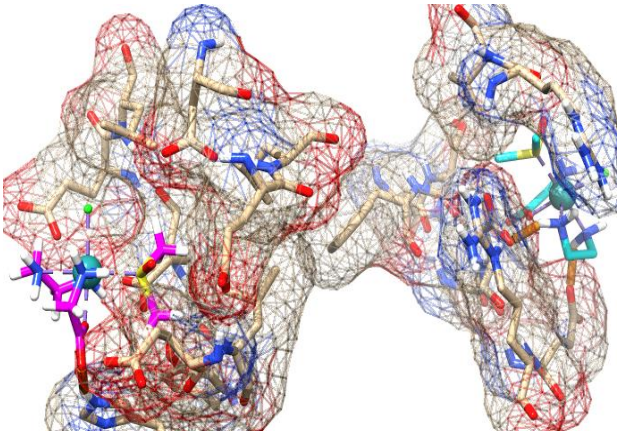

a). The interaction of etdiaglydmso with HP-NCP (in surface mesh) using Autodock and Glide.

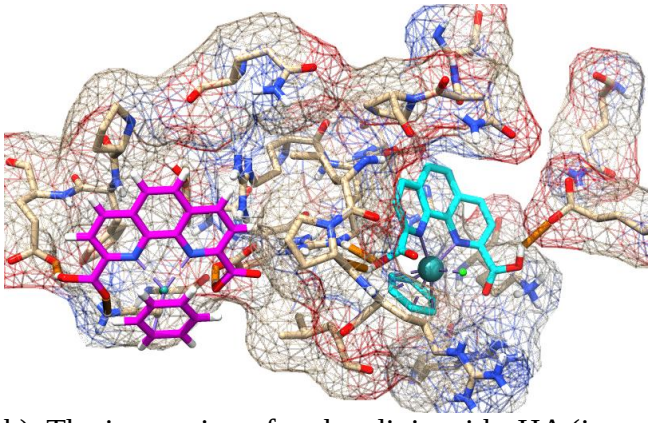

b). The interaction of raphendioic with rHA (in surface mesh) using Autodock and Glide.

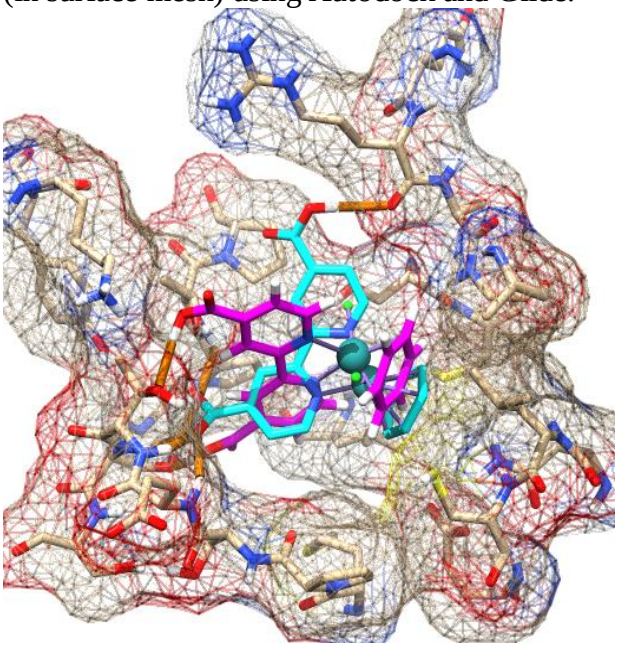

c). The interaction of radipyrdioic with RNR (in surface mesh) using Autodock (Cyan) and Glide.

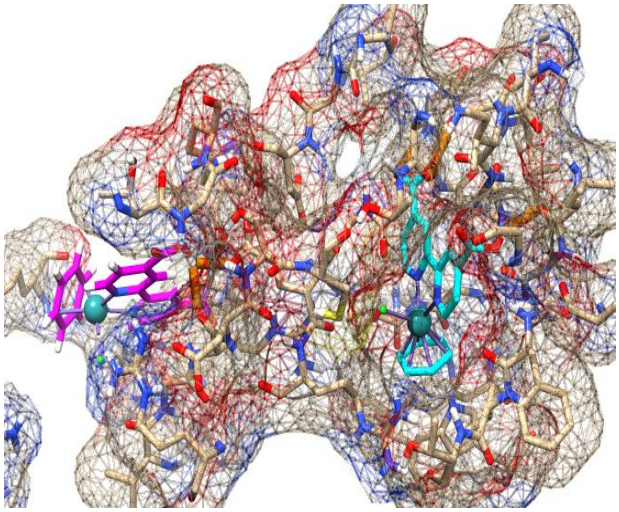

d). The interaction of radipyrdioic with TrXR (in surface mesh) using Autodock and Glide.

Figure 3.23: The binding site interactions of one of the best two inhibitors of HP-NCP, rHA, RNR and TrXR as predicted by the Autodock (right with C atoms in Cyan) and Glide (left with C atoms in Magenta) showing hydrogen bond (orange cylinder form).

3.5.2 Comparative study of the suitability of Autodock, Gold and Glide for the docking and predicting the possible targets of Ru(II)-based complexes as anticancer agents

In this subsection, the binding modes, the best possible targets and binding site interactions of Ru-based complexes with ten receptors were predicted using Glide, Autodock and Gold docking. Even though a little comparison of the ranking obtained from the three methods are considered but the interest is to understand and to predict the optimal orientation and conformation of the complexes embedded in proteins which is the primary objective of all the research efforts in the area of protein-ligand interactions, development of many different techniques and the associated software tools [354]. The results of the docking presented in this work is the best binding results out of the 20 favourably predicted by Autodock, 10 predicted by Gold and 26 predicted by Glide. The structures of all the metal-based complexes that were used in the docking study are presented in Figure 3.24.

The general features from the prediction of glide docking (table 3.93) show that the best predicted targets for most of the complexes are Top II followed by Kinase, RNR and Cat B accordingly. Some of the complexes like **6**, **5**, **13**, **9**, **16** and **21** respectively bind to Kinase preferentially than many other possible targets that are considered in this research. Also, **17**, **8** and **5** prefer to target TS than many other targets. Some of the least targeted receptors are rHA (except complex **21**), HDAC7, DNA-Gyrase, TrxR (except complex **21**).

The results obtained from the docking of these metal-based complexes with the ten choice receptors using Gold package are presented in the Table 3.94. The Gold docking results are reported in terms of the values of fitness which means the higher the fitness the better the docked interaction of the complexes unlike the other two docking packages (Glide and Autodock) which are reported in terms of

the docking energy score which means the lower the score the better the interaction. The most targeted receptors from Gold results are Top II, Cat B and Kinase respectively. This is in good agreement with the prediction from the Glide package which equally suggested Top II and Cat B as part of the most probable targets for the complexes. The receptors that are moderately targeted are TS, TrxR, rHA and DNA-Gyrase. The receptors that are predicted to be least targeted by the complexes are HP-NCP, RNR (except **1** and **5**) and occasionally HDAC7 especially by **1**, **5**, **11**, **12** and **17**. The prediction of Cat B as a better target than TrxR is in good agreement with experimental finding [9].

The receptors that are recorded to be the most targets by many of the metal-based complexes from Autodock prediction (Table 3.95) are Cat B followed by HDAC7, DNA-Gyrase, HP-NCP and Kinase except **6** and **7** that bind poorly with most of the receptors while TS and rHA are predicted as average targets. The receptors that are predicted to be least targeted by the complexes are Top II (with the exception of **5**, **17**), RNR and TrxR (with the exception of **21**, **5**, **20**, **4** accordingly). In all cases, Glide, Gold and Autodock commonly predicted Cat B as one of the most possible target of the complexes and TrXR as far less target compared to Cat B which is in good agreement with reported experimental results [9]. Also, Glide/Gold included Top II and Gold/Autodock included Kinase as one of the best targets. There is very close relationship in the predictions through the three packages except for the receptors Top II and RNR which are predicted as rarely targeted by Autodock but predicted to be one of the most targeted by Glide/Gold and Glide respectively. There is further agreement between Autodock and Gold as TS, rHA and DNA-Gyrase are either predicted as one of the best or average targets for most of the metal-based complexes. The complexes that are predicted to have the best activities against most of the chosen targets are **1**, **5**, **3**, **2**, **4**, **17**, **8**, **12**, **20**, **10** and **14** accordingly. The metal-based complexes that are predicted to have poor activity against most of the receptors are **6**, **7**, **18** and **21**. Just like the activities of the hydrated complexes are predicted to be highly enhanced using Glide and Gold, so also are **8**, **12**, **20** and **19** predicted to be more active than the respective parent

complexes.

A critical look at the general behaviour of the complexes towards the targets according to the Glide prediction shows that **6** is predicted as the best inhibitor of Kinase than any other complexes considered, while **8**, **13**, **17** and **20** respectively predicted as the best inhibitors of Top II than any other complexes. The feature of the Gold prediction shows that **4**, **3**, **16**, **11** and **12** are respectively predicted to have the best activities toward the Top II.

There is a very good agreement between our docked results and the reported experimental behaviour of some of the RAPTA as inhibitors of Cat B and TrxR [9]. Selecting the RAPTA complexes that are common with our models, the reported experimental results shows that the inhibitory strength against TrxR starting from the greatest to lowest are in this order: **1**, **5**, **11** and **14** respectively with little or no effect of **7** on TrxR. While that of the Cat B are in this order: **14**, **11** and **1** respectively with little or no effect of **5** and **7** on Cat B [9]. Also, the inhibition of Cat B is predicted to be high with RAPTA complexes than TrxR which is in agreement with the results from all the three packages used. According to Autodock prediction the inhibition of Cat B follows this order: **3**, **4**, **1**, **5**, **12**, **20** and **8**. Also **14** and **11** recorded significant effect far better than **7** which is in line with the experimental findings. Compounds **5**, **20**, **17**, **4**, **1**, **8** and **12** are predicted as TrxR inhibitors in that order. Gold predicted **1**, **4**, **15**, **16**, **7** and **10** for Cat B while the general behaviour of inhibitors toward TrxR are very low compared to Cat B just as it was in the reported experimental result. From Glide, the inhibition of Cat B by the inhibitors considered is low compared to some other receptors like Top II. However, **20**, **19**, **18**, **8**, **7** are predicted to take the lead accordingly. While TrxR inhibition is reported to be very poor by most of the complexes except **21**.

In summary, combining the three methods together, just as in the experimental result, **1, 5**, **12** and **20** are included as part of the best TrxR inhibitor and **1** is specifically rated among the best inhibitors of TrxR by the three docking methods which is in good agreement with the experimental

report. Also, almost all the experimentally found inhibitors of Cat B such as **1**, **12** and **20** are included except **5** which is predicted as one of the better inhibitors contrary to the experimental finding.

Further analysis of the interactions of some Ru(II)-based complexes with the receptors is presented in Table 3.96 where the binding site interactions of the two best ranked complexes for each receptor are shown in terms of the noticeable hydrogen bond (HB) and metal-receptor residues (MR) interactions. The two best ranked complexes are **5** and **12** for TrxR respectively are almost superimposed and the site of their binding is buried inside the receptor. The stronger interaction of **1** with TS (without any noticeable HB and MR) than complex **5** that is ranked second which has two HB suggests that the metal may not necessarily has direct interaction with the receptor residues but just act as holder of ligands for better and stronger ligand-receptor interactions which may include van der Waals, electrostatic, steric and others. A critical look at the interaction from Gold prediction (Table 3.96) give further insight into the mode of the complex-receptor interaction and the reason while some are rank better inhibitor than the others. The binding site located by the three docking suites are the same for many of the receptor with that of Gold and Autodock docking specifically in Cat B almost having superposition of the **1** (Figure 3.25). The structures with NH_2 like **10** and **4** which are ranked either first or second as inhibitors of rHA, TrxR and HDAC7 respectively show that there is very strong metal to receptor residues interactions as the NH_2 group was seriously pushed off for better direct interaction of Ru atom with the CH_3 part of $S(CH_3)$ group of MET 87A, arene part of phenol group of TYR 200 and arene of PHE 679A respectively. But in the case where there is an existence of HB between the NH_2 and receptor as in Top II where one of the H atom of NH_2 and O atom of CO group of ASN 129 are interacting through hydrogen bond, the NH_2 is well fixed in a right position with metal. This suggest that NH_2 can be a good leaving group where it does not make any HB contribution to the binding of the metal complexes. Another interesting feature indicates the significance of other form of interactions order than HB and MR that are analysed (Table 3.96) as in the case of RNR where **1** which

was ranked first has no HB while the second ranked complex **5** as five noticeable HB interactions. In Glide, the first two ranked complexes as inhibitors of rHA namely **21** and **17** locate two different binding sites. The presence of more than one binding sites observed in our docking studies is not far from the experimental report of multiple binding sites for Ru(II) complexes with HP-NCP [15] and Kinase [74].

The similarity in the three methods of predicting the interaction is also demonstrated from the binding site interaction of complexes **1**, **3**, **4**, **20** with Cat B, Top II, Gyrase and Kinase respectively as shown in Figure 3.25. Taking a critical look at complex **1** in Figure 3.25(a), the cyclobutyl di-carboxylate of the three predictions are towards the boundary of the hydrophilic and hydrophobic part of Cat B but the arene and PTA direction of the Glide is different from that of Autodock and Gold. Further agreement is seen in the prediction of Autodock (Cyan) and Gold (Magenta) as the PTA groups are directed toward an inner hydrophilic large pocket of Cat B and the arene groups of the complex are toward the hydrophilic end. The three packages predicted almost the same binding site interaction for complex **3** with Top II residues as shown in Figure 3.25(b) while there is a difference in the prediction of the interaction of complexes **4** and **20** with Gyrase and Kinase respectively (Figure 25c & d).

Very good agreement has been observed in the structural interaction of the complexes with the receptors using the three methods but the ranking of the three methods are not the same. On the average, there is a better agreement between the ranking of the docked metal-based complexes using Autodock and Gold (Table 3.97) with correlation of one of the receptors (i.e. RNR) up to 0.76. The correlation of the Glide with both Autodock and Gold is poor mainly because Glide did not recognise the Ru atom properly and most of the complexes geometrical orientations on the binding sites of the receptors vary significantly from that of Autodock and Gold as in Figure 3.25(a).

In order to further understand the properties that are prevalent in the determination of the docking score of Glide and the possible causes for wide difference in ranking from the other two

methods, the COMSIA properties was also carried out using the Field-based QSAR in Maestro (Table 3.98). The major defining factor of the docking score of Glide is predicted to be gaussian steric property which defines the steric hindrance of the molecule. Another property that define the docking score of the Glide for the metal-based complexes is the hydrogen bond followed by electrostatic property. The predicted activities agree well with the docked activities based on the statistical properties of significantly high value of R^2-value ranges from 0.49 to 0.72, high stability ranges from 0.31 to 0.94 and very low P-value ranges from 1.83E-011 to 1.07E-004 (Table 3.98).

No	Structure /Name	No	Structure /Name	No	Structure /Name	No	Structure /Name
1	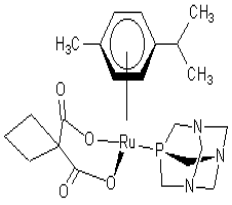 Carbo-RAPTA-C	7	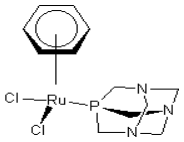 RAPTA-B	12	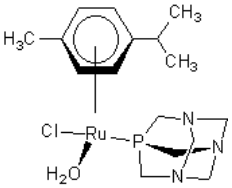 RAPTA-C-H_2O	17	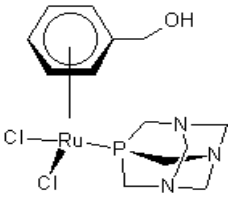 RAPTA-Ta-OH
2	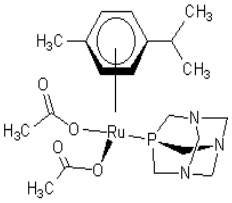 RAPTA-C-COOH	8	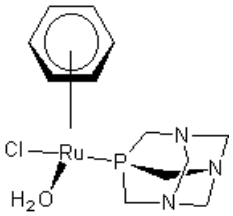 RAPTA-B-H_2O	13	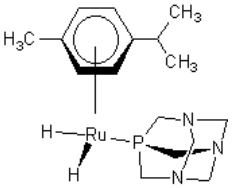 RAPTA-C-H	18	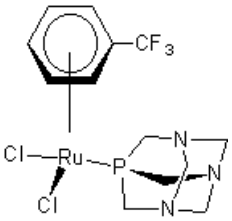 RAPTA-T-CF_3
3	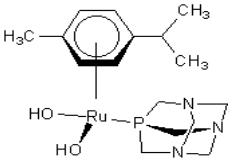 RAPTA-C-$(OH)_2$	9	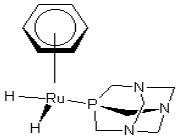 RAPTA-B-H	14	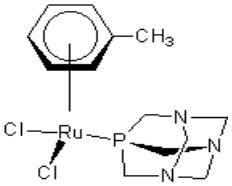 RAPTA-T	19	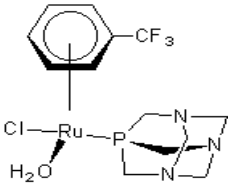 RAPTA-T-$CF_3(H_2O)$
4	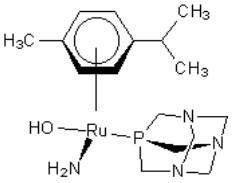 RAPTA-C-NH_2(OH)	10	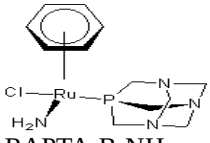 RAPTA-B-NH_2	15	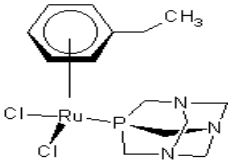 RAPTA-Ta-CH_3	20	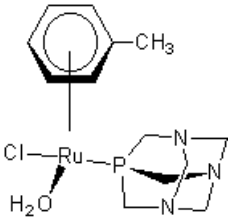 RAPTA-T-H_2O
5	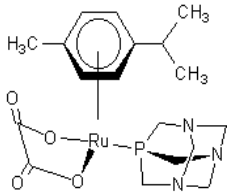 oxalo-RAPTA-C	11	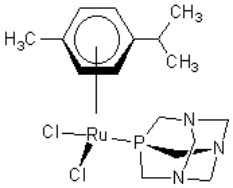 RAPTA-C	16	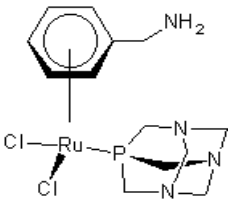 RAPTA-Ta-NH_2	21	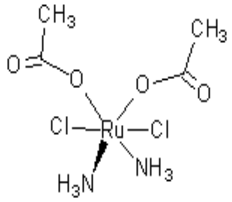 rClCOO-NH_3
6	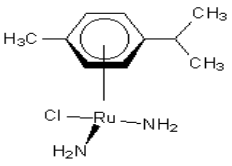 raC-NH_2						

Figure 3.24: The structures of the metal-based complexes

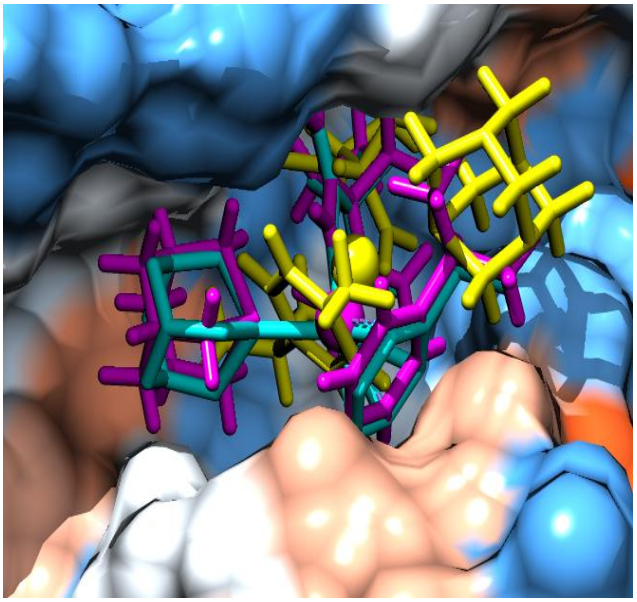

a). Complex **1** in Cat B

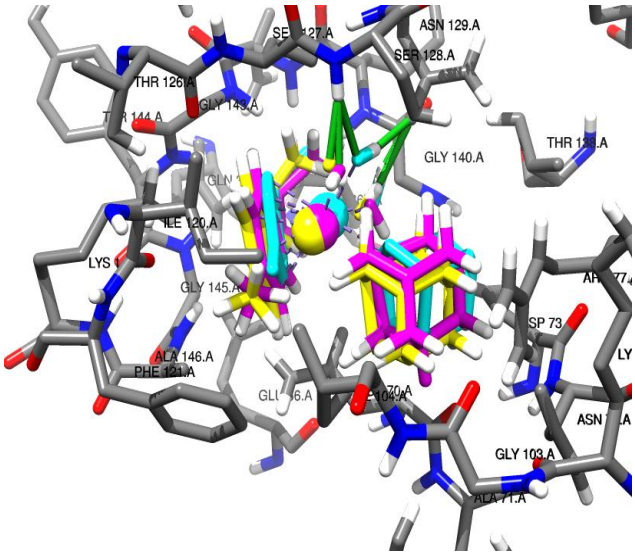

b). Complex **3** in Top II

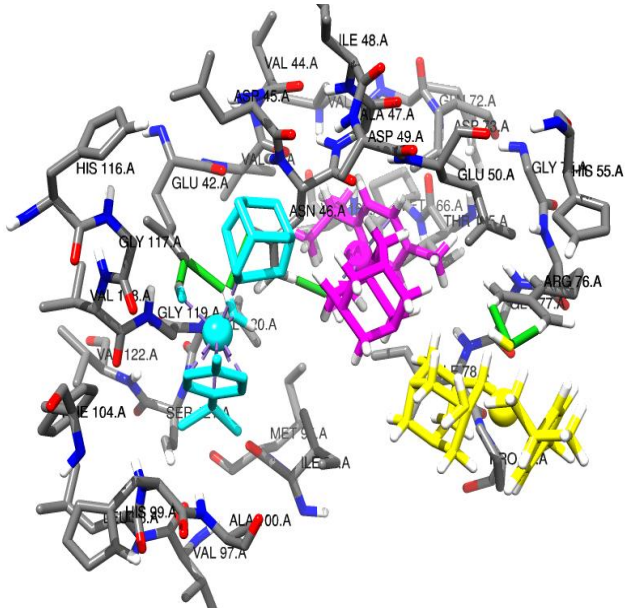

c). Complex **4** in Gyrase

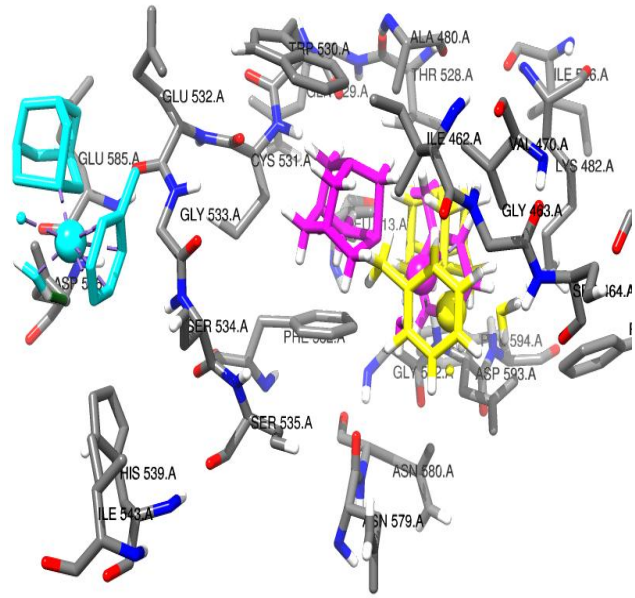

d). Complex **20** in Kinase

Figure 3.25: The binding site interaction of complexes **1**, **3**, **4** and **20** with Cat B, Top II, Gyrase and Kinase respectively using Autodcock (Cyan), Gold (Magenta) and Glide (yellow) Docking Predictions. The colouring of Cat B Surface is from the hydrophilic (red) to hydrophobic (blue) and the HB is represented with green cylinder in the figures.

3.5.3 Insight into the anticancer activities of Ru(II) based metallocompounds using docking methods

3.5.3.1 General features of the binding activities of the metallocompounds

In this subsection, the binding affinities and conformations of 30 metallocompounds including their hydrolytic forms are presented. The 30 metallocompounds (Figure 3.26) are docked against twelve receptors using relax Molegro, constraint Molegro and Autodock docking approaches. The summary of 72 poses of the best two metallocompounds in their interaction with the receptors are shown in Table 3.99 indicating the hydrogen bonding (HB) interactions with the binding sites receptor residues and the possible metal-receptor (MR) interactions. The results obtained from the docking of metallocompounds to twelve receptors using Autodock, relax Molegro without metal-residue covalent constraint and constraint Molegro with covalent constraint are shown in Table 3.100(a&b), 3.101(a&b) and 3.102(a&b) respectively. The docking results obtained from both relax and constraint Molegro docking (Table 3.101(a&b) and 3.102(a&b)) gives a better ranking than the Autodock which cannot not be easily ranked since many of the Autodock values (Table 3.100(a&b)) are within its standard error margin of ~2.177 kcal/mol [354, 353]. Table 3.100(a), 3.101(a) and 3.102(a) contain binding affinities of non-hydrolytic complexes while Tables 3.100(b), 3.101(b) and 3.102(b) contain the affinities of their respective hydrolytic complexes. The hydrolytic complexes are named after their respective non-hydrolytic type with suffix "a". Generally, we observed that some of the new metallocompounds like complexes **1**, **1a**, **8**, **8a**, **9**, **9a**, **10**, **10a**, **11** and **12** (Table 3.101(a&b)) are found to have better binding affinities than the co-crystallized compounds of Cat B, HDAC7, TS and BRAF Kinase receptors. Though co-crystallized compounds bind better in TrXR, Top II, RNR and Gyrase than all the metallocompounds (Table 3.101(a&b) and 3.102(a&b)), yet many of our modelled metallocompounds

(occasionally the bidentate RAPTA complexes **2** and **3**) are found to be highly competitive to the co-crystallized compounds in their binding affinities (Table 3.101(a&b) and 3.102(a&b)). The newly modelled metallocompounds especially **1 & 1a**, **9 & 9a**, **10 & 10a**, **11** and **12** followed by the bidentate RAPTA (**2** and **3**) and hydrated RAPTA (**13a**, **14a**, **15a** and **16a**) complexes are predicted to have stronger binding affinity to many of the receptors (Table 3.101(a&b) and 3.102(a&b)).

The proposed mechanism of activation of the metallocompounds through hydrolysis [8, 17, 37, 397] is further confirmed through the docking results. In most of the receptor interactions, autodock indicates an enhanced binding energy with receptors for all the hydrolytic complexes (Table 3.100(a&b)). The same is observed for the covalent constraint docking of metallocompounds to DNA-1,DNA-2, Cat B, RNR and TrXR and also for relax Molegro docking to DNA-1 and DNA-2 (Table 3.100(a&b) and 3.101(a&b)). In other receptors, only few hydrolytic metallocompounds increase binding energy as a result of the hydrolysis which depends on the type of receptor targets. The binding activities of the hydrated forms of RAPTA complexes are found to be greatly enhanced. Also, the bidentate form of RAPTA complexes are suggested to competitively bind strongly to receptors as the hydrated forms of RAPTA complexes especially metallocompound **14a** though their activities are still lower than the modelled metallocompounds using the results of the three docking methods (Table 3.100(a&b), 3.101(a&b) and 3.102(a&b)). In many of the receptor interactions, metallocompounds **16** and **16a** are predicted to have better binding affinity than **15** and **15a** (Table 3.101(a&b)) except for receptors RNR which further support the experimental report for higher anticancer activities of the first pair [17].

In many instances, the binding of the relax Molegro docking are stronger than the constrained Molegro docking, also the relax Molegro agree better with the available experimental reports (Table 3.103(a&b)) and the experimentally proposed activation of metallocompounds by hydrolysis (Table 3.101(a&b) and 3.102(a&b)).

All docking methods clearly indicate that the best target of the hydrolytic *cis*-platin (Cisp-W1 and Cisp-W2) is DNA as they are found having higher binding energy with DNA compared to other receptors. The hydrolytic cis-platin especially the doubly hydrolized (Cisp-W2) has the highest DNA binding compared to the other forms of cis-platin which further confirm the need for hydrolysis before activation [37, 51]. However, in protein receptors, there is decrease in binding affinity of hydrolytic cis-platin compared to its non-hydrolytic type which further confirms that protein is not its target. Considering the ranking of both relax and constrained Molegro docking, the best targets of the metallo complexes follow the order HDAC7 > DNA-1 > rHA > Cat B > DNA-2 > Gyrase > TrXR > Top II > TS > RNR > HiS > Kinase except in few cases like complex **12** that prefers Cat B to rHA. The poorest binding affinity of the complexes is observed in the covalent constrained docking to rHA receptor.

3.5.3.2 The interacting poses of the best two metallocompounds in the receptor binding sites.

To have a better understanding of the binding site orientation poses and interaction of the metallocompounds with the residues of each receptor, we have selected two metallocompounds predicted by relax Molegro, covalent constraint Molegro and Autodock methods to have the best binding to each of the receptors (Table 3.99). The binding site interactions are elaborated in terms of the hydrogen bonds (HB) and the metal-residues (MR). The MR considers possible covalent bonding interaction of the metal with a nucleophilic centre of receptor residue which was considered during the constrained docking. There is the possibility of metal-residue (MR) interaction of complex **4a** with DNA-1 according to Autodock prediction [Table 3.99]. The relax Molegro and Autodock dockings suggest different binding sites from that of constrain docking in the binding of metallocompound to DNA-1 (Figure 3.27(a)). Interestingly, the suggested conformation of complex **12** binding to DNA-2 from both relax and covalent constrain dockings is perfectly superimposed (Figure 3.27(b)). There is

also an interesting feature of possible intercalation of complex **12** with the two based pair nitrogen atoms (N7) of the Guanine in DNA-2 by both relax and constrained docking as shown in Figure 3.27(b). The tridentate ligand part of metallocompound **12** in the relax Molegro docking (cyan) and Autodock (magenta) perfectly fits into the hydrophobic pocket of the Cat B as shown in Figure 3.27(c) which was not the case in the constrained docking (green). This further suggest the possible reason why the binding affinities of the relax docking are higher than that of the constrained docking.

Both relax and constrained Molegro docking show a superimposed comformation for complex **10a** of which the arene unit pointing toward the mouth of the inner pocket of the HDAC7 while the Autodock preferentially locate the outer pocket (Figure 3.27(d)). Complex **1a** is rated to have the best binding affinity to HP-NCP in relax Molegro docking but it has no visible H-bond nor metal-receptor interaction. The conformation of complex **1a** as suggested by the relax Molegro docking fits in totally into one side of the binding site pockets than the conformation suggested by the constrained Molegro and Autodock docking to HP-NCP. In Figure 3.27(e), the experimental conformation from the crystal structure of RAPTA complex **14a** in the HP-NCP binding site is compared to the conformation obtained from the docking results.

In Autodock docking of complex **10** to rHA we observed possible covalent interaction of ruthenium with the NH_3 unit of residue LYS 195A characterised by a distance of 1.78 (Table 3.99). The three docking methods suggest either the hydrolytic complex **10a** or non-hydrolytic complex **10** as the best binding metallocompound to rHA. The conformation suggested for the docking of RAPTA complex **3** to RNR is shown in Figure 3.27(f), both Autodock and Molegro suggest a very close position for the ruthenium atom but different position for its coordinated ligands. In the constrained docking of complexes **9a** and **8a** to TrXR, there is the possibility of ruthenium atom forming covalent bond with the bridged sulfur (SG) residue CYS 64A or strong close contact van der Waal interactions with the two bridged sulfur (SG) atoms of the residues CYS 64A and CYS 59A.

3.5.3.3 The binding affinity of the metallocompounds to DNA

An insight into the interaction of the metallocompounds with two types of DNA (DNA-1 and DNA-2) is given for the Autodock (Table 3.100(a&b)), relaxes Molegro (Table 3.101(a&b)) and constrained Molegro (Table 3.102(a&b)). There is improvement in the binding of many of the complexes to DNA-1 and DNA-2 due to their hydrolysis. Typical examples are complexes **1a**, **8a**, **9a**, **10a** and all the hydrolytic RAPTA complexes. In agreement with literatures [5, 6], the best target of Cis-platin is DNA as their binding affinity decrease significantly in protein receptors compared to DNA-1 and DNA-2. The features of cis-platin in all the dockings show that their activities significantly increase when it is doubly hydrolized (Cisp-W2) than when it is singly hydrolyse (Cisp-W1). The newly proposed model complexes appear to have strong DNA interaction which suggests DNA as part of their possible targets. Most of the RAPTA complexes will target Cat B or HDAC7 preferentially to DNA. The spectrum of the interactions of RAPTA complexes with DNA ranges from -116.96 to -49.53, while Cat B ranges from -124.88 to -60.05 and HDAC7 ranges from -127.16 to -55.13, considering both the relax and constrained docking further confirm that RAPTA complexes will target proteins preferentially to DNA [9, 15].

3.5.3.4 The binding affinities of the metallocompounds to Cat B and TrxR

The results obtained from relax Molegro and Autodock docking (Table 3.100(a&b) and 3.101(a&b)) shows that **12**, **1** & **1a**, **10** & **10a**, **9** & **9a** and **11** bind strongly to Cat B than its co-crystallized compound. The experimental activities of the RAPTA complexes against Cat B follow the order **15**, **14**, **2** while **3** and **13** rarely show any appreciable binding affinity and that of TrXR followed the order **2**, **3**, **14** and **15** while **13** has the lowest activity (Table 3.103) [9]. Selecting only the metallocompounds that have experimental values, the predicted binding affinities of the metallocompounds against TrXR using Molegro agree better with the experimental order of their

inhibitory activities as metallocompound **13** is rated least in activities toward TrXR follow by metallocompound **15**. Contrary to the experimental report, metallocompound **3** was predicted to bind strongly to Cat B. However, ranking of metallocompounds **14a** and **15a** among those that have the best binding to Cat B and metallocompound **13** rated least agrees well with the experimental results (Table 3.103). The rating of both hydrated and non-hydrated forms of metallocompound **14a** among those that bind strongly to Cat B, further give insight into the experimental findings as the best anticancer among the RAPTA complexes [13]. The three docking methods show that the interaction of the metallocompounds with Cat B is stronger than with TrXR which agree well with the experimental report [9]. The binding affinities of the hydrated metallocompounds with Cat B and TrXR are significantly enhanced (Table 3.100(a&b), 3.101(a&b) and 3.102(a&b)).

3.5.3.5 The binding affinity of the metallocompounds with Gyrase, HDAC7, HP-NCP, BRAF Kinase, rHA, RNR, Top II and TS

The features of the binding affinities of the metallocompounds against Gyrase from both docking methods show that co-crystallized compounds still preferentially bind to Gyrase than any of the metallocompounds even though the activities of the new modelled metallocompounds are competitively close to that of its co-crystallized analogues. The metallocompounds that have the best binding to Gyrase using Molegro are **1** & **1a**, **9** & **9a**, **10** & **10a**, **11** and **12** (Table 3.101(a&b) and 3.102(a&b)). Autodock included the hydrated metallocompounds **14a**, **13a** and **15a** immediately after metallocompounds **12**, **9a**, **10, 4a, 8a, 1a, 10a** and **5a** (Table 3.100(a&b)). The binding affinities of the metallocompounds to HDAC7 show that the model **1**, **12**, **11**, **10, 9** and their respective hydrolytic forms (where applicable) have the best binding than its co-crystallized compound. This is also applicable to the RAPTA complexes.

There are experimental reports on HP-NCP also being a possible target of RAPTA complexes

[15], but the new model metallocompounds **1**, **9**, **10**, **11**, **12** and their hydrolytic forms (where applicable) are predicted to bind better than RAPTA complexes in all the three docking methods. The crystal structure of HP-NCP shows RAPTA-C (metallocompound 14a) binding to two different sites on chain G and H of the receptor (Figure 3.27(e)). In order to make parallel comparison of the poses of metallocompound 14a with the available experimental crystal structure, its docking features is shown in Figure 3.27(f). The constrained Molegro and Autodock docking of complex **14a** gives preference to the first binding site which suggest that complex **14a** will bind preferentially to the first site than the second. Also, the constrained Molegro docking shows that the PTA unit of this metallocompound locate the same receptor pocket as the crystal structures (Figure 3.27(e)). The new models of metallocompounds **1**, **9**, **10**, **11, 12** and **8** (include their hydrated forms) are predicted among those that have the best binding to BRAF Kinase (Table 3.101(a&b)). The rHA is predicted as an average target suggesting that many of the Ru(II)-based complexes that are considered will be on the average kinetically favourable which further support the experimental findings [13, 17, 51].

In the interaction of the metallocompounds with RNR, the co-crystallized compound is found to bind preferentially to all the metallocompounds. The predicted best binding metallocompounds to RNR are **1**, **10**, **8**, **11**, **12** and **9** including the bidentate RAPTA complexes **3**, **2** and hydrated **14a**. The suggested best binding metallocompounds to Top II after the co-crystallized compound are **1**, **10**, **9**, **12**, **11** and the RAPTA complexes **2**, **3**, **14a** and **16a**. Commonly predicted best binding metallocompounds to TS by the three methods of docking are **12**, **10**, **11, 9** and the bidentate RAPTA complexes **2** and **3** while only Molegro rated **1** as part of the best for TS.

3.5.3.6 Metal-Receptor residues covalent interaction using constraint Molegro docking

In this study, based on the available information on the binding site residues of each receptor, a nucleophilic atom was selected as centre of covalent interaction with the metal centre of the

metallocompounds. Cysteine sulfur atom (SG) was selected for the Cat B (Cys A 29) [398], BRAF Kinase (CYS A 531) [74], RNR (CYS B 439) [399], TrXR (CYS A 59) [400] and TS (CYS A 198) [401]; histidine nitrogen atom was used for the HDAC7 (HIS A 709) [402], HP-NCP (HIS H 106) [403] and Top II (HIS B 20) [404]; while for the Gyrase [73] and rHA [405] where none of the HIS, CYS and MET are within the binding site residues, nucleophilic nitrogen atom of ASN A 46 and ARG A 144 were used respectively. For the DNA (4DL7) [406], the nitrogen atom (N7) of the Guanine (DG T 7) was used.

The general features is that the binding affinity is lower when the covalent constraint is applied (Table 3.102(a&b)) compared to when it is not (Table 3.101(a&b)). This therefore shows that the ruthenium metal in many of the metallocompounds will prefer positioning the ligands for optimum receptor interactions than forming covalent bonds with the residues of protein receptors. However, the binding affinities of some metallocomponds against targets like DNA-1, DNA-2, HDAC7, HIS and RNR during the covalent constrained docking is competitively high as that of the relax docking indicating the possibility of the ruthenium atom forming covalent interaction with the receptor residues.

In summary, the new models especially complexes **1**, **9**, **10** and **12** (and their respective hydrolytic form where applicable) are predicted by all the methods of docking among the best two inhibitors of all the receptors. Also, complex **11** is rated among the best three by the relax docking for Gyrase and the constrained docking for Cat B and HDAC7. However, none of the RAPTA complexes appearing among the best two proposed inhibitors of the receptors considered in this work using the three docking methods (Table 3.99) except in rHA and RNR where the first and the second ranked complexes are the non-hydrolytic and hydrolytic forms of the same compound (Table 3.101(a&b) and 3.102(a&b)). This suggests the possibility of the new models acting as better anticancer agents than the RAPTA complexes.

3.5.3.7 The correlation of factors that determined the binding activities of the metallocompounds

The docking method of Molegro gives a more comprehensive insight into the factors that determine the binding affinities of the metallocompounds. Their correlations Tables 3.104(a&b) are constructed using the statistical package R [407]. The most significant factors that influence the metallocompounds interaction with the DNA and many of the protein receptors are intra-molecular van der Waal (E.Intra.vdw.), pose energy, steric and long range electrostatic interaction (ElectroLong in Table 3.104(a&b). In all the protein receptors, the inter protein-ligand and the pose energies significantly determine the total binding energy of the metallocompounds.

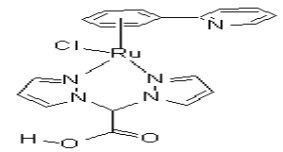

1. PPpyrazoic

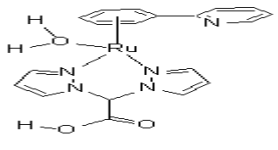

a. PPpyrazoic

1

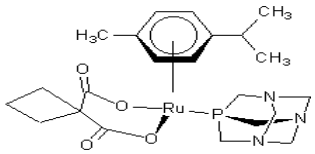

2. *Carbo*-RAPTA-C

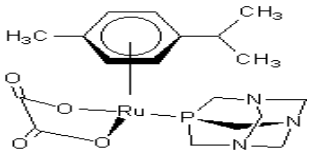

3. *Oxalo*-RAPTA-C

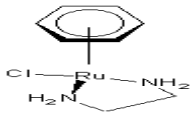

4. piano

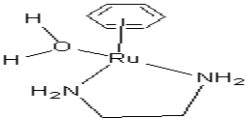

4a. piano

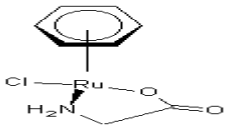

5. RAgly

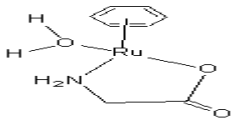

5a. RAgly

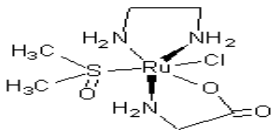

6. etdiaglydmso

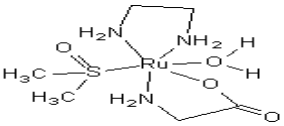

6a. etdiaglydmso

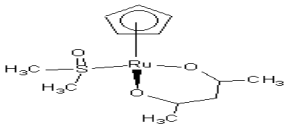

7. rCpBkdmso

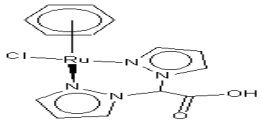

8. RAdipyrazoic

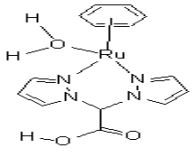

8a. RAdipyrazoic

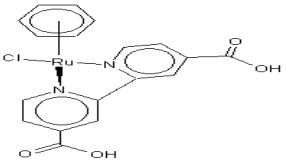

9. RAdiPyrdioic

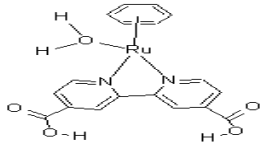

9a. RAdiPyrdioic

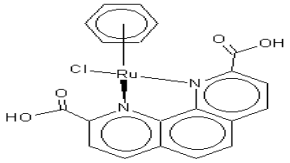

10. RAphendioic

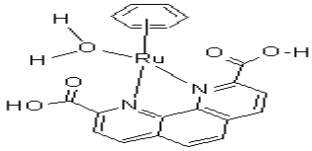

10a. RAphendioic

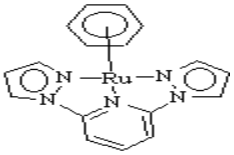

11. Rapyrdipyrazole

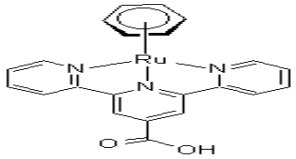

12. RAterpyrnic

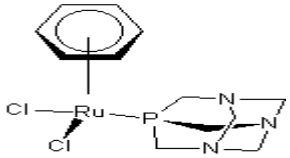

13. RAPTAB

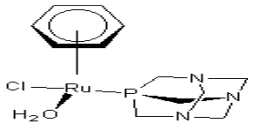

13a. RAPTAB-H_2O

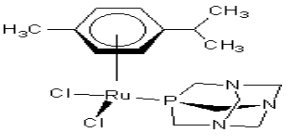

14. RAPTA-C

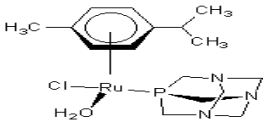

14a. RAPTA-C-H_2O

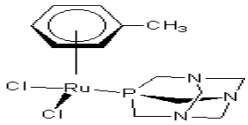

15. RAPTAT

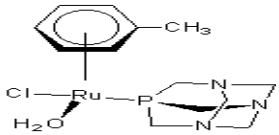

15a. RAPTAT-H_2O

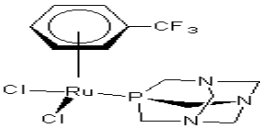

16. RAPTAT-CF_3

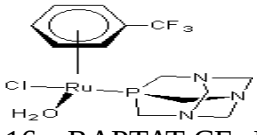

16a. RAPTAT-CF_3-H_2O

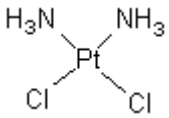

Cis-platin

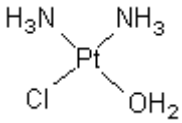

Cisp-W1

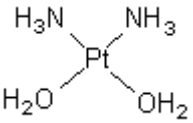

Cisp-W2

The PP = 4-Phenylpyridine, RA = Ruthenium-(η6-arene); etdia = ethylenediamine, phen = phenanthroline; pyr = pyridine; pyraz = pyrazole, PTA = 1,3,5-triaza-7-phosphaadamantane; Cp = cyclopentadienyl, Bk = β-diketone, piano = model of piano-stool

Figure 3.26: The schematic structures of the anticancer metal-based complexes

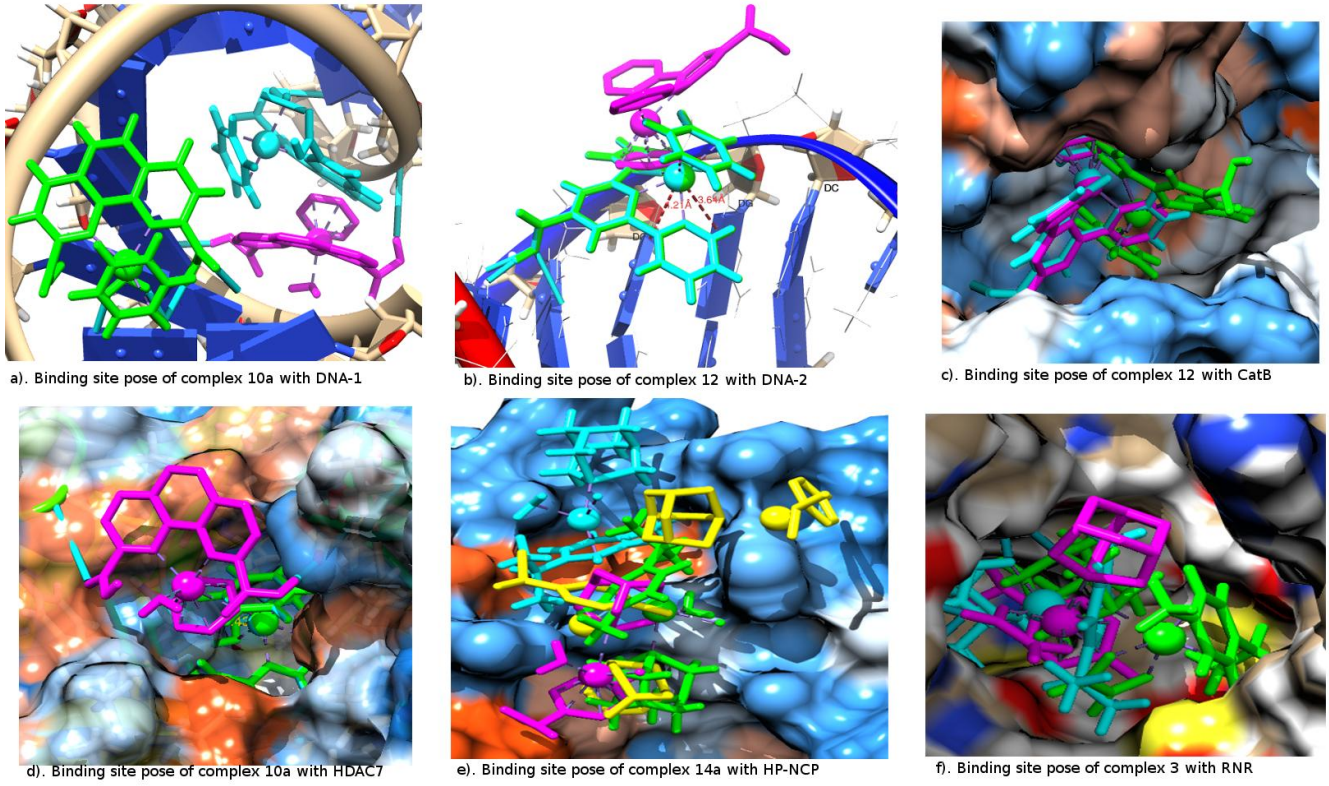

Figure 3.27: The receptor binding site interaction of the selected best binding metallocompounds from Autodock (magenta), Molegro unconstrained (cyan), constrained (green) and the experimental crystal structure in yellow.

CHAPTER FOUR

4 SYNTHESIS OF LIGANDS AND THEIR COMPUTATIONAL PROPERTIES

4.1 Background of the chapter

This chapter describes the synthesis and theoretical properties of the ligands that were used for the synthesis of Ru(II)-based complexes in Chapter Five. The atomic, molecular, spectroscopic and non-linear properties of the ligands and their derivatives were elucidated through molecular simulation using DFT methods of computation. For ease of comparison, the ligands are grouped into four sections 4.3, 4.4, 4.5 and 4.6. These sections describe the synthesis and computational studies of methylpyrazole, pyrazole, pyridine and phenathroline derivatives.

Sections 4.3 and 4.4 are respectively the studies on methylpyrazole (Figure 4.1) and pyrazole (Figure 4.6) derivatives which are usually referred to as scorpionates and have become one of the most versatile types of tridentate/bidentate ligands that can coordinate to a wide variety of elements ranging from early to late transition metals [408, 409]. These type of compounds have a wide application especially in the field of transition metal carbonyl chemistry [408]. Since the introduction of the scopionates compounds by Trofimenko more than 30 years ago [410, 411], several subset of these types have been synthesised where the R–B–R moiety has been changed to R–C–R [409]. There have been synthesis of several scopionates derivatives which are not necessarily linked with boron atom but with different organic linkers like CHCOOH, CH_2 and pyridine derivatives [412, 409]. Many of the pyrazoles derivatives are designed as bidentates, tridentates and tetradentates [413, 294-300]. The dimethypyrazole derivatives are significantly important in the formation of several metal complexes through the available lone pair of electron on the N atom [408, 414-416]. There have been syntheses of

many metal complexes of pyrazole derivatives especially that of ruthenium complexes [294-300] for various applications. Therefore in the two sections, we have considered the spectroscopic and the electronic properties of the methylpyrazole and pyrazole derivatives using both experimental and computational tools. The changes in the properties of the lone pair of electron on N2 atom which may affect its coordination to metal atom were probed theoretically. The four ligands considered in section 4.3 are shown in Figure 4.1. The ligands of interest in section 4.4 are pyrazole (pz), bis(pyrazol-1-yl)methane (bpzm), bis(pyrazol-1-yl)acetic (bpza) and bis(pyrazol-1-yl)pyridinic (bpzpya) as shown in Figure 4.6.

In section 4.5, another seven derivatives of pyrazole (Figure 4.11) were studied in order to show the effect of methyl, carboxylic, pyridine and phenyl on the stabilities, conductivity, availability of the nitrogen atom of pyrazole for metal coordination (denoted as *N) and the strength of the *N-N bonds of the pyrazole. Effort was also made to correlate the theoretical spectroscopic properties with the experimental values in an attempt to get the distinguishing features from the IR, Raman, ^{1}H-NMR, ^{13}C-NMR, ^{15}N-NMR and UV of the derivatives. We envisage that the information provided from experimental and theoretical studies will be of tremendous help in the design of pyrazole based organometallic complexes for specific uses in biomedical and non-linear optical (NLO) applications.

Lastly in section 4.6 of this chapter, we carried out a study on the pyridine (pyr) and phenanthroline (phn). The pyridine and phenanthroline derivatives are the most widely used bidentates ligands in metal coordination. They have received research attention in the application of their metal complexes as electro-chemiluminescence, catalyst, photochemical and anticancer [273-279, 417, 281-284]. Due to the wide application of pyr and phn derivatives, it is imperative to understand their relative properties in order to bring about a more rational combination in metal complexes. The interest of this section is to give at a glance the spectroscopic and electronic properties of pyr and phn derivatives. The schematic representation of the six ligands is shown in Figure 4.16.

4.2 Experimental Synthesis of the ligands

4.2.1 Chemicals and solvents

The chemicals and solvents used for the synthesis of the ligands were purchased from Sigma aldrich and were used as purchased without any further purification. The chemicals used for the synthesis of the ligands are pyrazole, 3,5-dimethylpyrazole, 3-phenylpyrazole and dibromoacetic acid. The solvents used during the synthesis are dichloromethane, tetrahydrofuran (THF), acetone, diethyl ether (Et_2O) methane and acetonitrile.

4.2.2 Physical measurements

The physical methods used for the characterisation of the ligands are IR, Raman, UV, NMR and Elemental analyser.

4.2.2.1 The IR measurement

The Fourier Transform Infra Red (FTIR) spectra of the ligands were measured using a Brukers Vector 22 spectrophotometer and the values are given in cm^{-1}. The solid samples of the ligands were used in all the IR analysis.

4.2.2.2 The Raman measurement

The Raman spectra were obtained for the ligands using Bruker Fourier Transform Raman spectrometer (model FRA 106). The solid samples of the ligands were also used.

4.2.2.3 The UV measurement

The absorption spectroscopic properties of the ligands were determined using Hewlett–Packard 8452A diode array spectrophotometer. The solids were dissolved in methanol.

4.2.2.4 The NMR measurement

The NMR chemical shifts of the ligands were determined using Bruker-AVANCE NMR spectrometer at 600 MHz. The samples were dissolved in deuterorated methanol (CD_3OD) or DMSO (DMSO-D_6). Both ^{1}H-NMR and ^{13}C-NMR chemical shifts are reported in δ relative to tetramethylsilane (TMS) as reference.

4.2.2.5 The elemental analysis

The elemental analyses of the ligands were performed using Perkin Elmer 2400 Series II CHNS Elemental analyzer.

4.2.3 Synthesis of bis(3,5-dimethylpyrazol-1-ly)acetic (bdmpza)

The method employed for the synthesis of this ligand is very similar to the method reported in the literature [408]. Both 3,5-dimethylpyrazole (40 mmol, 3.84 g) and dibromoacetic acid (20 mmol, 4.355 g) were added to THF solvent with K_2CO_3 (75.7 mmol, 10.45 g), KOH (77.7 mmol, 4.35 g) and BTEA (1.0 g) as phase transfer agent. The reaction was refluxed for 5-6 hours. The product was dried in vacuo, 80 ml of water was added and then acidified with half diluted HCl first to a pH of 7.0 and extracted with Et_2O (200 mL). It was further acidified to pH 1.0 and extracted twice with Et_2O (2 x 150 mL). The organic solvent was dried with Na_2SO_4 and evaporated in vacuo. Acetone was added to the oily product and then dried in vacuo to afford a white powder which was further recrystalized with

acetonitrile.

4.2.4 Synthesis of bis(methylpyrazol-1-ly)methane (bdmpzm)

The same method employed for the synthesis of bis(methylpyrazol-1-ly)methane is similar to that reported in the literature [418] with slight modification. Methylpyrazole (40 mmol, 3.84 g) was added to CH_2Cl_2 solvent for the synthesis. The same process as in bdmpza was equally followed for the separation of the product.

4.2.5 Synthesis of bis(pyrazol-1-ly)methane (bpzm)

Ligand bpzm was prepared as described in the literature [418]. Pyrazole (40 mmol, 2.725 g) was dissolved in dichloromethane solvent with K_2CO_3 (75.7 mmol, 10.45 g), KOH (77.7 mmol, 4.35 g) and BTEA (1.0 g) as phase transfer agent were added. The reaction mixture was refluxed for 5-6 hours. The product was dried in vacuo, 80 mL of water was added and was acidified with half diluted HCl first to a pH of 7.0 and extracted with Et_2O (200 mL). It was further acidified to pH 1.0 and extracted twice with Et_2O (2 x 100 mL). The organic solvent was dried with Na_2SO_4 and evaporated in vacuo. To the oily product was added acetone and dried in vacuo to afford white microcrystals of bpzm.

4.2.6 Synthesis of bis(pyrazol-1-ly)acetic (bpza)

Ligand bpza was prepared as reported in the literature [408]. Both pyrazole (40 mmol, 2.725 g) and Dibromoacetic (20 mmol, 4.355 g) were added to THF with K_2CO_3 (75.7 mmol, 10.45 g), KOH (77.7 mmol, 4.35 g) and BTEA (1.0 g) as phase transfer agent. The reaction mixture was refluxed for 5-6 h. The product then dried in vacuo, 80 mL of water was added and then acidified with 50% HCl first to a pH of 7.0 and extracted with Et_2O (200 mL). The reaction mixture was further acidified to pH 1.0 and

extracted twice with Et_2O (2 x 100 mL). The organic solvent was dry with Na_2SO_4 and evaporated in vacuo. To the oily product was added acetone and dry in vacuo to afford a white powder which was further recrystalized with acetonitrile.

4.2.7 Synthesis of 3,5-diaceticpyrazole (dcpz)

The ligand 3,5-dicarboxylpyrazole (dcpz) was synthesised by oxidation of the 3,5-dimethylpyrazole. The method used is similar to that method reported for the oxidation of the methyl group of 4-methyl-1,10-phenanthroline [280]. 3,5-dimethylpyrazole (1 g) was refluxed for 4 h with selenium oxide (2.5 g) in dioxane containing 4% water and filtered through celite 521 while hot. The aldehyde obtained was oxidized with HNO_3 to give 3,5-dicarboxylpyrazole (dcpz).

4.2.8 Synthesis of bis(phenylpyrazol-1-ly)acetic (bphpza)

The method used for the synthesis of bis(phenylpyrazol-1-ly)acetic is as reported in the literature [408] with slight modification. Both phenylpyrazole (40 mmol, 5.76 g) and dibromoacetic (20 mmol, 4.355 g) were added to THF solvent in a conical flask. The reaction mixture was reflux for 5-6 h. The product was dry in vacuo, 80 mL of water was added and was acidified with 50% HCl first to a pH of 7.0 and extracted with Et_2O (200 mL). It was further acidified to pH 1.0 and extracted twice with Et_2O (2 x 100 mL). The organic solvent was dry with Na_2SO_4 and evaporated in vacuo. To the oily product was added acetone and dry in vacuo to afford a white powder which was further recrystalized with acetonitrile.

4.2.9 Synthesis of bis(pyrazol-1-ly)pyridine (bpzpy)

The method employed for the synthesis of bis(pyrazol-1-ly)pyridine is a combination of different

methods reported in the literatures [413, 418] with slight modifications. The method used here is a bit similar to the method used for the synthesis of bis(pyrazo-1-ly)acetic [408]. Pyrazole (30 mmol, 2.044 g) and dichloropyridine (5.21 mmol, 1.235 g) were added to THF with K_2CO_3 (75.7 mmol, 10.45 g), KOH (77.7 mmol, 4.35 g) and BTEA (1.0 g) as phase transition. To allow complete replacement of the bromides, a 6:1 moles of pyrazole:bromopyridine was used. The reaction mixture was refluxed for 24 h. The product was dried in vacuo, 80 mL of water was added and was acidified with HCl to form precipitate which was filtered and washed with water.

4.2.10 Synthesis of bis(methylpyrazol-1-ly)pyridine (bmpzpy)

The same method as described for the synthesis of bis(pyrazo-1-ly)pyridine (bpzpy) was employed. In the synthesis of bis(methylpyrazol-1-ly)pyridine, methylpyrazole (30 mmol, 2.88 g) was reacted with dichloropyridine (5.21 mmol, 1.235 g).

4.3 Spectroscopic and electronic properties of 3,5-dimethylpyrazole based ligands using the experimental and computational methods

4.3.1 The infra red spectral

The schematic representation of 3,5-dimethylpyrazole based ligands are shown in Figure 4.1. The results of the experimental Raman, IR and the theoretical IR are shown in Figure 4.2 with the assigned vibrations. The assignment of the IR vibration was done based on potential energy distribution (PED) contributions using the package VEDA [419] as explained in the literatures [420, 421]. The best two vibrations which define all the prominent peaks in the ligands are shown in Table 4.1. The prominent peaks at 2927.75 cm^{-1} (dmpz), 2923.89 cm^{-1} (bdmpzm), 2929.68 cm^{-1} (bdmpza) which can

be ascribed to υ(C-H_{pz}) are highly Raman active and are very weak peaks in the experimental IR spectra but relatively stronger in the theoretical IR. Peculiar to Raman spectra is the strong vibrational peaks at 590.00 cm^{-1} (assigned to out of plane CCNN) and around 1000 cm^{-1} (assigned to bending of either CNN or CCN) in the three ligands. Another Raman active vibration common to dmpz, bdmpzm and bdmpza are the peaks around 1425.48 cm^{-1} which are ascribed to the bending vibration of CH_3 deformation. A prominent experimental and theoretical IR vibration at 1739.00 cm^{-1} is peculiar to only bdmpza and bdcpzm but absent in dmpz and bdmpzm is assigned to the ν(C=O) vibration in agreement with literature on a similar ligand [408].

4.3.2 The NMR properties

The experimental proton and carboN-NMR for bdmpzm and bdmpza with the proton for dmpz are presented in Table 4.2. The available values as reported in the literatures are shown in bracket. The two synthesised derivatives bdmpzm and bdmpza has no proton shift at 11.99 that is observed in the precursor dmpz indicating that the hydrogen atom at N1 has been successfully substituted with CH_2 and CHCOOH in the two derivatives respectively. The observed C-NMR shift at 169.71 is an indication of the formation of the CHCOOH group of ligand bdmpza which is absent in the complex bdmpzm which as CH_2 as linking unit of the two dmpz. Experimental ^{1}H-NMR shift for the CH_3 ranges from 1.703 to 2.49, the CH_2 or C*H*COO of the linking ranges from 6.13 to 7.27, CH_{pz} ranges from 5.73 to 5.88, COO*H* is found at 7.45 while the highest shift is found in dmpz at 11.99 which is ascribed to its NH_{pz} unit.

The results obtained are shown in Tables 4.3 and 4.4. Using the direct method, ^{1}H-NMR shift for the CH_3 ranges from 1.68 to 2.52, the CH_2 or C*H*COO of the linking ranges from 5.62 to 7.39, CH_{pz} ranges from 5.94 to 7.03, COO*H* ranges from 5.76 to 6.56 while the highest shift is found in dmpz at 8.68 which is ascribed to proton shift of its NH_{pz} unit. The fitting method gives the ^{1}H-NMR shift for

the C*H*$_3$ ranges from 2.15 to 2.97, the CH_2 of C*H*COO of the linking ranges from 5.97 to 7.69, CH_{pz} ranges from 6.29 to 7.34, COO*H* ranges from 6.11 to 6.88 while highest shift of 8.94 is also obtained for the NH_{pz} proton shift that is present in dmpz.

The experimental ^{13}C-NMR shift for all the CH_3 ranges from 11.13 to 13.54, CH_2 was found at 60.46, the C_{pz} ranges from 104.37 to 148.58 and the highest shift is 169.71 for COOH. Using the direct method, the ^{13}C-NMR shift for all the CH_3 ranges from 11.87 to 15.67, CH_2 or ***C***HCOOH ranges from 63.10 to 76.5, the C_{pz} ranges from 101.37 to 148.40 and the highest shifts also predicted for COOH ranges from 151.70 to 166.00. The fitting method for the ^{13}C-NMR shift predicted 3.082 to 6.747 for CH_3, 52.50 to 67.20 for CH_2 or ***C***HCOOH, 89.08 to 134.5 for C_{pz} and 137.7 to 152.00 for COOH.

The values obtained for the Rasey terms and the spin-spin coupling (J-coupling) are shown in Table 4.5. As indicated in Table 4.5, among the four Ramsey terms, FC term has the highest magnitudes followed by the PSO while the SD and DSO have the smallest. The magnitude of FC in the bonded *N-N are higher in bdmpzm than the precursor dmpz while bdcpzm has the lowest. The SD has the highest magnitude in the precursor dmpz than the derivatives. The order of the magnitude of the *N-N J-coupling in the four ligands are bdmpza > bmpm > bdcpzm > dmpz. Though bdcpzm have relatively lower FC and SD but it has the highest magnitude of PSO properties due to its higher conjugative features. The non-bonding *N···*N interaction in bdcpzm has the highest coupling properties which may be attributed to the electronic field effects on the *N atoms from the nearby carboxylic units.

4.3.3 The geometries

The changes in the *N-N bonds from the precursor to the derivatives are computed using the QTAIM method as shown in Table 4.6. Comparing *N-N bond in the precursor dmpz to the derivatives, there is a slight elongation in bdmpzm and bdmpza which result to a weaker feature of the bond as

indicated with a lower magnitude of the Laplacian of electron density ($\nabla^2\rho(r)$) (Figure 4.3). A pair of *N-N bond in each bdmpzm, bdmpza and bdcpzm indicate that there is a slight variation within each pair (Figure 4.3). It is interesting to point out that within a pair of *N-N in each ligand, the one with shorter distance is associated with higher magnitude of $\nabla^2\rho(r)$, $\rho(r)$ and V indicating the characteristic features of a stronger bond. The variations within a pair of *N-N bonds of each derivative is an indication that there will be significant difference in the properties of the two *N atoms that are available for the metal coordination of the derivatives. The ring electron density (in red) of the pyrazole unit are observed to have significantly changes from the precursor to the derivatives in the order dmpz < bdmpzm < bdmpza < bdcpzm (Figure 4.3).

As shown in Table 4.7, the *N atoms that are available for metal coordination are characterised with lower atomic charge (q(A)), intraatomic magnetizability ($\chi_{Intra\_Iso}(A)$), bonding magnetizability ($\chi_{bond\_Iso}(A)$), total magnetizability ($\chi_{Iso}(A)$), bond isotropic shielding tensor ($\sigma_{Iso}(A',A)$) and energy level compared to N atoms that are not accessible for metal coordination. These *N atoms are also characterised by higher magnitude of intraatomic dipole of an atom ($\mu_{intra}(A)$), bonding dipole of an atom ($\mu_{bond}(A)$), total atomic dipole ($\mu(A)$), atomic volume (Vol(A)), out of plane magnetizability of atoms ($\chi_{zz}(A)$), intraatomic isotropic shielding tensor ($\sigma_{Iso}(A,A)$), total shielding tensor of an atom ($\sigma_{Iso}(A)$) (except in dmpz), electron occupation and an extremely higher anisotropic values.

The characteristic properties of the *N atoms in the ligands suggest the possibility of poor metal coordination of bdcpzm compared to the others. This observation is further confirm with the lower number of localized electrons on the *N atoms of the ligand bdcpzm compared to other ligands (Figure 4.3). Considering the total values of the computed properties as shown in Table 4.7, the dipole properties of the ligands varies in the order of dmpz < bdmpzm < bdmpza < bdcpzm.

4.3.4 The hydrogen bonding

H-bonding is known to be the most widely studied non-covalent interactions in both chemical and biological systems due to its significant roles in the stability and biological functions of compounds [380-383]. The molecule bdmpza has the highest number of intramolecular H-bonding networks (Table 4.8 and Figure 4.3). There are no intraatomic H-bonding in the precursor dmpz but two are found in bdmpzm, five in bdmpza and two in bdcpzm. There is one unusual H-bonding in bdmpzm (H24···H28) and two in bdmpza (C2···C7 and H28···H33). This type of unusual interaction is not completely strange as H-bonding was found present in H_2···HH non-covalent interaction [381, 382]. The unusual H-bonding of H···H in both bdmpzm and bdmpza have relatively high bcp which is a clear indication that it is not a van der Waals interaction since it lies within the range proposed for H-bonding interactions [382].

4.3.5 The UV absorption and electronic transition

The experimental λ_{max} of the UV absorption for dmpz, bdmpza and bdmpza are found at 273.00, 270.00 and 269.00 nm respectively. The theoretical λ_{max} UV absorption are found at 213.36 (0.0241), 227.46 (0.0092), 272.98 (0.027) and 282.21 (0.0099) nm for the dmpz, bdmpzm, bdmpza and bdcpzm respectively (the oscillatory strength are in bracket). Contrary to the red shift observed in the experimental UV absorption, the theoretical method predicted a blue shift from dmpz to bdmpza (Figure 4.4). The computed triplet states have zero oscillatory strength (*f*) which is an indication that the excitation of the electrons are mostly into the singlet excited states in all the ligands. As shown in Figure 4.4 and Table 4.9, only two singlet excited states are visible for bdmpzm and bacpza among three predicted singlet states while one is visible in dmpz and bdmpza. In this case, the experimental absorption for dmpz at 273.00 is found theoretically to be predominantly characterised by HOMO to LUMO+1 transition, that of bdmpzm at 270.00 is found to be HOMO to LUMO while that of the

bdmpza at 269.00 is as a result of HOMO-1 to LUMO transition (Table 4.9). Both the experimental and theoretical λ_{max} UV absorption of bdmpza are in very good agreement and the features of the isodensity of its three HOMO and three LUMO energy levels are shown in Figure 4.5. The isodensity surface in Figure 4.5 gives a more comprehensive features of the levels of HOMO and LUMO contributions of the two *N atoms. Just as shown in Table 4.9, the first of the two *N atoms significantly determine the HOMO-4 (53%) while the second determine the HOMO-5 orbital (50%) (Figure 4.5). The experimental absorption of bdmpza at 269.00 can best be explained as the excitation of electron from one of the pyrazole ring that dominates HOMO-1 to the carboxylic unit that dominates the LUMO.

In order to further illustrate the variations in the properties of the two *N atoms that make up a pair of bidentate properties of the ligands, the contribution of each *N atom to the electronic transition are illustrated in Table 4.10. The *N atom in dmpz make highest contribution to the occupied low energy level H-2 (70%) and unoccupied higher energy level L+3 (26%). The two *N atoms in bdmpzm contribute to different energy levels where *N12 contributes to H-5 (50%) and L+3 (26) and *N14 contributes to H-4 (53%) and L-5 (53%).

4.3.6 The conductive properties of the ligands

The values of η calculated with other computed polarizabilities and hyperpolarizabilities are shown in Table 4.11. In agreement with the relative energies, the most stable isomer is predicted to be the hardest one [345]. However, the molecules having a small energy gap are known as soft and having a large energy gap is known as hard molecules [347].

The NLO properties of the derivatives are enhanced compared to the precursor. The computed properties show that bdmpza is the best NLO materials out of the four ligands because of its lower band gap and higher hyperpolarizabilities. Despite the higher number of H-bonding found in bdmpza, it has the lowest percentage of non-Lewis orbital while bdcpzm have the highest. However, the precursor is

predicted as the most stable based on the highest value of its Γ [345] but not the most reactive because of its higher band gap (very hard) [395]. The NLO properties therefore follow the order of bdmpza < bdmpzm < bdcpzm < dmpz which is also the order obtained for the magnitude of the *N-N J-coupling.

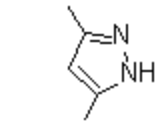

1. dmpz

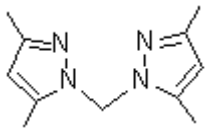

2. bdmpzm

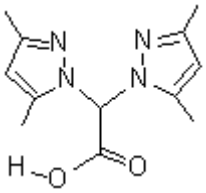

3. bdmpza

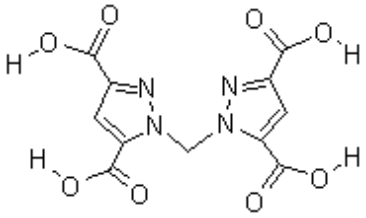

4. bdcpzm

Figure 4.1: The schematic diagram of methylpyrazole (dmpz), bis(dimethylpyrazol-1-yl)methane (bdmpzm), bis(dimethylpyrazol-1-yl)acetic (bdmpza) and bis(diaceticpyrazol-1-yl)methane (bdcpzm).

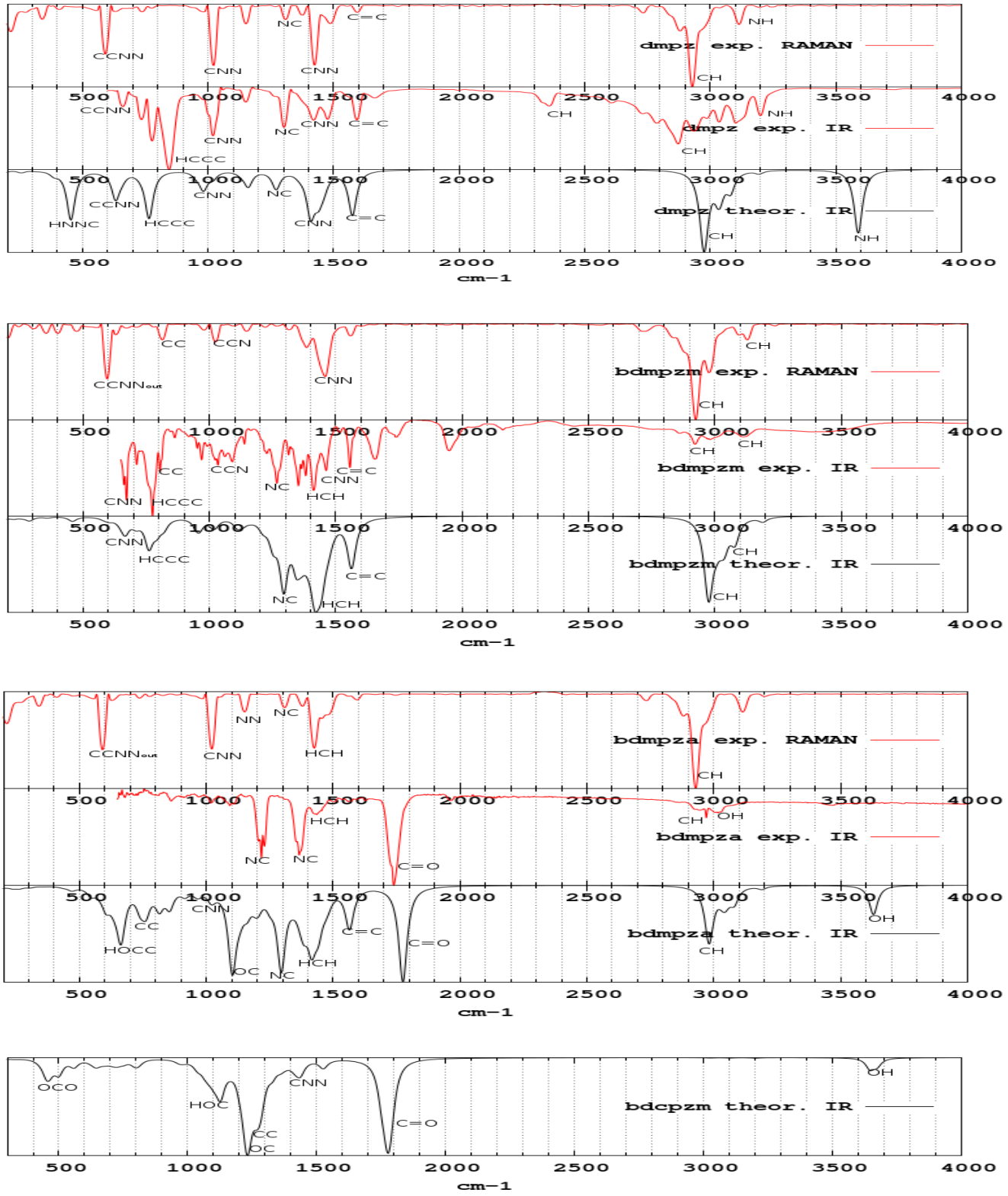

Figure 4.2: The experimental IR and Raman (in red) with the theoretical IR (in black) spectral of the ligands

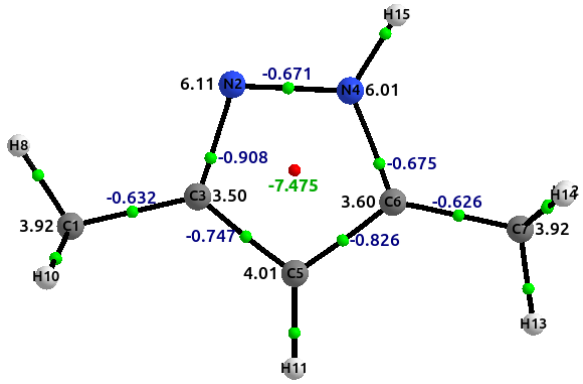

1. dmpz

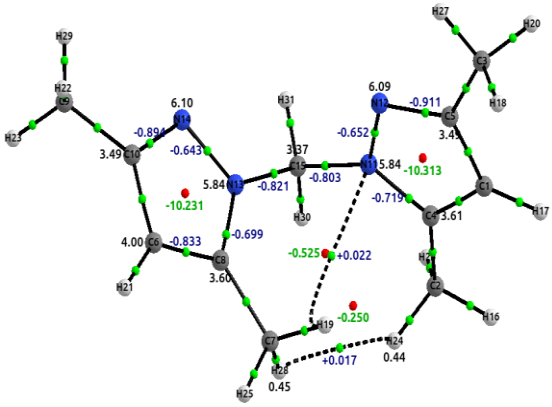

2. bdmpzm

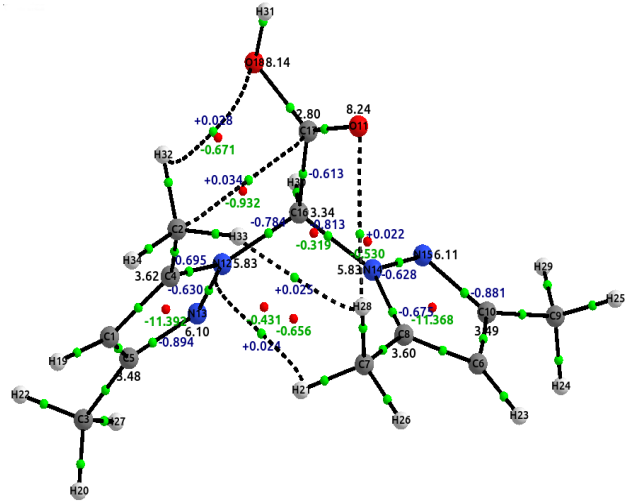

3. bdmpza

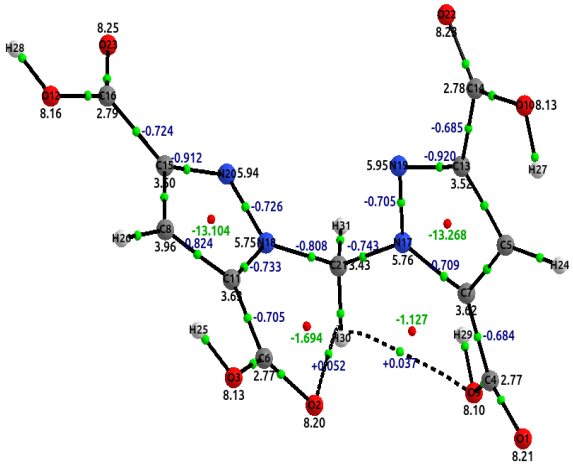

4. bdcpzm

Figure 4.3: The features of the QTAIM properties of the ligands showing the atomic localized electrons, Laplacian of electron density of the bonds and the ring electron density.

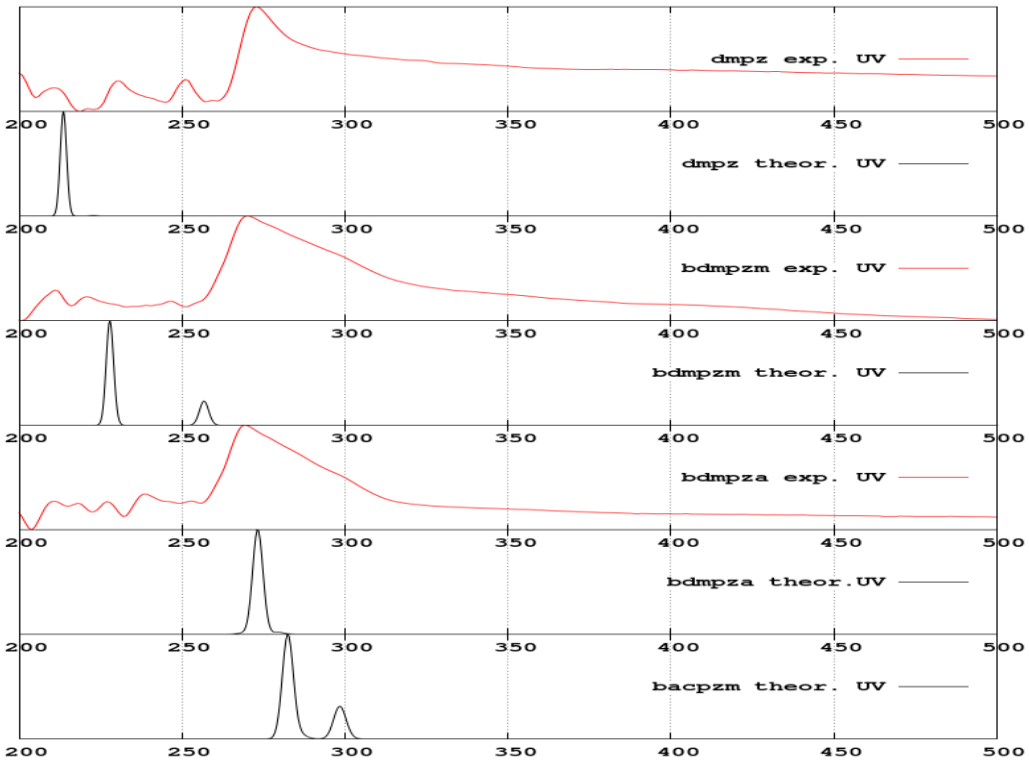

Figure 4.4: The experimental and theoretical UV absorption of the ligands in nm

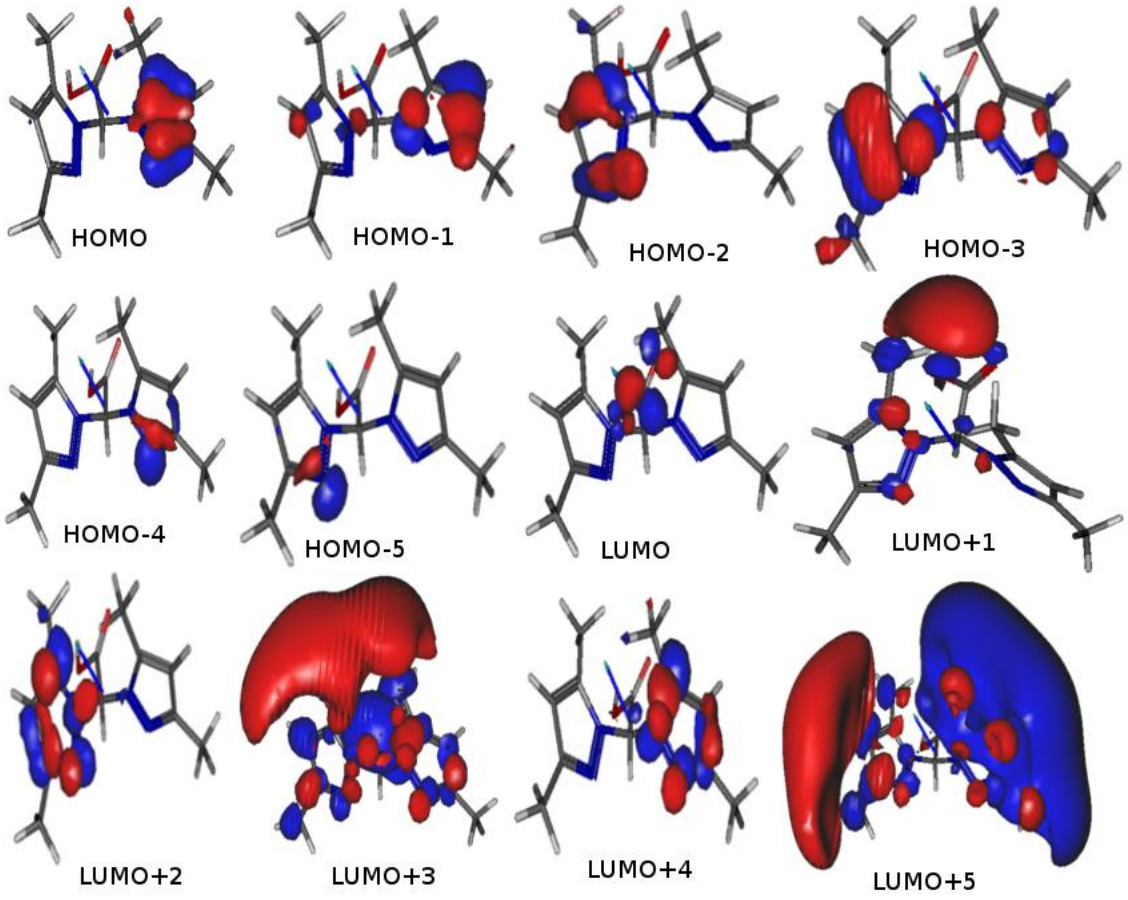

Figure 4.5: Electronic isodensity surface of six levels of HOMO and LUMO of bdmpza

4.4 Synthesis of pyrazole derivatives and their spectroscopic properties

The geometrical structures of the Ru complexes that were studied are shown in Figure 4.6. Comparing the computed geometries of bpza with the reported experimental crystal structure [408] (in bracket), the bond distance N9-C11 is 1.457 (1.468), N10-C11 is 1.457 (1.467), C11-C13 is 1.451(1.554), C13-O12 is 1.222 (1.215), C13-O14 is 1.353 (1.318) and the bond angle N9-C11-N10 is 114.08 (111.82). This shows a very good agreement between the computed geometry and the crystal structure of bpza.

4.4.1 The infra red spectra

The potential energy distribution (PED) contributions are employed for the assignment of the spectra using VEDA [419] as explained in the literatures [420, 421]. The experimental and theoretical IR vibration help to distinguished bpza from the rest of the ligands with a unique vibration at 1720 cm^{-1} (assigned for υ(C=O)) which is very close to the reported 1761 cm^{-1} in the literature [408]. The Raman spectra also distinguishes bpza from bpzm with the a weak vibration at 1720 cm^{-1} (i.e. C=O vibration) and a moderate vibration at 2990 cm^{-1} ascribed to the C-H vibration of the CHCOOH unit of bpza. Peculiar to bpza is the vibration at 3750 cm^{-1} (theoretically found at 3610 cm^{-1}) which is assigned to O-H vibration. The theoretical and experimental IR further distinguished bpza from other ligands with the strong vibration at 1100 cm^{-1} which is assigned to C-O vibration. Another distinguishing feature in the Raman spectra that is peculiar to bpza only is the vibration at 380 cm^{-1} assigned to the CCO which is completely absent in bpzm. The Raman active vibrations are 1400 cm^{-1}(assigned to the vibration of NC and CCN as shown in Table 4.12), the strongest peaks 1150 cm^{-1} (NN vibration) in bpzm and at 1300 cm^{-1} (NC vibration) in bpza. In bpza, there is a strong Raman peak at 1100 cm^{-1} which corresponds to both experimental and theoretical IR vibrations assigned to the stretching vibration of the OC. Also, all

the vibrations found within 500 to 1000 cm^{-1} which are assigned to the vibrations OCO, HOCC, CCN, NC and HCCN as shown in Figure 4.7 and Table 4.12 are not Raman active vibrations. The experimental N-H vibration in pz lies within the broad vibration of C-H but has a very sharp feature which distinguishes pz from bpzm and bpza. The theoretical comparison of bpza with bpzpya shows a red shift in most of the IR vibrations in bpzpya due to the presence of the pyridinic linking unit.

4.4.2 The NMR properties

The experimental protoN-NMR clearly shows that in bpzm and bpza, there is no high shift of 12.81 ascribed to N-H in pz which is an indication that the respective linking units CH_2 and CHCOOH have been successfully introduced into the bidentate ligands. The proton chemical shift at 7.20 in bpza also indicate the presence of carboxylic unit and CHCOO at 7.22 which is very close to the reported value 7.27 in the literature [408]. Most of the proton and carbon chemical shift obtained are very closer to the previously reported shift in the literatures which are shown in bracket in Table 4.13 [418, 408].

The theoretical proton chemical shifts obtained using the two methods are shown in Table 4.14 while that of the carbon chemical shifts are shown in Table 4.15 for each of the ligand. The H-bonding in bpza that involves H19 and H20 results in higher proton shifts compared to other hydrogen atoms in the ligands (Table 4.14).

The experimental protoN-NMR shift of C3-H is found within the range of 7.60 to 7.65, C4-H within 5.89 to 6.37, C5-H within 7.28 to 7.81, CH_2 at 6.41, CHCOO at 7.22, COOH at 7.20, N-H at 12.81. Using the direct method, the protoN-NMR shift of C3-H is found within the range of 7.58 to 7.97, C4-H within 6.34 to 6.67, C5-H within 7.07 to 8.37, CH_2 within 5.83 to 6.51, CHCOO at 7.29, COOH within 6.52 to 7.02, N-H at 9.51 and the H_{py} in bpzpya within 6.89 to 7.93. By making use of the fitting equation, the protoN-NMR shift of C3-H is found within the range of 7.87 to 8.26, C4-H 6.67 to 6.99, C5-H within 7.38 to 8.64, CH_2 within 6.18 to 6.84, CHCOO at 7.59, COOH within 6.85 to

7.34, N-H at 9.75 and the H_{py} in bpzpya within 7.20 to 8.22. It is evidently clear that the two theoretical methods give a perfect correlation with the experimental proton chemical shift but direct method gives values which are much closer to the experimental than the fitting method except for the COOH and N-H where fitting method is closer.

The experimental ^{13}C-NMR shift of C_{pz} is found within the range of 104.67 to 133.85, CH_2 at 77.00, **C**HCOO at 74.18 and **C**OOH at 140.94. Using the direct method, the ^{13}C-NMR shift of C_{pz} is found within the range of 101.65 to 140.64, **C**H_2 at 68.41, CHCOO at 76.49, **C**OOH within 160.13 to 166.09 and C_{py} in bpzpya within 101.05 to 152.00. Using the direct method, the ^{13}C-NMR shift of C_{pz} is found within the range of 89.54 to 127.09, **C**H_2 at 57.53, **C**HCOO at 65.31, **C**OOH within 145.86 to 151.60 and C_{py} in bpzpya within 88.96 to 138.02. There is a perfect correlation also between the experimental and computed ^{13}C-NMR shift. The direct method equally gives values close to the experimental than fitting method except for the COOH where the fitting method performed better.

4.4.3 The nuclear spin-spin coupling

The Ramsey terms are considered for the bonding *N-N and none bonding *N-*N where *N is the nitrogen available for metal coordination and N is the one not available for metal coordination (Table 4.16). The J-coupling of the *N-N bonds are stronger in the derivatives than the precursor pz and the two bonds in bpza have the highest values. The J coupling between the two *N atoms of the pyrazole unit in bpza is higher than what is found in bpzm and bpzpya. However considering the J-coupling of the *N atoms with the N_{py} of the pyridinic unit (*N-N_{py}) in bpzpya, the value is significantly higher than what is found in *N-*N coupling. It is interesting to observe in bpza a kind of symmetry in the properties of the two *N-N bonds which is not observed in the bpzm and bpzpya.

4.4.4 The bond properties

The bond properties of the *N-N are presented in Table 4.17. There is a gradual increase in the *N-N bonds from the precursor pz to the derivatives (GBL_I) which consequentially results to a weaker nature of these bonds in derivatives indicated with a lower Laplacian values of their electrons ($\nabla^2\rho(r)$). Generally, the features of *N-N in the ligands show that as the bond length increases from the pz to bpzpya, there in a corresponding decrease in electron density, strength of the bonds in term of the values of the Laplacian of electrons ($\nabla^2\rho(r)$) and the magnitude of the ratio of potential energy and Lagrangian kinetic energy (|V/G|). Only bpza have two intramolecular H-bonding while other ligands have none. The two H-bonding are also found to have NMR J-coupling of -2.58E-001 which is stronger than what is observed for the *N-*N coupling (Table 4.16).

4.4.5 The intra- and inter-atomic properties

There is also a unique pattern of the symmetrical features in both intra- and inter-atomic properties of the two *N atoms in bpza when compared to other ligands (Table 4.18). Comparing the *N with the N atoms in all the ligands, the *N atoms are characterised with lower atomic charge (q(A)), bonding magnetizability ($\chi_{bond\_Iso}(A)$), total magnetizability ($\chi_{Iso}(A)$), bond isotropic shielding tensor ($\sigma_{Iso}(A',A)$) (except in bpzpya) and lower energy level. These *N atoms are also characterised with higher magnitude of intraatomic dipole of an atom ($\mu_{intra}(A)$), bonding dipole of an atom ($\mu_{bond}(A)$), total atomic dipole ($\mu(A)$), atomic volume (Vol(A)), intraatomic isotropic shielding tensor ($\sigma_{Iso}(A,A)$), total shielding tensor of an atom ($\sigma_{Iso}(A)$) (except in pz), electron occupation and also have an extremely higher anisotropic values. The number of the localized electron on the *N is higher than that of the N atoms (Figure 4.8). A lower energy level of the *N atoms and their higher charges, $\mu_{bond}(A)$, $\chi_{Intra\_Iso}(A)$, $\sigma_{Iso}(A,A)$ and $\sigma_{Iso}(A)$ can be responsible for observed bond strength in the order bpzpya >

bpza > bpzm > pz. Also the total molecular dipole properties (μ_{intra}(A), μ_{bond}(A), μ(A)) follow the order bpzpya > bpza > bpzm > pz.

4.4.6 The Excitation properties

The experimental λmax is found at 211.00, 275.00 and 275.00 for pz, bpzm and bpza respectively. The theoretical is found at 205.26, 214.20, 248.42 and 338.64 for pz, bpzm, bpza and bpzpya respectively (Figure 4.9 and Table 4.19). There is a blue shift in both the experimental and theoretical UV from pz to bpza. A much more blue shift is observed in the theoretical study of bpzpya. The theoretical λmax for the ligands are underestimated compared to the experimental. Considering the theoretical λmax in relation to the experimental λmax, the type of the transitions is predicted as shown in Table 4.19. The experimental absorptions at 211.00, 275.00 and 275.00 are as a result of the predominant nature of HOMO-1→LUMO+1, HOMO-1→LUMO and HOMO-2→LUMO respectively for pz, bpzm and bpza.

Comparing energy level contribution of the coordinating point *N in pz with N, it contributes significantly to the HOMO than N and contributes 77% of the electrons occupying HOMO-2 energy level when compared to other atoms in the ligand. Interestingly, in all other ligands except in bpzpya, at least one of the *N atom makes significant contribution to the HOMO energy level. Also, comparing the two coordinating centre of *N atoms in bpzm and bpza as bidentate and three in bpzpya as tridentate, there are different contribution to the molecular energy levels (Table 4.20). The contributions of the *N atoms in bpzm, bpza and bpzpya are very similar. Their highest contribution are found at HOMO-4 and HOMO-5 where the two in bpzm contributes 73% in both energy levels, the two in bpza contribute 37% and 39% respectively, while the three in bpzpy contribute 36 to HOMO-4 and 28 and 47 to HOMO-5 (Table 4.20). The electronic isodensity surface of bpzm is shown in Figure 4.10. The isodensity feature of the HOMO-4 and HOMO-5 shows that the coordinating *N atoms dominate the

surface. It is interesting to also point out that one of the two pyrazole units in bpzm dominates the HOMO while the second dominate the LUMO (Figure 4.10). The variation in the properties of the *N atoms in both bidentate (bpzm and bpza) and tridentate (bpzpya) indicates the possibility of differences in the affinity for metal coordination of the *N atoms within a ligand.

4.4.7 The electrical properties

In agreement with literature [345], the most stable ligand (i.e. pz) is also the hardest ligand characterised with the highest magnitude of Γ and η. However, the most stable are less valuable material in terms of the NLO properties based on its lower hyperpolarizability (ß). The possible application of the ligands as NLO material is in order of bpzpya > bpza > bpzm >pz according to the values of their hyperpolarizability (Table 4.21). The order of their band gap and $\Sigma_i<\alpha>_i$ also agree with the order of their hyperpolarizability. It is interesting to point out that the tridentate bpzpya is more stable in terms of higher magnitude of Γ than bpza and bpzm and yet is better NLO material in terms of the higher ß and lower band gap.

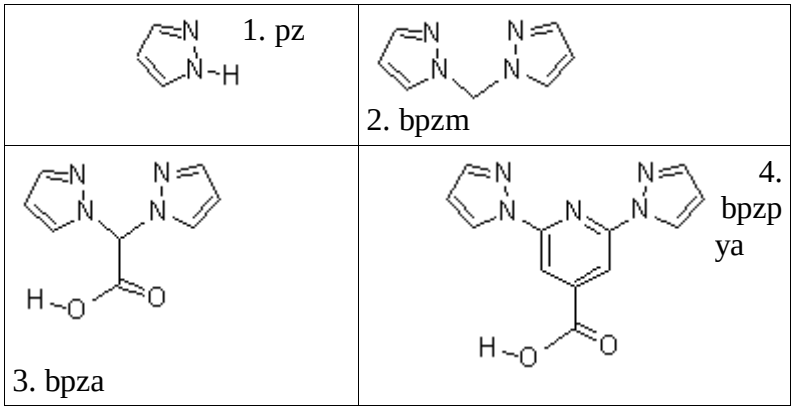

Figure 4.6: The schematic diagram of pyrazole (pz), bis(pyrazol-1-yl)methane (bpzm), bis(pyrazol-1-yl)acetic (bpza) and bis(pyrazol-1-yl)pyridinic (bpzpya).

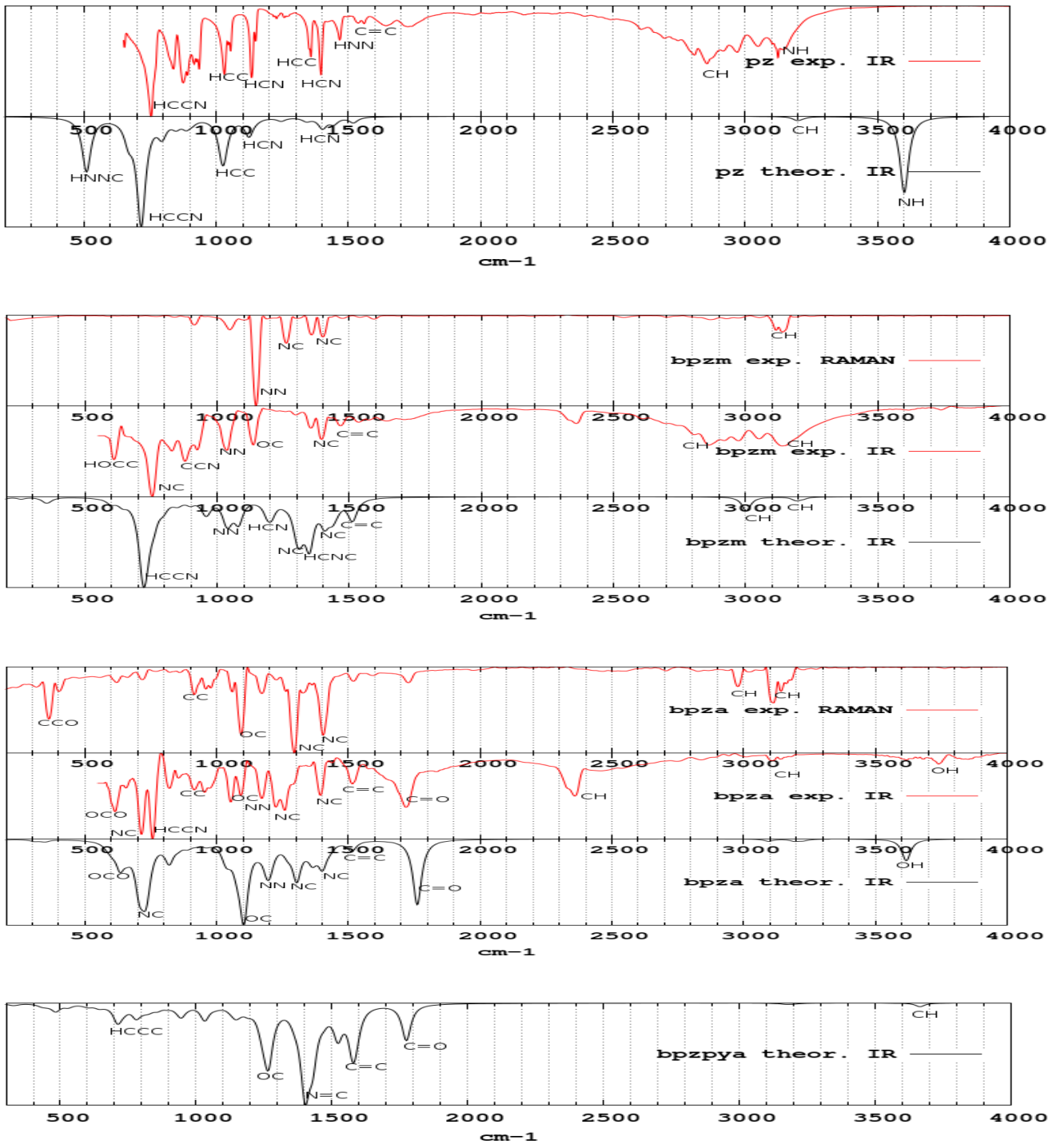

Figure 4.7: The experimental IR and Raman (in red) with the theoretical IR (in black) spectral of the ligands

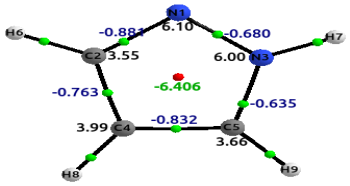

1. pz

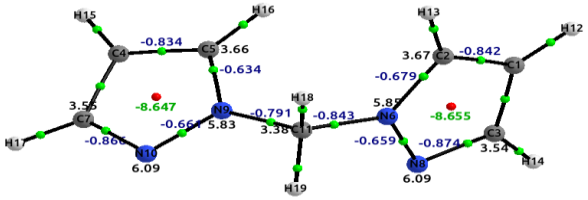

2. bpzm

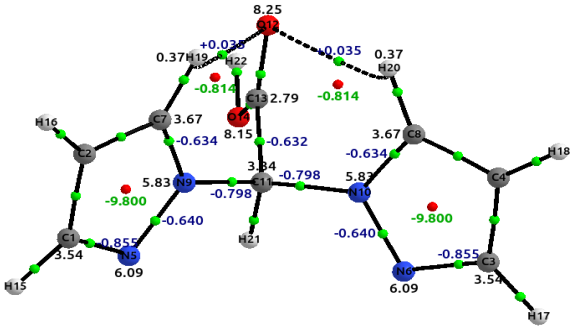

3. bpza

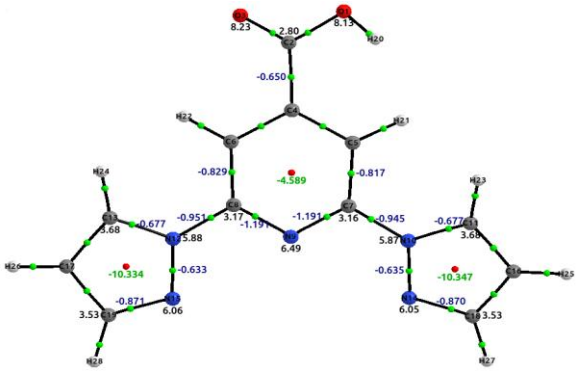

4. bpzpya

Figure 4.8: The features of the QTAIM properties of the ligands showing the atomic localized electrons, Laplacian of electron density of the bonds and the ring electron density.

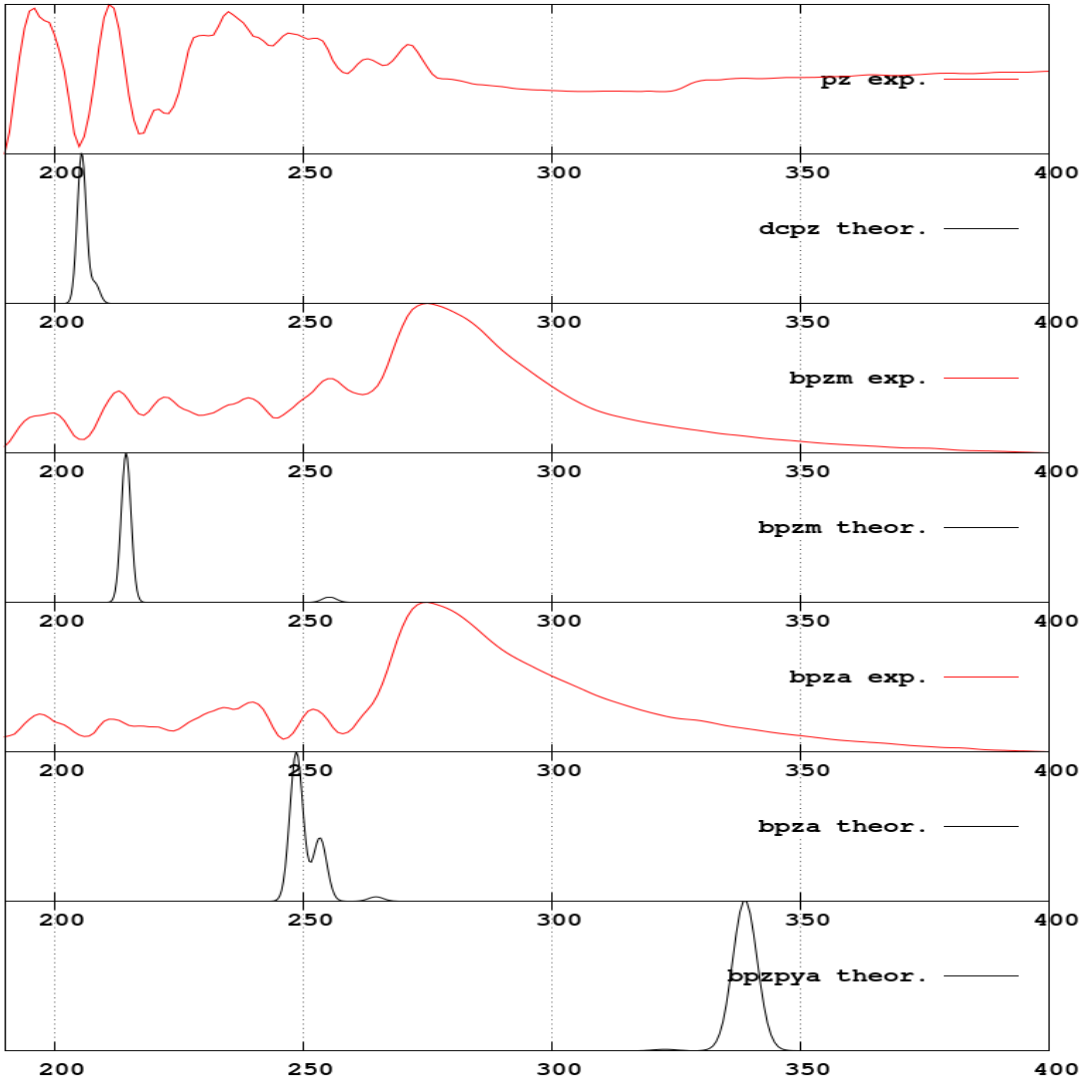

Figure 4.9: The experimental and theoretical UV absorption of the ligands in nm.

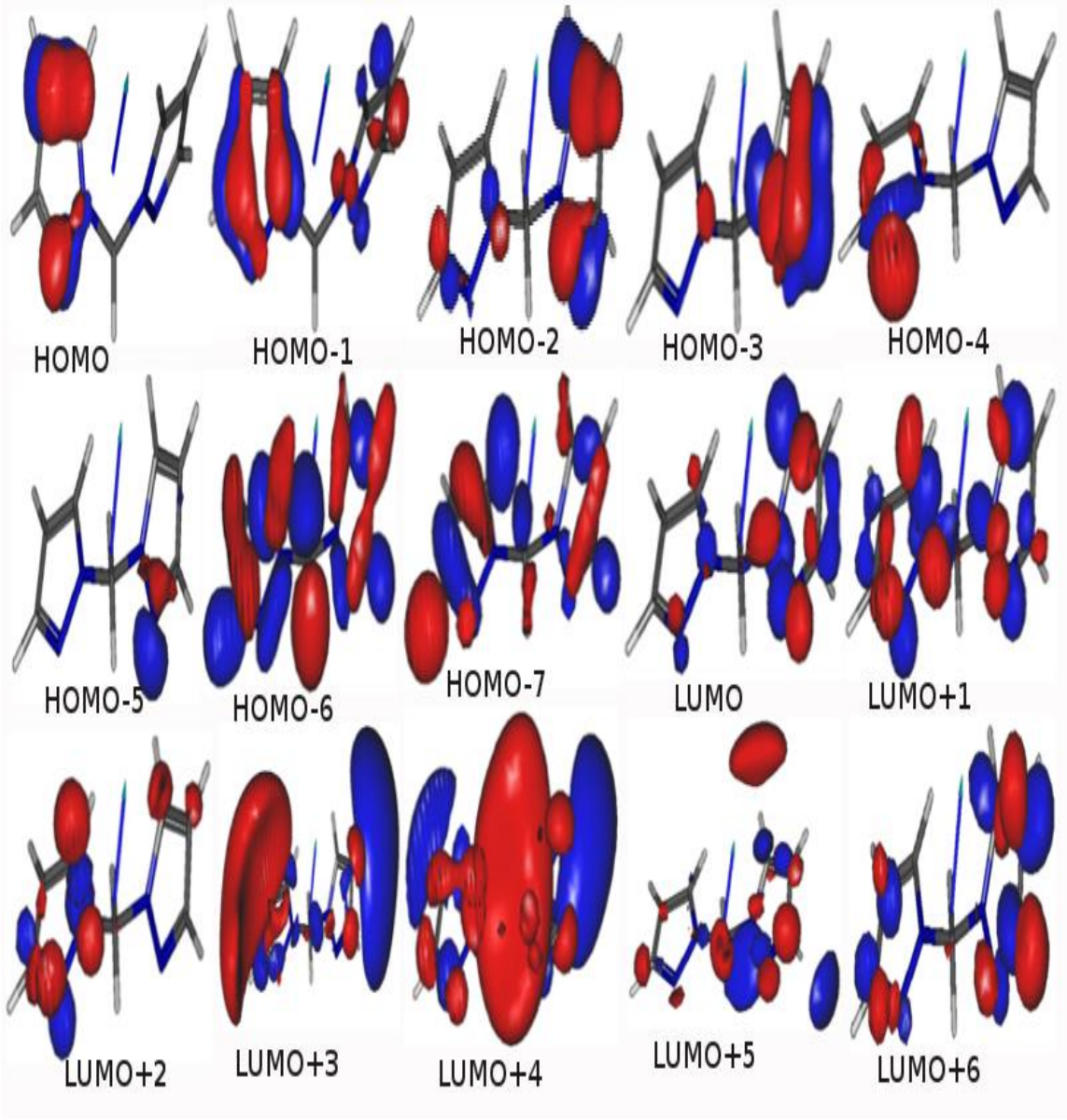

Figure 4.10: Electronic isodensity surface of six levels of HOMO and LUMO of bpzm

4.5 The substituent effects on the spectroscopic and electronic properties of pyrazole derivatives using experimental and computational approaches

4.5.1 The IR and Raman spectra

The experimental and theoretical IR spectra of the ligands (Figure 4.11) are shown in Figure 4.12. The spectra of the ligands are assigned as shown in Table 4.22 using the method of the potential energy distribution (PED) contributions as implemented in package VEDA [419] and explained in the literatures [420, 421]. Besides the OH and NH vibrations which are theoretically overestimated, there is a very strong correlation betweeen the theoretical and the experimental spectra (Figure 4.12) which help to establish the successful synthesis of the ligands. Starting from the ligands dcpz, there is an evidence of successful oxidation of the methyl group of the 3,5-dimethylpyrazole with the presence of C=O vibration at 1750 cm^{-1}. In bphpza, the distinguishing features theoretically and experimentally is the C=O vibration at 1750 cm^{-1} which is observed to be Raman inactive. In the presence of the C=O vibration in ligands like dcpz, bphpza and bdcpzpy, the C=C vibrations around 1600 cm^{-1} remain invisible in the experimental and theoretical IR but very strong in the experimental Raman spectra. Other vibrations in the ligands bphpza, bpzpy and bdmpzpy which were found to be Raman active are CH, HCC, CC, NC, NN, CCN, $CCNC_{out}$ and CCC as shown in Figure 4.12 for the ligands bphpza, bpzpy and bdmpzpy. A distingushing feature of the tridentate bpzpy and bdmpzpy from bidentate bphpza is the experimental Raman vibration within 270 to 300 cm^{-1} which are assigned to the CCN and $CCNC_{out}$ respectively. In both theoretical and experimental IR, the C-H vibration around 3100 cm^{-1} is very weak in bpzpy.

4.5.2 The 13C-NMR shift

There is a perfect correlation between the ^{13}C-NMR shifts obtained from the experimental

(Table 4.23) and from the two theoretical methods (Table 4.24). In the ligand bdmpzpy, the experimental carbon shift of CH_3 ranges from 13.72 to 14.89, direct methods gives a range of 15.11 to 15.49 while fitting method gives 6.20 to 6.57. The experimental ranges of ^{13}C-NMR shift of C4 are 105.04 to 109.79, C5 is 125.19 to 138.99 and C3 is 132.23 to 140.79. The theoretical direct method gives 101.91 to 105.71 for C4, 122.80 to 136.64 for C5 and 139.60 to 151.20 for C3 while the fitting method gives the ranges 89.79 to 93.45, 109.91 to 123.24 and 126.08 to 137.20 respectively for same set of carbon shifts. In many of the ^{13}C-NMR shifts, the direct method gives better values within the experimental ranges than the fitting method.

The order of the chemical shift of C4 within the ligands is phpz < dphpzm < dphpza < dcpz < bpzpy < bdmpzpy < bdcpzpy. The order of ^{13}C-NMR shift in tridentate ligands bpzpy, bdmpzpy and bdcpzpy which are made up of two pz and one pyr units are C4 < $C_{py\text{-}meta}$ < C5 < $C_{pyr\text{-}para}$ < C3 < $C_{pyr\text{-}ortho}$ except in bdmpzpy where $C_{pyr\text{-}para}$ of pyr is lower than C5 of pz. The order in the two bidnetate bphpzm and bphpza with phenyl (ph) and two pyrazole (pz) units is CH_2 < **C**HCOOH < C4 < $C_{ph\text{-}ortho}$ < $C_{ph\text{-}para}$ < $C_{ph\text{-}meta}$ < C5 < C_{ph} < C3 < CH**C**OOH. When considering all the carbon atoms across the seven ligands, CH_3 has the lowest chemical shift while CH**C**OOH has the highest.

4.5.3 The ^{1}H-NMR shift

There is very high correlation between the experimental (Table 4.25) and theoretical (Table 4.26) proton shifts. The theoretical direct method gives a range of 2.07 to 2.52 for the proton shift of CH_3, the fitting gives the range 2.53 to 2.96 while the experimental values obtained is within 2.317 to 2.673 for ligand bdmpzpy. The direct method shift for the COOH unit of bphpza is 6.56, the fitting method gives 6.89 while the experimental is 6.452. The order of the proton shift does not directly follow the order of the corresponding carbon atoms. Considering the level of proton across the ligands, the lowest shift is observed in CH_3 of bdmpzpy followed by those from CH_2 linking unit. The proton shift in the bidentate bphpzm and bphpza follows the order CH_2 < COOH < C4-H < CHCOO < $C_{ph\text{-}para}$-

H < $C_{ph\text{-}meta}$-H < $^{f}C_{ph\text{-}ortho}$-H < C5-H < $^{c}C_{ph\text{-}ortho}$-H except for C5-H that is lower than $C_{ph\text{-}para}$-H and C5-H' lower than $C_{ph\text{-}ortho}$-H in bphpzm (the superscript "c" and "f" on $C_{ph\text{-}ortho}$ mean close to and far from the nitrogen which is the coordination centre of the pyrazole). In tridentates bpzpy, bdmpzpy and bdcpzpy, the proton shift follow the order CH_3 < COOH < C4-H < $C_{pyr\text{-}meta}$-H < $C_{pyr\text{-}para}$-H < C5-H < C3-H except in bdcpzpy where the $C_{pyr\text{-}para}$-H is lower than one of the $C_{pyr\text{-}meta}$-H that is closed to the coordinating centre nitrogen atom due to twisting of one of the pyrazole units (Figure 4.13).

4.5.4 The ^{15}N-NMR shift

The nitrogen shift of the nitrogen atom that is not available for metal coordination (N) is far higher than that of the coordinating centre that is available for metal coordination (*N) as shown in Table 4.27 which indicates that the N are more shielded than the *N atoms. In the tridentate, which contain an extra coordinating centre on pyridine, the nitrogen shift of the coordinating centre on pyridine (^{pyr}N) is higher than the other two in pyrazole units. The two *N coordination centre on two pz units of bidentate and tridentate ligands have equal shift only bpzpy and bdmpzpy but different shift in other ligands with the highest difference observed in bdcpzpy. The *N atom of the pz units in bdcpzpy with the higher shift from the reference is the one that face the pyridine nitrogen while the one twisted away is lower. Across the ligands, the nitrogen shift of *N atoms is in the order of bdcpzpy < dcpz < bpzpy < bdmpzpy < bphpza < bphpzm < phpz. This order shows that carboxylic and pyridine units have significant de-shielding effect on the *N atoms of the pyrazole units.

4.5.5 The nuclear spin-spin coupling

In all the ligands, the FC is the most significant Ramsey term that determines the J-coupling of the *N-N bonds. The two *N-N bonds in the bidentate ligands bphpzm and bphpza have significantly different Ramsey terms and J-coupling compared to those in tridentates bpzpy, bmpzpy, bdcpzpy (Table 4.28). The FC and J-coupling of *N-N in the ligands are in the order of bpzpy > bdmpzpy > bphpza >

bphpzm > bdcpzpy > phpz > dcpz if the highest value is considered in each ligand. The H-bonding N···C interactions in bdcpzpy have J-coupling of -1.41E-001 while O···H H-bonding in bphpza have the J-coupling of -2.18E-001 which are higher in magnitude than the non-bonding *N-*N J-coupling. The corresponding strength of interactions of the three H-bonding in the bdcpzpy and bphpza are predicted to be 0.051 and 0.038 from the QTAIM properties (Figure 4.13 and Table 4.29). The J-coupling and the corresponding strength of H-bonding interactions are not in the same order.

4.5.6 The bond and atomic properties

The geometrical features with the strength of selected bonds and the amount of localized electrons on the selected atoms which are obtained through QTAIM analysis are shown in Figure 4.13. The strength of the *N-N bonds of the pyrazole unit in the ligands is in the order of dcpz > bdcpzpy > phpz > bphpzm > bphpza > bpzpy > bdmpzpy (Figure 4.13 and Table 4.29). The stronger *N-N bonds are also associated with shorter bond distance (GBL_I), bond stretch (BPL – GBL_I) and higher electron density ($\rho(r)$) as shown in Table 4.29. Considering the Laplacian of the electron density on the pyrazole ring in the ligands, the order is bdcpzpy > bphpza > bphpzm > bdmpzpy > bpzpy > dcpz > phpz. One intramolecular H-bonding is found in both bdcpzpy and bphpza while others have none. The strength of the H-bonding ranges from 0.038 to 0.051 which is within the suggested range of H-bonding in the literature [382].

Generally, the coordinating centre *N atoms are distinguished from the other N atom with the characteristic features of higher magnitude of intraatomic dipole ($\mu_{intra}(A)$), bonding dipole ($\mu_{bond}(A)$), total dipole ($\mu(A)$), atomic volume (Vol(A)), intraatomic magnetizability ($\chi_{Intra\_Iso}(A)$), intraatomic shielding tensor ($\sigma_{Iso}(A,A)$), total isotropic shielding tensor ($\sigma_{Iso}(A)$), anisotropy, total electron occupation (Occ) but lower atomic charge q(A), bonding magnetizability ($\chi_{bond\_Iso}(A)$), total magnetizability ($\chi_{Iso}(A)$), bonding shielding tensor ($\sigma_{Iso}(A',A)$), energy level (Table 4.30). The sum total of the computed atomic QTAIM properties over all the atoms in each of the ligands shows that

bdcpzpy and bphpza are having the highest dipole properties (μ_{intra}(A), μ_{bond}(A) and μ(A)) while phpz have the lowest (Table 4.30).

4.5.7 The electronic spectral

The experimental and theoretical UV absorption for the ligands are shown in Figure 4.14. A very broad experimental absorption was observed for bpzpy but found theoretically to be two distinct peaks (at 283.79 and 327.49 nm) of almost the same strength within the range of the broad experimental spectra. Experimentally, we observed a bathocromic (blue) shift from bphpza to bpzpy but red shift from bpzpy to bdmpzpy. In the theoretical absorption, there is a blue shift in the λmax in the order of bdmpzpy > bphpza> bdcpzpy >bpzpy > bphpzm > phpz > dcpz. The experimental λmax observed for dcpz, bphpza, bpzpy and bdmpzpy at 276.00, 286.00, 308.00 and 288.00 nm respectively can be ascribed to the theoretical λmax at 257.58, 299.56, 283.79 and 331.82 nm (Table 4.31). These experimental λmax absorption are found to be dominated with H-2→LUMO, HOMO→L+1, HOMO→L+1 and HOMO→LUMO for the bphpza, bpzpy and bdmpzpy respectively (Table 4.31). Also, in ligand phpz, bphpzm and bdcpzpy which are considered only theoretically, the λmax absorption are predominately HOMO→LUMO, H-1→LUMO and HOMO→L+1 respectively.

The level of the contribution of the *N atoms to the energy level are also considered for each of the ligands (Table 4.32). The *N atoms contributes significantly to the HOMO levels than the N atoms. Most of the orbital contributions of the *N atoms are found at the HOMO-4 or HOMO-5 except in ligand bdcpzpy where the highest *N atoms contribution is found at HOMO-1. The features of the high contribution of the *N atoms to HOMO and ^{py}N to the LUMO is shown in Figure 4.15 for ligand bpzpy. It is obvious from Figure 4.15 that the HOMO-5 are predominantly the *N atoms of the pyrazole while the LUMO is predominantly the pyridine unit.

4.5.8 The conductive properties

The conductive properties of the ligands are shown in Table 4.33. The ligand bdmpzpy have the highest molecular dipole moment while bphpza have the lowest. The trend of the conductive properties of the ligands in terms of the hyperpolarizability is bdmpzpy > bpzpy > bphpza > phpz> bdcpzpy > bphpzm > dcpz. It is obvious that the tridentate bdmpzpy and bpzpy have more potential for the application as non-linear optical (NLO) materials than the rest of the ligands. The most stable ligand is phpz which is characterised by the highest magnitude of Γ but it is not the hardest ligand since its η is lower than that of dcpz contrary to the expectation [345].

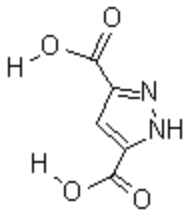

1. dcpz

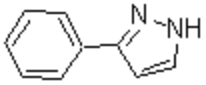

2. phpz

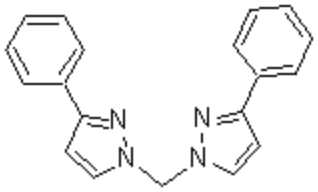

3.bphpzm

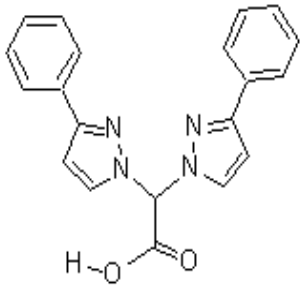

4. bphpza

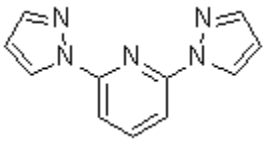

5. bpzpy

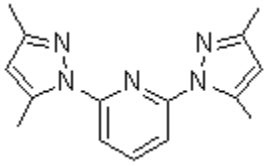

6. bdmpzpy

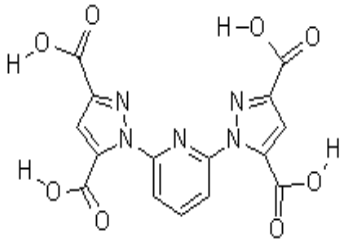

7. bdcpzpy

Figure 4.11: The schematic diagram of 3,5-dicarboxylpyrazole (dcpz), 3-phenylpyrazole (phpz), bis(3-phenylpyrazol-1-yl)methane (bphpzm), bis(3-phenylpyrazol-1-yl)acetic (bphpza), bis(pyrazol-1-yl)pyridine (bpzpy), bis(3,5-dimethylpyrazol-1-yl)pyridine (bdmpzpy), bis(3,5-dicarboxylpyrazol-1-yl)pyridine (bdcpzpy)

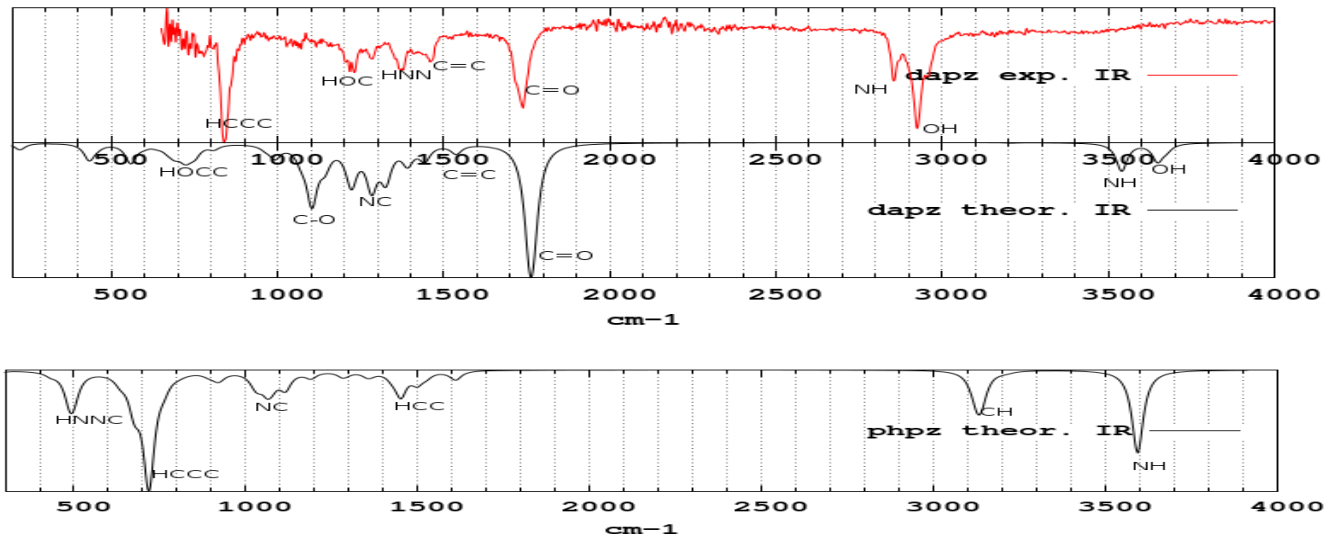

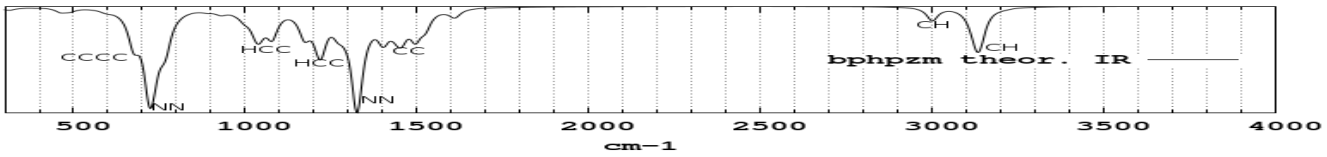
CCCC
NN
HCC
HCC
CC
NN
CH
CH
bphpzm theor. IR
500
1000
1500
2000
2500
3000
3500
4000
cm−1

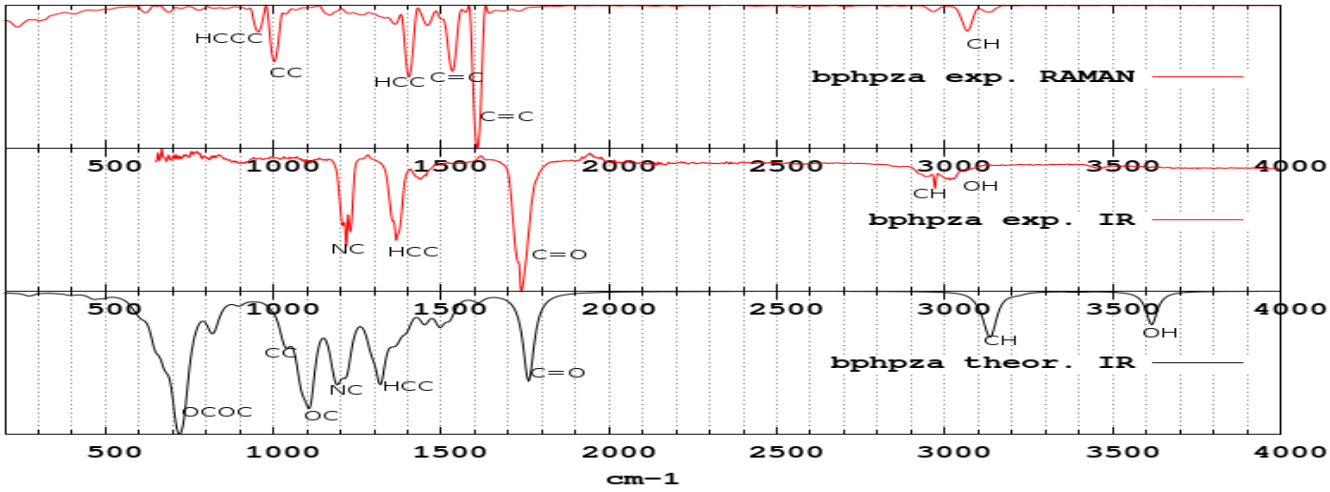
HCCC
CC
HCC
C=C
C=C
CH
bphpza exp. RAMAN
NC
HCC
C=O
CH
OH
bphpza exp. IR
CC
NC
HCC
C=O
OCOC
OC
CH
OH
bphpza theor. IR
500
1000
1500
2000
2500
3000
3500
4000
cm−1

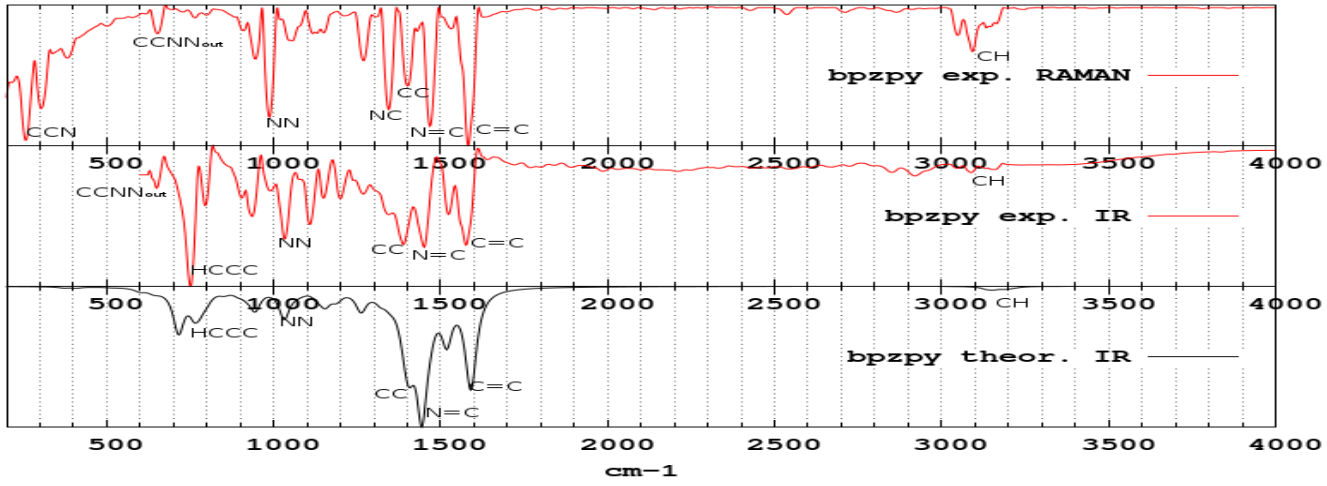
CCNNout
CCN
NN
NC
CC
N=C
C=C
CH
bpzpy exp. RAMAN
CCNNout
NN
CC
N=C
C=C
CH
bpzpy exp. IR
HCCC
HCCC
NN
CC
N=C
C=C
CH
bpzpy theor. IR
500
1000
1500
2000
2500
3000
3500
4000
cm−1

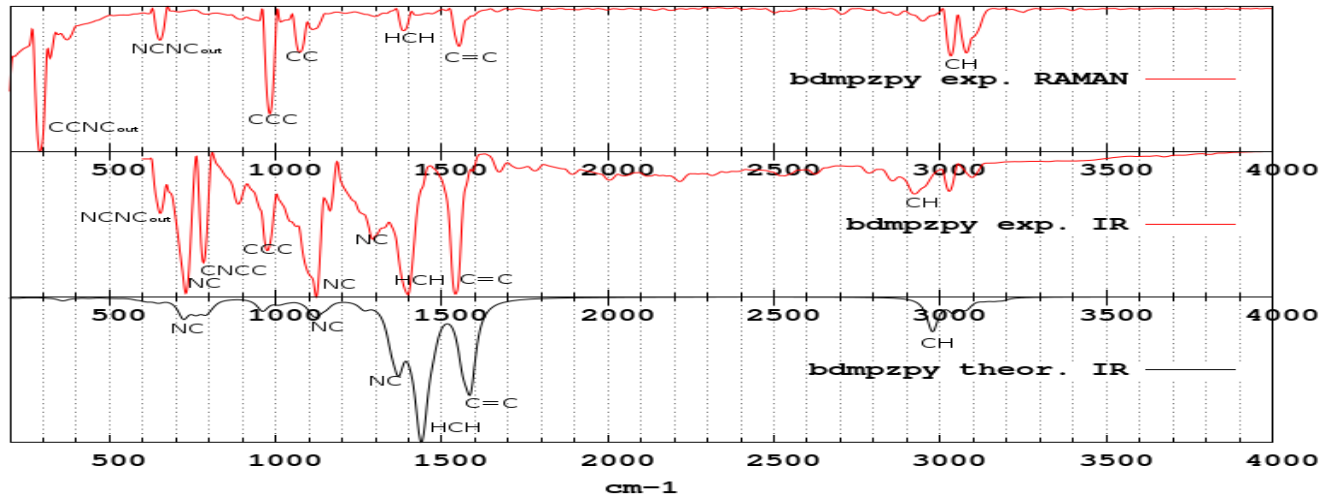
NCNCout
CCNCout
CC
CCC
HCH
C=C
CH
bdmpzpy exp. RAMAN
NCNCout
CCC
CNCC
NC
NC
NC
HCH
C=C
CH
bdmpzpy exp. IR
NC
NC
NC
C=C
HCH
CH
bdmpzpy theor. IR
500
1000
1500
2000
2500
3000
3500
4000
cm−1

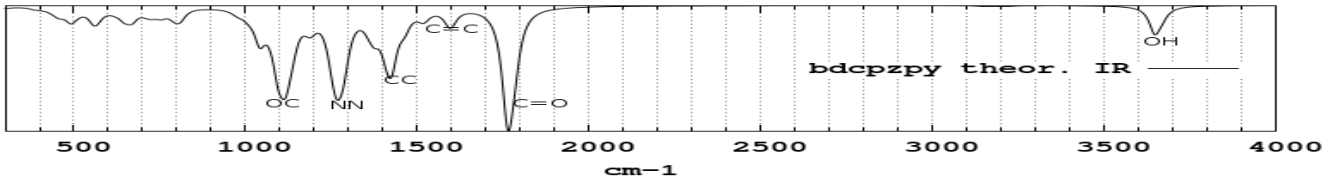

Figure 4.12: The experimental IR and Raman (in red) with the theoretical IR (in black) spectral of the ligands

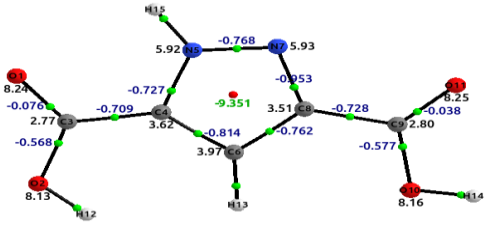

1. dcpz

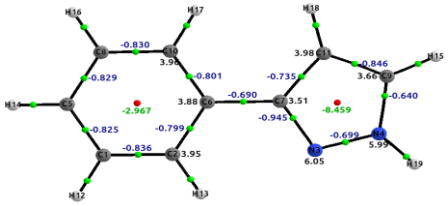

2. phpz

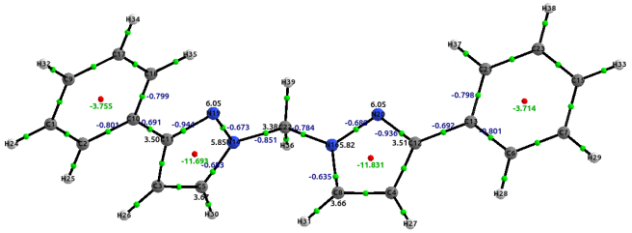

3. bphpzm

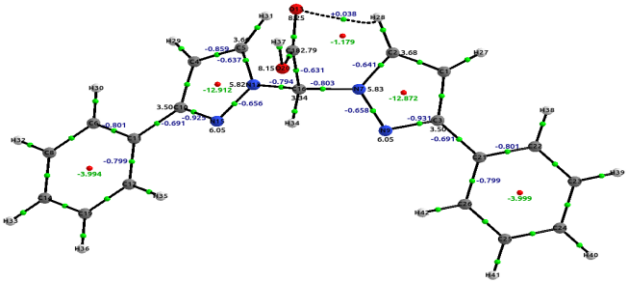

4. bphpza

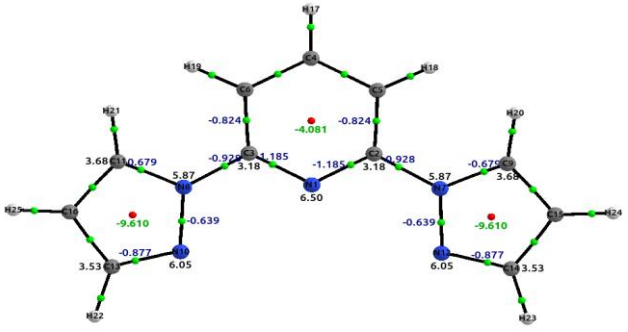

5. bpzpy

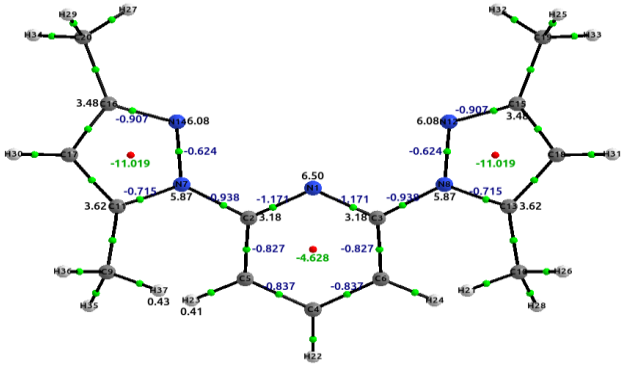

6. bdmpzpy

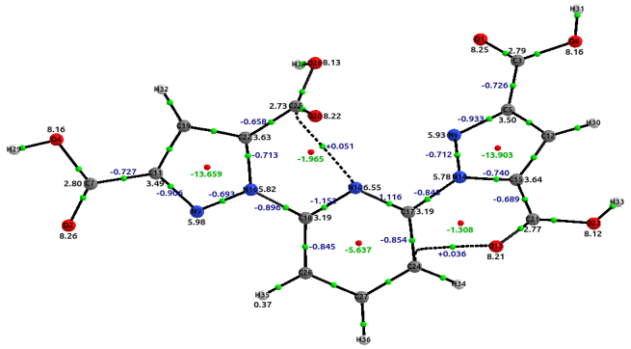

7. bdcpzpy

Figure 4.13: The features of the QTAIM properties of the ligands showing the atomic localized electrons, Laplacian of electron density of the bonds and the ring electron density.

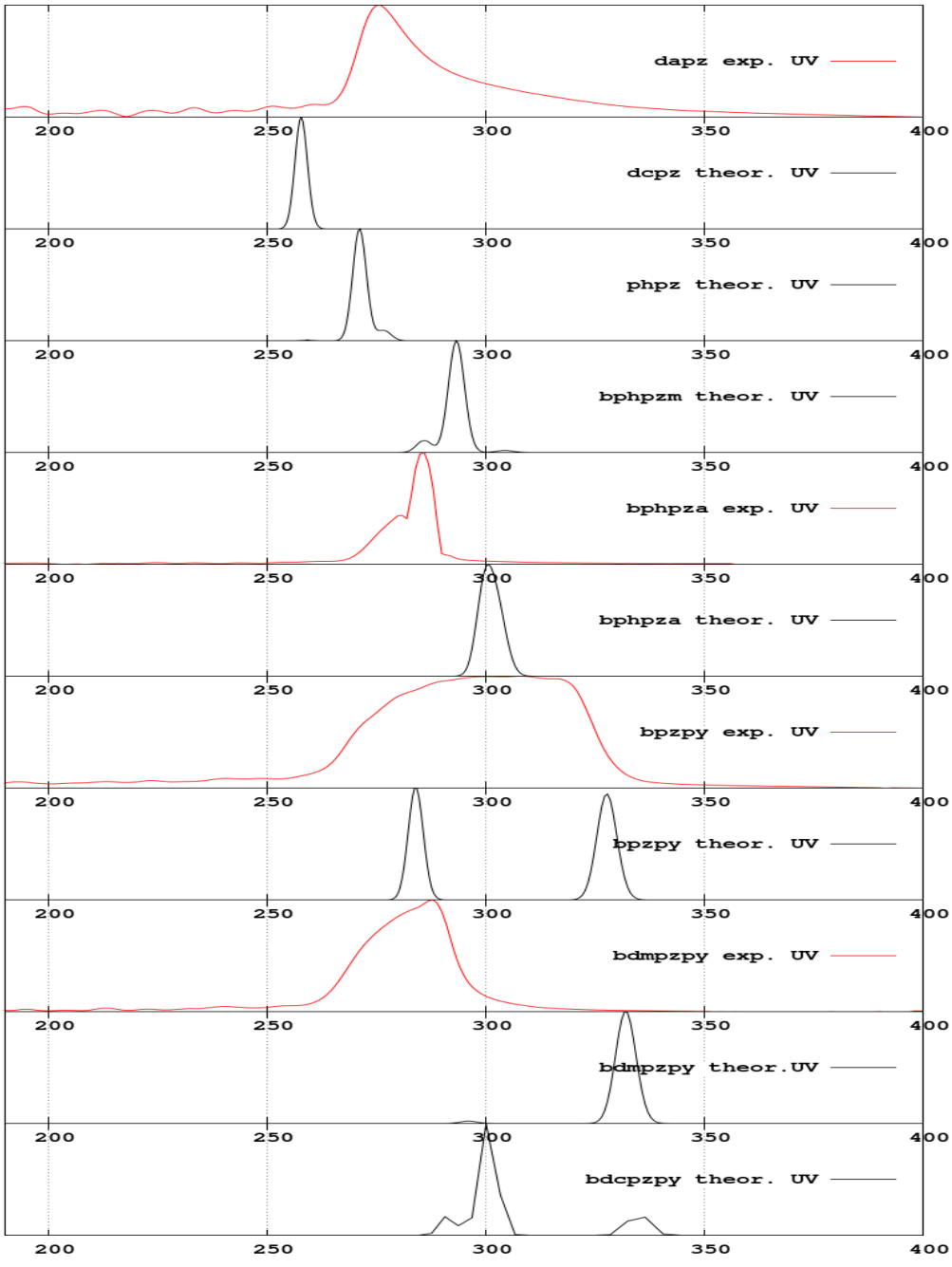

Figure 4.14: The experimental and theoretical UV absorption of the ligands in nm.

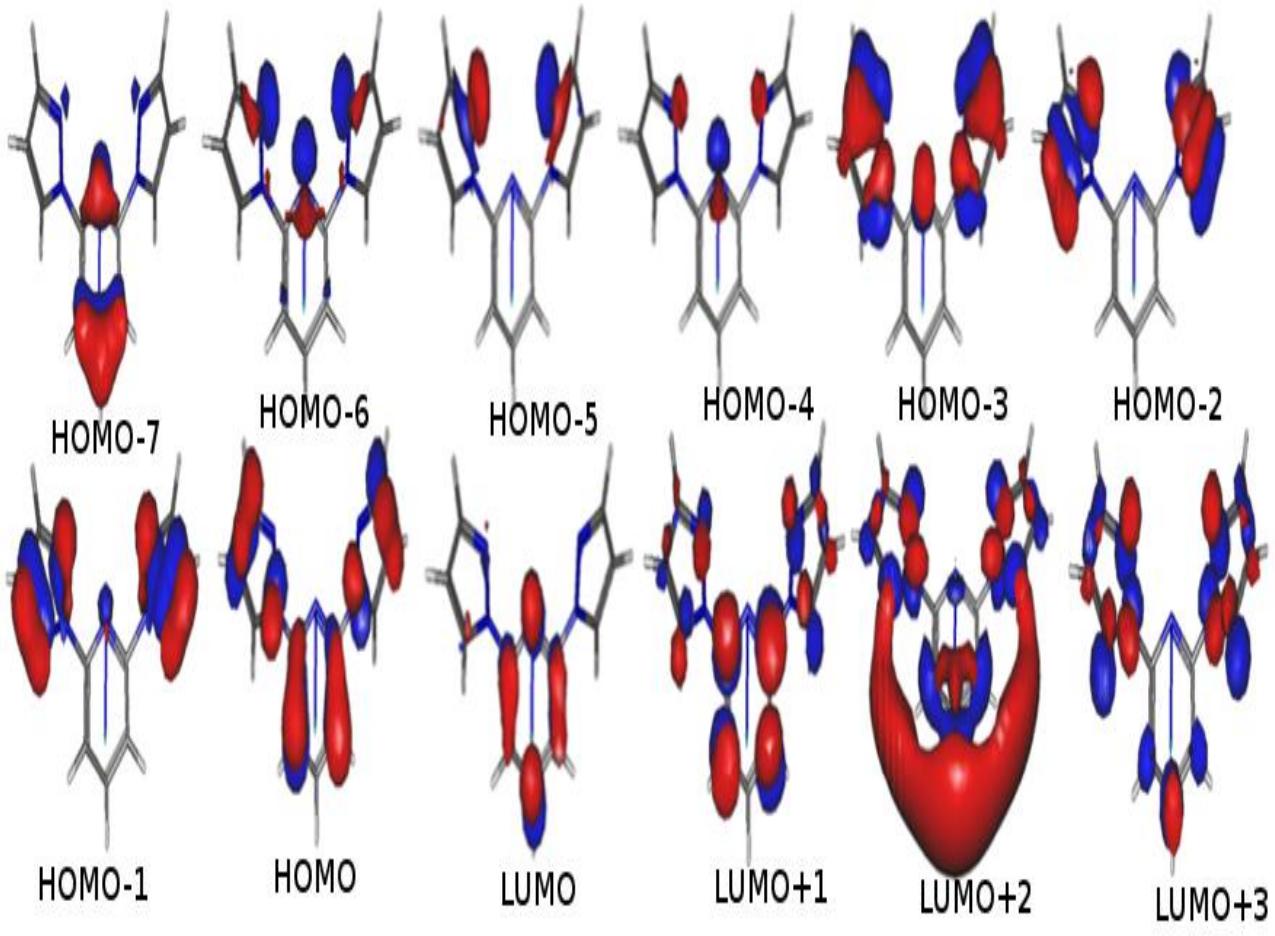

Figure 4.15: Electronic isodensity surface of six levels of HOMO and LUMO of bpzpy

4.6 The spectroscopic and the QTAIM properties of pyridine and phenanthroline derivatives using experimental and computational methods

4.6.1 The IR spectra

The structures of the ligands bpyr, dmbpr, dcbpyr, phn, dmphn and dcphn are shown in Figure 4.16 and their IR spectra in Figure 4.17. The spectra were analyzed in terms of the potential energy distribution (PED) contributions using the package VEDA [419] as explained in the literatures [420, 421]. The best peaks based on the level of the intensity and their corresponding best two vibrations are presented in Table 4.34. The unique difference in the experimental IR of the bpyr and dmbpyr compared to the phn and dmphn is the vibration around 1730 cm^{-1} which is ascribed is still assigned to the C=C vibration. The unique features in all the ligands bpyr, dmbpyr, dcbpyr, phn, dmphn and dcphn is the C=C vibration around 1500 - 1620 cm^{-1} but found experimentally in pyr and dmbpyr around 1730 cm^{-1}. The C-H vibrations in the ligands are found experimentally to be a weak vibration but theoretical found to be strong vibrations. Also, C-H vibrations in pyr derivatives are found experimentally around 3000 while the phn derivatives are found around 3400 cm^{-1}.

4.6.2 The ^{1}H-NMR shift

Both the experimental (Table 4.35) and theoretical ^{1}H-NMR chemical shift of the ligands bmpyr, phn and dmphn (Table 4.36) are in perfect agreement. It is interesting to point out that both experimental and theoretical methods clearly show that the proton chemical shift of CH_3 is higher in dmphn than dmbpyr. Also the range of proton shift on $C_{px\text{-}meta}$-H in dmbpyr, phn and dmphn using the direct method is 7.15 to 7.64 and that of the fitting method is 7.45 to 7.93 which are very close to the experimental range of 7.27 to 7.77. The ^{1}H-NMR chemical shift follows the same trend as observed for the ^{13}C-NMR shift in both bpyr and phn derivatives except for the proton atom of the COOH group which is characterised to have the lowest shift. The order of proton shift in pyr derivatives is CH_3 <

COOH < $C_{pyr\text{-}meta}$-H < $C_{pyr\text{-}para}$-H < $C_{pyr\text{-}ortho}$-H while that of phn derivatives is CH_3 < COOH < $C_{phn\text{-}meta}$-H < C_{base}-H < $C_{phn\text{-}para}$-H < $C_{phn\text{-}ortho}$-H. The little exception to the order of proton chemical shift in phn derivatives is the $C_{phn\text{-}meta}$ in dcphn which is found higher than the C_{base} and $C_{phn\text{-}para}$ due to the presence of carboxylic group on its $C_{phn\text{-}ortho}$.

4.6.3 The ^{15}N-NMR shift

The values of the ^{15}N-NMR chemical shift computed using the direct and the fitting methods are shown in Table 4.37. The experimental nitrogen shift observed for dmbpyr in the literature is -81.60 [344] but the direct method in our calculation gives a lower shift of -64.74 while the fitting method gives a higher shift of -91.24. In another type of dmphn in the literature [344] though the methyl substituent position is completely different, the experimental nitrogen shift is reported to be -76.00 but the direct method gives -68.36 while the fitting method gives -94.67. The direct method gives values lower than the experimental while the fitting gives values higher than the experimental. The order of the nitrogen chemical shift in the six ligands is dmphn > dmbpyr > phn > bpyr > dcphn > dapyr. The implication of this order is that the nitrogen atoms of the phn derivatives are more shielded than those of the pyr derivatives.

4.6.4 The ^{13}C-NMR shift

The theoretical ^{13}C-NMR of the six ligands are shown in Table 4.38. The ^{13}C-NMR chemical shifts in the three bipyridine (bpyr) and three phenanthroline (phn) derivatives follow predictable trends. The carbon atoms around the nitrogen atom in each of the rings in bpyr and phn derivatives will be considered as ortho, meta and para for easy explanation while the last two carbon atoms at the base of phenathroline (i.e. C5 and C6 from conventional numbering) will be referred to as C_{base}. Considering the pyr derivatives, the order of the carbon shift is CH_3 < $C_{pyr\text{-}meta}$ < $C_{pyr\text{-}para}$ < $C_{pyr\text{-}ortho}$ < $^{c}C_{pyr\text{-}ortho}$ < COOH where the superscript "c" represent the ortho carbon that connect the two units of pyridine. A

wide difference is observed between the shifts of $C_{pyr\text{-}ortho}$ and $^{c}C_{pyr\text{-}ortho}$.

The ^{13}C-NMR shift observed in the derivatives of phn is in the order of $CH_3 < C_{phn\text{-}meta} < C_{base} < {}^{c}C_{phn\text{-}meta} < C_{phn\text{-}para} < {}^{c}C_{phn\text{-}ortho} < C_{phn\text{-}ortho} <$ COOH where the superscript "c" on the $C_{phn\text{-}meta}$ and $C_{phn\text{-}ortho}$ indicates the one connected with another ring. The presence of the carboxylic unit on the $C_{phn\text{-}ortho}$ of the dcphn does not make significant change on its chemical shift (145.38 and 145.97) when compared to the parent compound phn (147.21 and 147.22) but the presence of methyl group results in a longer chemical shift of $C_{phn\text{-}ortho}$ (157.20).

It is worth pointing out that the order observed in both bpyr and phn derivatives for the ^{13}C-NMR is in perfect agreement with the experimental order observed for the similar bpyr and phn in the literature [344].

4.6.5 The Ramsey terms and the total nuclear spin-spin coupling

The most significant Ramsey term is the PSO in the six ligands followed by the FC. The values of the PSO and FC of the pyr derivatives are higher than the phn derivatives except in dcphn where FC is a little competitively high as that of pyr derivatives (Table 4.39). The J-coupling of the dcphn is significantly low compared to the remaining ligands. The values of the SD are also very significant compared to the values of the DSO which appear to be the less important in all the C-N bonds. Contrary to the bonding C-N interaction, FC is the most significant Ramsey term in the non-bonding N-N which also determines the total J-coupling. The Ramsey term FC and J-coupling of N-N are lower and positive in values compared to the C-N that are higher and negative. The order of the J-coupling for the C-N bonds is phn > dmphn > dcbpyr > bpyr > dmbpyr > dcphn while that of the N-N bond is dcbpyr > dmbpyr > bpyr > dmphn > phn > dcphn.

4.6.6 The bond and atom QTAIM properties

The Laplacian of the bond and ring electron density with the number of the localized electrons

are shown in Figure 4.18. There is an unusual H-bonding H···H in ligand dcbpyr which has the smallest bcp electron density, yet the value is a clear indication that it is not a van der Waals interaction since it lies within the range proposed for H-bonding interactions [382]. There is a gradual decrease in C-N bond strength from the phn to dmphn and to dcphn. In pyr derivatives, the strongest C-N bond is in dmbpyr while bpyr have the lowest. There is an increase in the Laplacian of the ring electron density from bpyr < dmbpyr < dcbpyr. Likewise in phn derivatives, the Laplacian of the ring electron density also follows the same trend as phn < dmphn < dcphn but little higher than what was found in pyr derivatives.

The details of the QTAIM properties of the two C-N bonds in each of the ligand and the linking C-C bonds are shown Table 4.40 while that of the selected atoms are shown in Table 4.41. In all the ligands, the C-N bond lengths are in a close range of 2.555 to 2.569. Likewise also the electron density ($\rho(r)$) and Laplacian of electron density ($\nabla^2\rho(r)$) of the C-N are in a very close range. Considering the sum total of the computed QTAIM properties over all the atoms in each of the ligand (Table 4.41), the ligands dcbpyr and dcphn with carboxylic unit have the highest magnitude of the sum total of the QTAIM atomic properties except for the $\chi_{bond\_Iso}(A)$, $\sigma_{Iso}(A,A)$, $\sigma_{Iso}(A',A)$ and $\sigma_{Iso}(A)$ where the ligands dmbpyr and dmphn with methyl group are taking the lead. The implication is that the carboxylic units in the ligands result to increase in the dipole and anisotropic properties of the molecules while the methyl group result to increase in the isotropic shielding tensor of the molecules.

4.6.7 The UV absorption

There is a very high correlation between the experimental and theoretical UV absorptions as shown in Figure 4.19. The experimental λmax of ligands bpyr, dmbpyr, phn and dmphn are found at 309.00, 299.00, 307.00 and 310.00 nm while the theoretical are found at 292.28, 286.60, 321.38 and 349.04 nm. It is interesting to point out that both the experimental and theoretical values indicate a red shift in the absorptions of bpyr to dmbpyr but a blue shift from phn to dmphn. The ligands dcbpyr and

dcphn are only considered theoretically are their respective λmax is found at 348.79 and 358.76 nm. The phn derivatives are characterised with broader and higher wavelength of absorption than the pyr derivatives (Figure 4.19). The features of the electronic excitation which define the observed absorptions are shown in Table 4.42 and the contributions of the N atoms to each of the energy levels are shown in Table 4.43.

The experimentally observed λmax for the ligands bpyr, dmbpyr, phn and dmphn are found through the theoretical methods to be predominantly defined with electronic excitations of the type HOMO-2→LUMO, HOMO→LUMO, HOMO-1→LUMO and HOMO→LUMO respectively (Table 4.42). The λmax of ligands dcbpyr and dcphn that were treated only theoretically are found to be predominately HOMO→LUMO and HOMO→LUMO respectively. The features of the electron excitations in the ligands show that most of the significant electron excitations are from either HOMO-2, HOMO-1 or HOMO to the LUMO of the ligands. The nitrogen atoms which served as the coordinating centres on the ligands contributes significantly to the HOMO energy levels of the ligands than the LUMO has shown in Table 4.43. A typical feature of the contributions of the atoms to the different energy levels of the ligand dmbpyr is shown in Figure 4.20. The features of the isodensity surface of the dmbpyr show that the N atoms significantly determine the surface of the HOMO-1 and HOMO-2.

4.6.8 The conductive properties

The order of their non-linear optical properties (NLO) is dcphn > dmphn > dcbpyr > dmbpyr > bpyr > phn. As seen in Table 4.44, the hyperpolarizability tensor of dcphn is far higher than other ligands. Interestingly also, dcphn has the lowest band gap and also appear to be the most stable based on the its high negative value of Γ. Contrary to the expectation, ligand dcphn that is the most stable is not the hardest [345]. In addition, the ligands dcphn and dmphn which are predicted as the best NLO material are also characterised with the highest values of Dipole and polarization

(<α>, Δα1, Δα2, Δα3) except for the properties Δα3 which is low in dmphn.

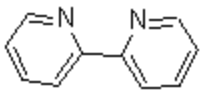 1. bpyr	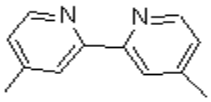 2. dmbpyr	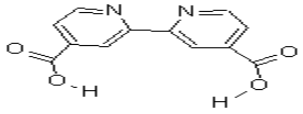 3. dcbpyr
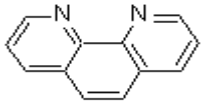 4. phn	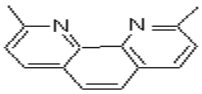 5. dmphn	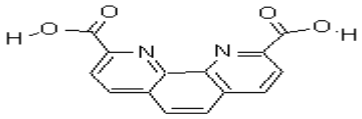 6. dcphn

Figure 4.16: The schematic diagram of 2,2'-bipyridine (bpyr), 4,4'-dimethyl-2,2'-bipyridine (dmbpyr), 4,4'-dicarboxyl-2,2'-bipyridine (dcbpyr), phenanthroline (phn), 2,9-dimethylphenanthroline (dmphn), 2,9-dicarboxylphenanthroline (dcphn)

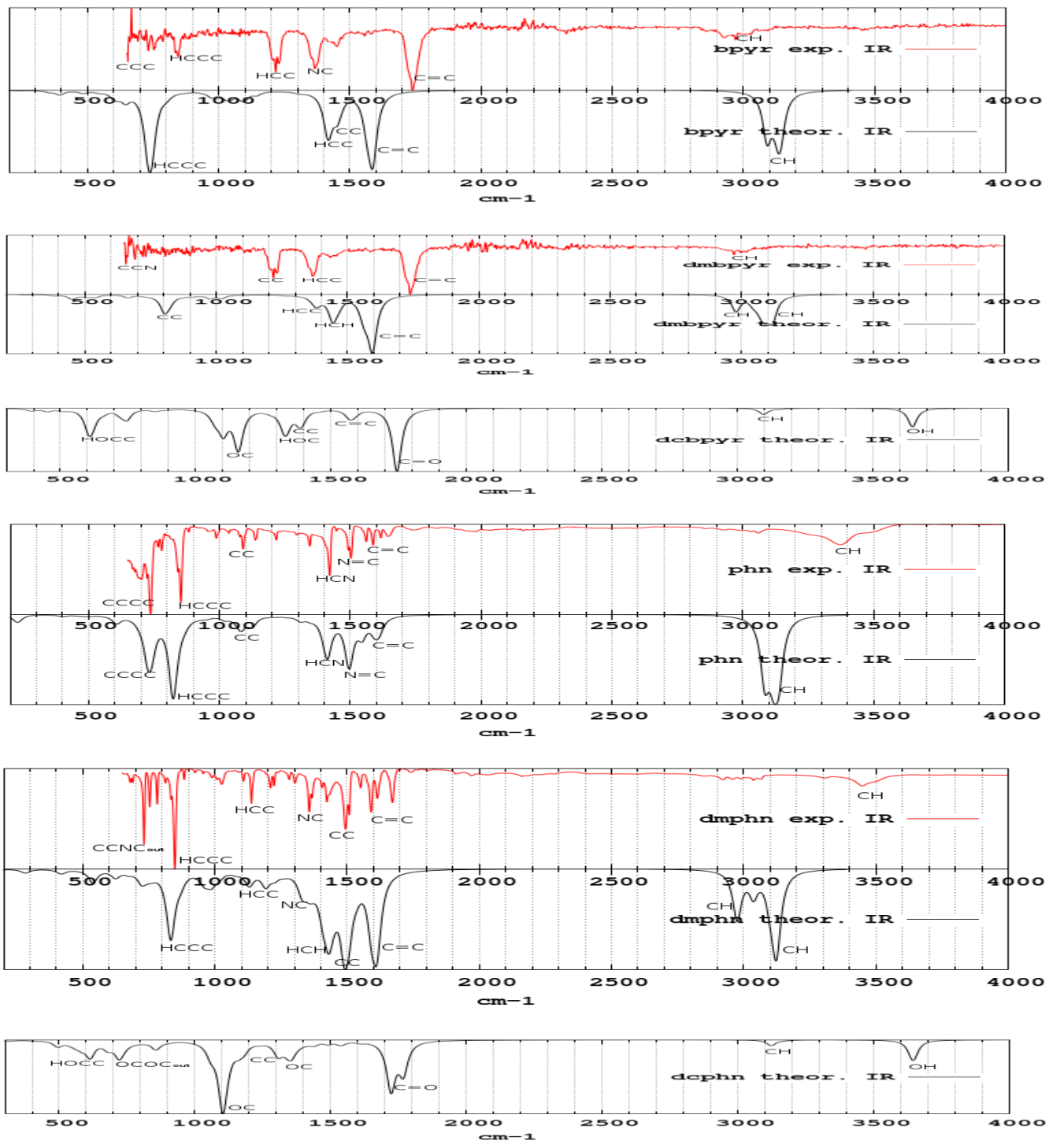

Figure 4.17: The experimental IR with the theoretical IR (in black) spectral of the ligands

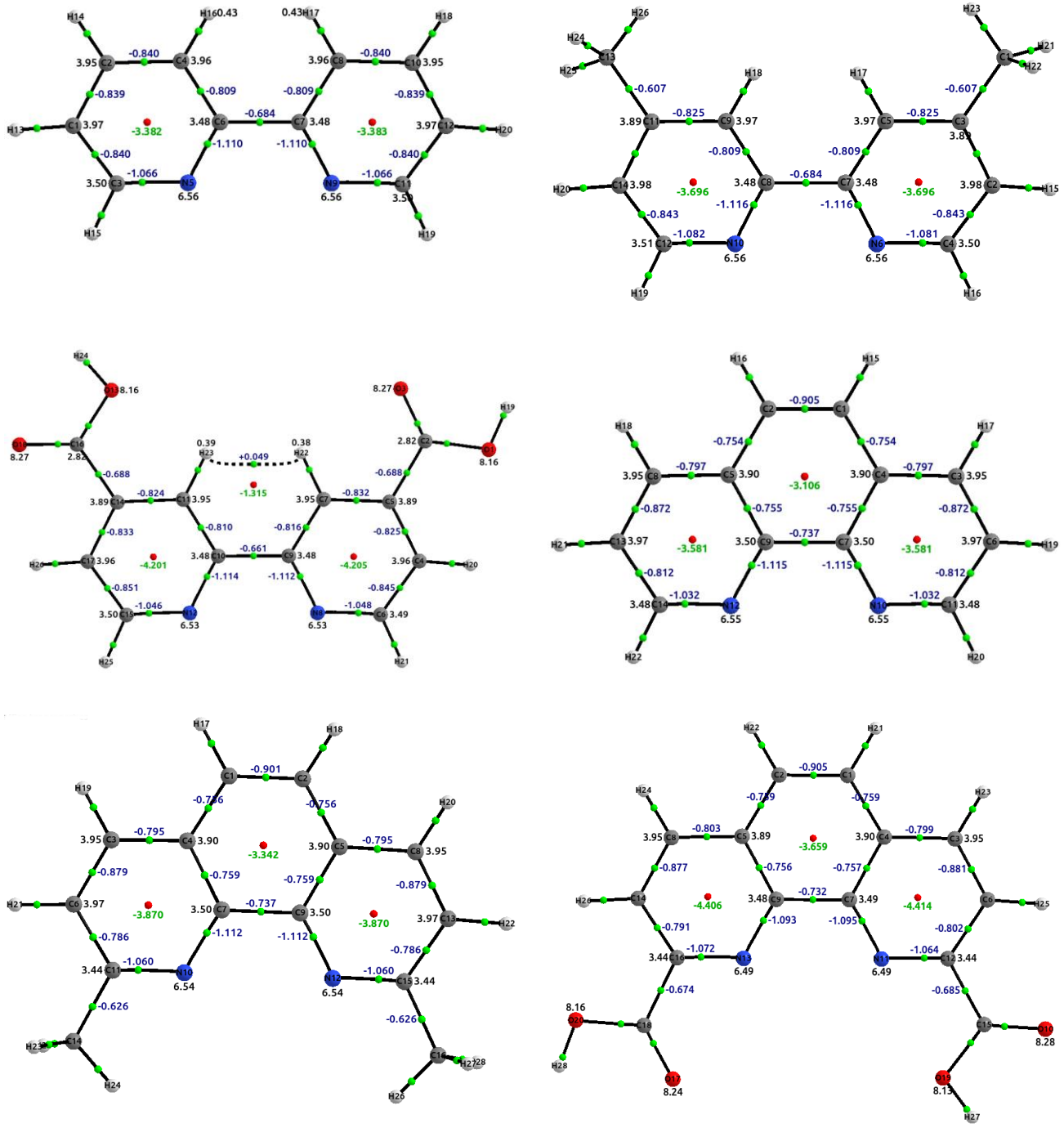

Figure 4.18: The features of the QTAIM properties of the ligands showing the atomic localized electrons, Laplacian of electron density of the bonds and the ring electron density.

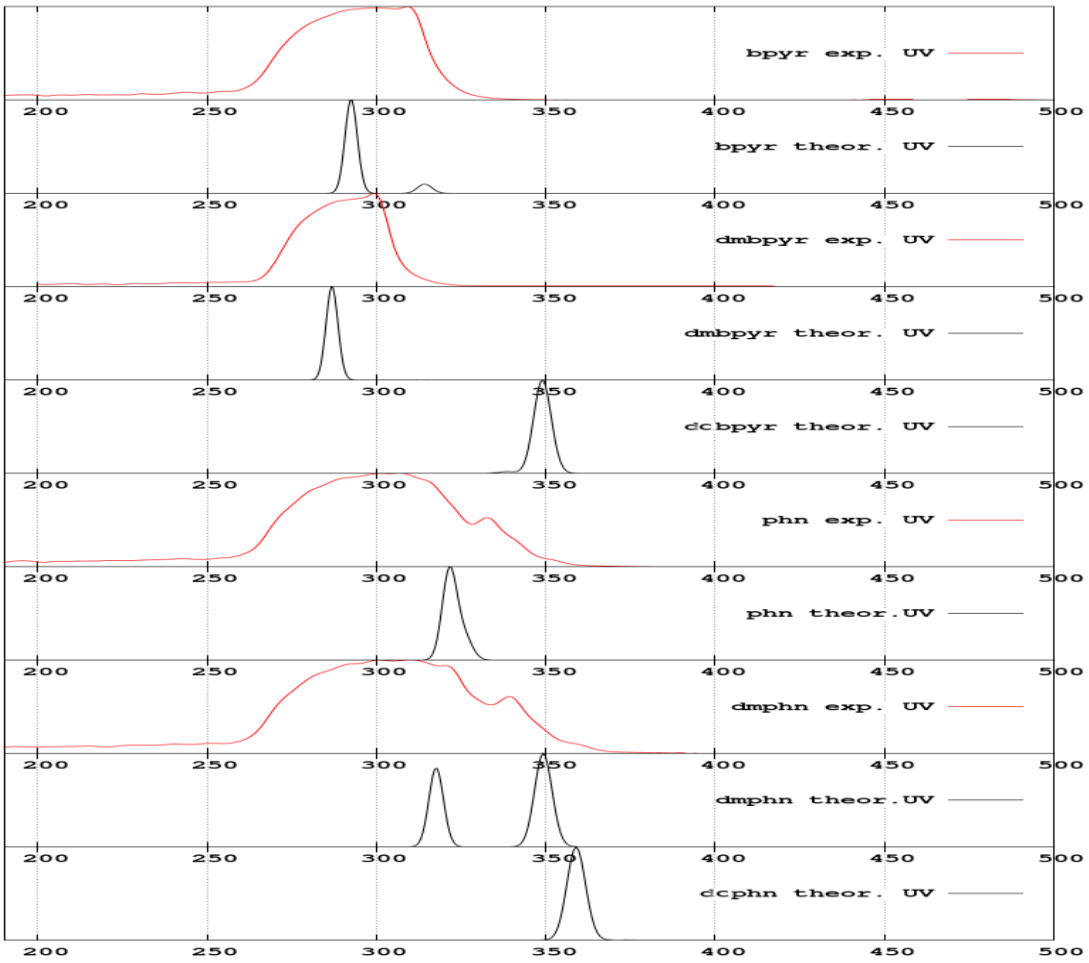

Figure 4.19: The experimental and theoretical UV absorption of the ligands in nm

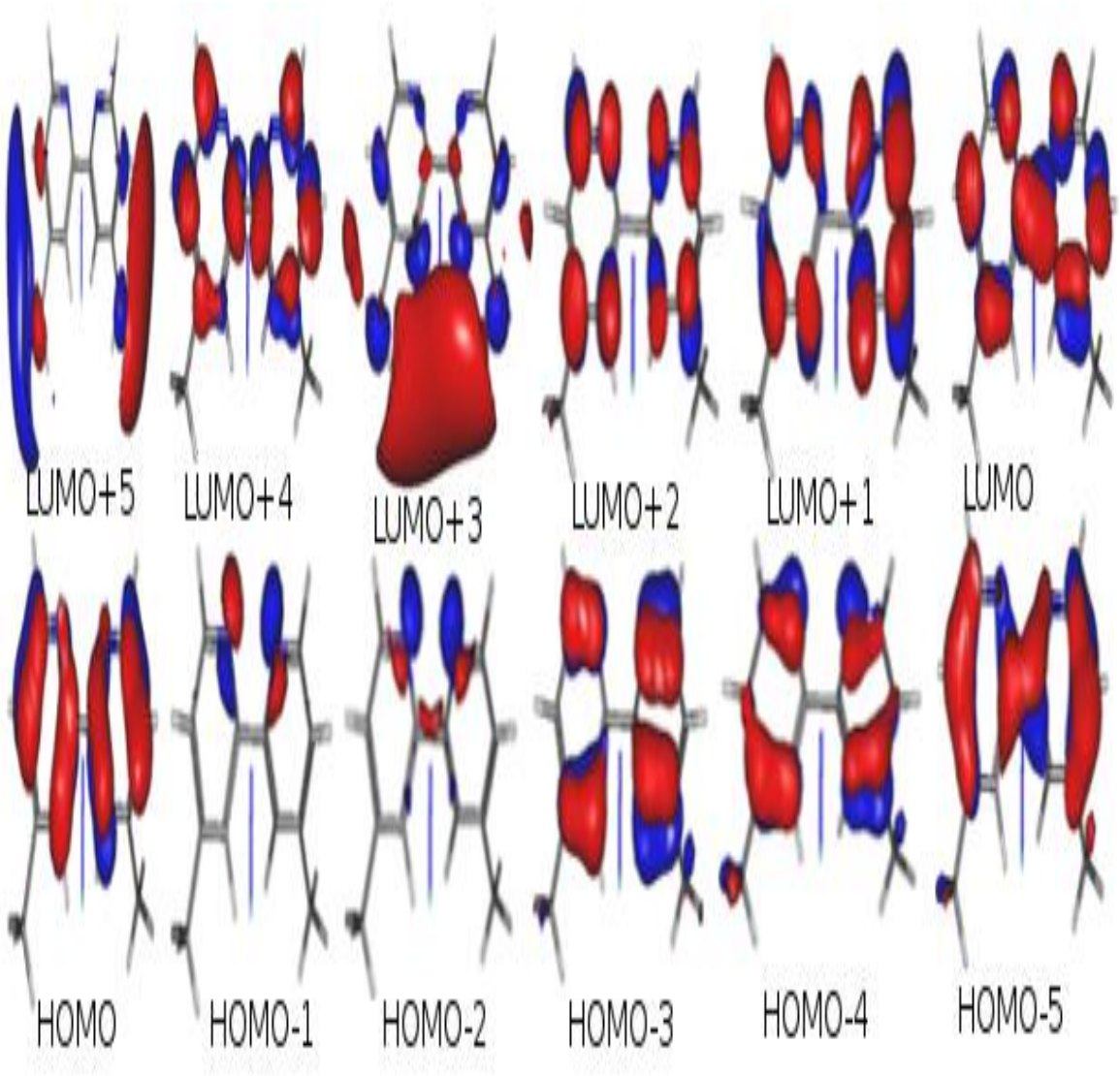

Figure 4.20: Electronic isodensity surface of six levels of HOMO and LUMO of dmbpyr

CHAPTER FIVE

5 SYNTHESIS, CHARACTERISATION AND COMPUTATIONAL ELUCIDATION OF RUTHENIUM(II) COMPLEXES

5.1 Background of the chapter

In this chapter, the synthesis, characterisation and computational spectroscopic properties of forty Ru(II)-based (**C1-C40**) complexes and four precursor (**ST1-ST4**) complexes are presented. The computational models were used to confirm the successful synthesis of the complexes and were also used to elucidate and interpret the experimental spectroscopic properties of the synthesised complexes. The different ligands that were used in this project are shown in Figure 5.1. Four different methods were used in the synthesis of the complexes based on the type of the starting materials as presented in Table 5.1. The method used was based on each starting material as detailed in the experimental section. All the syntheses were carried out in vacuum and the cationic complexes are precipitated using NH_4PF_6. The unique target in all our synthesised complexes is to have the pyrazole (pz) derivatives or have cymene (cym) unit or combination of both. The intention in all the pyrazole derivatives with the linker CHCOOH (i.e. bpza, bdmpza and bphpza) is to make sure the carboxylic unit is not coordinated to the metal but free for biological interactions. It is very rare to prevent the carboxylic unit of pyrazole derivatives participating in metal coordination. In fact, we have only come across one in the literature [422] where this was done compared to many other publications using the conventional method of forming tridentate through coordination of the carboxylic group. To afford the free carboxylic unit of the pyrazole derivatives, no deprotonation was allowed before or during their synthesis which is similar to the method reported in the literature [422].

5.2 Experimental methods for the synthesis of Ru-based complexes

5.2.1 Chemical and solvents for the synthesis of R(II)-based complexes

The ruthenium salt $RuCl_3 \cdot 3H_2O$, p-phenanthroline and the solvents dichloromethane, tetrahydrofuran (THF), DMSO, DMF, acetone, diethyl ether (Et_2O) and methanol and acetonitrile were used as purchased from Aldrich Chemical. Also the ligands 2,2'-bipyridine, 4,4'dimethyl-2,2'-bipyridine, 1,10-phenanthroline and 2,9-dimethyl-1,10-phenanthroline were used as purchased from Aldrich Chemical. The other ligands that were used for the sysnthesis of the Ru(II)-based complexes were synthesised as discribed in section 4.2 of this project. The synthesised ligands are bis(3,5-dimethylpyrazol-1-ly)acetic, bis(3,5-dimethylpyrazol-1-ly)methane, bis(pyrazol-1-ly)acetic, bis(pyrazol-1-ly)methane and bis(3-phenylpyrazol-1-ly)acetic.

5.2.2 Physical measurements

The same physical methods used for the characterisation of the ligands as described in subsection 4.2.2 are also used for the characterisation of the ruthenium complexes.

5.2.3 *Synthesis of ruthenium complexes*

The starting material $RuCl_2(dmso)_4$, $[(cym)RuCl_2]_2$, $Ru(bdmpzm)Cl_4$ and $Ru(bpzm)Cl_4$ were synthesised and used as precursors for the synthesis of the different forms of Ru complexes. The number of moles and the percentage yields of complexes are shown in Table 5.1. The complexes **C1** to **C4** and **C5** to **C8** were synthesised directly from the reaction of $RuCl_3 \cdot 3H_2O$ with equivalent of 3.1 and 2.1 mmol of ligands respectively.

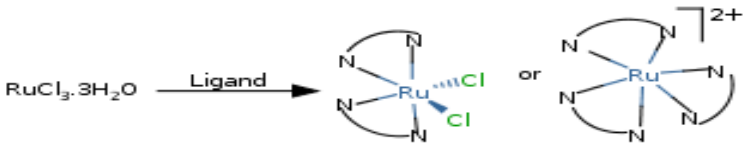

The method used for the synthesis of the precursor $RuCl_2(dmso)_4$ and all the Ru complexes synthesised from its application as starting material are shown below. The starting material $RuCl_2(dmso)_4$ was synthesised from the $RuCl_3.3H_2O$ (2 g, 7.62 mmol) added to 7 mL DMSO and reflux for 10 min. The solvent was reduced to half of its volume in vacuum and 40 mL acetone was added to give yellow precipitate which was filtered, wash with acetone and Et_2O and dry in vacuum [423]. All the Ru complexes synthesised from $RuCl_2(dmso)_4$ as starting material follow the same method as reported in literature [280]. As given in Table 5.1, a mixture of indicated amount of $RuCl_2(dmso)_4$ and equivalent 1.05 each of the two ligands L1 and L2 were heated for 6-12 h in DMF (except otherwise state) to form the different complexes as shown in Table 5.1. The DMF solvent was dried in vacuum and the product re-precipitated in CH_2Cl_2 and Et_2O.

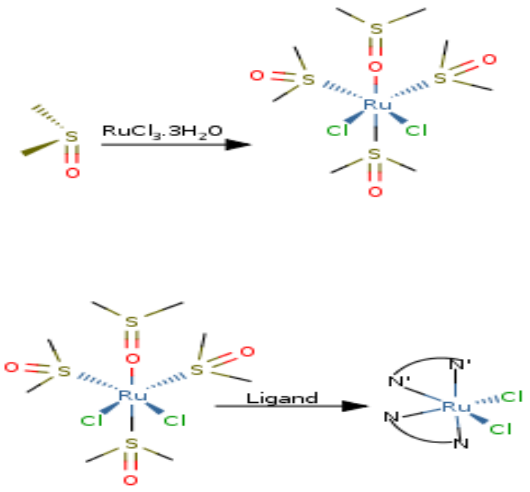

The preparation of both $Ru(bdmpzm)Cl_4$ and $Ru(bpzm)Cl_4$ follow similar way as reported in the literature [280]. The indicated mmol of $RuCl_3.3H_2O$ together with 1.18 equivalents of the respective ligands bdmpzm and bpzm (Table 5.1) are added to 70 mL of 1 N HCl and allow the reaction to stand over night. In all the complexes where $Ru(bdmpzm)Cl_4$ was used as starting material, the stated mmol of the starting material with 1.05 equivalent of the ligand were dissolved in 50 mL of DMF (except

otherwise state) and refluxed 6-12 h under a nitrogen atmosphere [280]. The solid products were obtained by drying the solvent in vacuum and the product washed with solvents like acetone and Et_2O.

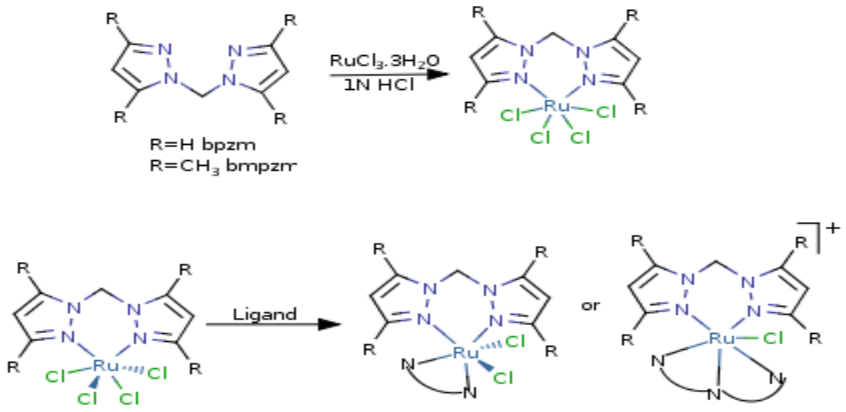

The precursor $[(cym)RuCl_2]_2$ was synthesised by reacting $RuCl_3 \cdot 3H_2O$ (1.834 g, 7.016 mmol) and p-phellandrene (7.646 g, 56.129 mmol) in ethanol (70 mL). The method used is similar to the literature report [201] except that 8.0 mmol equivalent of p-phellandrene was used instead of approximately 10 mmol equivalent in the literature [201]. The precursor $[(cym)RuCl_2]_2$ was used for the synthesis of $[(cym)RuLCl_2]$, $[(cym)RuLCl]^+$ or $[(cym)RuL]^{2+}$ derivatives. The synthesis of (cym)RuL derivatives followed a similar method used for the synthesis of RAPTA complexes [9, 424]. As stated for each of the (cym)RuL derivatives in Table 5.1, the stated mmol of the precursor $[(cym)RuCl_2]_2$ was mixed with 2.2 mmol equivalent of the ligand in the respective solvents as shown in the table and reflux for 6-12 h.

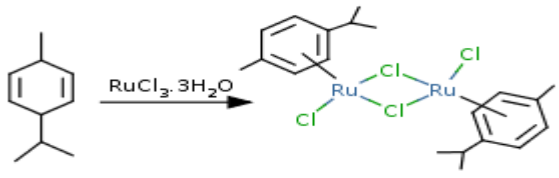

5.3 Characterisation and elucidation of the structures

The synthesised Ru complexes were analysed using Elemental Analysis, IR, ProtoN-NMR and

^{31}P-NMR. In order to have a better understanding of the structures, all the complexes were characterised theoretically using the computed IR, ^{1}H-NMR, ^{13}C-NMR, ^{15}N-NMR and ^{99}Ru-NMR. The chemical shift were computed for the ^{1}H-NMR and ^{13}C-NMR using TMS as reference, for ^{15}N-NMR using CH_3NO_2 [343, 344] and for ^{99}Ru-NMR using $[Ru(CN)_6]^{4-}$ [334] as reference in place of $K_4Ru(CN)_6$ [425, 426] which is difficult to compute [426].

5.3.1 *The elemental analysis and mass spectroscopic*

Directly from the elemental analysis (Table 5.2), there is an evidence that 25 complexes **C2**-**C4**, **C6**, **C8**-**C15**, **C17**-**C20**, **C25**, **C27**, **C28**, **C30**-**C32** and **C34**-**C36** are pure enough while 11 complexes **C1**, **C5**, **C7**, **C16**, **C21**-**C23** and **C37**-**C40** appears not to be pure enough. The starting materials **ST1**-**ST4** appear also to be pure enough. There is no result for 4 complexes **C24**, **C26**, **C29** and **C33** because of their instability of their mass during the analysis. Since the interest is to interpret the complexity of these organometallic using the computational methods, the Ru complexes that appears in the elemental analysis to be uncertain were still further purified and analysed.

5.3.2 *The IR spectra*

Both the experimental and theoretical IR spectra are shown in parallel for each of the complexes in Table 5.3 and Figure 5.2. There is a very high similarity and correlation between the observed experimental and theoretical IR. Interestingly, much peaks intensity is reproduced theoretically. The major differences between the experimental and theoretical are the OH vibration which is observed theoretically at higher frequency and well separated from the CH vibration. Also, the theoretically predicted high intensity of vibration around 2600 to 2700 cm^{-1} in complexes like **C6**, **C8**, **C9** and **C11** which are experimentally found to be very weak. Peculiar to only the experimental spectra is the

vibration found within 2300 to 2400 cm^{-1} as found in complexes like **C1**, **C22**, **C24**, **C26**, **C29** which can be interpreted to associate with the anionic PF_6^- in the cationic complexes except for complex **C22**.

The assignment of all the prominent peaks is shown in Table 5.3 while the peaks that are associated with the Ru atom are shown in Table 5.4. The IR vibrations that are dominantly strong in the complexes are stretching υ(SO), υ(C=O), υ(C-O) υ(NN), υ(CH), υ(NC), υ(CC), υ(OH), bending β(OCO), β(HOC), β(HCC) and torsional τ(HCSRu), τ(HCCO), τ(HCCC), τ(HCCN), τ(HOCC). In the starting complexes **ST3**-**ST4**, the υ(RuCl) IR vibration is very strong but its intensity in the complexes is lower. The carbonyl υ(C=O) vibrations are found within 1700 to 1860 cm^{-1} in the complexes while υ(C-O) is found within 1050 to 1400 cm^{-1} (Table 5.3). The υ(CO) are also found at very low frequency around 664 as found in complex **C27**. Many of the IR vibrations that are associated with Ru atom are found to be low frequency and weak vibration with low intensity (Table 5.4). However, some ruthenium vibrations like out(NRuNC) or out(CNRuN) as in complexes **C6**, **C9**-**C11**, **C15** are among the prominent vibrations. Also, in complexes with cymene unit (**C25** to **C40**), the vibrations like τ(HCCRu) are found to occur at high frequencies (around 1370 to 1000 cm^{-1}) though with low intensity. As shown in Table 5.4, in many of the complexes, the RuN vibrations are weaker and found at lower frequency than RuCl.

5.3.3 *The ^{1}H-NMR chemical shift of the complexes*

The theoretical and the experimental ^{1}H-NMR shifts of the complexes are shown in Table 5.5. The computational values were obtained through direct subtraction of the proton isotropic shielding tensor of the TMS from that of the each of the proton in the complexes while the fitting values were obtained using the fitting equation. The experimental and theoretical ^{1}H-NMR shifts for many of the complexes are in good agreement. The computation gives significant insight into the NMR spectra of the complexes. The general observation is that the proton that are directed towards the Ru metal centre are characterised with more shielding effect which results in lower shift while reverse is the case of the

protons that are directed towards the chloride or carbonyl group. The common trend in the proton shift of the complexes follow the order CH_3 < C_{cym}-H < $C_{cym\text{-}arene}$-H < CH_2 < C4-H < C_{pz}-H < COOH < C_{bpyr}-H < CHOO < NH. In some complexes the strong effect of the Ru atom shielding effect and Cl or carbonyl deshielding effect cause a change in the order. In many of the complexes, the proton shift of the CH_2 linker of the pyrazole derivatives are low and very close to that of the methyl shift except where any of the protons is directed toward the Cl atom. The proton shifts of the CH_2 group in complexes **C10** and **C21** are having a very wide variation as a result of one of the two hydrogen atoms being very close to the Cl atom. The proton shift of the CHCOO in complex **C6** is found be far higher theoretically (11.4349, 12.0581) than what is observed experimentally (8.5) because the theoretical model is pointing toward the Cl atom. Also, in many other complexes like **C9**, **C11**, the proton shift of CHOO is very high when directed toward the Cl atom. The reverse is the case for the proton shift of the CHOO and H_{meta} (i.e. C3-H) which are sometimes found lower than the C4-H because of their close range to metal atom especially in complexes like **C2** without Cl atom. Also very low proton shift is observed in precursor complex **ST3** for the methyl H atom that is pointed towards Ru atom while those pointing towards the Cl atom have a very high shift. Likewise in complex **C36** a higher proton shifts (>4.00) were observed for some of the methyl group protons because of being directed towards the Cl atom. In the complexes with the pyrazole derivatives with CHCOOH as linker, the proton shift of the CHCOO and COOH are within a close range of which either of the two can be smaller than the other.

There are many peculiar features observed in some of the complexes. In the experimental proton shift of complex **C8**, only the methyl and hydroxyl shift are very obvious while the rest are not observed. This observation can best be explained from the computed theoretical shift which shows that there is a very high possibility that the other proton shifts are within the same value of the OH. In complex **C19**, the methyl H atom that is pointing towards the C=O have higher proton shift compared to the one pointing toward the Cl atom. We observed in complex **C7** that if the H atom of the methyl is pointing towards the Ru atom, then a very low shift is usually observed which could be responsible for

the lower shift observed experimentally (as low as 0.5318) for some of the methyl H atoms. This lower proton shift as a result of being close to the Ru atom is observed theoretically and experimentally in complex **C3** where the methyl H atoms pointing towards the Ru atom have a very low shift (theor. 0.0440, exp. 0.4400). The strong singlet shift at 6.60 observed experimentally in the precursor complex **ST4** is an indication that one of the linking CH_2 hydrogen atom is very close to the Ru but those of the theoretical method are very close to the Cl atoms leading to a higher shift (11.1008 and 18.5331). The computational proton shift of the $C_{cy\text{-}H}$ in complex **C38** is lower than the experimental because it is pointing towards the direction of the Ru atom which enhances its shielding. There is possibility that the experimental proton shift for COOH in complex **C38** is pointing toward the direction of the Ru atom which result to its experimental shift being lower than the theoretical. The proton shift of the CH_3 and also that of the CH in cym group is lower than those of bdmpzpy group as observed in complexes **C40**. Also, the proton shift of the CH in cymene ring of complex **C39** are within the range of 5.00 to 6.50 while the CH of bpzpy unit is having the highest shift of 7.30 to 8.94. The CH of the para proton of the phenyl group and the ortho of the pz group of the bphpza are having the highest proton shift in complex **C32**. In complexes **C25**-**C27**, possibly the experimental NH is pointing towards Ru atom which resulted in significant lower proton shift compared to the theoretical.

5.3.4 *^{31}P-NMR chemical shift*

The phosphorus chemical shift of some of the synthesised cationic complexes were carried out experimentally only to confirm successful stabilization of the cationic complexes with PF_6^- ion. The ^{31}P-NMR shift obtained for the complexes **C2**-**C4**, **C28** and **C30**-**C40** are -144.5958, -144.6007, -144.6131, -144.5888, -144.6079, -144.6171, -144.6129, -144.6127, -144.6026, -144.6019, -144.6138, -144.6138, -144.6145, -144.6137 and -144.6153 respectively. This is a clear indication that the cationic complexes were successfully synthesised and stabilized with PF_6^- counter ion. The values obtained for

^{31}P-NMR shift of the cationic ruthenium complexes are very similar to what have been reported in the literature for the cationic complexes stabilized with PF_6^- [427].

5.3.5 *^{13}C-NMR chemical shift*

Since a very high correlation was observed between the theoretical and experimental proton shift, the structures of the complexes were further elucidated using the theoretical ^{13}C-NMR chemical shift as shown in Table 5.6. Just as was observed in the proton shift, the Ru atom causes a lower shift effect of carbon atoms that are directed toward it while the Cl or carbonyl atom causes a higher shift. Despite the effects of the Ru, Cl and carbonyl group on the carbon shift, these effects do not significantly alter the order of the carbon shifts which make the ^{13}C-NMR more predictable than the ^{1}H-NMR. The carbon shifts commonly follow the order $CH_3 < C_{cym}$-H $< CH_2 <$ **C**HCOOH $< C_{cym\text{-}arene} < C_{pyr\text{-}meta} <$ C4 $<$ C3 $<$ C5 $< C_{others} <$ CH**C**OOH. There are little exceptions to the given order. The carbon shift of C3 in the complex **C8** is having the highest shift while COOH carbon shift is in between the C3 and C5 shifts. Just as shown in the order, the $C_{pyr\text{-}meta}$ atoms that are at meta position of the pyridine unit of the tridentates as found in complexes **C23** and **C24** are having shift lower than the C4 of the pyrazole unit. The methyl group of the precursor complex **ST1** have the highest carbon shifts among all the methyl group in the complexes. As can be seen in complex **C15**, the methyl group results to the de-shielding of its anchoring C atom which consequentially results to high ^{13}C-NMR shift. The two methyl group in complex **C13** have the same carbon shift as the two C4 of complex **C12**.

5.3.6 ^{15}N-NMR chemical shift

In order to study the differences in the shielding of the nitrogen atoms based on their chemical environment, we have computed the nitrogen shift of the coordinating nitrogen on pyrazole derivatives

(*N), on the phn or pyr derivative (**N) and the nitrogen on the pyrazole derivatives that are not available for metal coordination (N). The general observation as presented in Table 5.7 is that in many of the complexes the nitrogen shift of the N atoms are higher in magnitude than both *N and **N atoms which is an indication that N is more shielded than the coordinating *N and **N atoms. However, in complexes with tridentates ligands (bdmpzpy and bpzpy), there are variation to the observation. The **N coordinating centre on the pyridine unit of the tridentates are having the highest magnitude of nitrogen shift (more shielded) among all the nitrogen atoms presence in cymene containing Ru complexes (**C39** and **C40**) while the reverse is the case in the Ru complexes without cymene as found in complexes **C23** and **C24**. The coordinating **N of the other bidentates like the dmbpyr, bpyr, dcbpyr, phn, dmphn and dcphn are having the nitrogen shift lower in magnitude (highly de-shielded) than both non-coordinating (N) and coordinating (*N) of the pz derivatives.

5.3.7 ^{99}Ru-NMR chemical shift

The ^{99}Ru-NMR chemical shifts of the complexes are shown in Table 5.8. The interesting features of the ruthenium chemical shift is that the **ST3** and **ST4** which have four chloride atoms have the highest shielding of the Ru atom which consequentially leads to lower chemical shifts. Also, the Ru atom of the complexes with the cymene group (i.e. **C25-C40**) are more shielded (characterised with lower shift) while those with bdmpza, bdmpzm and bphpza have the lowest shielding of Ru atom which consequentially lead to their highest shift of ^{99}Ru-NMR.

Bis(pyrazol-1-ly)methane (bpzm)

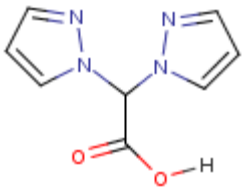

Bis(pyrazol-1-ly)acetic (bpza)

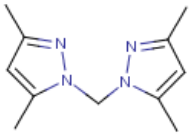

Bis(3,5-dimethylpyrazol-1-ly)methane (bdmpzm)

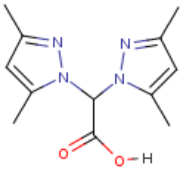

Bis(3,5-dimethylpyrazol-1-ly)acetic (bdmpza)

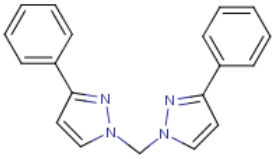

bis(3-phenylpyrazol-1-ly)methane (bphpzm)

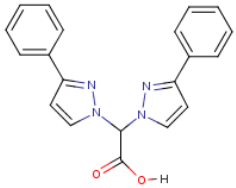

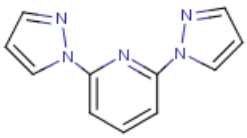

bis(pyrazol-1-ly)pyridine (bpzpy)

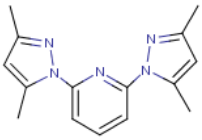

Bis(3,5-dimethylpyrazol-

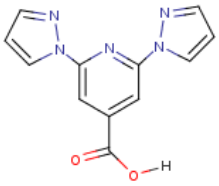

bis(pyrazol-1-

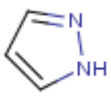

pyrazole (pz)

bis(3-phenylpyrazol-1-ly)acetic (bphpza)

1-ly)pyridine (bdmpzpy)

ly)pyridinic (bpzpya)

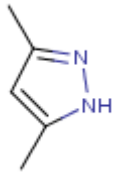

3,5-dimethylpyrazole (dmpz)

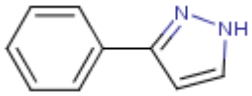

3-phenylpyrazole (phpz)

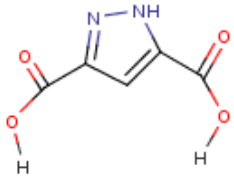

3,5-carboxylpyrazole (dcpz)

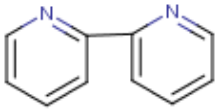

2,2'-Bipyridine (bpyr)

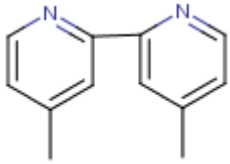

4,4'-dimethy-2,2'-bipyridine (dmbpyr)

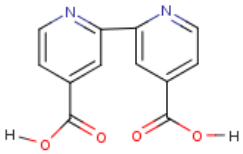

4,4'-dicarboxyl-2,2'-bipyridine (dcbpyr)

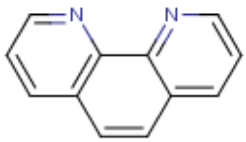

phenanthroline (phn)

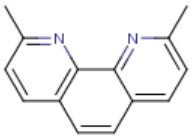

2,9-dimethylphenanthroline (dmphn)

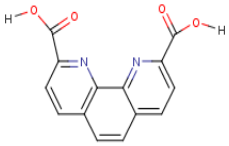

2,9-dicarboxylphenanthroline (dcphn)

Figure 5.1: The representation of the ligands which where used in the syntheses of the Ru complexes

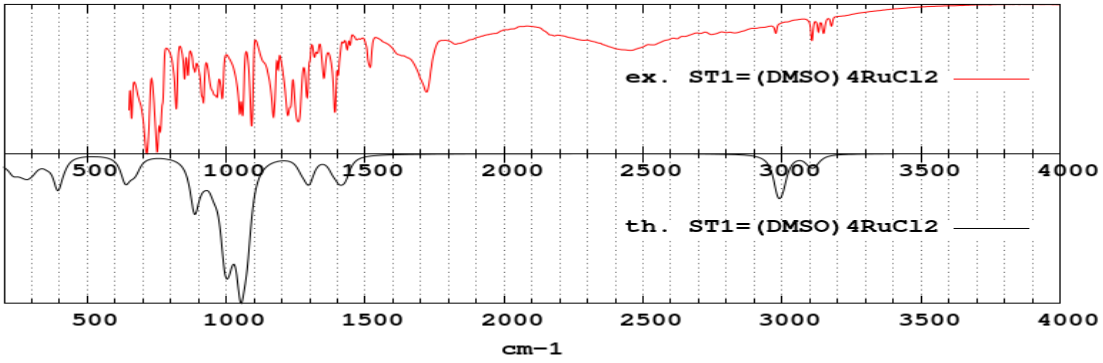
ex. ST1=(DMSO)4RuCl2
th. ST1=(DMSO)4RuCl2
500
1000
1500
2000
2500
3000
3500
4000
cm-1

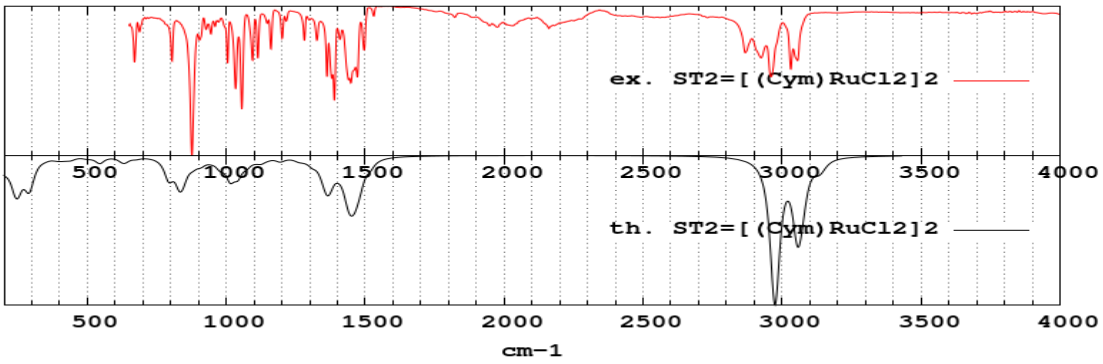
ex. ST2=[(Cym)RuCl2]2
th. ST2=[(Cym)RuCl2]2
500
1000
1500
2000
2500
3000
3500
4000
cm-1

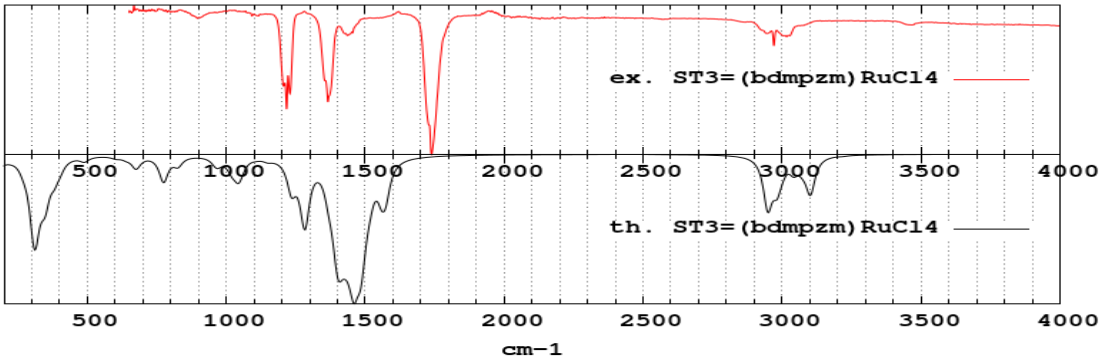
ex. ST3=(bdmpzm)RuCl4
th. ST3=(bdmpzm)RuCl4
500
1000
1500
2000
2500
3000
3500
4000
cm-1

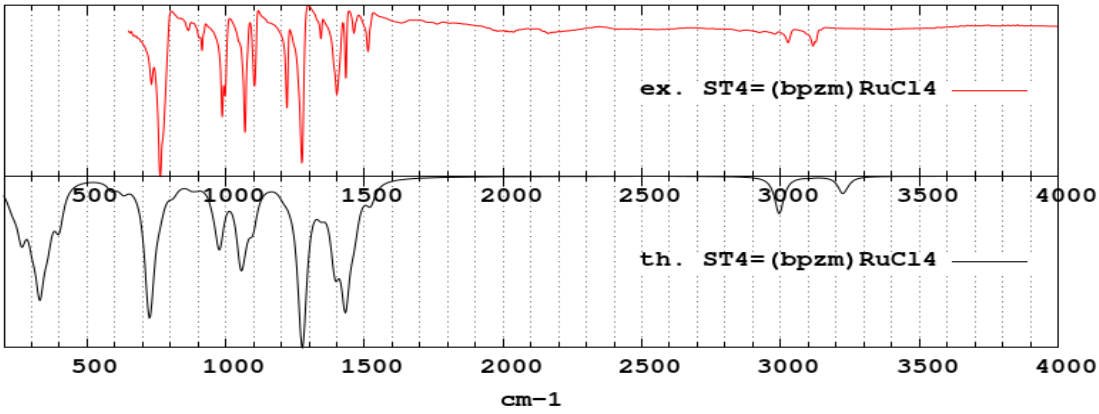
ex. ST4=(bpzm)RuCl4
th. ST4=(bpzm)RuCl4
500
1000
1500
2000
2500
3000
3500
4000
cm-1

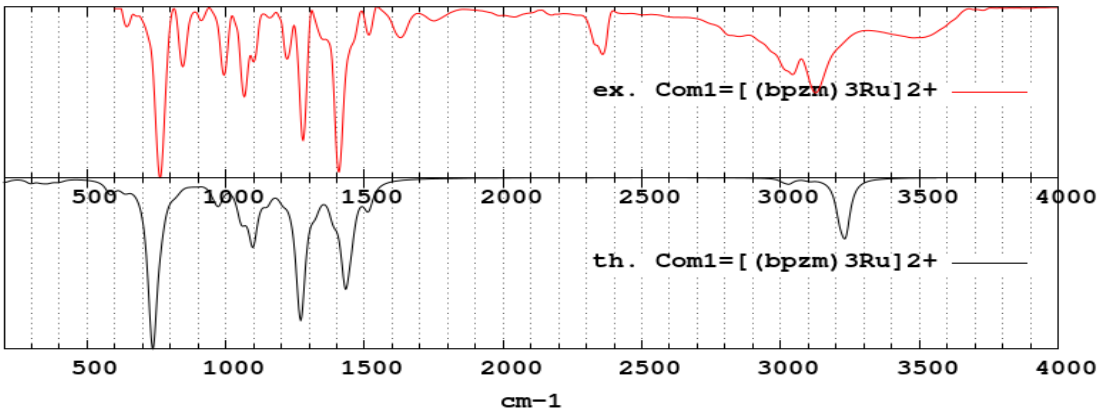
ex. Com1=[(bpzm)3Ru]2+
th. Com1=[(bpzm)3Ru]2+
500
1000
1500
2000
2500
3000
3500
4000
cm-1

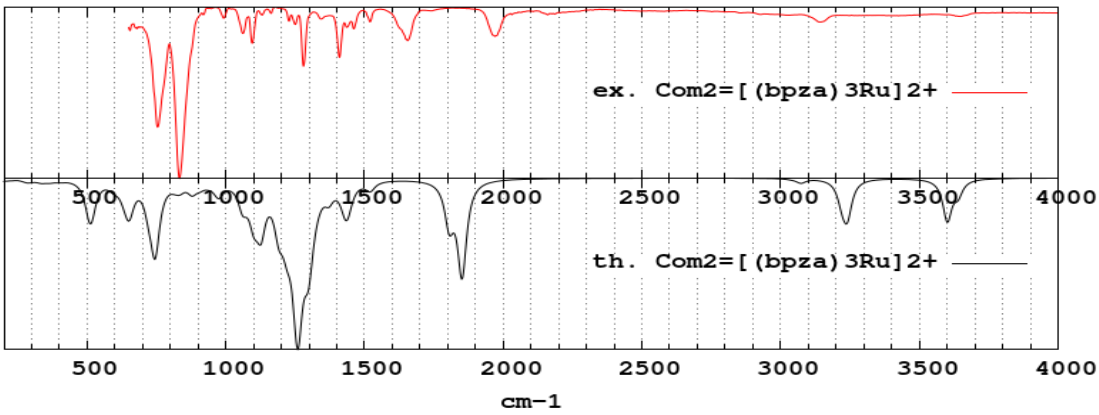
ex. Com2=[(bpza)3Ru]2+
th. Com2=[(bpza)3Ru]2+
500
1000
1500
2000
2500
3000
3500
4000
cm-1

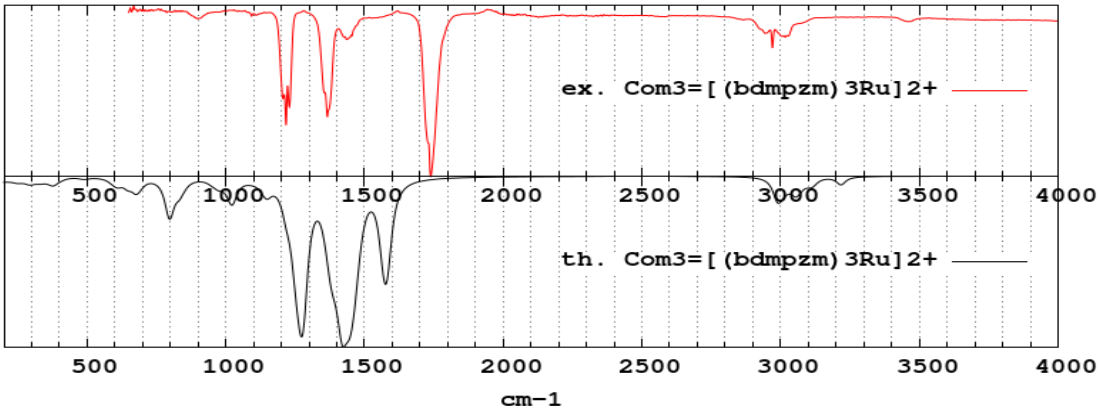
ex. Com3=[(bdmpzm)3Ru]2+
th. Com3=[(bdmpzm)3Ru]2+
500
1000
1500
2000
2500
3000
3500
4000
cm-1

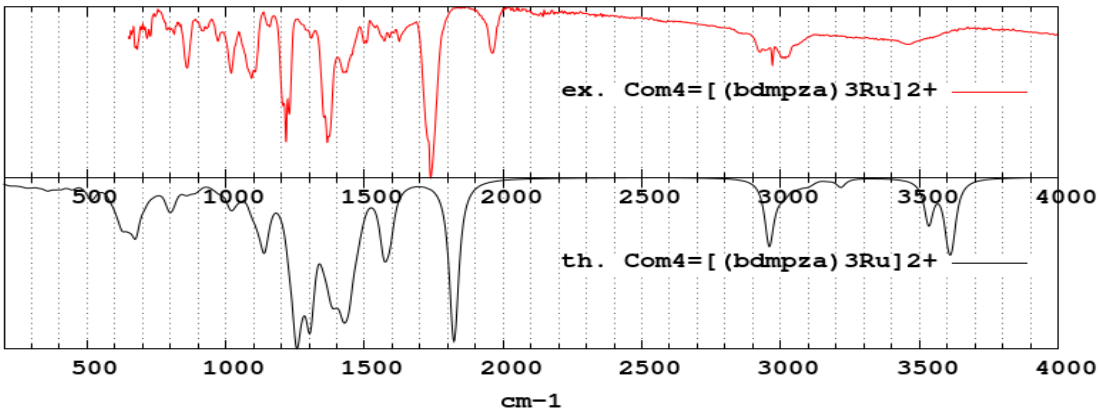
ex. Com4=[(bdmpza)3Ru]2+
th. Com4=[(bdmpza)3Ru]2+
500
1000
1500
2000
2500
3000
3500
4000
cm-1

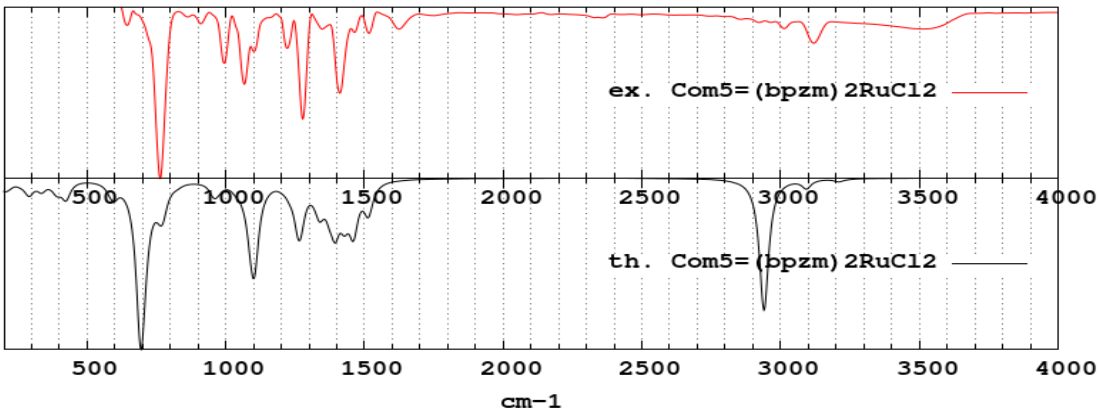
ex. Com5=(bpzm)2RuCl2
th. Com5=(bpzm)2RuCl2
500
1000
1500
2000
2500
3000
3500
4000
cm-1

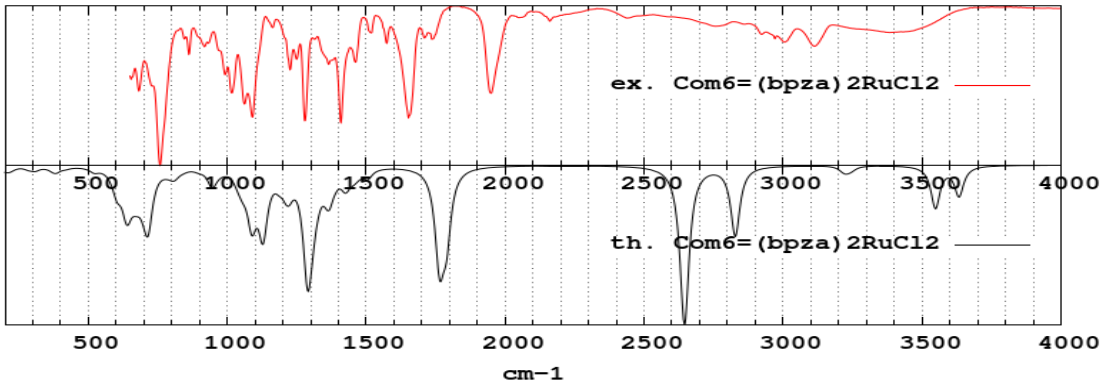
ex. Com6=(bpza)2RuCl2
th. Com6=(bpza)2RuCl2
500
1000
1500
2000
2500
3000
3500
4000
cm-1

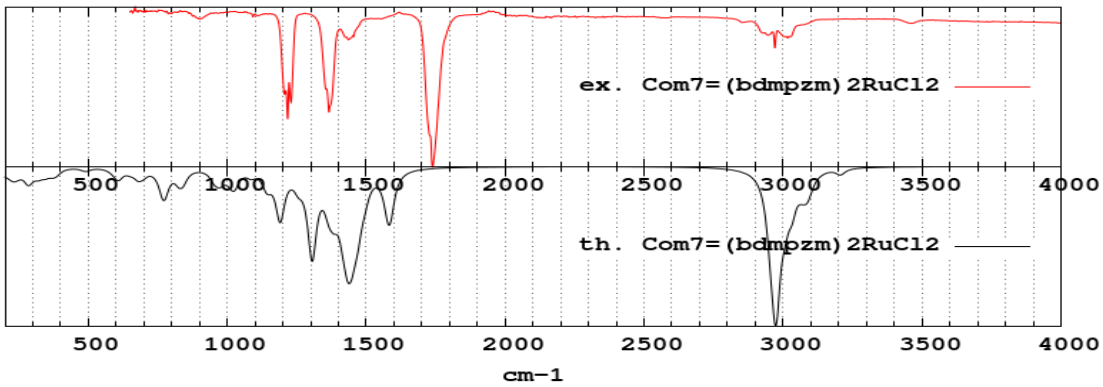
ex. Com7=(bdmpzm)2RuCl2
th. Com7=(bdmpzm)2RuCl2
500
1000
1500
2000
2500
3000
3500
4000
cm-1

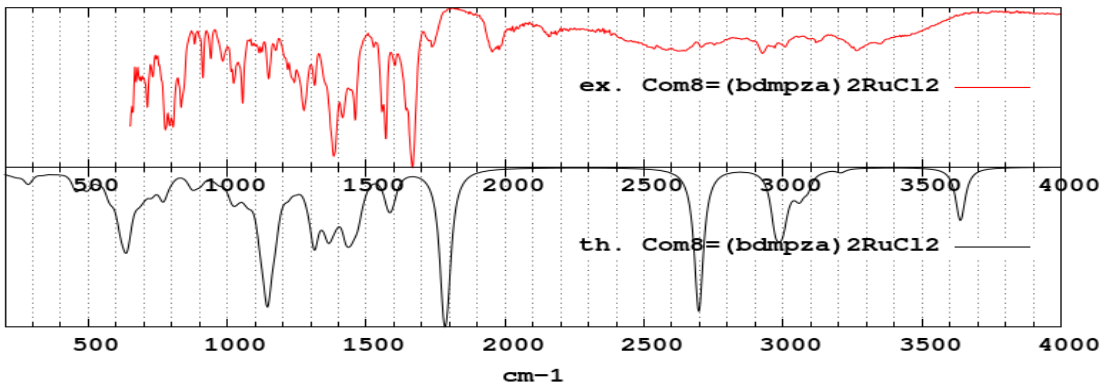
ex. Com8=(bdmpza)2RuCl2
th. Com8=(bdmpza)2RuCl2
500
1000
1500
2000
2500
3000
3500
4000
cm-1

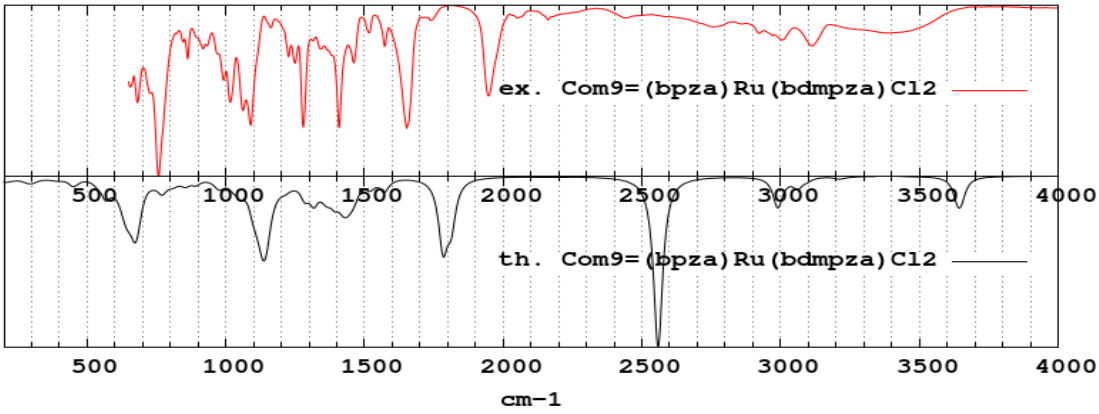
ex. Com9=(bpza)Ru(bdmpza)Cl2
th. Com9=(bpza)Ru(bdmpza)Cl2
500
1000
1500
2000
2500
3000
3500
4000
cm-1

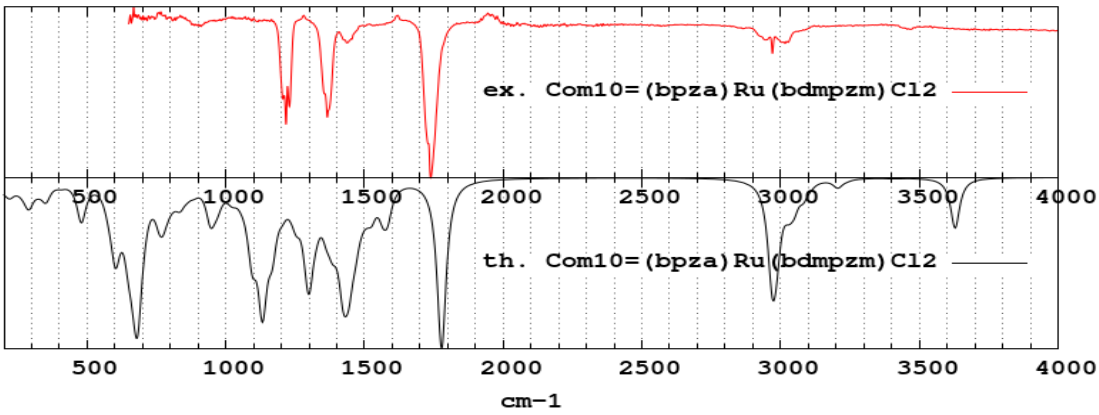
ex. Com10=(bpza)Ru(bdmpzm)Cl2
th. Com10=(bpza)Ru(bdmpzm)Cl2
500
1000
1500
2000
2500
3000
3500
4000
cm-1

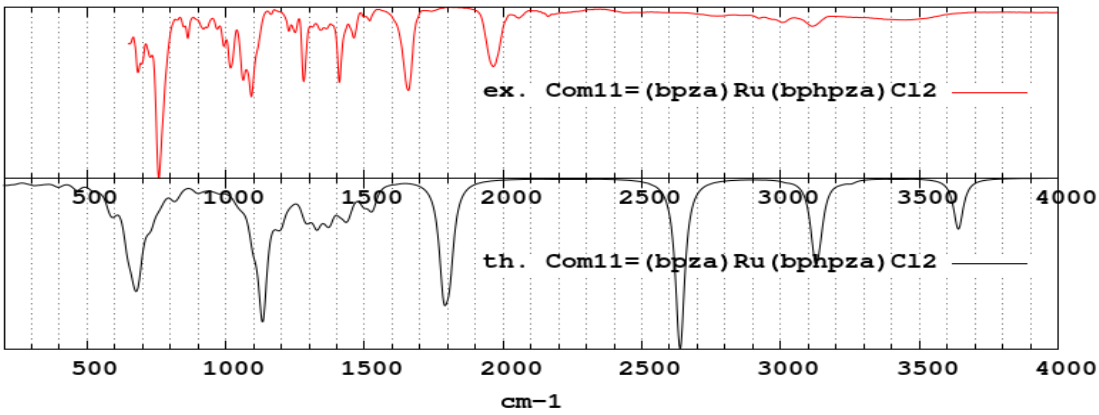
ex. Com11=(bpza)Ru(bphpza)Cl2
th. Com11=(bpza)Ru(bphpza)Cl2
500
1000
1500
2000
2500
3000
3500
4000
cm-1

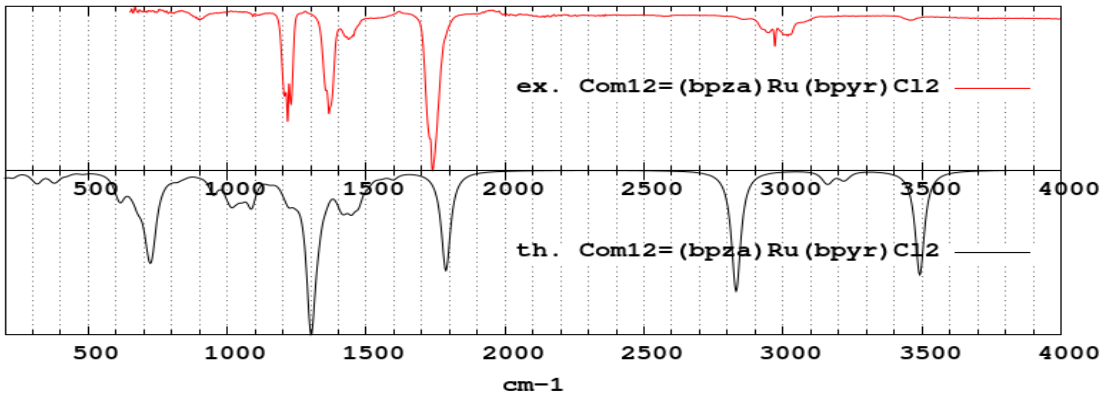
ex. Com12=(bpza)Ru(bpyr)Cl2
th. Com12=(bpza)Ru(bpyr)Cl2
500
1000
1500
2000
2500
3000
3500
4000
cm-1

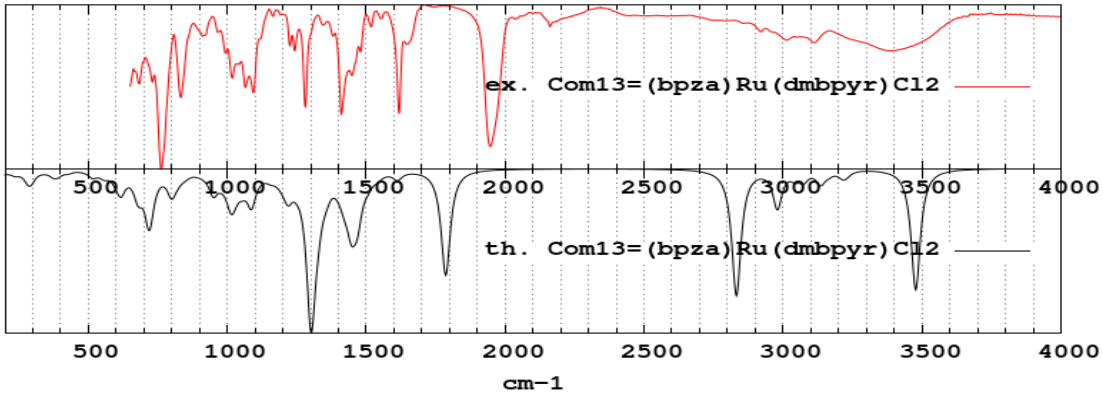
ex. Com13=(bpza)Ru(dmbpyr)Cl2
th. Com13=(bpza)Ru(dmbpyr)Cl2
500
1000
1500
2000
2500
3000
3500
4000
cm-1

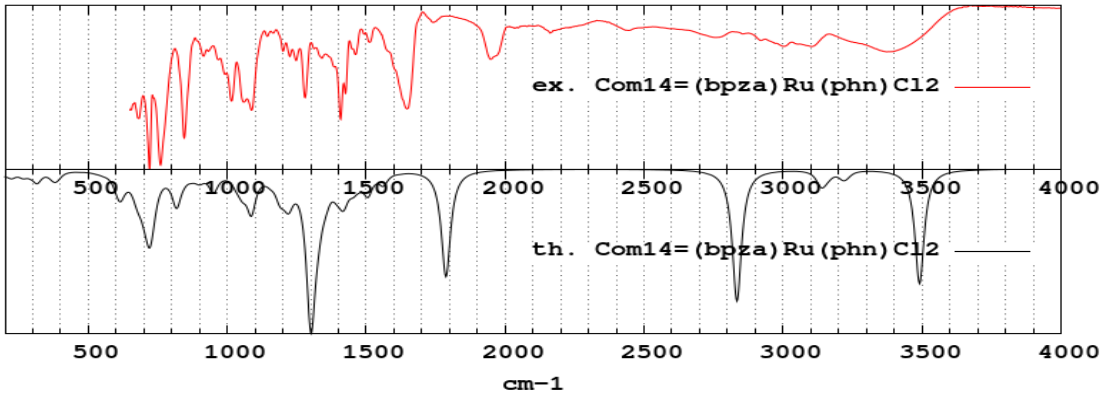
ex. Com14=(bpza)Ru(phn)Cl2
th. Com14=(bpza)Ru(phn)Cl2
500
1000
1500
2000
2500
3000
3500
4000
cm-1

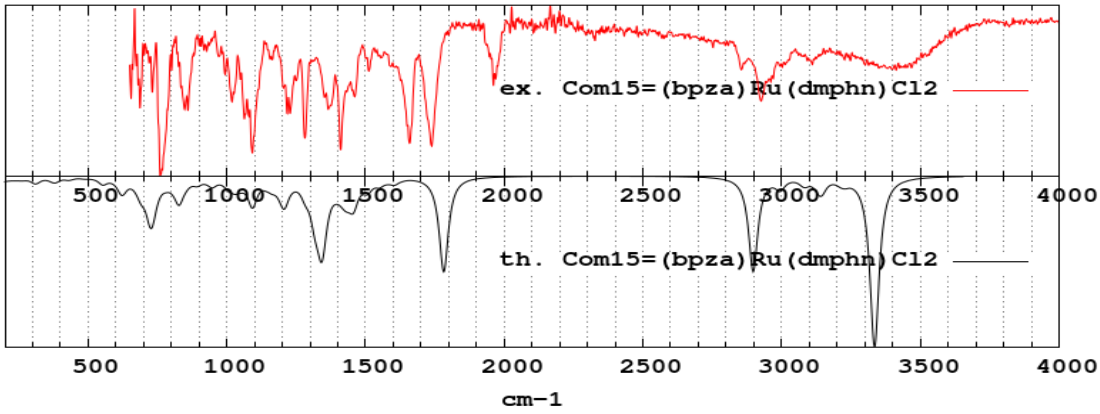
ex. Com15=(bpza)Ru(dmphn)Cl2
th. Com15=(bpza)Ru(dmphn)Cl2
500
1000
1500
2000
2500
3000
3500
4000
cm-1

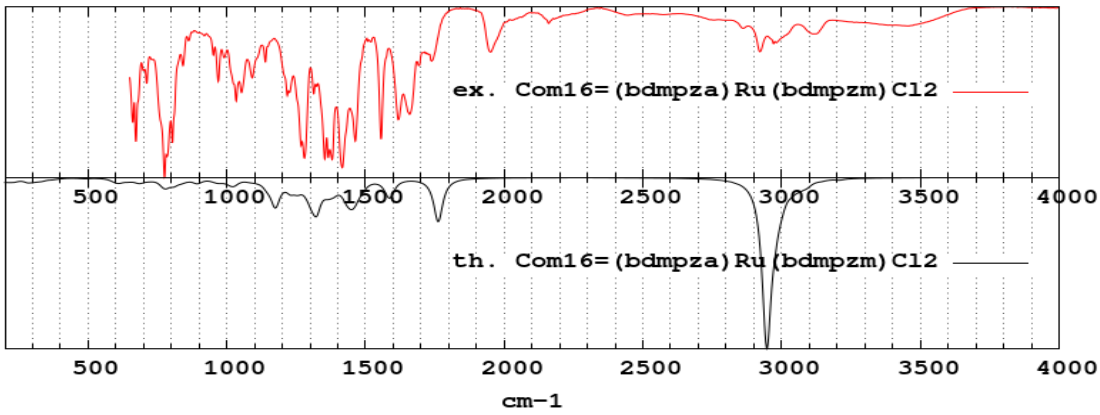
ex. Com16=(bdmpza)Ru(bdmpzm)Cl2
th. Com16=(bdmpza)Ru(bdmpzm)Cl2
500
1000
1500
2000
2500
3000
3500
4000
cm-1

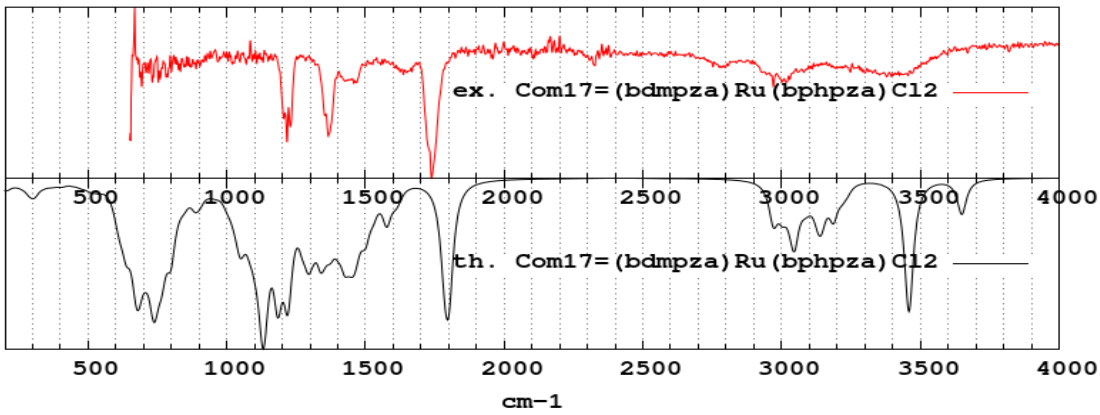
ex. Com17=(bdmpza)Ru(bphpza)Cl2
th. Com17=(bdmpza)Ru(bphpza)Cl2
500
1000
1500
2000
2500
3000
3500
4000
cm-1

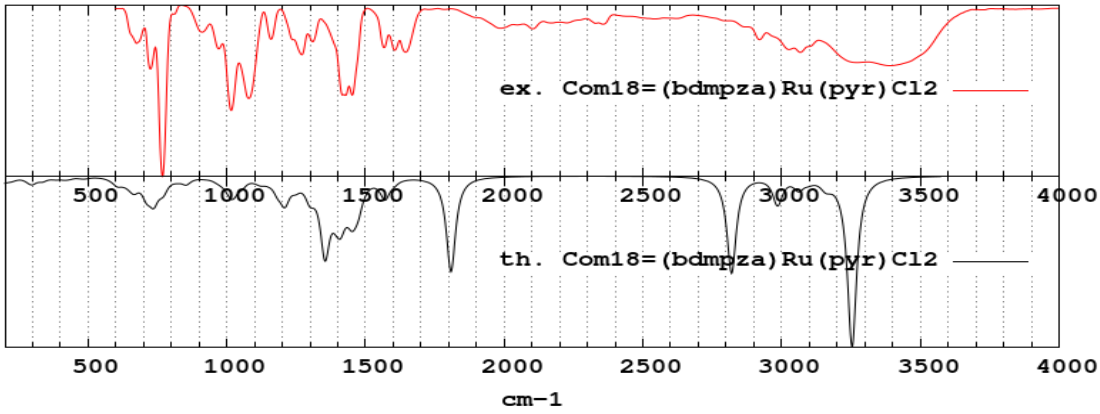
ex. Com18=(bdmpza)Ru(pyr)Cl2
th. Com18=(bdmpza)Ru(pyr)Cl2
500
1000
1500
2000
2500
3000
3500
4000
cm-1

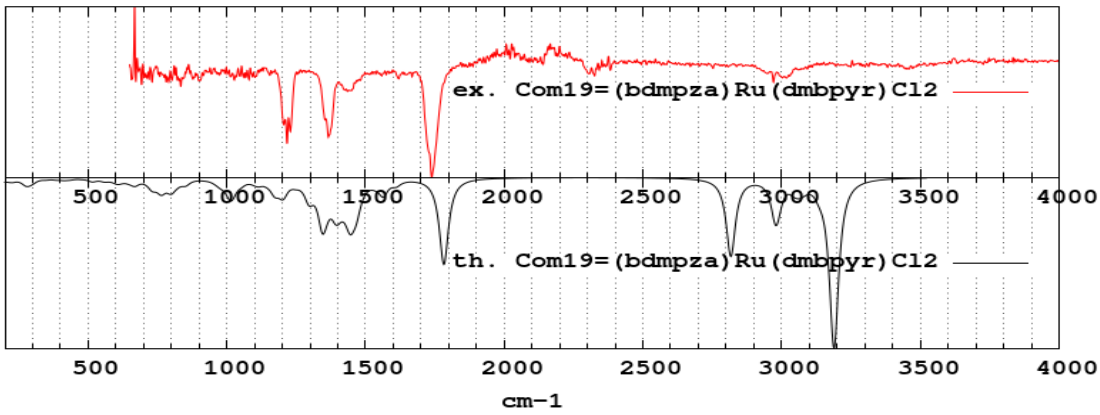
ex. Com19=(bdmpza)Ru(dmbpyr)Cl2
th. Com19=(bdmpza)Ru(dmbpyr)Cl2
500
1000
1500
2000
2500
3000
3500
4000
cm-1

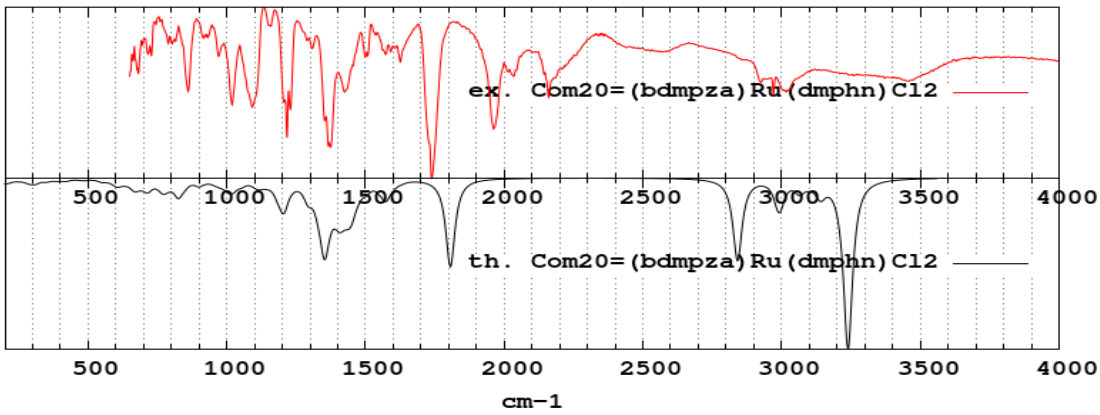
ex. Com20=(bdmpza)Ru(dmphn)Cl2
th. Com20=(bdmpza)Ru(dmphn)Cl2
500
1000
1500
2000
2500
3000
3500
4000
cm-1

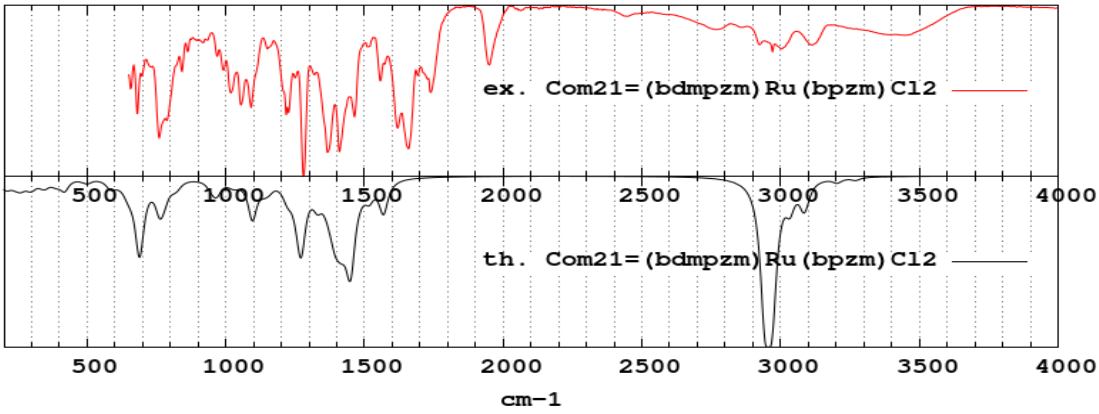
ex. Com21=(bdmpzm)Ru(bpzm)Cl2
th. Com21=(bdmpzm)Ru(bpzm)Cl2
500
1000
1500
2000
2500
3000
3500
4000
cm-1

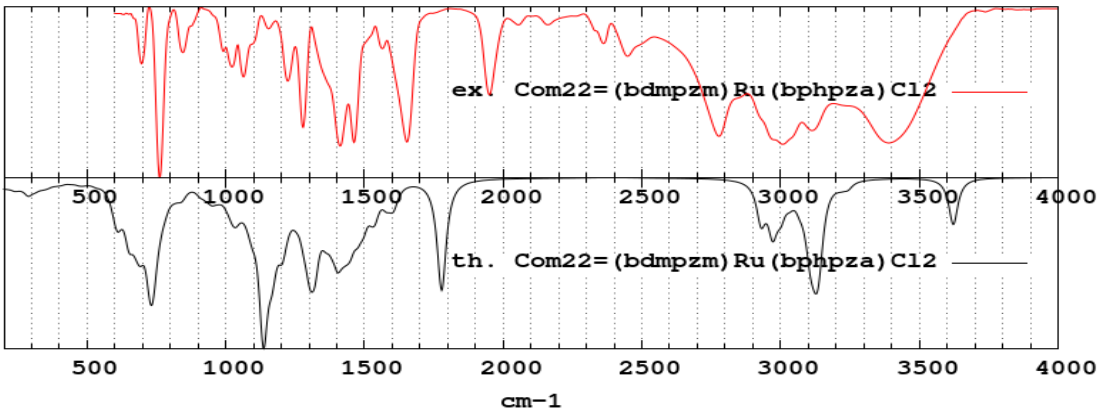
ex. Com22=(bdmpzm)Ru(bphpza)Cl2
th. Com22=(bdmpzm)Ru(bphpza)Cl2
500
1000
1500
2000
2500
3000
3500
4000
cm-1

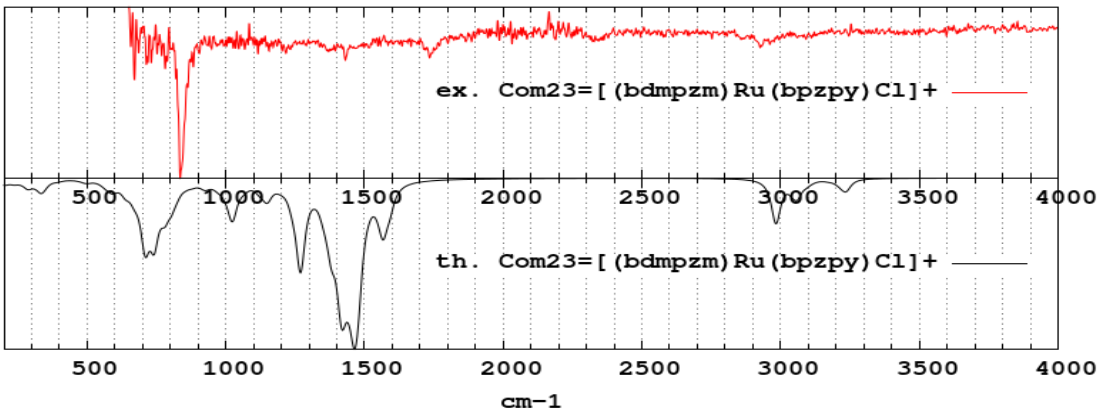
ex. Com23=[(bdmpzm)Ru(bpzpy)Cl]+
th. Com23=[(bdmpzm)Ru(bpzpy)Cl]+
500
1000
1500
2000
2500
3000
3500
4000
cm-1

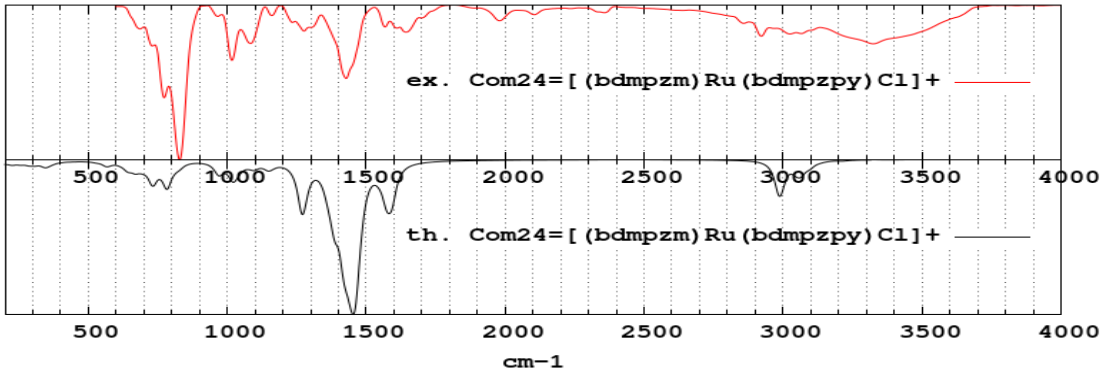
ex. Com24=[(bdmpzm)Ru(bdmpzpy)Cl]+
th. Com24=[(bdmpzm)Ru(bdmpzpy)Cl]+
500
1000
1500
2000
2500
3000
3500
4000
cm-1

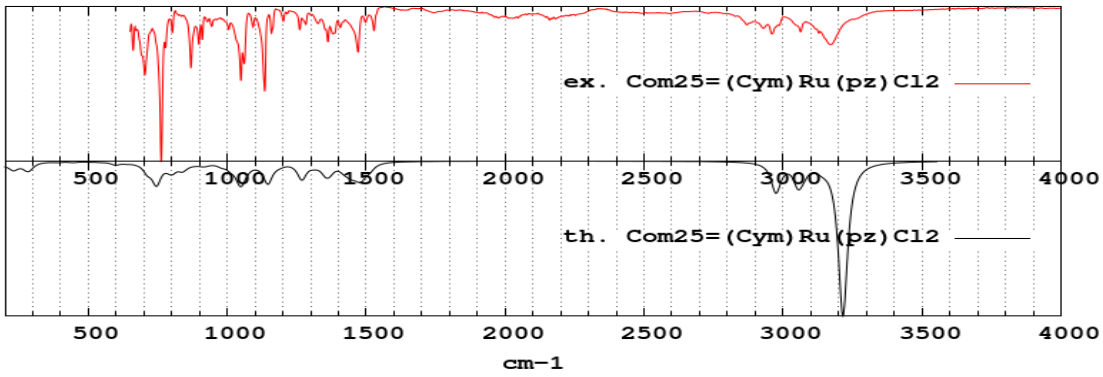
ex. Com25=(Cym)Ru(pz)Cl2
th. Com25=(Cym)Ru(pz)Cl2
500
1000
1500
2000
2500
3000
3500
4000
cm-1

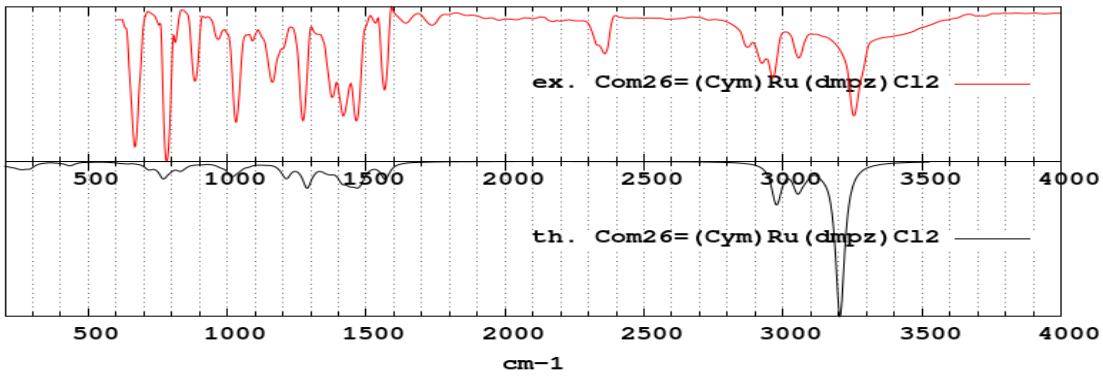
ex. Com26=(Cym)Ru(dmpz)Cl2
th. Com26=(Cym)Ru(dmpz)Cl2
500
1000
1500
2000
2500
3000
3500
4000
cm-1

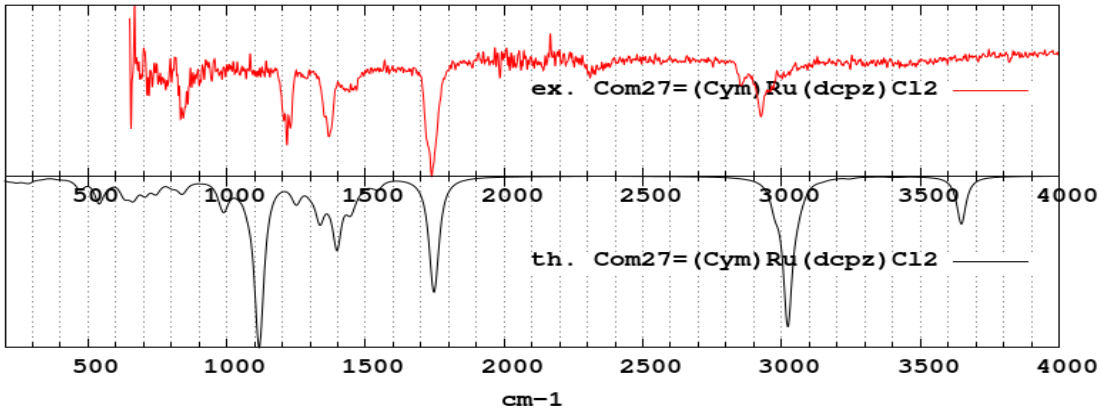
ex. Com27=(Cym)Ru(dcpz)Cl2
th. Com27=(Cym)Ru(dcpz)Cl2
500
1000
1500
2000
2500
3000
3500
4000
cm-1

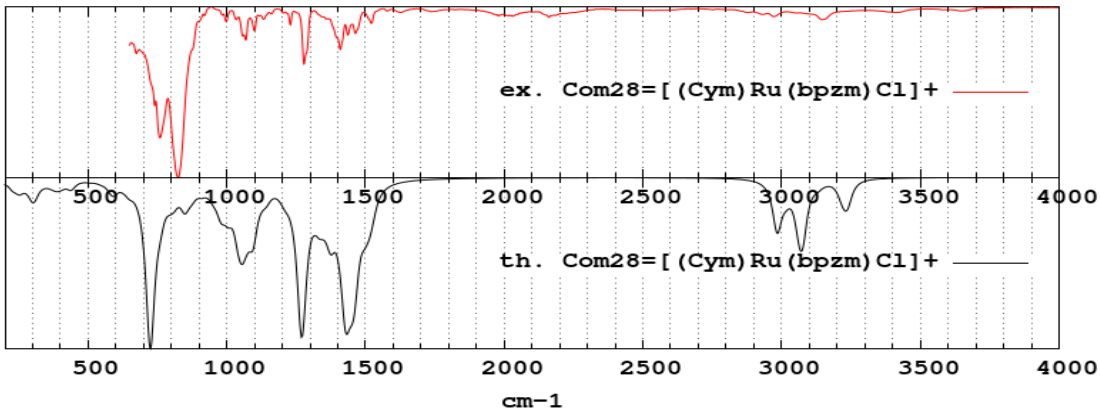
ex. Com28=[(Cym)Ru(bpzm)Cl]+
th. Com28=[(Cym)Ru(bpzm)Cl]+
500
1000
1500
2000
2500
3000
3500
4000
cm-1

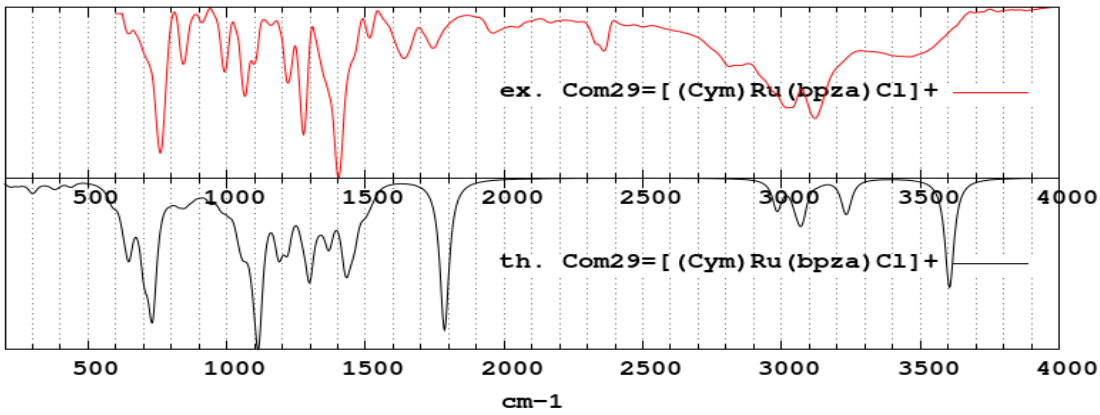
ex. Com29=[(Cym)Ru(bpza)Cl]+
th. Com29=[(Cym)Ru(bpza)Cl]+
500
1000
1500
2000
2500
3000
3500
4000
cm-1

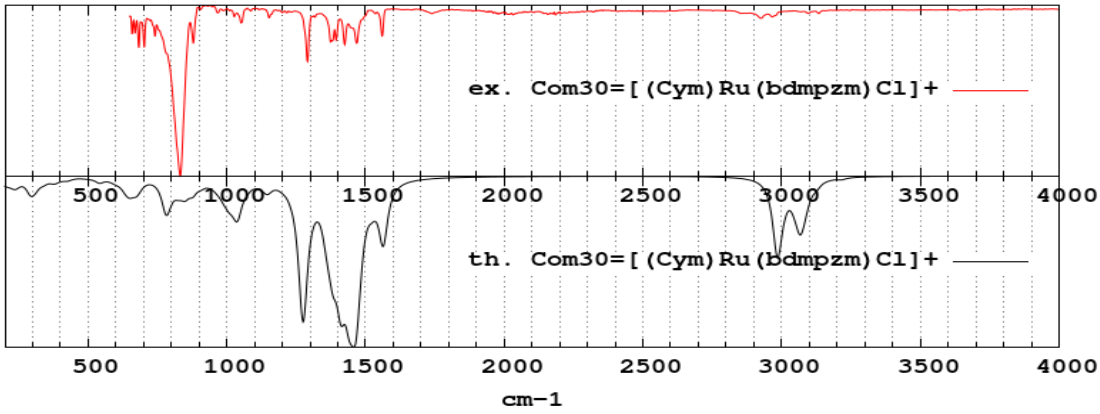
ex. Com30=[(Cym)Ru(bdmpzm)Cl]+
th. Com30=[(Cym)Ru(bdmpzm)Cl]+
500
1000
1500
2000
2500
3000
3500
4000
cm-1

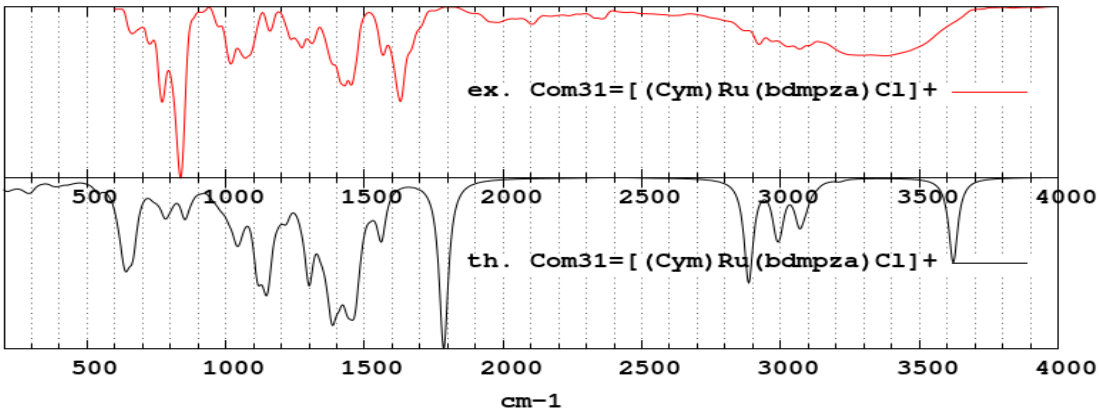
ex. Com31=[(Cym)Ru(bdmpza)Cl]+
th. Com31=[(Cym)Ru(bdmpza)Cl]+
500
1000
1500
2000
2500
3000
3500
4000
cm-1

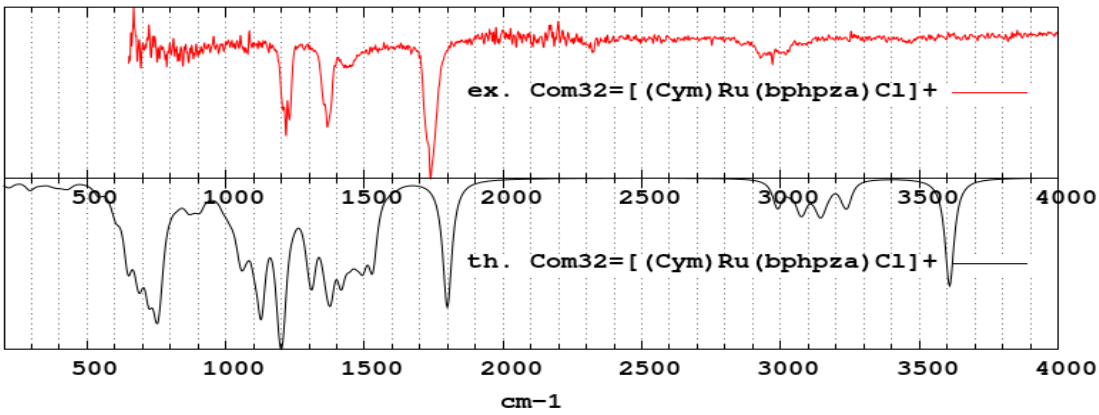
ex. Com32=[(Cym)Ru(bphpza)Cl]+
th. Com32=[(Cym)Ru(bphpza)Cl]+
500
1000
1500
2000
2500
3000
3500
4000
cm-1

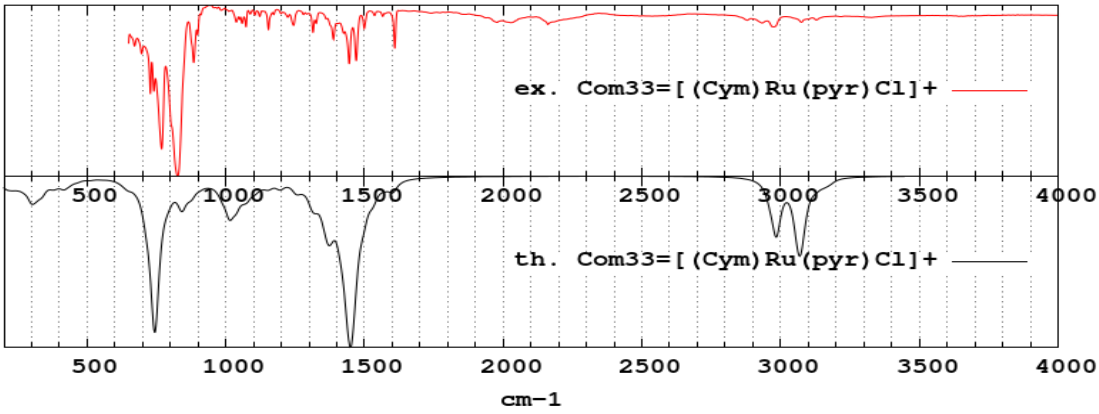
ex. Com33=[(Cym)Ru(pyr)Cl]+
th. Com33=[(Cym)Ru(pyr)Cl]+
500
1000
1500
2000
2500
3000
3500
4000
cm-1

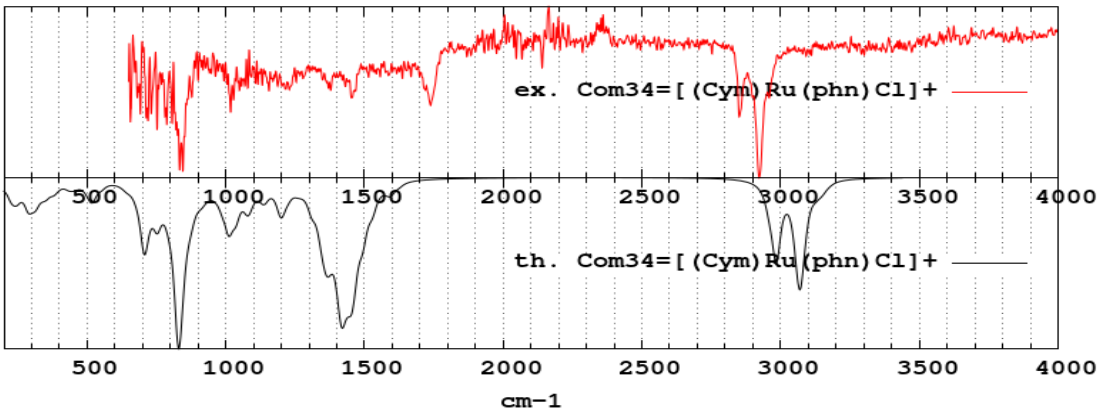
ex. Com34=[(Cym)Ru(phn)Cl]+
th. Com34=[(Cym)Ru(phn)Cl]+
500
1000
1500
2000
2500
3000
3500
4000
cm-1

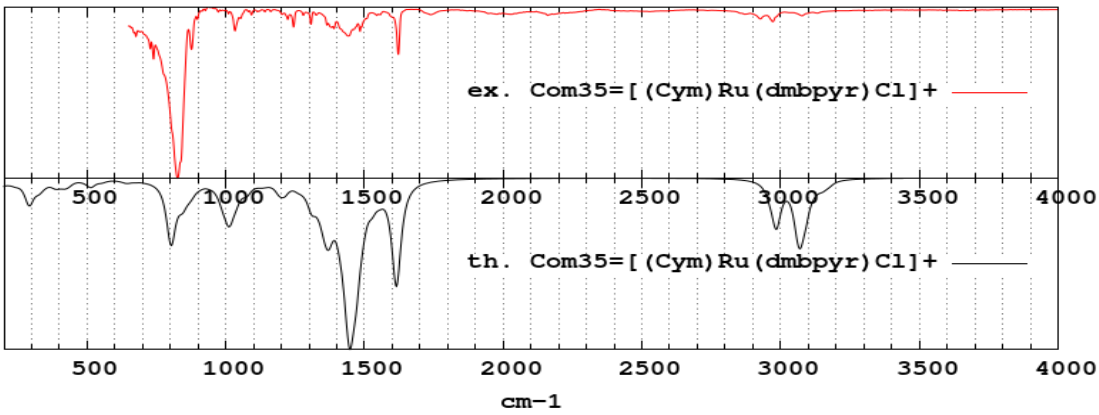
ex. Com35=[(Cym)Ru(dmbpyr)Cl]+
th. Com35=[(Cym)Ru(dmbpyr)Cl]+
500
1000
1500
2000
2500
3000
3500
4000
cm-1

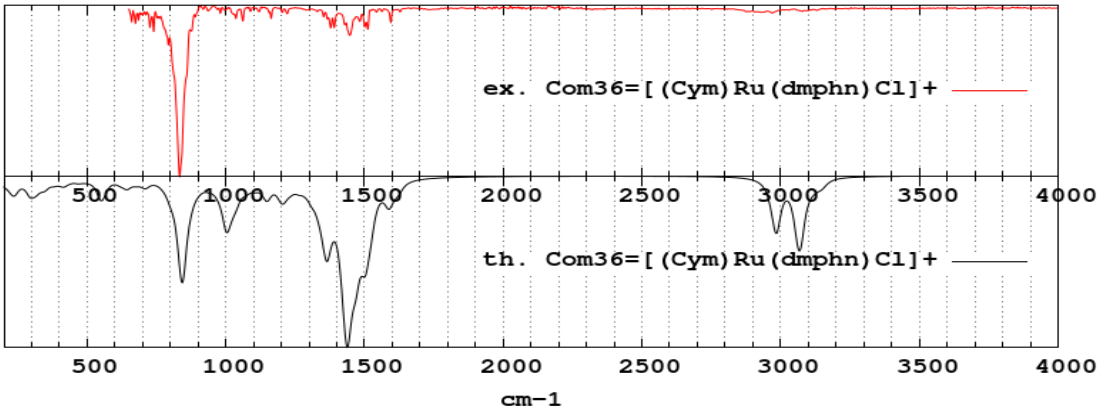
ex. Com36=[(Cym)Ru(dmphn)Cl]+
th. Com36=[(Cym)Ru(dmphn)Cl]+
500
1000
1500
2000
2500
3000
3500
4000
cm-1

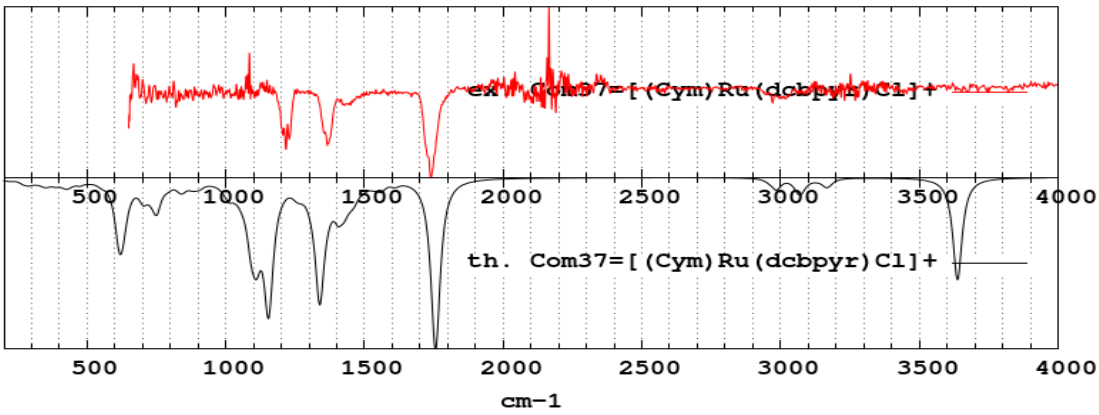
th. Com37=[(Cym)Ru(dcbpyr)Cl]+
500
1000
1500
2000
2500
3000
3500
4000
cm-1

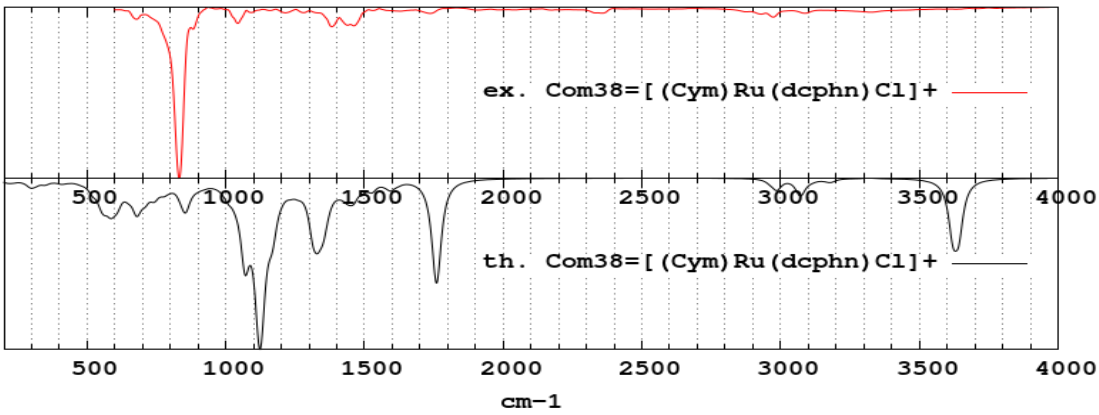
ex. Com38=[(Cym)Ru(dcphn)Cl]+
th. Com38=[(Cym)Ru(dcphn)Cl]+
500
1000
1500
2000
2500
3000
3500
4000
cm-1

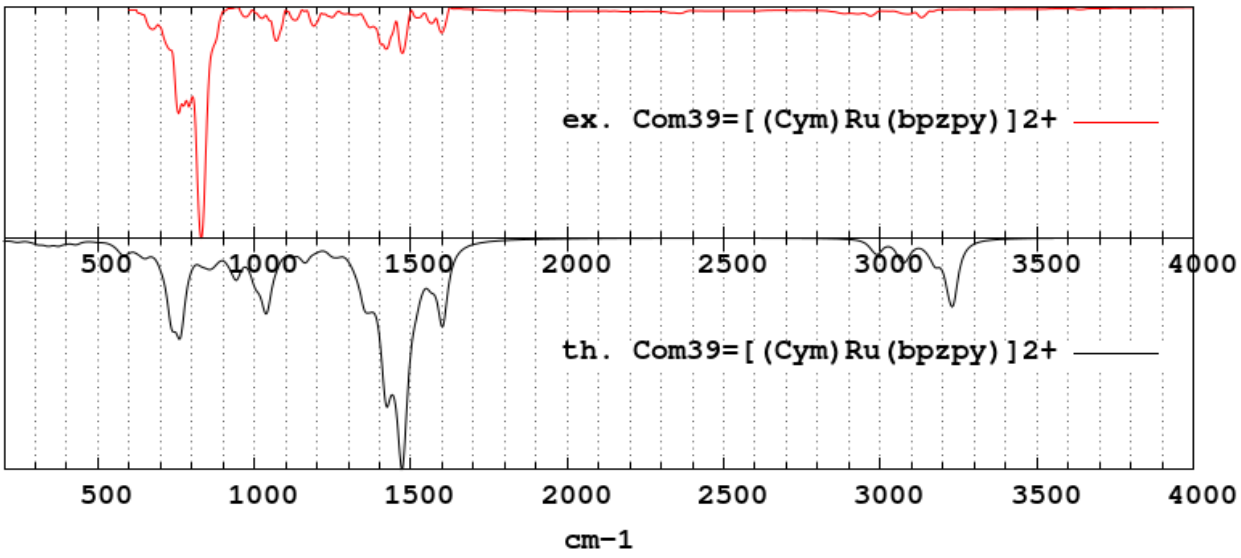

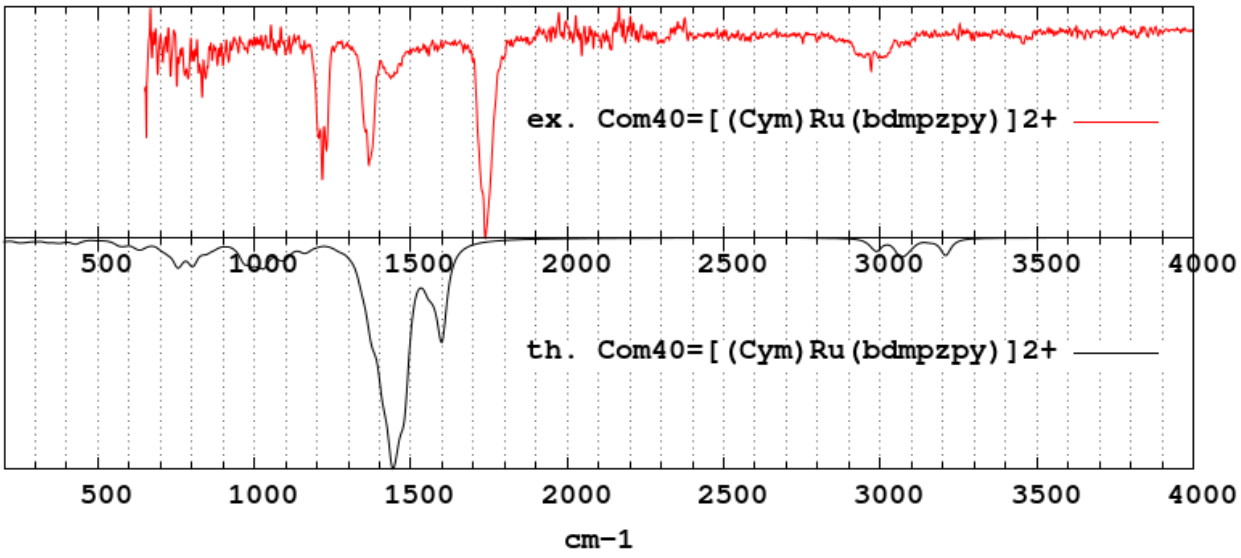

Figure 5.2: The IR plots of the complexes showing the correlation of the experimental (red) and the theoretical (black).

CHAPTER SIX

6 SUMMARY, CONCLUSION AND RECOMMENDATION

6.1 Summary

In this thesis, the literature review of the Ru-based complexes as promising alternative to *cis*-platin were presented in Chapter One and Two. In addressing some of the pressing challenges like lack of proper knowledge of the targets of Ru-based complexes, complication of their chemistry and instability, we have adopted different theoretical methods to elucidate the geometrical stability, spectroscopic properties and predicting the possible targets through docking as presented in Chapter Three. The experimental methods use for the synthesis of the ligands used for the synthesis of all our Ru complexes and their computational studies are presented in Chapter Four while Chapter Five gives information about the experimental synthesis, characterization and theoretical elucidation of the synthesised complexes.

In subsection 3.3.1, several quantum properties including the NEDA and QTAIM are computed on three models of RAPTA-C complexes using DFT with hybrid functional and basis set with ECP and without ECP. Several interesting correlations within the observed properties and also with the reported experimental behaviours of these complexes including their biological activities presented. The study shows that the stability of the two complexes with bidentate ligands is associated with their high hydrogen bonding stability and existence of stronger non-covalent metal-ligand bonds. The energy decomposition analysis indicated that inter-atomic interactions in the three forms of RAPTA-C complexes and their stability are governed by the charge transfer term with significant contributions from polarization and electrostatic terms. The higher stability of complex **1** and **2** over **3** comes from the lower exchange repulsion and a higher polarization contributions to their stability which agree

perfectly with the experimental observation. Our results provide insight into the nature of intramolecular forces that influence the structural stability of the three complexes [313].

In subsection 3.3.2, the computational properties of the η^6-toluene and η^6-trifluorotoluene half-sandwich Ru(II) anticancer complexes and their respective hydrated complexes were computed using DFT method and the quantum theory of atoms in a molecule (QTAIM) analysis. The interatomic properties that are crucial in understanding the non-covalent interactions and the stability of these complexes were considered. We observed that high polarization, charge transfer and strong networks of intramolecular hydrogen bond (HB) interactions significant influenced the stability of these complexes. The trifluorotoluene and the hydrated models are characterised with higher charge transfer, polarizability, synergistic effect of ligand fragments, stronger and higher HB interactions that support their reported experimental anticancer activities and the mechanism of their activation by hydrolysis. The complexes are predominantly characterised with metal to ligand charge transfer [314].

In subsection 3.3.3, the factors that determine the stability and the effects of non-covalent interaction on the η^6-arene ruthenium anticancer complexes are determined using DFT method. The intramolecular and intra-atomic properties were computed for two models of these half-sandwich ruthenium anticancer complexes and their respective hydrated forms. The results showed that the stability of these complexes depends largely on the network of hydrogen bonds (HB), strong nature of charge transfer, polarizability and electrostatic energies that exist within the complexes. The hydrogen bonds strength was found to be related to the reported anticancer activities and the activation of the complexes by hydration. The metal-ligand bonds were found to be a closed shell systems characterised by high positive Laplacian values of electron density. Two of the complexes are found to be predominantly characterised with LMCT while the other two are predominately characterised with MLCT [315].

In subsection 3.3.4, the intramolecular properties of five sets of ruthenium based anticancer

complexes have been theoretically studied using DFT method. The values of the energies show that PBE0 functional is good for the optimization of the metal complexes. The computed properties with minimal basis set or ECP basis sets reproduce the orders in reference higher basis set. The results shows that these complexes are thermodynamically stable and the stability is significantly enhanced through the high level of polarizability (POL), charge transfer (CT) and electrostatic (ES) contributions which may contribute to their biological effects. The presence of carboxylic unit waS found to enhance the contributions of these factors. The QTAIM atomic properties of ruthenium changed significantly with changes in the chemical environment of the complexes. The NEDA analysis shows that these type of complexes are predominantly characterised with ligand to metal charge transfer (LMCT).

DFT method was applied to study the thermodynamic and spectroscopic properties of three Ru-based complexes in Subsection 3.4.1. Possible reasons for the reported experimental stability of complexes **1** and **2** with bidentate chelating ligands over complex **3** were explained using the computed properties. The results show that the trend in their thermodynamic, hyperpolarizabilities, magnetizabilities and the NMR isotropic shielding agree well with many of their experimental properties which can be used to explain the reported differences in their stability, hydrolysis and anticancer activities. We also found out that these complexes that were originally designed as anticancer agents have high hyperpolarizabilities which suggest that they can also act as good non-linear optical (NLO) materials [316].

In subsection 3.4.2, computational method was used to study the correlation between the hydrolysis and the anticancer activities of selected Ru(II)-based complexes. Interestingly, the mechanism of activation by hydrolysis and their consequential anticancer activities was found to be associated with favourable thermodynamic changes, higher hyperpolarizability (ß), lower band-gap and higher first-order net current. The Fermi Contact (FC) and Spin Dipole (SD) were found to be the two most significant Ramsey terms that determine the spin-spin couplings (J(HZ)) of most of the existing bonds in the complexes. Many of the computed properties give insights into the change in the

chemistry of the complexes due to hydrolysis. Besides strong correlations of the computed properties to the anticancer activities of the complexes, using the quantum theory of atoms in a molecule (QTAIM) to analysed the spectroscopic properties shows a stronger correlation between the spectroscopic properties of Ru atom to the reported anticancer activities than the sum over of the spectroscopic properties of all atoms in the complexes [317].

In subsection 3.4.3, different density functional methods (DFT) were used to optimize and study the chemistry of five potential anticancer complexes in terms of their electronic, conductive and spectroscopic properties. Many of the computed properties in addition to the IR and QTAIM analysis of the NMR are dipole moment vector (μ_i), linear polarizability tensor (α_{ij}), first hyperpolarizability tensors (β_{ijk}), polarizability exaltation index (Γ) and chemical hardness (η) of the complexes. A stable low energy geometries were obtained using basis set with effective core potential (ECP) approximation but in the computation of atomic or molecular properties, the Ru metal atom is better treated with higher all electron basis set like DGDZVP. The spectroscopic features like the IR of the metal-ligand bonds, the isotropiC-NMR shielding tensor of the coordinated atoms are significantly influenced by the chemical environment of the participating atoms. The carboxylic and pyrazole units were found to significantly enhance the polarizabilities and hyperpolarizabilities of the complexes while the chloride only improves the polarity of the complexes. Fermi contact (FC) have the highest effect followed by the PSO among all the four Ramsey term which defined the total spin-spin coupling constant J(HZ) of these complexes.

In subsection 3.5.1, the interactions of selected Ru(II)-based complexes with different cancer receptors were carried out through computational docking. In an effort to search for better alternatives to *cis*-platin and its derivatives that are nonselective cytotoxic anticancer agents, many metal based complexes especially that of Ru(II)-based complexes with potential alternative targets other than universal target like DNA have been suggested. This subsection focus more on finding alternative

protein targets other than DNA for some Ru(II)-based complexes using computational docking as a means of addressing commonly reported research challenges on the lack of proper understanding of the anticancer targets of Ru-based complexes. The observed interactions through our docking study show that, besides predicted targets like Cat B, HP-NCP and Kinase which is in good agreement with what they have been experimentally suggested as possible target of Ru-based anticancer agents, other targets like RNR and HDAC7 were proposed. The fast majority of the complexes are on the average have good interaction with rHA which will enhance their pharmacokinetic properties and some of the complexes also are suggested to have the potential for dual roles of acting as anticancer and as antimalarial agents because they are found to bind favourably with DNA-Gyrase [318].

In subsection 3.5.2, some promising anticancer complexes of Ru(II) such as RAPTA based complexes formulated as [Ru(η^6-p-cymene)L_2(pta)] and those with unusual ligands were docked against receptors using Autodock, Glide and Gold. Cat B and Kinases receptors have been experimentally confirmed as possible targets of the complexes and are also predicted by the three methods as one of the most targeted receptors while Top II and HDAC7 are predicted by two and one of the methods as the best targets. The interesting features of the binding of the complexes show that some of the complexes preferentially target specific macromolecule unlike the other which is an indication of their specificity and probable therapeutic combination without severe side effect that may come from competition for the same target. Also, introduction of unusual ligands were found to significantly improve the activities of most of the complexes studied. Strong correlations were observed for the predicted binding sites and the orientation of the complexes within the binding site by the three methods of docking. However there were observable disparities in the ranking of the complexes by the three method of docking especially that of Glide [319].

In subsection 3.5.3, Molegro and Autodock were used to predict the anticancer activities of selected Ru(II) complexes against twelve anticancer targets. Unlike the organic molecules, reports on docking of metal complexes are very few mainly due to inadequacy of force fields in docking packages

to appropriately characterised the metal atoms which thus hinder their use in rational design of metal-based drugs. We observed that introducing the quantum calculated atomic charges of the optimized geometries significantly improved the docking predictions of these anticancer metallocompounds. Most of our newly proposed metallocompounds were found theoretically as better anticancer metallocompounds than all the experimentally proposed RAPTA complexes. An interesting features of strong interactions of new modelled of metallocompounds against both base edge of DNA strands suggest similar mechanisms of anticancer activities to *cis*-platin. There is possibility of covalent bonding between the metal centre of the metallocompounds and the residues of the receptor DNA-1, DNA-2, HDAC7, HIS and RNR. However, the results suggest the possibility of metals positioning the coordinated ligands for optimal receptor interactions and synergistic effects rather than forming covalent bond [320].

In section 4.3, the spectroscopic and the geometric properties of four ligands with pyrazole unit were studied at both experimental and computational levels. The computational results are perfectly in agreement with the experimental results especially in terms of the spectroscopic properties. The spectroscopic features as well as the computed properties were used to establish the successful synthesis of bdmpzm and bdmpza ligands. The theoretical and the experimental IR and Raman spectra significantly help in distinguishing the four ligands. The results show that the Raman spectra is better applicable in characterising the CH_3 deformation, the C-H, CNN and $CCNN_{out}$ of the ligands but vibrations like N-H in dmpz and O-H, C=O in bdmpza were observed to be Raman inactive. Significant variations were observed among the two available *N atoms characterising the bidentate features of bdmpzm, bdmpza and bdcpzm which indicate possible different affinities for metal coordination. Also the result suggest that bdmpza will be the best starting material for NLO application than other while bdcpzm is predicted to have potential of been a poor coordinating ligand.

In section 4.4, two pyrazole (pz) derivatives (bpzm and bpza) were synthesised and characterised by spectroscopic analysis. Many of the functional groups in these ligands were found to

be Raman active which also helps in their spectroscopic elucidation. The electronic, spectroscopic and conductivity properties of pz, bpzm, bpza and bpzpya were further studied using DFT methods. The computed properties such as the IR, ^{1}H-NMR, ^{13}C-NMR and UV are found to be highly correlated with the experimental values. Many of the computed properties like the dipole, band gap, hyperpolarizability and reactivity are in the order of bpzpya > bpza > bpzm > pz.

In section 4.5, the electronic and spectroscopic properties of seven pyrazole derivatives were studied. Four out of the seven ligands were synthesised and characterised experimentally. The excitation properties computed using the TDDFT shows that most of the experimentally observed absorptions of the ligands are predominantly from either the HOMO or HOMO-1 to LUMO or LUMO+1. The characteristic features of the *N atoms (i.e. metal available coordinating centre) shows that the carboxylic unit may possibly decrease the metal affinity of the pyrazole unit while the pyridine unit will increase the affinity. The conductivity properties of the seven ligands are in the order of bdmpzpy > bpzpy > bphpza > bdcpzpy > phpz > dcpz.

In section 4.6, the experimental and theoretical properties of six ligands comprising of three bipyridine and three phenanthroline derivatives were studied. The carboxylic units in the ligands result to increase in the dipole and anisotropic properties of the molecules while the methyl group result to increase in the isotropic shielding tensor of the molecules. Most of the observed UV λmax in the ligands are predominantly excitation of electrons from the HOMO-2 or HOMO-1 or HOMO to the LUMO of the ligands. The ligand dcphn is predicted to be the best starting material for non-linear optical (NLO) application due to its far higher first static hyperpolarizability tensor compared to other ligands and its lowest band gap.

In Chapter Five, forty Ru(II) complexes were synthesised from four ruthenium precursors and their spectroscopic features are elucidated using theoretical methods. A very high correlation was observed between experimental and theoretical characterisation of the complexes which is an indication of strong agreement between the experimentally synthesised and theoretically predicted complexes.

The theoretical approach significantly helps to elucidate and give more detail insight into the complicated chemistry of the complexes. The experimentally observed IR peaks are reproduced theoretically for many of the complexes. All the peaks including the fingerprint region that is know to be relevant for the structural peculiarities and equally known to be difficult are successfully assigned using the potential energy distribution (PED) method. The general trend in the ^{1}H-NMR chemical shift is $CH_3 < C_{cym}$-H $< C_{cym\text{-}arene}$-H $< CH_2 <$ C4-H $< C_{pz}$-H $<$ COOH $< C_{bpyr}$-H $<$ CHOO $<$ NH; in ^{13}C-NMR is $CH_3 < C_{cym}$-H $< CH_2 <$ **C**HCOOH $< C_{cym\text{-}arene} < C_{pyr\text{-}meta} <$ C4 $<$ C3 $<$ C5 $< C_{others} <$ CH**C**OOH, in ^{15}N-NMR N > **N > *N while the ^{99}Ru-NMR chemical shift in Cymene containing complexes are lower than the complexes without Cymene group. However, the presence of Ru atom in the complexes results to a more shielding effect and consequential lower shift of the 1H-NMR and 13C-NMR of the respective H and C atoms that are pointing toward the Ru atom while reverse is the case of those that are directed towards the Cl and carbonyl groups in the complexes.

6.2 Conclusion

In the subsection 3.3.1, an insight into the molecular properties like NBO, NEDA and QTAIM analysis of three Ru-based complexes named RAPTA-C derivatives were provided using DFT method. From the NBO analysis, we observed that the three complexes are characterised mainly with MLCT specifically from the Ru atom to the lone pair C atoms of arene π-ligand. The NEDA analysis shows that the stability of the complexes is most significantly determined by charge transfer followed by strong polarization and electrostatic. There is a high synergistic effect of the metal coordinated ligands on each other resulted to high induced dipole and induced stabilization energy which further support the reported differences in their stability and anticancer activities. The QTAIM analyses show that the metal-ligand bond are characterised with non-sharing bonds. We equally found out that the presence of NNA in our system with ECP basis set is a complete computational artefact which suggests the application of ECP will be appropriate in computing intramolecular properties if limited to metal atom only in these complexes. In addition to the significant effect of the bonds $\rho(r)$ and $\nabla^2\rho(r)$, bond ellipticity and the ratio of the potential energy density and Lagrangian form of kinetic energy density (V/G) are found to significantly influence the reported differences in the hydrolysis of the complexes. The intraatomic properties computed show that the atomic electrons are largely localized except for the H atoms which are highly delocalized and can be easily perturbed. The atomic volume V(A) of the Ru atom is found higher in complex RAPTA-C than complexes *carbo*-RAPTA-C ans *oxalo*-RAPTA-C derivatives which can further enhance its reported higher hydrolysis and anticancer activities.

The computed geometrical properties of the ruthenium complexes named RAPTA-T, RAPTA-CF3 and their hydrated models in subsection 3.3.2 give additional features. The hydrolysed complexes are characterised with higher values of induced dipole and hydrogen bond stabilization energy which gives a rational behind the reported activation of the complexes by hydrolysis. The complexes with trifluorotoluene are found to be characterised with stronger and higher number of intramolecular HB

interactions which consequently resulted in higher charge transfer, polarizability and synergistic effects (higher induced dipole and induced wavefunction) of the different units of ligands that made up the complexes. The synergistic effects can lead to highly cytotoxic species as it was experimentally suggested [62]. The computed properties of four ruthenium complexes named RAPTA-B and RAPTA-C and their respective hydrated forms were also studied in subsection 3.3.3. The hydrated form of RAPTA-C have the highest interaction energy as a result of its significant high CT, ES and POL which gives a possible distinguishing features that can contribute to its reported higher anticancer activities above the other [13].

The results obtained in subsection 3.3.4 for five different complexes shows that the PBE0 functional combined with ECP basis set is the most appropriate for the geometry optimization of these type of metal complexes in agreement with the literature [332, 333] because it gives the energy values closed to that of higher perturbation MP2 method. The set of complexes considered here can be described in terms of ligand to metal charge transfer (LMCT). The strength of the Ru-N bonds in the complexes follows the order 5>2>4>3>1 if only the mid Ru-N bond is considered in complexes 4 and 5 which agrees with the experimental report of stronger Ru-N_{bpyr} bonds than R-N_{phn} [379]. The presence of the carboxylic unit in the ligands significantly contributes to the H-bonding networks and the total hydrogen stability of the complexes.

In subsection 3.4.1, we have been able to establish the possible relationship between the reported experimental properties of three RAPTA complexes and the computed properties like the thermodynamic, magnetizabilities, spin-spin coupling, NMR shielding, dipole moment and hyperpolarizabilities. More significantly, inferences are made to the reported anticancer activities of the three complexes based on the correlation of the computed properties to the trend of their anticancer activities. The possibility of these complexes also acting as good NLO materials was also suggested giving indication that higher polarizability may play significant role in their anticancer activities. In subsection 3.4.2, the electronic, conductive and spectroscopic properties of the eight Ru(II)-based

complexes were computed. Also, we point out significant changes in the computed properties from the unhydrated to the hydrated complexes as a known mechanism of activation of ruthenium anticancer complexes. Other properties computed are the magnetizability contribution ($\chi_{Iso}(A)$), dipole ($\mu(A)$) and magnetic shielding tensor ($\sigma_{Iso}(A)$) using QTAIM analysis as implemented in AIMAll. There is a high relation between the anticancer activities and the conductivities of the complexes as the activated complexes which are the hydrated forms are characterised with higher hyperpolarizability (ß) and lower band-gap. We observed that the properties of the Ru atom in each of the complexes like higher $\chi_{Intra\_Iso}(A)$ and lower magnitude of $\chi_{Iso}(A)$ correlate significantly with their reported anticancer activities. Similarly, five different ruthenium complexes were studied in subsection 3.4.3. The difference in the IR features of these complexes shows that there is either bathochromic or hypsochromic shift in the IR vibration modes of the metal-ligand bonds like Ru-N as a result of the change in the chemical environment of participating atoms. Among the Ramsey terms, the FC was found to have the greatest values and also have the highest effect on the computed spin-spin coupling constant J(HZ) followed by the PSO and SD while the DSO is least. Complexes 2 and 3 are predicted as the most stable characterised with the highest value of Γ [345] and the most reactive with lowest band gap (very soft) [395].

In subsection 3.5.1, metal complexes are docked against receptors using Autodock and Glide docking packages. The general feature of the docking shows that the inhibitory activities do not directly depend on the number of the HB nor number of the MR but on their strength and other possible interactions that could not be directly accounted for. Also, there is preference for better HB in the interactions of the complexes with receptor residues than assuming an orientation that would allow close MR interaction. Autodock and Glide docking give preference to some of the newly proposed complexes like **8**, **9, 10** and **11** as inhibitors of most of the receptors than many of the RAPTA's complexes. One of the observed reasons for the preferential binding of the newly proposed structures is

observed to be as a result of enhanced HB especially through the presence of carboxilic group in some of the new complexes. Besides experimentally established possible anticancer target of Ru(II)-based complexes like Cat B, other suggested targets are HDAC7, Kinase, TS and HP-NCP. Also, RNR as a rare anticancer target of many complexes is predicted as alternative anticancer target for the newly proposed complexes **9** and**10**. A similar study was carried out in subsection 3.5.2 using Autodock, Glide and Gold on different sets of ruthenium complexes in relation to RAPTA complexes. Cat B was found to be the most possible target for these complexes as predicted by the three packages. Also, Top II and Kinase are predicted by two of the packages as some of the best targets while HP-NCP, HDAC7, DNA-Gyrase and RNR are suggested by one of the packages as part of the best targets. It is equally interesting to point out the three docking packages clearly show that the activities of the RAPTA complexes are enhanced when hydrolysed which is in good agreement with the experimental reports [8, 17, 37, 38]. Predictions from Autodock and Gold correlate better with experimental and each other than Glide. Also in subsection 3.5.3, we have presented the binding affinities of new model metallocompounds and that of RAPTA complexes using Molegro and Autodock methods of docking. Making use of the atomic charges of the metallocompounds obtained from the optimized quantum calculation significantly improved the predicted activities and ranking of the metallocompounds which strongly agree with the available experimental results. In summary, the new models are predicted by all the methods of docking among the best two inhibitors of all the receptors. Considering the ranking of both relax and constrained Molegro docking, the best targets of the metallocompounds are of the order HDAC7 > DNA-1 > rHA > Cat B > DNA-2 > Gyrase > TrXR > Top II > TS > RNR > HiS > Kinase except in few cases like complex **12** that prefers Cat B to rHA. The RAPTA complexes are suggested to target protein like Cat B and HDAC7 better than DNA which further confirms the experimental suggestion that DNA may not be the target of RAPTA complexes [9].

In section 4.3-4.6 of chapter four, the electronic and spectroscopic properties of the different sets of ligands were studied experimentally and computationally. Very strong agreements were

observed between the experimental and theoretical results. The finger print region of the IR and Raman spectra helps in distinguishing the ligands. Some of the vibration which are very prominent in Raman spectral are CH_3 deformation, the C-H, CNN and $CCNN_{out}$ of the ligands. However, some vibrations like N-H in dmpz and O-H, C=O in bdmpza is observed to be Raman inactive. Both the experimentally and theoretical obtained proton and carbon shifts significantly distinguishes the ligands. Using both the direct method and fitting methods, the calculated ^{1}H-NMR shift agrees strongly with the experiment. Also, the experimental values of the ^{13}C-NMR shift were better reproduced using the direct method but the fitting method underestimate the shifts. The most contributing part of the Ramsey terms to the J-coupling of the bonds is the FC followed by the PSO while the SD and DSO have the smallest contribution. The stronger *N-N bond within a pair is characterised with shorter bond length, higher magnitude of $\nabla^2\rho(r)$, $\rho(r)$, V and ∇^2Ven and lower ellipticity (ε). The usual H-bonding are characterised with negative values of J-Coupling compared to the unusual types that have positive values. In many of the ligands, the absorptions are found to be the result of the predominant nature of HOMO→LUMO, HOMO-1→LUMO+1, HOMO-1→LUMO and HOMO-2→LUMO.

In the Chapter Five, we have reported the successful synthesis of forty Ru(II)-based (**C1-C40**) complexes from four precursors (**ST1-ST4**). Their spectroscopic with the geometrical properties are elucidated using the computational methods. A very strong agreement between the experimental and theoretical IR and ^{1}H-NMR which further confirm that the expected Ru(II)-based complexes were successfully synthesised. Deeper insights into the complicated chemistry of the complexes are obtained through the theoretical studies of their ^{13}C-NMR, ^{15}N-NMR and ^{99}Ru-NMR. Interestingly, many of IR peak intensities which were observed experimentally were also reproduced theoretically. The major difference between the experimental and theoretical is the OH vibration which is observed theoretically at higher frequency and well separated from the CH vibration compared to the experimental. Also, the theoretical predicted high intensity of vibration around 2600 to 2700 cm^{-1} in complexes like **C6**, **C8**, **C9** and **C11** are experimentally found to be very weak. With the application of potential energy

distribution (PED) methods on the theoretical IR, the experimentally observed peaks including the difficult fingerprint region are fully assigned. The IR vibrations that are dominantly strong in the complexes are stretching υ(SO), υ(C=O), υ(C-O) υ(NN), υ(CH), υ(NC), υ(CC), υ(OH), bending β(OCO), β(HOC), β(HCC) and torsional τ(HCSRu), τ(HCCO), τ(HCCC), τ(HCCN), τ(HOCC). In the starting complexes **ST3**-**ST4**, the υ(RuCl) IR vibration is very strong but its intensity in the complexes **C1**-**C40** is lower. Both experimental and theoretical ^{1}H-NMR shift are in good agreement as found in many of the complexes. The general observation is that the protons that are directed towards the Ru metal centre are characterised with more shielding effect which results to lower shift while the reverse is the case of the protons that are directed towards the chloride or carbonyl group. The common trend in the proton shift of the complexes follow the order CH_3 < C_{cym}-H < $C_{cym\text{-}arene}$-H < CH_2 < C4-H < C_{pz}-H < COOH < C_{bpyr}-H < CHOO < NH. However, in some complexes the strong effect of the Ru atom shielding effect and Cl or carbonyl deshielding effect cause a change in the order. In many of the complexes, the proton shift of the linker CH_2 of the pyrazole derivatives are low and very close to that of the methyl shift except where any of its protons is directed toward the Cl atom.

6.3 Recommendation for further study

One of the major barrier in the rational design of the Ru(II)-based complexes as anticancer agent is the lack of the proper knowledge of their targets. Also many of the complexes that are found to be active *in vivo* are not active *in vitro*. It is therefore recommended that beyond the cytotoxic screening of the Ru(II) complexes to determine their anticancer activity, there should be more detail screening of the complexes against enzymes like Cat B, Top II, BRAF Kinases, HDAC7 which have been found in this study as probably the best possible targets.

This study shows that there is high possibility of improving the anticancer activities of Ru(II)-based complexes by the introduction of functional group like carboxylic unit. It is therefore recommend that more research effort need to be concentrated on the functionalization of the promising Ru(II)-based complexes, synthesis and study of their anticancer activity.

Many of the originally designed Ru(II)-based anticancer complexes have very high hyperpolarizability properties and lower band gap which are found to correlate with some of their anticancer activities. It will be necessary to study the electronic properties like the conductivity of some of these complexes which may shed some light about their potentials as anticancer agents.

In this study, it was established that stability of the complexes are greatly influence by properties like charge transfer, polarizability and electro static interactions. It is recommended that electronic properties be put into consideration in the design of Ru(II)-based complexes for application in cancer chemotherapy.

In addressing the problems associated with complicated chemistry of Ru(II)-based complexes, this study has found out that computational models can be useful tools to better understand the chemistry and interpretation of the spectroscopic properties of the complexes. It is therefore recommended that the computational modelling of the Ru(II)-based complexes should be given priority

in the rational design of potential anticancer compounds in order to understand their chemistry and get lead compounds.

There is a clear evidence that despite the limitations of docking methods to accurately predict the activities of metal complexes unlike their organic counterparts due to lack of appropriate force fields to represent heavy metal atoms, relativity problem of heavy metal and their polarizability, this study has been able to show that very good experimental correlation of the activities of these complexes can be found theoretically especially if the quantum parameter like the atomic charge is introduced into the docking. It is recommended that more research be carried out on the application of docking packages for the prediction of biological activities of metal-based complexes.

References

1. Sivakumar, R.; Karnan, M. Euro. *J. Sci. Research* **2012**, 88, 89-98.

2. Boulassel, M.R.; Galal, A.; Qaboos, S. *Univ. Med. J.* **2012**, 12, 273-285.

3. Kadioglu, H.; Ersoy, Y.E.; Bozkurt, S.; Memmi, N.; Cipe, G.; Gucin, Z.; Muslumanoglu, M. *Surg. Infect.* (*Larchmt*.) **2012**, 13, 413-414.

4. Seminog, O.O.; Goldacre, M.J. *Br. J. Cancer* **2013**, 108, 193–198.

5. Allardyce, C.S.; Dorcier, A.; Scolaro, C.; Dyson P.J. *Appl. Organomet. Chem*. **2005**, 19, 1–10.

6. Dyson, P.J.; Sava, G. *Dalton Trans.* **2006**, 23, 1929–1933.

7. Sava, G.; Bergamoa, A.; Dyson P.J. *Dalton Trans.* **2011**, 40, 9069-9075.

8. Gasser, G.; Ott, I.; Metzler-Nolte, N. *J. Med. Chem*. **2011**, 54, 3–25.

9. Casini, A.; Gabbiani, C.; Sorrentino, F.; Rigobello, M. P.; Bindoli, A.; Geldbach, T.J.; Marrone, A.; Re, N.; Hartinger, C.G.; Dyson, P.J.; Messori, L. *J. Med. Chem*. **2008**, 51, 6773–6781.

10. Page S. Ruthenium compounds as anticancer agents. *Education in Chemistry* **2012**, www.rsc.org/eic, 22 May 2012.

11. Allardyce, C.S.; Dyson, P.J. *Platium Metal* **2001**, 45, 62-69.

12. Heffeter, P.; Bock, K; Atil, B.; Hoda, M.A.R.; Korner, W.; Bartel, C.; Jungwirth, U.; Keppler, B.K.; Micksche, M.; Berger, W.; Koellensperger, G. *J. Biol. Inorg. Chem*. **2010**, 15, 737–748.

13. Chatterjee, S.; Kundu, S.; Bhattacharyya, A.; Hartinger, C.G.; Dyson, P.J. *J. Biol. Inorg. Chem*. **2008**, 13, 1149–1155.

14. Hartinger, C.G.; Jakupec, M.A.; Zorbas-Seifried, S.; Groessl, M.; Egger, A.; Berger, W.; Zorbas, H.; Dyson, P.J.; Keppler, B.K. *Chem. Biodiver*. **2008**, 5, 2140-2155.

15. Wu, B.; Ong, M.S.; Groessl, M.; Adhireksan, Z.; Hartinger, C.G.; Dyson, P.J.; Davey, C.A. *Chem. Euro. J*. **2011**, 17, 3562-3566.

16. Groessl, M.; Tsybin, Y.O.; Hartinger, C.G.; Keppler, B.K.; Dyson, P.J. J. *Biol. Inorg. Chem*. **2009**, 15, 677–688.

17. Egger, A.E.; Hartinger, C.G.; Renfrew, A.K.; Dyson, P.J. *J. Biol. Inorg. Chem*. **2010**, 15, 919–927.

18. Allardyce, C.S.; Dyson, P.J.; Ellis, D.J.; Heath, S.L. *Chem. Commun*. **2001**, 1396–1397.

19. Dutta, B.; Scolaro, C.; Scopelliti, R.; Dyson, P.J.; Severin, K. *Organometallics* **2008**, 27, 1355-1357.

20. Barragán, F.; López-Senín, P.; Salassa, L.; Betanzos-Lara, S.; Habtemariam, A.; Moreno, V.; Sadler, P.J.; Marchán, V. *J. Am. Chem. Soc*. **2011**, 133, 14098-14108.

21. Bugarcic, T.; Habtemariam, A.; Stepankova, J.; Heringova, P.; Kasparkova, J.; Deeth, R.J.; Johnstone, R.D.; Prescimone, A.; Parkin, A.; Parsons, S.; Brabec, V.; Sadler, P.J. *Inorg. Chem.* **2008**, 47, 11470-11486.

22. Castellano-Castillo, M.; Kostrhunova, H.; Marini, V.; Kasparkova, J.; Sadler, P.J.; Malinge, J.M.; Brabec, V. *J. Biol. Inorg. Chem.* **2008**, 13, 993-999.

23. Dougan, S.J.; Habtemariam, A.; McHale, S.E.; Parsons, S.; Sadler, P.J. *PNAS* **2008**, 105, 11628-11633.

24. Dougan, S.J.; Melchart, M.; Habtemariam, A.; Parsons, S.; Sadler, P.J. *Inorg. Chem.* **2006**, 45, 10882-10894.

25. Fernández, R.; Melchart, M.; Habtemariam, A.; Parsons, S.; Sadler, P.J. *Chem. Euro. J.* **2004**, 10, 5173-5179.

26. Fu, Y.; Habtemariam, A.; Basri, A.M.; Braddick, D.; Clarkson, G.J.; Sadler, P.J. *Dalton Trans.* **2011**, 40, 10553-10562.

27. Habtemariam, A.; Melchart, M.; Fernandez, R.; Parsons, S.; Oswald, I.D.; Parkin, A.; Fabbiani, F.P.; Davidson, J.E.; Dawson, A.; Aird, R.E.; Jodrell, D.I.; Sadler, P.J. *J. Med. Chem.* **2006**, 49, 6858-6868.

28. Kostrhunova, H.; Florian, J.; Novakova, O.; Peacock, A.F.; Sadler, P.J.; Brabec, V. *J. Med. Chem.* **2008**, 51, 3635-3643.

29. Liu, H.K.; Wang, F.; Parkinson, J.A.; Bella, J.; Sadler, P.J. *Chem. Euro. J.* **2006**, 12, 6151-6165.

30. Magennis, S.W.; Habtemariam, A.; Novakova, O.; Henry, J.B.; Meier, S.; Parsons, S.; Oswald, I.D.; Brabec, V.; Sadler, P.J. *Inorg. Chem.* **2007**, 46, 5059-5068.

31. Melchart, M.; Habtemariam, A.; Parsons, S.; Sadler, P.J. J. *Inorg. Biochem.* **2007**, 101(11-12), 1903-1912.

32. Morris, R.E.; Aird, R.E.; Murdoch Pdel, S.; Chen, H.; Cummings, J.; Hughes, N.D.; Parsons, S.; Parkin, A.; Boyd, G.; Jodrell, D.I.; Sadler, P.J. *J. Med. Chem.* **2001**, 44, 3616-3621.

33. Novakova, O.; Chen, H.; Vrana, O.; Rodger, A.; Sadler, P.J.; Brabec, V. *Biochemistry* **2003**, 42, 11544-11554.

34. Novakova, O.; Kasparkova, J.; Bursova, V.; Hofr, C.; Vojtiskova, M.; Chen, H.; Sadler, P.J.; Brabec, V. *Chem. Biol.* **2005**, 12, 121-129.

35. Novakova, O.; Malina, J.; Suchankova, T.; Kasparkova, J.; Bugarcic, T.; Sadler, P.J.; Brabec, V. *Chem. Euro. J.* **2010**, 16, 5744-5754.

36. Hu, W; Luo, Q; Ma, X; Wu, K; Liu, J; Chen, Y; Xiong, S; Wang, J; Sadler, P.J; Wang, F. *Chem. Euro. J.* **2009**, 15, 6586 – 6594.

37. Wang, F.; Habtemariam, A.; van der Geer, E.P.L.; Fernandez, R.; Melchart, M.; Deeth, R.J.; Aird, R.; Guichard, S.; Fabbiani, F.P.A.; Lozano-Casal, P.; Oswald, I.D.H.; Jodrell, D.I.; Parsons, S.; Sadler, P.J. *PNAS* **2005**, 102, 18269 –18274.

38. Hanif, M.; Henke, H.; Meier, S.M.; Martic, S.; Labib, M.; Kandioller, W.; Jakupec, M.A.; Arion, V.B.; Kraatz, H.; Keppler, B.K.; Hartinger, C.G. *Inorg*. *Chem*. **2010**, 49, 7953–7963.

39. Sanchez-Delgado, R.A.; Lazardi, K.; Rincon, L.; Urbina, J.A. *J*. *Med*. *Chem*. **1993**, 36, 2041-2045.

40. Bharti, S.K.; Singh, S.K. *Inter*. *J*. *Pharm.Tech*. *Research* **2009**, 1, 1406-1420.

41. Deubel, D.V.; Lau, J.K. *Chem*. *Commun*. **2006**, 23, 2451–2453.

42. Pizarro, A.M.; Habtemariam, A.; Sadler, P.J. *Top*. *Organomet*. *Chem*. **2010**, 32, 21–56.

43. Hinchlinffe A. (ed). Chemical modelling: Applications and theory, the Royal Society of Chemistry, **2008**; Vol. 5, pp 13-15.

44. Pratuangdejkul, J.; Pascale Jaudon, P.; Ducrocq, O.C. *J*. *Chem*. *Theory Comput*. **2006**, 2, 746-760.

45. http://www.cancer.gov/cancertopics/treatment/types-of-treatment 10 May 2012.

46. Blagosklonny, M.V. *Cell Cycle* **2004**, 3, 1035-1042.

47. Blagosklonny, M.V. *Cell Cycle* **2005**, 4, 269-278.

48. NCI cancer drug information: http://www.cancer.gov/cancertopics/druginfo/alphalist, 12 June 2012.

49. Meggers, E. *Chem*. *Commun*. **2009**, 1001–1010.

50. Dale, L.D.; Tocher, J.H.; Dyson, T.M.; Edwards, D.I.; Tocher, D.A. *Anti-Cancer Drug Des*. **1992**, 7, 3–14.

51. Ang, W.H.; Daldini, E.; Scolaro, C.; Scopelliti, R.; Juillerat-Jeannerat, L.; Dyson, P.J. *Inorg*. *Chem*. **2006**, 45, 9006−9013.

52. Gopal, Y.N.V.; Jayaraju, D.; Kondapi, A.K. *Biochemistry* **1999**, 38, 4382-4388.

53. Rajapakse, C.S.K.; Martinez, A.; Naoulou, B.; Jarzecki, A.A.; Suarez, L.; Deregnaucourt, C.; Sinou, V.; Schrével, J.; Musi, E.; Ambrosini, G.; Schwartz, G.K.; Sanchez-Delgado, R.A. *Inorg*. *Chem*. **2009**, 48, 1122–1131.

54. Vock, C.A.; Ang, W.H.; Scolaro, C.; Phillips, A.D.; Lagopoulos, L.; Juillerat-Jeanneret, L.; Sava, G.; Scopelliti, R.; Dyson, P.J. *J*. *Med*. *Chem*. **2007**, 50, 2166-2175.

55. Che, C.; Siu, F. *Cur*. *Opin*. *Chem*. *Biol*. **2010**, 14, 255–261.

56. Khanna, C.; Hunter, K. *Carcinogenesis* **2005**, 26, 513-523.

57. Pohl, J.; Goldfinger, N.; Radler-pohl, A.; Rotter, V.; Schirrmacher, V. *Mol*. *Cell*. *Biol*. **1988**, 8, 2078-2081.

58. Arpino, G.; Ciocca, D.R.; Weiss, H.; Allred, D.C.; Daguerre, P.; Vargas-Roig, L.; Leuzzi, M.; Gago, F.; Elledge, R.; and Mohsin, S.K. *Breast Cancer Research and Treatment* **2005**, 92, 69–75.

59. Malla, R.R.; Gopinath, S;, Gondi, C.S.; Alapati, K.; Dinh, D.H.; Tsung, A.J.; Rao, J.S. *J*.

Neurooncol. **2012**, 107, 69–80.

60. Kettmann, V. ; Kost'alova, D.; Holtje, H. *J. Comp*.-*Aided Mol*. *Design* **2004**, 18 785–796.

61. Choi,Y.J.; Rho, J.K.; Lee, S.J.; Jang, W.S.; Lee, S.S.; Kim, C.H.; Lee, J.C. *J*. *Cancer Res. Clin*. *Oncol*. **2009**, 135,1047–1053.

62. Stepanenko, I.N.; Casini, A.; Edafe, F.; Novak, M.S.; Arion, V.B.; Dyson, P.J.; Jakupec, M.A.; Keppler, B.K. *Inorg*. *Chem*. **2011**, 50, 12669−12679.

63. Ang, W.H.; Daldini, E.; Juillerat-Jeanneret, L.; Dyson, P.J. *Inorg*. *Chem*. **2007,** 46, 9048−9050.

64. Rapisarda, A; Uranchimeg, B; Scudiero, D.A; Selby, M; Sausville, E.A; Shoemaker, R.H; Melillo, G. *Cancer Res*. **2002**, 62, 4316–4324.

65. Campbell, K.J.; O'Shea, J.M.; Perkins, N.D. *BMC Cancer* **2006**, 6, 101-109.

66. Berg, J.M.; Tymoczko, J.L.; Stryer, L. Biochemistry (Fifth Edition). New York: W.H. Freeman, ISBN-10: 0-7167-3051-0, **2002.**

67. Matsuzaki, Y.; Sowa, Y.; Hirose, T.; Yokota, T; Sakai, T. *Environ*. *Health Prev*. *Med*. **2003**, 8, 157–160.

68. Ciancetta, A.; Genheden, S.; Ryde, U. *J*. *Comput*. *Aided*. *Mol*. *Des*. **2011**, 25, 729–742.

69. World, C.J., Yamawaki, H.; Berk, B.C. *J*. *Mol*. *Med*. **2006**, 84, 997–1003.

70. Wagner, C.; Sudati, J.H.; Nogueira, C.W.; Rocha, J.B.T. *Biometals* **2010**, 23, 1171–1177.

71. Zhuang, W.; Wu, X.; Zhou, Y.; Liu, G.; Wu, T.; Yao, X.; Du, L.; Wei, *M*. *Dig*. *Dis*. *Sci*. **2009**, 54,1379–1385.

72. Ghaneya, S.; Hassan, G.S.; Nahla, A; Farag, N.A.; Gehan, H.; Hegazy, G.H.; Reem, K.; Arafa, R.K. *Arch*. *Pharm*. *Chem*. *Life Sci*. **2008**, 341, 725-733.

73. Holdgate, G.A.; Tunnicliffe, A.; Ward, W.H.J.; Weston, S.A.; Rosenbrock, G.; Barth, P.T.; Taylor, I.W.F.; Pauptit, R.A.; Timms, D. *Biochemistry* **1997**, 36, 9663-9673.

74. Xie, P.; Streu, C.; Qin, J.; Bregman, H.; Pagano, N.; Meggers, E.; Marmorstein, R. *Biochemistry*. **2009**, 48, 5187-5198.

75. Landau R.H; José M.; Mejia P, Kowallik H.; Jensen H. Computational Physics: Problem Solving with Computers, *John Wiley and Sons Inc*. *International Publication*, New York, **1997**; pp 3-4.

76. Hecht, D.; Fogel, G.B. *Cur*. *Comput*. *Aided Drug Des*. **2009**, 5, 56-68.

77. Beerenwinkel, N.; Sing, T.; Lengauer, T.; Rahnenfuhrer, J.; Roomp, K.; Savenkov, I.; Fischer, R.; Hoffmann, D.; Selbig, J.; Korn, K.; Walter, H.; Berg, T.; Braun, P.; Fatkenheuer, G.; Oette, M. ; Rockstroh, J.; Kupfer, B.; Kaiser, R.; Daumer, M. *Bioinformatics* **2005**, 21, 3943–3950.

78. Alonso, H.; Bliznyuk, A.A.; Gready, J.E. *Med*. *Res*. *Reviews*. **2006**, 26, 531-568.

79. Kapetanovic, I.M. *Chem. Biol. Interact.* **2008**, 171, 165–176.

80. Cobb, K. *Biomed. Comp. Review* **2007**, 20-30.

81. Harvey, A.L. *Drug Discovery Today* **2008**, 13, 894-901.

82. Gossens, C.; Dorcier, A.; Dyson, P.J.; Rothlisberger, U. *Organometallics* **2007**, 26, 3969-3975.

83. Hu, X.; Shelver, W.H. *J. Mol. Graphics Model.* **2003**, 22, 115–126

84. Hannon, M.J. *Pure Appl. Chem.* **2007**, 79, 2243–2261.

85. Giannini, F.; Suss-Fink, G.; Furrer, J. *Inorg. Chem.* **2011**, 50, 10552–10554.

86. Zhao, G.; Lin, H. *Curr. Med. Chem. Anticancer Agents* **2005**, 5, 137-147.

87. Bacac, M.; Hotze, A.C.; van der Schilden, K.; Haasnoot, J.G.; Pacor, S.; Alessio, E.; Sava, G.; Reedijk, J. *J. Inorg. Biochem.* **2004**, 98, 402-412.

88. Velders, A.H.; Bergamo, A.; Alessio, E.; Zangrando, E.; Haasnoot, J.G.; Casarsa, C.; Cocchietto, M.; Zorzet, S.; Sava, G. *J. Med. Chem.* **2004**, 47, 1110-1121.

89. Vargiu, A.V.; Robertazzi, A.; Magistrato, A.; Ruggerone, P.; Carloni, P. *J. Phys. Chem.* B. **2008**, 112, 4401-4409.

90. Mura, P.; Camalli, M.; Messori, L.; Piccioli, F.; Zanello, P.; Corsini, M. *Inorg. Chem.* **2004**, 43, 3863-3670.

91. Hostetter, A.A.; Miranda, M.L.; DeRose, V.J.; McFarlane Holman, K.L. *J. Biol. Inorg. Chem.* **2011**, 16, 1177-1185.

92. Bergamo, A.; Gava, B.; Alessio, E.; Mestroni, G.; Serli, B.; Cocchietto, M.; Zorzet, S.; Sava, G. Int. *J. Oncol.* **2002**, 21, 1331-1338.

93. Alessio, E.; Mestroni, G.; Bergamo, A.; Sava, G. *Curr. Top. Med. Chem.* **2004**, 4, 1525-1535.

94. Bergamo, A.; Gaiddon, C.; Schellens, J.H.; Beijnen, J.H.; Sava, G. *J. Inorg. Biochem.* **2012**, 106, 90-99.

95. Bratsos, I.; Urankar, D.; Zangrando, E.; Genova-Kalou, P.; Košmrlj, J.; Alessio, E.; Turel, I. *Dalton Trans.* **2011**, 40, 5188-5199.

96. Brindell, M.; Kuliś, E.; Elmroth, S.K.; Urbańska, K.; Stochel, G. *J. Med. Chem.* **2005**, 48, 7298-7304.

97. Cabrera, E.; Cerecetto, H.; González, M.; Gambino, D.; Noblia, P.; Otero, L.; Parajón-Costa, B.; Anzellotti, A.; Sánchez-Delgado, R.; Azqueta, A.; López de Ceráin, A.; Monge, A. *Eur. J. Med. Chem.* **2004**, 39, 377-382.

98. Camm, K.D.; El-Sokkary, A.; Gott, A.L.; Stockley, P.G.; Belyaeva, T.; McGowan, P.C. *Dalton Trans.* **2009**, 10914-10925.

99. Corral, E.; Hotze, A.C.; den Dulk, H.; Leczkowska, A.; Rodger, A.; Hannon, M.J.; Reedijk, J. J. *Biol*. *Inorg*. *Chem*. **2009**, 14, 439-348.

100. Fetzer, L.; Boff, B.; Ali, M.; Xiangjun, M.; Collin, J.P.; Sirlin, C.; Gaiddon, C.; Pfeffer, M. *Dalton Trans*. **2011**, 40, 8869-8878.

101. Giovagnini, L.; Sitran, S.; Castagliuolo, I.; Brun, P.; Corsini, M.; Zanello, P.; Zoleo, A.; Maniero, A.; Biondi, B.; Fregona, D. *Dalton Trans*. **2008**, 6699-6708.

102. Grguric-Sipka, S.R.; Vilaplana, R.A.; Pérez, J.M.; Fuertes, M.A.; Alonso, C.; Alvarez, Y.; Sabo, T.J.; González-Vílchez, F. *J. Inorg*. *Biochem*. **2003**, 97, 215-220.

103. Helena, G.M.; Morais, T.S.; Florindo, P.; Piedade, M.F.; Moreno, V.; Ciudad, C.; Noe, V. *J. Inorg*. *Biochem*. **2009**, 103, 354-361.

104. Herman, A.; Tanski, J.M.; Tibbetts, M.F.; Anderson, C.M. *Inorg*. *Chem*. **2008**, 47, 274-280.

105. Hotze, A.C.; Bacac, M.; Velders, A.H.; Jansen, B.A.; Kooijman, H.; Spek, A.L.; Haasnoot, J.G.; Reedijk, J. *J. Med. Chem*. **2003**, 46, 1743-1750.

106. Jakupec, M.A.; Reisner, E.; Eichinger, A.; Pongratz, M.; Arion, V.B.; Galanski, M.; Hartinger, C.G.; Keppler, B.K. *J. Med. Chem*. **2005**, 48, 2831-2837.

107. Kamatchi, T.S.; Chitrapriya, N.; Lee, H.; Fronczek, C.F.; Fronczek, F.R.; Natarajan, K. Dalton *Trans*. **2012**, 4, 2066-2077.

108. Kandioller, W.; Hartinger, C.G.; Nazarov, A.A.; Bartel, C.; Skocic, M.; Jakupec, M.A.; Arion, V.B.; Keppler, B.K. *Chem*. *Euro*. *J*. **2009**, 15, 12283-12291.

109. Karki, S.S.; Thota, S.; Darj, S.Y.; Balzarini, J.; De Clercq, E. *Bioorg*. *Med. Chem*. **2007**, 15, 6632-6641.

110. Kowol, C.R.; Reisner, E.; Chiorescu, I.; Arion, V.B.; Galanski, M.; Deubel, D.V.; Keppler, B.K. *Inorg*. *Chem*. **2008**, 47, 11032-11047.

111. Liu, J.; Zheng, W.; Shi, S.; Tan, C.; Chen, J.; Zheng, K.; Ji, L. *J. Inorg*. *Biochem*. **2008,** 102, 193-202.

112. Loughrey, B.T.; Cunning, B.V.; Healy, P.C.; Brown, C.L.; Parsons, P.G.; Williams, M.L. *Chem*. *Asian J*. **2012**, 7, 112-121.

113. Mazumder, U.K.; Gupta, M.; Karki, S.S.; Bhattacharya, S.; Rathinasamy, S.; Thangavel, S. *Chem*. *Pharm*. *Bull*. (Tokyo). **2004**, 52, 178-185.

114. Mendoza-Ferri, M.G.; Hartinger, C.G.; Mendoza, M.A.; Groessl, M.; Egger, A.E.; Eichinger, R.E.; Mangrum, J.B.; Farrell, N.P.; Maruszak, M.; Bednarski, P.J.; Klein, F.; Jakupec, M.A.; Nazarov, A.A.; Severin, K.; Keppler, B.K. *J. Med. Chem*. **2009**, 52, 916-925.

115. Pascu, G.I.; Hotze, A.C.; Sanchez-Cano, C.; Kariuki, B.M.; Hannon, M.J. *Angew Chem*. *Int*. *Ed*. **2007**, 46, 4374-4378.

116. Rajendiran, V.; Murali, M.; Suresh, E.; Palaniandavar, M.; Periasamy, V.S.; Akbarsha, M.A.

Dalton Trans. **2008**, 2157-2170.

117. Romerosa, A.; Campos-Malpartida, T.; Lidrissi, C.; Saoud, M.; Serrano-Ruiz, M.; Peruzzini, M.; Garrido-Cárdenas, J.A.; García-Maroto, F. *Inorg*. *Chem*. **2006**, 45, 1289-1298.

118. Schmid, W.F.; John, R.O.; Mühlgassner, G.; Heffeter, P.; Jakupec, M.A.; Galanski, M.; Berger, W.; Arion, V.B.; Keppler, B.K. *J*. *Med*. *Chem*. **2007**, 50, 6343-6355.

119. Singh, S.K.; Joshi, S.; Singh, A.R.; Saxena, J.K.; Pandey, D.S. *Inorg*. *Chem*. **2007**, 46, 10869-10876.

120. Tan, C.; Liu, J.; Chen, L.; Shi, S.; Ji, L. *J*. *Inorg*. *Biochem*. **2008**, 102, 1644-1653.

121. Vrábel, M.; Pohl, R.; Votruba, I.; Sajadi, M.; Kovalenko, S.A.; Ernsting, N.P.; Hocek, M. *Org*. *Biomol*. *Chem*. **2008**, 6, 2852-2860.

122. Waern, J.B.; Dillon, C.T.; Harding, M.M. *J*. *Med*. Chem. **2005**, 48, 2093-2099.

123. Wu, A.; Kennedy, D.C.; Patrick, B.O.; James, B.R. *Inorg*. *Chem*. **2003**, 42, 7579-7586.

124. Wu, D.H.; Wu, C.H.; Li, Y.Z.; Guo, D.D.; Wang, X.M.; Yan, H. *Dalton Trans*., **2009**, 285-290.

125. Therrien, B.; Ang, W.H.; Cherioux, F.; Vieille-Petit, L.; Juillerat-Jeanneret, L.; Suss-Fink, G.; Dyson, P.J. *J*. *Cluster Sci*. **2007**, 18, 741-752.

126. Casini, A.; Gabbiani, C.; Michelucci, E.; Pieraccini, G.; Moneti, G.; Dyson, P.J.; Messori, L.J. Biol. *Inorg*. *Chem*. **2009**, 14, 761–770.

127. Ang, W.H.; De Luca, A.; Chapuis-Bernasconi, C.; Juillerat-Jeanneret, L.; Lo Bello, M.; Dyson, P.J. *Chem*. *Med*. *Chem*. **2007**, 2, 1799-1806.

128. Barry, N.P.; Zava, O.; Dyson, P.J.; Therrien, B. *Chem*. *Euro*. *J*. **2011**, 17, 9669-9677.

129. Barry, N.P.; Zava, O.; Furrer, J.; Dyson, P.J.; Therrien, B. *Dalton Trans*. **2010**, 39, 5272-5277.

130. Bergamo, A.; Masi, A.; Dyson, P.J.; Sava, G. *Int*. *J*. *Oncol*. **2008**, 33, 1281-1289.

131. Berger, I.; Hanif, M.; Nazarov, A.A.; Hartinger, C.G.; John, R.O.; Kuznetsov, M.L.; Groessl, M.; Schmitt, F.; Zava, O.; Biba, F.; Arion, V.B.; Galanski, M.; Jakupec, M.A.; Juillerat-Jeanneret, L.; Dyson, P.J.; Keppler, B.K. *Chem*. *Euro*. *J*. **2008**, 14, 9046-9057.

132. Casini, A.; Karotki, A.; Gabbiani, C.; Rugi, F.; Vašák, M.; Messori, L.; Dyson, P.J. *Metallomics* **2009**, 1, 434-441.

133. Casini, A.; Mastrobuoni, G.; Ang, W.H.; Gabbiani, C.; Pieraccini, G.; Moneti, G.; Dyson, P.J.; Messori, L. *Chem*. *Med*. *Chem*. **2007**, 2, 631-635.

134. Dorcier, A.; Hartinger, C.G.; Scopelliti, R.; Fish, R.H.; Keppler, B.K.; Dyson, P.J. *J*. *Inorg*. *Biochem*. **2008**, 102, 1066-1076.

135. Gras, M.; Therrien, B.; Süss-Fink, G.; Zava, O.; Dyson, P.J. *Dalton Trans*. **2010**, 39, 10305-10313.

136. Groessl, M.; Hartinger, C.G.; Dyson, P.J.; Keppler, B.K. *J. Inorg. Biochem.* **2008**, 102, 1060-1065.

137. Hanif, M.; Meier, S.M.; Kandioller, W.; Bytzek, A.; Hejl, M.; Hartinger, C.G.; Nazarov, A.A.; Arion, V.B.; Jakupec, M.A.; Dyson, P.J.; Keppler, B.K. *J. Inorg. Biochem.* **2011**, 105, 224-231.

138. Hanif, M.; Nazarov, A.A.; Hartinger, C.G.; Kandioller, W.; Jakupec, M.A.; Arion, V.B.; Dyson, P.J.; Keppler, B.K. *Dalton Trans.* **2010**, 39, 7345-7352.

139. Hanif, M.; Nazarov, A.A.; Legin, A.; Groessl, M.; Arion, V.B.; Jakupec, M.A.; Tsybin, Y.O.; Dyson, P.J.; Keppler, B.K.; Hartinger, C.G. *Chem. Commun.* **2012**, 48, 1475-1477.

140. Hartinger, C.G.; Casini, A.; Duhot, C.; Tsybin, Y.O.; Messori, L.; Dyson, P.J. *J. Inorg. Biochem.* **2008**, 102, 2136-2141.

141. Kilpin, K.J.; Cammack, S.M.; Clavel, C.M.; Dyson, P.J. *Dalton Trans.* **2013**, 42, 2008-2014.

142. Vajpayee, V.; Yang, Y.J.; Kang, S.C.; Kim, H.; Kim, I.S.; Wang, M.; Stang, P.J.; Chi, K.W. *Chem. Commun.* **2011**, 47, 5184-5186.

143. Schmitt, F.; Govindaswamy, P.; Zava, O.; Süss-Fink, G.; Juillerat-Jeanneret, L.; Therrien, B. *J. Biol. Inorg. Chem.* **2009**, 14, 101-109.

144. Süss-Fink, G. *Dalton Trans.* **2010**, 39, 1673-1688.

145. Ruiz, J.; Vicente, C.; de Haro, C.; Bautista, D. *Dalton Trans.* **2009**, 5071-5073.

146. Martínez, A.; Suárez, J.; Shand, T.; Magliozzo, R.S.; Sánchez-Delgado, R.A. *J. Inorg. Biochem.* **2011**, 105, 39-45.

147. Gossens, C.; Tavernelli, I.; Rothlisberger, U. *J. Am. Chem. Soc.* **2008**, 130, 10921-10928.

148. Gligorijević, N.; Aranđelović, S.; Filipović, L.; Jakovljević, K.; Janković, R.; Grgurić-Šipka, S.; Ivanović, I.; Radulović, S.; Tešić, Z.L.j. *J. Inorg. Biochem.* **2012**, 108, 53-61.

149. Grgurić-Sipka, S.; Ivanović, I.; Rakić, G.; Todorović, N.; Gligorijević, N.; Radulović, S.; Arion, V.B.; Keppler, B.K.; Tesić, Z.L.j. *Eur. J. Med. Chem.* **2010**, 45, 1051-1058.

150. Biersack, B.; Zoldakova, M.; Effenberger, K.; Schobert, R. *Eur. J. Med. Chem.* **2010**, 45, 1972-1975.

151. Mitra, R.; Das, S.; Shinde, S.V; Sinha, S.; Somasundaram K.; Samuelson, A.G. *Chem. Euro. J.* **2012**, 18, 12278-12291.

152. Bratsos, I.; Mitri, E.; Ravalico, F.; Zangrando, E.; Gianferrara, T.; Bergamo, A.; Alessio, E. *Dalton Trans.* **2012**, 41, 7358-7371.

153. Barry, N.P.; Sadler, P.J. *Chem. Soc. Rev.* **2012**, 41, 264-279.

154. Caruso, F.; Rossi, M.; Benson, A.; Opazo, C.; Freedman, D.; Monti, E.; Gariboldi, M.B.; Shaulky, J.; Marchetti, F.; Pettinari, R.; Pettinari, C. *J. Med. Chem.* **2012**, 55, 1072−1081.

155. Garcıa-Fernandez, A.; Dıez, J.; Manteca, A.; Sanchez, J.; Gamasa, M.P.; Lastra, E. *Polyhedron*

2008, 27, 1214–1228.

156. García-Fernandez, A.; Díez, J.; Gamasa, M.P.; Lastra, E. *Inorg*. *Chem*. **2009**, 48, 2471-2481.

157. Bergamo, A.; Sava, G. *Dalton Trans*. **2011**, 40, 7817–7823.

158. Bugarcic, T.; Habtemariam, A.; Deeth, R.J.; Fabbiani, F.P.A.; Parsons, S.; Sadler, P.J. *Inorg*. *Chem*. **2009**, 48, 9444–9453.

159. Bruijnincx, P.C.A; Sadler, P.J. *Cur. Opin*. *Chem*. *Biol*. **2008**, 12:197–206.

160. Betanzos-Lara, S.; Salassa, L.; Habtemariam, A.; Novakova, O.; Pizarro, A.M.; Clarkson, G.J.; Liskova, B.; Brabec, V.; Sadler, P.J. *Organometallics* **2012**, 31(9), 3466–3479.

161. Hillard, E.A.; Jaouen, G. *Organometallics* **2011**, 30, 20–27.

162. Schluter, A.; Bieber, K.; Sheldrick, W.S. *Inorg*. *Chim*. *Acta* **2002**, 340, 35-43.

163. Melchart, M.; Sadler, P.J. Ruthenium Arene Anticancer Complexes. *In Bioorganometallics, Jaouen, G., (ed). WILEY-VCH Verlag GmbH 6 Co. KGAA, Weinheim,* **2006,** pp 39-62.

164. Ang, W.H.; Dyson, P.J. *Eur*. *J*. *Inorg*. *Chem*. **2006**, 20, 4003–4018.

165. Meggers, E. *Cur*. *Opin*. *Chem*. *Biol*. **2007**, 11, 287–292.

166. Gaur, R.; Mishra, L. *Inorg*. *Chem*. **2012**, 51, 3059−3070.

167. Loughrey, B.T.; Healy, P.C.; Parsons, P.G.; Williams, M.L. *Inorg*. *Chem*. **2008**, 47, 8589-8591.

168. Micallef, L.S.; Loughrey, B.T.; Healy, P.C.; Parsons, P.G; Williams, M.L. *Organometallics* **2011**, 30, 1395–1403.

169. Walsh, J.L.; McCrackin, R.; McPhail, A.T. *Polyhedron* **1998**, 17, 3221-3226.

170. Wang, Q.; Yu, L. *J*. *Am*. *Chem*. *Soc*. **2000**, 122, 11806-11811.

171. Sanchez-Delgado, R.A.; Navarro, M.; Perez, H.; Urbina, J.A. *J*. *Med*. *Chem*. **1996**, 39, 1095-1099.

172. Cini, R.; Tamasi, G.; Defazio, S.; Corsini, M.; Zanello, P.; Messori, L.; Marcon, G.; Piccioli, F.; Orioli, P. *Inorg*. *Chem*. **2003**, 42, 8038-8052.

173. Hirano, M.; Sakate, Y.; Inoue, H.; Arai, Y.; Komine, N.; Komiya, S.; Wang, X.; Bennett, M.A. *J*. *Organomet*. *Chem*. 2012, 708–709, 46-57.

174. Bennett, M.A.; Byrnes, M.J.; Chung, G.; Edwards, A.J.; Willis, A.C. *Inorg*. *Chim*. *Acta* **2005**, 358, 1692-1708.

175. Pertici, P.; Verrazzani, A.; Vitulli, G.; Baldwin, R.; Bennett, M.A. *J*. *Organomet*. *Chem*. **1998**, 551, 37-47.

176. Bennett, M.A.; Edwards, A.J.; Harper, J.R.; Khimyak, T.; Willis, A.C. *J*. *Organomet*. *Chem*. **2001**, 629, 7-18.

177. Bennett, M.A.; Clark, A.M.; Contel, M.; Rickard, C.E.F.; Roper, W.R.; Wright, L.J. *J. Organomet. Chem.* **2000**, 601, 299-304.

178. Bennett, M.A. *Coord. Chem. Rev.* **1997**, 166, 225-254.

179. Bennett, M.A.; Bown, M.; Byrnes, M.J. *J. Organomet. Chem.* **1998**, 571, 139-144.

180. Bennett, M.A. *Compre. Organomet. Chem. II* **1995**, 7, 441-472.

181. Bennett, M.A. *Compre. Organomet. Chem. II* **1995**, 7, 549-602.

182. Bennett, M.A.; Khan, K.; Wenger, E. *Compre. Organomet. Chem. II* **1995**, 7, 473-548.

183. Bennett, M.A.; Willis, A.C.; Goh, L.Y.; Chen, W. *Polyhedron* **1996**, 15, 3559-3567.

184. Adams, J.R.; Bennett, M.A. *Advances Organomet. Chem.* **2006**, 54, 293-331.

185. Bennett, M.A. *Advances Organomet. Chem.* **1966**, 4, 353-387.

186. Bennett, M.A.; Matheson, T.W.; Robertson, G.B.; Smith, A.K.; Tucker, P.A. *Inorg. Chem.* **1980**, 19, 1014–1021.

187. Bennett, M.A.; Neumann, H.; Thomas, M.; Wang, X.Q.; Pertici, P.; Salvadori, P.; Vitulli, G. *Organometallics* **1991**, 10, 3237–3245.

188. Bennett, M.A.; Goh, L.Y.; McMahon, I.J.; Mitchell, T.R.B.; Robertson, G.B.; Turney, T.W.; Wasantha, W.A. *Organometallics* **1992**, 11, 3069–3085.

189. Bennett, M.A.; Pelling, S.; Robertson, G.B.; Wickramasinghe, W.A. *Organometallics* **1991**, 10, 2166–2172.

190. Bennett, M.A.; Goh, L.Y.; Willis, A.C. *J. Am. Chem. Soc.* **1996**, 118, 4984–4992.

191. Shin, R.Y.C.; Bennett, M.A.; Goh, L.Y.; Chen, W.; Hockless, D.C.R.; Leong, W.K.; Mashima, K.; Willis A.C. *Inorg. Chem.* **2003**, 42, 96–106.

192. Bennett, M.A.; Matheson, T.W.; Robertson, G.B.; Smith, A.K.; Tucker, P.A. *Inorg. Chem.* **1981**, 20, 2353–2365.

193. Bennett, M.A.; McMahon, I.J.; Pelling, S.; Robertson, G.B.; Wickramasinghe, W.A. *Organometallics* **1985**, 4, 754–761.

194. Bennett, M.A.; Neumann, H.; Willis, A.C.; Ballantini, V.; Pertici, P.; Mann, B.E. *Organometallics* **1997**, 16, 2868–2878.

195. Hirano, M.; Sakate, Y.; Komine, N.; Komiya, S.; Wang, X.; Bennett, M.A. *Organometallics* **2011**, 30, 768–777.

196. Widegren, J.A.; Bennett, M.A.; Finke, R.G. *J. Am. Chem. Soc.* **2003**, 125, 10301–10310.

197. Hirano, M.; Sakate, Y.; Komine, N.; Komiya, S.; Bennett, M.A. *Organometallics* **2009**, 28, 4902–4905.

198. Hirano, M.; Shibasaki, T.; Komiya, S.; Bennett, M.A. *Organometallics* **2002**, 21, 5738–5745.

199. Bennett, M.A.; Lu, Z.; Wang, X.; Bown, M.; Hockless, D.C.R. *J. Am. Chem. Soc*. **1998**, 120, 10409–10415.

200. Gollas, B.; Speiser, B.; Zagos, I.; Maichle-Mossmer, C. *J. Organomet. Chem*. **2000**, 602, 75 – 90.

201. Komiya, S.; Hurano, M. Group 8 (Fe, Ru, Os) metal compounds. In synthesis of organometallic compounds: A practical Guide*; Komiya, S., Ed. John Wiley & Sons, England*, **1997**; pp 159-203.

202. Suss-Fink, G.; Khan, F-A.; Juillerat-Jeanneret, L.; Dyson, P.J.; Renfrew, A.K. *J. Clust. Sci*. **2010**, 21, 313–324.

203. Dutta, B.; Scopelliti, R.; Severin, K. *Organometallics* **2008**, 27, 423–429.

204. Furrer, M.A.; Schmitt, F.; Wiederkehr, M.; Juillerat-Jeanneret, L.; Therrien, B. *Dalton Trans*. **2012**, 41, 7201-7211.

205. Zhou, Q.; Lei, W.; Chen, Y.; Li, C.; Hou, Y.; Zhang, B.; Wang, X. *Chem. Euro. J*. **2012**, 18, 8617-8621.

206. Bíró, L.; Farkas, E.; Buglyó, P. *Dalton Trans*. **2012**, 41, 285-291.

207. Boutadla, Y.; Davies, D.L.; Jones, R.C.; Singh, K. *Chem. Euro. J*. **2011**, 17, 3438-3448.

208. Han, Y.F.; Li, H.; Fei, Y.; Lin, Y.J.; Zhang, W.Z.; Jin, G.X. *Dalton Trans*. **2010**, 39, 7119-7124.

209. Dutta, B.; Curchod, B.F.; Campomanes, P.; Solari, E.; Scopelliti, R.; Rothlisberger, U.; Severin, K. *Chem. Euro. J*. **2010**, 16, 8400-8409.

210. Jiménez-Tenorio, M.; Puerta, M.C.; Valerga, P.; Moncho, S.; Ujaque, G.; Lledós, A. *Inorg. Chem*. **2010**, 49, 6035-6057.

211. Han, Y.F.; Jia, W.G.; Yu, W.B.; Jin, G.X. *Chem. Soc. Rev*. **2009**, 38, 3419-3434.

212. Jerphagnon, T.; Gayet, A.J.; Berthiol, F.; Ritleng, V.; Mrsić, N.; Meetsma, A.; Pfeffer, M.; Minnaard, A.J.; Feringa, B.L.; de Vries, J.G. *Chem. Euro. J*. **2009**, 15, 12780-12790.

213. Zhang, W.Z.; Han,Y.F.; Lin, Y.J.; Jin, G.X. *Dalton Trans*. **2009**, 8426-8431.

214. Buglyó, P.; Farkas, E. *Dalton Trans*. **2009**, 8063-8070.

215. Yasuda, H.; Lee, V.Y.; Sekiguchi, A. *J. Am. Chem. Soc*. **2009**, 131, 9902-9903.

216. Streu, C.; Carroll, P.J.; Kohli, R.K.; Meggers, E. *J. Organomet. Chem*. **2008**, 693, 551-556.

217. Marchetti, F.; Pettinari, C.; Pettinari, R.; Cerquetella, A.; Di Nicola, C.; Macchioni, A.; Zuccaccia, D.; Monari, M.; Piccinelli, F. *Inorg. Chem*. **2008**, 47, 11593-11603.

218. Galindo, M.A.; Quirós, M.; Romero, M.A.; Navarro, J.A. *J. Inorg. Biochem*. **2008**, 102, 1025-1032.

219. Herberhold, M.; Yan, H.; Milius, W.; Wrackmeyer, B. *Chem*. *Euro*. *J*. **2000**, 6, 3026-3032.

220. Ritleng, V.; Bertani, P.; Pfeffer, M.; Sirlin, C.; Hirschinger, J. *Inorg*. *Chem*. **2001**, 40, 5117-5122.

221. Sunada, Y.; Hayashi, Y.; Kawaguchi, H.; Tatsumi, K. *Inorg*. *Chem*. **2001**, 40, 7072-7078.

222. Yamanari, K.; Ito, R.; Yamamoto, S.; Konno, T.; Fuyuhiro, A.; Fujioka, K.; Arakawa, R. *Chem*. *Euro*. *J*. **2002**, 41, 6824-6830.

223. Ohki, Y.; Sadohara, H.; Takikawa, Y.; Tatsumi, K. *Angew Chem*. *Int*. *Ed*. **2004**, 43, 2290-2293.

224. Zuccaccia, D.; Bellachioma, G.; Cardaci, G.; Zuccaccia, C.; Macchioni, A. *Dalton Trans*. **2006**, 1963-1971.

225. Wang, X.; Liu, S.; Weng, L.H.; Jin, G.X. *Chem*. *Euro*. *J*. **2007**, 13, 188-195.

226. Jiménez-Tenorio, M.; Palacios, M.D.; Puerta, M.C.; Valerga, P. *Inorg*. *Chem*. **2007**, 46, 1001-1012.

227. Gauthier, S.; Solari, E.; Dutta, B.; Scopelliti, R.; Severin, K. *Chem*. *Commun*. **2007,** 1837-1839.

228. Bratsos, I.; Birarda, G.; Jedner, S.; Zangrando, E.; Alessio, E. *Dalton Trans*. **2007**, 4048-4058.

229. Beckford, F.; Dourth, D.; Shaloski, M.Jr.; Didion, J.; Thessing, J.; Woods, J.; Crowell, V.; Gerasimchuk, N.; Gonzalez-Sarrías, A.; Seeram, N.P. *J*. *Inorg*. *Biochem*. **2011**, 105, 1019-1029.

230. Bíró; L.; Farkas, E.; Buglyó, P. *Dalton Trans*. **2010**, 39, 10272-10278.

231. Atilla-Gokcumen, G.E.; Di Costanzo, L.; Meggers, E. *J*. *Biol*. *Inorg*. *Chem*. **2011**, 16, 45-50.

232. Beckford, F.A.; Leblanc, G.; Thessing, J.; Shaloski, M.; Frost, B.J.; Li, L.; Seeram, N.P. *Inorg*. *Chem*. *Commun*. **2009**, 12, 1094-1098.

233. Bregman, H.; Meggers, E. *Org*. *Lett*. **2006**, 8, 5465-5468.

234. McNae, I.W.; Fishburne, K.; Habtemariam, A.; Hunter, T.M.; Melchart, M.; Wang, F.; Walkinshaw, M.D.; Sadler, P.J. *Chem*. *Commun*. **2004**, 1786-1787.

235. Debreczeni, J.E.; Bullock, A.N.; Atilla, G.E.; Williams, D.S.; Bregman, H.; Knapp, S.; Meggers, E. *Angew Chem*. *Int*. *Ed*. *Engl*. **2006**, 45, 1580-1585.

236. Pagano, N.; Maksimoska, J.; Bregman, H.; Williams, DS.; Webster, RD.; Xue, F.; Meggers, E. *Org*. *Biomol*. *Chem*. **2007**, 5, 1218-1227.

237. Hoeschele, J.D.; Habtemariam, A.; Muir, J.; Sadler, P.J. *Dalton Trans*. 2007, 4974-4979.

238. Linares, F.; Galindo, M.A.; Galli, S.; Romero, M.A.; Navarro, J.A.; Barea, E. *Inorg*. *Chem*. **2009**, 48, 7413-7420.

239. Das, S.; Sinha, S.; Britto, R.; Somasundaram, K.; Samuelson, A.G. *J*. *Inorg*. *Biochem*. **2010**, 104, 93-104.

240. Gianferrara, T.; Bratsos, I.; Iengo, E.; Milani, B.; Ostrić, A.; Spagnul, C.; Zangrando, E.; Alessio,

E. *Dalton Trans*. **2009**, 10742-10756.

241. Meggers, E.; Atilla-Gokcumen, G.E.; Gründler, K.; Frias, C.; Prokop, A. *Dalton Trans*. **2009**, 10882-10888.

242. Nazarov, A.A.; Risse, J.; Ang, W.H.; Schmitt, F.; Zava, O.; Ruggi, A.; Groessl, M.; Scopelitti, R.; Juillerat-Jeanneret, L.; Hartinger, C.G.; Dyson, P.J. *Inorg*. *Chem*. **2012**, 51, 3633-3639.

243. Nowak-Sliwinska, P.; van Beijnum, J.R.; Casini, A.; Nazarov, A.A.; Wagnieres, G.; van den Bergh, H.; Dyson, P.J.; Griffioen, A.W. *J*. *Med*. *Chem*. **2011**, 54, 3895-3902.

244. Pelletier, F.; Comte, V.; Massard, A.; Wenzel, M.; Toulot, S.; Richard, P.; Picquet, M.; Le Gendre, P.; Zava, O.; Edafe, F.; Casini, A.; Dyson, P.J. *J*. *Med*. *Chem*. **2010**, 53, 6923-6933.

245. Pitto-Barry, A.; Barry, N.P.; Zava, O.; Deschenaux, R.; Dyson, P.J.; Therrien, B. *Chem*. *Euro*. *J*. **2011**, 17, 1966-1971.

246. Pitto-Barry, A.; Zava, O.; Dyson, P.J.; Deschenaux, R.; Therrien, B. *Inorg*. *Chem*. **2012**, 51, 7119-7124.

247. Ratanaphan, A.; Temboot, P.; Dyson, P.J. *Chem*. *Biodivers*. **2010**, 7, 1290-1302.

248. Renfrew, A.K.; Scopelliti, R.; Dyson, P.J. *Inorg*. *Chem*. **2010**, 49, 2239-2246.

249. Schmitt, F.; Govindaswamy, P.; Süss-Fink, G.; Ang, WH.; Dyson, P.J.; Juillerat-Jeanneret, L.; Therrien, B. *J*. *Med*. *Chem*. **2008**, 51, 1811-1816.

250. Scolaro, C.; Bergamo, A.; Brescacin, L.; Delfino, R.; Cocchietto, M.; Laurenczy, G.; Geldbach, T.J.; Sava, G.; Dyson, P.J. *J*. *Med*. *Chem*. **2005**, 48, 4161-4171.

251. Scolaro, C.; Chaplin, A.B.; Hartinger, C.G.; Bergamo, A.; Cocchietto, M.; Keppler, B.K.; Sava, G.; Dyson, P.J. *Dalton Trans*. **2007**, 5065-5072.

252. Scolaro, C.; Hartinger, C.G.; Allardyce, C.S.; Keppler, B.K.; Dyson, P.J. *J*. *Inorg*. *Biochem*. **2008**, 102, 1743-1748.

253. Vock, C.A.; Scolaro, C.; Phillips, A.D.; Scopelliti, R.; Sava, G.; Dyson, P.J. *J*. *Med*. *Chem*. **2006**, 49, 5552-5561.

254. Procopio, E.Q.; Rojas, S.; Padial, N.M.; Galli, S.; Masciocchi, N.; Linares, F.; Miguel, D.; Oltra, J.E.; Navarro, J.A.; Barea, E. *Chem*. *Commun*. **2011**, 47, 11751-11753.

255. Chval, Z.; Futera, Z.; Burda, J.V. *J*. *Chem*. *Phys*. **2011,** 134, 024520.

256. Akbayeva, D.N.; Gonsalvi, L.; Oberhauser, W.; Peruzzini, M.; Vizza, F.; Brüggeller, P.; Romerosa, A.; Sava, G.; Bergamo, A. *Chem*. *Commun*. **2003**, 264-265.

257. García-Fernández, A.; Díez, J.; Manteca, A.; Sánchez, J.; García-Navas, R.; Sierra, B.G.; Mollinedo, F.; Gamasa, M.P.; Lastra, E. *Dalton Trans*. **2010**, 39, 10186-10196.

258. Peacock, A.F.; Habtemariam, A.; Fernández, R.; Walland, V.; Fabbiani, F.P.; Parsons, S.; Aird, R.E.; Jodrell, D.I.; Sadler, P.J. *J*. *Am*. *Chem*. *Soc*. **2006**, 128, 1739-1748.

259. Peacock, A.F.; Habtemariam, A.; Moggach, S.A.; Prescimone, A.; Parsons, S.; Sadler, P.J. *Inorg. Chem.* **2007**, 46, 4049-4059.

260. Peacock, A.F.; Parsons, S.; Sadler, P.J. *J. Am. Chem. Soc.* **2007**, 129, 3348-3357.

261. Peacock, A.F.; Sadler, P.J. *Chem. Asian. J.* **2008**, 3, 1890-1899.

262. van Rijt, S.H.; Hebden, A.J.; Amaresekera, T.; Deeth, R.J.; Clarkson, G.J.; Parsons, S.; McGowan, P.C.; Sadler, P.J. *J. Med. Chem.* **2009**, 52, 7753-7764.

263. van Rijt, S.H.; Peacock, A.F.; Johnstone, R.D.; Parsons, S.; Sadler, P.J. *Inorg. Chem.* **2009**, 48, 1753-1762.

264. Wang, F.; Chen, H.; Parsons, S.; Oswald, I.D.; Davidson, J.E.; Sadler, P.J. *Chem. Euro. J.* **2003**, 9, 5810-5820.

265. Wang, F.; Habtemariam, A.; van der Geer, E.P.; Deeth, R.J.; Gould, R.; Parsons, S.; Sadler, P.J. *J. Biol. Inorg. Chem.* **2009**, 14, 1065-1076.

266. Wang, F.; Xu, J.; Habtemariam, A.; Bella, J.; Sadler, P.J. *J. Am Chem. Soc.* **2005**, 127, 17734-17743.

267. Williams, J.P.; Lough, J.A.; Campuzano, I.; Richardson, K.; Sadler, P.J. *Rapid Commun. Mass Spectrom.* **2009**, 23, 3563-3569.

268. Wu, K.; Luo, Q.; Hu, W.; Li, X.; Wang, F.; Xiong, S.; Sadler, P.J. *Metallomics* **2012**, 4, 139-148.

269. Yan YK.; Melchart M.; Habtemariam A.; Peacock AF.; Sadler P.J. *J. Biol. Inorg. Chem.* **2006**, 11, 483-488.

270. Yan, Y.K.; Melchart, M.; Habtemariam, A.; Sadler, P.J. *Chem. Commun.* **2005**, 4764-4776.

271. Bratsos, I.; Jedner, S.; Bergamo, A.; Sava, G.; Gianferrara, T.; Zangrando, E.; Alessio, E. *J. Inorg. Biochem.* **2008**, 102(5-6), 1120-1133.

272. Futera, Z.; Klenko, J.; Sponer, J.E.; Sponer, J.; Burda, J.V. *J. Comput. Chem.* **2009**, 30, 1758-1770.

273. Byabartta, P.; Jasimuddin, S.K.; Mostafa, G.; Lu, T.-H.; Sinha, C. *Polyhedron* **2003**, 22, 849-859.

274. Al-Lawati, H.A.J.; Suliman, F.E.O.; Al Kindy, S.M.Z.; Al-Lawati, A.M.; Varma, G.B.; Nour, I.E.M. *Talanta* **2010**, 82, 1999-2002.

275. Chen, X.-M.; Wu, G.-H.; Chen, J.-M.; Jiang, Y.-Q.; Chen, G.-N.; Oyama, M.; Chen, X.; Wang, X.-R. *Biosen. Bioelec.* **2010**, 26, 872-876.

276. Nakabayashi, Y.; Watanabe, Y.; Nakao, T.; Yamauchi, O. *Inorg. Chim. Acta* **2004**, 357, 2553-2560.

277. Małecki, J.G.; Kruszynski, R.; Mazurak, Z. *Polyhedron* **2009**, 28, 3891-3898.

278. Canivet, J.; Karmazin-Brelot, L.; Süss-Fink, G. *J. Organomet. Chem.* **2005**, 690, 3202-3211.

279. Himeda, Y.; Onozawa-Komatsuzaki, N.; Sugihara, H.; Arakawa, H.; Kasuga, K. *Organometallics*

2004, 23, 1480–1483.

280. Hara, K.; Sugihara, H.; Tachibana, Y.; Islam, A.;Yanagida, M.; Sayama, K.; Arakawa, H.; Fujihashi, G.; Horiguchi, T.; Kinoshita, T. *Langmuir* **2001**, 17, 5992–5999.

281. Mitsopoulou, C.A.; Veroni, I.; Philippopoulos, A.I.; Falaras, P. *J. Photochem. Photobio. A*: *Chem.* **2007**, 191, 6-12.

282. Wei, H.; Yin, J.; Wang, E. *Anal. Chem.* **2008**, 80, 5635–5639.

283. Tomaz, A.I.; Jakusch, T.; Morais, T.S.; Marques, F.; de Almeida, R.F.; Mendes, F.; Enyedy, E.A.; Santos, I.; Pessoa, J.C.; Kiss, T.; Garcia, M.H. *J.* Inorg. *Biochem.* **2012**, 117, 261-269.

284. Pruchnik, F.P.; Gałdecka, E.; Gałdecki, Z.; Kowalski, A. *Polyhedron* **1999**, 18, 2091-2097.

285. Hofmeier, H.; Andres, P.R.; Schubert, U.S. Metal-Contain. and Metallosupramol. *Polymers and Materials, ACS Symposium Series*, Chapter 7, **2006**, 928, 86-96.

286. Zhou, G.; Harruna, I.I. *Macromol.* **2005**, 38, 4114–4123.

287. Jain, A.; Wang, J.; Mashack, E.R.; Winkel, B.S.J.; Brewer, K.J. *Inorg. Chem.* **2009**, 48, 9077–9084.

288. Rajalakshmanan, E.; Alexander, V. *Inorg. Chem.* **2007**, 46, 6252–6260.

289. Goze, C.; Sabatini, C.; Barbieri, A.; Barigelletti, F.; Ziessel, R. *Inorg. Chem.* **2007**, 46, 7341–7350.

290. Etienne, S.; Beley, M. *Inorg. Chem. Com.* **2006**, 9, 68-71.

291. Sharma, S.; Singh, S.K.; Chandra, M.; Pandey, D.S. *J. Inorg. Biochem.* **2005**, 99, 458-466.

292. Bolink, H.J.; Cappelli, L.; Coronado, E.; Gaviña, P. *Inorg. Chem.* **2005**, 44, 5966–5968.

293. Koizumi, T.; Tomon, T.; Tanaka, K. *Organometallics* **2003**, 22, 970–975.

294. Zhao, M.; Yu, Z.; Yan, S.; Li, Y. *J. Organomet. Chem.* **2009**, 694, 3068-3075.

295. Blasberg, F.; Bats, J.W.; Bolte, M.; Lerner, H-W.;Wagner M. *Inorg. Chem.* **2010**, 49, 7435–7445.

296. Türkoglu, G.; Tampier, S.; Strinitz, F.; Heinemann, F.W.; Hübner, E.; Burzlaff, N. *Organometallics* **2012**, 31, 2166–2174.

297. Burns, I.D.; Hill, A.F.; White, A.J.P.; Williams, D.J.; Wilton-Ely J.D.E.T. *Organometallics* **1998**, 17, 1552–1557.

298. Tampier, S.; Müller, R.;Andrea Thorn, A.; Hübner, E.; Burzlaff, N. *Inorg. Chem.* **2008**, 47, 9624–9641.

299. Kopf, H.; Pietraszuk, C.; Hübner, E.; Burzlaff, N. *Organometallics* **2006**, 25, 2533–2546.

300. Kopf, H.; Holzberger, B.; Pietraszuk, C.; Hübner, E.; Burzlaff, N. *Organometallics* **2008**, 27, 5894–5905.

301. Xu, L.; Zhong, N.J.; Huang, H.L.; Liang, Z.H.; Li, Z.Z.; Liu, Y.J. *Nucleos. Nucleot. Nucleic Acids* **2012**, 31, 575-591.

302. Yu, H.J.; Chen, Y.; Yu, L.; Hao, Z.F.; Zhou, L.H. *J. Med. Chem.* **2012**, 55, 146-154.

303. Niyazi, H.; Hall, J.P.; O'Sullivan, K.; Winter, G.; Sorensen, T.; Kelly, J.M.; Cardin, C.J. *Nat. Chem.* 2012, 4, 621-628.

304. Liu, X.W.; Chen, Z.G.; Li, L.; Chen, Y.D.; Lu, J.L.; Zhang, D.S. *Spectrochim. Acta Part A: Mol. Biomol. Spect.* **2012**, 102C, 142-149.

305. Gu, S.; Liu, B.; Chen, J.; Wu, H.; Chen, W. *Dalton Trans.* **2012**, 41, 962-970.

306. Henke, H.; Kandioller, W.; Hanif, M.; Keppler, B.K.; Hartinger, C.G. *Chem. Biodivers.* **2012**, 9, 1718-1727.

307. David, S.; Perkins, R.S.; Fronczek, F.R.; Kasiri, S.; Mandal, S.S.; Srivastava, R.S. *J. Inorg. Biochem.* **2012**, 111, 33-39.

308. Sun, R.W.; Ng, M.F.; Wong, E.L.; Zhang, J.; Chui, S.S.; Shek, L.; Lau, T.C.; Che, C.M. *Dalton Trans.* **2009**, 10712-10716.

309. Zhu, X.J.; Holliday, B.J. *Macromol. Rapid Commun.* **2010**, 31, 904-909.

310. Bhat, S.S.; Kumbhar, A.S.; Kumbhar, A.A.; Khan, A. *Chem. Euro. J.* **2012**, 18, 16383-16392.

311. Kou, J.F.; Qian, C.; Wang, J.Q.; Chen, X.; Wang, L.L.; Chao, H.; Ji, L.N. *J. Biol. Inorg. Chem.* **2012**, 17, 81-96.

312. Concepcion, J.; Loeb, B.; Simon-Manso, Y.; Zuloaga, F. *Polyhedron*, **2000**, 19, 2297– 2302.

313. Adeniyi, A.A.; Ajibade, P.A. *J. Mol. Model.* **2013**, 19, 1325-1338.

314. Adeniyi, A.A.; Ajibade, P.A. *J. Biomol. Struc. Dynamics*, **2013**, 1-15, http://dx.doi.org/10.1080/07391102.2013.819299

315. Adeniyi, A.A.; Ajibade, P.A. *J. Chem.*, **2013**, 1-25.

316. Adeniyi, A.A.; Ajibade, P.A. *Spectrochim. Acta Part A: Mol. Biomol. Spect.* **2013**, 105, 456–465.

317. Adeniyi, A.A.; Ajibade, P.A. *Spectrochim. Acta Part A: Mol. Biomol. Spect.* **2013**, 115, 426–436.

318. Adeniyi, A.A.; Ajibade, P.A. *J. Mol. Graph. Model.* **2012**, 38, 60-69.

319. Adeniyi, A.A.; Ajibade, P.A. *Molecules* **2013**, 18, 3760-3778.

320. Adeniyi, A.A.; Ajibade, P.A. *Molecules*, **2013**, 18, 10829-10856.

321. Granovsky, A.A. Firefly version 7.1.G, www http://classic.chem.msu.su/gran/firefly/index.html 12 March 2012

322. Frisch, M.J.; Trucks, G.W.; Schlegel, H.B.; Scuseria, G.E.; Robb, M.A.; Cheeseman, J.R.;

Montgomery, J.A., Jr.; Vreven, T.; Kudin, K.N.; Burant, J.C.; Millam, J.M.; Iyengar, S.S.; Tomasi, J.; Barone, V.; Mennucci, B.; Cossi, M.; Scalmani, G.; Rega, N.; Petersson, G.A.; Nakatsuji, H.; Hada, M.; Ehara, M.; Toyota, K.; Fukuda, R.; Hasegawa, J.; Ishida, M.; Nakajima, T.; Honda, Y.; Kitao, O.; Nakai, H.; Klene, M.; Li, X.; Knox, J.E.; Hratchian, H.P.; Cross, J.B.; Adamo, C.; Jaramillo, J.; Gomperts, R.; Stratmann, R.E.; Yazyev, O.; Austin, A.J.; Cammi, R.; Pomelli, C.; Ochterski, J.W.; Ayala, P.Y.; Morokuma, K.; Voth, G.A.; Salvador, P.; Dannenberg, J.J.; Zakrzewski, V.G.; Dapprich, S.; Daniels, A.D.; Strain, M.C.; Farkas, O.; Malick, D.K.; Rabuck, A.D.; Raghavachari, K.; Foresman, J.B.; Ortiz, J.V.; Cui, Q.; Baboul, A.G.; Clifford, S.; Cioslowski, J.; Stefanov, B.B.; Liu, G.; Liashenko, A.; Piskorz, P.; Komaromi, I.; Martin, R.L.; Fox, D.J.; Keith, T.; Al-Laham, M.A.; Peng, C.Y.; Nanayakkara, A.; Challacombe, M.; Gill, P.M.W.; Johnson, B.; Chen, W.; Wong, M.W.; Gonzalez, C.; Pople, J.A.; Gaussian 03, *Gaussian Inc*., *Pittsburgh PA*, **2003**.

323. Frisch, M.J.; Trucks, G.W.; Schlegel, H.B.; Scuseria, G.E.; Robb, M.A.; Cheeseman, J.R.; Scalmani, G.; Barone, V.; Mennucci, B.; Petersson, G.A.; Nakatsuji, H.; Caricato, M.; Li, X.; Hratchian, H.P.; Izmaylov, A.F.; Bloino, J.; Zheng, G.; Sonnenberg, J.L.; Hada, M.; Ehara, M.; Toyota, K.; Fukuda, R.; Hasegawa, J.; Ishida, M.; Nakajima, T.; Honda, Y.; Kitao, O.; Nakai, H.; Vreven, T.; Montgomery, J.; J.A.;, Peralta, J.E.; Ogliaro, F.; Bearpark, M.; Heyd, J.J.; Brothers, E.; Kudin, K.N.; Staroverov, V.N.; Kobayashi, R.; Normand, J.; Raghavachari, K.; Rendell, A.; Burant, J.C.; Iyengar, S.S.; Tomasi, J.; Cossi, M.; Rega, N.; Millam, N.J.; Klene, M.; Knox, J.E.; Cross, J.B.; Bakken, V.; Adamo, C.; Jaramillo, J.; Gomperts, R.; Stratmann, R.E.; Yazyev, O.; Austin, A.J.; Cammi, R.; Pomelli, C.; Ochterski, J.W.; Martin, R.L.; Morokuma, K.; Zakrzewski, V.G.; Voth, G.A.; Salvador, P.; Dannenberg, J.J.; Dapprich, S.; Daniels, A.D.; Farkas, Ö.; Foresman, J.B.; Ortiz, J.V.; Cioslowski, J.; Fox, D.J. Gaussian 09, *Gaussian Inc*.: *Wallingford CT*, **2009**.

324. Keith, T.A. AIMAll (Version 12.06.03), TK Gristmill Software, Overland Park KS, USA, aim.tkgristmill.com 12 June 2012

325. Schmidt, M.W. Baldridge, K.K.; Boatz, J.A.; Elbert, S.T.; Gordon, M.S.; Jensen, J.H.; Koseki, S.; Matsunaga, N.; Nguyen, K.A.; Su, S.; Windus, T.L.; Dupuis, M.; Montgomery, J.A. Gamess (US). *J*. *Comput*. *Chem*. **1993**, 14, 1347-1363.

326. Adamo, C.; Barone V. *J*. *Chem*. *Phys*. **1999**, 110, 6158–6170.

327. Stevens, W.J.; Krauss, M.; Basch, H.; Jasien, P.G *J*. *Chem*. **1992**, 70, 612-630.

328. Becke, A.D. *J*. *Chem*. *Phys*. **1993**, 98, 5648-5652.

329. Dobbs, K.D., Hehre, W.J. *J*. *Comp*. *Chem*. **1987**, 6, 861–879.

330. Feller, D.J. *Comp*. *Chem*. **1996**, 17, 1571-1586.

331. Schuchardt, K.L.; Didier, B.T.; Elsethagen, T.; Sun, L.; Gurumoorthi, V.; Chase, J.; Li, J.; Windus, T.L. *J*. *Chem*. *Inf*. *Model*. **2007**, 47, 1045-1052.

332. Marchal, B.; Carbonniére, P.; Begue, D.; Pouchan, C. *Chem*. *Phy*. *Letters* **2008**, 453, 49–54.

333. Marchal, R.; Carbonnière, P.; Pouchan, C. *Comput*. *Theoret*. *Chem*. **2012**, 990, 100-105.

334. Bagno, A; Bonchio, M. *Eur*. *J*. *Inorg*. *Chem*. **2002**, 1475-1483.

335. Reed, A.E.; Curtiss, L.A.; Weinhold, F. *Chem*. *Rev*. **1988**, 88, 899–926.

336. Foster, J.P.; Weinhold, F. *J. Am. Chem. Soc.* **1980**, 102, 7211-7218.

337. Glendening, E.D.; Streitwieser, A.J. *Chem. Phys.* **1994**, 100, 2900-2909.

338. Liu, Y.; Liu, C-G.; Sun, S-L.;Yang, G-C.; Qiu, Y-Q. *Comp. Theoret. Chem.* **2012**, 979, 112–118.

339. Labello, N.P.; Ferreira, A.M.; Kurtz, H.A. *J. Phys. Chem. A* **2006**, 110, 13507-13513.

340. Helgaker, T.; Watson, M.; Handy, N.C. *J. Chem. Phys.* **2000**, 113, 9402-9409.

341. Sychrovsky, V.; Grafenstein, J.; Cremer, D. *J. Chem. Phys.* **2000**, 113, 3530-3547.

342. Wolinski, K.; Hilton, J.F.; Pulay, P. *J. Am. Chem. Soc.* **1990**, 112, 8251–8260

343. Sanz, D.; Claramunt, R.M.; Alkorta, I.; Sánchez-Sanz, G.; Elguero, J. *Magn. Reson. Chem.* **2012**, 50, 246–255.

344. Pazderski, L.; Tousek, J.; Sitkowski, J.; Kozerski, L.; Szłyk, E. *Magn. Reson.* Chem. **2007**, 45, 1045–1058.

345. Alparone, A. J. *Fluorine Chem.* **2012**,144, 94–101.

346. Liyanage, P.S.; de Silva, R.M.; de Silva, K.M.N. *J. Mol. Struc.* (*Theochem*) **2003**, 639, 195–201.

347. Karabacak, M.; Cinar, M. *Spectrochim. Acta Part A*: *Mol. Biomol. Spect.* **2012**, 86, 590–599.

348. Morris, G.M.; Huey, R.; Lindstrom, W.; Sanner, M.F.; Belew, R.K.; Goodsell, D.S.; Olson, A.J. *J. Comput. Chem.* **2009**, 30, 2785-2791.

349. Cole, J.C.; Nissink, J.W.M.; Taylor, R. Protein-Ligand Docking and Virtual Screening with GOLD in Virtual Screening in Drug Discovery (Eds. B. Shoichet, J. Alvarez), *Taylor & Francis CRC Press, Boca Raton*, Florida, USA, **2005**.

350. Thomsen, R.; Christensen, M.H. *J. Med. Chem.* **2006**, 49, 3315-3321.

351. Friesner, R.A.; Banks, J.L.; Murphy, R.B.; Halgren, T.A.; Klicic, J.J.; Mainz, D.T.; Repasky, M.P.; Knoll, E.H.; Shaw, D.E.; Shelley, M.; Perry, J.K.; Francis, P.; Shenkin, P.S. *J. Med. Chem.* **2004**, 47, 1739–1749.

352. Pettersen, E.F.; Goddard, T.D.; Huang, C.C.; Couch. G.S.; Greenblatt, D.M.; Meng, E.C.; Ferrin, T.E. *J. Comp. Chem.* **2004**, 25,1605-1612.

353. Morris, G.M.; Goodsell, D.S.; Halliday, R.S.; Huey, R.; Hart, W.E.; Belew, R.K.; Olson, A.J. *J. Comp. Chem.* **1998**, 19, 1639-1662.

354. Caballero, N.A.; Meléndez, F.J.; Niño, A.; Muñoz-Caro, C. *J. Mol. Model* **2007**, 13, 579–586.

355. Sapre, N.S; Gupta, S.; Sapre, N. *J. Chem. Sci.* **2008**, 120, 395–404.

356. Research Collaboratory for Structural Bioinformatics (RCSB) online pdb database, **2012**: www.rcsb.org 12 February 2012

357. Halgren, T.A.; Murphy, R.B.; Friesner, R.A.; Beard, H.S.; Frye, L.L.; Pollard, W.T.; Banks, J.L. *J. Med. Chem.* **2004**, 47, 1750–1759.

358. Corbeil, C.R.; Moitessier, N. *J. Chem. Inf. Model.* **2009**, 49, 997–1009.

359. Jacobson, M.P.; Pincus, D.L.; Rapp, C.S.; Day, T.J.F.; Honig, B.; Shaw, D.E.; Friesner, R.A. *Proteins* **2004**, 55, 351-367.

360. Alkorta, I.; Blanco, F.; Elguero, J. *J. Chem. Theory Comput.*, **2009**, 5, 1186–1194.

361. Calhorda, M.J.; Lopes, P.E.M. *J. Organomet. Chem.* **2000**, 609, 53 – 59.

362. Tiana, D. Organometallic chemistry from the interacting quantum atoms approach, Ph.D. Thesis, Università degli Studi di Milano, Milano, **2009**/**2010**, pp 18-19, 46.

363. Platts, J.A.; Overgaard, J.; Jones, C.; Iversen, B.B.; Stasch, A. *J. Phys. Chem. A* **2011**, 115, 194–200.

364. Farrugia, L.J.; Senn, H.M. *J. Phys. Chem. A* **2012**, 116, 738–746.

365. Renfrew, A.K.; Phillips, A.D.; Tapavicza, E.; Scopelliti, R.; Rothlisberger, U.; Dyson, P.J. *Organometallics* **2009**, 28, 5061–5071.

366. Nikolaienko, T.Y.; Bulavina, L.A.; Hovorun, D.M. *Phys. Chem. Chem. Phys.* **2012**, 14, 7441–7447.

367. Brovarets', O.O.; Yurenko, Y.P.; Hovorun, D.M. *J. Biomol. Struct. Dyn.* **2013**, 31, 913-936.

368. Yurenko, Y.P.; Zhurakivsky, R.O.; Samijlenko, S.P.; Hovorun, D.M. *J. Biomol. Struct. Dynam.* **2011**, 29, 51–65.

369. de Silva, I.C.; de Silva, R.M.; de Silva, K.M.N. *J. Mol. Struct. (Theochem)* **2005**, 728, 141–145.

370. Mendesa, P.J.; Ramalho, J.P.P.; Candeias, A.J.E.; Robalod, M.P.; Garcia, M.H. *J. Mol. Struct.* (*Theochem*) **2005**, 729, 109–113.

371. Rozas, I.; Alkorta, I.; Elguero. J. *J. Am. Chem. Soc.* **2000**, 122, 11154-11161.

372. Alkorta, I.; Rozas, I.; Elguero, *J. Chem. Soc. Rev.* **1998**, 27, 163-170.

373. Hammerum, S. *J. Am. Chem. Soc.*, **2009**, 131, 8627–8635.

374. Bene, J.E.D.; Alkorta, I.; Sanchez-Sanz, G.; Elguero, *J. Chem. Phy. Let.* **2012**, 538, 5–9.

375. Tang, K.; Shi, F.Q. *Int. J. Quan. Chem.*, **2007**, 107, 665–669.

376. Shubina, E.S.; Belkova, N.V.; Epstein, L.M. *J. Organomet. Chem.* **1997**, 536-537, 17-29.

377. Solimannejad, M.; Malekani, M.; Alkorta, I. *J. Mol. Struc.* (*Theochem*) **2010**, 955, 140–144.

378. Tognetti, V.; Joubert, L. *J. Phys. Chem. A* **2011**, 115, 5505–5515.

379. Maheswari, P.U.; Rajendiran, V.; Palaniandavar, M.; Thomas, R.; Kulkarni, G.U. *Inorg. Chim.*

Acta **2006**, 359, 4601–4612.

380. Parthasarathi, R.; Subramanian, V. Characterization of hydrogen bonding: From van der waals interactions to covalency. In Hydrogen Bonding—New Insights, *Springer* **2006**, Chapter 1, pp 1–50.

381. Grabowski, S.J.; Sokalski, W.A.; Leszczynski, *J. Chem. Phys. Lett.* **2006**, 432, 33-39.

382. Alkorta, I.; Elguero, J.; Bene, J.E.D. *Chem. Phys. Let.* **2010**, 489, 159–163.

383. Koch, U.; Popelier, P.L.A. *J. Phys. Chem.* **1995**, 99, 9747.

384. Lavallee, R.J.; Kutal, C. *J. Organomet. Chem.* **1998**, 562, 97 – 104.

385. Cremer, D.; Grafenstein *J. Phys. Chem. Chem. Phys.* **2007**, 9, 2791–2816.

386. Pratuangdejkul, J.; Jaudon, P.; Ducrocq, O.C.; Nosoongnoen, W.; Guerin, G-A.; Conti, M.; Loric, S.; Launay, J-M.; Manivet, P. *J. Chem. Theory Comput.* **2006**, 2, 746-760.

387. Crandles, D.A.; Eftekhari, F.; Faust, R.; Rao, G.S.; Reedyk, M.; Razavi, F.S. J. Phys. D: *Appl. Phys.* **2008**, 41, 135007- 135012.

388. Roscioli, J.R.; Hammer, N.I.; Johnson, M.A. *J. Phys. Chem. A* **2006**, 11, 7517-7520.

389. Venegas-Yazigi, D.; Campos-Vallette, M.; Lever, A.B.P.; Costamagna, J.; Latorre, R.O.; Hernández, W.G. *J. Chil. Chem. Soc.* **2003**, 48, ISSN 0717-9324, doi:10.4067/S0717-97072003000300016

390 Bor, G.; Dietler, U.K.; Stanghellini, P.L.; Gervasio, G.; Rossetti, R.; Sbrignadello, G.; Battison, G.A. *Chem. Euro. J.* **1981**, 213, 277-292.

391. Stanghellini, P.L.; Cognolato, L.; Bor, G.; Kettle, S.F.A. *J. Crys. Spec. Res.* **1983**, 13, 127-133.

392. Omberg, K.M.; Schoonover, J.R.; Treadway, J.A.; Leasure, R.M.; Dyer, R.B.; Meyer, T.J. *J. Am. Chem. Soc.* **1997**, 119, 7013-7018.

393. Yoshizawa, T.; Hada, M. *Chem. Phy. Let.* **2008**, 458, 223–226.

394. Foroutan-Nejad, C. *J. Phys. Chem. A* **2011**, 115, 12555–12560.

395. Ebenso, E.E.; Isabirye, D.A.; Eddy, N.O. *Int. J. Mol. Sci.* **2010**, 11, 2473-2498.

396. Page S. Education in Chemistry **2012**, 26-29, www.rsc.org/eic 22 May 2012.

397. Musil, D.; Zucic, D.; Turk, D.; Engh, R.A.; Mayr, I.; Huber, R.; Popovic, T.; Turk, V.; Towatari, T.; Katunuma, N.; Bode, W. *EMBO J.* **1991**, 10: 2321-2330.

398. Xie, P.; Streu, C.; Qin, J.; Bregman, H.; Pagano, N.; Meggers, E.; Marmorstein, R. *Biochemistry* **2009**, 48, 5187-5198.

399. Eriksson, M.; Uhlin, U.; Ramaswamy, S.; Ekberg, M.; Regnström, K.; Sjöberg, B.M.; Eklund, H. *Structure* **1997**, 5, 1077-1092.

400. Sandalova, T.; Zhong, L.; Lindqvist, Y.; Holmgren, A.; Schneider, G. *PNAS* **2001**, 98, 9533-9538.

401. Newby, Z.; Lee, T.T.; Morse, R.J.; Liu, Y.; Liu, L.; Venkatraman, P.; Santi, D.V.; Finer-Moore, J.S.; Stroud, R.M. *Biochemistry* **2006**, 45, 7415-7428.

402. Schuetz, A.; Min, J.; Allali-Hassani, A.; Schapira, M.; Shuen, M.; Loppnau, P.; Mazitschek, R.; Kwiatkowski, N.P.; Lewis, T.A.; Maglathin, R.L.; McLean, T.H.; Bochkarev, A.; Plotnikov, A.N.; Vedadi, M.; Arrowsmith, C.H. *J. Biol. Chem.* **2008**, 283, 11355-11363.

403. Zu, B.; Ong, M.S.; Groessl, M.; Adhireksan, Z.; Hartinger, C.G.; Dyson, P.J.; Davey, C.A. *Chem. Euro. J.* **2011**, 17, 3562-3566.

404. Classen, S.; Olland, S.; Berger, J.M. *PNAS* **2003**, 100, 10629-10634.

405. Sugio, S.; Kashima, A.; Mochizuki, S.; Noda, M.; Kobayashi, K. *Protein Eng.* **1999**, 12, 439-446.

406. Zhao, Y.; Biertümpfel, C.; Gregory, M.T.; Hua, Y.J.; Hanaoka, F.; Yang, W. *PNAS* **2012**, 109, 7269-7274.

407. R Development Core Team. R: A language and environment for statistical computing. R Foundation for Statistical Computing, Vienna, Austria. ISBN 3-900051-07-0, URL http://www.R-project.org 12 January 2012.

408. Burzlaff, N.; Hegelmann, I.; Weibert, B. *J. Organomet. Chem.* **2001**, 626, 16 – 23.

409. Otero, A.; Fernández-Baeza, J.; Antiñolo, A.; Tejeda, J.; Lara-Sánchez, A. *Dalton Trans.* **2004**, 1499–1510.

410. Trofimenko, S. *J. Am. Chem. Soc.* **1967**, 89, 3165–3170.

411. Trofimenko, S. *Chem. Rev.*, **1993**, 93, 943-980.

412. Tang, L-F.; Jia, W.-L.; Zhao, X.-M.; Yang, P.; Wang, J.-T. *J. Organomet. Chem.* **2002**, 658, 198-203.

413. Klein, C.; Baranoff, E.; Grätzel, M.; Nazeeruddin, Md.K. *Tetrahedron Let.* **2011**, 52, 584–587.

414. Masaguer, J.R.; Freijanes, E.; Sordo, J.; Casas, J.S.; Bermejo, M.R. *Inorg. Chim. Acta* **1977**, 25, 203–206.

415. Liang, S.; Wang, H.; Deb, T.; Petersen, J.L.; Yee, G.T.; Jensen, M.P. *Inorg. Chem.* **2012**, 51, 12707-12719.

416. Chou, C.-C.; Su, C.-C-; Yeh, A. *Inorg. Chem.* **2005**, 44, 6122−6128.

417. Díez-Barra, E.; García-Martínez, J.C.; Guerra, J.; Hornillos, V.; Merino, S.; del Rey, R.; Rodríguez-Curiel, R.I.; Rodríguez-López, J.; Sánchez-Verdú, P.; Tejeda, J.; Tolosa, J. *ARKIVOC* **2002**, (v) 17-25.

418. Hara, K.; Sugihara, H.; Tachibana, Y.; Islam, A.; Yanagida, M.; Sayama, K.; Arakawa, H. *Langmuir* **2001**, 17, 5992-5999.

419. Jamróz, M.H. Vibrational Energy Distribution Analysis: VEDA 4, program,Warsaw, **2004**–**2010**. http://www.smmg.pl. 15 October 2013.

420. Jamróz, M.H.; Dobrowolski, J.Cz.; Brzozowski, R. *Mol. Struc.* **2006**, 787, 172–183.

421. Jamróz, M.H. *Spectrochim. Acta Part A: Mol. Biomol. Spect.* **2013**, 114, 220–230.

422. Marchetti, F.; Pettinari, C.; Cerquetella, A.; Cingolani, A.; Pettinari, R.; Monari, M.; Wanke, R.; Kuznetsov, M.L.; Pombeiro, A.J.L. *Inorg. Chem.* **2009**, 48, 6096–6108.

423. Evans, I.P.; Spencer, A.; Wilkinson, G. J. Chem. Soc., *Dalton Trans.* **1973**, 204-209.

424. Renfrew, A.K.; Phillips, A.D.; Tapavicza, E.; Scopelliti, R.; Rothlisberger, U.; Dyson, P.J. *Organometallics* **2009**, 28, 5061–5071.

425. Ooms, K.J.; Wasylishen, R.E. *J. Am. Chem. Soc.* **2004**, 126, 10972-10980.

426. Bühl, M.; Gaemers, S.; Elsevier, C.J. *Chem. Eur. J.* **2000**, 6, 3272 - 3280.

427. Binotti, B.; Bellachioma, G.; Cardaci, G.; Macchioni, A.; Zuccaccia, C.; Foresti, E.; Sabatino, P. *Organometallics* **2002**, 21, 346-354.

Appendix

Table 3.1: Hybridization and Lewis properties in terms of percentage total electron density distribution of the complexes

Molecule	Ru(II) Valence rating	Total Lewis	Val non-Lewis	Rydberg non-Lewis
1	4d7 < 5s1	97.536% of 138	2.28%	0.18%
2	4d7< 5s1	97.384% of 123	2.44%	0.18%
3	4d7< 5s1	97.692% of 118	2.17%	0.14%

Table 3.2: The polarization of the bonding and the antibonding interaction of Ru(II) with ligand atoms

Comp.	**Lewis Bonding**	**(*c*A-squared) *c*A → (*c*A-squared) *c*A**	**Non-Lewis Antibonding**	**(*c*A-squared) *c*A ← (*c*A-squared) *c*A**
1	σ(Ru-P)	(33.77%) 0.5811*→ (66.23%) 0.8138*	σ*(Ru-O)	(66.23%) 0.8138* ← (33.77%) -0.5811*
	σ(Ru-O)	(23.78%) 0.4876* → (76.22%) 0.8731*	σ*(Ru-O)	(76.22%) 0.8731* ← (23.78%) -0.4876*
2	σ(Ru-O)	(21.12%) 0.4595*→ (78.88%) 0.8882*	σ*(Ru-O)	(78.88%) 0.8882* ← (21.12%) -0.4595*
	σ(Ru-O)	(21.12%) 0.4595* → (78.88%) 0.8882*	σ*(Ru-O)	(78.88%) 0.8882* ← (21.12%) -0.4595*
	σ(Ru-P)	(27.65%) 0.5258* → (72.35%) 0.8506*	σ*(Ru-P)	(72.35%) 0.8506* ← (27.65%) -0.5258*
3	σ(Ru-P)	(31.47%) 0.5610*→(68.53%) 0.8278*	σ*(Ru-P)	(68.53%) 0.8278*Ru ← (31.47%) -0.5610*
	σ(Ru-Cl)	(25.01%) 0.5001* → (74.99%) 0.8660*	σ*(Ru-Cl)	(74.99%) 0.8660* ← (25.01%) -0.5001*
	σ(Ru-Cl)	(24.81%) 0.4981* → (75.19%) 0.8671*	σ*(Ru-Cl)	(75.19%) 0.8671* ← (24.81%) -0.4981*

Polarization coefficient *c*A is the values with starred superscript and the square of it is percentage of the NBO (*c*A-squared) on each hybrid orbitals (in parentheses).

Table 3.3: The delocalization orbitals with their second perturbation energies ($E^{(2)}$) and the principal delocalizing acceptor orbitals associated with each donor NBO

Comp.	**Delocalization of Electrons**		**Delocalization donor orbitals**				**Delocalization acceptor orbitals**		
	Donor → Acceptor	**$E^{(2)}$ kcal/mol**	**Donor**	**occ**	**E**	**Pda**	**Acceptor**	**e^- gain**	**E**
1	1. σ(Ru-O) → 14. σ*(C^u=O^u)	15.28	1. ♦(Ru – O)	0.91961	-0.40736	14(v)	8. LP*(Ru)	0.18716e	0.62863
	2. LP(Ru) → 10. LP*(C)	22.72	2 LP(Ru)	0.87731	-0.24553	5(r)	10. LP*(C)	0.46262e	-0.16897
	3. LP(Ru) → 9. LP*(C)	22.81	3. LP(Ru)	0.86880	-0.24643	9(r)	11. LP*(C)	0.44596e	-0.15605
	3. LP(Ru) → 11. LP*(C)	16.20	5. LP(C)	0.49558	-0.17000	10(v)	12. σ*(Ru-P)	0.24037e	0.09092
	4. LP(O) → 8. LP*(Ru)	28.12	6. LP(C)	0.47745	-0.15262	11(v)	13. σ*(Ru–O)	0.23514e	-0.02340
	5. LP(C) → 13. ♦*(Ru-O)	43.01	7. LP(C)	0.49089	-0.16396	10(v)	14. σ*(C^u =O^u)	0.11939e	0.05793
	6. LP(C) → 12. ♦*(Ru-P)	22.70							
	7. LP(C) → 8. LP*(Ru)	10.43							
2	1. σ(Ru-O) →13. σ*(Ru–O)	11.05	1. σ(Ru-O)	0.95924	-0.45566	14(g)	12. σ*(Ru-O)	0.19245e	0.15949
	1. σ(Ru-O) →14. σ*(Ru–P)	16.36	2. σ(Ru-O)	0.95720	-0.45611	14(g)	13. σ*(Ru-O)	0.19124e	0.16517
	2. σ(Ru-O) →12. σ*(Ru-O)	11.16	3. σ(Ru-P)	0.93212	-0.37226	13(g)	14. σ*(Ru-P)	0.16022e	0.37628
	2. σ(Ru–O) →14. σ*(Ru-P)	16.63	4. LP(Ru)	0.87205	-0.24879	11(r)	9. LP*(C)	0.47318e	-0.16517
	3. σ(Ru-P) →12. σ*(Ru-O)	18.88	5. LP(Ru)	0.86829	-0.25044	9(r)	10. LP*(C)	0.46416e	-0.16617
	3. σ(Ru-P)→13. σ*(Ru-O)	19.15	6. LP(C)	0.47536	-0.16503	10(v)	11. LP*(C)	0.46586e	-0.16623
	3. σ(Ru-P) → 14. σ*(Ru-P)	10.82	7. LP(C)	0.48942	-0.17244	8(v)	7. LP(C)	0.48942e	-0.17244
	4. LP(Ru) → 7. LP(C)	10.60	8. LP(C)	0.48061	-0.17301	7(v)	8. LP(C)	0.48061e	-0.17301
	4. LP(Ru) → 11. LP*(C)	20.77							
	5. LP(Ru) → 8. LP(C)	12.47							
	5. LP (3)Ru → 9.	15.31							

	LP*(C)								
	5. LP (3)Ru → 10. LP*(C)	13.19							
	6. LP (1) C →12. σ*(Ru-O)	19.17							
	7. LP (1) C →13. σ*(Ru-O)	22.04							
	8. LP (1) C →12. σ*(Ru-O)	20.45							
3	1. σ(Ru-P) → 13. σ*(Ru-Cl)	19.10	1. σ(Ru-P)	0.93656	-0.37418	13(g)	12. σ*(Ru-P)	0.17416e	0.25537
	1. σ(Ru-P) → 14. σ*(Ru-Cl)	18.99	2. σ(Ru-Cl)	0.96973	-0.35980	12(g)	13. σ*(Ru-Cl)	0.18941e	0.18579
	2. σ(Ru-Cl) → 12. σ*(Ru-P)	15.19	3. σ(Ru-Cl)	0.97066	-0.36016	12(g)	14. σ*(Ru-Cl)	0.18893e	0.19315
	2. σ (Ru-Cl) → 14. σ*(Ru-Cl)	10.97	4. LP(Ru)	0.88393	-0.24641	6(r)	6. LP(C)	0.47037e	-0.16731
	3. σ (Ru-Cl) →12. σ*(Ru-P)	15.34	5. LP(Ru)	0.85983	-0.24181	9(r)	7. LP(C)	0.48229e	-0.17163
	3. σ(Ru-Cl) → 13. σ*(Ru-Cl)	11.19	6. LP(C)	0.47037	-0.16731	8(v)	8. LP(C)	0.47524e	-0.16572
	4. LP(Ru) → 6. LP(C)	14.58	7. LP(C)	0.48229	-0.17163	6(v)	9. LP*(C)	0.46719e	-0.16497
	4. LP(Ru) → 10. LP*(C)	10.36	8. LP(C)	0.47524	-0.16572	6(v)	10. LP*(C)	0.46930e	-0.15866
	4. LP(Ru) → 11. LP*(C)	10.12					11. LP*(C)	0.46202e	-0.15019
	5. LP(Ru) → 7. LP(C)	16.75							
	5. LP(Ru) → 8. LP(C)	11.72							
	5. LP(Ru) → 9. LP*(C)	22.31							
	6. LP(C) → 14. σ*(Ru-Cl)	16.80							
	7. LP(C) →13. σ*(Ru-Cl)	19.99							
	8. LP(C)→ 14. σ*(Ru-Cl)	20.25							

The orbital analyses in the table are defined in terms donor orbital, acceptor orbital, second perturbation energy or stability energy ($E^{(2)}$ in kcal/mol), occupancy (occ), principal delocalizing acceptor (Pda), quantity of electron gain (e^- gain) and energy level (E). The topological relationship to the NBO if attached to the same atom (geminal, "g"), to an adjacent bonded atom (vicinal, "v"), or to a more remote ("r") site. The amount of electron loss is calculated on the basis of NPA at the same level. The supercript “u” is on atoms that are not bonded to metal atom.

Table 3.4: Bond Order shows other atoms in the molecule that are interacting with the metal centre.

	Complex **1**		Complex **2**		Complex **3**	
	Bond length	Bond order	Bond length	Bond order	Bond length	Bond order
Ru-P	2.430	0.590	2.429	0.594	2.420	0.725
Ru-C	2.211	0.439	2.230	0.382	2.231	0.416
	2.233	0.423	2.225	0.390	2.205	0.441
	2.266	0.348	2.232	0.413	2.198	0.446
	2.249	0.429	2.241	0.411	2.205	0.452
	2.213	0.433	2.239	0.429	2.236	0.392
	2.232	0.425	2.231	0.442	2.295	0.332
Ru-Cl			2.500	0.966		
			2.496	0.947		
Ru-O	2.100	0.659	2.090	0.682		
	2.119	0.667	2.086	0.673		

Table 3.5: Electron density critical point analysis of selected bonds in the complexes

	Bonds	ρ(r)	$\nabla^2\rho$	Ellipticity	K	BPL-GBL_I	V	G	L	V/G
Complex 1										
pta	Ru1-P16	0.073	0.155	0.186	0.017	0.011	-0.072	0.055	-0.039	-1.300
arene	Ru1-C9	0.077	0.265	0.214	0.011	0.010	-0.089	0.078	-0.066	-1.146
	Ru1-C14	0.071	0.291	1.009	0.008	0.029	-0.089	0.081	-0.073	-1.098
	Ru1-C19	0.068	0.277	2.574	0.007	0.027	-0.083	0.076	-0.069	-1.091
	Ru1-C24	0.072	0.256	0.400	0.009	0.013	-0.083	0.073	-0.064	-1.129
	Ru1-C31	0.071	0.295	1.647	0.007	0.046	-0.088	0.081	-0.074	-1.088
	Ru1-C29	0.077	0.262	0.331	0.011	0.010	-0.089	0.077	-0.066	-1.149
bidentate	Ru1-O8	0.086	0.379	0.215	0.011	0.005	-0.118	0.106	-0.095	-1.107
	Ru1-O27	0.083	0.351	0.296	0.012	0.001	-0.112	0.100	-0.088	-1.121
HB	O8-H35	0.006	0.032	0.259	-0.002	0.009	-0.004	0.006	-0.008	-0.627
	C11-H49	0.003	0.013	1.235	-0.001	0.028	-0.002	0.003	-0.003	-0.723
	O30-H47	0.008	0.039	0.090	-0.002	0.016	-0.005	0.007	-0.010	-0.687
	H42-H54	0.005	0.019	0.213	-0.001	0.026	-0.002	0.003	-0.005	-0.608
	H58-H62	0.003	0.011	0.603	-0.001	0.133	-0.001	0.002	-0.003	-0.681
	O30-H61	0.010	0.047	0.672	-0.002	0.096	-0.007	0.009	-0.012	-0.739
Complex 2										
pta	Ru1-P17	0.073	0.162	0.166	0.016	0.010	-0.073	0.057	-0.041	-1.287
arene	Ru1-C2	0.073	0.281	0.767	0.009	0.017	-0.088	0.079	-0.070	-1.114
	Ru1-C6	0.074	0.265	0.397	0.010	0.016	-0.086	0.076	-0.066	-1.129
	Ru1-C5	0.074	0.274	0.561	0.010	0.015	-0.088	0.078	-0.069	-1.125
	Ru1-C7	0.072	0.272	0.627	0.009	0.023	-0.085	0.077	-0.068	-1.113
	Ru1-C10	0.073	0.274	0.414	0.009	0.018	-0.087	0.078	-0.068	-1.121
	Ru1-C8	0.071	0.282	0.865	0.008	0.027	-0.087	0.079	-0.071	-1.103
bidentate	Ru1-O12	0.090	0.383	0.194	0.013	0.003	-0.122	0.109	-0.096	-1.121
	Ru1-O16	0.091	0.386	0.196	0.013	0.004	-0.123	0.110	-0.096	-1.122
HB	C15-H41	0.007	0.027	1.073	-0.001	0.057	-0.004	0.005	-0.007	-0.740
	H45-H51	0.003	0.011	0.200	-0.001	0.015	-0.001	0.002	-0.003	-0.572
Complex 3										
pta	Ru1-P13	0.076	0.149	0.143	0.018	0.008	-0.073	0.055	-0.037	-1.327
arene	Ru1-C6	0.074	0.278	0.691	0.010	0.017	-0.089	0.079	-0.070	-1.121
	Ru1-C9	0.077	0.290	0.425	0.011	0.017	-0.094	0.083	-0.072	-1.130
	Ru1-C10	0.077	0.282	0.266	0.012	0.014	-0.094	0.082	-0.071	-1.141
	Ru1-C14	0.077	0.269	0.263	0.012	0.013	-0.091	0.079	-0.067	-1.149
	Ru1-C16	0.072	0.277	1.380	0.008	0.030	-0.086	0.077	-0.069	-1.106
mono	Ru1-Cl19	0.056	0.182	0.203	0.005	0.002	-0.055	0.050	-0.046	-1.094
	Ru1-Cl20	0.056	0.184	0.169	0.005	0.001	-0.056	0.051	-0.046	-1.095
HB	C2-H29	0.006	0.019	0.854	-0.001	0.121	-0.003	0.004	-0.005	-0.768
	Cl20-H43	0.010	0.034	0.911	-0.001	0.113	-0.006	0.007	-0.009	-0.814
	Cl20-H46	0.010	0.032	0.043	-0.001	0.006	-0.005	0.007	-0.008	-0.775

ρ(r) is electron density, $\nabla^2\rho$ is the Laplancian of ρ(r), BPL – GBL_I is Bond strain, V is virial field (potential energy density), G is Lagrangian form of kinetic energy density, K is hamiltonian form of kinetic energy density, L (i.e. K – G) is lagrangian density which is (-1/4) $\nabla^2\rho$ while "Ratio" is V/G i.e. PE/KE (the higher its magnitude the stronger the Bond).

Table 3.6. The summary of the natural energy decomposition analysis showing the components of interaction energy in kcal/mol.

Mol.	CT	ES	POL	XC	DEF	SE	Electrical	Core	E
CraptaC	-402.36	-157.67	-169.20	-176.52	834.49	82.1	-244.77	575.87	-71.26
OraptaC	-1079.81	-151.05	-162.92	512.35	810.4	78.58	-235.39	1244.16	-71.04
raptaC	-819.55	-162.03	-133.42	28.28	818.81	63.52	-231.93	983.58	-67.90

The components of energy are defines in terms of charge transfer (CT), electrostatic interaction (ES); polarization (POL); electrical self-energy (SE); exchange interaction (XC); deformation energy (DEF), Electrical (ES+POL+SE), Core (XC+DEF-SE) and Total Interaction energy which is the final net H-bond energy (E = Electrical + Core + CT)

Table 3.7: The correlation in the properties of the electron density critical point analysis of complexes **1**, **2** and **3**

$\rho(r)$#	$\nabla^2\rho$	Ellipticity	K	BPL.GBL_I	V	G	L	Ratio
1	-0.85	-0.57	0.96	-0.62	-0.86	0.39	0.85	-0.71
2	-0.83	-0.72	0.96	-0.74	-0.83	0.36	0.83	-0.64
3	-0.92	-0.65	0.98	-0.60	-0.95	0.23	0.92	-0.80
$\nabla^2\rho$#	Ellipticity	K	BPL.GBL_I	V	G	L	Ratio	
1	0.57	-0.81	0.47	0.54	0.09	-1.00	0.90	
2	0.65	-0.76	0.62	0.45	0.16	-1.00	0.88	
3	0.60	-0.95	0.43	0.82	0.13	-1.00	0.90	
Ellipticity#	K	BPL.GBL_I	V	G	L	Ratio		
1	-0.53	0.51	0.41	-0.06	-0.57	0.48		
2	-0.62	0.93	0.46	-0.07	-0.65	0.57		
3	-0.61	0.74	0.56	-0.05	-0.60	0.55		
K#	BPL.GBL_I	V	G	L	Ratio			
1	-0.53	-0.93	0.51	0.81	-0.60			
2	-0.62	-0.92	0.52	0.76	-0.50			
3	-0.51	-0.96	0.19	0.95	-0.77			
BPL.GBL_I #	V	G	L	Ratio	V#	G	L	Ratio
1	0.46	-0.20	-0.47	0.48	**1**	-0.79	-0.54	0.31
2	0.49	-0.13	-0.62	0.57	**2**	-0.81	-0.45	0.16
3	0.55	-0.29	-0.43	0.44	**3**	-0.46	-0.82	0.59
G#	L	Ratio	L#	Ratio				
1	-0.09	0.29	**1**	-0.90				
2	-0.16	0.40	**2**	-0.88				
3	-0.13	0.37	**3**	-0.90				

The parameters that are denoted with "#" shows they are in correlation with every other parameters that are in that row except where "#" appears again.

Table 3.8: Selected atomic properties derived through the quantum theory of atoms in molecules

analysis of the complexes

Complex 1												
	Name	q(A)	L(A)	K(A)	K_Scaled(A)	μ_{Intra}(A)	μ_{Bond}(A)	μμ(A)	N(A)	%Loc(A)	%Deloc(A,A')	Vol(A), 0.001
	Ru1	0.86	9.73E-04	4402.36	-4426.58	0.30	1.64	1.34	43.14	94.18	5.82	98.66
arene	C9	-0.11	-4.40E-05	37.63	-37.83	0.22	0.20	0.21	6.11	65.89	34.11	72.17
	C14	-0.14	4.30E-05	37.62	-37.83	0.24	0.11	0.17	6.14	65.99	34.01	76.94
	C19	-0.08	7.00E-06	37.63	-37.83	0.21	0.40	0.59	6.08	64.89	35.11	59.57
	C24	-0.10	-1.72E-04	37.62	-37.83	0.09	0.27	0.18	6.10	64.87	35.13	61.55
	C29	-0.12	-1.13E-04	37.65	-37.85	0.26	0.36	0.62	6.12	66.00	34.00	71.17
	C31	-0.12	4.70E-05	37.62	-37.83	0.25	0.18	0.23	6.12	65.96	34.04	76.32
pta	P16	0.89	2.52E-04	338.04	-339.90	1.03	0.56	1.59	14.11	86.02	13.98	102.66
Bidentate	O8	-0.95	-7.00E-06	74.55	-74.96	0.13	0.79	0.85	8.95	86.36	13.64	93.88
	O27	-0.95	1.75E-04	74.54	-74.95	0.17	1.01	1.14	8.95	86.87	13.13	96.01
Complex 2												
	Ru1	0.85	-1.02E-04	4402.39	-4426.23	0.37	1.83	1.65	43.15	94.12	5.88	99.40
arene	C2	-0.11	-1.10E-04	37.62	-37.82	0.24	0.18	0.10	6.11	65.99	34.01	75.24
	C5	-0.12	-1.64E-04	37.63	-37.83	0.22	0.16	0.11	6.12	65.92	34.08	73.72
	C6	-0.07	-1.78E-04	37.61	-37.82	0.16	0.30	0.16	6.07	64.86	35.14	61.43
	C7	-0.08	-3.30E-05	37.63	-37.83	0.19	0.20	0.05	6.08	64.80	35.20	58.62
	C8	-0.14	-8.80E-05	37.62	-37.82	0.22	0.11	0.14	6.14	65.93	34.07	76.13
	C10	-0.15	-6.10E-05	37.62	-37.83	0.20	0.10	0.13	6.15	65.89	34.11	74.16
pta	P17	0.82	-3.60E-05	338.07	-339.90	1.05	0.21	1.18	14.18	85.99	14.01	106.82
Bidentate	O12	-0.92	1.64E-04	74.54	-74.95	0.14	0.97	1.05	8.92	86.23	13.77	95.79
	O16	-0.92	1.57E-04	74.54	-74.95	0.15	1.02	1.10	8.92	86.23	13.77	96.49
Complex 3												
	Ru1	0.64	-7.21E-04	4402.59	-4424.39	0.37	1.39	1.48	43.36	94.05	5.95	107.89
arene	C6	-0.09	-2.56E-04	37.62	-37.80	0.12	0.17	0.05	6.09	64.84	35.16	61.85
	C9	-0.13	-1.78E-04	37.62	-37.81	0.23	0.11	0.14	6.13	65.90	34.10	74.95
	C10	-0.11	-3.14E-04	37.63	-37.81	0.24	0.17	0.10	6.11	65.85	34.15	73.23
	C14	-0.12	-1.86E-04	37.63	-37.81	0.23	0.18	0.09	6.12	65.84	34.16	71.88
	C16	-0.12	-1.28E-04	37.63	-37.81	0.23	0.18	0.11	6.12	65.87	34.13	72.90
	C17	-0.06	4.70E-05	37.61	-37.80	0.19	0.05	0.15	6.06	64.88	35.12	59.93
pta	P13	0.86	-2.50E-05	338.02	-339.70	1.02	0.11	0.96	14.14	85.74	14.26	99.49
mono	Cl19	-0.58	9.80E-05	456.63	-458.89	0.14	1.40	1.54	17.58	96.71	3.29	237.25
	Cl20	-0.57	7.60E-05	456.63	-458.89	0.14	0.66	0.79	17.57	96.55	3.45	231.48

q(A) is net charge of atom A, L(A) is Lagrangian of Atom A, N(A) is average number of electrons in atom A, K(A) is electronic kinetic energy of atom A (Hamiltonian Form), %Loc(A) is percentage of average number of electrons localized in atom A, K_Scaled(A) is approximation to virial-based total energy of atom A, μ_{Intra}(A) is magnitude of Intraatomic dipole moment of atom A, Ee(A) is contribution of atom A to electronic energy of molecule, %Deloc(A,A') is the percentage of electron delocalization index of atom A and Vol(A) is the volume bounded by an isosurface of the electron density distribution (0.001) and by interatomic surfaces of atom A.

Table 3.9: Bond Order shows the metal-ligand bonds for the B3LYP/DGDZVP(Ru)|6-31+G(d,p)

treated systems

	Complex 1			Complex 2			Complex 3			Complex 4		
	Bonds	**Bond distance (Å)**	**Bond Order**	**Bonds**	**Bond distance (Å)**	**Bond Order**	**Bonds**	**Bond distance (Å)**	**Bond Order**	**Bonds**	**Bond distance (Å)**	**Bond Order**
arene	Ru-C6	2.198	0.424	Ru-C2	2.221	0.396	Ru-C6	2.215	0.4	Ru-C6	2.223	0.383
	Ru-C9	2.216	0.407	Ru-C3	2.218	0.446	Ru-C8	2.213	0.411	Ru-C8	2.241	0.42
	Ru-C10	2.246	0.331	Ru-C7	2.229	0.415	Ru-C12	2.197	0.4	Ru-C12	2.182	0.418
	Ru-C14	2.235	0.41	Ru-C8	2.272	0.35	Ru-C17	2.254	0.329	Ru-C17	2.277	0.361
	Ru-C16	2.235	0.343	Ru-C13	2.181	0.463	Ru-C21	2.2	0.412	Ru-C21	2.18	0.446
	Ru-C19	2.209	0.409	Ru-C14	2.261	0.328	Ru-C22	2.257	0.32	Ru-C22	2.283	0.31
PTA	Ru-P11	2.419	0.781	Ru-P12	2.435	0.744	Ru-P14	2.423	0.798	Ru-P14	2.443	0.754
Others	Ru-Cl2	2.496	0.834	Ru-O11	2.251	0.41	Ru-Cl11	2.483	0.875	Ru-O11	2.239	0.416
	Ru-Cl20	2.493	0.834	Ru-Cl20	2.481	0.908	Ru-Cl23	2.487	0.854	Ru-Cl23	2.475	0.928

1 Table 3.10: The polarization of the bonding interaction of Ru(II) with ligand atoms using B3LYP/DGDZVP(Ru)|6-31+G(d,p)

				Complex 1			
	Bondσ	**cA-squared**	**cA**	**Atom**	**cA-squared**	**cA**	**Atom**
σ(1)	Ru-Cl2	22.71%	0.4765*	Ru	77.29%	0.8792*	Cl2
σ(1)	Ru-P11	28.37%	0.5326*	Ru	71.63%	0.8463*	P11
σ	Ru-Cl20	22.58%	0.4752*	Ru	77.42%	0.8799*	Cl20
				Complex 2			
σ(1)	Ru-P12	33.18%	0.5761*	Ru	66.82%	0.8174*	P12
σ(1)	Ru-Cl20	23.42%	0.4839*	Ru	76.58%	0.8751*	Cl20
				Complex 3			
σ(1)	Ru-Cl11	23.55%	0.4853*	Ru	76.45%	0.8744*	Cl11
σ(1)	Ru-P14	29.82%	0.5461*	Ru	70.18%	0.8377*	P14
σ(1)	Ru-Cl23	23.41%	0.4838*	Ru	76.59%	0.8752*	Cl23
				Complex 4			
σ(1)	Ru-P14	34.92%	0.5909*	Ru	65.08%	0.8067*	P14
σ(1)	Ru-Cl13	24.37%	0.4937*	Ru	75.63%	0.8696*	Cl23

Polarization coefficient c_A is the values with superscript "*" and its percentage NBO is "*c*A-squared" on each hybrid orbitals.

Table 3.11: The delocalization orbitals for the charge transfer with second perturbation energies (E_2) greater than or equals to 10 Kcal/mol

Donor		Acceptor		E^2 Kcal/mol
Complex 1				
94 n(2)	Ru	101 n(1)	C9	15.66
94 n(2)	Ru	108 n*(1)	C14	33.35
94 n(2)	Ru	417 σ*(2)	C10-C16	26.01
95 n(3)	Ru	101 n(1)	C9	32.66
95 n(3)	Ru	103 n(1)	C19	39.92
95 n(3)	Ru	107 n(1)	C6	73.57
95 n(3)	Ru	108 n(1)	C14	27.19
13 σ(1)	C6-C9	396 σ*(1)	Ru-Cl20	15.32
23 σ(1)	C10-C16	395 σ*	Ru-p11	12.79
24 σ(2)	C10-C16	395 σ*	Ru-P11	39.25
34 σ(1)	C14-C19	394 σ*	Ru-Cl2	14.99
101 n(1)	C9	396 σ*	Ru-Cl20	44.44
103 n(1)	C19	394 σ*	Ru-Cl2	46.59
Complex 2				
91 n(2)	Ru	93 n(1)	C2	17.27
91 n(2)	Ru	104 n*(1)	C7	22.37
91 n(2)	Ru	418 σ*(2)	C8-C14	23.14
92 n(3)	Ru	93 n(1)	C2	25.99
92 n(3)	Ru	94 n(1)	C3	45.94
92 n(3)	Ru	104 n(1)	C7	19.22
92 n(3)	Ru	105 n(1)	C13	52.84
3 σ(1)	C2-C3	400 σ*(1)	Ru-Cl20	14.54
18 σ(1)	C7-C13	103 n*(4)	Ru	14.17
19 σ(1)	C8-C14	399 σ*(1)	Ru-P12	10.73
20 σ(2)	C8-C14	399 σ*(1)	Ru-P12	43.33
93 n(1)	C2	399 σ*(1)	Ru-P12	12.04
93 n(1)	C2	400 σ*(1)	Ru-Cl20	51.77
94 n(1)	C3	400 σ*(1)	Ru-Cl20	60.44
97 n(2)	O11	103 n*(4)	Ru	51.84
Complex 3				
2 σ(1)	Ru-P14	423 σ*(1)	Ru-Cl11	10.92
2 σ(1)	Ru-P14	425 σ*(1)	Ru-Cl23	10.91
98 n(2)	Ru	101 n(1)	C6	51.02
98 n(2)	Ru	119 n*(1)	C8	31.34
98 n(2)	Ru	458 σ*(2)	C17-C22	20.1
99 n(3)	Ru	119 n*(1)	C8	25.77
99 n(3)	Ru	448 σ*(2)	C12-C21	38.13
25 σ(1)	C12-C21	423 σ*(1)	Ru-Cl11	16.13
26 σ(2)	C12-C21	423 σ*(1)	Ru-Cl11	52.33
35 σ(1)	C17-C22	424 σ*(1)	Ru-P14	12.46
36 σ(2)	C17-C22	424 σ*(1)	Ru-P14	36.97
101 n(1)	C6	425 σ*(1)	Ru-Cl23	39.08
Complex 4				
94 n(2)	Ru	100 n(1)	C8	18.7
94 n(2)	Ru	116 n*(1)	C6	49.12
94 n(2)	Ru	464 σ*(2)	C17-C22	15.43
95 n(3)	Ru	100 n(1)	C8	12.15
95 n(3)	Ru	106 n(1)	C12	50.7

95 n(3)	Ru	117 n*(1)	C21	77.09
15 σ(1)	C6-C8	430 σ*(1)	Ru-Cl23	13.46
26 σ(1)	C12-C21	115 n*(4)	Ru	14.63
35 σ(1)	C17-C22	429 σ*(1)	Ru-P14	10.5
36 σ(2)	C17-C22	429 σ*(1)	Ru-P14	40.48
100 n(1)	C8	430 σ*(1)	Ru-Cl23	66.76
106 n(1)	C12	115 n*(4)	Ru	45.44
106 n(1)	C12	429 σ*(1)	Ru-P14	22.62
105 n(2)	O11	115 n*(4)	Ru	53.44

$E^{(2)}$ in kcal/mol is the second perturbation energy or stability energy, "n" is lone pair and "σ" is sigma bond

Table 3.12: The principal delocalizing acceptor orbitals associated showing only the non-Lewis charge-transfer acceptors from the for B3LYP/DGDZVP(Ru)|6-31G+(d,p) systems

Complex 1	Acceptor orbitalσ	e- gain	Energy (Hatree)
394 σ*(1)	Ru-Cl2	0.31608	-0.02839
395 σ*(1)	Ru-P11	0.29782	0.01188
396 σ*(1)	Ru-Cl20	0.31292	-0.027
108 n*(1)	C14	0.96795	-0.17992
417 σ*(2)	C10-C16	0.33081	-0.00328
Complex 2			
103 n*(4)	Ru	0.349	-0.12843
399 σ*(1)	Ru-P12	0.37892	-0.18713
400 σ*(1)	Ru-Cl20	0.37243	-0.20633
Complex 3			
423 σ*	Ru-Cl11	0.30699	-0.03781
424 σ*	Ru-P14	0.29048	0.0009
425 σ*(1)	Ru-Cl23	0.31061	-0.03811
119 n*(1)	C8	0.96704	-0.19129
448 σ*(2)	C12-C21	0.43603	-0.036
Complex 4			
115 n*(4)	Ru	0.33789	-0.13532
429 σ*(1)	Ru-P14	0.37099	-0.20007
430 σ*(1)	Ru-Cl23	0.36914	-0.21941
116 n*(1)	C6	0.94061	-0.31983
117 n*(1)	C21	0.91202	-0.32273
464 σ*(2)	C17-C22	0.31585	-0.15262

"n" is lone pair and "σ" is sigma bond

Table 3.13: The summary of the natural energy decomposition analysis (NEDA) showing the components of interaction energy in kcal/mol for the B3LYP/DGDZVP(Ru)|6-31+G(d,p) treated systems

		Complex 1	Complex 2	Complex 3	Complex 4
Electrostatic	**ES**	-202.73	-238.05	-199.29	-232.16
Polarizability	**POL**	-617.07	-759.26	-622.79	-755.71
	XC	-178.19	219.22	-180.5	-178.96
	DEF	1331.71	1635.67	1360.91	2119.7
	SE	304.74	372.58	306.57	355.55
Electrical	**ES+POL+SE**	-515.06	-624.73	-515.51	-632.33
Charge Transfer	**CT**	-374.59	-955.54	-394.74	-1041.52
Core	**XC+DEF-SE**	848.77	1482.33	873.84	1585.19
Total Interaction	**E**	-40.87	-97.94	-36.4	-88.66

The components of energy are defines in terms of electrostatic interaction (ES); polarization (POL); electrical self-energy (SE); exchange interaction (XC); deformation energy (DEF), Electrical (ES+POL+SE), Core (XC+DEF-SE) and Total Interaction energy which is the final net H-bond energy (E = Electrical + Core + CT)

Table 3.14: The summary of the natural energy decomposition analysis (NEDA) showing the components of interaction energy in kcal/mol for the PBE0/ECP(Ru, Cl, P)|6-31G* treated systems

		1	2	3	4
Electrostatic	**ES**	-160.57		-157.95	-180.9
Polarizability	**POL**	-129.94		-134.23	-209.87
Exchange interaction	**XC**	251.3		266.41	-391.41
lectrical self-energy	**DEF**	818.35		845.39	1550.57
lectrical self-energy	**SE**	61.96		63.7	87.98
Electrical	ES+POL+SE	-228.55		-228.47	-302.78
Charge Transfer	**CT**	-844.65		-880.49	-883.95
Core	XC+DEF-SE	1007.7		1048.09	1071.19
Total Interaction	**E**	-65.5		-60.88	-115.55

The components of energy are defines in terms of electrostatic interaction (ES); polarization (POL); electrical self-energy (SE); exchange interaction (XC); deformation energy (DEF), Electrical (ES+POL+SE), Core (XC+DEF-SE) and Total Interaction energy which is the final net H-Bond energy (E = Electrical + Core + CT)

Table 3.15: The induced energy (Hatree) and dipole values (Debye) due to synergistic effect of fragments on each other for B3LYP/DGDZVP(Ru)|6-31+G(d,p) treated systems

	Fragments	Induced Energy	Induced Dipole
	Complex 1		
1	C6H12N3PCl	-0.602871	1.38
2	C7H8	-1.519335	0.78
	Complex 2		
1	C6H12N3PCl	-0.740521	10.70
2	C7H8	-1.404810	1.23
3	H2O	-0.461211	0.56
	Complex 3		
1	C6H12N3PCl	-0.628114	2.34
2	C7H5F3	-1.540632	0.84
	Complex 4		
1	C6H12N3PCl	-1.484898	33.56
2	C7H5F3	-1.422444	1.07
3	H2O	-0.470609	0.57

Table 3.16: Electron density critical point analysis of selected bonds in the four complexes using combined basis sets DGDZVP(Ru)|6-31+G(d,p) (all the data in atomic units)

Bonds	ρ(r) (e/bohr^3)	$\nabla^2\rho(r)$	ε	K	BPL - GBL_I	V	G	L	GBL_I (bohr)	|V/G|
Complex 1										
Ru1 - C6	0.081	0.248	0.545	0.016	0.012	-0.095	0.079	-0.062	4.154	1.209
Ru1 - C9	0.077	0.267	1.555	0.014	0.023	-0.094	0.081	-0.067	4.187	1.171
Ru1 - C14	0.076	0.251	1.805	0.013	0.030	-0.090	0.076	-0.063	4.225	1.176
Ru1 - C19	0.078	0.259	0.952	0.014	0.025	-0.093	0.079	-0.065	4.176	1.180
Ru1 - P11	0.080	0.143	0.205	0.021	0.008	-0.077	0.056	-0.036	4.572	1.365
Ru1 - Cl2	0.058	0.183	0.173	0.006	0.006	-0.057	0.051	-0.046	4.717	1.111
Ru1 - Cl20	0.058	0.184	0.209	0.006	0.005	-0.058	0.052	-0.046	4.711	1.111
Complex 2										
Ru1 - C2	0.077	0.254	1.321	0.014	0.023	-0.092	0.078	-0.064	4.197	1.182
Ru1 - C3	0.077	0.248	0.707	0.014	0.017	-0.090	0.076	-0.062	4.192	1.187
Ru1 - C7	0.076	0.252	1.974	0.013	0.021	-0.089	0.076	-0.063	4.213	1.172
Ru1 - C13	0.083	0.239	0.353	0.019	0.013	-0.097	0.078	-0.060	4.123	1.237
Ru1 - P12	0.080	0.127	0.183	0.021	0.003	-0.073	0.052	-0.032	4.602	1.396
Ru1 - O11	0.055	0.313	0.505	-0.004	0.004	-0.071	0.075	-0.078	4.254	0.950
Ru1 - Cl20	0.060	0.192	0.338	0.006	0.003	-0.060	0.054	-0.048	4.688	1.115
Complex 3										
Ru1 - C6	0.078	0.269	2.184	0.014	0.035	-0.095	0.081	-0.067	4.186	1.171
Ru1 - C8	0.078	0.252	0.773	0.015	0.015	-0.092	0.078	-0.063	4.181	1.187
Ru1 - C12	0.080	0.276	0.927	0.016	0.019	-0.100	0.085	-0.069	4.152	1.185
Ru1 - C21	0.080	0.252	0.592	0.016	0.014	-0.095	0.079	-0.063	4.158	1.202
Ru1 - P14	0.081	0.132	0.181	0.021	0.006	-0.075	0.054	-0.033	4.580	1.392
Ru1 - Cl11	0.060	0.184	0.184	0.006	0.005	-0.059	0.052	-0.046	4.692	1.121
Ru1 - Cl23	0.059	0.184	0.193	0.006	0.002	-0.058	0.052	-0.046	4.700	1.117
Complex 4										
Ru1 - C6	0.078	0.260	3.049	0.014	0.058	-0.093	0.079	-0.065	4.201	1.175
Ru1 - C8	0.072	0.255	1.593	0.012	0.023	-0.087	0.075	-0.064	4.234	1.153
Ru1 - C12	0.082	0.282	0.947	0.016	0.017	-0.102	0.086	-0.071	4.123	1.185
Ru1 - C17	0.069	0.237	6.641	0.010	0.122	-0.079	0.069	-0.059	4.303	1.140
Ru1 - C21	0.085	0.235	0.420	0.019	0.013	-0.098	0.078	-0.059	4.118	1.248
Ru1 - P14	0.080	0.113	0.176	0.021	0.003	-0.071	0.050	-0.028	4.615	1.428
Ru1 - O11	0.057	0.324	0.475	-0.004	0.003	-0.073	0.077	-0.081	4.231	0.950
Ru1 - Cl23	0.061	0.191	0.279	0.007	0.003	-0.061	0.055	-0.048	4.677	1.123

ρ(r) is electron density, $\nabla^2\rho(r)$ is the Laplancian of Rho, BPL – GBL_I is Bond strain, V is virial field (potential energy density), G is Lagrangian form of kinetic energy density, K is hamiltonian form of kinetic energy density, L (i.e. K – G) is lagrangian density which is $(-1/4)\nabla^2\rho(r)$ while |V/G| is the ratio of PE to KE and the higher its magnitude the stronger the Bond.

Table 3.17: Correlation among the computed QTAIM Bond properties for the systems using combined basis sets DGDZVP(Ru)|6-31+G(d,p)

	Complex 1			Complex 2			Complex 3			Complex 4		
	$\nabla^2\rho(r)$	ε	|V/G|	$\nabla^2\rho(r)$	ε	|V/G|	$\nabla^2\rho(r)$	ε	|V/G|	$\nabla^2\rho(r)$	ε	|V/G|
ρ(r)	-0.94	-0.70	0.74	-0.91	-0.62	0.74	-0.90	-0.46	0.69	-0.88	-0.39	0.70
$\nabla^2\rho(r)$	1.00	0.71	-0.87	1.00	0.64	-0.85	1.00	0.58	-0.87	1.00	0.44	-0.85
ε	0.71	1.00	-0.58	0.64	1.00	-0.55	0.58	1.00	-0.43	0.44	1.00	-0.33
K	-0.96	-0.70	0.73	-0.97	-0.61	0.72	-0.84	-0.49	0.59	-0.88	-0.40	0.63
BPL - GBL_I	0.41	0.65	-0.39	0.27	0.34	-0.29	0.46	0.42	-0.40	0.54	0.83	-0.46
V	0.86	0.65	-0.56	0.89	0.55	-0.58	0.60	0.35	-0.31	0.66	0.32	-0.37
G	0.01	-0.07	-0.38	0.01	0.05	-0.40	0.09	0.05	-0.34	0.10	0.01	-0.34
L	-1.00	-0.71	0.87	-1.00	-0.64	0.85	-1.00	-0.58	0.87	-1.00	-0.44	0.85
GBL_I	0.94	0.68	-0.88	0.93	0.61	-0.90	0.93	0.44	-0.84	0.91	0.37	-0.85
V/G	-0.87	-0.58	1.00	-0.85	-0.55	1.00	-0.87	-0.43	1.00	-0.85	-0.33	1.00

Table 3.18: Electron density critical point analysis of selected bonds in the four complexes using 3-21G (all the data in atomic units)

						Complex 1					
	Bond	ρ(r)	$\nabla^2\rho(r)$	ε	K	BPL - GBL_I	V	G	L	GBL_I (Hatree)	V/G
arene	Ru1-C6	7.83E-02	2.72E-01	2.17E-01	1.22E-02	1.16E-02	-9.23E-02	8.01E-02	-6.79E-02	4.15	-1.15
	Ru1-C9	7.48E-02	2.90E-01	5.81E-01	9.87E-03	1.94E-02	-9.22E-02	8.23E-02	-7.24E-02	4.19	-1.12
	Ru1-C10	7.00E-02	2.82E-01	2.72E+0 0	6.97E-03	3.78E-02	-8.45E-02	7.75E-02	-7.05E-02	4.24	-1.09
	Ru1-C14	7.38E-02	2.73E-01	5.92E-01	9.60E-03	1.65E-02	-8.75E-02	7.79E-02	-6.83E-02	4.22	-1.12
	Ru1-C16	7.21E-02	2.74E-01	9.95E-01	8.55E-03	2.03E-02	-8.57E-02	7.72E-02	-6.86E-02	4.22	-1.11
	Ru1-C19	7.57E-02	2.81E-01	3.54E-01	1.06E-02	1.64E-02	-9.15E-02	8.09E-02	-7.03E-02	4.17	-1.13
mono	Ru1-Cl2	5.65E-02	1.83E-01	1.55E-01	4.95E-03	2.54E-03	-5.56E-02	5.06E-02	-4.57E-02	4.72	-1.10
	Ru1-Cl20	5.67E-02	1.84E-01	1.84E-01	5.02E-03	2.03E-03	-5.59E-02	5.09E-02	-4.59E-02	4.71	-1.10
pta	Ru1-P11	7.59E-02	1.46E-01	1.34E-01	1.84E-02	1.02E-02	-7.33E-02	5.50E-02	-3.66E-02	4.57	-1.33
HB	Cl2-H25*	9.96E-03	3.37E-02	9.72E-01	-1.35E-03	8.95E-02	-5.72E-03	7.07E-03	-8.43E-03	5.30	-0.81
	C18-H37*	5.18E-03	1.81E-02	7.60E-01	-8.48E-04	6.10E-02	-2.82E-03	3.67E-03	-4.52E-03	5.65	-0.77
						Complex 2					
arene	Ru1-C2	7.49E-02	2.75E-01	5.25E-01	1.04E-02	1.61E-02	-8.95E-02	7.91E-02	-6.87E-02	4.20	-1.13
	Ru1-C3	7.46E-02	2.67E-01	2.88E-01	1.05E-02	1.75E-02	-8.77E-02	7.72E-02	-6.68E-02	4.19	-1.14
	Ru1-C7	7.43E-02	2.69E-01	6.75E-01	9.89E-03	1.93E-02	-8.70E-	7.71E-02	-6.72E-	4.21	-1.13

						02		02		
				2.17E+0		-7.90E-		-6.59E-		
	Ru1-C8	6.73E-02	2.64E-01	0	6.52E-03	3.51E-02	02	7.24E-02	02	4.29	-1.09
						-9.43E-		-6.67E-		
	Ru1-C13	8.10E-02	2.67E-01	1.17E-01	1.38E-02	1.44E-02	02	8.05E-02	02	4.12	-1.17
						-8.83E-		-7.36E-		
mono	Ru1-O11	6.04E-02	2.94E-01	3.42E-01	7.36E-03	3.85E-03	02	8.09E-02	02	4.25	-1.09
	Ru1-Cl20	5.88E-02	1.89E-01	2.37E-01	5.98E-03	3.66E-03	-5.91E-02	5.32E-02	-4.72E-02	4.69	-1.11
						-6.88E-		-3.26E-		
pta	Ru1-P12	7.46E-02	1.30E-01	1.22E-01	1.81E-02	5.04E-03	02	5.07E-02	02	4.60	-1.36
	Cl20-				-1.78E-		-1.89E-		-2.24E-		
HB	H41*	2.35E-02	8.97E-02	4.45E-01	03	1.30E-02	02	2.06E-02	02	4.35	-0.91
					-7.83E-		-2.21E-		-3.78E-		
	C6-H33*	4.17E-03	1.51E-02	6.57E-01	04	3.90E-01	03	2.99E-03	03	5.84	-0.74
	H23-				-9.30E-		-1.51E-		-3.37E-		
	H26*	3.63E-03	1.35E-02	4.72E-01	04	5.36E-02	03	2.44E-03	03	4.79	-0.62
						Complex 3					
						-9.24E-		-7.28E-		
arene	Ru1-C6	7.51E-02	2.91E-01	6.36E-01	9.79E-03	1.82E-02	02	8.26E-02	02	4.19	-1.12
						-8.95E-		-6.82E-		
	Ru1-C8	7.54E-02	2.73E-01	3.22E-01	1.06E-02	1.38E-02	02	7.88E-02	02	4.18	-1.13
						-9.89E-		-7.58E-		
	Ru1-C12	7.82E-02	3.03E-01	2.97E-01	1.16E-02	1.47E-02	02	8.74E-02	02	4.15	-1.13
				1.80E+0		-8.18E-		-6.76E-		
	Ru1-C17	6.93E-02	2.70E-01	0	7.11E-03	3.16E-02	02	7.47E-02	02	4.26	-1.10
						-9.24E-		-6.89E-		
	Ru1-C21	7.76E-02	2.76E-01	2.42E-01	1.17E-02	1.35E-02	02	8.06E-02	02	4.16	-1.15
	Ru1-						-5.65E-		-4.56E-		
mono	Cl23	5.78E-02	1.82E-01	1.56E-01	5.45E-03	7.20E-04	02	5.10E-02	02	4.70	-1.11
	Ru1-						-5.70E-		-4.57E-		
	Cl11	5.85E-02	1.83E-01	1.56E-01	5.68E-03	2.50E-03	02	5.13E-02	02	4.69	-1.11
							-7.15E-		-3.39E-		
pta	Ru1-P14	7.62E-02	1.36E-01	1.19E-01	1.88E-02	8.93E-03	02	5.27E-02	02	4.58	-1.36
	Cl11-			1.23E+0	-1.25E-		-5.76E-		-8.26E-		
HB	H32*	9.90E-03	3.30E-02	0	03	1.60E-01	03	7.01E-03	03	5.34	-0.82
	F18-				-2.87E-		-3.65E-		-9.39E-		
	H34*	5.78E-03	3.76E-02	5.42E-02	03	1.05E-02	03	6.52E-03	03	4.83	-0.56
					-2.37E-		-2.59E-		-7.32E-		
	F7-H34*	4.47E-03	2.93E-02	2.03E-01	03	2.57E-02	03	4.95E-03	03	5.04	-0.52
					-2.22E-		-2.33E-		-6.77E-		
	F7-H25*	3.89E-03	2.71E-02	2.93E-01	03	3.13E-02	03	4.55E-03	03	5.05	-0.51
						Complex 4					
						-8.93E-		-6.93E-		
arene	Ru1-C6	7.50E-02	2.77E-01	7.88E-01	9.97E-03	1.68E-02	02	7.93E-02	02	4.20	-1.13
						-8.41E-		-6.75E-		
	Ru1-C8	7.03E-02	2.70E-01	6.29E-01	8.31E-03	2.23E-02	02	7.58E-02	02	4.23	-1.11
						-1.00E-		-7.58E-		
	Ru1-C12	7.97E-02	3.03E-01	2.87E-01	1.23E-02	1.79E-02	01	8.81E-02	02	4.12	-1.14
						-7.65E-		-6.22E-		
	Ru1-C17	6.72E-02	2.49E-01	9.69E-01	7.13E-03	2.17E-02	02	6.93E-02	02	4.30	-1.10
						-9.39E-		-6.53E-		
	Ru1-C21	8.19E-02	2.61E-01	1.65E-01	1.43E-02	1.31E-02	02	7.96E-02	02	4.12	-1.18
						-9.07E-		-7.54E-		
mono	Ru1-O11	6.19E-02	3.02E-01	3.19E-01	7.61E-03	3.00E-03	02	8.30E-02	02	4.23	-1.09
	Ru1-						-5.96E-		-4.68E-		
	Cl23	5.98E-02	1.87E-01	1.91E-01	6.38E-03	4.32E-03	02	5.32E-02	02	4.68	-1.12

pta	Ru1-P14	7.44E-02	1.18E-01	1.18E-01	1.83E-02	4.66E-03	-6.61E-02	4.78E-02	-2.95E-02	4.62	-1.38
HB	Cl23-H42*	2.35E-02	9.06E-02	4.70E-01	-1.81E-03	1.41E-02	-1.90E-02	2.08E-02	-2.26E-02	4.34	-0.91
	F18-H34*	4.77E-03	3.16E-02	8.86E-02	-2.52E-03	1.79E-02	-2.85E-03	5.37E-03	-7.89E-03	4.96	-0.53
	F7-H34*	4.68E-03	3.14E-02	1.15E-01	-2.50E-03	2.63E-02	-2.83E-03	5.34E-03	-7.84E-03	4.98	-0.53
	F7-H25*	4.01E-03	2.82E-02	3.89E-01	-2.29E-03	4.10E-02	-2.47E-03	4.76E-03	-7.04E-03	5.03	-0.52

$\rho(r)$ is electron density, $\nabla^2\rho(r)$ is the Laplancian of Rho, BPL – GBL_I is Bond strain, V is virial field (potential energy density), G is Lagrangian form of kinetic energy density, K is hamiltonian form of kinetic energy density, L (i.e. K – G) is lagrangian density which is $(-1/4)\nabla^2\rho(r)$ while V/G is the ratio of PE to KE and the higher its magnitude the stronger the Bond.

Table 3.19: Selected atomic properties derived through the quantum theory of atoms in molecules analysis for the four complexes using combined basis sets DGDZVP(Ru)|6-31+G(d,p) (all the data in atomic units)

	q(A)	L(A)	K(A)	K_Scaled (A)	$\|\mu_{Intra}(A)\|$	$\|\mu_{Bond}(A)\|$	|μ(A)|	N(A)	LI(A)	%Loc(A)	DI(A,A')/2	%Deloc (A,A')	Vol(A), 0.001
Complex 1													
Ru1	0.78	-3.86E-04	4435.17	-4445.88	0.43	1.39	1.55	43.22	40.56	93.85	2.66	6.15	110.75
C6	-0.06	-7.00E-05	37.85	-37.94	0.11	0.14	0.07	6.06	3.96	65.39	2.10	34.61	71.16
C9	-0.08	-9.20E-05	37.85	-37.94	0.10	0.04	0.08	6.08	3.98	65.43	2.10	34.57	73.61
C10	-0.05	-6.70E-05	37.84	-37.93	0.14	0.12	0.08	6.05	3.97	65.54	2.08	34.46	74.57
C14	-0.05	-5.00E-06	37.85	-37.94	0.06	0.04	0.02	6.05	3.90	64.47	2.15	35.53	60.56
C16	-0.05	-1.36E-04	37.84	-37.93	0.13	0.13	0.08	6.05	3.96	65.46	2.09	34.54	72.87
C19	-0.07	2.28E-04	37.86	-37.95	0.10	0.10	0.07	6.07	3.97	65.43	2.10	34.57	71.83
P11	0.94	-5.00E-04	340.20	-341.02	1.11	0.46	0.72	14.06	12.03	85.53	2.04	14.47	99.10
Cl2	-0.59	9.30E-05	459.38	-460.49	0.12	1.20	1.29	17.59	17.00	96.62	0.60	3.38	243.78
Cl20	-0.59	9.90E-05	459.38	-460.49	0.12	1.23	1.31	17.59	17.00	96.62	0.59	3.38	244.32
Complex 2													
Ru1	0.78	-1.21E-04	4435.16	-4446.25	0.37	0.64	0.78	43.22	40.65	94.07	2.56	5.93	113.29
C2	-0.06	-2.82E-04	37.85	-37.94	0.10	0.06	0.09	6.06	3.97	65.44	2.09	34.56	71.86
C3	-0.07	-2.94E-04	37.84	-37.94	0.12	0.08	0.08	6.07	3.97	65.52	2.09	34.48	73.55
C7	-0.05	-4.15E-04	37.85	-37.94	0.09	0.14	0.21	6.05	3.90	64.55	2.14	35.45	59.94
C8	-0.05	-4.40E-05	37.84	-37.93	0.11	0.07	0.05	6.05	3.97	65.58	2.08	34.42	74.85
C13	-0.06	-1.12E-04	37.86	-37.96	0.10	0.11	0.09	6.06	3.97	65.45	2.09	34.55	69.95
C14	-0.03	1.90E-05	37.83	-37.93	0.14	0.13	0.05	6.03	3.95	65.56	2.08	34.44	73.59
P12	0.75	-2.42E-04	340.29	-341.15	1.01	0.57	0.44	14.25	12.18	85.46	2.07	14.54	106.96
O11	-1.16	6.70E-05	75.20	-75.39	0.32	0.87	0.70	9.16	8.22	89.77	0.94	10.23	119.81
Cl20	-0.56	4.80E-05	459.40	-460.55	0.07	1.31	1.25	17.56	16.92	96.39	0.63	3.61	233.67
Complex 3													
Ru1	0.79	6.95E-04	4435.15	-4446.40	0.43	1.92	2.14	43.21	40.53	93.79	2.68	6.21	109.65
C6	-0.06	-1.17E-04	37.84	-37.93	0.14	0.15	0.04	6.06	3.96	65.40	2.10	34.60	72.23
C8	-0.05	-2.00E-04	37.84	-37.94	0.12	0.20	0.09	6.05	3.96	65.41	2.09	34.59	71.76
C12	-0.04	-1.08E-04	37.89	-37.99	0.14	0.10	0.23	6.04	3.89	64.47	2.14	35.53	57.49
C17	-0.04	-1.49E-04	37.84	-37.93	0.13	0.15	0.08	6.04	3.96	65.51	2.08	34.49	73.39

C21	-0.05	-4.57E-04	37.85	-37.95	0.14	0.23	0.10	6.05	3.95	65.38	2.09	34.62	69.96
C22	-0.04	-9.00E-06	37.83	-37.93	0.15	0.15	0.08	6.04	3.95	65.51	2.08	34.49	74.06
P14	0.92	2.71E-04	340.21	-341.07	1.07	0.64	0.45	14.08	12.03	85.44	2.05	14.56	98.55
Cl11	-0.58	9.90E-05	459.39	-460.55	0.12	1.17	1.23	17.58	16.97	96.57	0.60	3.43	241.92
Cl23	-0.58	9.90E-05	459.38	-460.54	0.10	1.41	1.46	17.58	16.97	96.54	0.61	3.46	241.45
						Complex 4							
Ru1	0.79	5.90E-04	4435.13	-4446.80	0.37	0.98	1.24	43.21	40.63	94.03	2.58	5.97	112.26
C6	-0.04	-1.39E-04	37.84	-37.94	0.14	0.14	0.03	6.04	3.95	65.42	2.09	34.58	70.42
C8	-0.06	-3.21E-04	37.84	-37.94	0.14	0.09	0.07	6.06	3.97	65.56	2.09	34.44	74.48
C12	-0.04	1.36E-04	37.90	-38.00	0.11	0.10	0.05	6.04	3.90	64.52	2.14	35.48	56.69
C17	-0.05	3.00E-06	37.84	-37.94	0.10	0.09	0.05	6.05	3.97	65.57	2.08	34.43	73.76
C21	-0.03	-1.56E-04	37.85	-37.95	0.13	0.19	0.06	6.03	3.95	65.44	2.09	34.56	68.14
C22	-0.02	-4.80E-05	37.83	-37.92	0.15	0.15	0.06	6.02	3.95	65.59	2.07	34.41	74.92
P14	0.72	7.66E-04	340.30	-341.20	0.96	1.13	0.25	14.28	12.20	85.42	2.08	14.58	106.84
O11	-1.16	7.30E-05	75.20	-75.40	0.32	0.86	0.67	9.16	8.22	89.74	0.94	10.26	119.23
Cl23	-0.54	8.90E-05	459.39	-460.60	0.08	1.27	1.19	17.54	16.89	96.32	0.65	3.68	231.84

q(A) is net charge of atom A, L(A) is Lagrangian of Atom A, N(A) is average number of electrons in atom A, K(A) is electronic kinetic energy of atom A (Hamiltonian Form), %Loc(A) is percentage of average number of electrons localized in atom A, K_Scaled(A) is approximation to virial-based total energy of atom A, μ_{Intra}(A) is magnitude of Intraatomic dipole moment of atom A, %Deloc(A,A') is the percentage of electron delocalization index of atom A and Vol(A) is the volume bounded by an isosurface of the electron density distribution (0.001) and by interatomic surfaces of atom A.

2

3

Table 3.20: Correlation among the computed QTAIM Intra- and inter-atomic properties for the systems using combined basis sets DGDZVP(Ru)|6-31+G(d,p)

	Complex 1		**Complex 2**		**Complex 3**		**Complex 4**	
	|μ(A)|	**Vol(A),0.001**	**|μ(A)|**	**Vol(A),0.001**	**|μ(A)|**	**Vol(A),0.001**	**|μ(A)|**	**Vol(A),0.001**
q(A)	-0.07	-0.04	0.22	0.29	-0.05	-0.04	0.18	0.23
L(A)	-0.79	-0.78	-0.74	-0.76	0.91	0.88	0.89	0.88
K(A)	0.87	0.83	0.83	0.81	0.89	0.84	0.86	0.82
K_Scaled(A)	-0.87	-0.83	-0.83	-0.81	-0.89	-0.84	-0.86	-0.82
$\|\mu_{Intra}(A)\|$	0.97	0.98	0.97	0.99	0.97	0.98	0.97	0.99
$\|\mu_{Bond}(A)\|$	0.99	0.99	0.99	0.99	0.99	0.99	0.99	0.99
|μ(A)|	1.00	0.99	1.00	0.99	1.00	0.99	1.00	0.99
N(A)	0.99	0.98	0.98	0.98	0.99	0.99	0.99	0.99
LI(A)	0.99	0.97	0.98	0.97	0.99	0.98	0.99	0.98
%Loc(A)	0.98	1.00	0.98	1.00	0.98	1.00	0.99	1.00
DI(A,A')/2	0.98	0.99	0.98	0.99	0.98	0.99	0.98	0.99
%Deloc(A,A')	0.96	0.99	0.97	0.99	0.96	0.99	0.97	0.99
Vol(A),0.001	0.99	1.00	0.99	1.00	0.99	1.00	0.99	1.00

Table 3.21: Selected atomic properties derived through the quantum theory of atoms in molecules analysis for the four complexes using 3-21G basis set (all the data in atomic units)

	Atom	q(A)	L(A)	K(A)	K_Scaled(A)	$\|\mu_{Intra}(A)\|$	$\|\mu_{Bond}(A)\|$	|μ(A)|	N(A)	LI(A)	%Loc(A)	DI(A,A')/2	%Deloc(A,A')	Vol(A), 0.001
Complex 1														
	Ru1	0.65	7.41E-04	4402.64	-4424.04	0.39	1.56	1.71	43.35	40.77	94.03	2.59	5.97	107.30
arene	C6	-0.11	-1.39E-04	37.61	-37.80	0.25	0.21	0.07	6.11	4.02	65.90	2.08	34.10	73.62
	C9	-0.13	-2.10E-05	37.62	-37.80	0.23	0.12	0.12	6.13	4.04	65.93	2.09	34.07	75.60
	C10	-0.09	-6.60E-05	37.60	-37.78	0.27	0.23	0.07	6.09	4.02	66.01	2.07	33.99	76.65
	C14	-0.09	-1.80E-04	37.61	-37.79	0.12	0.16	0.04	6.09	3.95	64.85	2.14	35.15	61.84
	C16	-0.10	-7.10E-05	37.61	-37.79	0.26	0.23	0.07	6.10	4.02	65.97	2.07	34.03	75.11
	C19	-0.11	-1.02E-04	37.62	-37.80	0.24	0.18	0.08	6.11	4.03	65.88	2.09	34.12	73.86
	C18*	-0.06	-1.91E-04	37.52	-37.70	0.21	0.22	0.09	6.06	4.05	66.79	2.01	33.21	74.52
mono	Cl2#	-0.57	8.10E-05	456.64	-458.86	0.14	1.13	1.26	17.57	16.99	96.69	0.58	3.31	235.93
	Cl20	-0.57	8.00E-06	456.64	-458.85	0.14	1.38	1.51	17.57	16.99	96.70	0.58	3.30	236.66
pta	P11	0.86	-2.75E-04	338.03	-339.67	1.02	0.18	0.90	14.14	12.13	85.74	2.02	14.26	100.02
	N5	-0.85	6.70E-05	54.40	-54.66	0.38	0.47	0.85	7.85	6.07	77.36	1.78	22.64	74.29
	N7	-0.86	-9.00E-05	54.41	-54.68	0.37	0.49	0.84	7.86	6.08	77.33	1.78	22.67	74.16
	N15	-0.85	1.55E-04	54.40	-54.67	0.38	0.47	0.84	7.85	6.07	77.35	1.78	22.65	74.23
	H25*	0.12	7.50E-05	0.56	-0.57	0.15	0.44	0.50	0.88	0.34	38.92	0.54	61.08	39.83
	H37*	0.06	6.20E-05	0.59	-0.59	0.16	0.10	0.09	0.94	0.39	41.62	0.55	58.38	44.45
Complex 2														
	Ru1	0.68	5.60E-05	4402.57	-4424.80	0.31	0.72	0.78	43.32	40.83	94.25	2.49	5.75	108.66
arene	C2	-0.11	-1.36E-04	37.62	-37.81	0.24	0.13	0.13	6.11	4.03	65.93	2.08	34.07	74.20
	C3	-0.12	-1.65E-04	37.61	-37.80	0.24	0.15	0.12	6.12	4.04	66.06	2.08	33.94	76.49
	C7	-0.09	4.00E-05	37.62	-37.81	0.16	0.07	0.20	6.09	3.95	64.93	2.13	35.07	61.27

	C8	-0.11	-3.00E-06	37.60	-37.79	0.24	0.14	0.12	6.11	4.04	66.11	2.07	33.89	78.02
	C13	-0.11	-1.04E-04	37.63	-37.82	0.24	0.18	0.11	6.11	4.03	65.94	2.08	34.06	72.67
	C14	-0.08	3.80E-05	37.59	-37.78	0.27	0.22	0.09	6.08	4.01	66.02	2.06	33.98	76.20
	C6*	-0.06	-8.30E-05	37.52	-37.71	0.25	0.20	0.24	6.06	4.06	66.96	2.00	33.04	75.28
	H26*	0.06	7.20E-05	0.58	-0.58	0.16	0.09	0.23	0.94	0.39	41.93	0.55	58.07	45.74
mono	O11	-0.93	-1.50E-05	74.48	-74.86	0.13	0.67	0.75	8.93	7.88	88.24	1.05	11.76	99.90
	Cl20#	-0.53	5.40E-05	456.65	-458.95	0.11	1.21	1.31	17.53	16.91	96.49	0.62	3.51	230.54
	H41*	0.51	7.00E-05	0.40	-0.40	0.15	0.35	0.41	0.49	0.10	20.38	0.39	79.62	20.69
pta	P12	0.73	-2.28E-04	338.10	-339.80	0.94	0.43	0.51	14.27	12.24	85.74	2.03	14.26	107.07
	N15	-0.85	1.70E-05	54.41	-54.68	0.36	0.46	0.81	7.85	6.06	77.21	1.79	22.79	73.77
	N16	-0.85	7.90E-05	54.41	-54.69	0.35	0.45	0.81	7.85	6.06	77.21	1.79	22.79	73.70
	N5	-0.85	1.49E-04	54.41	-54.68	0.36	0.45	0.81	7.85	6.06	77.21	1.79	22.79	73.69
	H23*	0.07	7.40E-05	0.58	-0.58	0.16	0.12	0.09	0.93	0.39	41.41	0.55	58.59	45.34
	H33*	0.07	7.20E-05	0.58	-0.58	0.16	0.10	0.08	0.93	0.38	41.11	0.55	58.89	44.11
							Complex 3							
	Ru1	0.65	5.60E-05	4402.62	-4424.54	0.40	1.85	2.08	43.35	40.74	93.97	2.61	6.03	107.21
arene	C6	-0.10	-5.10E-05	37.60	-37.79	0.28	0.22	0.07	6.10	4.02	65.88	2.08	34.12	74.51
	C8	-0.09	-2.25E-04	37.60	-37.79	0.26	0.25	0.02	6.09	4.01	65.89	2.08	34.11	74.30
	C12	-0.11	-2.55E-04	37.69	-37.88	0.10	0.12	0.21	6.11	3.97	65.03	2.14	34.97	60.38
	C17	-0.09	-9.60E-05	37.60	-37.79	0.26	0.29	0.05	6.09	4.02	65.98	2.07	34.02	75.66
	C21	-0.08	-1.20E-05	37.60	-37.79	0.29	0.30	0.03	6.08	4.01	65.84	2.08	34.16	72.40
	C22	-0.08	-1.35E-04	37.59	-37.78	0.28	0.23	0.11	6.08	4.01	65.98	2.07	34.02	76.36
	F7*	-0.52	1.54E-04	98.81	-99.30	0.07	0.53	0.47	9.52	8.88	93.30	0.64	6.70	83.90
	F18*	-0.50	1.61E-	98.81	-99.30	0.07	0.68	0.61	9.50	8.86	93.28	0.64	6.72	83.31

			04										
	F9	-0.49	9.10E-05	98.84	-99.34	0.08	0.77	0.69	9.49	8.87	93.45	0.62	6.55	81.17
mono	Cl11#	-0.55	7.60E-05	456.64	-458.92	0.14	1.10	1.23	17.55	16.96	96.62	0.59	3.38	234.34
	Cl23	-0.55	7.80E-05	456.63	-458.91	0.14	1.33	1.46	17.55	16.96	96.61	0.59	3.39	234.96
pta	P14	0.84	-6.90E-05	338.04	-339.72	0.98	0.50	0.48	14.16	12.13	85.66	2.03	14.34	100.28
	N15	-0.85	1.20E-05	54.41	-54.68	0.37	0.47	0.84	7.85	6.07	77.32	1.78	22.68	74.20
	N13	-0.86	3.70E-05	54.41	-54.68	0.37	0.47	0.83	7.86	6.08	77.33	1.78	22.67	74.23
	N2	-0.85	-3.00E-06	54.40	-54.67	0.38	0.47	0.84	7.85	6.07	77.34	1.78	22.66	74.19
	H25*	0.07	5.60E-05	0.58	-0.58	0.16	0.18	0.29	0.93	0.38	41.38	0.54	58.62	44.22
	H32*	0.11	6.20E-05	0.57	-0.57	0.15	0.34	0.39	0.89	0.35	39.21	0.54	60.79	40.25
	H34*	0.08	5.20E-05	0.58	-0.58	0.15	0.26	0.37	0.92	0.37	40.73	0.54	59.27	41.12
							Complex 4							
	Ru1	0.69	-4.50E-04	4402.55	-4425.31	0.32	0.97	1.16	43.31	40.80	94.21	2.51	5.79	108.44
arene	C6	-0.08	-1.21E-04	37.60	-37.79	0.27	0.22	0.06	6.08	4.00	65.89	2.07	34.11	73.07
	C8	-0.10	-8.50E-05	37.60	-37.79	0.27	0.18	0.09	6.10	4.03	66.06	2.07	33.94	77.22
	C12	-0.11	-5.10E-05	37.70	-37.90	0.06	0.07	0.03	6.11	3.97	65.04	2.13	34.96	59.54
	C17	-0.11	-7.00E-06	37.61	-37.80	0.22	0.17	0.08	6.11	4.04	66.11	2.07	33.89	77.18
	C21	-0.07	-2.77E-04	37.61	-37.81	0.28	0.28	0.04	6.07	4.00	65.92	2.07	34.08	71.17
	C22	-0.06	3.00E-05	37.58	-37.77	0.30	0.24	0.10	6.06	4.00	66.02	2.06	33.98	77.52
mono	O11	-0.93	6.50E-05	74.48	-74.87	0.13	0.66	0.74	8.93	7.87	88.20	1.05	11.80	99.59
	Cl23#	-0.51	7.20E-05	456.65	-459.01	0.11	1.17	1.26	17.51	16.88	96.41	0.63	3.59	229.50
	H42*	0.51	1.20E-05	0.40	-0.40	0.15	0.35	0.40	0.49	0.10	20.29	0.39	79.71	20.62
pta	P14	0.70	-2.19E-04	338.10	-339.85	0.91	0.94	0.19	14.30	12.25	85.70	2.04	14.30	107.80
	N15	-0.85	-7.40E-05	54.42	-54.70	0.35	0.45	0.80	7.85	6.06	77.16	1.79	22.84	73.62
	N13	-0.85	2.90E-05	54.41	-54.69	0.35	0.46	0.81	7.85	6.06	77.19	1.79	22.81	73.73

N2	-0.85	-7.50E-05	54.41	-54.69	0.35	0.45	0.80	7.85	6.06	77.17	1.79	22.83	73.68
F18*	-0.49	1.35E-04	98.80	-99.31	0.07	0.69	0.62	9.49	8.85	93.23	0.64	6.77	83.61
F7*	-0.51	8.30E-05	98.80	-99.31	0.07	0.58	0.52	9.51	8.87	93.25	0.64	6.75	83.67
F9	-0.47	8.40E-05	98.83	-99.34	0.08	0.75	0.67	9.47	8.84	93.33	0.63	6.67	81.07
H25*	0.09	7.00E-05	0.57	-0.58	0.15	0.16	0.26	0.91	0.37	40.70	0.54	59.30	42.95
H34*	0.10	6.30E-05	0.57	-0.58	0.15	0.27	0.37	0.90	0.36	40.12	0.54	59.88	40.55

q(A) is net charge of atom A, L(A) is Lagrangian of Atom A, N(A) is average number of electrons in atom A, K(A) is electronic kinetic energy of atom A (Hamiltonian Form), %Loc(A) is percentage of average number of electrons localized in atom A, K_Scaled(A) is approximation to virial-based total energy of atom A, μ_{Intra}(A) is magnitude of Intraatomic dipole moment of atom A, %Deloc(A,A') is the percentage of electron delocalization index of atom A and Vol(A) is the volume bounded by an isosurface of the electron density distribution (0.001) and by interatomic surfaces of atom A.

Table 3.22: The sum total of computed atomic properties derived through the quantum theory of atoms in molecules analysis for the four complexes using two methods (all the data in atomic units)

					DGDZVP(Ru)|6-31+G(d,p)						
	q(A)	L(A)	K(A)	K_Scaled(A)	$\|\mu_{Intra}(A)\|$	$\|\mu_{Bond}(A)\|$	$\|\mu(A)\|$	N(A)	Loc(A)	DI(A,A')/2	Vol(A), 0.001
1	0.00	-1.59E-03	6360.99	-6376.34	9.67	11.59	11.52	212.00	163.28	2314.08	48.72
2	1.00	-1.26E-03	5977.39	-5992.34	9.63	10.63	9.08	204.00	154.43	2332.33	49.57
3	0.00	2.10E-03	6657.18	-6674.07	10.68	16.01	13.77	236.00	187.60	2455.78	48.40
4	1.00	4.52E-03	6273.56	-6290.06	10.64	15.26	11.33	228.00	178.76	2475.23	49.23
					3-21G						
1	0.00	1.43E-03	6316.25	-6346.95	10.91	12.03	11.43	212.00	163.62	48.37	2626.01
2	1.00	-2.10E-04	5934.77	-5964.72	10.95	10.86	9.23	204.00	154.54	49.46	2523.74
3	0.00	-3.80E-04	6610.15	-6643.07	11.06	15.26	13.29	236.00	187.63	48.37	2669.61
4	1.00	-5.95E-04	6228.64	-6260.83	9.61	14.35	11.01	228.00	178.54	49.46	2572.07

Table 3.23: Bond lengths and Orders of the Ruthenium-ligand bonds in the complexes when optimized with PBE0/ECP(Ru,P,Cl)|6-31G* and PBE0/ECP(Ru)|6-31+G(d,p)

PBE0/ECP(Ru,P,Cl)|6-31G*												
Complex 1			**Complex 2**			**Complex 3**			**Complex 4**			
Bond	Length	Order	Bond	Length	Order	Bond	Length	Order	Bond	Length	Order	
Ru-C2	2.206	0.451	Ru-C6	2.224	0.427	Ru-C6	2.231	0.416	Ru-C6	2.211	0.445	
Ru-C3	2.249	0.375	Ru-C9	2.223	0.467	Ru-C17	2.205	0.441	Ru-C19	2.217	0.468	
Ru-C4	2.210	0.444	Ru-C7	2.196	0.482	Ru-C9	2.198	0.446	Ru-C10	2.228	0.440	
Ru-C6	2.250	0.374	Ru-C18	2.277	0.391	Ru-C14	2.205	0.452	Ru-C21	2.304	0.366	
Ru-C7	2.210	0.444	Ru-C14	2.183	0.492	Ru-C10	2.236	0.392	Ru-C11	2.176	0.483	
Ru-C9	2.206	0.451	Ru-C17	2.265	0.359	Ru-C16	2.295	0.332	Ru-C18	2.252	0.373	
Ru-P11	2.406	0.727	Ru-P11	2.433	0.706	Ru-P13	2.420	0.725	Ru-P12	2.437	0.712	
Ru-Cl5	2.490	0.967	Ru-O8	2.244	0.503	Ru-Cl19	2.500	0.966	Ru-O16	2.253	0.509	
Ru-Cl17	2.490	0.967	Ru-Cl19	2.480	1.024	Ru-Cl20	2.496	0.947	Ru-Cl23	2.486	1.028	
PBE0/ECP(Ru)|6-31+G(d,p)												
Ru-C2	2.215	0.415	Ru-C6	2.244	0.378	Ru-C6	2.251	0.387	Ru-C6	2.222	0.393	
Ru-C3	2.28	0.295	Ru-C9	2.201	0.435	Ru-C17	2.325	0.27	Ru-C19	2.182	0.449	
Ru-C4	2.221	0.405	Ru-C7	2.229	0.442	Ru-C9	2.215	0.404	Ru-C10	2.239	0.419	
Ru-C6	2.28	0.295	Ru-C18	2.282	0.309	Ru-C14	2.216	0.413	Ru-C21	2.28	0.308	
Ru-C7	2.221	0.405	Ru-C14	2.309	0.305	Ru-C10	2.208	0.408	Ru-C11	2.235	0.418	
Ru-C9	2.215	0.415	Ru-C17	2.187	0.478	Ru-C16	2.268	0.31	Ru-C18	2.326	0.307	
Ru-P11	2.332	0.854	Ru-P11	2.362	0.799	Ru-P13	2.341	0.853	Ru-P12	2.368	0.789	
Ru-Cl5	2.443	0.853	Ru-O8	2.254	0.413	Ru-Cl19	2.451	0.837	Ru-O16	2.259	0.408	
Ru-Cl17	2.443	0.853	Ru-Cl19	2.423	0.934	Ru-Cl20	2.447	0.836	Ru-Cl23	2.437	0.912	

4

5

6

7

8

9

Table 3.24: The polarization of the bonding interaction of Ru(II) with ligand atoms

Bonds	**(NBO %) Polarization of Pair Atoms**
Complex 1	
Ru- P11	(37.49%) 0.6123*Ru → (62.51%) 0.7906* P11
Complex 2	
Ru- P11	(35.61%) 0.5967*Ru → (64.39%) 0.8024* P11
Ru-Cl19	(24.42%) 0.4941*Ru → (75.58%) 0.8694*Cl19
Complex 3	
Ru- P13	(30.40%) 0.5514*Ru → (69.60%) 0.8343* P13
Ru-Cl19	(22.81%) 0.4776*Ru → (77.19%) 0.8786*Cl19
Ru-Cl20	(22.72%) 0.4767*Ru → (77.28%) 0.8791*Cl20
Complex 4	
Ru- P12	(36.46%) 0.6038*Ru → (63.54%) 0.7971* P12

Polarization coefficient c_A is the values with starred superscript and the square of it is percentage of the NBO (c_A-squared) on each hybrid orbitals (in parentheses).

Table 3.25: The delocalization orbitals with their second perturbation energies ($E^{(2)}$).

Complex 1			**Complex 2**			**Complex 3**			**Complex 4**		
Donor	Acceptor	$E^{(2)}$	Donor	Acceptor	$E^{(2)}$	Donor	Acceptor	$E^{(2)}$	Donor	Acceptor	$E^{(2)}$
90. LP (2)Ru	378. BD*(2) C3-C6	22.42	87. LP (2)Ru	90. LP (1) C6	14.91	1. BD (1)Ru-P13	460. BD*(1)Ru-Cl19	11.88	102. LP (2)Ru	494. BD*(2) C11-C19	10.06
91. LP (3)Ru	375. BD*(2) C2-C4	25.07	87. LP (2)Ru	100. LP*(1) C7	11.99	1. BD (1)Ru-P13	461. BD*(1)Ru-Cl20	11.88	102. LP (2)Ru	509. BD*(2) C18-C21	18.79
91. LP (3)Ru	385. BD*(2) C7-C9	25.08	87. LP (2)Ru	101. LP*(1) C9	23	107. LP (2)Ru	111. LP (1) C10	18.88	103. LP (3)Ru	480. BD*(2) C6-C10	22.1
4. BD (2) C2-C4	103. LP*(4)Ru	67.13	87. LP (2)Ru	409. BD*(2) C14-C18	19.88	107. LP (2)Ru	119. LP*(1) C6	29.14	103. LP (3)Ru	494. BD*(2) C11-C19	21.2
4. BD (2) C2-C4	104. LP*(5)Ru	20.9	88. LP (3)Ru	90. LP (1) C6	10.98	107. LP (2)Ru	498. BD*(2) C16-C17	19.25	15. BD (2) C6-C10	115. LP*(4)Ru	64.38
4. BD (2) C2-C4	372. BD*(1)Ru -P11	10.22	88. LP (3)Ru	95. LP (1) C17	46.13	108. LP (3)Ru	111. LP (1) C10	38	15. BD (2) C6-C10	116. LP*(5)Ru	16.97
6. BD (1) C3-C6	372. BD*(1)Ru -P11	10.83	88. LP (3)Ru	100. LP*(1) C7	49.06	108. LP (3)Ru	119. LP*(1) C6	16.16	15. BD (2) C6-C10	466. BD*(1)Ru-P12	14.65
7. BD (2) C3-C6	372. BD*(1)Ru -P11	39.87	88. LP (3)Ru	101. LP*(1) C9	41.74	108. LP (3)Ru	483. BD*(2) C9-C14	31.27	16. BD (1) C6-C11	116. LP*(5)Ru	10.69

14. BD (2) C7-C9	103. LP*(4)Ru	67.15	15. BD (1) C6-C7	378. BD*(1)Ru -Cl19	13.76	17. BD (1) C6-C10	461. BD*(1)Ru-Cl20	15.15	29. BD (2) C11-C19	115. LP*(4)Ru	69.89
14. BD (2) C7-C9	104. LP*(5)Ru	20.9	22. BD (1) C9-C17	99. LP*(4)Ru	14.48	24. BD (1) C9-C14	460. BD*(1)Ru-Cl19	16.07	29. BD (2) C11-C19	116. LP*(5)Ru	23.38
14. BD (2) C7-C9	372. BD*(1)Ru -P11	10.21	33. BD (2) C14-C18	377. BD*(1)Ru -P11	35.44	25. BD (2) C9-C14	460. BD*(1)Ru-Cl19	52.3	44. BD (2) C18-C21	466. BD*(1)Ru-P12	38.6
92. LP (1)Cl5	103. LP*(4)Ru	10.93	95. LP (1) C17	99. LP*(4)Ru	45.96	39. BD (1) C16-C17	459. BD*(1)Ru-P13	11.35	108. LP (2) O16	115. LP*(4)Ru	22.23
92. LP (1)Cl5	104. LP*(5)Ru	13.01	95. LP (1) C17	378. BD*(1)Ru -Cl19	13.17	40. BD (2) C16-C17	459. BD*(1)Ru-P13	31.97	108. LP (2) O16	116. LP*(5)Ru	33.01
95. LP (4)Cl5	103. LP*(4)Ru	105.18	92. LP (2) O 8	99. LP*(4)Ru	51.52	111. LP (1) C10	461. BD*(1)Ru-Cl20	41.72	111. LP (1)Cl23	115. LP*(4)Ru	12.65
95. LP (4)Cl5	104. LP*(5)Ru	54.32							111. LP (1)Cl23	116. LP*(5)Ru	11.17
95. LP (4)Cl5	372. BD*(1)Ru -P11	13.89							114. LP (4)Cl23	115. LP*(4)Ru	104.34
98. LP (1)Cl17	103. LP*(4)Ru	10.93							114. LP (4)Cl23	116. LP*(5)Ru	44.64
98. LP (1)Cl17	104. LP*(5)Ru	13.01							114. LP (4)Cl23	466. BD*(1)Ru-P12	12.83
101. LP (4)Cl17	103. LP*(4)Ru	105.16									
101. LP (4)Cl17	104. LP*(5)Ru	54.31									
101. LP (4)Cl17	372. BD*(1)Ru -P11	13.89									

The orbital analyses in the table are defined in terms of the second perturbation energy or stability energy ($E^{(2)}$ in kcal/mol).

Table 3.26: The amount of electron transferred to the acceptor orbitals and their energy level values for the four complexes

Complex 1			Complex 2			Complex 3			Complex 4		
Acceptor	**e^-**	**Energy**	**Acceptor**	**e^-**	**Energy**	**Acceptor**	**e^-**	**Energy**	**Acceptor**	**e^-**	**Energy**
103. LP*(4)Ru	0.86632	-0.23304	99. LP*(4)Ru	0.34162	-0.12373	459. BD*(1)Ru-P13	0.28052	0.0264	115. LP*(4)Ru	0.7717	-0.34383
104. LP*(5)Ru	0.29265	0.09026	377. BD*(1)Ru-P11	0.36076	-0.18575	460. BD*(1)Ru-Cl19	0.31342	-0.0177	116. LP*(5)Ru	0.25086	-0.04602
372. BD*(1)Ru-P11	0.4201	-0.08239	378. BD*(1)Ru-Cl19	0.3616	-0.20458	461. BD*(1)Ru-Cl20	0.31388	-0.01498	466. BD*(1)Ru-P12	0.41636	-0.20332
375. BD*(2) C2-C4	0.3873	-0.0176	100. LP*(1) C7	0.95425	-0.319	119. LP*(1) C6	0.97701	-0.1717	480. BD*(2) C6-C10	0.38112	-0.14052
378. BD*(2) C3-C6	0.30743	-0.00519	101. LP*(1) C9	0.94513	-0.31816	483. BD*(2) C9-C14	0.3977	-0.01059	494. BD*(2) C11-C19	0.39198	-0.13302
385. BD*(2) C7-C9	0.38731	-0.0176	409. BD*(2) C14-C18	0.2906	-0.14131	498. BD*(2) C16-C17	0.31534	0.00534	509. BD*(2) C18-C21	0.31948	-0.12782

Table 3.27: The NEDA analysis of the complexes showing the contribution of different factors to the total interaction energies (i.e. stability energies)

	Complex 1	**Complex 2**	**Complex 3**	**Complex 4**
ES	-613.65	-232.72	-195.41	-1180.24
POL	-1005.45	-755.32	-631.22	-1056.91
XC	-865.43	-200.66	-178.08	-923.35
DEF	2694.41	1567.78	1317.34	3295.35
SE	488.65	373.76	312.37	454.75
Electrical (ES+POL+SE)	-1130.45	-614.27	-514.26	-1782.4
Charge Transfer (CT)	-661.56	-472.22	-351.67	-1441.76
Core (XC+DEF-SE)	1340.33	993.36	826.89	1917.24
Total Interaction (E)	-451.67	-93.14	-39.04	-1306.93

Table 3.28: The induced energy and dipole of each fragment of ligands coordinated to metal through

NEDA analysis for the four complexes

		Fragment 1	Fragment 2	Fragment 3	Fragment 4
1	E(ind)	-1.292	-1.506	-0.748	-0.748
	Dipole (ind)	24.135	0.854	1.163	1.163
2	E(ind)	-0.652	-1.388	-0.458	
	Dipole (ind)	6.816	0.927	0.544	
3	E(ind)	-0.576	-1.524		
	Dipole (ind)	0.655	1.133		
4	E(ind)	-1.411	-1.420	-1.695	-0.726
	Dipole (ind)	28.107	1.755	14.771	1.135

Table 3.29: The QTAIM properties of selected bonds in complex **1**, **2**, **3** and **4** that are associated with metal using DGDZVP

	$\rho(r)$	$\nabla^2\rho(r)$	ε	K	BPL-GBL_I	V	G	L	GBL_I	∇^2Ven	|V/G|
Complex 1											
Ru1 - P11	0.096	0.147	0.156	0.030	0.005	-0.097	0.067	-0.037	4.408	-7.633	1.450
Ru1 - C2	0.077	0.247	0.585	0.014	0.014	-0.091	0.076	-0.062	4.186	-11.882	1.189
Ru1 - C4	0.077	0.263	1.723	0.014	0.037	-0.093	0.079	-0.066	4.198	-12.781	1.170
Ru1 - C9	0.077	0.247	0.584	0.014	0.014	-0.091	0.076	-0.062	4.186	-11.880	1.189
Ru1 - C7	0.077	0.263	1.728	0.014	0.037	-0.093	0.079	-0.066	4.198	-12.783	1.170
Ru1 - Cl5	0.064	0.208	0.194	0.007	0.003	-0.067	0.059	-0.052	4.616	-10.204	1.122
Ru1 - Cl17	0.064	0.208	0.194	0.007	0.003	-0.067	0.059	-0.052	4.616	-10.205	1.122
Complex 2											
Ru1 - P11	0.092	0.131	0.147	0.028	0.002	-0.089	0.061	-0.033	4.463	-6.546	1.463
Ru1 - C7	0.076	0.227	0.394	0.015	0.015	-0.086	0.071	-0.057	4.212	-10.511	1.206
Ru1 - C9	0.081	0.249	0.744	0.016	0.014	-0.095	0.079	-0.062	4.160	-11.938	1.209
Ru1 - C17	0.081	0.250	0.496	0.017	0.017	-0.096	0.079	-0.063	4.133	-11.911	1.211
Ru1 - O8	0.054	0.311	0.504	-0.004	0.005	-0.070	0.074	-0.078	4.260	-14.561	0.946
Ru1 - Cl19	0.067	0.218	0.298	0.008	0.003	-0.071	0.063	-0.054	4.580	-10.442	1.133
Complex 3											
Ru1 - P13	0.094	0.151	0.162	0.029	0.006	-0.095	0.067	-0.038	4.424	-8.327	1.433
Ru1 - C9	0.077	0.258	0.981	0.015	0.020	-0.094	0.079	-0.065	4.187	-13.648	1.184
Ru1 - C10	0.078	0.248	0.476	0.015	0.016	-0.092	0.077	-0.062	4.173	-13.001	1.197
Ru1 - C14	0.077	0.241	0.623	0.015	0.015	-0.090	0.075	-0.060	4.188	-12.683	1.199
Ru1 - Cl19	0.063	0.206	0.219	0.007	0.004	-0.065	0.058	-0.052	4.632	-10.869	1.117
Ru1 - Cl20	0.063	0.209	0.182	0.007	0.003	-0.066	0.059	-0.052	4.624	-11.039	1.118
Complex 4											
Ru1 - P12	0.090	0.138	0.154	0.027	0.003	-0.088	0.061	-0.034	4.475	-7.374	1.439

Ru1 - C6	0.078	0.243	0.868	0.015	0.016	-0.091	0.076	-0.061	4.199	-12.578	1.198
Ru1 - C11	0.074	0.262	3.945	0.012	0.029	-0.089	0.077	-0.065	4.223	-13.605	1.150
Ru1 - C10	0.073	0.250	1.462	0.012	0.026	-0.087	0.075	-0.063	4.231	-12.862	1.161
Ru1 - C19	0.084	0.228	0.279	0.020	0.011	-0.096	0.077	-0.057	4.123	-11.721	1.257
Ru1 - O16	0.054	0.305	0.490	-0.004	0.006	-0.069	0.073	-0.076	4.268	-15.482	0.950
Ru1 - Cl23	0.065	0.215	0.313	0.008	0.003	-0.069	0.061	-0.054	4.605	-11.089	1.124

∇^2Ven=Laplacian of the electron-nuclear attractive contribution to virial field, $\nabla^2\rho(r)$= Laplacian of the electron density.

Table 3.30: The QTAIM properties of selected bonds in complex **1**, **2**, **3** and **4** that are associated with metal using 3-21G

					Complex 1						
	$\rho(r)$	$\nabla^2\rho(r)$	ε	K	BPL-GBL_I	V	G	L	GBL_I	∇^2Ven	|V/G|
Ru1 - P11	0.090	0.150	0.104	0.027	0.008	-0.091	0.065	-0.038	4.408	-7.737	1.418
Ru1 - C2	0.075	0.268	0.240	0.011	0.014	-0.089	0.078	-0.067	4.186	-12.842	1.140
Ru1 - C4	0.074	0.285	0.543	0.010	0.019	-0.091	0.081	-0.071	4.198	-13.801	1.121
Ru1 - C7	0.074	0.285	0.544	0.010	0.019	-0.091	0.081	-0.071	4.198	-13.803	1.121
Ru1 - C9	0.075	0.268	0.240	0.011	0.014	-0.089	0.078	-0.067	4.186	-12.841	1.140
Ru1 - Cl5	0.063	0.206	0.167	0.007	0.001	-0.065	0.058	-0.051	4.616	-10.030	1.117
Ru1 - Cl17	0.063	0.206	0.167	0.007	0.001	-0.065	0.058	-0.051	4.616	-10.030	1.117
					Complex 2						
Ru1 - P11	0.086	0.136	0.101	0.025	0.003	-0.083	0.059	-0.034	4.463	-6.746	1.422
Ru1 - C6	0.071	0.284	2.624	0.007	0.048	-0.086	0.078	-0.071	4.240	-13.389	1.094
Ru1 - C7	0.074	0.248	0.168	0.011	0.015	-0.084	0.073	-0.062	4.212	-11.473	1.148
Ru1 - C9	0.079	0.270	0.295	0.012	0.014	-0.092	0.080	-0.068	4.160	-12.885	1.155
Ru1 - C17	0.079	0.273	0.178	0.013	0.018	-0.094	0.081	-0.068	4.133	-12.968	1.156
Ru1 - O8	0.059	0.295	0.349	0.007	0.005	-0.087	0.081	-0.074	4.260	-13.772	1.086
Ru1 - Cl19	0.066	0.212	0.220	0.008	0.004	-0.070	0.061	-0.053	4.579	-10.127	1.136
					Complex 3						
Ru1 - P13	0.088	0.154	0.110	0.026	0.009	-0.090	0.064	-0.039	4.424	-8.486	1.400
Ru1 - C6	0.071	0.274	1.012	0.008	0.023	-0.085	0.077	-0.068	4.254	-14.381	1.107
Ru1 - C9	0.075	0.283	0.394	0.010	0.018	-0.092	0.081	-0.071	4.187	-14.913	1.128
Ru1 - C10	0.076	0.272	0.183	0.011	0.014	-0.090	0.079	-0.068	4.173	-14.209	1.143
Ru1 - C14	0.075	0.262	0.276	0.011	0.013	-0.088	0.077	-0.066	4.188	-13.769	1.145
Ru1 - Cl19	0.061	0.205	0.192	0.006	0.001	-0.064	0.057	-0.051	4.632	-10.728	1.110
Ru1 - Cl20	0.062	0.206	0.154	0.006	0.001	-0.065	0.058	-0.052	4.624	-10.861	1.112
					Complex 4						
Ru1 - P12	0.084	0.142	0.103	0.024	0.004	-0.083	0.059	-0.036	4.475	-7.569	1.400
Ru1 - C6	0.076	0.266	0.372	0.011	0.012	-0.088	0.077	-0.066	4.199	-13.683	1.142
Ru1 - C11	0.072	0.276	1.018	0.009	0.024	-0.087	0.078	-0.069	4.223	-14.275	1.113
Ru1 - C10	0.071	0.267	0.592	0.009	0.023	-0.084	0.075	-0.067	4.231	-13.640	1.116
Ru1 - C19	0.082	0.257	0.090	0.015	0.012	-0.093	0.079	-0.064	4.123	-13.179	1.186
Ru1 - O16	0.059	0.289	0.350	0.007	0.005	-0.086	0.079	-0.072	4.268	-14.667	1.089
Ru1 - Cl23	0.064	0.211	0.230	0.007	0.004	-0.068	0.060	-0.053	4.605	-10.815	1.123

Table 3.31: The correlation in the properties of the electron density critical point analysis of complexes

1, **2**, **3** and **4**

	Complex 1				Complex 2				Complex 3				Complex 4			
	ρ(r)	$\nabla^2\rho(r)$	ε	∇^2Ven	ρ(r)	$\nabla^2\rho(r)$	ε	∇^2Ven	ρ(r)	$\nabla^2\rho(r)$	ε	∇^2Ven	ρ(r)	$\nabla^2\rho(r)$	ε	∇^2Ven
ρ(r)	1.00	-0.94	-0.72	0.95	1.00	-0.92	-0.73	0.92	1.00	-0.93	-0.60	0.93	1.00	-0.90	-0.54	0.89
$\nabla^2\rho(r)$	-0.94	1.00	0.66	-0.99	-0.92	1.00	0.73	-0.99	-0.93	1.00	0.57	-0.97	-0.90	1.00	0.52	-0.98
Ellipticity	-0.72	0.66	1.00	-0.67	-0.73	0.73	1.00	-0.74	-0.60	0.57	1.00	-0.56	-0.54	0.52	1.00	-0.51
K	0.99	-0.96	-0.72	0.98	0.94	-0.97	-0.71	0.98	0.98	-0.96	-0.60	0.96	0.94	-0.97	-0.52	0.97
BPL-GBL_I	-0.63	0.44	0.80	-0.43	-0.58	0.44	0.52	-0.44	-0.64	0.49	0.46	-0.47	-0.66	0.47	0.62	-0.45
V	-0.96	0.86	0.72	-0.90	-0.91	0.89	0.66	-0.92	-0.95	0.85	0.58	-0.88	-0.93	0.90	0.49	-0.92
G	0.15	0.14	-0.20	-0.05	0.02	0.21	0.15	-0.12	0.24	0.07	-0.14	0.03	0.27	0.00	-0.06	0.08
L	0.94	-1.00	-0.66	0.99	0.92	-1.00	-0.73	0.99	0.93	-1.00	-0.57	0.97	0.90	-1.00	-0.52	0.98
GBL_I	-0.95	0.95	0.71	-0.92	-0.92	0.94	0.72	-0.91	-0.95	0.95	0.61	-0.90	-0.93	0.90	0.57	-0.85
∇^2Ven	0.95	-0.99	-0.67	1.00	0.92	-0.99	-0.74	1.00	0.93	-0.97	-0.56	1.00	0.89	-0.98	-0.51	1.00
|V/G|	0.73	-0.87	-0.54	0.80	0.71	-0.83	-0.64	0.77	0.76	-0.89	-0.50	0.81	0.78	-0.87	-0.45	0.80

Table 3.32: Selected atomic properties derived through QTAIM analysis for complex **1**, **2**, **3** and **4** using DGDZVP

	Complex 1														
	q(A)	**L(A)**	**K(A)**	**K_{Scaled} (A)**	**Ee(A)**	$\|\mu_{Intra}(A)\|$	$\|\mu_{Bond}(A)\|$	|μ(A)|	N(A)	λ(A)	**%λ(A)**	**δ(A,A')**	**%δ(A,A')**	Vol(A)	χ_{ZZ}(A)
Ru1	0.77	0.00	4435.29	-4445.63	-4435.29	0.41	1.60	1.70	43.23	40.56	93.81	2.68	6.19	108.10	-6.80
C2	-0.06	-1.94E-04	37.84	-37.93	-37.84	0.11	0.13	0.07	6.06	3.96	65.42	2.10	34.58	71.99	-10.67
C3	-0.04	-9.00E-05	37.83	-37.92	-37.83	0.13	0.12	0.07	6.04	3.96	65.52	2.08	34.48	74.58	-6.58
C4	-0.07	-1.75E-04	37.83	-37.92	-37.83	0.10	0.06	0.06	6.07	3.97	65.40	2.10	34.60	73.72	-10.43
C6	-0.04	8.70E-05	37.83	-37.92	-37.83	0.13	0.12	0.07	6.04	3.96	65.52	2.08	34.48	74.49	-6.57
C7	-0.07	-1.43E-04	37.83	-37.92	-37.83	0.10	0.06	0.06	6.07	3.97	65.40	2.10	34.60	73.67	-10.40
C9	-0.06	-2.27E-04	37.84	-37.93	-37.84	0.11	0.13	0.07	6.06	3.96	65.42	2.10	34.58	72.00	-10.63
P11	1.51	-6.77E-04	340.02	-340.81	-340.02	1.40	0.34	1.07	13.49	11.56	85.67	1.93	14.33	79.09	-10.43
Cl5	-0.58	1.05E-04	459.4	-	-	0.13	1.27	1.36	17.58	16.96	96.47	0.62	3.53	239.7	-26.11

			1	460.48	459.41								5		
Cl17	-0.58	1.03E-04	459.41	-460.48	-459.41	0.13	1.27	1.36	17.58	16.96	96.47	0.62	3.53	239.75	-26.11
Complex 2															
Ru1	0.77	-3.17E-04	4435.24	-4445.98	-4435.24	0.38	0.92	1.06	43.23	40.65	94.04	2.58	5.96	112.07	-5.80
C6	-0.05	-1.00E-05	37.83	-37.92	-37.83	0.13	0.08	0.09	6.05	3.96	65.52	2.09	34.48	74.04	-8.04
C7	-0.07	-2.46E-04	37.84	-37.93	-37.84	0.11	0.06	0.06	6.07	3.97	65.51	2.09	34.49	72.85	-12.96
C9	-0.06	-1.09E-04	37.84	-37.93	-37.84	0.09	0.09	0.11	6.06	3.96	65.41	2.09	34.59	70.53	-11.30
C14	-0.05	4.20E-05	37.83	-37.92	-37.83	0.13	0.08	0.06	6.05	3.97	65.65	2.08	34.35	76.53	-7.23
C17	-0.06	-3.69E-04	37.85	-37.94	-37.85	0.12	0.11	0.08	6.06	3.97	65.50	2.09	34.50	71.93	-11.11
C18	-0.02	1.22E-04	37.83	-37.92	-37.83	0.13	0.13	0.06	6.02	3.95	65.56	2.07	34.44	72.70	-6.69
P11	1.31	-3.08E-04	340.13	-340.96	-340.13	1.32	0.97	0.37	13.69	11.70	85.45	1.99	14.55	88.25	-11.43
O8	-1.17	4.40E-05	75.21	-75.39	-75.21	0.31	0.90	0.61	9.17	8.24	89.89	0.93	10.11	120.85	-12.65
Cl19	-0.54	6.20E-05	459.43	-460.54	-459.43	0.06	1.23	1.20	17.54	16.88	96.21	0.67	3.79	228.21	-26.04
Complex 3															
Ru1	0.75	5.80E-05	4435.21	-4446.21	-4435.21	0.42	1.61	1.66	43.25	40.58	93.85	2.66	6.15	108.97	-1.02
C9	-0.08	2.05E-04	37.85	-37.95	-37.85	0.09	0.02	0.07	6.08	3.97	65.37	2.11	34.63	72.50	-10.29
C10	-0.07	-2.39E-04	37.86	-37.95	-37.86	0.09	0.07	0.03	6.07	3.97	65.35	2.10	34.65	70.76	-12.64
C14	-0.07	-9.64E-04	37.86	-37.95	-37.86	0.09	0.10	0.05	6.07	3.97	65.35	2.10	34.65	70.15	-10.85
C16	-0.06	-1.10E-05	37.86	-37.95	-37.86	0.10	0.08	0.06	6.06	3.97	65.40	2.10	34.60	71.55	-7.97
C17	-0.04	1.58E-04	37.86	-37.95	-37.86	0.11	0.16	0.06	6.04	3.91	64.64	2.14	35.36	59.63	-6.69
P13	1.49	-6.44E-04	340.01	-340.86	-340.01	1.42	0.21	1.21	13.51	11.58	85.72	1.93	14.28	80.37	-10.30
Cl19	-0.59	1.22E-04	459.40	-460.54	-459.40	0.13	1.42	1.52	17.59	16.97	96.45	0.62	3.55	238.43	-23.78
Cl20	-0.59	1.12E-04	459.41	-460.55	-459.41	0.12	1.06	1.14	17.59	16.94	96.32	0.65	3.68	233.70	-28.24
Complex 4															
Ru1	0.76	-6.20E-05	4435.17	-4446.59	-4435.17	0.38	0.77	0.82	43.24	40.67	94.06	2.57	5.94	112.67	11.03

C6	-0.06	-1.85E-04	37.85	-37.95	-37.85	0.09	0.08	0.11	6.06	3.96	65.37	2.10	34.63	70.51	-9.00
C10	-0.08	1.71E-04	37.86	-37.95	-37.86	0.11	0.10	0.12	6.08	3.98	65.49	2.10	34.51	73.04	-10.70
C11	-0.05	1.09E-04	37.85	-37.95	-37.85	0.11	0.09	0.04	6.05	3.91	64.58	2.14	35.42	60.21	-9.43
C18	-0.05	1.24E-04	37.87	-37.97	-37.87	0.11	0.01	0.12	6.05	3.91	64.67	2.14	35.33	58.48	-6.52
C19	-0.06	-3.64E-04	37.87	-37.96	-37.87	0.09	0.13	0.12	6.06	3.96	65.38	2.10	34.62	68.72	-12.22
C21	-0.06	2.07E-04	37.85	-37.95	-37.85	0.12	0.12	0.12	6.06	3.97	65.50	2.09	34.50	73.24	-8.31
P12	1.31	1.50E-05	340.12	-341.00	-340.12	1.36	0.77	0.59	13.69	11.71	85.54	1.98	14.46	89.10	-10.46
O16	-1.17	1.17E-04	75.21	-75.41	-75.21	0.31	0.90	0.62	9.17	8.23	89.78	0.94	10.22	119.64	-13.16
Cl23	-0.55	7.40E-05	459.43	-460.61	-459.43	0.06	1.21	1.19	17.55	16.89	96.23	0.66	3.77	228.20	-23.81

q(A) is net charge of atom A, L(A) is Lagrangian of Atom A, N(A) is average number of electrons in atom A, K(A) is electronic kinetic energy of atom A (Hamiltonian Form), %λ(A) is percentage of average number of electrons localized in atom A, %δ(A,A') is the percentage of electron delocalization index of atom A, K_{Scaled}(A) is approximation to virial-based total energy of atom A, $|\mu_{Intra}(A)|$ is magnitude of Intraatomic dipole moment of atom A, Ee(A) is contribution of atom A to electronic energy of molecule, Vol(A) is the volume bounded by an isosurface of the electron density distribution (0.001) and by interatomic surfaces of atom A and χ_{zz}= Out of plane magnetizability contribution of atom A.

Table 3.33: Selected atomic properties derived through QTAIM analysis for complex **1**, **2**, **3** and **4** using 3-21G

Complex 1															
	q(A)	**L(A)**	**K(A)**	**K_{Scaled} (A)**	**Ee(A)**	**$\|\mu_{Intra}($ A)|**	**$\|\mu_{Bond}($ A)|**	**$\|\mu(A)\|$**	**N(A)**	**λ(A)**	**%λ(A)**	**δ(A,A ')**	**%δ(A, A')**	**Vol(A)**	**χ_{ZZ}(A)**
Ru1	0.61	3.10E-04	-4402.72	-4423.80	-4402.72	0.38	1.88	1.91	43.39	40.79	94.00	2.60	6.00	105.51	-4.67
C2	-0.10	-8.90E-05	37.61	-37.79	-37.61	0.25	0.22	0.09	6.10	4.02	65.90	2.08	34.10	74.18	-10.60
C3	-0.09	1.04E-04	37.59	-37.77	-37.59	0.25	0.21	0.11	6.09	4.02	66.00	2.07	34.00	76.48	-6.91
C4	-0.12	-7.80E-05	37.60	-37.78	-37.60	0.23	0.14	0.10	6.12	4.04	65.93	2.09	34.07	76.04	-10.63
C6	-0.09	-2.70E-05	37.59	-37.77	-37.59	0.26	0.21	0.11	6.09	4.02	66.00	2.07	34.00	76.53	-6.91
C7	-0.13	-1.41E-04	37.60	-37.78	-37.60	0.23	0.14	0.10	6.13	4.04	65.93	2.09	34.07	75.99	-10.62
C9	-0.10	-9.70E-05	37.61	-37.79	-37.61	0.25	0.22	0.09	6.10	4.02	65.90	2.08	34.10	74.21	-10.61
P11	1.19	-8.00E-04	337.98	-339.60	-337.98	1.14	0.36	1.50	13.81	11.80	85.50	2.00	14.50	85.10	-14.91
Cl5	-0.55	9.60E-05	456.65	-458.84	-456.65	0.17	1.31	1.48	17.55	16.95	96.56	0.60	3.44	232.43	-25.33

Cl17	-0.55	9.40E-05	-456.65	-458.84	-456.65	0.17	1.31	1.48	17.55	16.95	96.56	0.60	3.44	232.40	-25.33
Complex 2															
Ru1	0.66	3.18E-04	-4402.63	-4424.53	-4402.63	0.31	0.90	0.99	43.34	40.84	94.23	2.50	5.77	107.70	-3.04
C6	-0.10	1.16E-04	37.59	-37.78	-37.59	0.27	0.15	0.12	6.10	4.02	66.00	2.07	34.00	76.51	-11.14
C7	-0.12	-3.12E-04	37.61	-37.80	-37.61	0.22	0.13	0.10	6.12	4.04	66.06	2.08	33.94	75.90	-11.82
C9	-0.12	-3.15E-04	37.62	-37.80	-37.62	0.22	0.13	0.13	6.12	4.03	65.96	2.08	34.04	73.77	-10.11
C14	-0.10	1.39E-04	37.59	-37.77	-37.59	0.26	0.16	0.12	6.10	4.03	66.12	2.07	33.88	79.17	-7.57
C17	-0.10	-2.73E-04	37.61	-37.80	-37.61	0.26	0.18	0.11	6.10	4.03	66.01	2.07	33.99	74.92	-10.53
C18	-0.07	8.10E-05	37.59	-37.78	-37.59	0.26	0.22	0.10	6.07	4.01	66.03	2.06	33.97	75.48	-7.04
P11	1.02	1.31E-04	-338.08	-339.76	-338.08	1.06	0.67	0.40	13.98	11.95	85.46	2.03	14.54	93.48	-14.47
O8	-0.94	1.20E-05	74.50	-74.87	-74.50	0.14	0.66	0.77	8.94	7.90	88.36	1.04	11.64	100.57	-11.58
Cl19	-0.51	5.70E-05	-456.67	-458.94	-456.67	0.15	1.13	1.28	17.51	16.86	96.32	0.65	3.68	225.47	-25.46
Complex 3															
Ru1	0.61	-2.19E-04	-4402.64	-4424.27	-4402.64	0.38	1.62	1.67	43.39	40.81	94.04	2.59	5.96	106.26	1.22
C6	-0.09	4.70E-05	37.61	-37.79	-37.61	0.12	0.21	0.09	6.09	3.95	64.85	2.14	35.15	62.00	-9.97
C9	-0.13	5.00E-06	37.62	-37.81	-37.62	0.22	0.11	0.11	6.13	4.04	65.88	2.09	34.12	74.45	-9.49
C10	-0.11	-3.23E-04	37.62	-37.81	-37.62	0.23	0.17	0.07	6.11	4.02	65.83	2.09	34.17	72.73	-11.84
C14	-0.12	-2.76E-04	37.62	-37.81	-37.62	0.22	0.19	0.08	6.12	4.03	65.84	2.09	34.16	71.81	-10.51
C16	-0.11	-2.92E-04	37.62	-37.81	-37.62	0.23	0.17	0.10	6.11	4.03	65.88	2.09	34.12	73.50	-8.17
C17	-0.06	1.29E-04	37.61	-37.79	-37.61	0.19	0.20	0.06	6.06	3.93	64.88	2.13	35.12	59.99	-7.18
P13	1.18	-4.25E-04	-337.98	-339.64	-337.98	1.17	0.04	1.20	13.82	11.82	85.56	1.99	14.44	86.26	-13.55
Cl19	-0.56	9.90E-05	-456.64	-458.89	-456.64	0.18	1.34	1.51	17.56	16.96	96.55	0.61	3.45	232.12	-23.71
Cl20	-0.56	8.70E-05	-456.64	-458.89	-456.64	0.18	0.95	1.12	17.56	16.93	96.41	0.63	3.59	227.29	-28.25
Complex 4															
Ru1	0.66	-9.94E-04	-4402.56	-4425.01	-4402.56	0.32	0.83	0.83	43.34	40.85	94.26	2.49	5.74	108.27	13.22
C6	-0.12	-1.33E-04	37.62	-37.82	-37.62	0.21	0.13	0.14	6.12	4.03	65.89	2.09	34.11	72.94	-9.46

C10	-0.13	2.99E-04	37.62	-37.81	-37.62	0.23	0.14	0.15	6.13	4.04	65.98	2.08	34.02	74.94	-11.14
C11	-0.09	-1.85E-04	37.62	-37.81	-37.62	0.18	0.14	0.06	6.09	3.95	64.93	2.13	35.07	61.77	-10.48
C18	-0.08	-7.89E-04	37.63	-37.82	-37.63	0.17	0.02	0.17	6.08	3.95	64.97	2.13	35.03	59.74	-7.55
C19	-0.11	-1.06E-04	37.63	-37.83	-37.63	0.23	0.19	0.15	6.11	4.02	65.90	2.08	34.10	71.34	-12.70
C21	-0.10	-1.79E-04	37.61	-37.80	-37.61	0.25	0.20	0.15	6.10	4.02	65.93	2.08	34.07	75.47	-8.71
P12	1.01	-1.38E-04	338.07	-339.80	-338.07	1.10	0.44	0.66	13.99	11.96	85.54	2.02	14.46	94.56	-13.89
O16	-0.94	3.90E-05	74.50	-74.88	-74.50	0.14	0.66	0.77	8.94	7.90	88.30	1.05	11.70	100.27	-12.42
Cl23	-0.52	6.70E-05	456.66	-458.99	-456.66	0.16	1.16	1.31	17.52	16.88	96.34	0.64	3.66	225.69	-23.34

q(A) is net charge of atom A, L(A) is Lagrangian of Atom A, N(A) is average number of electrons in atom A, K(A) is electronic kinetic energy of atom A (Hamiltonian Form), %λ(A) is percentage of average number of electrons localized in atom A, %δ(A,A') is the percentage of electron delocalization index of atom A, $K_{Scaled}(A)$ is approximation to virial-based total energy of atom A, $|\mu_{Intra}(A)|$ is magnitude of Intraatomic dipole moment of atom A, Ee(A) is contribution of atom A to electronic energy of molecule, Vol(A) is the volume bounded by an isosurface of the electron density distribution (0.001) and by interatomic surfaces of atom A and χ_{zz}= Out of plane magnetizability contribution of atom A.

Table 3.34: The correlation in the atomic properties of complexes 1, 2, 3 and 4.

Complex 1	**Complex 2**	**Complex 3**	**Complex 4**

	K(A)	Ee(A)	$\|\mu_{Bond}$ (A)|	χ_{ZZ}(A)	K(A)	Ee(A)	$\|\mu_{Bond}$ (A)|	χ_{ZZ}(A)	K(A)	Ee(A)	$\|\mu_{Bond}$ (A)|	χ_{ZZ}(A)	K(A)	Ee(A)	$\|\mu_{Bond}$ (A)|	χ_{ZZ}(A)
q(A)	0.26	-0.26	-0.12	0.28	0.25	-0.25	-0.11	0.31	0.26	-0.26	-0.14	0.30	0.25	-0.25	-0.14	0.40
L(A)	0.07	-0.07	-0.16	0.19	-0.35	0.35	-0.36	0.38	0.03	-0.03	-0.16	0.13	-0.08	0.08	0.10	0.00
K(A)	1.00	-1.00	0.56	-0.17	1.00	-1.00	0.33	-0.13	1.00	-1.00	0.57	-0.03	1.00	-1.00	0.30	0.35
KScaled(A)	-1.00	1.00	-0.56	0.17	-1.00	1.00	-0.33	0.13	-1.00	1.00	-0.57	0.03	-1.00	1.00	-0.30	-0.35
Ee(A)	-1.00	1.00	-0.56	0.17	-1.00	1.00	-0.33	0.13	-1.00	1.00	-0.57	0.03	-1.00	1.00	-0.30	-0.35
$\|\mu_{Intra}$(A)|	0.11	-0.11	0.52	-0.06	0.11	-0.11	0.75	-0.13	0.13	-0.13	0.52	-0.05	0.13	-0.13	0.73	-0.07
$\|\mu_{Bond}$(A)|	0.56	-0.56	1.00	-0.57	0.33	-0.33	1.00	-0.54	0.57	-0.57	1.00	-0.48	0.30	-0.30	1.00	-0.38
|μ(A)|	0.64	-0.64	0.69	-0.66	0.53	-0.53	0.63	-0.60	0.63	-0.63	0.66	-0.52	0.43	-0.43	0.62	-0.38
N(A)	0.89	-0.89	0.77	-0.56	0.90	-0.90	0.61	-0.51	0.88	-0.88	0.77	-0.46	0.89	-0.89	0.58	-0.09
λ(A)	0.90	-0.90	0.76	-0.56	0.91	-0.91	0.59	-0.49	0.90	-0.90	0.77	-0.44	0.91	-0.91	0.56	-0.05
%λ(A)	0.45	-0.45	0.79	-0.83	0.40	-0.40	0.72	-0.79	0.44	-0.44	0.76	-0.79	0.40	-0.40	0.69	-0.59
δ(A,A')	0.33	-0.33	0.46	-0.30	0.33	-0.33	0.51	-0.47	0.30	-0.30	0.43	-0.35	0.30	-0.30	0.45	-0.39
%δ(A, A')	-0.45	0.45	-0.79	0.83	-0.40	0.40	-0.72	0.79	-0.44	0.44	-0.76	0.79	-0.40	0.40	-0.69	0.59
Vol(A)	0.29	-0.29	0.65	-0.94	0.34	-0.34	0.61	-0.90	0.31	-0.31	0.66	-0.87	0.35	-0.35	0.62	-0.65
χ_{ZZ}	-0.17	0.17	-0.57	1.00	-0.13	0.13	-0.54	1.00	-0.03	0.03	-0.48	1.00	0.35	-0.35	-0.38	1.00

Table 3.35: The sum total of the computed atomic properties over all the atoms in complexes **1**, **2**, **3** and **4** from DGDVZP(Ru)|6-31+G(d,p) systems.

	q(A)	L(A)	K(A)	K_{Scaled} (A)	Ee(A)	$\|\mu_{Intra}$(A)|	$\|\mu_{Bond}$(A)|	|μ(A)|	N(A)	λ(A)	%λ(A)	δ(A,A')	%δ(A,A')	Vol(A)	χ_{ZZ}(A)
1	0.00	-1.05E-03	6,322.29	6,337.02	6,322.29	10.42	12.09	10.96	204.00	158.50	58.48	45.50	41.52	2,541.90	-203.44
2	1.00	-6.96E-04	5,938.65	5,953.02	5,938.65	10.31	11.75	8.82	196.00	149.67	55.94	46.33	44.06	2,439.26	-190.77
3	0.00	-1.14E-03	6,478.23	6,494.30	6,478.23	11.73	12.20	12.53	236.00	177.64	56.73	58.36	43.27	3,156.67	-247.30
4	1.00	-1.82E-03	6,094.61	6,110.31	6,094.61	11.71	11.61	10.45	228.00	168.84	54.86	59.16	45.14	3,058.97	-219.51

Table 3.36: Thermodynamic properties of the complexes in KJ/mol or KJ/mol-K

	PBE0/ECP(Ru,Cl)[6-31G*]									
Complexes	E0	E	H	G	TC	E CV	S	KJ/mol-	Imaginary	No. Nor

					KJ/mol	KJ/mol-K	K		Vib Mode
1	-2.67E+06	-2.67E+06	-2.67E+06	-2.67E+06	7.51E+02	0.32	0.62	0	102
2	-3.18E+06	-3.18E+06	-3.18E+06	-3.18E+06	8.15E+02	0.37	0.69	0	114
3	-3.38E+06	-3.38E+06	-3.38E+06	-3.38E+06	8.48E+02	0.39	0.69	0	120
4	-2.68E+06	-2.68E+06	-2.68E+06	-2.69E+06	8.08E+02	0.31	0.55	1	108
5	-3.30E+06	-3.30E+06	-3.30E+06	-3.30E+06	9.52E+02	0.38	0.66	0	129
				PBE0/ECP(Ru)[6-31+G(d,p)]					
1	-3.84E+06	-3.84E+06	-3.84E+06	-3.84E+06	7.49E+02	0.32	0.62	0	102
2	-4.35E+06	-4.35E+06	-4.35E+06	-4.35E+06	8.13E+02	0.37	0.69	0	114
3	-4.55E+06	-4.55E+06	-4.55E+06	-4.55E+06	8.46E+02	0.70	0.39	0	120
4	-2.69E+06	-2.68E+06	-2.68E+06	-2.69E+06	8.06E+02	0.31	0.55	0	108
5	-3.30E+06	-3.30E+06	-3.30E+06	-3.30E+06	9.49E+02	0.38	0.66	0	129

Table 3.37: The total energy of the complexes in KJ/mol computed scaling up the functional and basis sets

Functional/Basis Sets	1	2	3	4	5
PBE0/ECP(Ru,Cl)[6-31G*]	-2.6733E+06	-3.1824E+06	-3.3823E+06	-2.6853E+06	-3.2957E+06
B3LYP/3-21G	-1.5195E+07	-1.5700E+07	-1.5899E+07	-1.4042E+07	-1.4649E+07
PBE0/ECP(Ru)[6-31+G(d,p)]	-3.8441E+06	-4.3515E+06	-4.5514E+06	-2.6858E+06	-3.2962E+06
B3LYP/ECP(Ru)[6-31+G(d,p)]	-1.5265E+07	-1.5773E+07	-1.5973E+07	-1.4107E+07	-1.4718E+07
MP2/ECP(Ru)[6-31+G(d,p)]	-3.8288E+06	-4.3340E+06	-4.5329E+06	-2.6712E+06	-3.2789E+06
B3LYP/DGDZVP(Ru)[6-31G*]	-1.5266E+07	-1.5774E+07	-1.5974E+07	-1.4108E+07	-1.4719E+07
B3LYP/DGDZVP(Ru)[6-31+G(d,p)]	-1.5265E+07	-1.5773E+07	-1.5973E+07	-1.4107E+07	-1.4718E+07
B3LYP/acc-pvtz	-1.5069E+07	-1.5576E+07	-1.5773E+07	-1.3907E+07	-1.4520E+07

The SCF of the both MP2/DGDZVP(Ru)[6-31+G(d,p) and B3LYP/aug-cc-pVTZ are prohibitively expensive and therefore is unconverged

Table 3.38: Bond distances (Å) and bond order of the ruthenium ligand bonds of the complexes

bpyr			dpy			pth			raz			ter		
Pair	Dist	Order	Pair	Dist	Order	Pair	Dist	Order	Pair	Distance	Order	Pair	Dist	Order

Ru-C9	2.267	0.387	Ru-C7	2.233	0.408	Ru-C13	2.236	0.376	Ru-C2	2.262	0.384	Ru-C20	2.269	0.399
Ru-C13	2.232	0.428	Ru-C8	2.254	0.371	Ru-C18	2.236	0.375	Ru-C5	2.241	0.435	Ru-C23	2.29	0.361
Ru-C18	2.236	0.401	Ru-C13	2.277	0.35	Ru-C25	2.261	0.414	Ru-C3	2.252	0.413	Ru-C26	2.269	0.399
Ru-C10	2.226	0.414	Ru-C18	2.233	0.408	Ru-C14	2.251	0.39	Ru-C6	2.252	0.412	Ru-C18	2.252	0.419
Ru-C16	2.228	0.405	Ru-C14	2.239	0.36	Ru-C21	2.264	0.411	Ru-C4	2.263	0.384	Ru-C22	2.252	0.419
Ru-C19	2.222	0.378	Ru-C19	2.254	0.372	Ru-C23	2.253	0.387	Ru-C7	2.242	0.435	Ru-C27	2.289	0.361
Ru-Cl22	2.394	1.007	Ru-Cl10	2.396	1.052	Ru-Cl7	2.39	0.996	Ru-N10	2.162	0.363	Ru-N14	2.152	0.423
Ru-N12	2.137	0.361	Ru-N11	2.096	0.431	Ru-N10	2.138	0.371	Ru-N13	2.162	0.363	Ru-N15	2.039	0.47
Ru-N17	2.139	0.361	Ru-N16	2.096	0.43	Ru-N16	2.138	0.371	Ru-N15	2.084	0.417	Ru-N21	2.153	0.424

Table 3.39: H-bonding properties of the complexes

	$\rho(r)$	$\nabla^2\rho(r)$	Ellipticity	K	BPL - GBL_I	V	G	L	GBL_I	V/G
Complex 1										
O2···H24	0.0101	0.0388	0.4777	-0.0016	0.1887	-0.0065	0.0081	-0.0097	4.7207	0.7994
O2···H29	0.0100	0.0384	0.5142	-0.0016	0.1942	-0.0064	0.0080	-0.0096	4.7341	0.7961
					0.0000					
H34···H38	0.0092	0.0403	1.7449	-0.0027	0.5505	-0.0047	0.0074	-0.0101	4.0818	0.6359
					0.0000					
O2···H31	0.0164	0.0614	0.3859	-0.0018	0.1265	-0.0118	0.0136	-0.0154	4.2711	0.8686
O28···H36	0.0168	0.0625	0.3248	-0.0017	0.1049	-0.0122	0.0139	-0.0156	4.2285	0.8778

Table 3.40: The C-H as H-Bonding donor represented with superscript "*" and another C-H in the same chemical environment but without taking part in H-Bonding

Bonds	$\rho(r)$	$\nabla^2\rho(r)$	Ellipticity	K	BPL - GBL_I	V	G	L	GBL_I	V/G

Complex 1										
*C5 - H24	0.2878	-1.1061	0.0325	0.3084	3.98E-04	-0.3403	0.0319	0.2765	2.0107	10.6741
*C15 - H29	0.2877	-1.1053	0.0325	0.3082	4.00E-04	-0.3402	0.0319	0.2763	2.0108	10.6583
C11 - H30	0.2883	-1.1066	0.0263	0.3079	1.09E-04	-0.3391	0.0312	0.2766	2.0123	10.8581
C21 - H35	0.2884	-1.1074	0.0262	0.3080	1.08E-04	-0.3392	0.0312	0.2768	2.0122	10.8735
Complex 2										
*C12 - H34	0.2853	-1.0584	0.0099	0.2998	8.50E-05	-0.3349	0.0351	0.2646	2.0199	9.5281
*C21 - H38	0.2845	-1.0570	0.0088	0.2987	1.47E-04	-0.3332	0.0345	0.2643	2.0224	9.6668
C3 - H27	0.2846	-1.0676	0.0088	0.2998	3.50E-05	-0.3328	0.0329	0.2669	2.0223	10.1006
C22 - H39	0.2850	-1.0639	0.0101	0.2998	1.20E-05	-0.3337	0.0339	0.2660	2.0206	9.8550
Complex 3										
*C14 - H31	0.2886	-1.1003	0.0080	0.3076	7.00E-05	-0.3402	0.0326	0.2751	2.0160	10.4485
*C23 - H36	0.2888	-1.1040	0.0081	0.3084	6.80E-05	-0.3409	0.0324	0.2760	2.0155	10.5077
C21 - H35	0.2832	-1.0352	0.0102	0.2941	1.80E-05	-0.3294	0.0353	0.2588	2.0245	9.3285
C25 - H37	0.2833	-1.0361	0.0096	0.2942	1.80E-05	-0.3294	0.0352	0.2590	2.0246	9.3567

Table 3.41: The second order perturbation of NBO donor and acceptor orbitals

bpy					dipy					phth					raz					ter				
obt	Donor	obt	Acceptor	$E^{(2)}$	obt	Donor	obt	Acceptor	$E^{(2)}$	obt	Donor	obt	Acceptor	$E^{(2)}$	obt	Donor	obt	Acceptor	$E^{(2)}$	obt	Donor	obt	Acceptor	$E^{(2)}$
			σ*(2)										σ*(2)					σ*(2)						
87	n(2)Ru	423	C18C19	26.81	95	n(1)Ru	109	n(2) N16 σ*(2)	12.9 10.8	103	n(2)Ru	488	C13C14 σ*(2)	18.25	91	n(2)Ru	398	C2C4 σ*(2)	23.17	103	n(1)Ru	114	n(2) N21 σ*(2)	10.29
88	n(3)Ru	403	σ*(2) C9C13 σ*(2)	18.9	96	n(2)Ru	456	C7C13 σ*(2)	1 18.5	103	n(2)Ru	500	C18C23 σ*(2)	19.23	92	n(3)Ru	401	C3C5 σ*(2)	19.8	104	n(2)Ru	519	C23C27 σ*(2)	21.54
88	n(3)Ru	406	C10C16	22.02	96	n(2)Ru	459	C8C14 σ*(2)	7 21.4	104	n(3)Ru	506	C21C25	25.94	92	n(3)Ru	408	C6C7	19.5	105	n(3)Ru	507	C18C20 σ*(2)	18.5
95	n(1) N12	102	n*(4)Ru	14.03	97	n(3)Ru	475	C18C19	1	114	n(1) N10	121	n*(4)Ru	16.2	2	σ(1) C2C4	99	n*(5)Ru	12.32	105	n(3)Ru	516	C22C26	18.81
95	n(1) N12	103	n*(5)Ru	58.16	107	n(1) N11	115	n*(4)Ru	18.1 70.4	114	n(1) N10	122	n*(5)Ru	59.16	3	σ(2) C2C4	99	n*(5)Ru	89.65	111	n(1) N14	115	n*(4)Ru	57.71
95	n(1) N12	104	n*(6)Ru	33.36	107	n(1) N11	116	n*(5)Ru	5 32.2	114	n(1) N10	123	n*(6)Ru	27.99	3	σ(2) C2C4	100	n*(6)Ru	15.13	111	n(1) N14	116	n*(5)Ru	17.3
97	n(1) N17	102	n*(4)Ru	14.78	107	n(1) N11 σ(1)	117	n*(6)Ru	1 12.2	115	n(1) N16	121	n*(4)Ru	16.38	6	σ(2) C3C5	98	n*(4)Ru	70.5	111	n(1) N14	117	n*(6)Ru	27.05
97	n(1) N17	103	n*(5)Ru	57.21	13	C7C8 σ(2)	116	n*(5)Ru	7	115	n(1) N16	122	n*(5)Ru	59.19	6	σ(2) C3C5	99	n*(5)Ru	19.76	112	n(1) N15	116	n*(5)Ru	118.46
97	n(1) N17 σ(1)	104	n*(6)Ru	33.1	15	C7C13 σ(2)	115	n*(4)Ru	69.11	115	n(1) N16	123	n*(6)Ru	28.02	6	σ(2) C3C5	100	n*(6)Ru	13.45	112	n(1) N15	117	n*(6)Ru	25.6
16	C9C13 σ(2)	102	n*(4)Ru	10.59	15	C7C13 σ(2)	116	n*(5)Ru	11.66 10.8	107	n(1)Cl7	121	n*(4)Ru	17.59	13	σ(2) C6C7	98	n*(4)Ru	70.86	113	n(1) N21	115	n*(4)Ru	63.65
17	C9C13 σ(1)	102	n*(4)Ru	87.37	15	C7C13 σ(2)	117	n*(6)Ru	4 47.1	108	n(2)Cl7	121	n*(4)Ru	17.78	13	σ(2) C6C7	99	n*(5)Ru	19.52	113	n(1) N21	116	n*(5)Ru	11.61
19	C10C16 σ(2)	103	n*(5)Ru	11.48	18	C8C14 σ(2)	115	n*(4)Ru	6 28.6	108	n(2)Cl7	123	n*(6)Ru	10.2	13	σ(2) C6C7	100	n*(6)Ru	13.47	113	n(1) N21 σ(2)	117	n*(6)Ru	26.95
20	C10C16 σ(2)	103	n*(5)Ru	77.73	18	C8C14 σ(2)	116	n*(5)Ru	3	110	n(4)Cl7	121	n*(4)Ru	185.27	93	n(1) N10	98	n*(4)Ru	48.83	35	C18C20 σ(2)	115	n*(4)Ru	70.99
20	C10C16 σ(1)	104	n*(6)Ru	16.06	18	C8C14 σ(1)	117	n*(6)Ru	17.11 10.7	110	n(4)Cl7 σ(2)	123	n*(6)Ru	37.72	93	n(1) N10	99	n*(5)Ru	9.9	35	C18C20 σ(2)	116	n*(5)Ru	15.15
25	C13C18 σ(2)	103	n*(5)Ru	10.83	33	C18C19 σ(2)	116	n*(5)Ru	1 73.2	22	C13C14 σ(2)	121	n*(4)Ru	20.94	93	n(1) N10	100	n*(6)Ru	28.72	35	C18C20 σ(2)	117	n*(6)Ru	13.12
37	C18C19 σ(2)	102	n*(4)Ru	32.3	34	C18C19 σ(2)	116	n*(5)Ru	4 15.2	22	C13C14 σ(2)	122	n*(5)Ru	70.12	95	n(1) N13	98	n*(4)Ru	48.81	44	C22C26 σ(2)	115	n*(4)Ru	63.72
37	C18C19 σ(2)	103	n*(5)Ru	52.5	34	C18C19	117	n*(6)Ru	6 16.4	22	C13C14 σ(2)	123	n*(6)Ru	15.69	95	n(1) N13	99	n*(5)Ru	9.86	44	C22C26 σ(2)	116	n*(5)Ru	22.29
37	C18C19	104	n*(6)Ru	16.34	103	n(1)Cl10	115	n*(4)Ru	9 16.9	34	C18C23 σ(2)	121	n*(4)Ru	22.57	95	n(1) N13	100	n*(6)Ru	28.71	44	C22C26 σ(1)	117	n*(6)Ru	13.12
98	n(1)Cl22	102	n*(4)Ru	17.04	104	n(2)Cl10	115	n*(4)Ru	3 201.	34	C18C23 σ(2)	122	n*(5)Ru	68.06	96	n(1) N15	99	n*(5)Ru	102.44	46	C23C27 σ(2)	116	n*(5)Ru	11.73
99	n(2)Cl22	102	n*(4)Ru	17.79	106	n(4)Cl10	115	n*(4)Ru	91 36.4	34	C18C23 σ(1)	123	n*(6)Ru	15.72	96	n(1) N15	100	n*(6)Ru	25.01	47	C23C27 σ(2)	116	n*(5)Ru	80.31
101	n(4)Cl22	102	n*(4)Ru	197.12	106	n(4)Cl10	117	n*(6)Ru	3	39	C21C25 σ(2)	121	n*(4)Ru	11.6						47	C23C27	117	n*(6)Ru	14.63
101	n(4)Cl22	104	n*(6)Ru	36.26						40	C21C25	121	n*(4)Ru	96.13										

Table 3.42: The amount of electron transferred to the acceptor orbitals and their energy level values for the five complexes

1				**2**				**3**			
Obt	Acceptor	e	Energy	Obt	Acceptor	e	Energy	Obt	Acceptor	e	Energy
102	n*(4)Ru	0.87434	0.35967	115	n*(4)Ru	0.87533	0.35947	121	n*(4)Ru	0.86496	0.34522
103	n*(5)Ru	0.74736	0.33432	116	n*(5)Ru	0.75181	0.33217	122	n*(5)Ru	0.74216	0.31543
104	n*(6)Ru	0.21177	0.01293	117	n*(6)Ru	0.21035	0.01637	123	n*(6)Ru	0.20406	0.02081
403	σ*(2) C9C13	0.36325	0.14514	456	σ*(2) C7C13	0.39975	0.14684	488	σ*(2) C13C14	0.32278	0.10755
406	σ*(2) C10C16	0.35698	0.13511	459	σ*(2) C8C14	0.38484	0.13694	500	σ*(2) C18C23	0.32044	0.10717
423	σ*(2) C18C19	0.33342	0.13002	475	σ*(2) C18C19	0.41816	0.14586	506	σ*(2) C21C25	0.34831	0.12365
	4				5						
Obt	Acceptor	e	Energy	Obt	Acceptor	e	Energy				
98	n*(4)Ru	0.76334	0.4648	115	n*(4)Ru	0.77615	0.45347				
99	*n*(5)Ru	0.75292	0.46237	116	n*(5)Ru	0.77258	0.45078				
100	n*(6)Ru	0.18956	0.12562	117	n*(6)Ru	0.18824	0.11449				
398	σ*(2) C2C4	0.30837	0.25545	114	n(2) N 21	1.31156	0.47767				
401	σ*(2) C3C5	0.31954	0.25861	507	σ*(2) C18C20	0.31805	0.24868				
408	σ*(2) C6C7	0.31948	0.25857	516	σ*(2) C22C26	0.31775	0.24853				
				519	σ*(2) C23C27	0.30475	0.24754				

Table 3.43: The induced energy and dipole of each fragment of ligands coordinated to metal through NEDA analysis for the five complexes

Complexes		Fragment 1	Fragment 2	Fragment 3	Fragment 4
1	E(ind)	-0.8162	-1.7613	-1.5040	-0.7680
	Dipole (ind)	0.3878	7.4842	1.1558	1.0618
2	E(ind)	-0.8371	-2.0440	-1.4205	-0.7389
	Dipole (ind)	0.3398	5.0347	1.0371	1.0819
3	E(ind)	-0.8263	2.1367	-0.7788	-1.4994
	Dipole (ind)	0.4199	11.5244	1.0331	1.3137
4	E(ind)	-0.8337	-1.2962	-1.7371	
	Dipole (ind)	0.3263	1.1486	6.7520	
5	E(ind)	-0.8695	-2.2202	-1.3309	
	Dipole (ind)	0.3455	6.2617	1.2446	

Table 3.44: The NEDA analysis of the complexes showing the contribution of different factors to the total interaction energies (i.e. stability energies)

	1	**2**	**3**	**4**	**5**
SE	818.92	760	835.99	747.73	794.78
ES	-825.88	-1121.16	-1087.51	-362.65	-589.75
POL	-1630.15	-1513.15	-1666.82	-1490.34	-1582.56
XC	-316.08	-307.19	-324.34	-272.18	-285.7
Electrical (Elec= ES+POL+SE)	-1637.11	-1874.31	-1918.35	-1105.26	-1377.52
Charge Transfer (CT)	-1197.82	-1566.92	-1559.06	-721.95	-1107.53
Core (XC+DEF-SE)	1908.05	2095.8	2128.62	1406.67	1693.56
Total Interaction (E=Elec + CT + Core)	-926.89	-1345.43	-1348.79	-420.55	-791.49

The components of energy are defines in terms of electrostatic interaction (ES); polarization (POL); electrical self-energy (SE); exchange interaction (XC); deformation energy (DEF), Electrical (ES+POL+SE), Core (XC+DEF-SE) and Total Interaction energy which is the final net H-bond energy (E = Electrical + Core + CT)

Table 3.45: Selected bond properties involving ruthenium or hydrogen bond (Bonds with superscript "#") obtained through QTAIM analysis of DGDZVP(Ru)[6-31+G(d,p)] basis set type of systems.

Bonds	ρ(r)	$\nabla^2\rho(r)$	Ellipticity	K	BPL - GBL_I	V	G	L	GBL_I	V/G
					Complex 1					
Ru1 - C10	0.077	0.235	0.621	0.015	1.50E-02	-0.088	0.073	-0.059	4.210	1.200
Ru1 - C13	0.077	0.231	0.658	0.015	1.84E-02	-0.088	0.073	-0.058	4.220	1.200
Ru1 - C19	0.078	0.237	1.030	0.015	1.99E-02	-0.089	0.074	-0.059	4.200	1.200
Ru1 - Cl22	0.073	0.216	0.162	0.011	1.06E-03	-0.075	0.065	-0.054	4.520	1.160
Ru1 - N17	0.082	0.415	0.428	0.005	1.88E-03	-0.114	0.109	-0.104	4.040	1.050
Ru1 - N12	0.082	0.417	0.417	0.005	2.00E-03	-0.114	0.109	-0.104	4.040	1.050
					Complex 2					
Ru1 - C7	0.077	0.222	0.399	0.015	9.17E-03	-0.086	0.071	-0.056	4.220	1.220
Ru1 - C14	0.076	0.223	0.786	0.014	1.17E-02	-0.084	0.070	-0.056	4.230	1.200
Ru1 - C18	0.077	0.222	0.400	0.015	9.20E-03	-0.086	0.071	-0.056	4.220	1.220
Ru1 - Cl10	0.073	0.214	0.172	0.011	6.59E-04	-0.075	0.064	-0.053	4.530	1.170
Ru1 - N11	0.094	0.445	0.319	0.011	5.10E-03	-0.133	0.122	-0.111	3.960	1.090
Ru1 - N16	0.093	0.446	0.319	0.011	5.36E-03	-0.133	0.122	-0.111	3.960	1.090
					Complex 3					
Ru1 - C13	0.074	0.248	1.930	0.012	5.19E-02	-0.086	0.074	-0.062	4.230	1.160
Ru1 - C14	0.072	0.240	1.600	0.011	3.01E-02	-0.083	0.071	-0.060	4.250	1.160
Ru1 - C18	0.074	0.246	1.800	0.012	4.85E-02	-0.086	0.074	-0.062	4.230	1.170
Ru1 - C23	0.072	0.241	2.010	0.011	3.73E-02	-0.082	0.071	-0.060	4.260	1.150
Ru1 - C21	0.071	0.241	2.940	0.011	8.17E-02	-0.081	0.071	-0.060	4.280	1.150
Ru1 - C25	0.071	0.238	2.000	0.011	5.91E-02	-0.082	0.070	-0.059	4.270	1.160
Ru1 - Cl7	0.073	0.222	0.195	0.011	7.90E-05	-0.077	0.066	-0.055	4.520	1.160
Ru1 - N10	0.083	0.418	0.434	0.006	3.61E-03	-0.116	0.110	-0.105	4.040	1.050
Ru1 - N16	0.082	0.418	0.439	0.006	3.50E-03	-0.116	0.110	-0.105	4.040	1.050
					Complex 4					
Ru1 - C2	0.070	0.240	9.190	0.009	1.67E-01	-0.079	0.069	-0.060	4.280	1.130
Ru1 - C3	0.072	0.235	1.560	0.012	2.42E-02	-0.082	0.070	-0.059	4.260	1.170
Ru1 - C4	0.070	0.241	14.500	0.009	1.92E-01	-0.079	0.069	-0.060	4.280	1.130
Ru1 - C5	0.075	0.241	1.670	0.013	3.95E-02	-0.087	0.074	-0.060	4.240	1.180
Ru1 - C6	0.073	0.234	1.530	0.012	2.38E-02	-0.082	0.070	-0.059	4.260	1.170
Ru1 - C7	0.075	0.242	1.720	0.013	4.08E-02	-0.087	0.074	-0.060	4.240	1.180
Ru1 - N10	0.080	0.372	0.185	0.006	2.11E-02	-0.105	0.099	-0.093	4.090	1.060
Ru1 - N13	0.080	0.372	0.185	0.006	2.11E-02	-0.105	0.099	-0.093	4.090	1.060
Ru1 - N15	0.097	0.433	0.314	0.013	1.50E-02	-0.135	0.122	-0.108	3.940	1.110
					Complex 5					
Ru1 - C18	0.073	0.238	1.790	0.012	4.69E-02	-0.084	0.072	-0.060	4.260	1.170
Ru1 - C20	0.070	0.227	1.520	0.011	2.19E-02	-0.078	0.068	-0.057	4.290	1.160
Ru1 - C22	0.073	0.238	1.720	0.013	4.50E-02	-0.084	0.072	-0.059	4.260	1.170
Ru1 - C26	0.070	0.228	1.550	0.011	2.23E-02	-0.078	0.068	-0.057	4.290	1.160
Ru1 - N14	0.084	0.372	0.146	0.008	1.83E-02	-0.109	0.101	-0.093	4.070	1.080
Ru1 - N15	0.109	0.469	0.285	0.021	9.59E-03	-0.158	0.138	-0.117	3.850	1.150
Ru1 - N21	0.084	0.371	0.144	0.008	1.83E-02	-0.109	0.101	-0.093	4.070	1.080

ρ(r) is electron density, $\nabla^2\rho$ is the Laplancian of ρ(r), BPL – GBL_I is Bond strain, V is virial field (potential energy density), G is Lagrangian form of kinetic energy density, K is hamiltonian form of kinetic energy density, L (i.e. K – G) is lagrangian density which is (-1/4) $\nabla^2\rho$ while "Ratio" is V/G i.e. PE/KE (the higher its magnitude the stronger the Bond).

Table 3.46: Selected bond properties involving ruthenium or hydrogen bond (Bonds with superscript "#") obtained through QTAIM analysis of 3-21G basis set type of systems.

Bonds	ρ(r)	$\nabla^2\rho(r)$	Ellipticity	K	BPL - GBL_I	V	G	L	GBL_I	V/G
					Complex 1					
Ru1 - C9	6.88E-02	2.75E-01	1.41E+00	7.05E-03	3.42E-02	-8.28E-02	7.58E-02	-6.87E-02	4.26E+00	1.09E+00
Ru1 - C10	7.31E-02	2.61E-01	3.77E-01	9.55E-03	1.79E-02	-8.43E-02	7.47E-02	-6.52E-02	4.22E+00	1.13E+00
Ru1 - C13	7.36E-02	2.58E-01	3.43E-01	9.97E-03	1.53E-02	-8.45E-02	7.46E-02	-6.46E-02	4.22E+00	1.13E+00
Ru1 - C16	7.24E-02	2.78E-01	7.42E-01	8.74E-03	2.80E-02	-8.69E-02	7.81E-02	-6.94E-02	4.21E+00	1.11E+00
Ru1 - C18	7.00E-02	2.81E-01	1.10E+00	7.53E-03	3.15E-02	-8.52E-02	7.77E-02	-7.02E-02	4.23E+00	1.10E+00
Ru1 - C19	7.45E-02	2.61E-01	4.84E-01	1.02E-02	1.71E-02	-8.56E-02	7.54E-02	-6.52E-02	4.20E+00	1.14E+00
Ru1 - Cl22	6.39E-02	1.89E-01	1.38E-01	7.52E-03	1.02E-03	-6.23E-02	5.48E-02	-4.72E-02	4.62E+00	1.14E+00
Ru1 - N12	8.34E-02	4.05E-01	3.50E-01	5.05E-03	3.38E-03	-1.11E-01	1.06E-01	-1.01E-01	4.03E+00	1.05E+00
Ru1 - N17	8.35E-02	4.09E-01	3.60E-01	4.98E-03	3.48E-03	-1.12E-01	1.07E-01	-1.02E-01	4.03E+00	1.05E+00
O2 - H24#	1.68E-02	7.59E-02	2.73E-01	-2.33E-03	5.97E-02	-1.43E-02	1.66E-02	-1.90E-02	4.30E+00	8.60E-01
					Complex 2					
Ru1 - C7	7.50E-02	2.48E-01	1.82E-01	1.10E-02	9.64E-03	-8.41E-02	7.31E-02	-6.20E-02	4.21E+00	1.15E+00
Ru1 - C8	6.73E-02	2.88E-01	2.43E+00	6.45E-03	3.28E-02	-8.50E-02	7.86E-02	-7.21E-02	4.25E+00	1.08E+00
Ru1 - C13	6.58E-02	2.83E-01	4.46E+00	5.63E-03	3.10E-02	-8.21E-02	7.65E-02	-7.08E-02	4.29E+00	1.07E+00
Ru1 - C14	7.41E-02	2.46E-01	4.02E-01	1.05E-02	1.15E-02	-8.25E-02	7.19E-02	-6.14E-02	4.22E+00	1.15E+00
Ru1 - C19	6.73E-02	2.88E-01	2.44E+00	6.45E-03	3.36E-02	-8.50E-02	7.85E-02	-7.21E-02	4.25E+00	1.08E+00
Ru1 - C18	7.50E-02	2.48E-01	1.82E-01	1.10E-02	9.69E-03	-8.41E-02	7.31E-02	-6.21E-02	4.21E+00	1.15E+00
Ru1 - Cl10	6.39E-02	1.88E-01	1.38E-01	7.53E-03	4.15E-04	-6.20E-02	5.44E-02	-4.69E-02	4.62E+00	1.14E+00
Ru1 - N11	9.24E-02	4.34E-01	2.67E-01	7.79E-03	6.65E-03	-1.24E-01	1.16E-01	-1.09E-01	3.97E+00	1.07E+00
Ru1 - N16	9.24E-02	4.35E-01	2.66E-01	7.77E-03	6.94E-03	-1.24E-01	1.16E-01	-1.09E-01	3.97E+00	1.07E+00
					Complex 3					
Ru1 - C13	7.25E-02	2.66E-01	6.54E-01	9.16E-03	2.49E-02	-8.48E-02	7.56E-02	-6.65E-02	4.22E+00	1.12E+00
Ru1 - C14	7.01E-02	2.58E-01	6.34E-01	8.05E-03	2.16E-02	-8.06E-02	7.25E-02	-6.45E-02	4.25E+00	1.11E+00
Ru1 - C18	7.30E-02	2.62E-01	5.70E-01	9.58E-03	2.18E-02	-8.47E-02	7.51E-02	-6.55E-02	4.22E+00	1.13E+00
Ru1 - C23	6.93E-02	2.61E-01	8.28E-01	7.55E-03	2.54E-02	-8.02E-02	7.27E-02	-6.51E-02	4.26E+00	1.10E+00
Ru1 - C21	6.93E-02	2.60E-01	7.20E-01	7.71E-03	2.33E-02	-8.04E-02	7.27E-02	-6.50E-02	4.27E+00	1.11E+00
Ru1 - C25	7.01E-02	2.57E-01	5.49E-01	8.21E-03	2.01E-02	-8.06E-02	7.24E-02	-6.42E-02	4.26E+00	1.11E+00
Ru1 - Cl7	6.39E-02	1.93E-01	1.65E-01	7.45E-03	7.57E-04	-6.31E-02	5.57E-02	-4.82E-02	4.61E+00	1.13E+00
Ru1 - N10	8.14E-02	4.03E-01	3.71E-01	4.63E-03	3.42E-03	-1.10E-01	1.05E-01	-1.01E-01	4.06E+00	1.04E+00
Ru1 - N16	8.26E-02	4.08E-01	3.72E-01	4.93E-03	3.48E-03	-1.12E-01	1.07E-01	-1.02E-01	4.04E+00	1.05E+00
O2 - H31#	1.60E-02	7.57E-02	7.35E-01	-2.64E-03	1.49E-01	-1.37E-02	1.63E-02	-1.89E-02	4.35E+00	8.38E-01
O28 - H36#	1.82E-02	8.48E-02	3.61E-01	-2.29E-03	5.16E-02	-1.66E-02	1.89E-02	-2.12E-02	4.20E+00	8.79E-01
					Complex 4					
Ru1 - C2	6.81E-02	2.50E-01	8.34E-01	7.33E-03	3.16E-02	-7.71E-02	6.98E-02	-6.24E-02	4.27E+00	1.11E+00
Ru1 - C3	7.01E-02	2.51E-01	6.89E-01	8.28E-03	2.14E-02	-7.94E-02	7.11E-02	-6.28E-02	4.25E+00	1.12E+00
Ru1 - C4	6.80E-02	2.50E-01	8.52E-01	7.29E-03	3.21E-02	-7.71E-02	6.98E-02	-6.25E-02	4.27E+00	1.10E+00
Ru1 - N15	9.48E-02	4.31E-01	2.81E-01	8.44E-03	1.65E-02	-1.25E-01	1.16E-01	-1.08E-01	3.95E+00	1.07E+00
Ru1 - C5	7.19E-02	2.63E-01	5.67E-01	8.84E-03	2.32E-02	-8.35E-02	7.46E-02	-6.58E-02	4.23E+00	1.12E+00
Ru1 - C6	7.01E-02	2.51E-01	6.77E-01	8.31E-03	2.12E-02	-7.93E-02	7.10E-02	-6.27E-02	4.25E+00	1.12E+00
Ru1 - C7	7.19E-02	2.63E-01	5.80E-01	8.78E-03	2.35E-02	-8.34E-02	7.46E-02	-6.59E-02	4.23E+00	1.12E+00
Ru1 - N10	7.92E-02	3.70E-01	2.39E-01	4.45E-03	1.84E-02	-1.01E-01	9.69E-02	-9.24E-02	4.09E+00	1.05E+00
Ru1 - N13	7.91E-02	3.69E-01	2.39E-01	4.45E-03	1.84E-02	-1.01E-01	9.68E-02	-9.24E-02	4.09E+00	1.05E+00
					Complex 5					
Ru1 - C18	7.03E-02	2.60E-01	6.01E-01	8.16E-03	2.34E-02	-8.13E-02	7.31E-02	-6.50E-02	4.25E+00	1.11E+00
Ru1 - C20	6.77E-02	2.44E-01	7.06E-01	7.52E-03	2.08E-02	-7.60E-02	6.85E-02	-6.10E-02	4.29E+00	1.11E+00
Ru1 - C22	7.03E-02	2.60E-01	5.91E-01	8.20E-03	2.31E-02	-8.13E-02	7.31E-02	-6.49E-02	4.25E+00	1.11E+00
Ru1 - C23	6.44E-02	2.42E-01	1.52E+00	5.76E-03	5.04E-02	-7.20E-02	6.62E-02	-6.05E-02	4.33E+00	1.09E+00
Ru1 - C27	6.45E-02	2.42E-01	1.48E+00	5.81E-03	4.95E-02	-7.20E-02	6.62E-02	-6.04E-02	4.33E+00	1.09E+00

Ru1 - C26	6.77E-02	2.44E-01	7.14E-01	7.51E-03	2.10E-02	-7.61E-02	6.85E-02	-6.10E-02	4.29E+00	1.11E+00
Ru1 - N14	8.27E-02	3.71E-01	1.83E-01	5.61E-03	1.65E-02	-1.04E-01	9.85E-02	-9.28E-02	4.08E+00	1.06E+00
Ru1 - N15	1.06E-01	4.68E-01	2.60E-01	1.30E-02	1.17E-02	-1.43E-01	1.30E-01	-1.17E-01	3.86E+00	1.10E+00
Ru1 - N21	8.26E-02	3.70E-01	1.81E-01	5.60E-03	1.65E-02	-1.04E-01	9.82E-02	-9.26E-02	4.08E+00	1.06E+00

10

11

Table 3.47: Selected bond properties involving ruthenium or hydrogen bond (Bonds with superscript "#") obtained through QTAIM analysis of ECP(Ru)[6-31+G(d,p)] basis set type of systems.

					Complex 1					
Bonds	$\rho(r)$	$\nabla^2\rho(r)$	Ellipticity	K	BPL - GBL_I	V	G	L	GBL_I	V/G
Ru1 - C19	7.99E-02	2.16E-01	1.04E+00	1.92E-02	1.50E-02	-9.24E-02	7.31E-02	-5.39E-02	4.20E+00	1.26E+00
Ru1 - C10	7.88E-02	2.13E-01	6.80E-01	1.90E-02	1.80E-02	-9.10E-02	7.21E-02	-5.31E-02	4.21E+00	1.26E+00
Ru1 - C13	7.87E-02	2.11E-01	7.01E-01	1.89E-02	1.88E-02	-9.05E-02	7.16E-02	-5.27E-02	4.22E+00	1.26E+00
Ru1 - C18	7.45E-02	2.46E-01	4.50E+00	1.50E-02	4.94E-02	-9.17E-02	7.66E-02	-6.16E-02	4.23E+00	1.20E+00
Ru1 - C16	7.65E-02	2.44E-01	3.71E+00	1.60E-02	6.56E-02	-9.28E-02	7.68E-02	-6.09E-02	4.21E+00	1.21E+00
Ru1 - Cl22	7.48E-02	1.84E-01	1.34E-01	1.54E-02	1.27E-03	-7.69E-02	6.15E-02	-4.61E-02	4.52E+00	1.25E+00
Ru1 - N17	8.41E-02	3.65E-01	3.74E-01	1.10E-02	2.72E-03	-1.13E-01	1.02E-01	-9.13E-02	4.04E+00	1.11E+00
Ru1 - N12	8.46E-02	3.67E-01	3.65E-01	1.12E-02	2.97E-03	-1.14E-01	1.03E-01	-9.18E-02	4.04E+00	1.11E+00
O2 - H24#	1.01E-02	3.87E-02	5.82E-01	-1.65E-03	2.04E-01	-6.37E-03	8.02E-03	-9.67E-03	4.72E+00	7.94E-01
O2 - H29#	1.00E-02	3.83E-02	6.32E-01	-1.66E-03	2.11E-01	-6.26E-03	7.92E-03	-9.58E-03	4.73E+00	7.91E-01
					Complex 2					
Ru1 - C7	7.86E-02	2.02E-01	4.65E-01	1.93E-02	9.77E-03	-8.92E-02	6.99E-02	-5.05E-02	4.22E+00	1.28E+00
Ru1 - C14	7.78E-02	2.04E-01	8.95E-01	1.82E-02	1.04E-02	-8.74E-02	6.92E-02	-5.09E-02	4.23E+00	1.26E+00
Ru1 - C18	7.85E-02	2.02E-01	4.66E-01	1.93E-02	9.88E-03	-8.92E-02	6.99E-02	-5.06E-02	4.22E+00	1.28E+00
Ru1 - Cl10	7.47E-02	1.82E-01	1.35E-01	1.54E-02	6.75E-04	-7.62E-02	6.08E-02	-4.54E-02	4.53E+00	1.25E+00
Ru1 - N11	9.63E-02	3.90E-01	2.81E-01	1.76E-02	7.50E-03	-1.33E-01	1.15E-01	-9.76E-02	3.96E+00	1.15E+00
Ru1 - N16	9.62E-02	3.91E-01	2.82E-01	1.76E-02	7.86E-03	-1.33E-01	1.15E-01	-9.77E-02	3.96E+00	1.15E+00
H34 - H38#	9.33E-03	4.07E-02	2.60E+00	-2.74E-03	6.30E-01	-4.69E-03	7.43E-03	-1.02E-02	4.08E+00	6.32E-01
					Complex 3					
Ru1 - C13	7.67E-02	2.23E-01	1.64E+00	1.70E-02	3.30E-02	-8.98E-02	7.28E-02	-5.59E-02	4.23E+00	1.23E+00
Ru1 - C14	7.43E-02	2.17E-01	1.48E+00	1.58E-02	2.56E-02	-8.59E-02	7.01E-02	-5.43E-02	4.25E+00	1.23E+00
Ru1 - C18	7.68E-02	2.22E-01	1.57E+00	1.71E-02	3.14E-02	-8.95E-02	7.25E-02	-5.54E-02	4.23E+00	1.24E+00
Ru1 - C23	7.38E-02	2.19E-01	1.73E+00	1.54E-02	2.83E-02	-8.55E-02	7.01E-02	-5.47E-02	4.26E+00	1.22E+00
Ru1 - C21	7.27E-02	2.21E-01	2.31E+00	1.45E-02	4.99E-02	-8.41E-02	6.96E-02	-5.52E-02	4.28E+00	1.21E+00
Ru1 - C25	7.31E-02	2.18E-01	1.79E+00	1.49E-02	4.02E-02	-8.43E-02	6.94E-02	-5.45E-02	4.27E+00	1.21E+00
Ru1 - Cl7	7.50E-02	1.88E-01	1.41E-01	1.55E-02	6.90E-05	-7.80E-02	6.26E-02	-4.71E-02	4.52E+00	1.25E+00
Ru1 - N10	8.54E-02	3.66E-01	3.58E-01	1.23E-02	3.22E-03	-1.16E-01	1.04E-01	-9.14E-02	4.04E+00	1.12E+00
Ru1 - N16	8.54E-02	3.66E-01	3.61E-01	1.23E-02	3.18E-03	-1.16E-01	1.04E-01	-9.14E-02	4.04E+00	1.12E+00
O2 - H31#	1.65E-02	6.08E-02	4.07E-01	-1.82E-03	1.29E-01	-1.16E-02	1.34E-02	-1.52E-02	4.27E+00	8.64E-01
O28 - H36#	1.69E-02	6.18E-02	3.41E-01	-1.74E-03	1.06E-01	-1.20E-02	1.37E-02	-1.55E-02	4.23E+00	8.73E-01
					Complex 4					
Ru1 - C2	7.22E-02	2.18E-01	3.44E+00	1.39E-02	7.45E-02	-8.23E-02	6.84E-02	-5.45E-02	4.28E+00	1.20E+00
Ru1 - C3	7.48E-02	2.11E-01	1.49E+00	1.62E-02	2.51E-02	-8.53E-02	6.90E-02	-5.28E-02	4.26E+00	1.23E+00
Ru1 - C4	7.21E-02	2.18E-01	3.66E+00	1.38E-02	7.78E-02	-8.23E-02	6.84E-02	-5.46E-02	4.28E+00	1.20E+00
Ru1 - C5	7.67E-02	2.21E-01	1.46E+00	1.72E-02	3.16E-02	-8.96E-02	7.24E-02	-5.52E-02	4.24E+00	1.24E+00
Ru1 - C6	7.48E-02	2.11E-01	1.46E+00	1.63E-02	2.47E-02	-8.52E-02	6.90E-02	-5.27E-02	4.26E+00	1.24E+00
Ru1 - C7	7.67E-02	2.21E-01	1.50E+00	1.71E-02	3.22E-02	-8.96E-02	7.24E-02	-5.53E-02	4.24E+00	1.24E+00
Ru1 - N10	8.22E-02	3.29E-01	1.93E-01	1.17E-02	2.05E-02	-1.06E-01	9.41E-02	-8.24E-02	4.09E+00	1.12E+00
Ru1 - N15	9.93E-02	3.83E-01	3.00E-01	1.97E-02	1.87E-02	-1.35E-01	1.16E-01	-9.59E-02	3.94E+00	1.17E+00

Ru1 - N13	8.21E-02	3.29E-01	1.93E-01	1.17E-02	2.05E-02	-1.06E-01	9.40E-02	-8.23E-02	4.09E+00	1.12E+00
					Complex 5					
Ru1 - C18	7.48E-02	2.18E-01	1.51E+00	1.62E-02	3.13E-02	-8.69E-02	7.07E-02	-5.45E-02	4.26E+00	1.23E+00
Ru1 - C20	7.22E-02	2.05E-01	1.50E+00	1.50E-02	2.22E-02	-8.13E-02	6.63E-02	-5.13E-02	4.29E+00	1.23E+00
Ru1 - C22	7.49E-02	2.18E-01	1.47E+00	1.63E-02	3.04E-02	-8.70E-02	7.07E-02	-5.44E-02	4.26E+00	1.23E+00
Ru1 - C26	7.22E-02	2.06E-01	1.52E+00	1.50E-02	2.24E-02	-8.14E-02	6.64E-02	-5.14E-02	4.29E+00	1.23E+00
Ru1 - N14	8.63E-02	3.26E-01	1.53E-01	1.40E-02	1.68E-02	-1.09E-01	9.55E-02	-8.15E-02	4.07E+00	1.15E+00
Ru1 - N15	1.12E-01	4.15E-01	2.63E-01	2.71E-02	1.17E-02	-1.58E-01	1.31E-01	-1.04E-01	3.85E+00	1.21E+00
Ru1 - N21	8.62E-02	3.25E-01	1.51E-01	1.39E-02	1.69E-02	-1.09E-01	9.52E-02	-8.13E-02	4.07E+00	1.15E+00

Table 3.48: The correlation between the computed Bond properties of complexes 1 to 5

	1			**2**			**3**			**4**			**5**		
	$\nabla^2\rho(r)$	Ellipticity	GBL_I	$\nabla^2\rho(r)$	Ellipticity	GBL_I	$\nabla^2\rho(r)$	Ellipticity	GBL_I	$\nabla^2\rho(r)$	Ellipticity	GBL_I	$\nabla^2\rho(r)$	Ellipticity	GBL_I
$\rho(r)$	-0.71	-0.71	-0.89	-0.65	-0.67	-0.86	-0.73	-0.69	-0.90	-0.88	-0.54	-0.88	-0.77	-0.73	-0.84
$\nabla^2\rho(r)$	1.00	0.74	0.87	1.00	0.51	0.83	1.00	0.64	0.87	1.00	0.48	0.96	1.00	0.64	0.89
Ellipticity	0.74	1.00	0.81	0.51	1.00	0.66	0.64	1.00	0.73	0.48	1.00	0.54	0.64	1.00	0.78
K	-0.54	-0.63	-0.76	-0.49	-0.51	-0.72	-0.59	-0.60	-0.79	-0.74	-0.46	-0.75	-0.59	-0.58	-0.69
BPL.GBL_I	0.35	0.41	0.59	0.23	0.87	0.32	0.55	0.62	0.70	0.58	0.98	0.62	0.73	0.89	0.82
V	0.17	0.39	0.49	0.11	0.35	0.44	0.24	0.42	0.54	0.44	0.35	0.48	0.22	0.38	0.39
G	0.29	-0.04	-0.09	0.33	-0.11	-0.06	0.24	-0.11	-0.12	0.12	-0.10	0.05	0.27	-0.06	0.05
L	-1.00	-0.74	-0.87	-1.00	-0.51	-0.83	-1.00	-0.64	-0.87	-1.00	-0.48	-0.96	-1.00	-0.64	-0.89
GBL_I	0.87	0.81	1.00	0.83	0.66	1.00	0.87	0.73	1.00	0.96	0.54	1.00	0.89	0.78	1.00
V/G	-0.82	-0.67	-0.77	-0.78	-0.52	-0.78	-0.80	-0.51	-0.80	-0.75	-0.31	-0.79	-0.74	-0.50	-0.80

Table 3.49: The Intra and inter atomic properties of atoms involve in Metal-Ligand and hydrogen bonding (atoms with superscript "#") of systems treated with DGDZVP(Ru)[6-31+G(d,p)] basis set using QTAIM analysis

						Complex 1							
	q(A)	L(A)	K(A)	K_Scaled(A)	μ_{Intra}(A)	μ_{Bond}(A)	|μ(A)|	N(A)	LI(A)	%Loc(A)	DI(A,A')/2	%Deloc(A,A')	Vol(A),0.001
Ru1	0.950	0.001	4440.000	-4450.000	0.126	1.140	1.200	43.100	40.500	94.100	2.540	5.900	101.000
C9	-0.063	0.000	37.800	-37.900	0.126	0.035	0.093	6.060	3.970	65.600	2.090	34.400	73.800
C10	-0.047	0.000	37.800	-37.900	0.089	0.080	0.061	6.050	3.960	65.500	2.090	34.500	71.400
C13	-0.050	0.000	37.800	-37.900	0.089	0.090	0.102	6.050	3.960	65.500	2.090	34.500	71.600
C16	-0.051	0.000	37.800	-37.900	0.134	0.099	0.055	6.050	3.970	65.600	2.080	34.400	73.700
C18	-0.058	0.000	37.800	-37.900	0.127	0.084	0.068	6.060	3.980	65.600	2.080	34.400	74.800
C19	-0.029	0.000	37.800	-37.900	0.118	0.136	0.102	6.030	3.950	65.500	2.080	34.500	69.900
Cl22	-0.527	0.000	459.000	-461.000	0.061	1.260	1.290	17.500	16.900	96.300	0.646	3.680	232.000
N12	-0.759	0.000	54.800	-54.900	0.695	0.810	0.658	7.760	5.900	76.100	1.860	23.900	78.100
N17	-0.759	0.000	54.800	-54.900	0.695	0.790	0.617	7.760	5.900	76.100	1.860	23.900	78.000
						Complex 2							
Ru1	0.959	0.000	4440.000	-4450.000	0.085	1.120	1.180	43.000	40.500	94.000	2.570	5.960	104.000
C7	-0.053	0.000	37.800	-38.000	0.075	0.066	0.061	6.050	3.960	65.400	2.090	34.600	70.100

C8	-0.063	0.000	37.800	-37.900	0.137	0.079	0.082	6.060	3.980	65.600	2.080	34.400	74.600
C13	-0.053	0.000	37.800	-37.900	0.146	0.068	0.078	6.050	3.970	65.600	2.080	34.400	76.400
C14	-0.027	-0.001	37.800	-37.900	0.111	0.144	0.092	6.030	3.950	65.500	2.080	34.500	69.600
C18	-0.054	-0.001	37.800	-38.000	0.073	0.087	0.093	6.050	3.960	65.400	2.090	34.600	70.200
C19	-0.063	0.000	37.800	-37.900	0.137	0.066	0.074	6.060	3.980	65.600	2.080	34.400	74.600
Cl10	-0.521	0.000	459.000	-461.000	0.019	1.250	1.260	17.500	16.900	96.400	0.623	3.560	237.000
N11	-1.220	0.000	55.100	-55.200	0.223	0.743	0.542	8.220	6.360	77.400	1.860	22.600	82.100
N16	-1.220	0.000	55.100	-55.200	0.224	0.710	0.510	8.220	6.360	77.400	1.860	22.600	82.100
Complex 3													
Ru1	0.955	0.000	4440.000	-4450.000	0.090	0.833	0.840	43.000	40.500	94.100	2.520	5.860	99.900
C13	-0.040	0.000	37.800	-38.000	0.121	0.145	0.081	6.040	3.960	65.500	2.080	34.500	70.600
C14	-0.049	0.000	37.900	-38.000	0.121	0.281	0.400	6.050	3.970	65.600	2.080	34.400	69.800
C18	-0.040	0.000	37.800	-38.000	0.118	0.136	0.086	6.040	3.960	65.500	2.080	34.500	70.700
C21	-0.060	0.000	37.800	-38.000	0.099	0.102	0.132	6.060	3.970	65.500	2.090	34.500	73.600
C23	-0.050	0.000	37.900	-38.000	0.128	0.287	0.412	6.050	3.970	65.600	2.080	34.400	70.200
C25	-0.059	0.000	37.800	-38.000	0.096	0.113	0.140	6.060	3.970	65.500	2.090	34.500	73.300
Cl7	-0.533	0.000	459.000	-461.000	0.035	1.270	1.300	17.500	16.900	96.400	0.631	3.600	236.000
N10	-1.200	0.000	55.000	-55.200	0.200	1.140	0.947	8.200	6.360	77.500	1.840	22.500	83.000
N16	-1.200	0.000	55.000	-55.200	0.201	1.100	0.912	8.200	6.360	77.500	1.840	22.500	83.000
Complex 4													
Ru1	0.992	-0.001	4430.000	-4450.000	0.147	0.442	0.399	43.000	40.600	94.300	2.460	5.710	110.000
C2	-0.046	0.000	37.800	-37.900	0.132	0.071	0.066	6.050	3.970	65.600	2.080	34.400	73.300
C3	-0.044	0.000	37.800	-37.900	0.107	0.081	0.066	6.040	3.960	65.600	2.080	34.400	70.700
C4	-0.046	0.000	37.800	-37.900	0.133	0.087	0.092	6.050	3.970	65.600	2.080	34.400	73.400
C5	-0.034	0.000	37.800	-37.900	0.127	0.096	0.091	6.030	3.960	65.600	2.080	34.400	72.700
C6	-0.044	0.000	37.800	-37.900	0.106	0.088	0.081	6.040	3.960	65.600	2.080	34.400	70.600
C7	-0.034	0.000	37.800	-37.900	0.127	0.100	0.098	6.030	3.960	65.600	2.080	34.400	72.600
N10	-0.771	0.000	54.700	-54.900	0.728	0.796	0.594	7.770	5.950	76.600	1.820	23.400	82.900
N13	-0.771	0.000	54.700	-54.900	0.728	0.791	0.581	7.770	5.950	76.600	1.820	23.400	82.900
N15	-1.240	0.000	55.100	-55.300	0.186	0.447	0.331	8.240	6.400	77.700	1.840	22.300	80.600
Complex 5													
Ru1	0.982	0.001	4430.000	-4450.000	0.192	0.583	0.562	43.000	40.500	94.200	2.500	5.820	108.000
C18	-0.036	0.000	37.800	-37.900	0.126	0.082	0.056	6.040	3.960	65.600	2.080	34.400	72.600
C20	-0.048	0.000	37.800	-38.000	0.106	0.095	0.089	6.050	3.970	65.600	2.080	34.400	70.900
C22	-0.036	0.000	37.800	-37.900	0.127	0.085	0.063	6.040	3.960	65.600	2.080	34.400	72.600
C23	-0.049	0.000	37.800	-37.900	0.132	0.068	0.081	6.050	3.970	65.600	2.080	34.400	73.000
C26	-0.048	-0.001	37.800	-38.000	0.107	0.128	0.127	6.050	3.970	65.600	2.080	34.400	71.000
C27	-0.049	0.000	37.800	-37.900	0.131	0.091	0.107	6.050	3.970	65.600	2.080	34.400	72.900
N14	-1.230	0.000	55.000	-55.200	0.199	0.621	0.462	8.230	6.400	77.800	1.830	22.200	85.800
N15	-1.230	0.000	55.100	-55.300	0.216	0.369	0.232	8.230	6.350	77.200	1.880	22.800	79.000
N21	-1.230	0.000	55.000	-55.200	0.199	0.517	0.370	8.230	6.400	77.800	1.830	22.200	85.800

q(A) is net charge of atom A, L(A) is Lagrangian of Atom A, N(A) is average number of electrons in atom A, K(A) is electronic kinetic energy of atom A (Hamiltonian Form), %Loc(A) is percentage of average number of electrons localized in atom A, K_Scaled(A) is approximation to virial-based total energy of atom A, μ_{Intra}(A) is magnitude of Intraatomic dipole moment of atom A, Ee(A) is contribution of atom A to electronic energy of molecule, %Deloc(A,A') is the percentage of electron delocalization index of atom A and Vol(A) is the volume bounded by an isosurface of the electron density distribution (0.001) and by interatomic surfaces of atom A.

Table 3.50: The Intra and inter atomic properties of atoms involve in Metal-Ligand and hydrogen bonding (atoms with superscript "#") of systems treated with 3-21G basis set using QTAIM analysis

Complex 1													
	q(A)	L(A)	K(A)	K_Scaled(A)	μ_{Intra}(A)	μ_{Bond}(A)	|μ(A)|	N(A)	LI(A)	%Loc(A)	DI(A,A')/2	%Deloc(A,A')	Vol(A),0.001
Ru1	8.63E-01	5.52E-04	4.40E+03	-4.43E+03	9.01E-02	1.10E+00	1.19E+00	4.31E+01	4.07E+01	9.43E+01	2.46E+00	5.71E+00	9.73E+01
C9	-1.14E-01	-7.00E-05	3.76E+01	-3.78E+01	2.51E-01	1.18E-01	1.35E-01	6.11E+00	4.04E+00	6.60E+01	2.08E+00	3.40E+01	7.66E+01
C10	-1.04E-01	-1.97E-04	3.76E+01	-3.78E+01	2.26E-01	1.65E-01	9.47E-02	6.10E+00	4.03E+00	6.61E+01	2.07E+00	3.39E+01	7.49E+01
C13	-1.09E-01	-1.11E-04	3.76E+01	-3.78E+01	2.25E-01	1.41E-01	1.16E-01	6.11E+00	4.03E+00	6.60E+01	2.08E+00	3.40E+01	7.52E+01
C16	-9.09E-02	-5.60E-05	3.76E+01	-3.78E+01	2.72E-01	2.03E-01	9.32E-02	6.09E+00	4.02E+00	6.60E+01	2.07E+00	3.40E+01	7.57E+01
C18	-1.04E-01	-4.80E-05	3.76E+01	-3.78E+01	2.56E-01	1.64E-01	1.14E-01	6.10E+00	4.04E+00	6.61E+01	2.07E+00	3.39E+01	7.71E+01
C19	-8.40E-02	-1.10E-04	3.76E+01	-3.78E+01	2.53E-01	2.18E-01	9.99E-02	6.08E+00	4.02E+00	6.60E+01	2.07E+00	3.40E+01	7.33E+01
Cl22	-4.89E-01	6.20E-05	4.57E+02	-4.59E+02	1.50E-01	1.18E+00	1.33E+00	1.75E+01	1.69E+01	9.65E+01	6.10E-01	3.49E+00	2.29E+02
N12	-6.13E-01	4.00E-05	5.43E+01	-5.45E+01	6.55E-01	5.13E-01	6.53E-01	7.61E+00	5.75E+00	7.56E+01	1.86E+00	2.44E+01	7.39E+01
N17	-6.03E-01	1.41E-04	5.43E+01	-5.45E+01	6.57E-01	6.91E-01	8.83E-01	7.60E+00	5.74E+00	7.55E+01	1.86E+00	2.45E+01	7.39E+01
$O2^{\#}$	-8.53E-01	8.40E-05	7.47E+01	-7.51E+01	1.11E-01	1.01E+00	9.06E-01	8.85E+00	7.78E+00	8.79E+01	1.07E+00	1.21E+01	1.04E+02
$H24^{\#}$	2.00E-01	3.70E-05	5.27E-01	-5.30E-01	1.25E-01	4.02E-01	4.44E-01	8.00E-01	2.92E-01	3.66E+01	5.07E-01	6.34E+01	3.41E+01
Complex 2													
Ru1	8.62E-01	4.02E-04	4.40E+03	-4.43E+03	7.85E-02	1.09E+00	1.17E+00	4.31E+01	4.06E+01	9.42E+01	2.49E+00	5.78E+00	9.91E+01
C7	-1.16E-01	-8.10E-05	3.76E+01	-3.78E+01	2.00E-01	1.33E-01	8.08E-02	6.12E+00	4.04E+00	6.60E+01	2.08E+00	3.40E+01	7.31E+01
C8	-1.05E-01	8.60E-05	3.76E+01	-3.78E+01	2.75E-01	1.67E-01	1.24E-01	6.11E+00	4.04E+00	6.61E+01	2.07E+00	3.39E+01	7.72E+01
C13	-9.59E-02	1.57E-04	3.76E+01	-3.78E+01	2.85E-01	1.60E-01	1.31E-01	6.10E+00	4.03E+00	6.61E+01	2.07E+00	3.39E+01	7.87E+01
C14	-8.33E-02	7.10E-05	3.76E+01	-3.78E+01	2.40E-01	2.33E-01	8.95E-02	6.08E+00	4.02E+00	6.60E+01	2.07E+00	3.40E+01	7.24E+01
C18	-1.16E-	-8.80E-	3.76E+0	-	1.99E-	1.29E-	1.08E-	6.12E+0	4.04E+0	6.60E+0	2.08E+0	3.40E+0	7.32E+0

	01	05	1	3.78E+01	01	01	01	0	0	1	0	1	1
C19	-1.05E-01	5.90E-05	3.76E+01	-3.78E+01	2.75E-01	1.55E-01	1.36E-01	6.11E+00	4.04E+00	6.61E+01	2.07E+00	3.39E+01	7.73E+01
Cl10	-4.78E-01	9.30E-05	4.57E+02	-4.59E+02	1.41E-01	1.15E+00	1.29E+00	1.75E+01	1.69E+01	9.66E+01	5.87E-01	3.36E+00	2.34E+02
N11	-9.49E-01	5.00E-05	5.45E+01	-5.48E+01	1.37E-01	5.27E-01	6.40E-01	7.95E+00	6.07E+00	7.63E+01	1.88E+00	2.37E+01	7.74E+01
N16	-9.49E-01	6.00E-05	5.45E+01	-5.48E+01	1.39E-01	4.93E-01	6.04E-01	7.95E+00	6.07E+00	7.63E+01	1.88E+00	2.37E+01	7.75E+01
Complex 3													
Ru1	8.73E-01	-6.31E-04	4.40E+03	-4.43E+03	8.46E-02	7.78E-01	8.55E-01	4.31E+01	4.07E+01	9.43E+01	2.45E+00	5.67E+00	9.61E+01
C13	-7.91E-02	-2.80E-05	3.76E+01	-3.78E+01	2.67E-01	2.44E-01	8.53E-02	6.08E+00	4.01E+00	6.60E+01	2.07E+00	3.40E+01	7.32E+01
C14	-9.33E-02	-4.90E-05	3.76E+01	-3.78E+01	2.41E-01	1.75E-01	4.11E-01	6.09E+00	4.02E+00	6.60E+01	2.07E+00	3.40E+01	7.21E+01
C18	-8.72E-02	8.60E-05	3.76E+01	-3.78E+01	2.57E-01	2.22E-01	9.86E-02	6.09E+00	4.02E+00	6.60E+01	2.07E+00	3.40E+01	7.36E+01
C21	-1.18E-01	-3.70E-05	3.76E+01	-3.78E+01	2.29E-01	1.33E-01	1.79E-01	6.12E+00	4.04E+00	6.61E+01	2.08E+00	3.39E+01	7.64E+01
C23	-9.43E-02	-8.40E-05	3.76E+01	-3.78E+01	2.66E-01	1.53E-01	4.09E-01	6.09E+00	4.03E+00	6.61E+01	2.06E+00	3.39E+01	7.27E+01
C25	-1.17E-01	1.72E-04	3.76E+01	-3.78E+01	2.23E-01	1.37E-01	1.83E-01	6.12E+00	4.04E+00	6.61E+01	2.08E+00	3.39E+01	7.61E+01
Cl7	-4.97E-01	7.30E-05	4.57E+02	-4.59E+02	1.53E-01	1.20E+00	1.35E+00	1.75E+01	1.69E+01	9.66E+01	5.90E-01	3.37E+00	2.32E+02
N10	-9.26E-01	2.83E-04	5.44E+01	-5.47E+01	1.73E-01	7.90E-01	9.41E-01	7.93E+00	6.06E+00	7.65E+01	1.86E+00	2.35E+01	7.82E+01
N16	-9.30E-01	2.81E-04	5.45E+01	-5.47E+01	1.71E-01	7.70E-01	9.13E-01	7.93E+00	6.06E+00	7.65E+01	1.87E+00	2.35E+01	7.78E+01
O2[#]	-8.96E-01	1.68E-04	7.47E+01	-7.51E+01	7.76E-02	1.00E+00	9.29E-01	8.90E+00	7.80E+00	8.77E+01	1.09E+00	1.23E+01	1.04E+02
O28[#]	-8.94E-01	1.36E-04	7.47E+01	-7.51E+01	8.16E-02	9.64E-01	8.86E-01	8.89E+00	7.81E+00	8.78E+01	1.09E+00	1.22E+01	1.05E+02
H31[#]	1.61E-01	3.80E-05	5.47E-01	-5.50E-01	1.38E-01	2.93E-01	3.16E-01	8.39E-01	3.19E-01	3.80E+01	5.20E-01	6.20E+01	3.65E+01
H36[#]	1.77E-01	1.80E-05	5.41E-01	-5.44E-01	1.34E-01	2.70E-01	3.08E-01	8.23E-01	3.05E-01	3.71E+01	5.17E-01	6.29E+01	3.48E+01
Complex 4													
Ru1	9.46E-01	-2.96E-04	4.40E+03	-4.43E+03	1.27E-01	5.11E-01	4.45E-01	4.31E+01	4.07E+01	9.45E+01	2.38E+00	5.52E+00	1.02E+02
C2	-9.53E-02	9.40E-05	3.76E+01	-3.78E+01	2.55E-01	1.64E-01	9.19E-02	6.10E+00	4.03E+00	6.62E+01	2.06E+00	3.38E+01	7.64E+01
C3	-9.30E-02	-9.30E-05	3.76E+01	-3.78E+01	2.35E-01	1.60E-01	1.09E-01	6.09E+00	4.03E+00	6.61E+01	2.06E+00	3.39E+01	7.35E+01

C4	-9.54E-02	-5.80E-05	3.76E+01	-3.78E+01	2.56E-01	1.61E-01	1.18E-01	6.10E+00	4.03E+00	6.62E+01	2.06E+00	3.38E+01	7.65E+01
C5	-8.74E-02	-7.70E-05	3.76E+01	-3.78E+01	2.58E-01	1.66E-01	1.29E-01	6.09E+00	4.03E+00	6.62E+01	2.06E+00	3.38E+01	7.61E+01
C6	-9.30E-02	-5.60E-05	3.76E+01	-3.78E+01	2.34E-01	1.58E-01	1.27E-01	6.09E+00	4.03E+00	6.61E+01	2.06E+00	3.39E+01	7.35E+01
C7	-8.74E-02	-8.00E-05	3.76E+01	-3.78E+01	2.59E-01	1.62E-01	1.46E-01	6.09E+00	4.03E+00	6.62E+01	2.06E+00	3.38E+01	7.61E+01
N10	-6.07E-01	1.22E-04	5.42E+01	-5.45E+01	6.88E-01	5.32E-01	6.51E-01	7.61E+00	5.78E+00	7.60E+01	1.82E+00	2.40E+01	7.84E+01
N13	-6.07E-01	-4.29E-04	5.42E+01	-5.45E+01	6.88E-01	5.29E-01	6.36E-01	7.61E+00	5.78E+00	7.60E+01	1.82E+00	2.40E+01	7.84E+01
N15	-9.65E-01	1.70E-04	5.46E+01	-5.49E+01	1.51E-01	2.33E-01	3.83E-01	7.97E+00	6.10E+00	7.66E+01	1.86E+00	2.34E+01	7.53E+01
Complex 5													
Ru1	9.26E-01	9.21E-04	4.40E+03	-4.43E+03	1.55E-01	4.97E-01	4.94E-01	4.31E+01	4.06E+01	9.44E+01	2.43E+00	5.63E+00	1.01E+02
C18	-8.75E-02	-2.80E-04	3.76E+01	-3.78E+01	2.57E-01	1.80E-01	7.76E-02	6.09E+00	4.03E+00	6.61E+01	2.06E+00	3.39E+01	7.60E+01
C20	-9.77E-02	-1.45E-04	3.76E+01	-3.78E+01	2.30E-01	1.54E-01	9.89E-02	6.10E+00	4.03E+00	6.61E+01	2.07E+00	3.39E+01	7.36E+01
C22	-8.70E-02	7.70E-05	3.76E+01	-3.78E+01	2.57E-01	1.74E-01	9.16E-02	6.09E+00	4.03E+00	6.61E+01	2.06E+00	3.39E+01	7.59E+01
C23	-1.01E-01	-4.40E-05	3.76E+01	-3.78E+01	2.49E-01	1.46E-01	1.18E-01	6.10E+00	4.03E+00	6.61E+01	2.07E+00	3.39E+01	7.60E+01
C26	-9.72E-02	-2.40E-05	3.76E+01	-3.78E+01	2.30E-01	1.53E-01	1.14E-01	6.10E+00	4.03E+00	6.61E+01	2.07E+00	3.39E+01	7.36E+01
C27	-1.01E-01	-1.10E-04	3.76E+01	-3.78E+01	2.48E-01	1.47E-01	1.38E-01	6.10E+00	4.03E+00	6.61E+01	2.07E+00	3.39E+01	7.59E+01
N14	-9.58E-01	1.32E-04	5.44E+01	-5.47E+01	1.96E-01	3.93E-01	5.43E-01	7.96E+00	6.10E+00	7.67E+01	1.85E+00	2.33E+01	8.06E+01
N15	-9.52E-01	3.41E-04	5.46E+01	-5.49E+01	1.07E-01	1.73E-01	2.78E-01	7.95E+00	6.05E+00	7.61E+01	1.90E+00	2.39E+01	7.36E+01
N21	-9.59E-01	8.90E-05	5.44E+01	-5.47E+01	1.96E-01	2.96E-01	4.49E-01	7.96E+00	6.11E+00	7.67E+01	1.85E+00	2.33E+01	8.06E+01

Table 3.51: The Intra and inter atomic properties of atoms involve in Metal-Ligand and hydrogen bonding (atoms with superscript "#") of systems treated with ECP(Ru)[6-31+G(d,p)] basis set using QTAIM analysis

Complex 1												
	q(A)	L(A)	K(A)	K_Scaled(A)	μ_{Intra}(A)	μ_{Bond}(A)	|μ(A)|	N(A)	LI(A)	%Loc(A)	DI(A,A')/2	%Deloc(A,A')	Vol(A),0.001

Ru1	9.40E-01	2.84E-04	3.27E+01	-3.43E+01	1.37E-01	1.02E+00	1.07E+00	1.51E+01	1.24E+01	8.21E+01	2.70E+00	1.79E+01	1.03E+02
C9	-7.56E-02	2.30E-05	3.78E+01	-3.97E+01	1.42E-01	4.25E-02	1.03E-01	6.08E+00	3.98E+00	6.56E+01	2.09E+00	3.44E+01	7.39E+01
C10	-5.98E-02	-2.78E-04	3.78E+01	-3.97E+01	1.04E-01	8.99E-02	5.74E-02	6.06E+00	3.97E+00	6.55E+01	2.09E+00	3.45E+01	7.16E+01
C13	-6.39E-02	-2.07E-04	3.78E+01	-3.97E+01	1.09E-01	9.96E-02	1.06E-01	6.06E+00	3.97E+00	6.55E+01	2.09E+00	3.45E+01	7.18E+01
C16	-6.54E-02	1.51E-04	3.78E+01	-3.97E+01	1.47E-01	1.03E-01	8.08E-02	6.07E+00	3.98E+00	6.56E+01	2.09E+00	3.44E+01	7.37E+01
C18	-7.15E-02	2.20E-05	3.78E+01	-3.97E+01	1.40E-01	9.20E-02	9.33E-02	6.07E+00	3.98E+00	6.56E+01	2.09E+00	3.44E+01	7.47E+01
C19	-4.23E-02	-2.32E-04	3.78E+01	-3.97E+01	1.25E-01	1.33E-01	8.09E-02	6.04E+00	3.96E+00	6.55E+01	2.09E+00	3.45E+01	7.01E+01
Cl22	-4.92E-01	6.40E-05	4.59E+02	-4.82E+02	4.86E-02	1.17E+00	1.16E+00	1.75E+01	1.68E+01	9.61E+01	6.81E-01	3.89E+00	2.30E+02
N12	-7.26E-01	2.69E-04	5.47E+01	-5.74E+01	6.62E-01	7.84E-01	6.76E-01	7.73E+00	5.84E+00	7.56E+01	1.89E+00	2.44E+01	7.72E+01
N17	-7.26E-01	2.02E-04	5.47E+01	-5.74E+01	6.63E-01	7.63E-01	6.36E-01	7.73E+00	5.84E+00	7.56E+01	1.89E+00	2.44E+01	7.72E+01
O2[#]	-1.13E+00	7.20E-05	7.54E+01	-7.90E+01	5.41E-01	1.46E+00	1.00E+00	9.13E+00	8.15E+00	8.92E+01	9.82E-01	1.08E+01	1.29E+02
H24[#]	1.28E-01	1.60E-05	5.64E-01	-5.92E-01	1.07E-01	4.19E-01	4.61E-01	8.72E-01	3.40E-01	3.90E+01	5.32E-01	6.10E+01	4.04E+01
H29[#]	1.27E-01	2.30E-05	5.64E-01	-5.92E-01	1.07E-01	4.30E-01	4.72E-01	8.73E-01	3.41E-01	3.90E+01	5.32E-01	6.10E+01	4.04E+01
						Complex 2							
Ru1	9.57E-01	4.83E-04	3.27E+01	-3.41E+01	9.03E-02	1.00E+00	1.06E+00	1.50E+01	1.23E+01	8.18E+01	2.73E+00	1.82E+01	1.05E+02
C7	-6.65E-02	4.00E-05	3.78E+01	-3.95E+01	9.49E-02	8.37E-02	7.96E-02	6.07E+00	3.97E+00	6.54E+01	2.10E+00	3.46E+01	7.04E+01
C8	-7.69E-02	-1.02E-04	3.78E+01	-3.95E+01	1.50E-01	8.40E-02	9.09E-02	6.08E+00	3.99E+00	6.56E+01	2.09E+00	3.44E+01	7.49E+01
C13	-6.59E-02	-2.96E-04	3.78E+01	-3.95E+01	1.58E-01	7.62E-02	8.29E-02	6.07E+00	3.98E+00	6.57E+01	2.08E+00	3.43E+01	7.67E+01
C14	-4.00E-02	-5.43E-04	3.78E+01	-3.95E+01	1.19E-01	1.43E-01	9.34E-02	6.04E+00	3.96E+00	6.55E+01	2.08E+00	3.45E+01	6.99E+01
C18	-6.67E-02	1.40E-05	3.78E+01	-3.95E+01	9.40E-02	1.02E-01	1.05E-01	6.07E+00	3.97E+00	6.54E+01	2.10E+00	3.46E+01	7.04E+01
C19	-7.67E-02	2.55E-04	3.78E+01	-3.95E+01	1.50E-01	7.10E-02	8.19E-02	6.08E+00	3.99E+00	6.56E+01	2.09E+00	3.44E+01	7.48E+01
Cl10	-4.84E-01	6.80E-05	4.59E+02	-4.79E+02	3.25E-02	1.15E+00	1.12E+00	1.75E+01	1.68E+01	9.62E+01	6.57E-01	3.76E+00	2.34E+02
N11	-1.16E+00	6.60E-05	5.50E+01	-5.74E+01	1.93E-01	6.93E-01	5.24E-01	8.16E+00	6.27E+00	7.69E+01	1.89E+00	2.31E+01	8.10E+01

N16	-1.16E+00	2.46E-04	5.50E+01	-5.74E+01	1.95E-01	6.59E-01	4.90E-01	8.16E+00	6.27E+00	7.69E+01	1.89E+00	2.31E+01	8.09E+01
H34#	9.67E-02	9.50E-05	5.81E-01	-6.06E-01	1.11E-01	5.69E-02	6.89E-02	9.03E-01	3.58E-01	3.96E+01	5.45E-01	6.04E+01	4.09E+01
H38#	1.03E-01	7.70E-05	5.76E-01	-6.01E-01	1.15E-01	6.54E-02	5.26E-02	8.97E-01	3.53E-01	3.93E+01	5.45E-01	6.07E+01	4.10E+01
Complex 3													
Ru1	9.59E-01	2.52E-04	3.27E+01	-3.41E+01	9.73E-02	7.73E-01	7.69E-01	1.50E+01	1.23E+01	8.20E+01	2.71E+00	1.80E+01	1.01E+02
C13	-5.37E-02	-6.10E-05	3.78E+01	-3.94E+01	1.31E-01	1.45E-01	7.69E-02	6.05E+00	3.97E+00	6.56E+01	2.09E+00	3.44E+01	7.08E+01
C14	-6.12E-02	-1.90E-04	3.78E+01	-3.94E+01	1.29E-01	2.77E-01	4.01E-01	6.06E+00	3.97E+00	6.56E+01	2.09E+00	3.44E+01	6.99E+01
C18	-5.33E-02	-1.48E-04	3.78E+01	-3.94E+01	1.29E-01	1.38E-01	8.25E-02	6.05E+00	3.97E+00	6.56E+01	2.09E+00	3.44E+01	7.09E+01
C21	-7.24E-02	-1.20E-04	3.78E+01	-3.94E+01	1.18E-01	1.10E-01	1.34E-01	6.07E+00	3.98E+00	6.56E+01	2.09E+00	3.44E+01	7.38E+01
C23	-6.28E-02	-2.92E-04	3.78E+01	-3.94E+01	1.35E-01	2.83E-01	4.12E-01	6.06E+00	3.98E+00	6.56E+01	2.09E+00	3.44E+01	7.02E+01
C25	-7.20E-02	-2.53E-04	3.78E+01	-3.94E+01	1.15E-01	1.20E-01	1.42E-01	6.07E+00	3.98E+00	6.55E+01	2.09E+00	3.45E+01	7.35E+01
Cl7	-4.94E-01	8.90E-05	4.59E+02	-4.78E+02	7.56E-03	1.17E+00	1.16E+00	1.75E+01	1.68E+01	9.62E+01	6.69E-01	3.83E+00	2.33E+02
N10	-1.14E+00	2.23E-04	5.49E+01	-5.72E+01	1.71E-01	1.06E+00	9.04E-01	8.14E+00	6.27E+00	7.70E+01	1.87E+00	2.30E+01	8.19E+01
N16	-1.14E+00	5.60E-05	5.49E+01	-5.72E+01	1.72E-01	1.03E+00	8.69E-01	8.14E+00	6.27E+00	7.70E+01	1.87E+00	2.30E+01	8.18E+01
O2#	-1.15E+00	1.11E-04	7.54E+01	-7.85E+01	5.23E-01	1.38E+00	8.93E-01	9.15E+00	8.14E+00	8.90E+01	1.01E+00	1.10E+01	1.27E+02
O28#	-1.15E+00	1.17E-04	7.54E+01	-7.85E+01	5.23E-01	1.37E+00	8.78E-01	9.15E+00	8.14E+00	8.90E+01	1.01E+00	1.10E+01	1.27E+02
H31#	1.18E-01	2.20E-05	5.75E-01	-5.99E-01	1.13E-01	3.22E-01	3.52E-01	8.82E-01	3.43E-01	3.89E+01	5.39E-01	6.11E+01	3.91E+01
H36#	1.22E-01	3.20E-05	5.74E-01	-5.98E-01	1.12E-01	3.21E-01	3.54E-01	8.78E-01	3.40E-01	3.87E+01	5.39E-01	6.13E+01	3.86E+01
Complex 4													
Ru1	9.82E-01	-8.61E-04	3.27E+01	-3.50E+01	1.46E-01	3.81E-01	3.23E-01	1.50E+01	1.24E+01	8.25E+01	2.63E+00	1.75E+01	1.12E+02
C2	-5.75E-02	-2.60E-05	3.78E+01	-4.05E+01	1.48E-01	7.65E-02	7.55E-02	6.06E+00	3.98E+00	6.56E+01	2.08E+00	3.44E+01	7.36E+01
C3	-5.54E-02	-2.19E-04	3.78E+01	-4.05E+01	1.22E-01	8.73E-02	7.39E-02	6.06E+00	3.97E+00	6.56E+01	2.08E+00	3.44E+01	7.08E+01
C4	-5.77E-02	-3.00E-05	3.78E+01	-4.05E+01	1.48E-01	9.24E-02	9.46E-02	6.06E+00	3.98E+00	6.57E+01	2.08E+00	3.43E+01	7.36E+01
C5	-4.58E-02	-9.20E-05	3.78E+01	-4.05E+01	1.42E-01	1.02E-01	9.35E-02	6.05E+00	3.97E+00	6.56E+01	2.08E+00	3.44E+01	7.27E+01
C6	-5.55E-	-3.53E-	3.78E+0	-	1.21E-	9.59E-	8.67E-	6.06E+0	3.97E+0	6.56E+0	2.08E+0	3.44E+0	7.07E+0

	02	04	1	4.05E+01	01	02	02	0	0	1	0	1	1
C7	-4.61E-02	-7.90E-05	3.78E+01	-4.05E+01	1.43E-01	1.08E-01	1.01E-01	6.05E+00	3.97E+00	6.56E+01	2.08E+00	3.44E+01	7.27E+01
N10	-7.38E-01	2.73E-04	5.47E+01	-5.85E+01	6.93E-01	7.59E-01	5.90E-01	7.74E+00	5.89E+00	7.61E+01	1.85E+00	2.39E+01	8.21E+01
N13	-7.38E-01	2.80E-04	5.47E+01	-5.85E+01	6.93E-01	7.53E-01	5.75E-01	7.74E+00	5.89E+00	7.61E+01	1.85E+00	2.39E+01	8.21E+01
N15	-1.18E+00	4.18E-04	5.51E+01	-5.89E+01	1.58E-01	4.22E-01	3.23E-01	8.18E+00	6.30E+00	7.71E+01	1.87E+00	2.29E+01	7.93E+01
						Complex 5							
Ru1	9.80E-01	1.36E-03	3.27E+01	-3.46E+01	1.99E-01	5.46E-01	5.13E-01	1.50E+01	1.23E+01	8.21E+01	2.69E+00	1.79E+01	1.09E+02
C18	-4.88E-02	-3.90E-04	3.78E+01	-4.00E+01	1.42E-01	9.08E-02	6.77E-02	6.05E+00	3.97E+00	6.56E+01	2.08E+00	3.44E+01	7.28E+01
C20	-5.86E-02	-3.20E-05	3.78E+01	-4.00E+01	1.19E-01	1.16E-01	1.08E-01	6.06E+00	3.97E+00	6.56E+01	2.08E+00	3.44E+01	7.09E+01
C22	-4.81E-02	4.30E-05	3.78E+01	-4.00E+01	1.42E-01	9.31E-02	6.63E-02	6.05E+00	3.97E+00	6.56E+01	2.08E+00	3.44E+01	7.26E+01
C23	-6.19E-02	-2.73E-04	3.78E+01	-4.00E+01	1.49E-01	7.92E-02	1.00E-01	6.06E+00	3.98E+00	6.56E+01	2.08E+00	3.44E+01	7.32E+01
C26	-5.90E-02	-3.44E-04	3.78E+01	-4.00E+01	1.20E-01	1.23E-01	1.17E-01	6.06E+00	3.97E+00	6.56E+01	2.08E+00	3.44E+01	7.11E+01
C27	-6.16E-02	-2.82E-04	3.78E+01	-4.00E+01	1.47E-01	7.98E-02	9.87E-02	6.06E+00	3.98E+00	6.56E+01	2.08E+00	3.44E+01	7.31E+01
N14	-1.17E+00	2.33E-04	5.49E+01	-5.81E+01	1.77E-01	5.85E-01	4.48E-01	8.17E+00	6.31E+00	7.72E+01	1.86E+00	2.28E+01	8.46E+01
N15	-1.17E+00	4.56E-04	5.51E+01	-5.82E+01	1.85E-01	3.33E-01	2.20E-01	8.17E+00	6.26E+00	7.66E+01	1.91E+00	2.34E+01	7.77E+01
N21	-1.17E+00	2.77E-04	5.49E+01	-5.81E+01	1.77E-01	4.82E-01	3.55E-01	8.17E+00	6.31E+00	7.72E+01	1.86E+00	2.28E+01	8.46E+01

Table 3.52: Correlation between the computed atomic properties for complexes 1 to 5

	1		**2**		**3**		**4**		**5**	
	$\|\mu_{Bond}(A)\|$	Vol(A), 0.001	$\|\mu_{Bond}(A)\|$	Vol(A), 0.001	$\|\mu_{Bond}(A)\|$	Vol(A), 0.001	$\|\mu_{Bond}(A)\|$	Vol(A), 0.001	$\|\mu_{Bond}(A)\|$	Vol(A), 0.001
q(A)	-0.40	-0.45	-0.31	-0.56	-0.45	-0.57	-0.15	-0.17	-0.21	-0.50
L(A)	0.48	0.23	0.23	0.05	0.44	0.23	-0.11	-0.21	0.22	0.12
K(A)	0.36	0.25	0.28	0.23	0.21	0.22	0.14	0.44	0.16	0.32
K_Scaled(A)	-0.36	-0.25	-0.28	-0.23	-0.21	-0.22	-0.14	-0.44	-0.16	-0.32
$\|\mu_{Intra}(A)\|$	0.46	0.09	0.53	0.01	0.50	-0.04	0.92	0.36	0.65	0.17

$\|\mu_{Bond}(A)\|$	1.00	0.65	1.00	0.67	1.00	0.65	1.00	0.50	1.00	0.61
$\|\mu(A)\|$	0.89	0.68	0.92	0.81	0.88	0.75	0.80	0.59	0.92	0.71
N(A)	0.60	0.57	0.54	0.58	0.49	0.57	0.37	0.72	0.38	0.63
LI(A)	0.61	0.58	0.55	0.59	0.51	0.58	0.33	0.66	0.38	0.60
%Loc(A)	0.73	0.80	0.73	0.83	0.71	0.82	0.68	0.94	0.64	0.93
DI(A,A')/2	0.22	0.25	0.07	0.19	0.06	0.19	0.53	0.91	0.21	0.63
%Deloc(A, A')	-0.73	-0.80	-0.73	-0.83	-0.71	-0.82	-0.68	-0.94	-0.64	-0.93
Vol(A), 0.001	0.65	1.00	0.67	1.00	0.65	1.00	0.50	1.00	0.61	1.00

12

Table 3.53: The thermodynamic properties and number of vibrational modes

	E^0 KJ/mol	E KJ/mol	H KJ/mol	G KJ/mol	CV KJ/mol-K	S KJ/mol-K	Imaginary	No. Nor Vib Mode
1	-3.73E+06	-3.73E+06	-3.73E+06	-3.73E+06	0.51	0.82	0	183
2	-3.32E+06	-3.32E+06	-3.32E+06	-3.32E+06	0.44	0.75	0	153
3	-2.41E+06	-2.41E+06	-2.41E+06	-2.41E+06	0.39	0.67	1	141

The notations in this Table are Zero-point energy (E_0) , Total energy (E), Enthalpy (H), Gibb free energy (G), Constant volume molar heat capacity (CV) and Entropy (S).

13

14

15

16

17

Table 3.54: Total hyperpolarizability, band gap, dipole moments and isotropic polarizability of complexes **1**, **2** and **3** when mixed basis set (SBKJC VDZ with ECP and 6-31g*) and single basis set 3-21g were used.

	B3lyp/3-21g				pb0/SBKJC VDZ(6-31g*)			
	ß in esu (1x10-30)	Gap KJ/mol	Dipole Debye	Isot. pol. Bohr**3	ß esu (1x10-30)	Gap KJ/mol	Dipole Debye	Isot. pol. Bohr**3
1	20.43	382.40	7.3726	122.81	22.17	209.46	8.11	134.32
2	19.63	366.26	10.9667	101.84	21.60	212.95	10.66	111.52
3	19.56	366.36	7.9075	110.73	20.48	208.94	7.37	121.14
3**	18.74	362.66	7.6025	110.73				

The superscript "**" represent the computation with polarized basis set 3-21g**.

Table 3.55: The effect of the four Ramsey terms in determining the shielding tensor of complexes 2 and 3 using the functional B3LYP and all electron basis set 3-21g

Complex 2					
	FC (HZ)	SD	PSO	DSO	J (HZ)
Ru-C	-2.20	-0.02	-1.32	-0.04	-3.58
	-2.37	0.02	-1.41	-0.04	-3.78
	-2.45	-0.13	-1.37	-0.04	-3.98
	-2.46	0.10	-1.32	-0.04	-3.72
	-2.80	-0.02	-1.08	-0.04	-3.94
	-2.96	0.14	-1.09	-0.04	-3.94
Ru-P	-73.12	-0.87	4.62	-0.06	-69.43
Ru-bO	6.77	1.16	10.22	0.02	18.17
	6.69	1.19	10.58	0.02	18.49
Complex 3					
	FC (HZ)	SD	PSO	DSO	J (HZ)
Ru-C	-1.67	0.10	-0.96	-0.04	-2.56
	-2.09	0.01	-1.14	-0.04	-3.26
	-2.46	-0.16	-1.72	-0.04	-4.38
	-2.63	-0.04	-1.67	-0.04	-4.38
	-2.96	-0.01	-1.66	-0.04	-4.66
	-3.16	0.04	-2.10	-0.04	-5.26
Ru-P	-61.68	-1.17	2.79	-0.06	-60.12
Ru-Cl	-0.94	-2.03	-19.73	-0.01	-22.71
	-1.16	-2.14	-20.18	-0.01	-23.48

Table 3.56: The effect of the four Ramsey terms in determining the shielding tensor of complex **3** using the hybrid DFT functional B3LYP and polarized all electron basis set 3-21g**

	FC (HZ)	SD	PSO	DSO	J (HZ)
Ru-C	-1.60	0.11	-0.91	-0.04	-2.44
	-2.03	0.01	-1.08	-0.04	-3.13
	-2.42	-0.16	-1.69	-0.04	-4.30
	-2.59	-0.03	-1.64	-0.04	-4.31
	-3.00	0.00	-1.65	-0.04	-4.68
	-3.19	0.04	-2.08	-0.04	-5.26
Ru-P	-62.54	-1.17	4.55	-0.06	-59.22
Ru-Cl	-0.64	-2.09	-19.82	-0.01	-22.56
	-0.89	-2.19	-20.22	-0.01	-23.30

Table 3.57: The correlation of Isotropic, Anisotropic, charges of all atoms and four Ramsey terms of all atoms to Ru atom.

Isotropic/	Anisotropy	Charges	FC	SD	PSO	DSO	J
2	-0.16	-0.30	-0.60	-0.15	0.35	-0.11	-0.52
3	0.91	-0.39	-0.24	-0.96	-0.90	-0.07	-0.64
3**	0.92	-0.47	-0.19	-0.95	-0.89	-0.06	-0.61
Anisotropy/	Charges	FC	SD	PSO	DSO	J	
2	-0.46	0.09	0.52	0.38	0.12	0.19	
3	-0.41	-0.04	-0.85	-0.95	-0.15	-0.47	
3**	-0.46	-0.10	-0.87	-0.92	-0.18	-0.53	
Charges/	FC	SD	PSO	DSO	J		
2	-0.30	-0.38	-0.12	-0.21	-0.34		
3	-0.33	0.12	0.33	-0.10	-0.16		
3**	-0.34	0.21	0.44	-0.09	-0.12		
FC/	SD	PSO	DSO	J			
2	0.59	-0.14	0.34	0.97			
3	0.36	-0.11	0.34	0.89			
3**	0.34	-0.18	0.34	0.88			
SD/	PSO	DSO	J				
2	0.67	0.36	0.74				
3	0.87	0.10	0.74				
3**	0.85	0.10	0.73				
PSO/	DSO	J	DSO/	J			
2	0.26	0.09	**2**	0.41			
3	0.02	0.36	**3**	0.33			
3**	0.00	0.31	**3****	0.33			

The sign "/" stands for correlation with the factors of the row and superscript "**" stands for the case where polarized basis

set 3-21g** is used

Table 3.58: The effect of the four Ramsey terms in determining the shielding tensor of complex **3** using the DFT functional pb0 and ECP basis set SBKJC VDZ for Ru, P and Cl while all electron basis set 6-31g* is used for other atoms

	FC (HZ)	SD	PSO	DSO	J (HZ)
Ru-C	-1.84E-006	3.28E-003	-2.58E-001	-3.01E-002	-2.84E-001
	-3.23E-006	2.07E-002	-2.28E-001	-3.07E-002	-2.38E-001
	-3.62E-006	1.70E-002	-2.50E-001	-2.93E-002	-2.63E-001
	-4.47E-006	2.21E-002	-3.00E-001	-2.92E-002	-3.07E-001
	2.58E-006	2.17E-002	-1.81E-001	-2.84E-002	-1.88E-001
	6.37E-006	3.35E-002	-1.52E-001	-2.97E-002	-1.48E-001
Ru-P	0.00E+000	-5.47E-003	-5.77E-003	-4.98E-002	-6.10E-002
Ru-Cl	0.00E+000	-9.32E-003	-2.04E-001	-8.22E-003	-2.22E-001
	0.00E+000	-1.03E-002	-2.06E-001	-8.43E-003	-2.24E-001

18

Table 3.59: Correlation of the charges, dipole, magnetizabilities and nmr shielding of complex **2** and **3**

q(A)	$\chi_{Intra\_Iso}(A)$	$\chi_{Bond\_Iso}(A)$	$\chi_{Iso}(A)$	$\mu_{Intra}(A)$	$\mu_{Bond}(A)$	$\mu(A)$	$\sigma_{Iso}(A,A)$	$\sigma_{Iso}(A',A)$	$\sigma_{Iso}(A)$
2	0.53	-0.19	0.33	0.4	-0.16	-0.31	-0.26	0.22	-0.26
3	0.55	-0.11	0.45	0.21	-0.17	-0.29	-0.44	0.1	-0.44
$\chi_{Intra\_Iso}(A)$	$\chi_{Bond\_Iso}(A)$	$\chi_{Iso}(A)$	$\mu_{Intra}(A)$	$\mu_{Bond}(A)$	$\mu(A)$	$\sigma_{Iso}(A,A)$	$\sigma_{Iso}(A',A)$	$\sigma_{Iso}(A)$	
2	-0.49	0.49	-0.09	0.22	0.06	-0.91	0.14	-0.91	
3	-0.25	0.78	-0.02	-0.18	-0.24	-0.93	0.29	-0.93	
$\chi_{Bond\_Iso}(A)$	$\chi_{Iso}(A)$	$\mu_{Intra}(A)$	$\mu_{Bond}(A)$	$\mu(A)$	$\sigma_{Iso}(A,A)$	$\sigma_{Iso}(A',A)$	$\sigma_{Iso}(A)$		
2	0.52	-0.33	-0.56	-0.48	0.68	-0.74	0.67		
3	0.41	-0.32	-0.63	-0.54	0.53	-0.7	0.52		
$\chi_{Iso}(A)$	$\mu_{Intra}(A)$	$\mu_{Bond}(A)$	$\mu(A)$	$\sigma_{Iso}(A,A)$	$\sigma_{Iso}(A',A)$	$\sigma_{Iso}(A)$			
2	-0.42	-0.35	-0.42	-0.22	-0.6	-0.22			
3	-0.23	-0.57	-0.57	-0.54	-0.18	-0.54			
$\mu_{Intra}(A)$	$\mu_{Bond}(A)$	$\mu(A)$	$\sigma_{Iso}(A,A)$	$\sigma_{Iso}(A',A)$	$\sigma_{Iso}(A)$				
2	0.28	0.24	0.09	0.27	0.09				
3	0.38	0.27	0	0.22	0.01				
$\mu_{Bond}(A)$	$\mu(A)$	$\sigma_{Iso}(A,A)$	$\sigma_{Iso}(A',A)$	$\sigma_{Iso}(A)$		$\mu(A)$	$\sigma_{Iso}(A,A)$	$\sigma_{Iso}(A',A)$	$\sigma_{Iso}(A)$
2	0.81	-0.52	0.13	-0.52		**2**	-0.4	-0.05	-0.4
3	0.76	-0.12	0.16	-0.12		**3**	-0.06	-0.01	-0.06
$\sigma_{Iso}(A,A)$	$\sigma_{Iso}(A',A)$	$\sigma_{Iso}(A)$		$\sigma_{Iso}(A',A)$	$\sigma_{Iso}(A)$				
2	-0.19	1		**2**	-0.18				
3	-0.37	1		**3**	-0.36				

The magnetic properties are define in terms of q(A)=Total charge on atom A; $\chi_{Intra\_Iso}(A)$= Intraatomic Magnetizability Contribution of Atom A (cgs-ppm); $\chi_{Bond\_Iso}(A)$ = Bonding Magnetizability Contribution of Atom A; $\chi_{Iso}(A)$= Total Magnetizability Contribution of Atom A ($\chi_{Intra}(A) + \chi_{Bond}(A)$); $\mu_{Intra}(A)$ = Intraatomic Dipole Moment Contribution of Atom A; $\mu_{Bond}(A)$ = Bonding Dipole Moment Contribution of Atom A; $\mu(A)$ =Total Dipole Moment Contribution of Atom A ($\mu_{Intra}(A) + \mu_{Bond}(A)$); $\sigma_{Iso}(A,A)$=The intraatomic shielding tensor; $\sigma_{Iso}(A',A)$= Total Induced Magnetic Field on Nucleus A by other nuclei A'; $\sigma_{Iso}(A)$= Total Magnetic shielding tensor of atom A.

Table 3.60: The sum over of the charges, dipole, magnetizabilities and nmr shielding of complexes **2** and **3**.

Complexes	q(A)	χ_{Intra_Iso}(A)	χ_{Bond_Iso}(A)	χ_{Iso}(A)	$\lvert\mu_{Intra}(A)\rvert$	$\lvert\mu_{Bond}(A)\rvert$	$\lvert\mu(A)\rvert$	σ_{Iso}(A,A)	σ_{Iso}(A',A)	σ_{Iso}(A)
2	0.00	-114.56	-147.91	-262.47	13.65	16.25	15.92	1391.42	653.97	2045.39
3	0.00	-132.96	-143.11	-276.07	12.23	11.72	12.62	3538.67	604.26	4142.93

Table 3.61: The charges, dipole, magnetizabilities and nmr shielding of selected atoms in complexes **2**

	Orapta	q(A)	χIntra_Iso$_{Intra_Iso}$_Iso$_{Intra_Iso}$(A)	χBond_Iso$_{Bond_Iso}$(A)	χ_{Iso}(A)	μ_{Intra}(A)	μ_{Bond}(A)	μ(A)	σ_{Iso}(A,A)	σ_{Iso}(A',A)	σ_{Iso}(A)
	Ru1	0.85	19.65	-24.07	-4.41	0.37	1.83	1.65	-2459.77	23.85	-2435.92
arene	C2	-0.11	-3.39	-6.03	-9.42	0.24	0.18	0.10	94.61	21.65	116.26
	C5	-0.12	-3.20	-6.01	-9.22	0.22	0.16	0.11	91.07	21.67	112.74
	C6	-0.07	-2.56	-6.89	-9.45	0.16	0.30	0.16	87.83	24.41	112.24
	C7	-0.08	-2.37	-6.89	-9.26	0.19	0.20	0.05	82.99	24.32	107.32
	C8	-0.14	-3.73	-6.33	-10.05	0.22	0.11	0.14	105.93	24.05	129.98
	C10	-0.15	-3.63	-6.28	-9.92	0.20	0.10	0.13	107.39	24.17	131.56
	H45*	0.04	-1.20	-0.26	-1.46	0.16	0.15	0.31	21.18	10.01	31.19
bidentate	O12	-0.92	-6.95	-3.12	-10.07	0.14	0.97	1.05	166.70	8.86	175.56
	O16	-0.92	-7.05	-3.11	-10.17	0.15	1.02	1.10	174.13	9.04	183.17
	O11u	-0.87	-5.10	-1.45	-6.55	0.09	1.29	1.20	-112.27	5.00	-107.26
	O23u	-0.87	-5.12	-1.45	-6.57	0.09	1.29	1.20	-111.17	5.00	-106.17
	C15*	1.14	-0.77	-3.48	-4.25	0.61	0.67	0.58	41.09	15.30	56.39
PTA	P17	0.82	-7.65	-7.25	-14.90	1.05	0.21	1.18	493.74	12.28	506.03
	N18	-0.86	-5.98	-3.44	-9.42	0.37	0.50	0.85	211.19	11.96	223.15
	N22	-0.85	-6.02	-3.17	-9.19	0.38	0.48	0.86	215.23	11.67	226.89
	N26	-0.86	-5.97	-3.08	-9.06	0.37	0.46	0.83	210.59	11.93	222.53
	H41*	0.11	-0.98	-1.35	-2.33	0.15	0.35	0.43	19.69	9.10	28.79
	H51*	0.07	-1.11	-0.23	-1.34	0.16	0.22	0.12	20.49	8.45	28.94

Table 3.62: The charges, dipole, magnetizabilities and nmr shielding of selected atoms in complexes **3**

	Atom	q(A)	χ_{Intra_Iso}(A)	χ_{Bond_Iso}(A)	$\chi_{\_Iso}$(A)	μ_{Intra}(A)	μ_{Bond}(A)	μ(A)	$\sigma_{\_Iso}$(A,A)	$\sigma_{\_Iso}$(A', A)	$\sigma_{\_Iso}$(A)
	Ru1	0.64	19.74	-23.48	-3.74	0.37	1.39	1.48	-2469.14	25.92	-2443.22
arene	C6	-0.09	-2.66	-6.76	-9.42	0.12	0.17	0.05	92.92	25.77	118.68
	C9	-0.13	-3.73	-6.51	-10.24	0.23	0.11	0.14	108.03	24.53	132.55
	C10	-0.11	-3.47	-6.33	-9.81	0.24	0.17	0.10	101.25	24.12	125.37
	C14	-0.12	-3.44	-6.88	-10.32	0.23	0.18	0.09	101.98	23.93	125.91
	C16	-0.12	-3.18	-6.71	-9.89	0.23	0.18	0.11	93.18	21.89	115.07
	C17	-0.06	-2.15	-4.16	-6.32	0.19	0.05	0.15	73.89	22.72	96.61
	C2*	-0.06	-4.69	-5.07	-9.76	0.21	0.22	0.06	163.69	15.51	179.20
	H46*	0.09	-1.03	-1.84	-2.88	0.15	0.30	0.42	19.98	9.77	29.74
mono	Cl19	-0.58	-23.11	-3.05	-26.16	0.14	1.40	1.54	1191.50	4.08	1195.58
	Cl20	-0.57	-22.80	-6.68	-29.48	0.14	0.66	0.79	1197.51	4.37	1201.88
pta	P13	0.86	-7.07	-6.37	-13.43	1.02	0.11	0.96	481.97	12.18	494.15
	N4	-0.85	-5.95	-3.25	-9.20	0.38	0.47	0.85	208.64	11.71	220.35
	N5	-0.85	-5.95	-3.05	-9.00	0.38	0.47	0.85	209.40	11.64	221.04
	N15	-0.86	-5.91	-3.46	-9.37	0.37	0.48	0.84	204.84	11.84	216.69
	H29*	0.06	-1.07	-1.25	-2.32	0.16	0.07	0.09	20.56	7.97	28.52
	H43*	0.11	-0.96	-1.59	-2.55	0.15	0.36	0.42	19.46	8.66	28.12

The atoms with "*" shows those that are involve in HB

Table 3.63: The thermodynamic properties and number of vibrational modes

Complex	E^0 KJ/mol	E KJ/mol	H KJ/mol	G KJ/mol	CV KJ/mol-K	S KJ/mol-K	Imaginary	No. Nor Vib Mode
1	-2.00E+06	-2.00E+06	-2.00E+06	-2.00E+06	0.31	0.59	0	105
2	-2.16E+06	-2.16E+06	-2.16E+06	-2.16E+06	0.31	0.57	1	111
3	-2.41E+06	-2.41E+06	-2.41E+06	-2.41E+06	0.39	0.67	1	141
4	-2.57E+06	-2.57E+06	-2.57E+06	-2.57E+06	0.42	0.73	0	147
5	-2.10E+06	-2.10E+06	-2.10E+06	-2.10E+06	0.33	0.59	1	114
6	-2.26E+06	-2.26E+06	-2.26E+06	-2.26E+06	0.35	0.62	0	120
7	-2.88E+06	-2.88E+06	-2.88E+06	-2.88E+06	0.36	0.67	0	114
8	-3.04E+06	-3.04E+06	-3.04E+06	-3.04E+06	0.38	0.66	0	120
Cl	-3.93E+04	-3.93E+04	-3.93E+04	-3.93E+04	0.01	0.15	0	0
H_2O	-2.00E+05	-2.00E+05	-2.00E+05	-2.00E+05	0.03	0.19	0	3

Table 3.64: The change in the thermodynamic properties due to hydrolysis

KJ/mol	ΔH	ΔG	ΔS
(**2**+Cl) – (**1**+H2O)	4.18E+02	4.38E+02	-6.63E-02
(**4**+Cl) – (**3**+H2O)	4.06E+02	4.01E+02	1.94E-02
(**6**+Cl) – (**5**+H2O)	4.16E+02	4.20E+02	-1.39E-02
(**8**+Cl) – (**7**+H2O)	4.32E+02	4.46E+02	-4.55E-02

Table 3.65: Total hyperpolarizability, band gap, and isotropic polarizability of complexes **1**, **2**, **3**, **4**, **5**, **6**, **7** and **8** when mixed basis set (SBKJC VDZ with ECP and 6-31g*) and single basis set 3-21g were used.

	B3lyp/3-21g			PBE0/mixes basis		
	ß in esu (1x10-30)	Gap in KJ/mol	Iso. pol. Bohr**3	ß in esu (1x10-30)	Gap in KJ/mol	Iso. pol. Bohr**3
1	19.24	363.37	88.84	19.95	208.86	226.9
2	34.39	264.76	93.65	56.74	132.01	227.56
3	19.56	362.00	110.73	20.48	208.94	277.85
4	32.96	274.39	115.47	53.30	140.81	277.87
5	19.59	362.98	91.97	19.92	208.73	238.95
6	33.06	268.64	95.74	52.99	135.27	238.02
7	22.10	335.91	93.2	23.50	196.39	240.87
8	39.21	237.42	97.72	66.97	111.85	243.51

Table 3.66: The effect of the four Ramsey terms in determining the shielding tensor of complexes using the functional b3lyp and all electron basis set 3-21g

	Bond	FC (HZ)	SD	PSO	DSO	J (HZ)
			Complex 1			
arene	Ru-C	-2.40E+000	-5.31E-002	-1.47E+000	-3.32E-002	-3.96E+000
		-1.87E+000	3.75E-002	-9.03E-001	-3.11E-002	-2.77E+000
		-2.95E+000	3.56E-002	-1.82E+000	-3.30E-002	-4.77E+000
		-1.87E+000	3.83E-002	-9.02E-001	-3.11E-002	-2.77E+000
		-2.95E+000	3.63E-002	-1.82E+000	-3.30E-002	-4.77E+000
		-2.40E+000	-5.36E-002	-1.47E+000	-3.32E-002	-3.96E+000
mono	Ru-Cl17	-1.04E+000	-2.17E+000	-2.06E+001	-9.64E-003	-2.38E+001
	Ru-Cl5	-1.04E+000	-2.17E+000	-2.06E+001	-9.64E-003	-2.38E+001
pta	Ru-P	-6.07E+001	-1.35E+000	2.59E+000	-5.63E-002	-5.96E+001
			Complex 2			
arene	Ru-C	-2.93E+000	2.93E-002	-1.76E+000	-3.12E-002	-4.69E+000
		-2.37E+000	-1.19E-001	-2.10E+000	-3.12E-002	-4.62E+000
		-3.58E+000	-1.22E-001	-2.13E+000	-3.28E-002	-5.87E+000
		-1.28E+000	1.21E-002	-1.26E+000	-2.87E-002	-2.56E+000
		-3.52E+000	-2.43E-001	-2.22E+000	-3.33E-002	-6.01E+000
		-1.52E+000	1.33E-002	-1.06E+000	-2.93E-002	-2.60E+000
mono	Ru-O	2.86E+000	6.28E-001	3.83E+000	1.58E-002	7.33E+000
	Ru-Cl#	-4.80E-001	-1.72E+000	-1.68E+001	-9.07E-003	-1.90E+001
pta	Ru-P	-5.69E+001	-1.77E+000	-1.53E+000	-5.24E-002	-6.02E+001
			Complex 3			
arene	Ru-C	-2.96E+00	-5.29E-03	-1.66E+00	-3.78E-02	-4.66E+00
		-3.16E+00	3.61E-02	-2.10E+00	-3.64E-02	-5.26E+00
		-2.63E+00	-3.71E-02	-1.67E+00	-3.67E-02	-4.38E+00
		-2.46E+00	-1.64E-01	-1.72E+00	-3.75E-02	-4.38E+00
		-2.09E+00	6.41E-03	-1.14E+00	-3.57E-02	-3.26E+00

		-1.67E+00	1.05E-01	-9.58E-01	-3.68E-02	-2.56E+00
mono	Ru-Cl19	-9.41E-01	-2.03E+00	-1.97E+01	-1.02E-02	-2.27E+01
	Ru-Cl20	-1.16E+00	-2.14E+00	-2.02E+01	-1.04E-02	-2.35E+01
pta	Ru-P13	-6.17E+01	-1.17E+00	2.79E+00	-5.83E-02	-6.01E+01
Complex 4						
arene	Ru-C	-2.94E+000	-1.24E-001	-1.97E+000	-3.53E-002	-5.07E+000
		-2.69E+000	-1.05E-001	-2.43E+000	-3.57E-002	-5.26E+000
		-3.75E+000	1.90E-003	-2.12E+000	-3.72E-002	-5.91E+000
		-1.17E+000	-1.07E-001	-1.40E+000	-3.53E-002	-2.71E+000
		-3.42E+000	-3.16E-001	-2.27E+000	-3.68E-002	-6.04E+000
		-1.76E+000	1.22E-001	-1.19E+000	-3.36E-002	-2.86E+000
mono	Ru-O	2.49E+000	6.09E-001	3.87E+000	1.70E-002	6.98E+000
	Ru-Cl#	-5.27E-001	-1.55E+000	-1.56E+001	-9.63E-003	-1.77E+001
pta	Ru-P12	-5.92E+001	-1.51E+000	-7.70E-001	-5.49E-002	-6.15E+001
Complex 5						
arene	Ru-C	-2.48E+000	-1.62E-001	-1.40E+000	-3.43E-002	-4.07E+000
		-2.90E+000	8.62E-002	-2.06E+000	-3.43E-002	-4.91E+000
		-1.93E+000	8.87E-002	-9.31E-001	-3.17E-002	-2.80E+000
		-3.00E+000	5.25E-003	-1.60E+000	-3.64E-002	-4.63E+000
		-2.09E+000	-1.04E-001	-9.20E-001	-3.25E-002	-3.14E+000
		-2.39E+000	6.14E-002	-1.75E+000	-3.48E-002	-4.12E+000
mono	Ru-Cl2#	-9.94E-001	-2.17E+000	-2.06E+001	-9.75E-003	-2.37E+001
	Ru-Cl20	-1.04E+000	-2.12E+000	-2.04E+001	-9.82E-003	-2.36E+001
pta	Ru-P	-6.19E+001	-1.29E+000	2.48E+000	-5.70E-002	-6.07E+001
Complex 6						
arene	Ru-C	-2.80E+000	-5.44E-002	-1.94E+000	-3.32E-002	-4.83E+000
		-2.61E+000	-1.05E-001	-2.16E+000	-3.22E-002	-4.91E+000
		-3.72E+000	-2.97E-002	-1.97E+000	-3.60E-002	-5.76E+000
		-1.35E+000	-5.93E-002	-1.39E+000	-2.95E-002	-2.83E+000
		-3.39E+000	-2.52E-001	-2.36E+000	-3.52E-002	-6.05E+000
		-1.67E+000	2.29E-002	-1.01E+000	-3.01E-002	-2.69E+000
mono	Ru-O11	2.53E+000	6.07E-001	3.80E+000	1.60E-002	6.95E+000
	Ru-Cl20#	-5.34E-001	-1.64E+000	-1.64E+001	-9.26E-003	-1.86E+001
pta	Ru-P12	-5.90E+001	-1.71E+000	-1.33E+000	-5.36E-002	-6.21E+001
Complex 7						
arene	Ru-C	-2.76E+000	1.04E-001	-1.72E+000	-3.74E-002	-4.42E+000
		-2.36E+000	-3.98E-002	-1.53E+000	-3.54E-002	-3.96E+000
		-3.71E+000	1.63E-001	-1.61E+000	-4.39E-002	-5.20E+000
		-1.66E+000	3.89E-002	-7.43E-001	-3.31E-002	-2.40E+000
		-2.16E+000	-4.85E-002	-1.50E+000	-3.83E-002	-3.74E+000
		-1.86E+000	6.14E-002	-8.73E-001	-3.33E-002	-2.71E+000
mono	Ru-Cl11#	-1.08E+000	-2.21E+000	-2.14E+001	-1.02E-002	-2.47E+001
	Ru-Cl23	-9.40E-001	-2.30E+000	-2.16E+001	-1.05E-002	-2.48E+001
pta	Ru-P14	-5.96E+001	-1.56E+000	9.82E-001	-6.04E-002	-6.03E+001

Table 3.67: The correlation within the four Ramsey terms that were used in determining the shielding tensor of the complexes **1**, **2**, **3**, **4**, **5**, **6** and **7** using the functional b3lyp and all electron basis set 3-21g

FC*	SD	PSO	DSO	J.HZ.
1	0.38	-0.12	0.43	0.88
2	0.7	0.08	0.37	0.95
3	0.36	-0.11	0.34	0.89
4	0.67	0.06	0.3	0.96
5	0.37	-0.11	0.39	0.89
6	0.7	0.07	0.34	0.96
7	0.41	-0.05	0.38	0.87

SD*	PSO	DSO	J.HZ.
1	0.86	0.14	0.77
2	0.74	0.27	0.87
3	0.87	0.1	0.74
4	0.73	0.23	0.84
5	0.86	0.12	0.75
6	0.73	0.26	0.87
7	0.83	0.04	0.78

PSO*	DSO	J.HZ.	DSO*	J.HZ.
1	0.01	0.37	**1**	0.4
2	0.2	0.38	**2**	0.4
3	0.02	0.36	**3**	0.33
4	0.19	0.34	**4**	0.33
5	0.01	0.36	**5**	0.37
6	0.2	0.36	**6**	0.38
7	0	0.44	**7**	0.33

The superscript "*" stands for the correlation of the factor with the rest of the factors on the same row except where another one appears.

Table 3.68: J_XY is X component of the first-order net current vector induced in the molecule by a uniform magnetic field along the Y axis in atomic units from QTAIM for complexes **1**, **2**, **3**, **4**, **5**, **6** and **7**

	1	**2**	**3**	**4**	**5**	**6**	**7**
J_XX	3.52E-08	-4.65E-04	-2.75E-04	-4.17E-04	2.07E-04	-2.76E-04	1.51E-04
J_YX	1.23E-06	1.63E-04	1.72E-03	-1.05E-04	5.79E-04	-7.38E-05	1.21E-03
J_ZX	1.67E-03	-4.10E-04	1.26E-03	8.27E-04	1.48E-03	2.95E-04	7.35E-04
J_XY	-6.03E-07	9.87E-04	-1.29E-03	8.57E-05	-1.50E-04	-7.05E-04	-3.81E-04
J_YY	-1.00E-07	6.47E-07	3.36E-04	-3.13E-04	3.92E-05	-9.09E-05	-1.79E-04
J_ZY	8.24E-04	-3.39E-03	-1.07E-03	-2.26E-03	-1.03E-03	-3.29E-03	-9.54E-04
J_XZ	-5.19E-04	-9.73E-04	-1.12E-04	9.10E-04	-1.43E-04	1.80E-03	-1.02E-04
J_YZ	-1.42E-03	2.14E-03	6.07E-04	2.15E-03	6.64E-04	2.39E-03	1.65E-03
J_ZZ	8.85E-03	1.14E-02	1.12E-02	1.30E-02	1.12E-02	1.14E-02	1.16E-02

Table 3.69: The charges, magnetizability contribution, dipole, magnetic shielding tensor and anisotropy of some selected atoms in complexes **1**

Atom	q(A)	χ_{Intra_Iso}(A)	χ_{Bond_Iso}(A)	$\chi_{\_Iso}$(A)	$\lvert\mu_{Intra}(A)\rvert$	$\lvert\mu_{Bond}(A)\rvert$	$\lvert\mu(A)\rvert$	$\sigma_{\_Iso}$(A,A)	$\sigma_{\_Iso}$(A',A)	$\sigma_{\_Iso}$(A)	Anisotropy
Ru1	0.64	17.13	-26.98	-9.85	0.38	1.85	1.94	-2172.26	26.08	-2146.18	5274.66
C2	-0.10	-3.47	-6.19	-9.66	0.25	0.21	0.06	100.03	23.86	123.89	118.23
C3	-0.09	-3.32	-6.07	-9.40	0.26	0.23	0.06	91.92	21.68	113.61	131.16
C4	-0.13	-3.72	-6.43	-10.15	0.23	0.13	0.11	107.86	24.39	132.25	108.80
C6	-0.09	-3.32	-6.08	-9.40	0.26	0.23	0.06	91.94	21.68	113.62	131.15
C7	-0.13	-3.72	-6.44	-10.16	0.23	0.13	0.11	107.87	24.39	132.26	108.80
C9	-0.10	-3.47	-6.20	-9.67	0.25	0.21	0.06	100.02	23.86	123.88	118.24
Cl17	-0.56	-23.02	-2.99	-26.01	0.14	1.37	1.50	1192.99	4.19	1197.18	411.30
Cl5	-0.56	-23.02	-2.99	-26.01	0.14	1.37	1.50	1193.03	4.19	1197.22	411.35
P11	0.88	-6.92	-8.08	-14.99	1.00	0.50	1.49	478.93	12.13	491.06	49.27
N16	-0.85	-5.92	-3.16	-9.09	0.38	0.48	0.85	206.92	11.60	218.52	24.48
N10	-0.85	-5.92	-3.16	-9.08	0.38	0.48	0.85	206.92	11.60	218.52	24.47
N18	-0.86	-5.88	-3.15	-9.03	0.37	0.46	0.83	202.83	11.78	214.61	28.90

The magnetic properties are define in terms of q(A)=Total charge on atom A; χ_{Intra_Iso}(A)= Intraatomic Magnetizability Contribution of Atom A (cgs-ppm); χ_{Bond_Iso}(A) = Bonding Magnetizability Contribution of Atom A; $\chi_{\_Iso}$(A)= Total Magnetizability Contribution of Atom A (χ_{Intra}(A) + χ_{Bond}(A)); μ_{Intra}(A) = Intraatomic Dipole Moment Contribution of Atom A; μ_{Bond}(A) = Bonding Dipole Moment Contribution of Atom A; μ(A) =Total Dipole Moment Contribution of Atom A (μ_{Intra}(A) + μ_{Bond}(A)); $\sigma_{\_Iso}$(A,A)=The Intraatomic shielding tensor; $\sigma_{\_Iso}$(A',A)= Total Induced Magnetic Field on Nucleus A by other nuclei A'; $\sigma_{\_Iso}$(A)= Total Magnetic shielding tensor of atom A. The superscript "*" stands for the correlation of the factor with the rest of the factors on the same row except where another one appears.

Table 3.70: The charges, magnetizability contribution, dipole, magnetic shielding tensor and anisotropy of some selected atoms in complexes **2**

Atom	q(A)	χ_{Intra_Iso}(A)	χ_{Bond_Iso}(A)	$\chi_{\_Iso}$(A)	$\lvert\mu_{Intra}(A)\rvert$	$\lvert\mu_{Bond}(A)\rvert$	$\lvert\mu(A)\rvert$	$\sigma_{\_Iso}$(A,A)	$\sigma_{\_Iso}$(A',A)	$\sigma_{\_Iso}$(A)	Anisotropy
Ru1	0.68	22.05	-23.81	-1.76	0.31	0.85	0.96	-2855.76	25.32	-2830.44	5682.70
C6	-0.10	-3.56	-6.48	-10.04	0.26	0.15	0.11	103.76	23.94	127.69	119.61
C7	-0.12	-3.64	-6.64	-10.28	0.24	0.14	0.11	103.50	23.85	127.35	112.19
C9	-0.11	-3.67	-6.90	-10.57	0.24	0.14	0.12	108.55	25.44	133.98	114.53
C14	-0.11	-3.43	-7.49	-10.92	0.24	0.15	0.12	93.72	21.71	115.43	127.89
C17	-0.10	-3.62	-7.52	-11.14	0.26	0.20	0.08	107.49	25.33	132.82	113.11
C18	-0.07	-3.18	-4.33	-7.51	0.27	0.22	0.09	89.67	21.59	111.25	137.72
O8	-0.93	-9.13	-2.85	-11.98	0.13	0.66	0.74	357.06	9.88	366.94	169.65
Cl19#	-0.52	-22.16	-3.59	-25.76	0.11	1.20	1.29	1066.93	4.18	1071.11	627.58
H39*	0.51	-0.47	-0.83	-1.30	0.15	0.35	0.40	13.84	18.08	31.92	18.56
P11	0.72	-7.34	-7.44	-14.79	0.93	0.62	0.33	465.02	10.76	475.78	86.83
N10	-0.85	-5.69	-2.93	-8.61	0.35	0.45	0.80	191.35	11.42	202.77	42.54
N2	-0.85	-5.66	-2.96	-8.62	0.36	0.45	0.81	189.80	11.23	201.03	45.90
N12	-0.85	-5.68	-2.95	-8.64	0.36	0.45	0.81	190.54	11.33	201.88	41.49

Table 3.71: The charges, magnetizability contribution, dipole, magnetic shielding tensor and anisotropy of some selected atoms in complexes **3**

Atom	q(A)	χ_{Intra_Iso}(A)	χ_{Bond_Iso}(A)	$\chi_{\_Iso}$(A)	$\lvert\mu_{Intra}(A)\rvert$	$\lvert\mu_{Bond}(A)\rvert$	$\lvert\mu(A)\rvert$	$\sigma_{\_Iso}$(A, A)	$\sigma_{\_Iso}$(A', A)	$\sigma_{\_Iso}$(A)	Anisotropy
Ru1	0.64	19.74	-23.48	-3.74	0.37	1.39	1.48	-2469.14	25.92	-2443.22	5352.17
C6	-0.09	-2.66	-6.76	-9.42	0.12	0.17	0.05	92.92	25.77	118.68	119.23
C9	-0.13	-3.73	-6.51	-10.24	0.23	0.11	0.14	108.03	24.53	132.55	91.39
C10	-0.11	-3.47	-6.33	-9.81	0.24	0.17	0.10	101.25	24.12	125.37	99.04
C14	-0.12	-3.44	-6.88	-10.32	0.23	0.18	0.09	101.98	23.93	125.91	108.16
C16	-0.12	-3.18	-6.71	-9.89	0.23	0.18	0.11	93.18	21.89	115.07	113.71
C17	-0.06	-2.15	-4.16	-6.32	0.19	0.05	0.15	73.89	22.72	96.61	136.40
C2*	-0.06	-4.69	-5.07	-9.76	0.21	0.22	0.06	163.69	15.51	179.20	33.03
H46*	0.09	-1.03	-1.84	-2.88	0.15	0.30	0.42	19.98	9.77	29.74	9.24
Cl19	-0.58	-23.11	-3.05	-26.16	0.14	1.40	1.54	1191.50	4.08	1195.58	423.85
Cl20	-0.57	-22.80	-6.68	-29.48	0.14	0.66	0.79	1197.51	4.37	1201.88	413.29
P13	0.86	-7.07	-6.37	-13.43	1.02	0.11	0.96	481.97	12.18	494.15	40.48
N4	-0.85	-5.95	-3.25	-9.20	0.38	0.47	0.85	208.64	11.71	220.35	22.80
N5	-0.85	-5.95	-3.05	-9.00	0.38	0.47	0.85	209.40	11.64	221.04	23.93
N15	-0.86	-5.91	-3.46	-9.37	0.37	0.48	0.84	204.84	11.84	216.69	26.24
H29*	0.06	-1.07	-1.25	-2.32	0.16	0.07	0.09	20.56	7.97	28.52	7.38
H43*	0.11	-0.96	-1.59	-2.55	0.15	0.36	0.42	19.46	8.66	28.12	8.76

Table 3.72: The charges, magnetizability contribution, dipole, magnetic shielding tensor and anisotropy of some selected atoms in complexes **4**

Atom	q(A)	χ_{Intra_Iso}(A)	χ_{Bond_Iso}(A)	$\chi_{\_Iso}$(A)	$\lvert\mu_{Intra}(A)\rvert$	$\lvert\mu_{Bond}(A)\rvert$	$\lvert\mu(A)\rvert$	$\sigma_{\_Iso}$(A, A)	$\sigma_{\_Iso}$(A', A)	$\sigma_{\_Iso}$(A)	Anisotropy
Ru1	0.68	23.69	-20.31	3.38	0.31	0.84	0.85	-3024.52	25.27	-2999.25	5722.50
C6	-0.11	-3.44	-6.63	-10.07	0.23	0.13	0.13	101.94	24.15	126.09	101.34
C10	-0.13	-3.71	-8.04	-11.75	0.22	0.13	0.13	108.63	24.14	132.77	101.98
C11	-0.09	-2.68	-7.28	-9.96	0.17	0.07	0.14	94.23	26.95	121.18	126.57
C18	-0.08	-2.06	-5.20	-7.26	0.18	0.12	0.06	71.21	23.14	94.35	137.73
C19	-0.11	-3.46	-8.15	-11.61	0.24	0.18	0.12	104.19	25.25	129.44	94.91
C21	-0.10	-3.21	-4.78	-8.00	0.25	0.18	0.11	94.13	21.65	115.78	114.93
C7*	-0.06	-4.79	-5.72	-10.51	0.25	0.19	0.16	165.34	15.82	181.16	34.35
H31*	0.06	-1.20	-1.09	-2.29	0.16	0.07	0.21	21.07	9.57	30.64	7.88
H39*	0.01	-1.30	-1.79	-3.09	0.16	0.12	0.10	21.72	10.25	31.97	6.80
O16	-0.93	-9.11	-3.96	-13.07	0.13	0.69	0.75	353.42	9.98	363.40	163.45
Cl23#	-0.54	-22.35	-3.67	-26.02	0.11	1.22	1.32	1072.63	4.11	1076.74	602.88
H50*	0.49	-0.52	-1.26	-1.78	0.15	0.14	0.08	15.52	15.78	31.30	19.15
H51*	0.50	-0.47	-0.95	-1.43	0.15	0.32	0.38	13.81	18.29	32.10	19.30
P12	0.73	-7.52	-6.77	-14.29	0.96	0.26	0.70	477.46	10.96	488.42	65.95
N2	-0.85	-5.74	-2.99	-8.72	0.36	0.45	0.81	195.39	11.31	206.69	39.66
N8	-0.85	-5.76	-3.17	-8.93	0.36	0.45	0.81	195.98	11.48	207.46	34.05
N9	-0.85	-5.78	-2.93	-8.72	0.36	0.45	0.81	198.20	11.54	209.74	34.91
H26*	0.07	-1.09	-1.02	-2.11	0.16	0.10	0.09	20.46	7.28	27.74	5.96
H35*	0.07	-1.07	-1.58	-2.65	0.16	0.06	0.10	20.36	7.84	28.20	5.35

Table 3.73: The charges, magnetizability contribution, dipole, magnetic shielding tensor and anisotropy of some selected atoms in complexes **5**

Atom	q(A)	χ_{Intra_Iso}(A)	χ_{Bond_Iso}(A)	$\chi_{\_Iso}$(A)	$\lvert\mu_{Intra}(A)\rvert$	$\lvert\mu_{Bond}(A)\rvert$	$\lvert\mu(A)\rvert$	$\sigma_{\_Iso}$(A, A)	$\sigma_{\_Iso}$(A', A)	$\sigma_{\_Iso}$(A)	Anisotropy
Ru1	0.65	18.61	-25.14	-6.53	0.39	1.56	1.71	-2345.90	25.97	-2319.93	5313.01
C6	-0.11	-3.37	-6.14	-9.51	0.25	0.21	0.07	97.78	23.80	121.58	116.49
C9	-0.13	-3.74	-6.32	-10.06	0.23	0.12	0.12	107.84	24.25	132.10	95.56
C10	-0.09	-3.44	-6.09	-9.53	0.27	0.23	0.07	94.64	21.69	116.33	129.12
C14	-0.09	-2.58	-6.72	-9.30	0.12	0.16	0.04	90.63	25.57	116.20	122.22
C16	-0.10	-3.24	-6.04	-9.28	0.26	0.23	0.07	90.66	22.00	112.66	129.03
C19	-0.11	-3.52	-6.12	-9.64	0.24	0.18	0.08	102.28	23.87	126.15	102.06
C18*	-0.06	-4.69	-5.08	-9.77	0.21	0.22	0.09	163.28	15.45	178.73	33.91
Cl2#	-0.57	-23.04	-4.20	-27.24	0.14	1.13	1.26	1197.33	4.27	1201.60	395.17
Cl20	-0.57	-23.06	-2.98	-26.03	0.14	1.38	1.51	1193.59	4.13	1197.72	416.52
P11	0.86	-7.10	-6.45	-13.54	1.02	0.18	0.90	482.52	11.99	494.50	39.20
N5	-0.85	-5.93	-3.05	-8.98	0.38	0.47	0.85	207.96	11.63	219.59	24.26
N7	-0.86	-5.90	-3.35	-9.25	0.37	0.49	0.84	204.07	11.84	215.91	27.50
N15	-0.85	-5.95	-3.24	-9.19	0.38	0.47	0.84	208.95	11.67	220.62	24.12
H25*	0.12	-0.95	-1.32	-2.28	0.15	0.44	0.50	19.43	8.70	28.13	7.97
H37*	0.06	-1.07	-1.22	-2.29	0.16	0.10	0.09	20.56	7.84	28.40	7.67

Table 3.74: The charges, magnetizability contribution, dipole, magnetic shielding tensor and anisotropy of some selected atoms in complexes **6**

Atom	q(A)	χ_{Intra_Iso}(A)	χ_{Bond_Iso}(A)	$\chi_{\_Iso}$(A)	$\lvert\mu_{Intra}(A)\rvert$	$\lvert\mu_{Bond}(A)\rvert$	$\lvert\mu(A)\rvert$	$\sigma_{\_Iso}$(A, A)	$\sigma_{\_Iso}$(A', A)	$\sigma_{\_Iso}$(A)	Anisotropy
Ru1	0.68	23.15	-22.34	0.82	0.31	0.72	0.78	-2970.53	25.12	-2945.40	5733.05
C2	-0.11	-3.46	-6.28	-9.74	0.24	0.13	0.12	102.45	23.77	126.22	106.28
C3	-0.12	-3.69	-6.58	-10.27	0.24	0.15	0.12	104.89	23.98	128.87	107.88
C7	-0.09	-2.58	-6.94	-9.52	0.16	0.07	0.21	91.48	26.60	118.08	129.93
C8	-0.11	-3.45	-7.45	-10.90	0.24	0.14	0.12	94.36	22.00	116.37	125.75
C13	-0.11	-3.53	-7.30	-10.83	0.24	0.18	0.11	106.84	25.21	132.05	98.20
C14	-0.08	-3.23	-4.31	-7.54	0.27	0.22	0.09	90.79	21.76	112.55	133.93
C6*	-0.06	-4.78	-5.35	-10.13	0.25	0.20	0.24	164.78	15.66	180.44	33.68
H26*	0.06	-1.19	-1.04	-2.23	0.16	0.09	0.23	21.04	9.44	30.48	7.55
O11	-0.93	-9.12	-2.85	-11.97	0.13	0.67	0.75	356.99	10.01	367.00	170.49
Cl20#	-0.53	-22.24	-3.59	-25.83	0.11	1.21	1.31	1069.96	4.10	1074.06	624.88
H41*	0.51	-0.47	-0.83	-1.30	0.15	0.35	0.41	13.88	18.24	32.12	18.46
P12	0.73	-7.44	-6.57	-14.00	0.94	0.43	0.51	469.82	10.77	480.59	76.75
N15	-0.85	-5.72	-3.09	-8.81	0.36	0.45	0.81	193.31	11.41	204.72	37.10
N16	-0.85	-5.73	-2.88	-8.61	0.35	0.45	0.81	194.52	11.50	206.02	38.83
N5	-0.85	-5.69	-2.94	-8.63	0.36	0.45	0.81	191.98	11.26	203.24	44.04
H23*	0.07	-1.09	-0.98	-2.06	0.16	0.12	0.09	20.44	7.18	27.62	5.98
H33*	0.07	-1.06	-1.41	-2.46	0.16	0.10	0.08	20.32	7.72	28.04	5.82

Table 3.75: The charges, magnetizability contribution, dipole, magnetic shielding tensor and anisotropy of some selected atoms in complexes **7**

Atom	q(A)	χ_{Intra_Iso}(A)	χ_{Bond_Iso}(A)	$\chi_{\_Iso}$(A)	$\lvert\mu_{Intra}(A)\rvert$	$\lvert\mu_{Bond}(A)\rvert$	$\lvert\mu(A)\rvert$	$\sigma_{\_Iso}$(A, A)	$\sigma_{\_Iso}$(A', A)	$\sigma_{\_Iso}$(A)	Anisotropy
Ru1	0.65	17.24	-23.87	-6.64	0.40	1.85	2.08	-2148.92	26.26	-2122.67	5122.76
C6	-0.10	-3.69	-6.34	-10.03	0.28	0.22	0.07	108.41	24.34	132.74	105.68
C8	-0.09	-3.45	-6.50	-9.95	0.26	0.25	0.02	100.02	23.76	123.77	118.80
C12	-0.11	-3.10	-6.72	-9.82	0.10	0.12	0.21	99.58	25.32	124.90	90.09
C17	-0.09	-3.24	-7.24	-10.48	0.26	0.29	0.05	89.86	21.53	111.38	135.87
C21	-0.08	-3.43	-7.23	-10.66	0.28	0.30	0.03	102.49	23.84	126.33	112.53
C22	-0.08	-3.35	-4.29	-7.64	0.28	0.23	0.11	92.87	21.58	114.44	131.45
F7*	-0.52	-6.91	-2.43	-9.33	0.07	0.53	0.47	281.25	3.59	284.84	133.19
F18*	-0.50	-6.90	-1.45	-8.35	0.07	0.68	0.61	272.91	4.03	276.95	120.71
F9	-0.49	-6.83	-1.06	-7.90	0.08	0.77	0.69	256.09	4.03	260.12	120.24
Cl11#	-0.55	-22.77	-4.23	-27.00	0.14	1.10	1.23	1171.99	4.38	1176.36	416.09
Cl23	-0.55	-22.78	-3.08	-25.86	0.14	1.33	1.46	1168.89	4.30	1173.19	423.99
P14	0.84	-7.00	-6.25	-13.25	0.98	0.50	0.48	473.02	12.00	485.02	55.06
N15	-0.85	-5.86	-3.08	-8.93	0.37	0.47	0.84	201.41	11.66	213.07	30.75
N13	-0.86	-5.85	-3.29	-9.15	0.37	0.47	0.83	200.41	11.78	212.19	31.52
N2	-0.85	-5.87	-3.00	-8.88	0.38	0.47	0.84	203.56	11.58	215.14	27.72
H25*	0.07	-1.10	-1.16	-2.26	0.16	0.18	0.30	20.50	7.71	28.21	5.99
H32*	0.11	-0.96	-1.37	-2.34	0.15	0.34	0.39	19.53	8.52	28.04	8.08
H34*	0.08	-1.05	-1.59	-2.63	0.15	0.26	0.37	20.32	7.95	28.27	8.66

Table 3.76: The sum total of the charges, magnetizability contribution, dipole, magnetic shielding tensor and anisotropy over all atoms in complexes **1**, **2**, **3**, **4**, **5**, **6** and **7**

	q(A)	χ_{Intra_Iso}(A)	χ_{Bond_Iso}(A)	$\chi_{\_Iso}$(A)	$\lvert\mu_{Intra}(A)\rvert$	$\lvert\mu_{Bond}(A)\rvert$	$\lvert\mu(A)\rvert$	$\sigma_{\_Iso}$(A, A)	$\sigma_{\_Iso}$(A', A)	$\sigma_{\_Iso}$(A)	Anisotropy
raptaB	0.001	-110.750	-117.580	-228.330	10.478	11.915	11.699	3038.482	453.272	3491.754	7253.739
raptaBh20	1.000	-91.203	-115.337	-206.540	10.470	10.873	8.596	1359.166	485.857	1845.024	7767.755
raptaC	-0.001	-132.964	-143.111	-276.075	12.231	11.723	12.618	3538.673	604.259	4142.932	7475.581
raptaCh2o	0.999	-114.947	-142.820	-257.767	12.299	11.078	10.343	2006.529	640.884	2647.412	7882.425
raptaT	0.000	-115.510	-123.627	-239.137	10.910	12.036	11.422	3068.983	491.212	3560.194	7300.437
raptaTh2o	0.998	-96.468	-121.308	-217.776	10.945	10.860	9.233	1454.307	524.732	1979.039	7825.634
raptaTcf3	0.000	-128.347	-124.585	-252.932	11.055	15.261	13.282	3834.681	476.175	4310.856	7487.330

Table 3.77: Correlation of the charges, magnetizability contribution, dipole, magnetic shielding tensor and anisotropy of complexes **1**, **2**, **3**, **4**, **5**, **6** and **7**

qA*	χ_{Intra_Iso}(A)	χ_{Bond_Iso}(A)	$\chi_{\_Iso}$(A)	μ_{Intra}(A)	μ_{Bond}(A)	μ(A)	$\sigma_{\_Iso}$(AA)	$\sigma_{\_Iso}$(A'A)	$\sigma_{\_Iso}$(A)	Anisotropy
raptaB	0.55	-0.21	0.38	0.21	-0.1	-0.18	-0.44	0.12	-0.44	0.25
raptaBh2o	0.54	-0.13	0.46	0.15	-0.18	-0.52	-0.38	0.11	-0.38	0.23
raptaC	0.55	-0.11	0.45	0.21	-0.17	-0.29	-0.44	0.1	-0.44	0.25
raptaCh2o	0.54	-0.06	0.5	0.16	-0.25	-0.47	-0.38	0.09	-0.38	0.24
raptaT	0.55	-0.17	0.43	0.21	-0.18	-0.29	-0.44	0.11	-0.44	0.25
raptaTh2o	0.54	-0.1	0.49	0.15	-0.24	-0.54	-0.38	0.1	-0.38	0.23
raptaTcf3	0.53	-0.16	0.42	0.38	-0.12	-0.29	-0.4	0.28	-0.39	0.19

χ_{Intra_Iso}(A)*	χ_{Bond_Iso}(A)	$\chi_{\_Iso}$(A)	μ_{Intra}(A)	μ_{Bond}(A)	μ(A)	$\sigma_{\_Iso}$(AA)	$\sigma_{\_Iso}$(A'A)	$\sigma_{\_Iso}$(A)	Anisotropy
raptaB	-0.36	0.71	0	-0.23	-0.29	-0.93	0.32	-0.93	0.47
raptaBh2o	-0.44	0.7	-0.08	-0.26	-0.23	-0.92	0.27	-0.92	0.65
raptaC	-0.25	0.78	-0.02	-0.18	-0.24	-0.93	0.29	-0.93	0.51
raptaCh2o	-0.34	0.77	-0.08	-0.23	-0.28	-0.93	0.24	-0.93	0.67
raptaT	-0.34	0.75	-0.01	-0.23	-0.27	-0.93	0.32	-0.93	0.5
raptaTh2o	-0.43	0.74	-0.08	-0.3	-0.31	-0.93	0.27	-0.93	0.67
raptaTcf3	-0.34	0.77	0.08	-0.19	-0.19	-0.93	0.37	-0.93	0.47

χ_{Bond_Iso}(A)*	$\chi_{\_Iso}$(A)	μ_{Intra}(A)	μ_{Bond}(A)	μ(A)	$\sigma_{\_Iso}$(AA)	$\sigma_{\_Iso}$(A'A)	$\sigma_{\_Iso}$(A)	Anisotropy
raptaB	0.4	-0.37	-0.68	-0.59	0.62	-0.7	0.62	-0.88
raptaBh2o	0.34	-0.33	-0.49	-0.4	0.68	-0.7	0.68	-0.84
raptaC	0.41	-0.32	-0.63	-0.54	0.53	-0.7	0.52	-0.83
raptaCh2o	0.34	-0.32	-0.47	-0.37	0.58	-0.75	0.58	-0.76
raptaT	0.36	-0.34	-0.64	-0.55	0.61	-0.71	0.6	-0.87
raptaTh2o	0.3	-0.32	-0.42	-0.35	0.67	-0.71	0.66	-0.82
raptaTcf3	0.34	-0.33	-0.67	-0.58	0.6	-0.7	0.59	-0.86

$\chi_{\_Iso}$(A)*	μ_{Intra}(A)	μ_{Bond}(A)	μ(A)	$\sigma_{\_Iso}$(AA)	$\sigma_{\_Iso}$(A'A)	$\sigma_{\_Iso}$(A)	Anisotropy
raptaB	-0.28	-0.75	-0.73	-0.44	-0.22	-0.45	-0.2
raptaBh2o	-0.35	-0.67	-0.56	-0.42	-0.28	-0.43	0.01
raptaC	-0.23	-0.57	-0.57	-0.54	-0.18	-0.54	-0.05
raptaCh2o	-0.3	-0.55	-0.53	-0.53	-0.27	-0.53	0.15
raptaT	-0.25	-0.68	-0.66	-0.5	-0.18	-0.5	-0.11
raptaTh2o	-0.32	-0.64	-0.6	-0.48	-0.25	-0.49	0.09
raptaTcf3	-0.15	-0.65	-0.58	-0.52	-0.11	-0.53	-0.12

μ_{Intra}(A)*	μ_{Bond}(A)	μ(A)	$\sigma_{\_Iso}$(AA)	$\sigma_{\_Iso}$(A'A)	$\sigma_{\_Iso}$(A)	Anisotropy
raptaB	0.32	0.29	0	0.31	0	0.08
raptaBh2o	0.56	0	0.05	0.24	0.06	0.03
raptaC	0.38	0.27	0	0.22	0.01	0.09
raptaCh2o	0.47	0.16	0.04	0.17	0.05	0.05
raptaT	0.32	0.22	-0.01	0.26	0	0.09
raptaTh2o	0.51	0.05	0.05	0.2	0.05	0.04
raptaTcf3	0.3	0.05	-0.05	0.39	-0.04	0.08

μ_{Bond}(A)*	μ(A)	$\sigma_{\_Iso}$(AA)	$\sigma_{\_Iso}$(A'A)	$\sigma_{\_Iso}$(A)	Anisotropy
raptaB	0.85	-0.1	0.18	-0.1	0.69
raptaBh2o	0.68	-0.03	0.15	-0.03	0.4

raptaC	0.76	-0.12	0.16	-0.12	0.6					
raptaCh2o	0.69	-0.07	0.12	-0.07	0.42					
raptaT	0.82	-0.09	0.16	-0.09	0.63					
raptaTh2o	0.67	0.01	0.11	0.01	0.35					
raptaTcf3	0.86	-0.13	0.12	-0.13	0.68					
μ(A)*	σ_{Iso}(AA)	σ_{Iso}(A'A)	σ_{Iso}(A)	Anisotropy		σ_{Iso}(AA)*	σ_{Iso}(A'A)	σ_{Iso}(A)	Anisotropy	
raptaB	-0.02	0.01	-0.02	0.6		raptaB	-0.41	1	-0.75	
raptaBh2o	-0.11	-0.01	-0.11	0.46		raptaBh2o	-0.35	1	-0.89	
raptaC	-0.06	-0.01	-0.06	0.56		raptaC	-0.37	1	-0.78	
raptaCh2o	-0.04	-0.05	-0.04	0.39		raptaCh2o	-0.31	1	-0.89	
raptaT	-0.05	-0.03	-0.05	0.6		raptaT	-0.4	1	-0.77	
raptaTh2o	-0.01	-0.02	-0.01	0.37		raptaTh2o	-0.33	1	-0.89	
raptaTcf3	-0.15	-0.04	-0.15	0.69		raptaTcf3	-0.42	1	-0.75	
σ_{Iso}(A'A)*	σ_{Iso}(A)	Anisotropy		σ_{Iso}(A)*	Anisotropy					
raptaB	-0.39	0.38		raptaB	-0.75					
raptaBh2o	-0.33	0.35		raptaBh2o	-0.89					
raptaC	-0.36	0.35		raptaC	-0.78					
raptaCh2o	-0.3	0.33		raptaCh2o	-0.89					
raptaT	-0.39	0.37		raptaT	-0.77					
raptaTh2o	-0.32	0.34		raptaTh2o	-0.89					
raptaTcf3	-0.4	0.35		raptaTcf3	-0.75					

20

21

22

Table 3.78: The selected bond lengths and angles of interest with the percentage of the alignment of each complexes optimized using different basis sets ECP(Ru,Cl)|6-31G* and ECP(Ru)|6-31+G(d,p).

		1	2	3	4	5
Ru-Cl	ECP(Ru,Cl)|6-31G*	2.444	2.444	2.390		
	ECP(Ru)|6-31+G(d,p)	2.394	2.396	2.440		
Ru-N	ECP(Ru,Cl)|6-31G*	2.133, 2.134	2.10, 2.10	2.140, 2.146	2.166, 2.166, *2.089	2.157, 2.158, *2.045
	ECP(Ru)|6-31+G(d,p)	2.137,2.139	2.096, 2.096	2.138, 2.138	2.162, 2.162, *2.084	2.152, 2.153, *2.039
Ru-C ranges	ECP(Ru,Cl)|6-31G*	2.225 - 2.234	2.229 - 2.251	2.233 – 2.252	2.240 – 2.251	2.251 – 2.268
	ECP(Ru)|6-31+G(d,p)	2.222 – 2.232	2.233 – 2.254	2.236 – 2.253	2.241 – 2.252	2.252 – 2.269
N-Ru-N	ECP(Ru,Cl)|6-31G*	83.045	76.995	77.375	107.984, *72.054, *72.051	108.839, *73.521, *73.568
	ECP(Ru)|6-31+G(d,p)	82.809	77.116	77.317	107.855, *72.159, *72.158	108.654, *73.632, *73.672
RMSD of atoms in Å		0.068	0.004	0.017	0.011	0.01

The values for the complexes 4 and 5 with superscript "*" indicated their association with the middle nitrogen of their tridentate.

Table 3.79: The assignment of the IR vibrations to different bonds in the complexes

Vibrations	Complex	Assignment
3600-3625	1, 2, 3, 5	O-H of carboxylic
1758-1784	1, 2, 3, 5	C=O [[Carusoetal2012]] of carboxylic
1050-1150	1, 2, 3, 5	O-C stretches (2-bands)
735-745	1, 2, 4, 5	O-H bend (out-of-plane)
3228	1, 4	C-H asymmetric vibration peculiar to pyrazol-1-ly unit
3050-3161	all	C-H arene asymmetric vibration
1419	all	charge transfer Ru-L [[Rajapakseetal2009]] C-C arene v(C-H) stretches
1337	All but prominent in complex 2	C-N stretches
597	complex 3 i.e. effect of carbonyl unit being very close to metal	Charge transfer
614-642	Complex 1, 2, 3, 5	O-H bend (out-of-plane) of carboxylic unit
300	Complex 1, 2, 3, 5	Peculiar to carboxylic
1477	4	Ru-L charge transfer [[Ombergetal1997]], C-C, C-N
1419	all	Ru-L charge transfer [[Ombergetal1997]], C-C, C-N
700	1,2,3	Ru-Cl
751	2,4,5 with pyridine has peculiar	Ru-N(py)
847	3	Ru-N(phen)
731	1, 4	Ru-N(pz)
765	4,5 (strong)	Ru-N(py) should result from the strong long bond of Ru with mid pyridine unit
797	all	Ru-C
3161	2,4,5	v(C-H) antisymmetric stretches (py)
3224	1,4	v(C-H) antisymmetric stretches (pz)
505	5	Ru-N(py) close to 424-428 assigned to v(Ru-S) [[Carusoetal2012]]
300	all	Bond deformations

Table 3.80: The values of the Ramsey terms that define all the metal-ligand spin spin coupling of the

complexes from two different systems treated with DGDZVP(Ru)|6-31+G(d,p) and 3-21G respectively

DGDZVP(Ru)|6-31+G(d,p) Complex **1**						3-21G Complex **1**					
	FC	SD	PSO	DSO	J (HZ)		FC	SD	PSO	DSO	J (HZ)
Ru-C9	-7.06E+00	3.62E-001	-1.71E+00	-3.20E-002	-8.44E+00	Ru-C9	-2.15E+00	1.81E-001	-1.74E+00	-3.21E-002	-3.74E+00
Ru-C10	-7.83E+00	-3.13E-001	-1.67E+00	-3.37E-002	-9.85E+00	Ru-C10	-2.32E+00	-2.63E-001	-1.65E+00	-3.31E-002	-4.26E+00
Ru-C13	-7.44E+00	-2.17E-001	-1.53E+00	-3.37E-002	-9.22E+00	Ru-C13	-2.14E+00	-1.73E-001	-1.60E+00	-3.32E-002	-3.95E+00
Ru-C16	-9.25E+00	2.82E-001	-1.38E+00	-3.31E-002	-1.04E+01	Ru-C16	-2.76E+00	9.19E-002	-1.31E+00	-3.30E-002	-4.01E+00
Ru-C18	-8.82E+00	2.44E-001	-1.74E+00	-3.29E-002	-1.03E+01	Ru-C18	-2.54E+00	7.33E-002	-1.69E+00	-3.26E-002	-4.19E+00
Ru-C19	-8.16E+00	-3.04E-001	-1.04E+00	-3.34E-002	-9.53E+00	Ru-C19	-2.55E+00	-2.52E-001	-1.12E+00	-3.31E-002	-3.96E+00
Ru-Cl22	-1.57E+00	-2.33E+00	-2.32E+00	-9.87E-003	-2.71E+01	Ru-Cl22	-1.11E+00	-2.49E+00	-2.20E+00	-9.88E-003	-2.56E+01
Ru-N12	-1.24E+01	-1.01E-001	-7.08E-001	-1.46E-002	-1.32E+01	Ru-N12	-8.92E+00	-1.07E-001	-6.04E-001	-1.42E-002	-9.65E+00
Ru-N17	-1.22E+01	-1.03E-001	-6.93E-001	-1.46E-002	-1.30E+01	Ru-N17	-8.86E+00	-1.04E-001	-5.18E-001	-1.42E-002	-9.49E+00
Complex **2**						Complex **2**					
Ru-C7	-7.31E+00	-3.58E-001	-1.31E+00	-3.33E-002	-9.01E+00	Ru-C7	-2.42E+00	-3.80E-001	-1.32E+00	-3.31E-002	-4.16E+00
Ru-C8	-8.36E+00	4.45E-001	-1.26E+00	-3.21E-002	-9.21E+00	Ru-C8	-2.76E+00	3.22E-001	-1.26E+00	-3.19E-002	-3.74E+00
Ru-C13	-6.18E+00	4.40E-001	-1.71E+00	-3.08E-002	-7.47E+00	Ru-C13	-2.13E+00	3.39E-001	-1.73E+00	-3.07E-002	-3.55E+00
Ru-C14	-7.30E+00	-4.17E-001	-8.50E-001	-3.30E-002	-8.61E+00	Ru-C14	-2.11E+00	-4.33E-001	-9.09E-001	-3.29E-002	-3.48E+00
Ru-C18	-7.30E+00	-3.58E-001	-1.31E+00	-3.33E-002	-9.01E+00	Ru-C18	-2.42E+00	-3.80E-001	-1.33E+00	-3.30E-002	-4.17E+00
Ru-C19	-8.34E+00	4.46E-001	-1.26E+00	-3.21E-002	-9.18E+00	Ru-C19	-2.75E+00	3.23E-001	-1.26E+00	-3.19E-002	-3.72E+00
Ru-Cl10	-1.17E+00	-2.36E+00	-2.40E+00	-9.72E-003	-2.76E+01	Ru-Cl10	9.17E-001	-2.48E+00	-2.26E+00	-9.71E-003	-2.60E+01
Ru-N11	-1.28E+01	-8.72E-002	-2.53E-002	-1.41E-002	-1.29E+01	Ru-N11	-8.59E+00	-1.01E-001	-1.99E-003	-1.37E-002	-8.71E+00
Ru-N16	-1.28E+01	-8.64E-002	-9.98E-003	-1.41E-002	-1.29E+01	Ru-N16	-8.59E+00	-1.01E-001	-1.20E-002	-1.37E-002	-8.69E+00
Complex **3**						Complex **3**					
Ru-C13	-	-1.31E-	-	-3.59E-	-	Ru-C13	-	-6.54E-	-	-3.59E-	-

	8.75E+00	002	1.30E+00	002	1.01E+00		2.83E+00	002	1.31E+00	002	4.25E+00
	0		0		1		0		0		0
	-		-		-		-		-		-
	7.71E+00	-7.27E-	1.84E+00	-3.59E-	9.66E+00		2.42E+00	-1.44E-	1.79E+00	-3.58E-	4.39E+00
Ru-C14	0	002	0	002	0	Ru-C14	0	001	0	002	0
	-		-		-		-		-		-
	8.63E+00	-5.35E-	1.29E+00	-3.58E-	1.00E+00		2.79E+00	-1.41E-	1.33E+00	-3.58E-	4.29E+00
Ru-C18	0	002	0	002	1	Ru-C18	0	001	0	002	0
	-		-		-		-		-		-
	7.02E+00	-2.37E-	1.63E+00	-3.47E-	8.68E+00		2.02E+00	-5.09E-	1.68E+00	-3.45E-	3.79E+00
Ru-C21	0	003	0	002	0	Ru-C21	0	002	0	002	0
	-		-		-		-		-		-
	7.68E+00	-2.66E-	1.86E+00	-3.57E-	9.60E+00		2.40E+00	-7.16E-	1.88E+00	-3.55E-	4.38E+00
Ru-C23	0	002	0	002	0	Ru-C23	0	002	0	002	0
	-		-		-		-		-		-
	7.09E+00	-4.84E-	1.62E+00	-3.48E-	8.80E+00		2.13E+00	-1.25E-	1.70E+00	-3.47E-	3.98E+00
Ru-C25	0	002	0	002	0	Ru-C25	0	001	0	002	0
	-	-	-		-		-	-	-		-
	2.06E+00	2.04E+00	2.29E+00	-1.11E-	2.70E+00		1.45E+00	2.17E+00	2.19E+00	-1.11E-	2.55E+00
Ru-Cl7	0	0	1	002	1	Ru-Cl7	0	0	1	002	1
	-			-	-		-				-
	1.15E+00	-5.83E-	3.27E-	-1.49E-	1.13E+00		8.07E+00	-6.77E-	3.26E-	-1.45E-	7.83E+00
Ru-N10	1	002	001	002	1	Ru-N10	0	002	001	002	0
	-			-	-		-				-
	1.15E+00	-6.05E-	3.14E-	-1.49E-	1.13E+00		8.01E+00	-7.72E-	2.97E-	-1.46E-	7.80E+00
Ru-N16	1	002	001	002	1	Ru-N16	0	002	001	002	0
		Complex **4**						Complex **4**			
	-		-		-		-		-		-
	7.36E+00	-2.69E-	1.17E+00	-3.17E-	8.56E+00		2.45E+00	-6.12E-	1.30E+00	-3.17E-	3.84E+00
Ru-C2	0	003	0	002	0	Ru-C2	0	002	0	002	0
	-		-		-		-		-		-
	6.27E+00	-1.82E-	1.65E+00	-3.24E-	8.13E+00		1.53E+00	-2.32E-	1.69E+00	-3.24E-	3.48E+00
Ru-C3	0	001	0	002	0	Ru-C3	0	001	0	002	0
	-		-		-		-		-		-
	7.37E+00	6.30E-	1.16E+00	-3.17E-	8.56E+00		2.46E+00	-5.27E-	1.30E+00	-3.17E-	3.84E+00
Ru-C4	0	003	0	002	0	Ru-C4	0	002	0	002	0
	-		-		-		-		-		-
	7.96E+00	-7.38E-	2.60E+00	-3.23E-	1.07E+00		2.91E+00	-1.26E-	2.50E+00	-3.22E-	5.57E+00
Ru-C5	0	002	0	002	1	Ru-C5	0	001	0	002	0
	-		-		-		-		-		-
	6.26E+00	-1.90E-	1.64E+00	-3.24E-	8.13E+00		1.53E+00	-2.40E-	1.68E+00	-3.24E-	3.48E+00
Ru-C6	0	001	0	002	0	Ru-C6	0	001	0	002	0
	-		-		-		-		-		-
	7.95E+00	-6.55E-	2.60E+00	-3.23E-	1.06E+00		2.90E+00	-1.19E-	2.51E+00	-3.22E-	5.55E+00
Ru-C7	0	002	0	002	1	Ru-C7	0	001	0	002	0
	-			-	-		-				-
	1.28E+00	3.65E-	-7.79E-	-1.33E-	1.35E+00		8.84E+00	2.47E-	-6.00E-	-1.30E-	9.43E+00
Ru-N10	1	002	001	002	1	Ru-N10	0	002	001	002	0
	-			-	-		-				-
	1.28E+00	3.67E-	-7.79E-	-1.33E-	1.35E+00		8.84E+00	2.50E-	-5.99E-	-1.30E-	9.43E+00
Ru-N13	1	002	001	002	1	Ru-N13	0	002	001	002	0
	-			-	-		-				-
	1.07E+00	-1.64E-	-6.73E-	-1.47E-	1.16E+00		6.86E+00	-1.59E-	-4.56E-	-1.45E-	7.49E+00
Ru-N15	1	001	001	002	1	Ru-N15	0	001	001	002	0
Complex **5**								Complex **5**			
	-		-		-		-		-		-
	7.94E+00	-8.67E-	2.14E+00	-3.26E-	1.01E+00		2.81E+00	-6.52E-	2.07E+00	-3.25E-	4.98E+00
Ru-C18	0	003	0	002	1	Ru-C18	0	002	0	002	0
	-		-		-		-		-		-
	6.08E+00	-1.52E-	1.42E+00	-3.27E-	7.69E+00		1.43E+00	-1.99E-	1.45E+00	-3.26E-	3.11E+00
Ru-C20	0	001	0	002	0	Ru-C20	0	001	0	002	0
	-		-		-		-		-		-
	7.95E+00	-1.74E-	2.14E+00	-3.26E-	1.01E+00		2.82E+00	-7.17E-	2.07E+00	-3.25E-	4.99E+00
Ru-C22	0	002	0	002	1	Ru-C22	0	002	0	002	0
Ru-C23	-	7.09E-	-8.44E-	-3.18E-	-	Ru-C23	-	1.27E-	-9.64E-	-3.17E-	-

	6.77E+000	002	001	002	7.57E+000		2.28E+000	002	001	002	3.26E+000
	-		-		-		-		-		-
Ru-C26	6.10E+000	-1.46E-001	1.43E+000	-3.27E-002	7.71E+000	Ru-C26	1.43E+000	-1.96E-001	1.45E+000	-3.26E-002	3.11E+000
	-				-		-				-
Ru-C27	6.75E+000	6.16E-002	-8.46E-001	-3.18E-002	7.57E+000	Ru-C27	2.27E+000	6.47E-003	-9.66E-001	-3.17E-002	3.26E+000
	-				-		-				-
Ru-N14	1.27E+001	1.90E-002	-2.15E-001	-1.33E-002	1.29E+001	Ru-N14	8.69E+000	5.82E-003	-9.55E-002	-1.30E-002	8.80E+000
	-				-		-				-
Ru-N15	1.24E+001	-1.60E-001	-3.08E-001	-1.50E-002	1.29E+001	Ru-N15	7.90E+000	-1.68E-001	-1.85E-001	-1.48E-002	8.26E+000
	-				-		-				-
Ru-N21	1.27E+001	1.81E-002	-2.34E-001	-1.33E-002	1.30E+001	Ru-N21	8.71E+000	5.23E-003	-1.08E-001	-1.30E-002	8.82E+000

Table 3.81: The values of the Ramsey terms that define all the metal-ligand spin spin coupling of the complexes from two different systems treated with ECP(Ru)|6-31+G(d,p) and ECP(Ru,Cl)|6-31G* respectively

	Ramsey Terms	ECP(6-31+G(d,p)					ECP(6-31G*)	Ramsey Terms			
	Complex **1**						Complex **1**				
	FC (HZ) for Ru	SD for Ru	PSO for Ru	DSO for Ru	J (HZ) for Ru		FC (HZ) for Ru	SD for Ru	PSO for Ru	DSO for Ru	J (HZ) for Ru
Ru-C9	-3.67E-006	4.55E-002	-2.43E-001	-3.18E-002	-2.29E-001	Ru-C9	-1.79E-006	3.65E-002	-2.55E-001	-3.00E-002	-2.48E-001
Ru-C10	-6.04E-006	-2.15E-002	-2.38E-001	-3.35E-002	-2.93E-001	Ru-C10	0.00E+000	-1.41E-002	-2.43E-001	-3.06E-002	-2.88E-001
Ru-C13	-6.00E-006	-7.58E-003	-2.17E-001	-3.35E-002	-2.58E-001	Ru-C13	-2.90E-006	8.14E-004	-2.34E-001	-3.09E-002	-2.64E-001
Ru-C16	-3.66E-006	4.04E-002	-2.09E-001	-3.29E-002	-2.01E-001	Ru-C16	0.00E+000	3.01E-002	-2.00E-001	-2.98E-002	-2.00E-001
Ru-C18	-3.00E-006	3.33E-002	-2.52E-001	-3.27E-002	-2.52E-001	Ru-C18	1.33E-006	2.31E-002	-2.51E-001	-2.99E-002	-2.58E-001
Ru-C19	-6.44E-006	-1.89E-002	-1.57E-001	-3.32E-002	-2.09E-001	Ru-C19	0.00E+000	-9.33E-003	-1.69E-001	-2.98E-002	-2.08E-001
Ru-Cl22	0.00E+000	-1.71E-001	3.17E+000	-9.93E-003	-3.35E+000	Ru-Cl22	0.00E+000	-1.17E-002	-2.17E-001	-9.88E-003	-2.38E-001
Ru-N12	-3.55E-006	-3.63E-003	-9.07E-002	-1.46E-002	-1.09E-001	Ru-N12	1.35E-006	-4.11E-003	-1.09E-001	-1.37E-002	-1.27E-001
Ru-N17	-3.49E-006	-3.73E-003	-8.93E-002	-1.46E-002	-1.08E-001	Ru-N17	1.18E-006	-3.82E-003	-9.36E-002	-1.37E-002	-1.11E-001
	Complex **2**						Complex **2**				
Ru-C7	-8.10E-006	-2.42E-002	-1.86E-001	-3.31E-002	-2.43E-001	Ru-C7	-5.02E-006	-2.49E-002	-1.95E-001	-3.06E-002	-2.51E-001
Ru-C8	-7.05E-006	5.42E-002	-1.89E-001	-3.18E-002	-1.67E-001	Ru-C8	0.00E+000	5.35E-002	-1.94E-001	-2.89E-002	-1.69E-001
Ru-C13	-6.10E-006	5.10E-002	-2.39E-001	-3.06E-002	-2.19E-001	Ru-C13	-5.93E-006	5.09E-002	-2.56E-001	-2.86E-002	-2.34E-001
Ru-C14	-4.52E-006	-2.90E-002	-1.27E-001	-3.28E-002	-1.89E-001	Ru-C14	-1.35E-006	-2.96E-002	-1.36E-001	-2.95E-002	-1.96E-001
Ru-C18	-8.10E-006	-2.42E-002	-1.87E-001	-3.31E-002	-2.44E-001	Ru-C18	-5.03E-006	-2.49E-002	-1.96E-001	-3.06E-002	-2.51E-001
Ru-C19	-7.04E-006	5.42E-002	-1.88E-001	-3.18E-002	-1.66E-001	Ru-C19	0.00E+000	5.36E-002	-1.93E-001	-2.89E-002	-1.69E-001

				-							
	0.00E+00	-1.69E-	3.28E+00	-9.78E-	3.46E+00		0.00E+00	-1.10E-	-2.25E-	-9.74E-	-2.46E-
Ru-Cl10	0	001	0	003	0	Ru-Cl10	0	002	001	003	001
	-3.33E-	-3.49E-	8.27E-	-1.41E-	-9.33E-		0.00E+00	-3.67E-	4.69E-	-1.30E-	-1.62E-
Ru-N11	006	003	003	002	003	Ru-N11	0	003	004	002	002
	-3.28E-	-3.57E-	1.05E-	-1.41E-	-7.21E-		0.00E+00	-3.73E-	2.52E-	-1.30E-	-1.42E-
Ru-N16	006	003	002	002	003	Ru-N16	0	003	003	002	002
		Complex **3**						Complex **3**			
	-6.29E-	8.47E-	-1.86E-	-3.57E-	-2.13E-		0.00E+00	9.88E-	-1.87E-	-3.27E-	-2.10E-
Ru-C13	006	003	001	002	001	Ru-C13	0	003	001	002	001
	-7.82E-	2.83E-	-2.47E-	-3.56E-	-2.79E-		-1.39E-	8.60E-	-2.42E-	-3.31E-	-2.74E-
Ru-C14	006	003	001	002	001	Ru-C14	006	004	001	002	001
	-6.23E-	4.71E-	-1.84E-	-3.56E-	-2.15E-		1.32E-	1.50E-	-1.89E-	-3.26E-	-2.20E-
Ru-C18	006	003	001	002	001	Ru-C18	006	003	001	002	001
	-7.37E-	1.06E-	-2.25E-	-3.45E-	-2.49E-		-2.65E-	1.08E-	-2.40E-	-3.24E-	-2.61E-
Ru-C21	006	002	001	002	001	Ru-C21	006	002	001	002	001
	-7.69E-	7.47E-	-2.49E-	-3.55E-	-2.77E-		-1.47E-	9.20E-	-2.54E-	-3.29E-	-2.78E-
Ru-C23	006	003	001	002	001	Ru-C23	006	003	001	002	001
	-7.51E-	6.02E-	-2.24E-	-3.46E-	-2.53E-		-2.80E-	2.72E-	-2.41E-	-3.25E-	-2.71E-
Ru-C25	006	003	001	002	001	Ru-C25	006	003	001	002	001
				-							
	0.00E+00	-1.24E-	3.06E+00	-1.11E-	3.20E+00		0.00E+00	-7.99E-	-2.11E-	-1.11E-	-2.30E-
Ru-Cl7	0	001	0	002	0	Ru-Cl7	0	003	001	002	001
	-3.25E-	-2.18E-	6.56E-	-1.49E-	4.85E-		-1.10E-	-1.94E-	6.08E-	-1.39E-	4.50E-
Ru-N10	006	003	002	002	002	Ru-N10	006	003	002	002	002
	-3.25E-	-2.24E-	6.39E-	-1.49E-	4.67E-		-1.02E-	-2.53E-	5.75E-	-1.39E-	
Ru-N16	006	003	002	002	002	Ru-N16	006	003	002	002	4.11E-002
		Complex **4**						Complex **4**			
	-3.54E-	8.88E-	-1.74E-	-3.14E-	-1.97E-		5.22E-	8.93E-	-1.80E-	-3.13E-	-2.03E-
Ru-C2	006	003	001	002	001	Ru-C2	006	003	001	002	001
	-8.33E-	-8.29E-	-2.29E-	-3.22E-	-2.70E-		-2.18E-	-8.75E-	-2.34E-	-3.21E-	-2.74E-
Ru-C3	006	003	001	002	001	Ru-C3	006	003	001	002	001
	-3.54E-	9.73E-	-1.74E-	-3.14E-	-1.96E-		5.25E-	9.81E-	-1.80E-	-3.13E-	-2.02E-
Ru-C4	006	003	001	002	001	Ru-C4	006	003	001	002	001
	-7.34E-	1.34E-	-3.43E-	-3.22E-	-3.75E-		0.00E+00	-5.09E-	-3.47E-	-3.21E-	-3.80E-
Ru-C5	006	004	001	002	001	Ru-C5	0	004	001	002	001
	-8.31E-	-9.04E-	-2.28E-	-3.22E-	-2.69E-		-2.17E-	-9.54E-	-2.32E-	-3.21E-	-2.74E-
Ru-C6	006	003	001	002	001	Ru-C6	006	003	001	002	001
	-7.33E-	9.98E-	-3.44E-	-3.22E-	-3.75E-		0.00E+00	3.83E-	-3.48E-	-3.21E-	-3.79E-
Ru-C7	006	004	001	002	001	Ru-C7	0	004	001	002	001
	-3.37E-	1.11E-	-1.07E-	-1.34E-	-1.09E-		0.00E+00	1.10E-	-1.10E-	-1.33E-	-1.13E-
Ru-N10	006	002	001	002	001	Ru-N10	0	002	001	002	001
	-3.37E-	1.11E-	-1.07E-	-1.34E-	-1.09E-		0.00E+00	1.10E-	-1.10E-	-1.33E-	-1.13E-
Ru-N13	006	002	001	002	001	Ru-N13	0	002	001	002	001
	-2.89E-	-1.15E-	-6.88E-	-1.47E-	-9.51E-		0.00E+00	-1.17E-	-7.21E-	-1.47E-	-9.84E-
Ru-N15	006	002	002	002	002	Ru-N15	0	002	002	002	002
		Complex **5**						Complex **5**			
	-6.68E-	7.27E-	-2.86E-	-3.25E-	-3.11E-		0.00E+00	6.50E-	-2.91E-	-3.24E-	-3.17E-
Ru-C18	006	003	001	002	001	Ru-C18	0	003	001	002	001
	-7.65E-	-5.87E-	-2.02E-	-3.24E-	-2.40E-		0.00E+00	-6.18E-	-2.07E-	-3.23E-	-2.45E-
Ru-C20	006	003	001	002	001	Ru-C20	0	003	001	002	001
	-6.70E-	6.32E-	-2.86E-	-3.25E-	-3.12E-		0.00E+00	5.75E-	-2.91E-	-3.24E-	-3.17E-
Ru-C22	006	003	001	002	001	Ru-C22	0	003	001	002	001
	-2.90E-	1.57E-	-1.33E-	-3.14E-	-1.49E-		4.56E-	1.59E-	-1.40E-	-3.13E-	-1.55E-
Ru-C23	006	002	001	002	001	Ru-C23	006	002	001	002	001
	-7.62E-	-5.40E-	-2.02E-	-3.24E-	-2.40E-		0.00E+00	-5.95E-	-2.07E-	-3.23E-	-2.45E-
Ru-C26	006	003	001	002	001	Ru-C26	0	003	001	002	001
	-2.93E-	1.49E-	-1.33E-	-3.14E-	-1.50E-		4.62E-	1.54E-	-1.40E-	-3.13E-	-1.56E-
Ru-C27	006	002	001	002	001	Ru-C27	006	002	001	002	001
	-3.40E-	1.07E-	-1.97E-	-1.33E-	-2.23E-		-1.06E-	1.08E-	-2.29E-	-1.33E-	-2.54E-
Ru-N14	006	002	002	002	002	Ru-N14	006	002	002	002	002
	-3.65E-	-1.37E-	-1.20E-	-1.51E-	-4.08E-		0.00E+00	-1.41E-	-1.94E-	-1.50E-	-4.84E-
Ru-N15	006	002	002	002	002	Ru-N15	0	002	002	002	002
	-3.39E-	1.07E-	-2.23E-	-1.33E-	-2.50E-		-1.08E-	1.08E-	-2.54E-	-1.33E-	-2.79E-
Ru-N21	006	002	002	002	002	Ru-N21	006	002	002	002	002

Table 3.82: Correlation of computed Ramsey Terms to the spin spin coupling over all atoms in each of the complexes

	1	**2**	**3**	**4**	**5**
	J(HZ)	J(HZ)	J(HZ)	J(HZ)	J(HZ)
FC	0.71	0.68	0.71	0.99	0.99
SD	0.66	0.64	0.72	0.28	0.15
PSO	0.77	0.77	0.77	0.76	0.64
DSO	0.24	0.34	0.47	0.59	0.48
J(HZ)	1.00	1.00	1.00	1.00	1.00

Table 3.83: The atomic NMR magnetazability and shielding for the selected atoms in the complexes using combined basis set DGDZVP(Ru)|6-31+G(d,p)

	Complex **1**														
	q(A)	Vol(A), 0.001	L(A)	K(A)	LI(A)	DI(A, A')/2	χ_{Intra_Iso} (A)	χ_{Bond_Iso}(A)	$\chi_{\_Iso}$(A)	μ(A)	$\sigma_{\_Iso}$(A,A)	$\sigma_{\_Iso}$(A',A)	$\sigma_{\_Iso}$(A)	Isotropic	Anisotropy
Ru1	9.50E-01	1.01E+02	6.36E-04	4.44E+03	4.05E+01	2.54E+00	2.24E+01	-2.27E+01	-3.35E-01	1.20E+00	-3.51E+03	-2.52E+01	3.49E+03	3.49E+03	6.16E+03
C9	-6.26E-02	7.38E+01	-5.40E-05	3.78E+01	3.97E+00	2.09E+00	-3.09E+00	-4.98E+00	-8.07E+00	9.26E-02	-8.50E+01	-2.29E+01	-1.08E+02	-1.08E+02	1.28E+02
C10	-4.68E-02	7.14E+01	-3.51E-04	3.78E+01	3.96E+00	2.09E+00	-2.65E+00	-9.19E+00	-1.18E+01	6.08E-02	-7.30E+01	-2.35E+01	-9.65E+01	-9.65E+01	1.35E+02
C13	-4.96E-02	7.16E+01	-7.50E-05	3.78E+01	3.96E+00	2.09E+00	-2.68E+00	-9.21E+00	-1.19E+01	1.02E-01	-7.55E+01	-2.33E+01	-9.88E+01	-9.88E+01	1.31E+02
C16	-5.13E-02	7.37E+01	-1.58E-04	3.78E+01	3.97E+00	2.08E+00	-3.09E+00	-4.90E+00	-7.99E+00	5.52E-02	-8.44E+01	-2.30E+01	-1.07E+02	-1.07E+02	1.32E+02
C18	-5.82E-02	7.48E+01	-1.32E-04	3.78E+01	3.98E+00	2.08E+00	-3.22E+00	-4.95E+00	-8.17E+00	6.78E-02	-8.75E+01	-2.35E+01	-1.11E+02	-1.11E+02	1.27E+02
C19	-2.85E-02	6.99E+01	-6.90E-05	3.78E+01	3.95E+00	2.08E+00	-2.34E+00	-9.02E+00	-1.14E+01	1.02E-01	-6.40E+01	-2.25E+01	-8.65E+01	-8.65E+01	1.51E+02
Cl22	-5.27E-01	2.32E+02	-8.30E-05	4.59E+02	1.69E+01	-6.46E-01	-2.15E+01	-3.69E+00	-2.52E+01	1.29E+00	-1.06E+03	-4.24E+00	-1.06E+03	-1.06E+03	5.20E+02
N12	-7.59E-01	7.81E+01	-2.16E-04	5.48E+01	5.90E+00	1.86E+00	-3.51E+00	-6.63E+00	-1.01E+01	6.58E-01	-3.46E+00	-1.70E+01	-1.35E+01	-1.35E+01	1.92E+02
N17	-7.59E-01	7.80E+01	-2.41E-04	5.48E+01	5.90E+00	1.86E+00	-3.50E+00	-6.64E+00	-1.01E+01	6.17E-01	-3.94E+00	-1.69E+01	-1.29E+01	-1.29E+01	1.93E+02

O2	-1.17E+00	1.30E+02	8.20E-05	7.54E+01	8.23E+00	9.47E-01	-6.12E+00	-3.48E+00	-9.60E+00	-1.03E+00	9.64E+01	-2.41E+00	9.40E+01	9.40E+01	5.67E+02
H24	1.23E-01	4.05E+01	2.40E-05	5.68E-01	3.45E-01	5.32E-01	-9.18E-01	-1.36E+00	-2.28E+00	-4.80E-01	1.77E+01	-5.68E+00	2.33E+01	2.33E+01	6.65E+00
H29	1.23E-01	4.06E+01	2.60E-05	5.68E-01	3.45E-01	5.32E-01	-9.20E-01	-1.36E+00	-2.29E+00	-4.92E-01	1.77E+01	-5.67E+00	2.33E+01	2.33E+01	6.63E+00
Complex **2**															
Ru1	-9.59E-01	1.04E+02	2.47E-04	4.44E+03	4.05E+01	2.57E+00	-2.00E+01	-2.28E+01	-2.79E+00	-1.18E+00	3.12E+03	-2.45E+01	3.09E+03	3.09E+03	5.61E+03
C7	-5.32E-02	7.01E+01	-2.27E-04	3.78E+01	3.96E+00	2.09E+00	-2.53E+00	-9.07E+00	-1.16E+01	-6.14E-02	6.95E+01	-2.28E+01	9.23E+01	9.23E+01	1.38E+02
C8	-6.29E-02	7.46E+01	-9.20E-05	3.78E+01	3.98E+00	2.08E+00	-3.26E+00	-4.86E+00	-8.12E+00	-8.23E-02	8.88E+01	-2.26E+01	1.11E+02	1.11E+02	1.30E+02
C13	-5.29E-02	7.64E+01	-6.00E-06	3.78E+01	3.97E+00	2.08E+00	-3.20E+00	-4.90E+00	-8.10E+00	-7.84E-02	8.70E+01	-2.27E+01	1.10E+02	1.10E+02	1.30E+02
C14	-2.67E-02	6.96E+01	-5.71E-04	3.78E+01	3.95E+00	2.08E+00	-2.13E+00	-8.85E+00	-1.10E+01	-9.18E-02	5.83E+01	-2.19E+01	8.02E+01	8.02E+01	1.57E+02
C18	-5.42E-02	7.02E+01	-8.17E-04	3.78E+01	3.96E+00	2.09E+00	-2.53E+00	-9.07E+00	-1.16E+01	-9.29E-02	6.96E+01	-2.29E+01	9.24E+01	9.24E+01	1.37E+02
C19	-6.30E-02	7.46E+01	-9.00E-05	3.78E+01	3.98E+00	2.08E+00	-3.26E+00	-4.86E+00	-8.12E+00	-7.40E-02	8.89E+01	-2.26E+01	1.11E+02	1.11E+02	1.30E+02
Cl10	-5.21E-01	2.37E+02	-8.60E-05	4.59E+02	1.69E+01	-6.23E-01	-2.20E+01	-3.76E+00	-2.57E+01	-1.26E+00	1.10E+03	-4.72E+00	1.10E+03	1.10E+03	4.20E+02
N11	-1.22E+00	8.21E+01	-8.40E-05	5.51E+01	6.36E+00	-1.86E+00	-3.55E+00	-7.30E+00	-1.09E+01	-5.42E-01	3.05E+01	-1.29E+01	1.76E+01	1.76E+01	3.87E+02
N16	-1.22E+00	8.21E+01	-1.68E-04	5.51E+01	6.36E+00	-1.86E+00	-3.54E+00	-7.32E+00	-1.09E+01	-5.10E-01	3.11E+01	-1.29E+01	1.82E+01	1.82E+01	3.89E+02
H34	8.99E-02	4.09E+01	8.10E-05	5.87E-01	3.64E-01	5.46E-01	-9.14E-01	-1.27E+00	-2.19E+00	-6.96E-02	1.82E+01	-4.25E+00	2.25E+01	2.25E+01	1.07E+01
H38	9.65E-02	4.10E+01	5.80E-05	5.81E-01	3.59E-01	5.45E-01	-9.15E-01	-1.28E+00	-2.19E+00	-5.34E-02	1.81E+01	-4.22E+00	2.23E+01	2.23E+01	1.01E+01
Complex **3**															
Ru1	-9.55E-01	9.99E+01	3.57E-04	4.44E+03	4.05E+01	2.52E+00	-2.45E+01	-2.56E+01	-1.05E+00	-8.40E-01	3.76E+03	-2.39E+01	3.73E+03	3.73E+03	6.00E+03
C13	-4.01E-02	7.06E+01	-1.19E-04	3.78E+01	3.96E+00	2.08E+00	-2.72E+00	-6.38E+00	-9.11E+00	-8.08E-02	7.46E+01	-2.26E+01	9.72E+01	9.72E+01	1.39E+02
C14	-4.85E-02	6.98E+01	-1.15E-04	3.79E+01	3.97E+00	2.08E+00	-2.69E+00	-6.81E+00	-9.50E+00	-4.00E-01	7.44E+01	-2.31E+01	9.75E+01	9.75E+01	1.39E+02
C18	-3.97E-02	7.07E+01	-9.40E-05	3.78E+01	3.96E+00	2.08E+00	-2.69E+00	-6.38E+00	-9.06E+00	-8.56E-02	7.35E+01	-2.26E+01	9.61E+01	9.61E+01	1.40E+02
C21	-5.97E-02	7.36E+01	-6.60E-05	3.78E+01	3.97E+00	2.09E+00	-2.89E+00	-6.48E+00	-9.37E+00	-1.32E-01	7.88E+01	-2.31E+01	1.02E+02	1.02E+02	1.34E+02
C23	-5.00E-02	7.02E+01	-1.81E-04	3.79E+01	3.97E+00	2.08E+00	-2.73E+00	-6.81E+00	-9.53E+00	-4.12E-01	7.53E+01	-2.31E+01	9.84E+01	9.84E+01	1.39E+02

C25	-5.93E-02	7.33E+01	-2.62E-04	3.78E+01	3.97E+00	2.09E+00	-2.87E+00	-6.46E+00	-9.33E+00	1.40E-01	7.81E+01	2.32E+01	1.01E+02	1.01E+02	1.34E+02
Cl7	-5.33E-01	2.36E+02	1.08E-04	4.59E+02	1.69E+01	6.31E-01	-2.18E+01	-3.57E+00	-2.54E+01	1.30E+00	1.08E+03	4.16E+00	1.09E+03	1.09E+03	5.79E+02
N10	-1.20E+00	8.30E+01	-2.90E-04	5.50E+01	6.36E+00	1.84E+00	-3.65E+00	-7.31E+00	-1.10E+01	9.47E-01	-2.31E+01	-1.21E+01	-1.11E+01	-1.11E+01	3.83E+02
N16	-1.20E+00	8.30E+01	-8.80E-05	5.50E+01	6.36E+00	1.84E+00	-3.65E+00	-7.31E+00	-1.10E+01	9.12E-01	-2.24E+01	-1.21E+01	-1.03E+01	-1.03E+01	3.81E+02
O2	-1.19E+00	1.28E+02	-1.16E-04	7.54E+01	8.22E+00	9.69E-01	-6.05E+00	-2.15E+00	-8.20E+00	9.26E-01	-8.06E+01	-2.34E+00	-7.83E+01	-7.83E+01	5.28E+02
O28	-1.19E+00	1.28E+02	-1.27E-04	7.54E+01	8.23E+00	9.67E-01	-6.07E+00	-2.15E+00	-8.22E+00	9.10E-01	-8.12E+01	-2.31E+00	-7.89E+01	-7.89E+01	5.26E+02
H31	1.12E-01	3.92E+01	-2.90E-05	5.80E-01	3.48E-01	5.39E-01	-9.26E-01	-1.24E+00	-2.16E+00	3.59E-01	-1.82E+01	-6.49E+00	-2.47E+01	-2.47E+01	6.46E+00
H36	1.17E-01	3.87E+01	-2.90E-05	5.79E-01	3.45E-01	5.39E-01	-9.12E-01	-1.23E+00	-2.15E+00	3.62E-01	-1.81E+01	-6.49E+00	-2.46E+01	-2.46E+01	6.83E+00
Complex **4**															
Ru1	9.92E-01	1.10E+02	-9.65E-04	4.43E+03	4.06E+01	2.46E+00	-2.65E+01	-2.59E+01	-5.96E-01	-3.99E-01	-4.14E+03	-2.40E+01	-4.12E+03	-4.12E+03	6.61E+03
C2	-4.55E-02	7.33E+01	-1.09E-04	3.78E+01	3.97E+00	2.08E+00	-2.80E+00	-6.45E+00	-9.25E+00	6.59E-02	-7.44E+01	-2.23E+01	-9.67E+01	-9.67E+01	1.37E+02
C3	-4.44E-02	7.07E+01	-1.18E-04	3.78E+01	3.96E+00	2.08E+00	-2.70E+00	-6.37E+00	-9.07E+00	6.64E-02	-7.52E+01	-2.36E+01	-9.87E+01	-9.87E+01	1.40E+02
C4	-4.58E-02	7.34E+01	-6.00E-06	3.78E+01	3.97E+00	2.08E+00	-2.81E+00	-6.45E+00	-9.26E+00	9.17E-02	-7.46E+01	-2.23E+01	-9.69E+01	-9.69E+01	1.37E+02
C5	-3.39E-02	7.27E+01	-2.15E-04	3.78E+01	3.96E+00	2.08E+00	-2.84E+00	-6.43E+00	-9.27E+00	9.10E-02	-8.08E+01	-2.38E+01	-1.05E+02	-1.05E+02	1.35E+02
C6	-4.44E-02	7.06E+01	-1.85E-04	3.78E+01	3.96E+00	2.08E+00	-2.69E+00	-6.37E+00	-9.05E+00	8.10E-02	-7.49E+01	-2.36E+01	-9.84E+01	-9.84E+01	1.40E+02
C7	-3.40E-02	7.26E+01	-7.40E-05	3.78E+01	3.96E+00	2.08E+00	-2.85E+00	-6.42E+00	-9.27E+00	9.80E-02	-8.10E+01	-2.38E+01	-1.05E+02	-1.05E+02	1.35E+02
N10	-7.71E-01	8.29E+01	-7.40E-05	5.47E+01	5.95E+00	1.82E+00	-3.69E+00	-6.67E+00	-1.04E+01	5.94E-01	-4.52E+00	-1.51E+01	-1.06E+01	-1.06E+01	1.47E+02
N13	-7.71E-01	8.29E+01	-3.03E-04	5.47E+01	5.95E+00	1.82E+00	-3.69E+00	-6.68E+00	-1.04E+01	5.81E-01	-4.53E+00	-1.51E+01	-1.06E+01	-1.06E+01	1.47E+02
N15	-1.24E+00	8.06E+01	-4.25E-04	5.51E+01	6.40E+00	1.84E+00	-4.55E+00	-6.84E+00	-1.14E+01	3.31E-01	-4.37E+01	-1.25E+01	-5.62E+01	-5.62E+01	2.20E+02
Complex **5**															
Ru1	9.82E-01	1.08E+02	-1.20E-03	4.43E+03	4.05E+01	2.50E+00	-2.53E+01	-2.34E+01	-1.86E+00	-5.62E-01	-3.94E+03	-2.31E+01	-3.92E+03	-3.92E+03	5.35E+03
C18	-3.61E-02	7.26E+01	-3.09E-04	3.78E+01	3.96E+00	2.08E+00	-2.80E+00	-7.46E+00	-1.03E+01	5.62E-02	-7.91E+01	-2.29E+01	-1.02E+02	-1.02E+02	1.38E+02
C20	-4.79E-02	7.09E+01	-3.12E-04	3.78E+01	3.97E+00	2.08E+00	-2.67E+00	-8.73E+00	-1.14E+01	8.92E-02	-7.42E+01	-2.28E+01	-9.70E+01	-9.70E+01	1.42E+02

C22	-3.57E-02	7.26E+01	-1.31E-04	3.78E+01	3.96E+00	2.08E+00	-2.79E+00	-7.45E+00	-1.02E+01	6.26E-02	7.89E+01	2.29E+01	1.02E+02	1.02E+02	1.38E+02
C23	-4.91E-02	7.30E+01	4.00E-06	3.78E+01	3.97E+00	2.08E+00	-2.72E+00	-3.64E+00	-6.36E+00	8.07E-02	7.14E+01	2.16E+01	9.29E+01	9.29E+01	1.42E+02
C26	-4.81E-02	7.10E+01	-6.86E-04	3.78E+01	3.97E+00	2.08E+00	-2.67E+00	-8.72E+00	-1.14E+01	1.27E-01	7.44E+01	2.28E+01	9.72E+01	9.72E+01	1.41E+02
C27	-4.90E-02	7.29E+01	-1.03E-04	3.78E+01	3.97E+00	2.08E+00	-2.71E+00	-3.64E+00	-6.35E+00	1.07E-01	7.11E+01	2.16E+01	9.26E+01	9.26E+01	1.43E+02
N14	-1.23E+00	8.58E+01	-2.21E-04	5.50E+01	6.40E+00	1.83E+00	-3.88E+00	-7.35E+00	-1.12E+01	4.62E-01	-1.31E+01	1.19E+01	-1.24E+00	-1.24E+00	3.37E+02
N15	-1.23E+00	7.90E+01	-4.56E-04	5.51E+01	6.35E+00	1.88E+00	-3.71E+00	-7.16E+00	-1.09E+01	2.32E-01	-1.01E+01	1.22E+01	-2.12E+00	-2.12E+00	3.05E+02
N21	-1.23E+00	8.58E+01	-2.75E-04	5.50E+01	6.40E+00	1.83E+00	-3.89E+00	-7.37E+00	-1.13E+01	3.70E-01	-1.23E+01	1.19E+01	-4.32E-01	-4.31E-01	3.35E+02

q(A) is total charge on atom A, Vol(A) is the volume bounded by an isosurface of the electron density distribution (0.001) and by interatomic surfaces of atom A; K(A) is electronic kinetic energy of atom A (Hamiltonian Form), Loc(A) is number of electrons localized in atom A, K_Scaled(A) is approximation to virial-based total energy of atom A, Deloc(A,A') is number of electron delocalization from atom A, $\chi_{Intra\_Iso}(A)$ is Intraatomic magnetizability contribution of atom A (cgs-ppm); $\chi_{Bond\_Iso}(A)$ is Bonding magnetizability contribution of atom A; $\chi_{\_Iso}(A)$ is total magnetizability contribution of atom A (i.e. magnetizability isotropic); $\mu(A)$ is total dipole moment contribution of atom A; $\sigma_{Iso}(A,A)$ is the Intraatomic shielding tensor; $\sigma_{Iso}(A',A)$ is total induced magnetic field on nucleus a by other nuclei A'; $\sigma_{\_Iso}(A)$ is total magnetic shielding tensor of atom A (i.e. nmr shielding isotropic).

Table 3.84: The correlation of the computed atomic NMR properties of the complexes

	Complex **1**		Complex **2**		Complex **3**		Complex **4**		Complex **5**	
	$\sigma_{\_Iso}(A)$	$\chi_{\_Iso}(A)$	$\sigma_{\_Iso}(A)$	$\chi_{\_Iso}(A)$	$\sigma_{\_Iso}(A)$	$\chi_{\_Iso}(A)$	$\sigma_{\_Iso}(A)$	$\chi_{\_Iso}(A)$	$\sigma_{\_Iso}(A)$	$\chi_{\_Iso}(A)$
q(A)	-0.30	0.53	-0.25	0.52	-0.25	0.54	-0.33	0.56	-0.25	0.58
Vol(A),	0.07	-0.83	0.10	-0.84	0.07	-0.85	-0.39	-0.68	-0.28	-0.64

0.001										
K(A)	-0.93	0.10	-0.91	0.01	-0.93	0.08	-1.00	0.24	-1.00	0.26
K_Scaled(A)	0.93	-0.10	0.91	-0.01	0.93	-0.08	1.00	-0.24	1.00	-0.26
LI(A)	-0.75	-0.27	-0.72	-0.36	-0.75	-0.30	-0.94	-0.04	-0.92	-0.05
DI(A,A')/2	-0.28	-0.40	-0.27	-0.38	-0.25	-0.40	-0.21	-0.78	-0.20	-0.67
χ_{Intra_Iso}(A)	-0.89	0.68	-0.86	0.66	-0.88	0.65	-0.98	0.45	-0.94	0.50
χ_{Bond_Iso}(A)	0.71	0.30	0.68	0.35	0.75	0.25	0.81	0.31	0.73	0.37
$\chi_{\_Iso}$(A)	-0.37	1.00	-0.33	1.00	-0.35	1.00	-0.29	1.00	-0.31	1.00
|μ(A)|	-0.29	-0.42	-0.25	-0.48	-0.14	-0.57	-0.33	-0.44	-0.28	-0.26
$\sigma_{\_Iso}$(A,A)	1.00	-0.37	1.00	-0.32	1.00	-0.34	1.00	-0.28	1.00	-0.30
$\sigma_{\_Iso}$(A',A)	-0.31	-0.31	-0.30	-0.28	-0.28	-0.26	-0.25	-0.71	-0.25	-0.57
$\sigma_{\_Iso}$(A)	1.00	-0.37	1.00	-0.33	1.00	-0.35	1.00	-0.29	1.00	-0.31
Anisotropy	-0.93	0.08	-0.92	-0.01	-0.93	0.04	-1.00	0.21	-0.99	0.17

Table 3.85: The atomic NMR magnetazability and shielding for the selected atoms in the complexes using combined basis sets 3-21G

Complex **1**															
	q(A)	Vol(A), 0.001	L(A)	K(A)	LI(A)	DI(A, A')/2	χ_{Intra_Iso} (A)	χ_{Bond_Iso}(A)	$\chi_{\_Iso}$(A)	μ(A)	$\sigma_{\_Iso}$(A,A)	$\sigma_{\_Iso}$(A',A)	$\sigma_{\_Iso}$(A)	Isotropic	Anisotropy
Ru1	8.63E-01	9.73E+01	5.52E-04	4.40E+03	4.07E+01	2.46E+00	2.47E+01	2.50E+01	-2.65E-01	1.19E+00	3.10E+03	2.41E+01	3.07E+03	3.07E+03	6.03E+03
C9	-1.14E-01	7.66E+01	-7.00E-05	3.76E+01	4.04E+00	2.08E+00	-3.64E+00	-6.30E+00	-9.95E+00	1.35E-01	1.04E+02	2.27E+01	1.26E+02	1.26E+02	1.19E+02
C10	-1.04E-01	7.49E+01	-1.97E-04	3.76E+01	4.03E+00	2.07E+00	-3.35E+00	-6.23E+00	-9.58E+00	9.47E-02	9.56E+01	2.30E+01	1.19E+02	1.19E+02	1.24E+02
C13	-1.09E-01	7.52E+01	-1.11E-04	3.76E+01	4.03E+00	2.08E+00	-3.37E+00	-6.24E+00	-9.61E+00	1.16E-01	9.77E+01	2.28E+01	1.20E+02	1.20E+02	1.21E+02
C16	-9.09E-02	7.57E+01	-5.60E-05	3.76E+01	4.02E+00	2.07E+00	-3.52E+00	-6.13E+00	-9.66E+00	9.32E-02	1.00E+02	2.24E+01	1.23E+02	1.23E+02	1.26E+02
C18	-1.04E-01	7.71E+01	-4.80E-05	3.76E+01	4.04E+00	2.07E+00	-3.71E+00	-6.23E+00	-9.94E+00	1.14E-01	1.04E+02	2.30E+01	1.27E+02	1.27E+02	1.21E+02
C19	-8.40E-02	7.33E+01	-1.10E-04	3.76E+01	4.02E+00	2.07E+00	-3.05E+00	-6.06E+00	-9.11E+00	9.99E-02	8.86E+01	2.21E+01	1.11E+02	1.11E+02	1.35E+02
Cl22	-4.89E-01	2.29E+02	6.20E-05	4.57E+02	1.69E+01	6.10E-01	-2.15E+01	-3.19E+00	-2.47E+01	1.33E+00	9.98E+02	3.76E+00	1.00E+03	1.00E+03	4.24E+02
N12	-6.13E-01	7.39E+01	4.00E-05	5.43E+01	5.75E+00	1.86E+00	-3.74E+00	-6.36E+00	-1.01E+01	6.53E-01	2.36E+01	1.74E+01	4.10E+01	4.10E+01	1.58E+02
N17	-6.03E-01	7.39E+01	1.41E-04	5.43E+01	5.74E+00	1.86E+00	-3.68E+00	-6.52E+00	-1.02E+01	8.83E-01	1.93E+01	1.74E+01	3.66E+01	3.66E+01	1.68E+02
O2	-8.53E-01	1.04E+02	8.40E-05	7.47E+01	7.78E+00	1.07E+00	-5.00E+00	-2.28E+00	-7.27E+00	9.06E-01	9.86E+01	4.65E+00	9.40E+01	9.40E+01	5.71E+02
H24	2.00E-01	3.41E+01	3.70E-05	5.27E-01	2.92E-01	5.07E-01	-8.31E-01	-9.37E-01	-1.77E+00	4.44E-01	1.80E+01	5.96E+00	2.40E+01	2.40E+01	6.47E+00
H29	1.55E-	3.93E+	4.10E-	5.43E-	3.30E-	5.14E-	-9.62E-	-4.06E-	-	3.57E-	1.90E+	6.38E+	2.54E+	2.54E+	5.79E+

	01	01	05	01	01	01	01	01	1.37E+00	02	01	00	01	01	00
							Complex **2**								
Ru1	8.62E-01	9.91E+01	4.02E-04	4.40E+03	4.06E+01	2.49E+00	2.21E+01	2.48E+01	2.66E+00	1.17E+00	2.71E+03	2.35E+01	2.69E+03	2.69E+03	5.42E+03
C7	-1.16E-01	7.31E+01	-8.10E-05	3.76E+01	4.04E+00	2.08E+00	3.14E+00	6.11E+00	9.25E+00	8.08E-02	9.07E+01	2.25E+01	1.13E+02	1.13E+02	1.27E+02
C8	-1.05E-01	7.72E+01	8.60E-05	3.76E+01	4.04E+00	2.07E+00	3.83E+00	6.13E+00	9.96E+00	1.24E-01	1.07E+02	2.23E+01	1.29E+02	1.29E+02	1.23E+02
C13	-9.59E-02	7.87E+01	1.57E-04	3.76E+01	4.03E+00	2.07E+00	3.78E+00	6.21E+00	9.99E+00	1.31E-01	1.05E+02	2.24E+01	1.28E+02	1.28E+02	1.24E+02
C14	-8.33E-02	7.24E+01	7.10E-05	3.76E+01	4.02E+00	2.07E+00	2.78E+00	5.96E+00	8.74E+00	8.95E-02	8.18E+01	2.17E+01	1.03E+02	1.03E+02	1.41E+02
C18	-1.16E-01	7.32E+01	-8.80E-05	3.76E+01	4.04E+00	2.08E+00	3.15E+00	6.13E+00	9.27E+00	1.08E-01	9.08E+01	2.25E+01	1.13E+02	1.13E+02	1.27E+02
C19	-1.05E-01	7.73E+01	5.90E-05	3.76E+01	4.04E+00	2.07E+00	3.83E+00	6.15E+00	9.97E+00	1.36E-01	1.07E+02	2.23E+01	1.29E+02	1.29E+02	1.23E+02
Cl10	-4.78E-01	2.34E+02	9.30E-05	4.57E+02	1.69E+01	5.87E-01	2.19E+01	3.41E+00	2.53E+01	1.29E+00	1.03E+03	4.26E+00	1.03E+03	1.03E+03	3.66E+02
N11	-9.49E-01	7.74E+01	5.00E-05	5.45E+01	6.07E+00	1.88E+00	3.67E+00	6.91E+00	1.06E+01	6.40E-01	1.00E+00	1.39E+01	1.49E+01	1.49E+01	3.56E+02
N16	-9.49E-01	7.75E+01	6.00E-05	5.45E+01	6.07E+00	1.88E+00	3.67E+00	6.90E+00	1.06E+01	6.04E-01	4.94E-01	1.39E+01	1.44E+01	1.44E+01	3.58E+02
H34	1.49E-01	3.72E+01	3.70E-05	5.50E-01	3.27E-01	5.25E-01	-9.03E-01	-4.11E-01	1.31E+00	3.97E-02	1.89E+01	4.77E+00	2.37E+01	2.37E+01	1.00E+01
H38	1.51E-01	3.74E+01	8.50E-05	5.47E-01	3.24E-01	5.25E-01	-9.09E-01	-4.18E-01	1.33E+00	4.12E-02	1.88E+01	4.70E+00	2.35E+01	2.35E+01	9.30E+00
							Complex **3**								
Ru1	8.73E-01	9.61E+01	-6.31E-04	4.40E+03	4.07E+01	2.45E+00	2.73E+01	2.50E+01	2.30E+00	8.55E-01	3.41E+03	2.29E+01	3.38E+03	3.38E+03	5.84E+03
C13	-7.91E-02	7.32E+01	-2.80E-05	3.76E+01	4.01E+00	2.07E+00	3.29E+00	6.18E+00	9.47E+00	8.53E-02	9.47E+01	2.23E+01	1.17E+02	1.17E+02	1.29E+02
C14	-9.33E-02	7.21E+01	-4.90E-05	3.76E+01	4.02E+00	2.07E+00	3.27E+00	6.65E+00	9.92E+00	4.11E-01	9.41E+01	2.29E+01	1.17E+02	1.17E+02	1.27E+02
C18	-8.72E-02	7.36E+01	8.60E-05	3.76E+01	4.02E+00	2.07E+00	3.26E+00	6.21E+00	9.47E+00	9.86E-02	9.37E+01	2.23E+01	1.16E+02	1.16E+02	1.29E+02
C21	-1.18E-01	7.64E+01	-3.70E-05	3.76E+01	4.04E+00	2.08E+00	3.50E+00	6.31E+00	9.81E+00	1.79E-01	9.88E+01	2.29E+01	1.22E+02	1.22E+02	1.25E+02
C23	-9.43E-02	7.27E+01	-8.40E-05	3.76E+01	4.03E+00	2.06E+00	3.35E+00	6.66E+00	1.00E+01	4.09E-01	9.62E+01	2.29E+01	1.19E+02	1.19E+02	1.29E+02
C25	-1.17E-01	7.61E+01	1.72E-04	3.76E+01	4.04E+00	2.08E+00	3.46E+00	6.30E+00	9.76E+00	1.83E-01	9.81E+01	2.30E+01	1.21E+02	1.21E+02	1.25E+02
Cl7	-4.97E-01	2.32E+02	7.30E-05	4.57E+02	1.69E+01	5.90E-01	2.18E+01	3.20E+00	2.50E+01	1.35E+00	1.01E+03	3.77E+00	1.02E+03	1.02E+03	4.99E+02
N10	-9.26E-	7.82E+	2.83E-	5.44E+	6.06E+	1.86E+	-	-	-	9.41E-	2.92E+	1.31E+	1.60E+	1.60E+	3.60E+

	01	01	04	01	00	00	3.72E+00	7.07E+00	1.08E+01	01	00	01	01	01	02
N16	-9.30E-01	7.78E+01	2.81E-04	5.45E+01	6.06E+00	1.87E+00	-3.73E+00	-6.99E+00	-1.07E+01	9.13E-01	4.52E+00	1.31E+01	1.76E+01	1.76E+01	3.55E+02
O2	-8.96E-01	1.04E+02	1.68E-04	7.47E+01	7.80E+00	1.09E+00	-5.04E+00	-2.27E+00	-7.31E+00	9.29E-01	7.73E+01	4.31E+00	7.30E+01	7.30E+01	5.56E+02
O28	-8.94E-01	1.05E+02	1.36E-04	7.47E+01	7.81E+00	1.09E+00	-5.06E+00	-2.21E+00	-7.27E+00	8.86E-01	8.26E+01	4.19E+00	7.84E+01	7.84E+01	5.53E+02
H31	1.61E-01	3.65E+01	3.80E-05	-5.47E-01	3.19E-01	-5.20E-01	9.69E-01	-1.06E+00	-2.03E+00	3.16E-01	1.93E+01	7.78E+00	2.71E+01	2.71E+01	5.20E+00
H36	1.77E-01	3.48E+01	1.80E-05	-5.41E-01	3.05E-01	-5.17E-01	9.20E-01	-1.05E+00	-1.98E+00	3.08E-01	1.89E+01	7.65E+00	2.66E+01	2.66E+01	6.36E+00
Complex **4**															
Ru1	9.46E-01	1.02E+02	-2.96E-04	4.40E+03	4.07E+01	2.38E+00	-2.97E+01	-2.51E+01	-4.51E+00	4.45E-01	-3.77E+03	-2.31E+01	-3.75E+03	-3.75E+03	6.50E+03
C2	-9.53E-02	7.64E+01	9.40E-05	3.76E+01	4.03E+00	2.06E+00	-3.39E+00	-6.18E+00	-9.57E+00	9.19E-02	9.45E+01	2.19E+01	1.16E+02	1.16E+02	1.28E+02
C3	-9.30E-02	7.35E+01	-9.30E-05	3.76E+01	4.03E+00	2.06E+00	-3.29E+00	-6.17E+00	-9.46E+00	1.09E-01	9.52E+01	2.33E+01	1.18E+02	1.18E+02	1.32E+02
C4	-9.54E-02	7.65E+01	-5.80E-05	3.76E+01	4.03E+00	2.06E+00	-3.40E+00	-6.18E+00	-9.58E+00	1.18E-01	9.46E+01	2.19E+01	1.17E+02	1.17E+02	1.28E+02
C5	-8.74E-02	7.61E+01	-7.70E-05	3.76E+01	4.03E+00	2.06E+00	-3.50E+00	-6.23E+00	-9.73E+00	1.29E-01	1.01E+02	2.36E+01	1.25E+02	1.25E+02	1.26E+02
C6	-9.30E-02	7.35E+01	-5.60E-05	3.76E+01	4.03E+00	2.06E+00	-3.28E+00	-6.16E+00	-9.45E+00	1.27E-01	9.49E+01	2.33E+01	1.18E+02	1.18E+02	1.32E+02
C7	-8.74E-02	7.61E+01	-8.00E-05	3.76E+01	4.03E+00	2.06E+00	-3.51E+00	-6.23E+00	-9.74E+00	1.46E-01	1.01E+02	2.36E+01	1.25E+02	1.25E+02	1.26E+02
N10	-6.07E-01	7.84E+01	1.22E-04	5.42E+01	5.78E+00	1.82E+00	-3.84E+00	-6.59E+00	-1.04E+01	6.51E-01	1.74E+01	1.59E+01	3.33E+01	3.33E+01	1.33E+02
N13	-6.07E-01	7.84E+01	-4.29E-04	5.42E+01	5.78E+00	1.82E+00	-3.84E+00	-6.59E+00	-1.04E+01	6.36E-01	1.74E+01	1.59E+01	3.33E+01	3.33E+01	1.33E+02
N15	-9.65E-01	7.53E+01	1.70E-04	5.46E+01	6.10E+00	1.86E+00	-4.55E+00	-6.58E+00	-1.11E+01	3.83E-01	6.20E+01	1.36E+01	7.56E+01	7.56E+01	2.10E+02
Complex **5**															
Ru1	9.26E-01	1.01E+02	9.21E-04	4.40E+03	4.06E+01	2.43E+00	-2.82E+01	-2.44E+01	-3.84E+00	4.94E-01	-3.57E+03	-2.23E+01	-3.55E+03	-3.55E+03	5.25E+03
C18	-8.75E-02	7.60E+01	-2.80E-04	3.76E+01	4.03E+00	2.06E+00	-3.44E+00	-6.11E+00	-9.55E+00	7.76E-02	9.92E+01	2.27E+01	1.22E+02	1.22E+02	1.29E+02
C20	-9.77E-02	7.36E+01	-1.45E-04	3.76E+01	4.03E+00	2.07E+00	-3.26E+00	-6.04E+00	-9.29E+00	9.89E-02	9.45E+01	2.26E+01	1.17E+02	1.17E+02	1.32E+02
C22	-8.70E-02	7.59E+01	7.70E-05	3.76E+01	4.03E+00	2.06E+00	-3.43E+00	-6.10E+00	-9.53E+00	9.16E-02	9.91E+01	2.27E+01	1.22E+02	1.22E+02	1.29E+02
C23	-1.01E-01	7.60E+01	-4.40E-05	3.76E+01	4.03E+00	2.07E+00	-3.31E+00	-6.03E+00	-9.34E+00	1.18E-01	9.15E+01	2.12E+01	1.13E+02	1.13E+02	1.33E+02
C26	-9.72E-	7.36E+	-2.40E-	3.76E+	4.03E+	2.07E+	-	-	-	1.14E-	9.46E+	2.26E+	1.17E+	1.17E+	1.32E+

	02	01	05	01	00	00	3.26E+00	6.03E+00	9.29E+00	01	01	01	02	02	02
C27	-1.01E-01	7.59E+01	-1.10E-04	3.76E+01	4.03E+00	2.07E+00	-3.30E+00	-6.03E+00	-9.33E+00	1.38E-01	9.13E+01	2.12E+01	1.13E+02	1.13E+02	1.33E+02
N14	-9.58E-01	8.06E+01	1.32E-04	5.44E+01	6.10E+00	1.85E+00	-3.97E+00	-7.06E+00	-1.10E+01	5.43E-01	1.27E+01	1.30E+01	2.57E+01	2.57E+01	3.17E+02
N15	-9.52E-01	7.36E+01	3.41E-04	5.46E+01	6.05E+00	1.90E+00	-3.79E+00	-6.70E+00	-1.05E+01	2.78E-01	1.69E+01	1.34E+01	3.04E+01	3.04E+01	2.83E+02
N21	-9.59E-01	8.06E+01	8.90E-05	5.44E+01	6.11E+00	1.85E+00	-3.97E+00	-7.07E+00	-1.10E+01	4.49E-01	1.32E+01	1.30E+01	2.62E+01	2.62E+01	3.16E+02

Table 3.86: The atomic NMR magnetazability and shielding for the selected atoms in the complexes using combined basis sets ECP(Ru)|6-31+G(d,p)

Complex **1**														
q(A)	Vol(A), 0.001	L(A)	K(A)	LI(A)	DI(A,A')/2	χ_{Intra_Iso} (A)	χ_{Bond_Iso} (A)	$\chi_{\_Iso}$(A)	μ(A)	$\sigma_{\_Iso}$(A, A)	$\sigma_{\_Iso}$(A', A)	$\sigma_{\_Iso}$(A)	Isotropic	Anisotropy
9.40E-01	1.03E+02	2.84E-04	3.27E+01	1.24E+01	2.70E+00	1.42E+01	-4.48E+01	-3.06E+01	1.07E+00	1.52E+03	2.53E+01	1.55E+03	-4.41E+02	6.61E+02
-7.56E-02	7.39E+01	2.30E-05	3.78E+01	3.98E+00	2.09E+00	-3.04E+00	-6.24E+00	-9.29E+00	1.03E-01	8.71E+01	1.29E+01	1.00E+02	-1.10E+02	1.21E+02
-5.98E-02	7.16E+01	-2.78E-04	3.78E+01	3.97E+00	2.09E+00	-2.69E+00	-6.57E+00	-9.26E+00	5.74E-02	7.77E+01	7.36E+00	7.04E+01	-1.01E+02	1.28E+02
-6.39E-02	7.18E+01	-2.07E-04	3.78E+01	3.97E+00	2.09E+00	-2.75E+00	-8.16E+00	-1.09E+01	1.06E-01	8.19E+01	6.66E+00	8.85E+01	-1.05E+02	1.23E+02
-6.54E-02	7.37E+01	1.51E-04	3.78E+01	3.98E+00	2.09E+00	-3.07E+00	-2.09E+00	-5.16E+00	8.08E-02	8.69E+01	-3.55E+01	5.14E+01	-1.09E+02	1.26E+02
-7.15E-02	7.47E+01	2.20E-05	3.78E+01	3.98E+00	2.09E+00	-3.17E+00	-3.53E+00	-6.70E+00	9.33E-02	8.93E+01	-2.09E+01	6.84E+01	-1.12E+02	1.21E+02
-4.23E-02	7.01E+01	-2.32E-04	3.78E+01	3.96E+00	2.09E+00	-2.42E+00	-7.31E-01	-1.69E+00	8.09E-02	7.01E+01	-4.33E+01	2.68E+01	-9.18E+01	1.43E+02
-4.92E-01	2.30E+02	6.40E-05	4.59E+02	1.68E+01	6.81E-01	-2.03E+01	-3.56E+00	-2.38E+01	1.16E+00	9.04E+02	-3.28E+00	9.01E+02	-9.08E+02	5.31E+02
-7.26E-01	7.72E+01	2.69E-04	5.47E+01	5.84E+00	1.89E+00	-3.36E+00	-3.66E+01	-3.99E+01	6.76E-01	2.99E+00	-6.84E+01	7.13E+01	-1.95E+01	1.73E+02
-7.26E-01	7.72E+01	2.02E-04	5.47E+01	5.84E+00	1.89E+00	-3.36E+00	-3.86E+01	-4.19E+01	6.36E-01	2.77E+00	-6.84E+01	7.12E+01	-1.93E+01	1.74E+02
-1.13E+00	1.29E+02	7.20E-05	7.54E+01	8.15E+00	9.82E-01	-5.90E+00	-4.31E+00	-1.02E+01	1.00E+00	8.96E+01	-1.29E+01	7.67E+01	-8.70E+01	5.43E+02
1.28E-01	4.04E+01	1.60E-05	5.64E-01	3.40E-01	5.32E-01	-9.11E-01	-2.81E+00	-3.72E+00	4.61E-01	1.75E+01	-1.67E+01	3.42E+01	-2.32E+01	6.57E+00
1.27E-01	4.04E+01	2.30E-05	5.64E-01	3.41E-01	5.32E-01	-9.13E-01	-3.04E+00	-3.95E+00	4.72E-01	1.75E+01	-1.67E+01	3.43E+01	-2.33E+01	6.51E+00
Complex **2**														

9.57E-01	1.05E+02	4.83E-04	3.27E+01	1.23E+01	2.73E+00	1.23E+01	-6.54E+01	-5.31E+01	1.06E+00	1.53E+03	2.44E+01	1.56E+03	-4.29E+02	5.46E+02
-6.65E-02	7.04E+01	4.00E-05	3.78E+01	3.97E+00	2.10E+00	2.58E+00	-1.72E+00	-4.30E+00	7.96E-02	7.53E+01	-3.11E+01	4.43E+01	9.75E+01	1.31E+02
-7.69E-02	7.49E+01	-1.02E-04	3.78E+01	3.99E+00	2.09E+00	3.19E+00	-4.54E+00	-7.73E+00	9.09E-02	8.97E+01	-5.68E+01	3.29E+01	1.11E+02	1.26E+02
-6.59E-02	7.67E+01	-2.96E-04	3.78E+01	3.98E+00	2.08E+00	3.15E+00	-6.68E+00	-9.83E+00	8.29E-02	8.70E+01	-1.67E+01	7.03E+01	1.09E+02	1.26E+02
-4.00E-02	6.99E+01	-5.43E-04	3.78E+01	3.96E+00	2.08E+00	2.20E+00	-4.69E+00	-2.49E+00	9.34E-02	6.43E+01	-7.19E+01	-7.61E+00	8.54E+01	1.50E+02
-6.67E-02	7.04E+01	1.40E-05	3.78E+01	3.97E+00	2.10E+00	2.58E+00	-3.40E-01	-2.24E+00	1.05E-01	7.54E+01	-3.10E+01	4.45E+01	9.75E+01	1.30E+02
-7.67E-02	7.48E+01	2.55E-04	3.78E+01	3.99E+00	2.09E+00	3.19E+00	-3.50E+00	-6.69E+00	8.19E-02	8.98E+01	-5.67E+01	3.31E+01	1.11E+02	1.26E+02
-4.84E-01	2.34E+02	6.80E-05	4.59E+02	1.68E+01	6.57E-01	2.08E+01	-4.12E+00	-2.49E+01	1.12E+00	9.50E+02	-1.89E+01	9.69E+02	-9.55E+02	4.05E+02
-1.16E+00	8.10E+01	6.60E-05	5.50E+01	6.27E+00	1.89E+00	3.34E+00	-5.67E+01	-6.00E+01	5.24E-01	2.40E+01	-9.76E+01	7.36E+01	-1.13E+01	3.45E+02
-1.16E+00	8.09E+01	2.46E-04	5.50E+01	6.27E+00	1.89E+00	3.34E+00	-5.92E+01	-6.25E+01	4.90E-01	2.44E+01	-9.81E+01	7.37E+01	-1.17E+01	3.47E+02
9.67E-02	4.09E+01	9.50E-05	5.81E-01	3.58E-01	5.45E-01	-9.04E-01	-1.89E+00	-2.80E+00	6.89E-02	1.80E+01	-2.20E+01	4.00E+01	-2.23E+01	1.05E+01
1.03E-01	4.10E+01	7.70E-05	5.76E-01	3.53E-01	5.45E-01	-9.10E-01	-1.87E+00	-2.78E+00	5.26E-02	1.79E+01	-2.19E+01	3.98E+01	-2.22E+01	9.71E+00

Complex **3**

9.59E-01	1.01E+02	2.52E-04	3.27E+01	1.23E+01	2.71E+00	1.57E+01	-2.51E+01	-9.33E+00	7.69E-01	1.45E+03	-2.38E+01	1.47E+03	-5.15E+02	5.85E+02
-5.37E-02	7.08E+01	-6.10E-05	3.78E+01	3.97E+00	2.09E+00	2.74E+00	-1.78E+00	-4.52E+00	7.69E-02	7.80E+01	-3.43E+01	4.37E+01	9.77E+01	1.36E+02
-6.12E-02	6.99E+01	-1.90E-04	3.78E+01	3.97E+00	2.09E+00	2.66E+00	-1.16E+00	-3.81E+00	4.01E-01	7.74E+01	-1.80E+01	5.94E+01	9.83E+01	1.35E+02
-5.33E-02	7.09E+01	-1.48E-04	3.78E+01	3.97E+00	2.09E+00	2.71E+00	8.01E-01	-3.52E+00	8.25E-02	7.71E+01	-3.46E+01	4.25E+01	9.68E+01	1.37E+02
-7.24E-02	7.38E+01	-1.20E-04	3.78E+01	3.98E+00	2.09E+00	2.90E+00	-3.34E+00	-6.24E+00	1.34E-01	8.08E+01	-2.52E+00	7.83E+01	-1.02E+02	1.32E+02
-6.28E-02	7.02E+01	-2.92E-04	3.78E+01	3.98E+00	2.09E+00	2.69E+00	3.87E-01	-3.08E+00	4.12E-01	7.80E+01	-1.87E+01	5.94E+01	-9.88E+01	1.36E+02
-7.20E-02	7.35E+01	-2.53E-04	3.78E+01	3.98E+00	2.09E+00	2.88E+00	-2.91E+00	-5.79E+00	1.42E-01	8.04E+01	-2.87E+00	7.76E+01	-1.02E+02	1.32E+02
-4.94E-01	2.33E+02	8.90E-05	4.59E+02	1.68E+01	6.69E-01	2.04E+01	-3.83E+00	-2.42E+01	1.16E+00	9.18E+02	-1.43E+01	9.32E+02	-9.23E+02	6.30E+02
-1.14E+00	8.19E+01	2.23E-04	5.49E+01	6.27E+00	1.87E+00	3.46E+00	-3.07E+01	-3.42E+01	9.04E-01	1.84E+01	-6.25E+01	4.41E+01	-4.93E+00	3.41E+02
-	8.18E+	5.60E-	5.49E+	6.27E+	1.87E+	-	-	-	8.69E-	-	6.25E+	4.46E+	-	3.41E+

1.14E+00	01	05	01	00	00	3.46E+00	3.25E+01	3.60E+01	01	1.79E+01	01	01	4.43E+00	02
-						-	-	-		-		-	-	
1.15E+00	1.27E+02	1.11E-04	7.54E+01	8.14E+00	1.01E+00	5.80E+00	1.14E+01	1.72E+01	8.93E-01	7.45E+01	-1.02E-01	7.46E+01	7.20E+01	5.01E+02
-						-	-	-		-		-	-	
1.15E+00	1.27E+02	1.17E-04	7.54E+01	8.14E+00	1.01E+00	5.82E+00	1.19E+01	1.77E+01	8.78E-01	7.53E+01	-5.23E-02	7.54E+01	7.28E+01	4.99E+02
							-	-			-			
1.18E-01	3.91E+01	2.20E-05	5.75E-01	3.43E-01	5.39E-01	-9.17E-01	5.56E+00	6.48E+00	3.52E-01	1.80E+01	9.34E+00	8.68E+00	2.41E+01	6.77E+00
							-	-			-			
1.22E-01	3.86E+01	3.20E-05	5.74E-01	3.40E-01	5.39E-01	-9.03E-01	5.80E+00	6.70E+00	3.54E-01	1.79E+01	9.83E+00	8.07E+00	2.40E+01	7.09E+00
Complex **4**														
							-	-					-	
9.82E-01	1.12E+02	-8.61E-04	3.27E+01	1.24E+01	2.63E+00	1.72E+01	3.72E+01	2.00E+01	3.23E-01	1.38E+03	2.40E+01	1.41E+03	5.81E+02	7.13E+02
							-	-	-			-		
-5.75E-02	7.36E+01	-2.60E-05	3.78E+01	3.98E+00	2.08E+00	2.80E+00	3.30E+00	6.10E+00	7.55E-02	7.77E+01	2.22E+01	5.55E+01	9.86E+01	1.32E+02
							-	-	-			-		
-5.54E-02	7.08E+01	-2.19E-04	3.78E+01	3.97E+00	2.08E+00	2.71E+00	3.84E+00	6.55E+00	7.39E-02	7.94E+01	7.69E+00	7.17E+01	1.02E+02	1.32E+02
							-	-	-			-		
-5.77E-02	7.36E+01	-3.00E-05	3.78E+01	3.98E+00	2.08E+00	2.81E+00	2.41E+00	5.22E+00	9.46E-02	7.79E+01	2.22E+01	5.57E+01	9.87E+01	1.32E+02
							-	-	-					
-4.58E-02	7.27E+01	-9.20E-05	3.78E+01	3.97E+00	2.08E+00	2.85E+00	5.17E+00	8.02E+00	9.35E-02	8.34E+01	6.44E+00	8.98E+01	1.07E+02	1.31E+02
							-	-	-			-		
-5.55E-02	7.07E+01	-3.53E-04	3.78E+01	3.97E+00	2.08E+00	2.71E+00	3.48E+00	6.19E+00	8.67E-02	7.92E+01	7.80E+00	7.14E+01	1.02E+02	1.32E+02
							-	-	-					
-4.61E-02	7.27E+01	-7.90E-05	3.78E+01	3.97E+00	2.08E+00	2.85E+00	4.95E+00	7.80E+00	1.01E-01	8.35E+01	6.38E+00	8.99E+01	1.07E+02	1.31E+02
							-	-	-					
-7.38E-01	8.21E+01	2.73E-04	5.47E+01	5.89E+00	1.85E+00	3.51E+00	1.44E+01	1.79E+01	5.90E-01	1.80E+00	3.50E+01	3.68E+01	1.66E+01	1.21E+02
							-	-	-					
-7.38E-01	8.21E+01	2.80E-04	5.47E+01	5.89E+00	1.85E+00	3.51E+00	1.46E+01	1.81E+01	5.75E-01	1.80E+00	3.50E+01	3.68E+01	1.66E+01	1.21E+02
-						-	-	-						
1.18E+00	7.93E+01	4.18E-04	5.51E+01	6.30E+00	1.87E+00	4.22E+00	2.86E+01	3.28E+01	3.23E-01	3.98E+01	6.59E+01	1.06E+02	5.34E+01	1.95E+02
Complex **5**														
							-	-					-	
9.80E-01	1.09E+02	1.36E-03	3.27E+01	1.23E+01	2.69E+00	1.65E+01	5.14E+01	3.49E+01	5.13E-01	1.36E+03	2.32E+01	1.38E+03	6.08E+02	4.66E+02
							-	-	-			-		
-4.88E-02	7.28E+01	-3.90E-04	3.78E+01	3.97E+00	2.08E+00	2.82E+00	5.26E+00	8.08E+00	6.77E-02	8.26E+01	1.05E+00	8.15E+01	1.04E+02	1.33E+02
							-	-	-			-		
-5.86E-02	7.09E+01	-3.20E-05	3.78E+01	3.97E+00	2.08E+00	2.72E+00	1.28E+00	4.00E+00	1.08E-01	7.85E+01	2.39E+01	5.46E+01	9.99E+01	1.34E+02
							-	-	-			-		
-4.81E-02	7.26E+01	4.30E-05	3.78E+01	3.97E+00	2.08E+00	2.81E+00	5.08E+00	7.89E+00	6.63E-02	8.24E+01	1.02E+00	8.14E+01	1.04E+02	1.33E+02
							-	-	-			-		
-6.19E-02	7.32E+01	-2.73E-04	3.78E+01	3.98E+00	2.08E+00	2.73E+00	2.89E+00	5.62E+00	1.00E-01	7.44E+01	4.68E+01	2.76E+01	9.43E+01	1.38E+02
							-	-	-			-		
-5.90E-02	7.11E+01	-3.44E-04	3.78E+01	3.97E+00	2.08E+00	2.72E+00	1.14E+00	3.86E+00	1.17E-01	7.88E+01	2.38E+01	5.49E+01	1.00E+02	1.34E+02
-6.16E-	7.31E+	-2.82E-	3.78E+	3.98E+	2.08E+	-	-	-	9.87E-	7.42E+	-	2.74E+	9.40E+	1.38E+

02	01	04	01	00	00	2.73E+00	2.89E+00	5.62E+00	02	01	4.68E+01	01	01	02
-1.17E+00	8.46E+01	2.33E-04	5.49E+01	6.31E+00	1.86E+00	-3.60E+00	-2.02E+01	-2.38E+01	4.48E-01	-6.06E+00	4.15E+01	3.55E+01	6.43E+00	2.96E+02
-1.17E+00	7.77E+01	4.56E-04	5.51E+01	6.26E+00	1.91E+00	-3.45E+00	-4.33E+01	-4.68E+01	2.20E-01	-9.09E+00	1.00E+02	9.11E+01	4.13E+00	2.62E+02
-1.17E+00	8.46E+01	2.77E-04	5.49E+01	6.31E+00	1.86E+00	-3.61E+00	-2.10E+01	-2.46E+01	3.55E-01	-5.54E+00	4.13E+01	3.57E+01	6.90E+00	2.94E+02

Table 3.87: The fitted properties of the factors used in the proposed isotropic shielding model

	1	2	3	4	5
(Intercept)	2.98E+001	3.95E+001	3.89E+001	-1.01E+002	35.19
abs(q(A))	-5.40E+001	-5.43E+001	-5.37E+001	4.22E+001	-5.32E+001
K(A)	4.04E+000	3.92E+000	3.97E+000	-1.35E+001	3.34
$(K\_Scaled(A))^2$	-1.01E-003	-9.74E-004	-1.01E-003	2.64E-003	-8.96E-004
LI(A)	-3.52E+001	-2.97E+001	-3.15E+001	7.71E+001	-2.43E+001
DI(A,A')/2	2.42E+001	3.81E+000	5.61E+000	1.89E+002	3.96E+000
R-squared	0.9968	0.9941	0.9966	0.9998	0.9974
p-value	2.20E-016	2.20E-016	2.20E-016	2.20E-016	2.20E-016
Min residue	-92.515	-104.098	-93.863	-37.232	-113.183
Max residue	117.752	114.178	100.135	12.616	117.111

Table 3.88: The conductive properties of the complexes

	ECP|6-31G*								
	Dipole	<α>	$\Delta\alpha_1$	$\Delta\alpha_2$	$\Delta\alpha_3$	Γ	ß in esu (1x10-30)	Gap in KJ/mol	η KJ/mol
bpyrazace	3.36	216.91	21.47	23.65	49.34	4.52E+00	5.19	156.35	78.17
dpynic	6.60	279.95	178.26	178.69	75.21	1.35E-02	21.58	173.10	86.55
phth	7.71	293.04	-57.11	147.14	9193.44	1.06E-02	14.22	159.95	79.97
razol	2.78	239.30	120.99	132.10	1405.16	6.07E-03	4.43	221.67	110.84
terpy	5.41	304.08	176.09	179.75	651.20	1.69E-02	4.66	210.70	105.35

				3-21G					
bpyrazace	6.78	191.82	30.93	42.17	410.65	-20.57	4.13	395.11	197.56
dpynic	6.60	248.11	157.78	157.85	12.16	-31.83	11.98	314.14	157.07
phth	8.43	262.55	-55.83	134.05	7426.85	-30.48	7.26	294.69	147.34
razol	3.15	218.38	112.59	126.98	1723.92	-20.91	3.08	391.80	195.90
terpy	4.96	274.65	165.37	170.87	923.74	-29.41	2.81	366.20	183.10
				DGDZVP|6-31+G(d,p)					
bpyrazace	6.85	224.50	-26.12	41.27	510.43	-8.50	3.60	405.87	202.93
dpynic	6.85	290.46	157.90	158.15	39.09	-17.15	12.96	307.11	153.55
phth	8.28	303.87	124.09	125.04	118.04	-16.09	6.66	301.63	150.82
razol	2.47	246.42	106.75	117.33	1184.90	-9.55	2.75	390.01	195.00
terpy	6.07	311.90	156.81	160.52	588.77	-14.47	3.12	358.54	179.27
				ECP|6-31+G(d,p)					
bpyrazace	5.80	233.00	-29.28	48.32	738.82	-1.89E-03		238.15	119.08
dpynic	5.89	307.61	179.09	179.83	133.67	6.16E-04		165.29	82.64
phth	6.95	319.96	138.24	138.69	62.08	-7.98E-04		162.12	81.06
razol	1.83	255.97	115.41	124.10	1040.71	-2.24E-04		221.85	110.92
terpy	4.65	326.37	168.22	170.74	427.26	2.45E-03		218.62	109.31

Table 3.89: The binding activities of the Ru(II)-based complexes as predicted suing Glide package

	CatB	DNA-Gyrase	HDAC7	HP-NCP	KINASE	rHA	RNR	Top11	TrXR	TS	
1 CraptaC	-2.14	-1.68	-1.41	-2.67	-3.45		-1.51		-1.70	-1.00	
2 OraptaC	-2.19	-2.19	-2.38	-2.15	-4.44	-2.12	-0.55		-2.69	-3.71	
3 raptaB-H_2O	-4.04	-3.18	-2.16	-3.41	-3.10	-2.40	-3.52	-5.68		-4.10	
4 raptaC-H_2O	-3.56	-2.49	-3.35	-2.99	-2.61	-2.61	-3.64	-3.97	-2.37	-2.82	
5 raptaT-H_2O	-3.98	-2.48	-2.61	-2.87	-3.38	-2.23	-3.75	-4.75	-2.57	-3.76	
6 piano	-4.35	-3.41	-3.72	-3.29	-3.48	-3.75	-3.40	-4.96	-3.45	-3.94	
7 ragly	-2.92	-3.63	-2.73	-3.90	-4.83	-3.35	-2.06	-4.42	-2.88	-3.32	
8 etdiaglydmso	-2.57	-2.88	-2.12	-4.17	-4.02		-2.42	-3.79	-3.60	-3.52	
9 radipyrazoic	-4.93	-3.88	-3.40	-5.11	-3.12	-3.10	-7.10	-5.15	-4.43	-4.10	
10 radipyrdioic	-3.22	-4.60	-4.06	-4.00	-5.97	-3.57	-6.87	-3.87	-4.69	-4.00	
11 raphendioic	-4.37	-4.39	-2.62	-3.20	-4.30	-3.85	-4.71	-4.58	-3.33	-4.97	

23

Table 3.90: The binding activities of the Ru(II)-based complexes as predicted suing Autodock package

	CatB	DNA_Gyrase	HDAC7	HP-NCP	KINASE	rHA	RNR	top11	TrXR	TS	
1 CraptaC	-9.29	-8.92	-8.33	-7.11	-6.57	-6.49	-5.49	-4.47	-5.22	-8.05	
2 OraptaC	-9.11	-8.35	-7.93	-7.59	-6.44	-5.52	-5.16	-5.6	-5.96	-7.15	
3 raptaBh2o	-7.16	-6.21	-6.95	-6.78	-6.3	-4.72	-3.79	-4.41	-5.1	-5.46	
4 raptaCh2o	-8.15	-6.58	-6.63	-6.75	-6.21	-5.11	-3.89	-4.14	-4.78	-5.17	
5 raptaTh2o	-7.27	-6.26	-6.61	-7.01	-6.32	-5.04	-3.62	-4.42	-5.05	-5.52	
6 piano	-5.83	-5.56	-6.49	-7.31	-6.45	-5.35	-3.72	-4.53	-4.72	-4.26	
7 ragly	-5.63	-5.05	-5.77	-6.6	-5.08	-4.88	-3.64	-4.38	-5.04	-4.5	

8	etdiaglydmso	-9.34	-7.57	-8.63	-8.5	-7.92	-6.37	-4.02	-6.46	-6.3	-5.62
9	radipyrazoic	-4.49	-3.77	-3.84	-3.94	-3.4	-4.3	-4.93	-4.73	-4.17	-4.5
10	radipyrdioic	-3.68	-4.4	-2.5	-5.01	-5.33	-6.09	-5.65	-6	-6.24	-4.91
11	raphendioic	-5.3	-5.58	-3.48	-5.49	-4.77	-6.52	-5.47	-5.48	-4.93	-5.04
12	rCpbkdmso	-6.16	-5.6	-6.05	-4.85	-4.18	-4.63	-4.69	-4.35	-4.39	-4.73

Table 3.91: The correlation between the ranking of the complexes activity as predicted from Autodock and Glide packages.

	Autodock/Glide
CatB	-0.65
DNA-Gyrase	-0.86
HDAC7	-0.69
HP-NCP	-0.55
KINASE	-0.12
rHA	0.46
RNR	0.24
TopII	-0.55
TrXR	0.11
TS	-0.66

Table 3.92: The interaction of the binding site residues with first two rank best inhibitors complexes from the three docking methods defining the Complex-receptor existing Hydrogen bond (HB) and Metal-Receptor (MR) possible interactions with residues within the range of 4.5Å.

Receptor	Autodock	Glide
CatB	etdiaglydmso[a]{[HB: 2.31 Å (H^1@NH_2EtNH_2)-(O@CO CYC 26D)], [HB: 1.72 Å (H^2@NH_2EtNH_2)-(O@COOH GLU 122E)], [HB: 1.93 Å (H@NH_2CH_2COO)-(O@COOH GLU 122E)], [HB: 2.73 Å (N@NH_2CH_2COO)-(H@COOH GLU 122E)], [HB: 2.87 Å (O@NH_2CH_2COO)-(S@CH_2S CYS 29D)], [HB: 2.13 Å (O@NH_2CH_2COO)-(H@NH	radipyrazoic[a]{[HB: 1.82 Å (H@COOH)-(O@COO GLU 122E)], [MR: 3.66Å (H@ar TRP 221E)]}; raphendioic[b]{[HB: 1.63 Å (H@COOH)-(O@COO GLU 122E)], [MR: 4.27 Å (H@ar TRP 221E)]};

	CYS 29D)], [MR: 3.38 Å (O@COOH GLU 122 E)], [MR: 4.36 Å (CH GLY 27 D)]}; CraptaC[b]{[HB: 1.92 Å (O@COO)-(H@im HIS 111E)], MR: 4.07Å (ar TRP 221E)};	
DNA-Gyrase	CraptaC[a] {[HB: 1.74Å (O@COO)-(H@NH VAL 120A)]; [MR: 4.35Å (NH_2 ASN 46A)}; OraptaC[b] {[HB: 1.78Å (O@COO)-(H@NH VAL 120A)], [MR: 4.41Å (CO GLY 117A)], [MR: 4.48Å (CH2 GLY 119A)]};	radipyrdioic[a] {[HB: 2.12 Å (H@$COOH^1$)-(O@CO ASP 49A)]; [HB: 1.92 Å (O@$COOH^2$)-(H@NH GLY 77A)];[HB: 2.08 Å (H@$COOH^2$)-(O@CO ASP 73A)]; raphendioic[b] {[HB: 1.67 Å (H@$COOH^1$)-(O@COO ASP 49A)], [HB: 2.48 Å (H@$COOH^2$)-(O@COO ASP 73A)], [MR: 4.14Å (CH_2 ASN 46A)], [MR: 4.09 Å (CH_2 ILE78A)]}
HDAC7	etdiaglydmso[a]{[HB: 1.67 Å (H@NH_2EtNH_2)-(O@COO ASP 626 A)], [MR: 4.06 Å (COO ASP 626 A)]}; CraptaC[b]{MR: 3.53Å (COO ASP 626 A)};	radipyrdioic[a] {[HB: 1.58 Å (H@COOH)-(O@COO ASP 626A)], [MR: 3.59 Å (H@CH_2 PHE 738 A)], [MR: 4.45 Å (H@NH PHE 738 A)], [MR: 4.36 Å (O@CO PRO 809 A)], [MR: 4.47 Å (H@CH_2 PRO 809 A)]}; piano[b] {[HB: 2.10 Å (H@NH_2)-(O@CO PRO 809 A)], [MR: 4.11 Å (H@CH_3 LEU 810 A)], [MR: 4.29 Å (O@CO PRO 809 A)], [MR: 4.35 Å ($H^{1,2}$@CH_2 PHE 738 A)]}
HP-NCP	etdiaglydmso[a]{[HB: 1.98 Å (O@dmso)-(H@NH ASP 478 A)], [MR: 3.96 Å (O@COO GLU 532 A)], [MR: 4.42Å (O@COO ASP 478 A)]}; OraptaC[b] {[IT: 2.90 (N@PTA)-(O@COO GLU 64G)],[MR: 3.73Å (COO GLU 61G)]},	radipyrazoic[a] {[HB: 2.12 Å (O@COOH)-(H@COOH GLU 61 G)], [MR: 4.50 Å (H@COOH ASP 90 G)]}; etdiaglydmso[b] {[HB: 2.09 Å (O@COOH)-(HN@im HIS 106H)]}
KINASE	etdiaglydmso[a]{[HB: 2.15 Å (H@NH_2EtNH_2[1])-(O@COO GLU 68 H)], [HB: 1.76 Å (H@NH_2EtNH_2[2])-(O@COO ASP 65 H)], [MR: 4.06 Å (CH_2COO ASP 65 H)]}; CraptaC[b] {[HB: 1.36 (O@COO)- (H@im HIS 584A)]};	radipyrdioic[a] {[HB: 2.55 Å (H@$COOH^1$)-(O@CO CYS 531A)], [HB: 2.10 Å (O@$COOH^1$)-(H@NH CYS 531A)], [HB: 2.67 Å (O@$COOH^2$)-(H@OH THR 528A)], [MR: 3.88 Å (H@CH_3 VAL 470 A)], [MR: 4.28 Å (H@ar PHE 582 A)]}; ragly[b] {[HB: 1.99 Å (O@COO)-(H@NH ASP 593 A)], [MR: 4.05 Å (H@CH_3 LEU 513 A)], [MR: 3.60 Å (H@NH ASP 593 A)], [MR: 3.40 Å (H@CH_2 LYS 482 A)], [MR: 4.06 Å (H@NH_3 LYS 482 A)]}
rHA	raphendioic[a] {[HB: 2.15 Å (H@$COOH^1$)-(H@COO GLU 425 A)], [HB: 1.72 Å (H@$COOH^2$)-(O@CO PRO 113 A)], [HB: 1.92 Å (O@$COOH^2$)-(H@NH ARG 145 A)], [MR: 4.45 Å (CH_2 ARG 145 A)]}; CraptaC[b] {[MR: 4.05Å (NH2 ASN 109A)], [MR: 4.21Å (COOH GLU 425A)]};	raphendioic[a] {[HB: 2.20 Å (O@$COOH^1$)-(H@NH_2 ARG 145 A)], [HB: 2.23 Å (O@$COOH^1$)-(H@OH GLU 141 A)], [HB: 1.84 Å (O@$COOH^2$)-(H@NH_3 LYS 137 A)], [HB: 1.67 Å (H@$COOH^2$)-(O@COOH GLU 37 A)], [MR: 4.45 Å (H@NH_3 LYS 137 A)]}; piano[b] {[HB: 1.99 Å (H@NH_2)-(O@COOH ASP 107 A)], [MR: 4.32 Å (O@COOH ASP 107 A)], [MR: 4.45 Å (H@NH_2 ASN 111 A)]}
RNR	radipyrdioic[a] {[HB: 2.32 Å (H@$COOH^1$)-(O@CO ARG 251A)], [HB: 2.60 Å (O^1@$COOH^2$)-(H@NH THR 209 A)], [HB: 1.99 Å (O^1@$COOH^2$)-(H@OH SER 625A)], [HB: 2.13 Å (O^2@$COOH^2$)-(H@NH SER 625A)], [HB: 2.26 Å (O^2@$COOH^2$)-(H@NH THR 624 A)], [HB: 2.43 Å (O^2@$COOH^2$)-(H@NH GLU 623 A)]}; CraptaC[b] {[HB: 1.99Å (O@COO)- (H@NH THR 209A)], [HB: 2.55Å (N@PTA)- (H@COOH GLU 441A], }	radipyrazoic[a] {[HB: 2.09 Å (O^1@$COOH^1$)-(H@NH GLU 633 A)], [HB: 1.89 Å (O^1@COOH)-(H@NH THR 624 A)], [HB: 1.95 Å (O^2@COOH)-(H@NH SER 625 A)], [MR: 3.59 Å (CH_3 LEU 464 A)], [MR: 4.46 Å (H@CH_2 SER 224 A)]}; radipyrdioic[b] {[HB: 2.51 Å (O^1@$COOH^1$)-(H@NH_3 LYS 154A)], [HB: 2.31 Å (O^2@$COOH^1$)-(H@NH_3 LYS 154A)], [HB: 2.50 Å (O^2@$COOH^1$)-(H@OH THR 209 A)], [HB: 1.70 Å (H@$COOH^2$)-(H@OH THR 624 A)],

		[HB: 1.44 Å (H@$COOH^2$)-(H@OH SER 224 A)], [MR: 3.90 Å (H@CH_2OH SER 224 A)]}
TopII	etdiaglydmso[a]{[HB: 2.17 Å (O@NH_2CH_2COO)-(H@NH LEU 124 A)], [MR: 3.85 Å (im HIS 123 A)]}; radipyrdioic[b] {[HB: 1.79 Å (H@$COOH^1$)-(O@CO PHE 362 A)], [HB: 2.00 Å (H@$COOH^2$)-(O@CO THR 27 A)]}	raptaB-H_2O[a]{[HB: 1.83Å (H@H_2O)- (O@OH SER 128A)], [HB: 2.04Å (H@H_2O)- (O@CO ASN 129A)], [IT: 2.97Å (N@PTA)- (O@CO ASN 70A)], [MR: 3.66Å (NH SER 128A)]}, radipyrazoic[b] {[HB: 2.28 Å (O@COOH)-(H@NH_3 LYS 147 A)], [HB: 2.23 Å (H@COOH)-(O@CO ASN 70 A)], [MR: 4.31 Å (H@CH_3 ILE 120A)], [MR: 4.01 Å (H@OH SER 128 A)]};
TrXR	etdiaglydmso[a]{[HB: 1.83 Å (H@NH_2EtNH_2)-(O@CO THR 161 A)], [MR: 3.66 Å (CO THR 161 A)], [MR: 3.97 Å (O@CO PHE 43 A)], [MR: 4.21 Å (H@NH PHE 43 A)], [MR: 4.15 Å (H@NH GLY 20 A)]}; radipyrdioic[b] {[HB: 2.30Å (H@$COOH^1$)-(O@CO LEU 41 A)], [HB: 1.91 Å (H@$COOH^2$)-(O@CO ALA 160 A)], [HB: 2.11 Å (O^1@$COOH^2$)-(H@NH GLY 24 A)], HB: 2.43 Å (O^2@$COOH^2$)-(H@NH GLY 23 A)], [MR: 3.82 Å (H@NH_2 ARG 164 A)], [MR: 4.33 Å (O@CO THR 161 A)], [MR: 4.00 Å (H@NH TRP 53 A)], [MR: 4.10 Å (NH THR 58 A)], [MR: 3.41 Å (OH THR 58 A)]}	radipyrdioic[a] {[HB: 1.92 Å (O@COOH)-(H@COOH GLU 163 A)], [HB: 2.22 Å (H@COOH)-(O@CO ARG 293 A)], [MR: 3.81 Å (H@NH_2 ARG 166 A)]}; radipyrazoic[b] {[HB: 2.60 Å (O@COOH)-(H@COOH GLU 163 A)], [HB: 2.29 Å (O@COOH)-(H@NH_2 ARG 166 A)]}
TS	CraptaC[a] {[no HB and MR]}, OraptaC[b] {[HB: 1.86Å (O@COO)-(H@SH CYS 198A], [HB: 2.22Å (CO)-(H@NH ASP 221A], [MR: 4.14Å (CH_2 GLY 225A)]}	raphendioic[a] {[HB: 2.91 Å (O@COOH)-(H@NH_2 ASN 229 A)], [MR: 3.94 Å (H@NH_2 ASN 229 A)]} raptaB-H_2O[b]{[HB: 1.69Å (H@H_2O)- (H@OH ASP 257A)], [MR: 3.73Å (OH SER 219A)]}

Table 3.93: The docking result of the metal-based complexes against ten receptors using Glide package in Maestro.

	CatB	DNA-Gyrase	HDAC7	HP-NCP	KINASE	rHA	RNR	Top11	TrxR	TS
1 carbo-rapta-C	-2.14	-1.68	-1.41	-2.67	-3.45	-0.97	-1.51		-1.70	-1.00
2 rapta-C-COOH	-1.24	-1.67		-1.35			-0.88		-2.12	-1.22
3 rapta-C-$(OH)_2$	-2.50	-2.14	-1.38	-3.02	-3.26	-1.49	-2.52	-3.12	-2.84	-1.91
4 rapta-C-NH_2(OH)	-2.12	-1.88	-1.63	-1.99	-3.49		-1.16	-3.03	-2.44	-1.65
5 oxalo-rapta-C	-2.19	-2.19	-2.38	-2.15	-4.44	-2.12	-0.55		-2.69	-3.71
6 raC-NH_2	-2.68	-2.51	-1.93	-3.56	-5.17	-2.91	-1.80	-3.44	-2.92	-2.93
7 rapta-B	-3.59	-2.53	-2.30	-2.84	-3.20	-2.49	-2.88	-3.75	-2.54	-1.74
8 rapta-B-H_2O	-4.04	-3.18	-2.16	-3.41	-3.10	-2.40	-3.52	-5.68		-4.10
9 rapta-B-H	-4.01	-2.63	-2.83	-3.03	-4.06	-2.96	-2.81	-4.67	-3.16	-2.56
11 rapta-C	-3.36	-2.34	-2.62	-2.46	-3.31	-1.88	-3.32	-4.18	-2.49	-3.09
12 rapta-C-H_2O	-3.56	-2.49	-3.35	-2.99	-2.61	-2.61	-3.64	-3.97	-2.37	-2.82
13 rapta-C-H	-3.68	-3.08	-3.44	-2.79	-4.34	-2.66	-3.82	-5.09	-3.00	-3.06
14 rapta-T	-3.25	-2.65		-2.71	-2.39	-2.01	-2.53	-3.91	-2.56	-2.74
15 rapta-Ta-CH_3	-3.21	-2.19	-2.44	-2.64	-2.25	-2.34	-3.41	-3.74	-2.84	-3.21
16 rapta-Ta-NH_2	-3.05	-2.56	-3.06	-2.97	-3.96	-2.68	-4.15	-4.76	-2.73	-3.22
17 rapta-Ta-OH	-3.83	-3.16	-3.19	-3.55	-3.24	-3.35	-4.75	-5.02	-2.87	-4.16
18 rapta-T-CF_3	-3.81	-2.21	-2.58	-2.33	-2.13	-2.31	-3.99	-4.19	-1.91	-2.73
19 rapta-T-CF_3(H_2O)	-3.92	-2.35	-2.43	-2.65	-2.47	-2.08	-4.21	-3.95	-2.56	-3.36
20 rapta-T-H_2O	-3.98	-2.48	-2.61	-2.87	-3.38	-2.23	-3.75	-4.75	-2.57	-3.76
21 rClCOO-NH_3	-3.18	-2.20	-1.92	-2.95	-3.79	-3.82	-1.96	-2.76	-3.79	-3.19

Table 3.94: The docking prediction for metal-based complexes using Gold

	CatB	DNA-Gyrase	HDAC7	HP-NCP	KINASE	rHA	RNR	Top11	TrxR	TS
1	carbo-rapta-C	50.37	40.79	-39.09	21.56	39	36.51	51.46	41.13	34.48	42.45
2	rapta-C-COOH	40.53	47.59	30.82	30.46	35.37	33.26	43.02	45.21	38.67	45.48
3	rapta-C-$(OH)_2$	45.53	39.29	37.14	21.63	42.04	39.06	38.54	60.73	41.92	52.63
4	rapta-C-$NH_2(OH)$	53.29	46.78	39.97	32.2	39.68	43.75	40.18	64.48	40.31	51.22
5	oxalo-rapta-C	40.94	42.48	18.01	25.28	42.51	46.79	46.62	49.95	40.75	40.28
6	raC-NH_2	32.39	26.92	30.46	25.81	27.59	29.22	24.97	30.63	35.56	30.02
7	rapta-B	45.14	31.96	32.91	22.01	34.92	29.49	28.93	41.53	37.1	34.2
8	rapta-B-H_2O	45.94	32.76	32.4	26.36	40.14	31.73	29.32	42.14	32.71	31.72
9	rapta-B-H	45.08	32.04	38.21		40.34	33.89		41.4		40.08
10	rapta-B-NH_2	47.66	37.76	40	28.61	42.27	42.57	36.13	47.9	48.6	38.03
11	rapta-C	44.84	41.05	1.63	24.02	46.02	35.18	27.07	53.56	33.47	38.49
12	rapta-C-H_2O	40.34	39.56	10.84	26.19	42.19	36.96	36.94	52.18	37.26	37.39
13	rapta-C-H	47.22	39.11	32.49	15.25	43.03	39.26	24.33	51.92	32.93	39.36
14	rapta-T	41.09	34.83	34.43	22.33	38.57	31.1	28.8	46.48	40.48	34.66
15	rapta-Ta-CH_3	50.09	38.46	38.59	25.11	39.04	35.87	29.64	48.55	30.9	38.84
16	rapta-Ta-NH_2	50.46	44.05	34.02	30.56	46.61	39.58	41.03	53.8	35.93	38.7
17	rapta-Ta-OH	49.51	43.87	-4.38	28.01	38.15	34.39	42	49.75	36.91	40.75
18	rapta-T-CF_3	45.33	32.37	33.2	22.83	39.65	30.95	31.99	43.82	37.93	35.02
19	rapta-T-$CF_3(H_2O)$	46.03	27.52	29.51	26.64	43.79	29.8	34.39	45.61	30.34	31.96
20	rapta-T-H_2O	45.13	33.69	26.55	26.86	44.12	29.71	37.95	46.1	28.8	34.72
21	rClCOO-NH_3	35.59	38.42	38.51	28.92	32.83	32.54	33.89	40.86	39.64	48.42

Table 3.95: The docking prediction for metal-based complexes using Autodock.

	CatB	DNA-Gyrase	HDAC7	HP-NCP	KINASE	rHA	RNR	Top11	TrxR	TS
1 carbo-rapta-C	-9.29	-8.92	-8.33	-3.93	-6.57	-6.49	-5.49	-4.94	-3.04	-8.05
2 rapta-C-COOH	-8.33	-6.63	-7.68	-3.06	-5.51	-5.02	-4.12	-2.63	-5.32	-6.66
3 rapta-C-$(OH)_2$	-9.96	-7.9	-8.1	-3.46	-6.65	-5.58	-4	-3.82	-6.43	-6.27
4 rapta-C-NH_2(OH)	-9.42	-6.79	-7.37	-2.95	-6.16	-5.25	-3.73	-3.1	-6.22	-5.79
5 oxalo-rapta-C	-9.11	-8.35	-7.93	-3.66	-6.44	-5.52	-5.16	-3.8	-7.26	-7.15
6 raC-NH_2	-3.22	-2.72	-3.69	-2.11	-3.41	-2.96	-2.94	-1.84	-2.78	-2.73
7 rapta-B	-5.01	-3.95	-4.09	-2.61	-3.82	-4.11	-2.65	-2.38	-2.84	-3.89
8 rapta-B-H_2O	-7.16	-6.21	-6.95	-2.98	-6.3	-4.72	-3.79	-3.22	-5.69	-5.46
9 rapta-B-H	-4.83	-4.77	-5.07	-2.71	-4.81	-4.4	-2.83	-2.42	-3.03	-4.01
10 rapta-B-NH_2	-7.09	-5.65	-6.76	-2.76	-5.76	-4.23	-3.31	-2.54	-4.24	-4.68
11 rapta-C	-5.73	-5.36	-5.2	-3.08	-4.71	-4.34	-3.46	-3.18	-2.18	-4.65
12 rapta-C-H_2O	-8.15	-6.58	-6.63	-3.61	-6.21	-5.11	-3.89	-2.78	-5.87	-5.17
13 rapta-C-H	-5.44	-5.14	-5.1	-2.83	-4.69	-4.24	-2.99	-2.65	-3.46	-4.32
14 rapta-T	-7.1	-6.15	-6.23	-2.79	-5.32	-4.62	-3.74	-3.23	-4.67	-5.31
15 rapta-Ta-CH_3	-5.42	-4.94	-4.49	-3.04	-4.18	-4.48	-3.68	-2.86	-2.64	-4.13
16 rapta-Ta-NH_2	-5.02	-4.76	-4.37	-2.96	-4	-4.21	-3.11	-2.7	-2.5	-3.77
17 rapta-Ta-OH	-7.15	-7.03	-7.51	-5.14	-6.48	-5.83	-5.32	-3.98	-4.58	-5.99
18 rapta-T-CF_3	-5.02	-4.59	-4.98	-1.86	-4.33	-3.89	-2.8	-2.04	-1.77	-3.91
19 rapta-T-CF_3(H_2O)	-6.57	-5.86	-5.91	-2.31	-5.87	-4.34	-3.07	-2.53	-4.41	-4.76
20 rapta-T-H_2O	-7.27	-6.26	-6.61	-2.9	-6.32	-5.04	-3.62	-3.23	-4.89	-5.52
21 rClCOO-NH_3	-5.74	-4.88	-5.57	-2.78	-5.32	-4.81	-3.37	-3.09	-4.25	-3.85

Table 3.96: The interaction of the binding site residues with first two rank best inhibitors complexes from the three docking methods defining the Complex-receptor existing Hydrogen bond (HB) and Metal-Receptor (MR) possible interactions with residues within the range of 4.5Å.

No	Method	Receptor Interactions
1	Autodock	CatB[b]{[HB: 1.92 Å (O@COO)-(H@imHIS 111E)], MR:4.07Å (arTRP 221E)}; Gyrase[a]{[HB:1.74Å (O@COO)-(H@NHVAL 120A)]; [MR:4.35Å (NH_2ASN 46A)}; HDAC7[a]{[MR:3.52Å (COOH ASP 626A)]}; Kinase[b]{[HB:1.36 (O@COO)- (H@imHIS 584A)]}; rHA[a]{[MR:4.05Å (NH2 ASN 109A)], [MR:4.21Å (COOH GLU 425A)]}; RNR[a] {[HB:1.99Å (O@COO)- (H@NHTHR 209A)], [HB:2.55Å (N@PTA)- (H@COOHGLU 441A], } TS[a] {[no HB and MR]}
	Gold	CatB[b]{[MR: 4.32Å (arTRP 221E)]}; RNR[a] {[MR:3.83Å (HOTHR 209A)]}
3	Autodock	CatB[a]{[HB:1.59Å (OH^1)-(O@COOGLU 122E)], [HB:1.52Å (OH^2)-(O@COOH GLU 122E)], [HB:2.52Å (HO^2)-(H@NH2GLN 23D)], [MR:3.88Å (CH_2GLY 121E)}; HDAC7[b]{[HB:1.69 (OH)-(O@COOASP 626A)],[MR:4.37Å (arPHE 738A)], [MR:4.39Å (COOH ASP 626A)] ; HP-NCP[a]{[HB:2.22 (OH)-(O@COOGLU 64G)],[MR:2.83Å (COOGLU 64G)], [MR:4.19Å (COOGLU 61G)]} Kinase[a]{[HB:1.96Å (H@OH^1)-(O@COOH ASP 586A)], [HB:2.54Å (H@HO^2)-(O@COOH ASP 586A)], [HB:3.02Å (O@HO^2)-(H@COOH ASP 586A)], }
	Gold	Gyrase[a]{[MR:4.48Å (COO GLU 50A)], } Top11[b] { [HB:2.11Å (O@OH)- (H@NH SER 128A)], [MR:3.97Å (CHSER 127A)], [MR:4.23Å (CO ASN 71A)]} TrxR[b]{ [HB:1.73Å (O@OH)-(H@NH2 ARG 166A)], [MR:3.67Å (NH_2ARG 166A)]} TS[a] {[HB:1.11Å (O@OH^1)-(H@NH_2ARG 218A], [HB:2.30Å (O@OH^1)-(H@OH SER 219A], [HB:2.52Å (O@OH^2)-(H@NH_2ARG 23A)][MR:3.47Å (CH_2ARG 23A)], [MR:3.20Å (NH_2ARG 218A)]}
4	Autodock	CatB[a]{[HB: 1.44 Å (NH_2)-(O@COOH GLU 122E)], MR:3.23Å (CH_2 GLY 29D)}; Gyrase[b]{HB: 1.87 Å (OH)-(H@NH_2 ASN 46A)], [MR:2.07Å (CH_2ASN 46A)], [MR:4.17Å (CH_3ILE 78A)]} HDAC7[a]{[MR:1.87Å (arPHE 679A)], [MR:3.73Å (im HIS 709A)] } TS[b] {[HB:2.57Å (N@PTA)-(H@OH SER 219A], [MR:2.90Å (SH CYS 198A)], [MR:3.48Å (CH_3LEU 195A)]}
5	Autodock	HP-NCP[a]{[IT:2.90 (N@PTA)-(O@COOGLU 64G)],[MR:3.73Å (COOGLU 61G)]} Gyrase[b]{[HB:1.78Å (O@COO)-(H@NHVAL 120A)], [MR:4.41Å (COGLY 117A)], [MR:4.48Å (CH2GLY 119A)]}; Top11[a]{[HB:2.08Å (O@COO)-(H@OHSER 128A)], [MR:3.18Å (COOGLU 134A)]} TrxR[a]{[HB:1.83Å (O@COO)-(H@NHSER 386A)], [MR:3.96Å (COGLY 38A)]} TS[b] {[HB:1.86Å (O@COO)-(H@SHCYS 198A], [HB:2.22Å (CO)-(H@NH ASP 221A], [MR:4.14Å (CH_2GLY 225A)]}
	Gold	rHA[a] {[HB:1.68Å (O@COO)-(H@NH_2ASN 111A], [HB:2.08Å (O@COO)-(H@NH ASN 111A], [MR:3.20Å (CH2 GLN 33A)]} RNR[b] {[HB:1.86Å (O@COO^1)- (H@NH GLU 623A)], [HB:1.98Å (O@COO^1)- (H@NH THR 624A)], HB:2.56Å (O@COO^1) - (H@OH THR 624A)], HB:1.98Å (O@COO^2)- (H@OH SER 625A)], [IT:2.81Å (N@PTA)- (O@COPRO 621A], [MR:3.40Å (HOTHR 209A)]}
6	Glide	HP-NCP[a]{[MR:2.42Å (NH3 LYS 113H)]} Kinase[a]{[MR:3.01Å (NH ASP 593A)]}
8	Glide	CatB[a]{[HB:1.96Å (H@H_2O)-(O@COOGLU 122E)]} Gyrase[a]{[HB:1.67Å (H@H_2O)-(O@COO ASP 49A)]} Top11[a]{[HB:1.83Å (H@H_2O)- (O@OHSER 128A)], [HB:2.04Å (H@H_2O)- (O@CO ASN 129A)], [IT:2.97Å (N@PTA)- (O@CO ASN 70A)], [MR:3.66Å (NH SER 128A)]} TS[b]{[HB:1.69Å (H@H_2O)- (H@OHASP 257A)], [MR:3.73Å (OH SER 219A)]}
9	Glide	CatB[b]{[MR:3.09Å (CH_2 GLY121E)], [MR:4.29Å (COOH GLY122E)]} TrxR[b]{[MR:3.42Å OH SER 199A]}
10	Gold	rHA[b] { [MR:1.55Å (CH_3@S(CH_3) MET 87A)]} TrxR[a]{ [MR:4.18Å (ar@ph TYR 200A)]}
12	Autodock	
	Glide	HDAC7[b]{[HB:1.64Å (H@H_2O)-(O@COOASP 626A)]}
13	Glide	HDAC7[a]{[MR:3.21Å (ar PHE 679A)], [MR:4.42Å (CH_3 LEV 810A)]} Kinase[a]{[MR:3.33Å (ar PHE 582A)], [MR:3.30Å (CH_3ILE 462A)] } Top11[b]{[MR:4.10Å (CH_2ASN 70A)], [MR:3.78Å (CH_3 ILE 104A)]}

15	Gold	HDAC7[b]{[MR:2.80Å (arPHE 679A)], [MR:3.52Å (im HIS 709A)]
16	Gold	HP-NCP[b]{[HB: 1.69Å(NH2@ar)-(O@COOH GLU 61G)]} Kinase[a]{[MR:4.24Å (ar TRP 530A)], [MR:4.34Å (ar PHE 582A)] }
17	Autodock	HP-NCP[a]{[HB:2.044Å(OH@ar)-(O@COTHR 101G)]}; rHA[b] {[HB:1.88Å (OH@ar)-(O@COPRO 113A], [HB:2.02Å (HO@ar)-(H@NH ARG 145A], [HB:2.11Å (HO@ar)-(H@NH LEU 115A], [HB:2.44Å (N@PTA)-(H@COOH GLU 425A]}; RNR[b] {[HB:1.89Å (HO@ar)-(H@NH SER 625A]} Top11[b] {[no HB and MR]}
	Glide	Gyrase[b]{[MR:3.26Å (CH_2 ILE 78A)], [MR:3.99Å (CH_2 ASN 46A)]} Top11[b]{[HB:1.69Å (OH@ar)- (O@COASP 73A)], [MR:4.33Å (COO GLU 134A)]} rHA[b] {[HB:1.77Å (OH@ar)-(O@CO PRO 110A]} RNR[a]{[HB:1.80Å (OH@ar)- (O@OHSER 625A)], [HB:1.86Å (OH@ar)- (H@NHSER 625A)], [MR:4.08Å (H@OH THR 209A)]} TS[a]{[HB:2.63Å (OH@ar)- (H@NH_3ARG 23A)], [MR:4.39Å (NH_2 ASP 221A)], [MR:3.43Å (SH CYS 198A)]}
19	Glide	RNR[b]{[HB andMR]}
20	Gold	Kinase[a]{[MR:2.83Å (ar PHE 582A)], [MR:3.46Å (CH_3VAL 470A)] }
21	Autodock	TrxR[b] {[HB:1.70Å (H@NH_3)-(O^1@COOGLU 341A], [HB:2.32Å (H@NH_3)-(O^2@COOGLU 341A)], [HB:1.70Å (H@NH_3)-(O@COARG 293A], [MR: 3.26Å (COOGLU 341A)], [MR: 3.88Å (COOARG 166A)], [MR: 4.09Å (NH_3LYS 315A)]}
	Glide	rHA[a] {[HB:1.74Å (O@COO^1)-(H@NH_2ARG 144A], [HB:2.03Å (O@COO^2)-(H@NH_2ARG 145A], [HB:1.95Å (O@COO)-(H@OH GLU 141A]} TrxR[a] {[HB:2.62Å (H@NH_3)-(O@CO VAL 291A], [HB:1.85Å (O@COO)-(H@NH ALA 198A], [MR:3.27Å NH_2ARG 221A], [MR:3.81Å CH_2ARG 226A]}

The type of the interaction: MR(Metal-Receptor define for any receptor residue within the range of 4.50Å), HB(Hydrogen bond Interaction) and IT (interaction predicted to be also HB). The signs im (imidazole group), ar (arene group which in some residues like TRP is part of benzopyrole), @ (part of). The superscript "a" and "b" on each receptors indicate the ranking of the ligand as first and second respectively, while superscript "1" and "2" indicates first and second respectively of the same functional group that exist on a residue, {} separate different receptor, [] separate different interaction in the same receptor while () define the atom with its residue that is involved in the interaction.

Table 3.97. The correlation of the docking result using Autodock, Gold and Glide Packages

	Autodock VS Gold	Autodock VS Glide	Gold VS Glide
CatB	0.27	-0.50	0.10
DNA-Gyrase	0.54	-0.32	-0.33
HDAC7	-0.13	-0.33	-0.38
HP-NCP	0.24	-0.17	-0.18
KINASE	0.32	-0.17	-0.26
rHA	0.45	-0.37	-0.20
RNR	0.76	-0.32	-0.36
topoII	0.41	-0.06	-0.11
TrxR	0.32	0.13	0.07
TS	0.42	-0.28	-0.46

Table 3.98. The statistical results of the QSAR analysis called COMSIA of the Glide docked result.

	Factors	gausσs	gausσe	gausσh	gausσa	gausσd	S.D	R^2	R^2-CV	R^2-Scramble	Stability	F	P
CatB	1	0.53	0.15	0.22	0.06	0.05	0.33	0.85	0.41	0.39	0.66	138.8	1.83E-011
DNA-Gyrase	1	0.52	0.17	0.19	0.08	0.04	0.53	0.53	0.19	0.39	0.86	27.2	2.41E-005
HDAC7	1	0.5	0.14	0.19	0.07	0.1	0.42	0.65	0.04	0.45	0.58	41.3	1.82E-006
HP-NCP	1	0.59	0.14	0.19	0.04	0.03	0.42	0.71	0.35	0.38	0.77	58.5	6.88E-008
KINASE	1	0.63	0.08	0.16	0.07	0.06	0.68	0.49	0.25	0.35	0.94	21.8	1.07E-004
rHA	1	0.53	0.16	0.22	0.04	0.05	0.41	0.72	0.02	0.55	0.48	52.9	3.68E-007
RNR	1	0.63	0.13	0.15	0.05	0.04	1	0.62	0.39	0.45	0.93	38.7	2.00E-006
topoII	1	0.43	0.18	0.18	0.07	0.14	0.45	0.65	0.27	0.45	0.72	38.4	3.78E-006
TrxR	1	0.48	0.15	0.23	0.08	0.06	0.32	0.8	0.03	0.55	0.31	92.6	1.57E-009
TS	1	0.6	0.16	0.15	0.05	0.03	0.7	0.49	0.27	0.36	0.94	23.4	6.35E-005

Table 3.99: The two best binding metallocomponds of each receptors from Molegro and Autodock showing the existing Hydrogen bond (HB) (in Å) and Metal-Residues (MR) interactions with binding site residues

DNA-1	Molegro	metallocompound **10a** {[HB: 2.39 O(COOH)^{i} H(DC 18.B)], [HB: 1.91 H(COOH)^{ii} N7(DG 16.B)]}; metallocompound **12** {[HB: 2.32 O(COOH) H(DA 17.B)], [HB: 1.44 H(COOH) O6(DG 7.A)]}
	Molegro-Constrain	metallocompound **10a** {[HB: 1.71 O(COOH)^{i} H(DC 2.A)], [HB: 1.89 H(COOH)^{i} O6(DG 23.B)], [HB: 1.66 H(H_2O) O6(DG 23.B)], [HB: 2.01 H(H_2O) N7(DG 23.B)], [MR 4.49 N7(DG 34.B)], [MR 4.60 N7(DA 22.B)]}; metallocompound **9a** {[HB: 2.05 H(COOH)^{i} O6(DG 23.B)], [HB: 2.02 H(COOH)^{ii} OP2(DG 23.B)], [HB: 2.11 H(H_2O) N7(DA 22.B)], [MR 4.60 N7(DA 22.B)]};
	Autodock	metallocompound **9a** {[HB: 2.00 H(COOH)^{i} OP1(DT 5.A)], [HB: 1.65 H(COOH)^{ii} OP2(DA 15.B)]} metallocompound 4**a** {[HB: 1.81 H(NH_2)^{i} OP1(DG 6.A)], [HB: 1.70 H(NH_2)^{ii} OP2(DG 7.A)], [MR 3.32 O(DG 6.A)], [MR 3.88 O(DG 6.A)]}
DNA-2	Molegro	Metallocompound **10a** {[HB: 1.92 O(COOH)^{i} H(DG 7.T)], [HB: 1.76 H(COOH)^{i} O4(DT 8.T)], [HB: 2.16 H(COOH)^{ii} O3(DC 9.T)]}; metallocompound **1a** {[HB: 1.75 H(COOH) O2(DC 8.P)], [HB: 2.12 H(H_2O) O4(DT 8.T)]}
	Molegro-Constrain	metallocompound **12** {[HB: 1.57 H(COOH) O6(DG 5.P)], [HB: 2.50 O(COOH) H(DC 9.T)], [HB: 2.80 O(COOH) H(DA 6.P)], [MR 3.64 N7(DG 6.T)], [MR 4.21 N7(DG 7.T)]}; metallocompound **1** {[HB: 1.95 N(arene) H(DA 6.P)], [MR 3.91 N7(DG 7.T)]}
	Autodock	metallocompound **1a** {[HB: 1.79 H(COOH) OP2(DG 6.T)]}; metallocompound **4a** {[HB: 1.76 H(H_2O) OP2(DG 7.T)], [HB: 1.96 H(NH_2)^{i} O3(DG 6.T)], [HB: 1.84 H(NH_2)^{i} OP1(DG 6.T)]}
CatB	Molegro	metallocompound **12** {[HB: 1.66 H(COOH) O(GLY 24 D)]} metallocompound **1** {[HB: 2.21 H(COOH) O(MET 196 E)]}

	Molegro-Constrain	metallocompound **1a** {[HB: 3.28 N(arene) SG(CYS 29D)], [HB: 2.61 H(COOH) O(GLY 198E)], [MR 4.60 SG(CYS 29D)]} metallocompound **8a** {[MR 4.60 SG(CYS 29D)]}
	Autodock	metallocompound **10a** {[HB: 2.99 O(COOH)^{i} SG(CYS 29 D)], [HB: 2.76 O(COOH)^{i} H(GLN 23 D)], [HB: 1.70 H(COOH)^{i} OE1(GLN 23D)], [HB: 2.14 H(COOH)^{ii} OE2(GLU 122D)]}; metallocompound **1a** {[HB: 1.72 H(COOH) OE1(GLU 122 E)], HB: 1.72 H(COOH) OE2(GLU 122E)]}
Gyrase	Molegro	metallocompound **10** {[HB: 2.17 H(COOH) O(ASP 73A)]} metallocompound **11** {[none]}
	Molegro-Constrain	metallocompound **10a** {[HB: 2.24 H(COOH)^{i} OD2(ASP 49A)], [HB: 1.92 H(COOH)^{ii} O(GLY 117A)], MR: 4.60 ND2(ASP 46 A)]} metallocompound **9a** {[HB: 1.50 H(H_2O) OD1(ASP 46A)], [HB: 2.08 H(COOH)^{i} O(ASP 46A)], [HB: 1.84 H(COOH)^{ii} O(ASP 45A)], MR: 4.27 ND2(ASP 46 A)]};
	Autodock	metallocompound **12** {[HB: 2.11 H(COOH) O(ASP 73A)], [HB: 1.81 H(COOH) O(ASP 73A)], [HB: 2.00 O(COOH) H(GLY 77A)]}; metallocompound **9a** {[HB: 1.90 O(H_2O) HD22(ASN 46A)], [HB: 1.63 H(COOH)^{i} O(LYS 103 A)], [HB: 2.05 O(COOH)^{ii} H(ALA 100 A)], [HB: 1.65 H(COOH)^{ii} O(ILE 94 A)], [HB: 2.14 O(COOH)^{ii} H(SER 121 A)]}
HDAC7	Molegro	metallocompound **1** {[HB: 1.82 N(arene) H(imi@HIS 709A)], [HB: 1.87 O(COOH) H(imi@HIS 669A)]}; metallocompound **12** {[HB: 2.36 H(COOH) O(ASP 707A)]}
	Molegro-Constrain	metallocompound **10a** {[HB: 1.89 H(COOH)^{i} O(GLY 678A)], [HB: 2.43 O(COOH)^{i} H(CYS 680A)], [HB: 1.99 O(COOH)^{i} HE2(HIS 669A)], [MR: 3.43 NE2(HIS 709A)]} metallocompound **11** {[MR: 3.60 N(HIS 709A)]}
	Autodock	metallocompound **1a** {[HB: 1.63 H(COOH) OD1(ASP 626A)], [HB: 1.90 H(H_2O) OD1(ASP 626A)]}; metallocompound **9a** {[HB: 1.80 O(COOH)^{i} H(PHE 738A)], [HB: 1.79 H(COOH)^{i} O(PRO 809 A)]}
HP-NCP	Molegro	metallocompound **1a** {[none]} metallocompound **11** {[MR: 3.38 OE(GLU 56G)]}
	Molegro-Constrain	metallocompound **10a** {[HB: 1.75 H(COOH)^{i} OE1(GLU 92 G)], [[HB: 2.17 H(COOH)^{ii} NE2(HIS 106 H)], [MR: 4.36 OE1(GLU 61 H)], MR: 4.44 NE2(HIS 106 H)]} metallocompound **11** {[MR: 4.36 OE1(GLU 61 H)], [MR: 4.60 NE2(HIS 106 H)]}
	Autodock	metallocompound **4a** {[HB: 1.67 H(H_2O) OE2(GLU 61 G)], [HB: 1.67 H(H_2O) OE1(GLU 64G)]}; metallocompound **5a** {[MR: 2.90 OE2(GLU 61 G)]}
BRAF Kinase	Molegro	metallocompound **1a** {[HB: 2.09 H(COOH) O(ASN 579A)]}; metallocompound **12** {[HB: 2.59 H(COOH) O(CYS 531A)], [HB: 1.66 O(COOH) H(CYS 531A)]}
	Molegro-Constrain	metallocompound **1** {[HB: 2.04 N(arene) H(SER 535A)], [MR: 4.61 SG(CYS 531 A)]} metallocompound **8** {[MR: 4.61 SG(CYS 531 A)]}
	Autodock	metallocompound **4a** {[HB: 1.91 H(NH_2)^{i} OD2(ASP 478A)], [HB: 2.03 H(H_2O) OD2(ASP 478A)], [HB: 1.84 H(NH_2)^{ii} OE2(GLU 532A)], [HB: 1.94 H(H_2O) OE2(GLU 532A)]}; metallocompound **5a** {[none]}
rHA	Molegro	metallocompound **10** {[HB: 2.24 O(COOH)^{i} H(ARG 117A)], [HB: 2.05 O(COOH)^{ii} H(ARG 186A)]};

		metallocompound **12** {[HB: 2.16 H(COOH) O(ASP 108A)], [MR: 4.27 O(SER 193A)]}
	Molegro-Constrain	metallocompound **10a** {[HB: 2.12 H(COOH)^{i} OE2(GLU 37A)], [HB: 1.68 O(COOH)^{ii} H(ARG 144A)], [HB: 1.82 H(COOH)^{ii} O(GLN 33A)], [MR: 4.59 NH1(ARG 144A)]} metallocompound **2** {[HB: 1.91 O(COO)^{i} H(ARG 144A)], [HB: 1.91 O(COO)^{i} H(ARG 144A)], [MR: 4.59 NH1(ARG 144A)]};
	Autodock	metallocompound **10** {[MR: 1.78 NZ(LYS 195A)], [MR: 4.52 NH_2(ARG 222A)]}; metallocompound **4a** {[HB: 1.85 H(H_2O) OD2(ASP 38A)], [HB: 1.73 H(H_2O) OH(TYR 84A)], [HB: 1.85 H(NH_2)^{i} OD2(ASP 34A)]}
RNR	Molegro	metallocompound **1a** {[HB: 1.59 H(H_2O) O(PRO 621A)], [HB: 1.98 H(COOH) OE1(GLU 441A)], [HB: 2.39 O(COOH) HD22(ASN 437A)]}; metallocompound **3** {[HB: 1.88 O(COO)^{i} H(GLU 623A)], [HB: 1.92 O(COO)^{i} H(SER 625A)], [HB: 2.34 O(COO)^{ii} H(THR 209A)]}
	Molegro-Constrain	metallocompound **1a** {[HB: 2.22 H(COOH) O(SER 224B)], [MR: 4.17 SG(CYS 439A)]}; metallocompound **10** {[HB: 2.27 H(COOH)^{i} O(PRO 621A)], [HB: 2.16 H(COOH)^{ii} O(SER 224A)], [MR: 4.26 S(CYS 439A)]}
	Autodock	metallocompound **1a** {[HB: 1.68 H(COOH) OE1(GLU 623A)], [HB: 2.00 O(H_2O) H(ARG 639A)], [MR: 3.69 NH_2(ARG 639A)]}; metallocompound **12** {[HB: 2.60 O(COOH) H(GLU 623A)], [HB: 1.95 O(COOH) N(SER 625A)], [HB: 2.02 O(COOH) HG(SER 625A)], [HB: 1.77 H(COOH) OG1(THR 209A)]}
TopII	Molegro	metallocompound **1** {[HB: 2.15 H(COOH) O(GLN 365B)], [HB: 3.38 O(COOH) O(THR 27A)]} metallocompound **10** {none};
	Molegro-Constrain	metallocompound **10a** {[HB: 2.47 H(COOH) O(ILE 15A)], [MR: 4.60 NE2(HIS 20B)]}; metallocompound **1a** {[MR: 4.60 NE2(HIS 20B)]}
	Autodock	metallocompound **5** {[HB: 2.21 O(COO) H(GLY)], [HB: 2.57 O(COO) NH_2(GLN 365A)], [HB: 2.53 O(COO) NH_3(LYS 367A)], [HB: 2.09 O(COO) H(ASN 142A)], [HB: 2.37 O(COO) H(ARG 141A)]}; metallocompound **9a** {[HB: 1.90 H(COOH)^{i} OD1(ASN 70A)], [HB: 1.88 O(COOH)^{i} HZ1(LYS 147A)], [HB: 1.85 H(COOH)^{ii} OD1(ASN 129A)], [HB: 2.15 O(COOH)^{ii} HD21(ASN 129A)]}
TrXR	Molegro	metallocompound **10** {[HB: 1.77 O(COOH)^{i} O(ALA 198A)], [HB: 2.60 O(COOH)^{ii} H(ARG 166A)], [HB: 2.19 O(COOH)^{ii} H(ARG 166A)]}; metallocompound **1** {[HB: 2.14 H(COOH) O(SER 222A)], [HB: 1.75 O(COOH) OH(SER 222A)]}
	Molegro-Constrain	metallocompound **9a** {[HB: 2.27 O(COOH)^{i} HZ1(LYS 67A)], [HB: 2.10 H(COOH)^{ii} O(THR 373A)], [MR: 3.59 SG(CYS 64A)], [MR: 4.60 SG(CYS 59A)]} metallocompound **8a** {[HB: 1.63 H(COOH) OD2(ASP 334A)], [HB: 2.11 O(COOH) HH21(ARG 293A)], [HB: 1.85 O(COOH) HE(ARG 293A)], [MR: 3.06 SG(CYS 64A)], [MR: 4.60 SG(CYS 59A)]}
	Autodock	metallocompound **5a** {[HB: 1.96 H(NH_2) O(GLU 341A)], [HB: 1.89 H(NH_2) OH(TYR 200A)], [HB: 2.10 O(COO) H(THR 343A)], [HB: 2.13 O(COO) H(THR 343A)], [HB: 2.02 H(H_2O) OD1(ASP 334A)], [HB: 2.48 H(H_2O) OD2(ASP 334A)]} metallocompound **12** {[HB: 1.69 H(COOH) O(GLU 341A)], [HB: 1.98 O(COOH) NH_3(LYS 315A)], [MR: 3.47 H(LEU 340A)]};
TS	Molegro	metallocompound **12** {[HB: 2.22 H(COOH) O(SER 232A)]}; metallocompound **10** {[HB: 1.53 O(COOH) H(ASN 229A)]}
	Molegro-Constrain	metallocompound **10a** {[HB: 2.40 O(COOH) H(CYS 198A)], [HB: 1.86 O(COOH)

		HH(TYR 146A)], [MR: 4.60 S(CYS 198A)]} metallocompound **1** {[HB: 2.13 H(COOH) O(SER 219A)], [HB: 2.70 O(COOH) H(ARG 218A)], [HB: 2.39 O(COOH) H(ARG 218A)], [HB: 2.38 O(COOH) H(ARG 23A)], [HB: 1.56 O(COOH) H(ARG 23A)], [MR: 3.55 S(CYS 198A)]};
	Autodock	metallocompound **9a** {[HB: 1.82 H(COOH)^{i} O(SER 219A)], [HB: 1.97 O(COOH)^{i} H(ASP 221A)], [HB: 2.45 O(COOH)^{i} HG(CYS 198A)], [HB: 2.08 O(COOH)^{ii} HD21(ASN 229A)], [HB: 1.63 H(COOH)^{ii} OE2(GLU 60A)]}; metallocompound **5a** {[HB: 2.36 O(COO) HH(TYR 146A)], [HB: 1.71 H(H_2O) OE1(GLU 60A)]}

Table 3.100(a): The binding energy of the metallocompounds from the Autodock docking

	DNA-1	**DNA-2**	**CatB**	**DNA_ Gyrase**	**HDAC 7**	**HP-NCP**	**BRAF KINASE**	**rHA**	**RNR**	**topoII**	**TrxR**	**TS**
1	-4.32	-3.3	-4.26	-3.68	-3.15	-3.44	-3.25	-3.45	-3.15	-3	-3.43	-3.03
2	-2.47	-3.08	-3.38	-3.21	-2.64	-3.43	-3.79	-4.19	-3.71	-2.65	-3.35	-4.14
3	-2.73	-2.5	-3.43	-3.49	-2.5	-3.82	-3.29	-3.91	-3.49	-3.84	-3.35	-3.7
4	-4.67	-3.88	-3.98	-3.49	-3.92	-4.16	-3.65	-3.86	-2.85	-3.05	-3.21	-2.84
5	-2.93	-2.7	-3.27	-3.01	-3.02	-3.54	-3.39	-3.62	-3.07	-4.08	-3.39	-3.21
6	-2.29	-1.9	-1.24	-1.31	-1.77	-2.46	-2.37	-2.32	-2.45	-1.62	-2.19	-1.31
7	-2.82	-2.79	-3.42	-3.38	-3.1	-2.59	-3.97	-3.97	-3.6	-3.47	-2.79	-2.96
8	-2.24	-3.41	-2.92	-3.09	-2.59	-3.29	-3.39	-3.4	-3.25	-3.03	-3.43	-2.53
9	-4.27	-3.73	-4.02	-3.24	-3.5	-3.63	-3.66	-3.34	-3.39	-3.1	-3.92	-3.67
10	-5.13	-4.94	-5.19	-4.86	-3.78	-5.14	-4.48	-5.24	-4.03	-3.86	-4.24	-4.51
11	-5.02	-3.81	-4.5	-3.68	-4.01	-3.85	-3.12	-2.98	-2.43	-2.19	-2.91	-3.65
12	-5.97	-4.65	-5.77	-5.12	-5.1	-4.56	-4.37	-4.16	-4.19	-3.4	-4.31	-5.23
13	-2.5	-2.44	-3.35	-2.94	-2.78	-2.84	-3.13	-3.38	-2.88	-2.88	-2.86	-2.78
14	-3.04	-3.14	-3.55	-3.54	-2.72	-3.83	-3.41	-4.29	-3.52	-3.98	-3.79	-3.7
15	-2.43	-2.56	-3.38	-3.1	-2.82	-3.05	-3.27	-3.39	-3.09	-3.13	-2.83	-2.96
16	-1.63	-1.87	-2.23	-2.15	-1.66	-2.22	-2.08	-2.59	-2.41	-2.08	-2.11	-2.4
cisplatin	-2.23	-2.94	-2.15	-1.34	-1.98	-2.18	-2.56	-1.65	-1.93	-1.95	-2.4	-1.23
co-crystallized compounds			-5.49	-8.68	-4.35				-7.01	-12.48	-4.79	-9.19

24

Table 3.100(b): The binding energy of the metallocompounds from the Autodock docking of hydrolytic complexes

	DNA-1	DNA-2	CatB	DNA_ Gyrase	HDAC 7	HP-NCP	BRAF KINASE	rHA	RNR	topoII	TrxR	TS
1a	-6.53	-5.65	-6.47	-4.67	-5.97	-4.95	-4.97	-4.04	-4.39	-3.16	-4.26	-4.9
4a	-6.85	-5.87	-6.29	-4.82	-5.55	-5.58	-5.27	-4.54	-3.16	-3.47	-4.23	-4.72
5a	-5.58	-4.75	-5.65	-4.55	-5.08	-5.26	-4.98	-4.33	-4.13	-3.96		-5.35
6a	-5.35	-3.6	-3.6	-2.3	-3.39	-4.51	-4.26	-2.6	-2.37	-2.38	-3.54	-2.96
8a	-6.44	-5.03	-5.78	-4.76	-5.25	-5.22	-3.96	-4.02	-3.02	-3.06	-2.98	-4.2
9a	-6.98	-5.96	-6.19	-5.03	-5.56	-5.05	-4.77	-3.3	-3.95	-4.07	-3.94	-6.09
10a	-6.38	-5.22	-6.7	-4.61	-5.21	-4.58	-4.03	-4.48	-3.49	-3.51	-4.17	-5.26
13a	-4.86	-4.06	-5.19	-4.05	-4.81	-4.29	-3.59	-3.74	-3.32	-3.65	-3.61	-3.39
14a	-4.39	-3.75	-4.84	-4.19	-4.59	-4.32	-3.33	-3.99	-3.65	-3.73	-3.76	-3.17
15a	-4.86	-4.03	-4.38	-3.8	-4.79	-4.27	-3.64	-3.41	-3.14	-3.6	-3.65	-3.05
16a	-4.12	-3.24	-3.1	-3.28	-3.75	-3.62	-3.1	-2.91	-2.16	-2.77	-2.65	-2.31
Cisp-W1	-4.31	-3.98	-2.1	-0.99	-2.55	-3.37	-3.25	-1.73	-1.04	-1.15	-2.63	-1.45
Cisp-W2	-4.92	-4.4	-2.15	-0.93	-2.76	-3.18	-3.47	-1.72	0.02	-0.33	-1.79	-1.2

Table 3.101(a): The binding energy of the metallocompounds from the relax Molgro docking

	DNA-1	DNA-2	CatB	Gyrase	HDAC 7	HP-NCP	BRAF Kinase	rHA	RNR	TopII	TrXR	TS
1	-137.57	-133.77	-136.37	-131.99	-166.09	-111.45	-118.79	-142.13	-126.87	-154.82	-137.87	-127.39
2	-113.84	-106.15	-124.88	-110.82	-127.16	-94.13	-110.31	-113.18	-98.90	-121.50	-103.71	-114.61
3	-116.96	-97.09	-114.43	-103.00	-110.06	-91.82	-105.79	-135.47	-124.93	-118.69	-104.43	-111.20
4	-77.36	-77.97	-72.59	-79.89	-83.51	-68.21	-67.34	-85.02	-74.88	-74.75	-75.04	-75.89
5	-71.22	-82.12	-78.61	-73.09	-90.05	-68.85	-74.96	-86.25	-83.41	-84.15	-82.63	-79.76
6	-86.14	-81.39	-88.78	-84.63	-95.90	-75.53	-84.76	-97.60	-88.56	-92.57	-100.22	-79.41
7	-87.95	-84.94	-93.69	-94.11	-102.98	-75.06	-99.78	-100.28	-92.07	-97.69	-106.18	-83.43
8	-119.77	-111.18	-118.67	-110.79	-107.93	-96.84	-117.76	-126.06	-116.02	-115.67	-121.37	-111.59
9	-124.03	-122.96	-125.25	-126.26	-131.56	-101.43	-115.00	-119.84	-106.90	-129.34	-119.82	-118.59
10	-141.56	-126.74	-135.89	-142.43	-147.55	-107.85	-114.94	-147.15	-121.72	-129.66	-138.35	-129.75
11	-143.11	-142.45	-131.53	-140.36	-157.61	-117.62	-114.61	-133.71	-114.68	-128.89	-121.04	-127.35
12	-153.94	-129.90	-144.21	-138.83	-160.63	-104.74	-122.12	-142.37	-113.66	-129.13	-120.89	-135.47
13	-62.98	-67.16	-83.32	-70.45	-90.53	-63.02	-73.54	-73.40	-74.49	-82.38	-70.73	-77.41
14	-82.56	-85.26	-100.23	-85.99	-113.53	-71.41	-89.94	-97.88	-91.04	-102.67	-89.64	-85.02
15	-66.45	-67.86	-89.21	-70.59	-101.13	-62.61	-74.58	-78.25	-81.13	-84.18	-78.17	-84.17
16	-73.52	-76.16	-95.70	-80.20	-94.92	-71.53	-87.20	-87.77	-80.40	-93.80	-84.48	-87.89
cisplatin	-47.86	-44.53	-38.09	-46.03	-45.22	-46.40	-39.91	-43.53	-40.83	-43.89	-38.82	-39.79
co-crystallized compounds			-117.36	-162.48	-70.17		-121.74		-152.80	-192.15	-160.24	-106.57

Table 3.101(b): The binding energy of the metallocompounds from the relax Molgro docking for hydrolytic

	DNA-1	DNA-2	CatB	Gyrase	HDAC 7	HP-NCP	BRAF Kinase	rHA	RNR	TopII	TrXR	TS
1a	-150.05	-145.76	-128.02	-136.31	-106.38	-129.59	-122.79	-137.56	-125.01	-84.25	-131.96	-127.11
4a	-94.36	-98.02	-77.65	-81.91	-81.50	-76.86	-61.37	-80.77	-73.66	-75.59	-87.09	-79.70
5a	-88.43	-96.33	-82.01	-76.01	-86.05	-75.74	-68.95	-87.31	-80.07	-82.79	-87.95	-86.37
6a	-100.04	-95.69	-91.02	-89.94	-96.65	-73.28	-85.05	-104.25	-86.02	-81.42	-99.80	-82.86
8a	-146.26	-127.46	-126.15	-136.28	-129.26	-113.66	-113.13	-129.33	-113.82	-116.42	-111.76	-118.85
9a	-144.54	-125.87	-123.34	-120.42	-90.58	-106.68	-109.38	-127.80	-106.99	-44.91	-131.76	-120.86
10a	-161.33	-145.84	-131.71	-142.22	-158.93	-113.82	-110.56	-121.54	-120.44	-79.33	-122.11	-126.24
13a	-77.52	-81.55	-90.06	-75.72	-94.57	-71.10	-71.20	-74.88	-80.32	-88.55	-71.37	-79.81
14a	-96.88	-106.30	-105.80	-99.03	-110.38	-80.03	-95.53	-86.14	-94.44	-106.7	-94.05	-86.26
15a	-84.66	-86.84	-91.02	-82.81	-101.74	-74.49	-74.40	-78.79	-83.59	-95.58	-80	-75.33
16a	-89.62	-89.80	-98.32	-85.32	-106.94	-81.19	-85.06	-90.37	-82.83	-99.96	-81.1	-84.77
Cisp-W1	-62.38	-58.09	-46.27	-50.24	-44.07	-44.94	-35.32	-44.08	-41.17	-42.72	-44.55	-42.56
Cisp-W2	-84.39	-70.95	-45.17	-57.47	-43.45	-42.73	-28.77	-37.91	-43.82	-42.74	-44.54	-41.68

Table 3.102(a): The binding affinities of the metallocompounds from the covalent constrain Molegro docking

	DNA-1	DNA-2	CatB	Gyrase	HDAC 7	HP-NCP	BRAF Kinase	rHA	RNR	TopII	TrXR	TS
1	-116.11	-128.23	-99.45	-107.80	-133.48	-95.08	-105.04	-27.44	-121.13	-43.60	-67.44	-110.86
2	-97.80	-85.91	-82.34	-84.02	-74.26	-72.24	-10.28	-86.36	-99.26	-8.38	-14.82	-98.92
3	-78.05	-72.06	-74.09	-72.94	-66.77	-76.14	-58.45	10.16	-90.08	-72.78	-40.92	-81.43
4	-68.50	-61.59	-67.53	-50.22	-71.28	-61.87	-63.35	-43.68	-60.08	-38.15	-39.06	-54.89
5	-61.04	-58.83	-63.33	-57.28	-76.44	-58.64	-70.82	26.31	-65.84	-44.97	-41.88	-61.54
6	-71.93	-66.06	-72.19	-62.16	-94.46	-61.01	-65.64	-70.29	-71.03	-43.94	-47.54	-69.91
7	-70.49	-65.18	-75.95	-67.76	-96.59	-67.18	-69.16	15.13	-75.00	-63.31	-53.38	-70.06
8	-90.84	-88.44	-79.93	-82.66	-83.25	-81.53	-96.36	-2.29	-96.45	-49.40	-63.45	-102.19
9	-111.80	-117.06	-99.06	-110.65	-87.96	-78.92	-79.57	-49.97	-104.49	-70.13	-62.38	-92.44
10	-122.46	-117.40	-90.07	-90.46	-141.61	-102.69	-74.46	-88.52	-113.02	-47.87	-45.13	-99.57
11	-124.47	-125.50	-111.86	-104.70	-144.86	-104.53	-92.96	-85.74	-107.52	-50.71	-91.01	-98.64
12	-125.54	-129.90	-104.35	-107.26	-112.43	-97.12	-75.51	-66.29	-106.43	-8.28	-66.59	-91.48
13	-49.78	-49.53	-60.05	-48.08	-55.13	-46.22	-59.27	-47.94	-62.99	-56.55	-28.91	-58.53
14	-66.71	-68.14	-79.05	-65.58	-66.86	-51.48	-50.64	19.86	-77.96	0.00	-52.96	-78.21
15	-54.61	-55.65	-64.40	-58.80	-58.83	-53.29	-63.23	-55.84	-64.54	-57.33	-36.73	-65.11
16	-65.29	-64.79	-70.31	-68.07	-72.82	-58.20	-58.63	-66.45	-73.20	-37.72	-35.54	-71.26
Cisplatin	-38.97	-34.23	-43.49	-33.31	-49.14	-29.06	-36.20	-26.49	-30.79	-35.58	-33.00	-30.63
co-crystallized compounds			-132.12	-120.11	-73.24	-30.80	-94.68		-126.37	-115.68	-144.33	-95.40

Table 3.102(b): The binding affinities of the metallocompounds from the covalent constrain Molegro docking of hydrolytic complexes

	DNA-1	DNA-2	CatB	Gyrase	HDAC 7	HP-NCP	BRAF Kinase	rHA	RNR	TopII	TrXR	TS
1a	-126.70	-122.83	-127.33	-117.35	-99.20	-104.06	-86.78	-7.23	-113.75	-81.83	-101.44	-108.38
4a	-85.71	-72.54	-69.40	-65.33	-81.49	29.93	-59.98	36.01	-59.88	-39.37	-63.58	-53.49
5a	-77.64	-71.78	-68.57	-63.59	-86.11	-57.75	-67.38	29.87	-63.13	-47.71	-67.64	-64.37
6a	-94.75	-84.34	-81.49	-74.57	-96.64	-66.72	-64.99	24.66	-76.07	-54.41	-69.31	-73.20
8a	-128.21	-111.69	-110.41	-112.41	-129.27	-99.85	-92.82	-78.11	-110.43	-69.52	-103.76	-94.83
9a	-134.05	-125.46	-103.79	-119.20	-65.16	-81.50	-74.88	-52.63	-106.48	-68.35	-118.89	-100.43
10a	-135.60	-126.76	-116.86	-120.84	-158.92	-115.24	-72.50	-91.28	-110.44	-82.45	-84.59	-113.85
13a	-63.52	-63.46	-69.71	-57.52	-73.39	-60.84	-58.70	35.82	-67.58	-59.59	-33.43	-55.79
14a	-84.65	-78.01	-92.77	-69.23	-74.84	-60.37	-54.22	23.16	-82.70	-5.71	-11.37	-78.60
15a	-71.57	-68.76	-75.77	-66.29	-72.91	-66.99	-64.27	-37.41	-72.72	-66.08	-36.32	-62.97
16a	-74.70	-74.07	-73.81	-74.55	-72.88	-69.08	-60.26	-34.70	-76.95	-46.59	-42.19	-66.71
Cisp-W1	-62.37	-45.20	-40.91	-36.93	-43.65	-35.62	-32.23	-31.06	-35.91	-29.93	-34.13	-29.65
Cisp-W2	-78.38	-55.98	-34.03	-38.27	-43.46	-40.96	-29.51	-24.29	-32.68	-25.48	-32.34	-26.43

Table 3.103: The docking results of metallocompounds with available experimental activities.

		CatB		
	Experiment	Moldock-non	Moldock-cons	Autodock
RAPTATh2o	1.5	-91.0243	-75.7655	-4.38
RAPTACh2o	2.5	-105.798	-92.7676	-4.84
CRAPTAC	5	-124.877	-82.3353	-3.38
ORAPTAC	200	-114.427	-74.0878	-3.43
RAPTABh2o	200	-90.0599	-69.7078	-5.19
		TrXR		
CRAPTAC	4.6	-103.714	-14.8246	-3.35
ORAPTAC	32.5	-104.425	-40.9218	-3.35
RAPTACh2o	37.1	-94.0454	-52.9618	-3.76
RAPTATh2o	144	-80.0042	-36.727	-3.65
RAPTABh2o	200	-71.3701	-28.9068	-3.61

Table 3.104(a):The correlation of the factors that determine the biding interaction of the

metallocompounds with the receptors using Molgro docking (unconstrained cocking)

	4DL7	CatB	Gyrase	HDAC7	HP-NCP	BRAF Kinase	rHA	RNR	TopII	TrXR	TS
E.Inter.protein.ligand.	0.28	0.91	0.93	0.93	0.89	0.89	0.93	0.92	0.81	0.90	0.90
E.Intertotal	0.84	0.91	0.93	0.93	0.89	0.89	0.93	0.92	0.81	0.90	0.90
E.Intra.steric.	0.12	0.42	0.39	0.46	0.68	0.49	0.66	0.58	0.45	0.31	0.55
E.Intra.tors.	0.26	-0.01	-0.11	0.07	0.20	0.05	0.15	-0.11	-0.10	-0.53	0.14
E.Intra.tors.ligand atoms.	0.16	0.37	0.30	0.43	0.65	0.46	0.63	0.51	0.36	-0.01	0.52
E.Intra.vdw.	-0.91	-0.77	-0.82	-0.79	-0.67	-0.65	-0.69	-0.50	-0.32	-0.58	-0.74
Electro	-0.35	0.22	0.45	-0.14	-0.07	-0.04	-0.12	0.61	-0.19	0.26	0.07
ElectroLong	-0.76	0.20	0.31	-0.08	-0.21	-0.06	-0.29	0.36	-0.20	0.53	0.51
HBond	-0.47	0.20	0.17	-0.44	0.03	-0.14	0.11	0.34	0.13	0.71	0.31
HeavyAtoms	-0.71	-0.91	-0.82	-0.84	-0.80	-0.85	-0.76	-0.78	-0.52	-0.82	-0.84
LE1	-0.13	-0.50	-0.20	-0.39	-0.21	-0.39	-0.11	-0.27	-0.23	-0.22	-0.30
LE3	-0.11	-0.63	-0.39	-0.45	-0.43	-0.41	-0.42	-0.27	-0.40	-0.52	-0.11
MW	-0.51	-0.69	-0.65	-0.64	-0.60	-0.67	-0.54	-0.53	-0.13	-0.71	-0.56
N	-0.51	-0.57	-0.35	-0.63	-0.59	-0.49	-0.47	-0.63	-0.60	-0.64	-0.53
NoHBond90	-0.35	0.19	0.15	-0.15	0.08	0.01	0.22	0.64	0.45	0.74	0.31
PoseEnergy	0.80	0.99	0.99	0.99	0.99	0.99	1.00	0.99	0.99	0.99	0.99
RerankScore	0.81	0.69	0.48	0.08	0.52	0.54	0.32	0.85	-0.23	0.38	0.53
Steric	0.48	0.85	0.90	0.94	0.89	0.87	0.92	0.77	0.80	0.85	0.86
Torsions	-0.31	-0.31	-0.55	-0.20	-0.41	-0.45	-0.38	-0.65	-0.27	-0.70	-0.37
VdW.LJ12.6.	0.32	-0.01	-0.17	-0.30	-0.11	0.04	-0.29	0.35	-0.34	-0.37	0.20
halogen	0.26	0.38	0.50	0.29	0.40	0.40	0.45	0.50	0.51	0.50	0.42

Table 3.104(b):The correlation of the factors that determine the binding interaction of the

metallocompounds with the receptors using Molgro docking (constrained cocking)

	4DL7	CatB	Gyrase	HDAC7	HP-NCP	BRAF Kinase	rHA	RNR	TopII	TrXR	TS
E.Inter.protein.ligand.	-0.43	0.87	0.87	0.94	0.83	-0.17	0.31	0.89	0.67	0.52	0.85
E.Intertotal	0.82	0.87	0.87	0.94	0.83	-0.17	0.31	0.89	0.67	0.52	0.85
E.Intra.steric.	0.15	0.32	0.25	0.67	0.71	-0.39	0.29	0.53	-0.04	-0.18	0.61
E.Intra.tors.	0.30	0.14	-0.01	0.46	0.35	-0.05	-0.21	-0.21	-0.25	-0.51	-0.04
E.Intra.tors.ligand atoms.	0.21	0.31	0.22	0.68	0.70	-0.37	0.22	0.44	-0.09	-0.28	0.54
E.Intra.vdw.	-0.71	-0.55	-0.79	-0.55	-0.65	-0.55	-0.43	-0.58	0.00	-0.71	-0.51
E.SoftConstraintPenalty	0.14	0.15	0.46	-0.01	-0.37	0.76	0.89	NA	0.33	0.41	-0.45
Electro	0.05	0.57	-0.33	-0.24	-0.07	-0.24	-0.10	0.19	0.06	-0.01	0.31
ElectroLong	-0.73	0.18	-0.33	0.16	0.72	0.17	0.08	-0.31	0.16	-0.33	-0.36
HBond	0.04	0.10	0.42	0.12	0.10	0.15	0.25	0.53	0.17	0.62	0.34
HeavyAtoms	-0.53	-0.71	-0.81	-0.47	-0.65	-0.37	-0.71	-0.84	0.15	-0.67	-0.82
LE1	0.08	-0.10	-0.20	0.16	0.06	0.78	0.79	-0.14	0.72	0.40	-0.10
LE3	-0.02	-0.15	-0.25	0.09	0.17	-0.42	-0.59	-0.54	0.45	-0.09	-0.47
MW	-0.39	-0.35	-0.67	-0.23	-0.40	-0.50	-0.75	-0.61	0.39	-0.57	-0.55
N	-0.26	-0.42	-0.38	-0.41	-0.49	-0.18	-0.43	-0.63	-0.08	-0.73	-0.57
NoHBond90	0.36	0.40	0.47	0.30	0.13	0.21	0.24	0.70	0.18	0.70	0.31
PoseEnergy	0.83	0.99	0.99	0.99	0.99	1.00	0.99	0.99	0.99	0.99	0.98
RerankScore	0.07	0.05	0.10	0.25	0.66	-0.40	-0.45	0.34	0.46	-0.03	-0.02
Steric	-0.20	0.81	0.85	0.92	0.72	-0.19	0.25	0.87	0.64	0.54	0.79
Torsions	-0.25	-0.62	-0.55	-0.04	-0.16	-0.17	-0.62	-0.63	-0.17	-0.70	-0.51
VdW.LJ12.6.	-0.11	-0.20	-0.23	0.08	0.48	-0.38	-0.44	-0.36	0.41	-0.17	-0.36
halogen	0.37	0.44	0.38	0.35	0.45	-0.32	0.14	0.44	0.17	0.33	0.38

Table 4.1: Assignment of the prominent IR picks of the ligands using the PED method

dmpz				bdmpzm			
Freq	Intensity	Vibration	Vibration	Freq	Intensity	Vibration	Vibration
3589.12	58.84	υ(NH)		3007.49	24.96	υ(CH)	
3080.63	14.85	υ(CH)		2979.19	43.12	υ(CH)	
3039.59	15.12	υ(CH)		2979.69	31.47	υ(CH)	υ(CH)
3029.52	13.11	υ(CH)		2972.01	36.22	υ(CH)	υ(CH)
2979.22	32.22	υ(CH)		2968.49	32.95	υ(CH)	υ(CH)
2972.32	42.98	υ(CH)		1564.26	42.14	υ(CC)	υ(CC)
1574.91	41.03	υ(CC)	β(HNN)	1560.38	42.94	υ(CC)	
1462.75	8.13	β(CNN)	β(HCH)	1446.85	19.42	β(CNN)	β(HCH)
1450.17	6.67	β(HCH)	τ(HCCC)	1444.59	32.48	β(CNN)	β(HCH)
1438.24	5.59	β(HCH)	τ(HCCC)	1424.05	37.84	β(HCH)	β(HCH)
1437.84	12.07	β(HCH)	τ(HCCN)	1414.81	26.55	β(HCH)	β(HCH)
1409.03	36.57	β(CNN)	β(HCH)	1413.02	45.24	β(HCH)	β(HCH)
1270.94	16.64	υ(NC)	β(HNN)	1392.69	19.24	υ(NC)	β(HCN)
1159.57	14.56	υ(NN)	υ(NC)	1343.57	55.23	β(HCH)	τ(HCNC)
981.5	16.75	β(CNN)	τ(HCCC)	1294.06	110.65	υ(NC)	β(HCN)
764.89	43.89	τ(HCCC)		1251.9	37.26	υ(NC)	
656.84	4.66	τ(CNNC)		792.24	20.33	υ(CC)	υ(CC)
631.81	25.35	τ(CCNN)		760.76	24.87	τ(HCCC)	τ(HCCC)
453.74	45.71	τ(HNNC)		760.33	24.34	τ(HCCC)	τ(HCCC)
175.21	4.78	ο(CCNC)		666.26	26.51	β(CNN)	β(CNN)
		bdmpza				bdcpzm	
3629.27	65.03	υ(OH)		3645.72	97.92	υ(OH)	
2987.94	25.11	υ(CH)		1791.4	199.66	υ(OC)	
2981.16	35.35	υ(CH)	υ(CH)	1780.25	376.25	υ(OC)	
2979.61	60.08	υ(CH)	υ(CH)	1771.02	324.55	υ(OC)	
1774.89	212.51	υ(OC)		1752.4	224.79	υ(OC)	
1565.7	45.07	υ(CC)	β(HCC)	1432.98	68.69	β(CNN)	τ(HCNC)
1562.87	45.09	υ(CC)	β(HCC)	1327.66	89.51	υ(NN)	
1418.12	53.16	β(HCH)	β(HCH)	1285.01	237.63	υ(OC)	β(HOC)
1412.14	52.72	β(HCH)	β(HCH)	1272.6	188.17	υ(OC)	β(HOC)
1385.44	33.5	υ(NC)		1262.45	139.57	υ(NN)	β(HOC)
1382.52	29.6	υ(CC)	τ(HCCO)	1237.44	369.46	υ(CC)	β(HOC)
1295.36	172.05	υ(NC)	τ(HCCO)	1225.77	432.86	υ(OC)	β(HOC)
1204.93	26.43	υ(NC)	β(CNN)	1204.6	100.07	υ(NN)	β(HCN)
1161.02	35.66	υ(NN)		1125.64	238.72	β(HOC)	β(HCC)
1102.19	177.16	υ(OC)	β(HOC)	1102.65	107.68	υ(OC)	β(HCC)
855.36	40.86	υ(CC)	υ(NC)	1083.83	75.29	υ(OC)	β(HCC)
814.87	41.6	β(CCN)	ο(CNNC)	1066.37	69.13	υ(OC)	
738.61	30.95	υ(CC)	β(CNN)	500.48	123.33	τ(HOCC)	
664.37	103.74	τ(HOCC)		457.1	86.89	β(OCO)	τ(HOCC)

605.52	30.88 β(OCO)	τ(CCNN)	448.41	64.62 β(OCC)	β(OCC)

Greek letters υ, β, τ, o denote stretching, bending, tortion and out of plane modes respectively

Table 4.2: The experimental H- and C-NMR shift in ligands bdmpzm and bdmpza

^{1}H-NMR (dmso-d6)		**^{1}H-NMR ($CHCl_3$-d, 250.00 MHz)**			
dmpz			bdmpzm		bdmpza
2.11	(s, 3H, $C3CH_3$)	2.44	(s, 6H, $C3CH_3$)	1.703 (1.94)	(s, 6H, $C3CH_3$) [[Díez-Barraetal2002]]
2.11	(s, 3H, $C5CH_3$)	2.44	(s, 6H, $C5CH_3$)	2.21 (2.21)	(s, 6H, $C5CH_3$) [[Díez-Barraetal2002]]
5.73	(s, H, H4)	5.86	(s, 2H, H4)	5.88 (5.82)	(s, 2H, H4) [[Díez-Barraetal2002]]
11.99	(s, H, H1)	6.13, 7.27	(s, 2H, C*H*$_2$)	7.27 (7.27)	(s, 1H, C*H*COOH) [[Burzlaffetal2001]]
				7.45	(s, 1H, COO*H*)
		^{13}C- NMR ($CHCl_3$-d, 62.5 MHz)			
		11.13, 13.54	(CH_3)	11.42, 12.03, 13.54 (11.40, 14.50)	(CH_3) [[Burzlaffetal2001]]
		60.46	(CH_2)		
		106.78, 140.46, 148.58	(C_{pz})	104.37, 106.78, 144.37, 147.98	(C_{pz})
				169.71 (165.90)	(CO_2H)

Table 4.3: The computed H-NMR shifts from the direct subtractions of TMS isotropic and from fitting equation

dmpz			bdmpzm			bdmpza			bdcpzm		
	direct	fitted		direct	fitted		direct	fitted		direct	fitted
H8	2.291	2.745	H16	2.35	2.8	H19	5.96	6.31	H24	6.89	7.21
H9	2.141	2.599	H17	5.94	6.29	H20	2.06	2.52	H25	6.56	6.88
H10	2.13	2.59	H18	2.05	2.51	H21	1.65	2.12	H26	7.03	7.34
H11	5.99	6.33	H19	1.68	2.15	H22	2.14	2.6	H27	6.46	6.78
H12	2.14	2.6	H20	2.11	2.57	H23	5.97	6.31	H28	6.29	6.63
H13	2.2	2.66	H21	5.96	6.3	H24	2.13	2.59	H29	5.76	6.11
H14	2.16	2.62	H22	2.16	2.62	H25	2.1	2.56	H30	7.39	7.69
H15	8.68	8.94	H23	2.1	2.56	H26	2.01	2.47	H31	6.34	6.68
			H24	2.28	2.74	H27	2.26	2.71			
			H25	2.05	2.51	H28	2.52	2.97			
			H26	2.2	2.66	H29	2.24	2.69			
			H27	2.23	2.69	H30	7.37	7.67			
			H28	1.99	2.45	H31	6.53	6.86			
			H29	2.29	2.75	H32	2.19	2.65			
			H30	5.62	5.97	H33	2.37	2.82			
			H31	6.12	6.46	H34	2.23	2.69			

Table 4.4: The computed C-NMR shifts from the direct subtractions of TMS isotropic and fitted equation

dmpz			bdmpzm			bdmpza			bdcpzm		
	direct	fitted		direct	fitted		direct	fitted		direct	fitted
C1	15.67	6.747	C1	102.5	90.36	C1	104.8	92.66	C4	151.7	137.7
C3	147.8	134	C2	13.42	4.575	C2	14.52	5.637	C5	109.1	96.77
C5	101.1	89.08	C3	15.41	6.499	C3	15.24	6.332	C6	154.3	140.2
C6	134	120.7	C4	137.2	123.7	C4	139.6	126.1	C7	138.5	125
C7	11.87	3.082	C5	148.1	134.3	C5	148.4	134.5	C8	109.4	97.09
			C6	104.4	92.22	C6	105.9	93.66	C11	130	117
			C7	12.78	3.967	C7	12.98	4.155	C13	143	129
			C8	135.9	122.6	C8	137.9	124.4	C14	153	139
			C9	15.35	6.435	C9	15.18	6.276	C15	141	127
			C10	145	131	C10	146	132	C16	155	141
			C15	63.1	52.5	C16	78.5	67.2	C21	68	57.1
						C17	166	152			

Table 4.5:The four Ramsey terms of the N-N bonds in the ligands

		dmpz			
	FC	**SD**	**PSO**	**DSO**	**J**
*N2-N4	-4.957	-0.039	-1.046	0.024	-6.018
		bdmpzm			
N11-*N12	-5.306	-0.028	-1.095	0.031	-6.398
N13-*N14	-5.120	-0.037	-0.155	0.031	-6.182
*N12⋯*N14	0.081	-0.001	-0.002	0.004	0.081
		bdmpza			
N12-*N13	-5.483	-0.029	-1.054	0.033	-6.534
N14-*N15	-5.156	-0.036	-1.009	0.032	-6.169
*N13⋯*N15	0.039	0.000	-0.003	0.004	0.039
		bdcpzm			
N18-*N20	-4.341	-0.005	-1.510	0.032	-5.824
*N19-N17	-4.901	-0.010	-1.462	0.033	-6.339
*N19⋯*N20	0.112	0.000	-0.001	0.007	0.116

The N atoms with superscript "*" represent the lone pair centre for the metal coordination

Table 4.6: The bonds properties of the four ligands

Bonds	GBL_I (au)	BPL - GBL_I	ρ(r)	$\nabla^2\rho(r)$	ε	V	G	∇^2Ven	V/G
dmpz									
*N2 - N4	2.570	1.02E-03	0.360	-0.671	0.128	-0.557	0.194	13.189	2.863
bdmpzm									
N11 - *N12	2.577	8.71E-04	0.357	-0.652	0.127	-0.553	0.195	18.473	2.836
N13 - *N14	2.582	5.42E-04	0.355	-0.643	0.132	-0.546	0.193	17.834	2.835
bdmpza									
N14 - *N15	2.592	4.55E-04	0.351	-0.628	0.133	-0.537	0.190	19.486	2.826
N12 - *N13	2.590	6.24E-04	0.352	-0.630	0.129	-0.540	0.191	19.751	2.824
bacpzpm									
N17 - *N19	2.537	1.24E-03	0.375	-0.705	0.134	-0.598	0.211	25.172	2.835
N18 - *N20	2.532	9.13E-04	0.378	-0.726	0.138	-0.603	0.211	25.088	2.860

Table 4.7: The QTAIM and NBO properties of the nitrogen atoms that are available (*N) and not

available (N) for metal coordination.

Atom	q(A)	$\|\mu_{intra}(A)\|$	$\|\mu_{bond}(A)\|$	$\|\mu(A)\|$	Vol(A),0.001	$\chi_{Intra\_Iso}(A)$	$\chi_{bond\_Iso}(A)$	$\chi_{Iso}(A)$	$\chi_{zz}(A)$	$\sigma_{Iso}(A,A)$	$\sigma_{Iso}(A',A)$	$\sigma_{Iso}(A)$	Anisotropy	Occ	Energy
dmpz															
*N2	-0.70	0.78	0.98	1.19	119.04	-3.98	-3.91	-7.90	-14.20	-55.57	11.55	-44.01	295.57	1.94615	-0.38847
N4	-0.84	0.60	0.81	0.21	92.40	-4.43	-4.60	-9.03	-13.75	53.52	12.24	65.76	94.68	1.58142	-0.25392
Total	0.00	4.28	3.43	3.06	952.33	-32.62	-32.93	-65.55	-89.63	620.52	169.77	790.29	849.46		
bdmpzm															
N11	-0.816	0.564	0.809	0.271	69.565	-3.331	-5.397	-8.728	-12.467	37.568	12.928	50.496	116.5493	1.5678	-0.25669
*N12	-0.698	0.769	0.986	1.142	115.451	-3.695	-3.877	-7.572	11.987	-62.467	11.339	-51.128	294.8341	1.94546	-0.38988
N13	-0.810	0.561	0.809	0.282	70.713	-3.367	-5.211	-8.578	-7.438	35.206	13.119	48.325	113.7568	1.56663	-0.24896
*N14	-0.707	0.774	0.989	1.171	116.239	-3.681	-3.916	-7.597	-6.661	-69.651	11.219	-58.432	252.5809	1.94618	-0.38905
Total	0.000	8.882	7.083	6.257	1923.584	-64.154	-71.124	-135.278	-144.812	1300.711	350.216	1650.927	1704.9506		
bdmpza															
N12	-0.797	0.558	0.750	0.216	68.782	-3.431	-5.208	-8.638	-10.699	42.143	12.613	54.757	107.6403	1.58165	-0.26522
*N13	-0.706	0.766	1.016	1.145	114.505	-3.587	-3.847	-7.434	-10.433	-70.142	11.171	-58.971	266.5736	1.9459	-0.39875
N14	-0.797	0.552	0.772	0.246	67.971	-3.386	-5.156	-8.541	-6.152	34.361	12.918	47.279	110.3655	1.57531	-0.25183
*N15	-0.720	0.773	1.013	1.179	115.671	-3.703	-3.885	-7.589	-5.217	-68.287	11.233	-57.053	240.267	1.94628	-0.39373
Total	0.000	10.391	11.077	8.396	2149.119	-75.759	-75.082	-150.841	-148.698	1318.551	370.533	1689.083	2476.2381		
bdcpzm															
N17	-0.756	0.540	0.747	0.287	68.060	-3.110	-5.514	-8.623	-13.084	27.889	13.099	40.988	135.3961	1.52297	-0.31378

N18	-0.744	0.533	0.708	0.236	66.449	-3.049	-5.408	-8.458	-5.950	19.933	13.133	33.066	146.3104	1.5131	-0.31374
*N19	-0.590	0.705	0.821	0.976	106.663	-2.900	-4.097	-6.997	-12.403	-86.523	-12.315	-74.208	365.0761	1.94536	-0.44307
*N20	-0.575	0.702	0.819	0.974	107.657	-2.685	-4.037	-6.722	-4.822	-108.564	11.575	-96.989	359.7227	1.94603	-0.44913
Total	0.000	13.241	21.040	13.195	2253.555	-86.530	-67.769	-154.298	-163.630	694.606	284.539	979.145	4947.7465		

Table 4.8: The Laplacian of electron density and the NMR J_coupling of the intramolecular H-bonding in the ligands

bdmpzm			**bdmpza**			**bdcpzm**		
	$\nabla^2\rho(r)$	**J_Coupling**		$\nabla^2\rho(r)$	**J_Coupling**		$\nabla^2\rho(r)$	**J_Coupling**
N11···H19	0.022	3.30E-002	C2···C17	0.034	2.49E-002	O2···H30	0.052	-5.10E-002
H24···H28	0.017	7.13E-001	O11···H28	0.022	-3.07E-001	O9···H30	0.037	-3.37E-001
			N12···H21	0.024	3.99E-002			
			O18···H32	0.028	-1.91E-001			
			H28···H33	0.025	7.86E-001			

Table 4.9: The electronic excitation of the ligands showing their triplet and singlet transitions

dmpz			
	λ	*f*	transitions
Triplet-A	298.67	0	HOMO→L+1 (116%), H-1→L+5 (4%), HOMO→L+5 (3%),
Triplet-A	249.49	0	H-1→L+1 (102%), H-1→L+7 (2%), HOMO→L+5 (3%),
Triplet-A	224.30	0	HOMO→LUMO (98%),
Singlet-A	222.61	0.0001	HOMO→LUMO (98%),
Singlet-A	214.55	0.0001	H-1→LUMO (96%),
Singlet-A	213.36	0.0241	H-1→L+1 (61%), HOMO→L+5 (18%), HOMO→L+1 (2%), HOMO→L+4 (5%),
bdmpzm			
Triplet-A	303.69	0	H-2→L+1 (98%), H-2→LUMO (2%), H-2→L+2 (2%), H-2→L+3 (2%),
Triplet-A	302.55	0	H-1→L+2 (11%), HOMO→L+2 (76%), H-3→L+2 (2%), H-2→L+1 (2%),
Triplet-A	261.18	0	H-3→L+1 (57%), H-1→L+1 (21%), HOMO→L+1 (20%), H-3→L+2 (2%),
Singlet-A	256.50	0.0028	HOMO→LUMO (83%),
Singlet-A	228.08	0.0033	H-1→LUMO (86%), HOMO→L+1 (3%),
Singlet-A	227.46	0.0092	H-2→LUMO (55%), HOMO→L+1 (34%), H-1→LUMO (4%),
bdmpza			
Triplet-A	311.63	0	HOMO→LUMO (30%), HOMO→L+4 (65%), H-2→L+4 (2%), HOMO→L+1 (3%),
Triplet-A	308.62	0	H-2→L+1 (14%), H-2→L+2 (88%), H-3→L+8 (2%), H-2→L+3 (3%),
Triplet-A	281.41	0	H-1→LUMO (81%), HOMO→LUMO (10%), H-6→LUMO (2%), H-1→L+4 (4%),
Singlet-A	279.59	0.0005	HOMO→LUMO (95%), H-1→LUMO (4%),
Singlet-A	272.98	0.027	H-1→LUMO (92%), HOMO→LUMO (4%),
Singlet-A	268.01	0.0003	H-2→LUMO (96%),
bdcpzm			
Triplet-A	352.51	0	H-4→LUMO (24%), H-2→LUMO (10%), H-1→L+1 (23%), HOMO→L+1 (31%),
Triplet-A	351.31	0	H-4→LUMO (33%), H-2→LUMO (18%), H-1→L+1 (17%), HOMO→L+1 (24%),
Triplet-A	299.77	0	H-1→L+1 (35%), HOMO→L+3 (36%), H-5→L+1 (8%), H-4→L+1 (9%),
Singlet-A	298.17	0.0031	H-1→L+1 (17%), HOMO→LUMO (12%), HOMO→L+1 (14%), HOMO→L+3 (20%),
Singlet-A	286.59	0.0003	H-7→LUMO (17%), H-3→LUMO (11%), H-2→LUMO (10%), HOMO→LUMO (23%),
Singlet-A	282.21	0.0099	H-6→L+1 (23%), H-5→L+1 (10%), H-1→L+1 (20%), HOMO→L+1 (12%),

Table 4.10: The molecular orbital (MO) contribution of the nitrogen atom(s) "*N" available for metal

coordination and nitrogen atom “N” in dmpz not available for metal coordination.

		dmpz			
MO	eV	*N2	N4	others	
L+5		1.03	11	0	89
L+4		1.02	3	-5	104
L+3		0.76	26	-37	112
L+2		0.52	15	-54	140
L+1		0.27	21	21	58
LUMO		-0.08	-104	13	191
HOMO		-6.49	38	3	59
H-1		-6.7	1	28	71
H-2		-7.84	70	9	22
H-3		-9.93	4	1	96
H-4		-10.49	8	5	88
H-5		-10.61	9	23	69
H-6		-11.13	1	7	92
H-7		-11.4	6	3	91
		bdmpzm			
MO	eV	*N12	*N14	others	
L+5		0.51	3	53	44
L+4		0.42	15	9	75
L+3		0.36	5	-19	115
L+2		0.21	10	17	74
L+1		-0.05	18	-1	83
LUMO		-0.28	-40	-32	174
HOMO		-6.38	2	28	70
H-1		-6.53	1	6	93
H-2		-6.64	35	2	63
H-3		-6.84	1	2	98
H-4		-7.78	15	53	32
H-5		-7.91	50	14	36
H-6		-9.86	0	3	97
H-7		-10.01	3	1	96
		bdmpza			
MO	eV	*N13	*N15	others	
L+5		0.39	-4	-29	135
L+4		0.2	0	18	83
L+3		0.09	-9	0	111
L+2		-0.22	24	-3	80
L+1		-0.45	-11	-9	122
LUMO		-1.24	9	1	91
HOMO		-6.46	2	34	64
H-1		-6.61	1	1	98

H-2		-6.82	35	2	63
H-3		-7.05	0	1	99
H-4		-7.91	2	63	35
H-5		-8.09	63	3	34
H-6		-8.59	2	1	97
H-7		-9.67	0	0	100
		bdcpzm			
MO	eV	*N20	*N19	others	
L+5		-0.88	-18	0	120
L+4		-1.03	4	-40	137
L+3		-1.82	0	8	92
L+2		-2.08	12	1	87
L+1		-2.48	0	19	81
LUMO		-2.74	19	0	81
HOMO		-8.12	0	13	86
H-1		-8.22	2	10	87
H-2		-8.42	7	2	91
H-3		-8.5	1	0	98
H-4		-8.56	18	1	81
H-5		-8.76	1	2	97
H-6		-8.86	1	12	88
H-7		-9.07	2	0	97

Table 4.11: The non-linear conductive properties of the ligands

	Dipole	<α>	Δα1	Δα2	Δα3	Γ	ß in esu (1x10-30)	HOMO	LUMO	Gap in KJ/mol	Non-Valence Lewis Orbitals
dmpz	2.61	74.42	-21.68	40.15	570.80	-43.15	0.34	-0.23835	-0.0029	618.28	1.87%
bdmpzm	4.02	162.68	10.35	61.51	1838.25	-4.98	1.36	-0.2345	-0.0103	588.78	1.84%
bdmpza	3.59	182.12	6.52	52.67	1365.72	-6.60	2.47	-0.2374	-0.0455	503.87	1.83%
bdcpzm	3.42	196.10	-22.50	88.84	3692.83	-8.99	1.31	-0.2984	-0.1006	519.29	2.23%

Table 4.12: Assignment of the prominent IR picks of the ligands using the PED method

	pz			**bpzm**	
3601.64	74.41 υ(NH)		3003.03	25.78 υ(CH)	υ(CH)
3203.74	1.7 υ(CH)	υ(CH)	1516.54	19.02 υ(CC)	
3193.24	2.19 υ(CH)	υ(CH)	1507.74	21.96 υ(CC)	β(HCC)
1518.85	5.49 β(HNN)	υ(CC)	1436.15	24.83 υ(NC)	β(HCC)
1444.72	6.06 β(HNN)	υ(NC)	1409.7	10.65 υ(NC)	β(CNN)
1401.82	10.65 β(HCN)	υ(NC)	1404.78	27.48 υ(NC)	β(CNN)
1341.32	3.61 β(HCC)	υ(NC)	1349.45	75.51 τ(HCNC)	
1245.72	3.32 β(HNN)	β(HCN)	1312.28	47.45 υ(NC)	τ(HCNC)
1154.22	0.83 β(HCC)	υ(NN)	1299.08	33.65 υ(NC)	υ(NC)
1124.08	17.65 β(HCN)	υ(NC)	1205.13	22.97 β(HCC)	β(HCN)
1031.5	11.21 β(HCC)	β(CNN)	1189.67	21.56 β(HCN)	
1024.07	36.48 β(HCC)	β(CNN)	1082.75	21.57 β(HCC)	β(NNC)
908.49	3.33 β(CCN)	β(CNN)	1078.25	19.56 β(HCC)	β(CNN)
886.66	7.58 β(CNN)		1045.82	19.31 β(HCC)	
848.44	7.16 τ(HCNN)		1033.64	30.12 υ(NN)	β(HCC)
795.2	15.77 τ(HCNN)		958.08	15.84 υ(NN)	β(CNN)
716.49	103.29 τ(HCCN)		759.18	28.62 υ(NN)	β(NCN)
668.81	18.72 τ(CCNN)		732.76	53.57 υ(NC)	β(NNC)
509.76	52.85 τ(HNNC)		720.53	44.07 τ(HCCN)	
			717.43	74.71 τ(HCCN)	
	bpza			**bpzpya**	
3617.19	67.3 υ(OH)		1773.99	246.25 υ(OC)	
1761.24	201.93 υ(OC)		1590.32	109.86 υ(CC)	β(HCC)
1511.96	24.72 υ(CC)	β(HCC)	1576.91	288.13 υ(CC)	
1404.28	36.29 υ(NC)	β(CCN)	1523.44	89.91 υ(CC)	
1398.39	39.14 υ(NC)	β(CCN)	1520.84	102.81 υ(CC)	
1363.89	49.98 υ(OC)	β(HCC)	1469.66	47.37 υ(NC)	
1303.66	111.35 υ(NC)	υ(NC)	1429.18	299.82 υ(NC)	
1269.37	24.85 υ(NC)	β(HOC)	1402.85	338.61 υ(NC)	β(CCN)
1197.96	53.15 υ(NN)	β(HCN)	1398.32	192.84 υ(CC)	
1188.49	40.96 β(HOC)	β(HCN)	1362.55	50.55 υ(CC)	β(HCC)
1102.94	234.02 υ(OC)	β(HOC)	1266.95	325.58 υ(OC)	β(HOC)
1076.39	29.98 υ(NC)	β(HCC)	1255.47	92.5 υ(CC)	β(HOC)
1033.2	38.2 υ(NN)	β(HCC)	1241.24	84.13 υ(NN)	β(HCC)
819.44	30.4 β(CNN)	ο(CNNC)	1145.19	60.4 υ(NN)	β(HCC)
819.98	28.03 β(CCN)	τ(HOCC)	1031.32	94.3 υ(NN)	β(HCC)
735.45	96.35 τ(HCCN)		944.81	76.94 υ(NC)	υ(NN)
725.23	75.06 τ(HCCN)		779.35	77.51 υ(NC)	β(CCC)
705.81	121.4 υ(NC)	τ(HOCC)	716.71	33.69 τ(HCCC)	
659.97	26.01 β(OCO)	ο(CCNN)	709.34	71.44 τ(HCCC)	
632.85	67.27 β(OCO)	τ(CNNC)	483.01	49.64 τ(HOCC)	

Greek letters υ, β, τ, ο denote stretching, bending, tortion and out of plane modes respectively

Table 4.13: The experimental H- and C-NMR shift in ligands bpzm and bpza

pz **^{1}H-NMR (dmso-d6)**		**bpzm** **^{1}H- NMR ($CHCl_3$-d, 250.00 MHz)**		**bpza** **^{1}H- NMR ($CHCl_3$-d, 250.00 MHz)**	
6.25	(t, 2H, H4) [[Díez-Barraetal2002]]	5.89 (5.82)	(t, 2H, H4) [[Díez-Barraetal2002]]	6.37 (6.39)	(t, 2H, H4), (dd, 2H, $^3J_{H-H}$ = 1.9 Hz, $^3J_{H-H}$ =1.6 Hz, H_{pz}) [[Burzlaffetal2001]]
7.60	(d, 2H, H5)	7.28	(d, 2H, H5)	7.81 (7.84)	(d, 2H, H5), (d, 2H, $^3J_{H-H}$ =1.3 Hz, H_{pz}) [[Burzlaffetal2001]]
7.60	(d, 2H, H3)	7.28	(d, 2H, H3)	7.65 (7.57)	(d, 2H, H3), (d, 2H, $^3J_{H-H}$ = 2.0 Hz, H_{pz}) [[Burzlaffetal2001]]
12.81	(s, H, NH)	6.41 (6.28)	(s, 1H, CH_2) [[Díez-Barraetal2002]]	7.22 (7.27)	(s, 1H, C*H*COOH) [[Burzlaffetal2001]]
				7.20	(s, 1H, COO*H*)
		^{13}C- NMR ($CHCl_3$-d, 62.50 MHz)		**^{13}C- NMR ($CHCl_3$-d, 62.50 MHz)**	
		77.00	(s, CH_2)	74.18 (74.70)	(s, CH) [[Burzlaffetal2001]]
		104.67, 104.97, 133.85	(C_{pz})	107.44 130.58 132.82	(C_{pz})
				140.94 (165.90)	(s, CO_2H) [[Burzlaffetal2001]]

Table 4.14: The computed H-NMR shifts from the direct subtractions of TMS isotropic and from fitting equation

pz			**bpzm**			**bpza**			**bpzpya**		
	direct	**fitted**		**direct**	**fitted**		**direct**	**fitted**		**direct**	**fitted**
H6	7.76	8.05	H12	6.49	6.82	H15	7.58	7.87	H20	7.02	7.34
H7	9.51	9.75	H13	7.69	7.98	H16	6.42	6.75	H21	6.89	7.20
H8	6.43	6.76	H14	7.77	8.06	H17	7.58	7.87	H22	7.93	8.22
H9	7.47	7.77	H15	6.34	6.67	H18	6.42	6.75	H23	7.84	8.13
			H16	7.07	7.38	H19	8.37	8.64	H24	8.11	8.39
			H17	7.59	7.89	H20	8.37	8.64	H25	6.66	6.98
			H18	5.83	6.18	H21	7.29	7.59	H26	6.67	6.99
			H19	6.51	6.84	H22	6.52	6.85	H27	7.97	8.26
									H28	7.95	8.23

Table 4.15: The computed C-NMR shifts from the direct subtractions of TMS isotropic and fitted equation

	pz			**bpzm**			**bpza**			**bpzpya**	
	direct	**fitted**		**direct**	**fitted**		**direct**	**fitted**		**direct**	**fitted**
C2	136.51	123.11	C1	103.42	91.25	C1	136.95	123.53	C2	160.13	145.86
C4	101.65	89.54	C2	126.27	113.25	C2	104.95	92.71	C4	140.97	127.41
C5	121.46	108.62	C3	139.04	125.55	C3	136.95	123.53	C5	101.05	88.96
			C4	103.82	91.63	C4	104.95	92.71	C6	107.47	95.15
			C5	120.87	108.05	C7	123.41	110.49	C7	152.00	138.02
			C7	135.70	122.33	C8	123.41	110.50	C8	151.87	137.90
			C11	68.41	57.53	C11	76.49	65.31	C11	122.47	109.59
						C13	166.09	151.60	C13	123.51	110.59
									C16	106.40	94.11
									C17	106.61	94.32
									C18	140.40	126.86
									C19	140.64	127.09

Table 4.16: The four Ramsey terms of the N-N bonds in the ligands

	FC	**SD**	**PSO**	**DSO**	**J**
			pz		
*N1-N3	-5.220	-0.018	-1.197	0.022	-6.414
			bpzm		
N6-*N8	-5.492	-0.010	-1.215	0.029	-6.688
N9-*N10	-5.265	-0.017	-1.222	0.028	-6.476
***N8-*N10**	0.018	0.000	0.000	0.000	0.018
			bpza		
*N5-N9	-5.753	-0.023	-1.162	0.030	-6.908
*N6-N10	-5.753	-0.023	-1.162	0.030	-6.908
*N5-*N6	0.032	0.000	0.001	0.003	0.035
			bpzpya		
N10-*N14	-5.793	0.005	-1.150	0.030	-6.908
N12-*N15	-5.776	0.009	-1.129	0.030	-6.867
***N14-*N15**	0.009	0.001	-0.002	0.004	0.011
N_{py}-*N14	0.541	0.003	0.014	0.008	0.566
N_{py}-*N15	0.607	0.010	0.015	0.009	0.641

Table 4.17: The *N-N bond and H-bond properties of the ligands

Bonds	GBL_I (au)	BPL - GBL_I	ρ(r)	$\nabla^2\rho(r)$	ε	V	G	∇^2Ven	V/G
				pz					
*N1 - N3	2.560	1.06E-03	0.364	-0.680	0.131	-0.569	0.200	11.646	2.852
				bpzm					
N6 - *N8	2.569	7.63E-04	0.361	-0.659	0.130	-0.562	0.199	15.718	2.830
N9 - *N10	2.566	7.17E-04	0.362	-0.661	0.135	-0.566	0.200	15.541	2.826
				bpza					
*N5 - N9	2.578	5.87E-04	0.356	-0.640	0.129	-0.553	0.196	17.204	2.816
*N6 - N10	2.578	5.87E-04	0.356	-0.640	0.129	-0.553	0.196	17.204	2.816
#O12⋯H19	4.890	0.2281	0.009	0.035	0.756	-0.006	0.007	-0.693	0.810
#O12⋯H20	4.890	0.2280	0.009	0.035	0.755	-0.006	0.007	-0.693	0.810
				bpzpya					
N10 - *N14	2.580	8.35E-04	0.355	-0.635	0.112	-0.550	0.196	18.235	2.811
N12 - *N15	2.583	8.26E-04	0.354	-0.633	0.108	-0.548	0.195	18.161	2.812

The bonds with "#" represent the H-bonds while an atom with "*" represent the nitrogen atom on pyrazole that is available for metal coordination.

Table 4.18: The QTAIM and NBO properties of the nitrogen atoms that are available (*N) and not available (N) for metal coordination.

Atom	q(A)	$\lvert\mu_{intra}$(A)$\rvert$	$\lvert\mu_{bond}$(A)$\rvert$	|μ(A)|	Vol(A),0.001	$\chi_{Intra\_Is_o}$(A)	$\chi_{bond\_Is_o}$(A)	χ_{Iso}(A)	χ_{zz}(A)	σ_{Iso}(A,A)	σ_{Iso}(A',A)	σ_{Iso}(A)	Anisotropy	Occ	Energy
pz															
*N1	-0.68	0.78	0.95	1.16	119.03	-3.92	-4.44	-8.36	-15.79	-62.54	12.31	-50.23	352.31	1.94672	-0.39917
N3	-0.83	0.62	0.79	0.17	93.03	-4.41	-5.18	-9.60	-15.43	47.91	12.98	60.89	126.34	1.56142	-0.26347
Total	0.00	3.61	3.11	2.30	629.67	-20.31	-24.21	-44.51	-74.36	221.44	97.48	318.91	860.52		
bpzm															
N6	-0.828	0.578	0.814	0.282	70.337	-3.292	-5.747	-9.038	-7.925	29.574	13.470	43.044	136.58	1.55382	-0.27289
*N8	-0.682	0.767	0.974	1.129	116.792	-3.670	-4.313	-7.983	-5.944	-71.654	11.792	-59.862	336.50	1.9466	-0.40814
N9	-0.806	0.577	0.815	0.287	72.037	-3.231	-5.649	-8.880	-14.030	24.643	13.689	38.332	130.27	1.54606	-0.26187

*N10	-0.690	0.775	0.963	1.155	117.064	-3.801	-4.333	-8.135	-14.038	-67.342	12.001	-55.342	317.04	1.94645	-0.40211
Total bpza	0.000	7.626	6.632	4.879	1293.130	-39.875	-51.939	-91.814	-106.811	499.094	203.463	702.557	1701.86		
*N5	-0.687	0.765	0.986	1.133	116.402	-3.653	-4.274	-7.927	-5.486	-72.499	11.779	-60.720	304.82	1.94717	-0.40943
*N6	-0.687	0.765	0.985	1.133	116.399	-3.653	-4.275	-7.928	-5.487	-72.498	11.779	-60.719	304.82	1.94717	-0.40944
N9	-0.807	0.569	0.779	0.257	70.689	-3.270	-5.515	-8.785	-6.248	24.740	13.415	38.155	125.43	1.55934	-0.27117
N10	-0.807	0.569	0.779	0.257	70.606	-3.269	-5.516	-8.785	-6.249	24.742	13.416	38.158	125.43	1.55934	-0.27117
Total bpzpy	0.000	9.101	10.499	7.032	1529.574	-51.928	-55.395	-107.322	-79.855	551.850	221.953	773.804	2412.24		
*N_{py}	-1.112	0.054	0.944	0.907	109.016	-4.083	-4.337	-8.420	-16.473	-34.897	7.237	-27.660	436.16	1.89676	-0.35529
N10	-0.840	0.572	0.738	0.166	73.055	-3.150	-5.450	-8.599	-12.754	15.536	10.781	26.317	134.65	1.53421	-0.27632
N12	-0.841	0.571	0.738	0.170	73.513	-3.174	-5.269	-8.443	-13.371	16.260	10.557	26.818	131.58	1.53172	-0.27416
*N14	-0.653	0.766	1.003	1.062	112.748	-3.473	-4.180	-7.653	-12.722	-73.521	10.806	-62.715	349.89	1.94652	-0.40698
*N15	-0.656	0.768	1.013	1.061	112.415	-3.510	-4.096	-7.606	-13.655	-70.411	10.662	-59.749	352.41	1.94658	-0.40432
Total	0.000	10.396	12.224	8.071	1989.531	-63.173	-78.125	-141.298	-221.200	649.805	273.183	922.988	3638.08		

Table 4.19: The electronic excitation of the ligands showing their triplet and singlet transitions

Ligang	State	Wavelength	*f*	Transitions
pz	Triplet-A	290.64	0	H-1→L+1 (16%); HOMO→L+1 (104%); H-1→L+4 (7%); HOMO→L+9 (2%)
	Triplet-A	244.49	0	H-1→L+1 (94%); HOMO→L+1 (15%); HOMO→L+4 (3%);
	Triplet-A	211.04	0	H-2→L+1 (95%); H-2→L+4 (8%); HOMO→LUMO (3%);
	Singlet-A	207.98	0.0071	HOMO→LUMO (99%);
	Singlet-A	206.79	0	H-1→LUMO (93%);
	Singlet-A	205.26	0.0551	H-1→L+1 (40%); HOMO→L+1 (29%); HOMO→L+4 (11%); H-1→L+4 (3%)
bpzm	Triplet-A	297.73	0	H-2→LUMO (60%); H-2→L+1 (24%); H-1→LUMO (19%); H-3→LUMO (8%)
	Triplet-A	296.03	0	H-1→L+1 (12%); HOMO→LUMO (17%); HOMO→L+1 (42%); HOMO→L+2 (22%)
	Triplet-A	257.18	0	H-1→LUMO (14%); H-1→L+1 (35%); H-1→L+2 (15%); HOMO→L+1 (14%)
	Singlet-A	255.04	0.0024	HOMO→LUMO (75%); HOMO→L+1 (8%);
	Singlet-A	214.20	0.0592	H-1→LUMO (90%); H-2→LUMO (3%);
	Singlet-A	214.03	0.0073	H-2→LUMO (11%); H-1→L+1 (76%);
bpzcooh	Triplet-A	307.69	0	H-1→LUMO (18%); H-1→L+3 (19%); HOMO→L+1 (47%); HOMO→L+2 (10%)
	Triplet-A	307.03	0	H-1→L+1 (32%); HOMO→LUMO (28%); HOMO→L+3 (24%); H-3→L+1 (7%)
	Triplet-A	265.21	0	H-6→LUMO (14%); H-3→LUMO (40%); H-2→L+1 (20%); H-1→LUMO (19%)
	Singlet-A	264.41	0.001	HOMO→LUMO (93%);
	Singlet-A	253.16	0.0145	H-1→LUMO (87%) H-6→LUMO (3%); H-3→LUMO (4%);
	Singlet-A	248.42	0.0342	H-2→LUMO (94%);
bpzpya	Triplet-A	406.98	0	HOMO→LUMO (104%); H-8→LUMO (2%);
	Triplet-A	386.82	0	H-3→LUMO (10%); HOMO→L+1 (82%); H-9→LUMO (7%); H-9→L+1 (3%)
	Triplet-A	349.08	0	H-1→LUMO (40%); H-1→L+1 (32%); H-1→L+2 (15%); H-2→L+1 (4%)
	Singlet-A	338.64	0.1315	HOMO→LUMO (88%);
	Singlet-A	334.79	0.001	H-1→LUMO (88%);
	Singlet-A	322.55	0.0012	H-2→LUMO (89%); H-3→LUMO (3%); ;

Table 4.20: The molecular orbital (MO) contribution of the nitrogen atom(s) "*N" available for metal coordination and nitrogen atom "N" in pz not available for metal coordination.

pz				
MO	eV	*N1	N3	others
L+5	1.41	-39	10	130
L+4	1.18	-4	0	106
L+3	0.82	71	-86	116
L+2	0.67	-18	15	105
L+1	-0.02	26	14	60
LUMO	-0.05	-54	-23	179
HOMO	-6.98	32	1	66
H-1	-7.26	7	32	61
H-2	-8.18	77	4	19
H-3	-11.03	3	2	95
H-4	-11.83	7	10	82
H-5	-12	23	45	33
H-6	-12.24	13	16	71
H-7	-14.97	10	12	77
bpzm				
MO	eV	*N8	*N10	others
L+5	0.69	37	9	55
L+4	0.51	-6	1	106
L+3	0.46	-4	-19	125
L+2	0.07	-41	-9	152
L+1	-0.37	2	6	93
LUMO	-0.54	18	4	78
HOMO	-7	0	29	71
H-1	-7.05	5	6	89
H-2	-7.33	28	2	70
H-3	-7.5	5	2	93
H-4	-8.25	2	73	25
H-5	-8.42	73	2	25
H-6	-10.89	2	6	92
H-7	-11.03	2	3	95
bpza				
MO	eV	*N5	*N6	others
L+5	0.47	-22	-21	145
L+4	0.25	-23	-23	148
L+3	0.15	13	13	75
L+2	-0.37	-6	-6	114
L+1	-0.71	8	8	84
LUMO	-1.45	1	1	99
HOMO	-7.11	17	16	67
H-1	-7.26	12	15	73
H-2	-7.27	4	2	95
H-3	-7.58	7	7	87
H-4	-8.38	37	34	29
H-5	-8.48	36	39	25
H-6	-8.92	2	2	97
H-7	-9.9	0	0	100
bpzpya				
MO	eV	*N9	*N15	*N14 others
L+5	0.23	2	2	-32 129
L+4	0.05	-6	-48	4 153

L+3	-0.83	0	4	-3	100
L+2	-0.86	4	5	-5	97
L+1	-2.01	1	3	4	92
LUMO	-2.66	16	0	0	85
HOMO	-6.93	0	0	0	100
H-1	-7.31	2	28	1	69
H-2	-7.39	1	3	29	67
H-3	-7.54	11	5	6	77
H-4	-7.99	36	26	12	25
H-5	-8.37	1	28	47	25
H-6	-8.41	3	3	0	94
H-7	-8.78	35	19	18	28

Table 4.21: The non-linear conductive properties of the ligands

	Dipole	$\Sigma_i\langle\alpha\rangle_i$	$\Delta\alpha1$	$\Delta\alpha2$	$\Delta\alpha3$	Γ	ß in esu (1x10-30)	HOMO	LUMO	Gap in KJ/mol	Non-Valence Lewis Orbitals
pz	2.42	47.89	-10.40	23.80	229.13	-29.52	0.86	-0.2564	-0.0017	668.85	2.46%
bpzm	3.58	109.44	5.65	46.37	1059.23	-2.61	1.69	-0.2571	-0.0200	622.64	2.36%
bpza	2.76	129.47	3.57	26.01	332.00	-4.45	2.40	-0.2612	-0.0536	545.07	2.22%
bpzpya	3.21	205.34	-80.24	160.82	9712.52	-8.53	11.21	-0.2546	-0.0979	411.44	2.61%

Table 4.22: Assignment of the prominent IR picks of the ligands using the PED method

apz		**phpz**		**bphpzm**		**bphpza**	
Freq	Int Vibration	Freq	Int Vibration	Freq	Int Vibration	Freq	Int Vibration
3648.54	82.4 2 υ(OH),	3593.44	98.3 1 υ(NH)	3129.09	25.59 υ(CH)	3616.33	77.78 υ(OH)
3540.35	131.49 υ(NH),	3138.03	20.3 υ(CH), 4 υ(CH)	3000.64	31.33 υ(CH), υ(CH)	1760.17	205.61 υ(OC)
1768.92	305.06 υ(OC),	3128.31	27.4 2 υ(CH)	1494.65	41.23 υ(CC), υ(CC)	1495.18	44.25 β(HCC)
1757.84	373.2 υ(OC),	1610.48	10.6 υ(CC), 6 β(HCC)	1458.92	β(HCC), 29.35 τ(HCNC)	1360.97	31.16 υ(NC), β(HCC)
1537.16	42.2 υ(CC), 9 β(HNN)	1498.5	13.1 β(HCC), 5 υ(CC)	1396.47	υ(NC), 25.73 β(HCH)	1319.14	161.6 β(HCC), 9 τ(HCCO)
1442.47	69.3 β(CNN), 5 υ(NN)	1450.73	β(HCC), 28.8 β(CNN)	1331.19	β(HCN), 51.15 τ(HCNC)	1294.65	υ(NN), 31.53 β(HCC)
1390.89	83.5 β(HNN), 5 υ(NC)	1189.52	υ(NC), 7.56 β(HNN)	1323.98	179.7 υ(NN), 4 τ(HCNC)	1218.14	120.2 9 υ(NC), β(HCC)
1325.35	153.82 υ(NC),	1114.88	19.4 υ(NC), 5 β(HCC)	1269.88	υ(NN), 31.67 β(HOC)	1192.55	70.32 β(HCC)
1282.98	192. υ(OC), 1 β(HOC)	1077.18	10.7 υ(CC), 3 β(HCC)	1221.44	β(HCC), 65.93 β(HCC)	1183.41	υ(NN), 78.99 τ(HCCO)
1222.05	175. β(HOC), 36 υ(NN)	1062.24	18.4 υ(NC), 1 β(HCC)	1211.55	38.26 υ(CC), β(HCC)	1109.45	186.7 υ(OC), 6 β(HOC)

1141.69	81.89	β(HOC), β(HCC)	1034.58	12.21	υ(NN), β(HCC)	1173.91	β(HCN), 33.52 τ(HCNC)
1102.96	265.59	υ(OC), β(HOC)	1023.39	6.59	υ(CC)	1078.52	β(HCC), 28.76 β(HCC)
1071.28	48.81	υ(OC), β(HCC)	923.28	7.89	β(CNN)	1076.91	27.27 υ(CC), β(HCC)
991.97	58.75	υ(OC), β(CNN)	761.53	11.5	τ(HCCC), τ(CCCC)	1037.52	β(HCC), 44.66 β(HCC)
750.49	44.99	τ(HOCC),	718.12	133.94	τ(HCCC)	769.06	υ(NC), 56.23 β(CNN)
728.55	40.05	o(OCOC), τ(HNNC)	676.43	29.4	τ(HCCC), τ(CCCC)	735.51	υ(NN), 60.47 β(CNN)
715.8	36.14	υ(OC), β(CCO)	673.86	8.15	υ(CC), β(CCC)	723.81	τ(HCCC), 72.56 τ(HCCC)
689.66	42.42	τ(HNNC),	635.07	8.11	τ(HNNC)	718.87	τ(HCCC), 99.7 τ(HCCC)
558.04	84.82	τ(HOCC), τ(CNNC)	500.13	20.06	τ(HNNC)	675.37	τ(CCCC), 27.06 τ(HCCC)
432.8	76.95	τ(HOCC),					
bpzpy			**bmpzpy**			**bdcpzpy**	
1592.97	209.02	υ(CC),	2979.18	43.5	υ(CH)	3647.99	97.65 υ(OH)
1585.64	121.33	υ(CC), β(HCC)	2974.42	61.5	υ(CH), υ(CH)	3646.99	101.65 υ(OH)
1518.25	138.22	υ(CC), β(HCN)	1586.88	164.64	υ(CC), β(HCC)	1784.33	237.14 υ(OC)
1466.34	53.07	υ(NC), β(HCC)	1585.83	139.1	υ(CC)	1770.78	184.51 υ(OC)
1443.46	372.02	υ(NC), β(HCC)	1562.89	142.13	υ(CC), υ(CC)	1764.3	328.22 υ(OC)
1408.63	60.09	υ(CC), β(HCC)	1472.69	62.89	υ(NC), β(HCH)	1761.17	380.46 υ(OC)
1408	55.38	β(CCN), β(HCC)	1448.29	56.14	β(HCH), τ(HCCC)	1463.43	102.81 υ(NC), β(HCC)
1398.39	120.44	υ(NC), β(HCN)	1445.37	177.85	β(HCH), β(HCH)	1428.08	υ(CC), 90.81 β(CNN)
1384.99	28.62	υ(NC), β(HCC)	1434.61	203.98	β(HCH), τ(HCCN)	1423.68	295.15 υ(CC), β(HCC)
1347.29	22.45	υ(NC), β(CCN)	1430.85	88.06	υ(CC), β(HCH)	1407.62	156.69 υ(NC)
1319.78	24.08	υ(NC), β(CCN)	1405.69	34.13	υ(NC), β(HCH)	1291.72	103.15 β(HOC)
1261.65	60.87	υ(NN), β(HCC)	1375.64	34.59	υ(NC), β(HCH)	1282.21	186.13 β(HOC), β(HOC)
1190.14	18.05	υ(NC), β(HCN)	1371.04	62.88	β(HCH)	1268.92	263.03 υ(CC)
1153.82	46.74	β(HCC),	1368.17	83.05	υ(NC), β(HCH)	1258.68	236.55 υ(NN), β(HOC)
1031.61	91.19	υ(NN), β(HCC)	1350.11	48.42	υ(NC), β(HCH)	1247.5	90.14 υ(NN)
944.	67.3	υ(NN),	1345.	36.0	υ(NC)	1130.4	117.1 β(HOC),

		β(HCC),
1088.7	60.09	β(NCN)
1080.2	31.23	υ(CC), β(HCC)
1078.24	43.6	β(HCC)
1036.02	59.94	β(HCC)
817.08	35.99	o(OCOC), τ(HCCC)
735.44	132.76	τ(HCCC), τ(HCCC)
722.11	113.5	τ(HCCC)
709.32	139.56	o(OCOC), τ(HOCC)
675.51	44.08	τ(HCCC)
647.56	74.3	o(CCNN), β(OCO)

02	2 β(CCN)	36	3	7	2 β(HCC)						
799.06	22.34 τ(HCNN),	1110.01	36.86 β(NCN)	1115.66	375.57 β(HOC)	υ(NC),	υ(OC),				
778.87	39.66 τ(CNCC)	790.01	46.22 τ(HCCC)	1098.52	227.46 β(OCO)	τ(HCCC),	υ(OC),				
762.8	65.56 β(CNN)	760.05	35.83 τ(HCCC)	1091.94	152.97 υ(CC), β(HCC)	β(CCC),					
715.31	131.94 τ(HCCC),	723.36	57.06 β(CNN)	1041.4	221.86 β(CCN)	υ(NC),	υ(OC),				

Greek letters υ, β, τ, o denote stretching, bending, tortion and out of plane modes respectively

Table 4.23: The experimental ^{13}C-NMR shifts obtained using d-chloroform as solvent

	bphpza	bpzpy	bdmpzpy
CH_3			13.724, 14.892
CHCOOH	74.015 (74.70 [[Burzlaffet al2001]])		
C4	105.040	108.27	109.791
$C_{px\text{-}meta}$	128.582	110.898	113.879
C5	128.947	125.188	138.991
C_{ph}	131.867		
$C_{px\text{-}para}$	126.392	127.158	124.683
C3	132.232	140.791	140.743
$C_{px\text{-}ortho}$	126.210	142.926	150.671
CH**C**OOH	153.219		

The subscript "px" represent the phenyl (ph) in bphpza and pyridine (pyr) in bpzpy and bdmpzpy. The value in bracket is from the cited reference for similar molecule.

Table 4.24: The computed ^{13}C-NMR shifts from the direct and fitting methods

dcpz		**phpz**		**bphpzm**		**bphpza**		**bpzpy**		**bmpzpy**		**bdcpzpy**	
Direct	Fitting	Direct	Fitting	Direct	Fitting	Direct	Fitting	Direct	Fitting	Direct	Fitting	Direct	Fitting

C3	153.80	139.76	C1	125.13	112.15	C1	124.57	111.61	C1	101.91	89.79	C2	151.38	137.43	C2	151.68	137.72	C3	156.61	142.47			
C4	131.35	118.14	C2	121.91	109.05	C2	121.34	108.50	C2	125.17	112.19	C3	151.37	137.42	C3	151.68	137.72	C5	141.69	128.10			
C6	104.06	91.86	C5	123.46	110.54	C3	100.34	88.28	C3	151.20	137.26	C4	135.40	122.04	C4	133.28	120.00	C7	157.20	143.04			
C8	143.68	130.02	C6	132.05	118.81	C4	100.77	88.69	C4	102.19	90.06	C5	106.74	94.44	C5	111.80	99.31	C11	143.05	129.41			
C9	156.57	142.43	C7	150.31	136.40	C5	128.10	115.02	C5	124.97	112.00	C6	106.72	94.42	C6	111.79	99.31	C12	109.84	97.43			
			C8	124.48	111.53	C6	121.27	108.43	C6	121.44	108.60	C9	122.81	109.92	C9	15.11	6.20	C15	131.75	118.52			
			C9	123.36	110.45	C7	124.51	111.56	C8	124.58	111.62	C11	122.80	109.91	C10	15.11	6.20	C17	148.07	134.24			
			C10	121.21	108.38	C8	122.70	109.81	C10	150.23	136.32	C13	139.60	126.08	C11	136.64	123.24	C18	148.62	134.77			
			C11	98.83	86.83	C9	124.13	111.19	C11	131.18	117.98	C14	139.60	126.08	C13	136.64	123.24	C19	109.06	96.67			
						C10	131.10	117.90	C14	123.84	110.91	C15	105.31	93.06	C15	148.65	134.80	C21	152.92	138.92			
						C11	153.01	139.00	C16	76.65	65.47	C16	105.31	93.07	C16	148.65	134.80	C22	136.23	122.85			
						C12	149.81	135.92	C17	122.72	109.83				C17	105.71	93.45	C24	116.99	104.31			
						C13	131.82	118.60	C18	165.95	151.46				C18	105.71	93.45	C25	157.36	143.19			
						C15	123.34	110.43	C19	125.34	112.36				C19	15.49	6.57	C26	112.41	99.90			
						C17	125.45	112.46	C21	130.94	117.75				C20	15.49	6.57	C27	136.29	122.90			
						C18	122.82	109.93	C22	121.44	108.60												
						C21	122.30	109.42	C23	124.54	111.59												
						C22	68.32	57.44	C24	124.02	111.08												
						C23	125.23	112.24	C25	125.37	112.38												
									C26	122.70	109.81												

Table 4.25: The experimental ^{1}H-NMR shifts using d-chloroform

	bphpza	bpzpy	bdmpzpy
CH_3			2.317, 2.673

COOH	6.452		
C4-H	7.174	6.497	6.040
CHCOO	7.354		
$C_{px\text{-}para}$-H	7.369	7.376	7.461
$C_{px\text{-}meta}$-H	7.429	7.292	7.309
$^{f}C_{px\text{-}ortho}$-H	7.520	7.681	7.647
C5-H	7.790	7.952	
$^{c}C_{px\text{-}ortho}$-H	7.850		
C3-H		8.561	

The subscript "px" represent the phenyl (ph) in bphpza and pyridine (pyr) in bpzpy and bdmpzpy. Also, the superscript "c" and "f" on $C_{ph\text{-}ortho}$ mean close to and far from the nitrogen which is the coordination centre of the pyrazole.

Table 4.26: The computed ^{1}H-NMR shifts from the direct and fitting methods

dcpz			phpz			bphpzm			bphpza			bpzpy			bmpzpy			bdcpzpy		
	Direct	Fitting		Direct	Fitting		Direct	Fitting		Direct	Fitting		Direct	Fitting		Direct	Fitting		Direct	Fitting
H12	6.54	6.87	H12	7.41	7.71	H24	7.43	7.73	H27	6.84	7.15	H17	7.75	8.04	H21	2.07	2.53	H29	6.25	6.59
H13	6.91	7.23	H13	8.64	8.91	H25	7.73	8.02	H28	8.43	8.70	H18	7.10	7.41	H22	7.75	8.04	H30	7.20	7.51
H14	6.16	6.50	H14	7.30	7.60	H26	6.88	7.20	H29	6.80	7.12	H19	7.11	7.41	H23	6.99	7.30	H31	6.29	6.63
H15	10.74	10.94	H15	7.48	7.78	H27	6.71	7.03	H30	7.67	7.96	H20	7.90	8.19	H24	6.99	7.30	H32	7.11	7.42
			H16	7.38	7.69	H28	7.69	7.98	H31	8.21	8.48	H21	7.91	8.19	H25	2.22	2.67	H33	6.78	7.10
			H17	7.72	8.01	H29	7.40	7.70	H32	7.40	7.70	H22	7.92	8.20	H26	2.41	2.86	H34	7.20	7.51
			H18	6.84	7.16	H30	7.68	7.97	H33	7.32	7.63	H23	7.92	8.20	H27	2.52	2.96	H35	8.38	8.65
			H19	9.32	9.56	H31	7.00	7.31	H34	7.27	7.57	H24	6.59	6.92	H28	2.40	2.85	H36	7.98	8.26
						H32	7.33	7.63	H35	8.67	8.93	H25	6.59	6.92	H29	2.22	2.67	H37	6.81	7.12
						H33	7.31	7.61	H36	7.50	7.80				H30	6.22	6.55			
						H34	7.44	7.74	H37	6.56	6.89				H31	6.22	6.55			
						H35	8.57	8.84	H38	7.69	7.98				H32	2.51	2.96			
						H36	5.83	6.18	H39	7.40	7.70				H33	2.21	2.66			
						H37	8.63	8.90	H40	7.32	7.62				H34	2.21	2.67			
						H38	7.48	7.78	H41	7.48	7.78				H35	2.40	2.85			
						H39	6.49	6.82	H42	8.63	8.90				H36	2.41	2.86			
															H37	2.07	2.53			

Table 4.27: The computed ^{15}N-NMR shifts from the direct and fitting methods

dcpz			**phpz**			**bphpzm**			**bphpza**			**bpzpy**			**bmpzpy**			**bdcpzpy**		
	Direct	Fitting		Direct	Fitting		Direct	Fitting		Direct	Fitting		Direct	Fitting		Direct	Fitting		Direct	Fitting
N5	-173.52	-194.15	*N3	-88.00	-113.25	N14	-178.81	-199.15	N7	-173.01	-193.66	^{pyr}N1	-106.43	-130.68	^{pyr}N1	-84.25	-109.70	*N6	-32.73	-60.96
*N7	-45.78	-73.31	N4	-193.87	-213.40	N16	-171.49	-192.23	*N9	-78.61	-104.36	N7	-154.15	-175.82	N7	-161.87	-183.13	*N9	-65.32	-91.80
						*N19	-79.52	-105.22	N12	-171.53	-192.27	N8	-154.16	-175.83	N8	-161.87	-183.13	^{pyr}N10	-109.55	-133.63
						*N20	-84.46	-109.90	*N15	-79.20	-104.92	*N10	-67.33	-93.70	*N12	-70.52	-96.71	N14	-147.55	-169.58
												*N12	-67.32	-93.68	*N14	-70.52	-96.71	N16	-153.33	-175.04

Table 4.28:The four Ramsey terms of the N-N bonds in the ligands

	FC	SD	PSO	DSO	J	
			dcpz			
N5-*N7		-3.947	0.000	-1.564	0.025	-5.486
			phpz			
*N3-N4		-4.535	-0.053	-1.175	0.024	-5.739
			bphpzm			
N14-*N19		-4.832	-0.044	-1.177	0.031	-6.022
N16-*N20		-4.499	-0.051	-1.205	0.030	-5.725
*N19-*N20		0.014	0.000	-0.001	0.000	0.014
			bphpza			
N7-*N9		-5.000	-0.056	-1.139	0.032	-6.163
N12-*N15		-4.940	-0.060	-1.128	0.032	-6.096
*N9-*N15		0.025	0.000	-0.001	0.004	0.027
			bpzpy			
N7-*N12		-5.712	0.005	-1.167	0.029	-6.844
N8-*N10		-5.712	0.005	-1.167	0.029	-6.844
*N10-*N12		0.006	0.000	-0.002	0.004	0.008
^{py}N1-*N10		0.531	0.004	0.016	0.008	0.559
^{py}N1-*N12		0.530	0.004	0.016	0.008	0.558
			bdmpzpy			
N7-*N14		-5.548	-0.015	-1.034	0.031	-6.566
N8-*N12		-5.549	-0.015	-1.034	0.031	-6.566
*N12-*N14		0.003	0.000	-0.002	0.004	0.005
^{py}N1-*N12		0.478	-0.005	-0.001	0.008	0.481
^{py}N1-*N14		0.478	-0.005	-0.001	0.008	0.480
			bdcpzpy			
*N6-*N9		-0.001	0.000	0.000	-0.001	-0.002
*N6-^{py}N10		0.497	-0.013	0.008	0.010	0.502
*N6-N14		-4.517	0.020	-1.526	0.033	-5.990
*N9-^{py}N10		0.350	0.007	0.030	-0.003	0.384
*N9-N16		-4.608	-0.008	-1.316	0.033	-5.900

Table 4.29: The *N-N bond and H-bond properties of the ligands

Bonds	GBL_I (au)	BPL - GBL_I	ρ(r)	$\nabla^2\rho(r)$	ε	V	G	∇^2Ven	V/G
apz									
N5 - *N7	2.514	1.50E-03	0.386	-0.768	0.137	-0.623	0.215	18.251	2.891
phpz									
*N3 - N4	2.552	1.15E-03	0.368	-0.699	0.137	-0.577	0.201	15.401	2.869
bphpzm									
N14 - *N19	2.562	8.32E-04	0.363	-0.673	0.135	-0.567	0.199	21.260	2.844
N16 - *N20	2.556	8.36E-04	0.366	-0.680	0.140	-0.574	0.202	21.317	2.842
bphpza									
N7 - *N9	2.569	6.84E-04	0.360	-0.658	0.134	-0.559	0.198	22.852	2.832
N12 - *N15	2.570	6.41E-04	0.359	-0.656	0.135	-0.559	0.197	22.803	2.831
bpzpy									
N8 - *N10	2.578	8.62E-04	0.356	-0.639	0.114	-0.552	0.196	17.120	2.815
N7 - *N12	2.578	8.62E-04	0.356	-0.639	0.114	-0.552	0.196	17.121	2.815
bmpzpy									
N8 - *N12	2.590	8.22E-04	0.351	-0.624	0.118	-0.538	0.191	19.062	2.818
N7 - *N14	2.590	8.22E-04	0.351	-0.624	0.118	-0.538	0.191	19.063	2.818
bdcpzpy									
N6 - N14	2.537	1.20E-03	0.375	-0.712	0.134	-0.598	0.210	26.683	2.849
N9 - N16	2.550	9.91E-04	0.369	-0.693	0.125	-0.582	0.205	24.986	2.847

Table 4.30: The QTAIM and NBO properties of the nitrogen atoms that are available (*N) and not available (N) for metal coordination.

Atom	q(A)	$\lvert\mu_{intra}$(A)$\rvert$	$\lvert\mu_{bond}$(A)$\rvert$	$\lvert\mu$(A)$\rvert$	Vol(A),0.001	χ_{Intra_Iso}(A)	χ_{bond_Iso}(A)	χ_{Iso}(A)	χ_{zz}(A)	σ_{Iso}(A,A)	σ_{Iso}(A',A)	σ_{Iso}(A)	Anisotropy	Occ	Energy
apz															
N5	-0.77	0.58	0.77	0.24	87.00	-3.97	-4.82	-8.78	-14.17	32.48	12.08	44.56	146.34	1.50121	-0.30083
*N7	-0.56	0.70	0.74	0.98	110.03	-2.96	-4.11	-7.07	-14.66	-95.22	12.03	-83.18	409.38	1.94621	-0.43617
Total	0.00	6.34	10.47	6.90	1119.40	-44.29	-32.12	-76.41	113.48	-361.02	137.12	498.14	2440.20		
phpz															

*N3	-0.66	0.74	0.92	1.13	113.65	-3.70	-3.93	-7.63	-14.21	-52.01	11.05	-40.96	328.93	1.94337	-0.3989
N4	-0.82	0.62	0.79	0.17	92.72	-4.40	-4.78	-9.18	-14.16	52.51	12.39	64.90	117.40	1.55871	-0.26706
Total	0.00	4.53	3.32	3.15	1297.55	-37.95	-54.03	-91.98	-156.74	617.95	194.60	812.55	1832.26		
							bphpzm								
N14	-0.826	0.583	0.811	0.273	69.83	-3.328	-5.412	-8.741	-12.160	36.886	12.958	49.843	123.0147	1.55459	-0.27659
N16	-0.797	0.584	0.818	0.289	71.77	-3.228	-5.296	-8.524	-5.813	29.389	13.138	42.527	116.5939	1.54285	-0.26537
*N19	-0.671	0.731	0.951	1.116	112.09	-3.475	-3.877	-7.352	-11.668	-59.958	10.510	-49.448	312.0204	1.94381	-0.40761
*N20	-0.677	0.738	0.928	1.138	112.21	-3.617	-3.895	-7.513	-4.970	-55.248	10.740	-44.507	299.3827	1.94349	-0.40137
Total	0.000	9.474	7.152	6.585	2629.01	-75.087	-112.691	-187.778	-202.274	1296.134	397.761	1693.895	3653.2171		
							bphpza								
N7	-0.803	0.577	0.775	0.257	70.50	-3.291	-5.200	-8.491	-8.983	-31.172	12.865	-44.038	115.044	1.9445	-0.40808
*N9	-0.674	0.731	0.958	1.119	111.58	-3.477	-3.861	-7.337	-8.488	-60.859	10.502	-50.357	285.9892	1.55658	-0.27211
N12	-0.799	0.571	0.783	0.226	69.98	-3.261	-5.279	-8.540	-7.281	29.661	12.905	42.566	113.2764		
*N15	-0.677	0.732	0.967	1.127	111.57	-3.487	-3.856	-7.343	-6.542	-60.265	10.497	-49.768	278.4442	1.94454	-0.40721
Total	0.002	10.960	11.139	8.735	2864.42	-87.220	-116.496	-203.716	-198.815	1347.838	416.7758	1764.596	4365.6132		
							bpzpy								
^{py}N1	-1.126	0.046	0.958	0.931	110.02	-4.225	-4.442	-8.667	-16.676	-29.865	7.329	-22.536	423.1244	1.89726	-0.3406
N7	-0.840	0.576	0.764	0.194	73.12	-3.123	-5.335	-8.458	-12.899	14.435	10.749	25.184	136.5511	1.53084	-0.26267
N8	-0.840	0.576	0.764	0.193	73.09	-3.123	-5.339	-8.462	-12.916	14.444	10.746	25.190	136.5213	1.53083	-0.26269
*N10	-0.655	0.768	0.983	1.066	113.07	-3.501	-4.162	-7.663	-13.159	72.487	10.854	61.633	351.3237	1.9467	-0.39493

*N12	-0.655	0.768	0.983	1.066	113.09	-3.501	-4.159	-7.660	-13.140	-72.500	-10.856	-61.644	351.2671	1.9467	-0.39493
Total	0.000	8.871	8.299	5.856	1751.24	-51.311	-73.404	-124.715	-199.399	-581.470	-254.378	-835.848	2838.5704		
bmpzpy															
^{py}N1	-1.121	0.057	0.956	0.944	111.11	-3.947	-4.623	-8.570	-15.292	-52.450	-7.734	-44.717	435.9292	1.90056	-0.3385
N7	-0.836	0.562	0.764	0.207	72.31	-3.225	-5.144	-8.369	-12.150	-22.544	-10.362	-32.905	116.6121	1.55471	-0.25168
N8	-0.836	0.562	0.764	0.208	72.34	-3.225	-5.148	-8.373	-12.156	-22.546	-10.362	-32.907	116.6045	1.55465	-0.25168
*N12	-0.681	0.765	1.007	1.108	112.86	-3.536	-3.823	-7.359	-11.679	-68.864	-10.419	-58.446	283.0056	1.94633	-0.38443
*N14	-0.681	0.765	1.007	1.108	112.89	-3.536	-3.820	-7.356	-11.673	-68.864	-10.417	-58.447	283.0162	1.94633	-0.38443
Total	0.001	10.107	8.876	7.304	2383.12	-74.999	-94.032	-169.031	-227.920	-1338.409	-401.525	-1739.934	2848.6794		
bdcpzpy															
*N6	-0.568	0.705	0.785	0.949	107.008	-2.585	-3.957	-6.541	-11.433	-107.350	-11.118	-96.232	378.8421	1.94663	-0.43694
*N9	-0.618	0.714	0.824	1.006	107.523	-3.155	-3.900	-7.056	-10.615	-74.426	-10.785	-63.641	350.7135	1.94312	-0.43333
^{py}N10	-1.188	0.045	0.966	0.926	105.196	-4.112	-4.784	-8.897	-15.209	-27.346	-7.929	-19.417	394.8674	1.89035	-0.3775
N14	-0.766	0.549	0.755	0.283	70.134	-2.915	-5.017	-7.932	-11.447	-8.119	-10.467	-18.586	156.3873	1.49714	-0.30068
N16	-0.800	0.552	0.866	0.363	71.356	-2.990	-4.965	-7.955	-10.144	-14.068	-10.292	-24.360	134.4276		
Total	-0.002	14.652	23.912	15.042	2722.229	-98.477	-88.933	-187.410	-249.824	-784.200	-336.632	-1120.832	6037.6538		

Table 4.31: The electronic excitation of the ligands showing their triplet and singlet transitions

Ligang	State	Wavelength	*f*	Transitions
apz	Triplet-A	342.05	0	HOMO→LUMO (100%); H-2→LUMO (8%); H-2→L+1 (6%); HOMO→L+1 (9%)
	Triplet-A	286.65	0	H-2→LUMO (90%); HOMO→L+1 (18%);
	Triplet-A	282.89	0	H-3→LUMO (75%); H-1→LUMO (22%); H-3→L+1 (5%); H-3→L+8 (2%)
	Singlet-A	278.48	0	H-3→LUMO (45%); H-1→LUMO (35%); H-3→L+1 (4%); H-1→L+1 (3%)
	Singlet-A	267.06	0	H-3→LUMO (13%); H-1→L+1 (74%);
	Singlet-A	257.58	0.0307	H-2→LUMO (38%); HOMO→LUMO (21%); HOMO→L+1 (25%); H-2→L+1 (4%)
phpz	Triplet-A	392.39	0	H-1→L+1 (16%); HOMO→LUMO (107%); H-3→L+11 (3%); H-2→L+4 (4%)
	Triplet-A	300.57	0	H-3→LUMO (11%); H-2→LUMO (12%); H-2→L+1 (10%); H-1→L+1 (36%)
	Triplet-A	292.00	0	H-1→LUMO (29%); HOMO→L+1 (55%); H-2→LUMO (6%); H-1→L+1 (5%)
	Singlet-A	276.51	0.0284	H-1→LUMO (33%); HOMO→LUMO (10%); HOMO→L+1 (49%);8-→8 (0)
	Singlet-A	270.94	0.3149	HOMO→LUMO (66%); H-1→LUMO (5%); H-1→L+1 (3%); HOMO→L+1 (7%)
	Singlet-A	259.01	0.0013	HOMO→L+2 (88%);11-→-95 (-106);11-→27 (16);78-→168 (90)
bphpzm	Triplet-A	396.80	0	H-2→L+3 (11%); HOMO→L+1 (102%); H-2→L+4 (4%);
	Triplet-A	394.73	0	H-3→L+2 (13%); H-1→LUMO (104%); H-5→LUMO (2%); H-5→L+5 (3%)
	Triplet-A	304.68	0	H-6→L+1 (11%); H-2→L+3 (18%); HOMO→L+3 (21%); H-5→LUMO (3%)
	Singlet-A	304.16	0.0099	HOMO→LUMO (89%);
	Singlet-A	293.09	0.5388	H-1→LUMO (21%); HOMO→L+1 (48%); H-2→L+1 (3%); HOMO→L+3 (5%)
	Singlet-A	285.71	0.0588	H-2→L+1 (19%); H-1→LUMO (15%); H-1→L+2 (11%); HOMO→L+3 (26%)
bphpza	Triplet-A	399.17	0	H-1→L+1 (10%); H-1→L+2 (14%); HOMO→LUMO (14%); HOMO→L+1 (37%)
	Triplet-A	398.24	0	H-1→LUMO (11%); H-1→L+1 (40%); H-1→L+2 (14%); HOMO→LUMO (11%)
	Triplet-A	314.89	0	H-2→L+5 (11%); HOMO→LUMO (40%); H-7→L+1 (2%); H-6→LUMO (4%)
	Singlet-A	303.52	0.0608	HOMO→LUMO (93%);
	Singlet-A	302.26	0.1404	H-1→LUMO (92%);
	Singlet-A	299.56	0.2834	HOMO→L+1 (81%);
bpzpy	Triplet-A	372.77	0	HOMO→L+1 (95%); H-8→L+1 (8%); H-7→LUMO (9%); H-3→LUMO (7%)
	Triplet-A	336.13	0	H-1→L+1 (10%); HOMO→LUMO (71%); H-3→L+1 (8%); H-2→LUMO (9%)
	Triplet-A	330.05	0	H-2→L+1 (53%); H-1→LUMO (26%); H-1→L+3 (13%); H-3→LUMO (4%)
	Singlet-A	327.49	0.1405	HOMO→LUMO (75%); H-7→L+1 (3%); H-3→L+1 (4%);
	Singlet-A	283.79	0.1472	HOMO→L+1 (78%);
	Singlet-A	283.01	0.0025	H-4→LUMO (11%); H-1→LUMO (68%); H-3→LUMO (7%);

bmpzpy	Triplet-A	365.15	0	H-8→LUMO (13%); H-7→L+1 (16%); HOMO→L+1 (83%); H-3→LUMO (7%)
	Triplet-A	339.28	0	H-1→L+1 (20%); HOMO→LUMO (63%); H-7→LUMO (3%); H-2→LUMO (7%)
	Triplet-A	334.68	0	H-2→L+1 (41%); H-1→LUMO (34%); H-1→L+4 (19%); H-2→L+6 (6%)
	Singlet-A	331.82	0.1454	HOMO→LUMO (81%); H-8→L+1 (3%);
	Singlet-A	295.94	0.0026	H-1→LUMO (91%);
	Singlet-A	295.40	0.0006	H-2→LUMO (87%); H-1→L+1 (4%);
bdcpzpy	Triplet-A	382.00	0	HOMO→LUMO (51%); HOMO→L+1 (36%); H-9→L+3 (5%); H-4→LUMO (2%)
	Triplet-A	356.50	0	H-1→L+1 (62%); H-6→L+1 (6%); H-3→LUMO (3%); H-2→LUMO (6%)
	Triplet-A	354.64	0	H-4→LUMO (21%); H-3→LUMO (33%); H-2→LUMO (33%); H-5→LUMO (3%)
	Singlet-A	334.57	0.0563	HOMO→LUMO (73%); HOMO→L+1 (8%)
	Singlet-A	300.35	0.2795	HOMO→L+1 (66%); H-1→LUMO (6%); HOMO→LUMO (5%);;
	Singlet-A	291.27	0.0499	H-1→LUMO (84%); HOMO→L+1 (4%)

Table 4.32: The molecular orbital (MO) contribution of the nitrogen atom(s) "*N" available for metal coordination.

		dcpz		
	eV	N5	*N7	others
L+5	0.93	7	6	87
L+4	0.18	-1	-81	184
L+3	-0.24	-33	21	113
L+2	-0.83	-1	-13	116
L+1	-1.88	3	13	85
LUMO	-2.37	15	18	68
HOMO	-8.2	5	28	67
H-1	-8.32	0	0	100
H-2	-8.51	24	2	74
H-3	-8.78	0	3	98
H-4	-9.36	12	65	22
H-5	-9.49	1	0	99
H-6	-9.73	0	2	98
H-7	-11.65	1	1	98
		phpz		
	eV	*N3	N4	others
L+5	0.56	3	-6	103
L+4	0.27	10	6	84
L+3	0.24	-5	1	105
L+2	-0.14	-94	27	168
L+1	-0.38	1	1	98

LUMO	-0.93	17	6	78
HOMO	-6.12	11	11	78
H-1	-6.85	2	1	97
H-2	-7.1	24	3	73
H-3	-8.06	3	17	80
H-4	-8.2	74	2	24
H-5	-9.35	6	0	95
H-6	-9.53	1	0	99
H-7	-10.06	0	5	95

bphpzm

	eV	*N20	*N19	others
L+5	-0.1	0	4	95
L+4	-0.26	-22	-19	143
L+3	-0.44	0	0	102
L+2	-0.56	0	1	99
L+1	-1.01	16	0	84
LUMO	-1.19	1	19	80
HOMO	-6.09	9	0	91
H-1	-6.33	1	10	89
H-2	-6.86	3	0	97
H-3	-7	0	1	99
H-4	-7.1	24	0	76
H-5	-7.36	0	25	76
H-6	-7.98	2	1	97
H-7	-8.23	9	2	89

bphpza

	eV	*N9	*N15	others
L+5	-0.43	0	-11	113
L+4	-0.45	-1	-8	111
L+3	-0.59	-2	-10	114
L+2	-0.88	4	2	94
L+1	-1.21	12	9	79
LUMO	-1.54	1	2	97
HOMO	-6.19	3	7	90
H-1	-6.34	7	4	89
H-2	-6.94	0	2	98
H-3	-6.97	1	0	99
H-4	-7.2	6	18	77
H-5	-7.34	18	6	76
H-6	-8.08	2	2	96
H-7	-8.2	4	5	90

bpzpy

	eV	*N12	^{py}N1	*N10	others	
L+5	0.43	-14	4	-14	126	
L+4	0.13	-21	-5	-21	150	

L+3	-0.11	1	-1	1	99
L+2	-0.3	-8	-14	-8	133
L+1	-1.53	4	0	4	92
LUMO	-1.53	0	22	1	77
HOMO	-6.57	0	0	0	100
H-1	-7.03	14	3	14	69
H-2	-7.06	18	0	18	65
H-3	-7.22	5	12	5	78
H-4	-7.67	16	44	16	25
H-5	-8.06	38	0	38	24
H-6	-8.33	22	28	22	28
H-7	-8.61	3	20	3	74
		bdmpzpy			
	eV	*N12	^{py}N1	*N14	others
L+5	0.37	-9	-1	-9	122
L+4	0.21	4	2	4	90
L+3	0.05	-27	-8	-27	166
L+2	-0.27	-20	-34	-20	177
L+1	-1.23	2	1	2	95
LUMO	-1.39	-1	23	-1	82
HOMO	-6.27	1	0	1	98
H-1	-6.48	19	2	18	61
H-2	-6.52	17	0	18	66
H-3	-6.7	0	7	0	93
H-4	-7.51	20	33	20	28
H-5	-7.7	35	0	35	31
H-6	-7.96	16	38	16	29
H-7	-8.07	2	0	2	95
		bdcpzpy			
	ev	*N6	*N9	^{py}N10	others
L+5	0.9	4	3	0	94
L+4	1.28	3	2	1	94
L+3	1.71	3	10	3	84
L+2	1.96	0	1	4	95
L+1	2.39	17	10	0	72
LUMO	2.66	1	2	18	80
HOMO	7.4	0	1	0	99
H-1	7.72	23	0	0	77
H-2	8.18	1	4	9	85
H-3	8.2	1	1	9	88
H-4	8.32	0	10	7	83
H-5	8.38	0	0	2	98
H-6	8.5	11	4	0	85
H-7	8.7	0	2	3	95

Table 4.24: Assignment of the prominent IR picks of the ligands using the PED method

bpyr				**dmbpyr**				**dcbpyr**			
Freq	Int	Vibration		Freq	Int	Vibration		Freq	Int	Vibration	
3143.43	5.05	υ(CH)		3118.65	41.42	υ(CH)	υ(CH)	3647.4	86.05	υ(OH)	
3142.75	30.16	υ(CH)		3116.37	14.03	υ(CH)		3645.65	85.75	υ(OH)	
3134.79	13.82	υ(CH)		3088.13	29.71	υ(CH)		3096.08	29.02	υ(CH)	
3132.07	17.5	υ(CH)		3087.84	19.95	υ(CH)		1744.04	334.41	υ(OC)	
3119.95	5.07	υ(CH)		3070.06	13.34	υ(CH)		1741.81	245.55	υ(OC)	
3090.23	28.13	υ(CH)		3070.44	13.05	υ(CH)		1572.05	70.3	υ(CC)	
3090.62	24.68	υ(CH)		2978.88	24.74	υ(CH)		1392.35	91.63	υ(CC)	β(CCC)
1587.35	73.62	υ(CC)		2978.41	23.91	υ(CH)		1380.49	67.75	β(HCC)	β(CCC)
1565.85	28	β(HCC)	υ(CC)	1595.18	107.12	υ(CC)		1338.5	77.81	υ(CC)	υ(CC)
1451.68	23.93	υ(CC)	β(HCN)	1593.63	53.65	υ(CC)	β(HCC)	1329.35	96.32	β(HOC)	β(HCC)
1417.84	46.82	β(HCC)	β(HCN)	1566.58	39.07	υ(CC)		1326.49	61.18	υ(CC)	β(HOC)
1406.33	5.39	υ(CC)	β(HCC)	1557	22.82	υ(CC)		1161.06	137.93	υ(CC)	β(HOC)
1098.16	7.81	υ(CC)	β(HCC)	1465.43	13.55	υ(NC)	β(HCC)	1155.19	237.45	υ(OC)	β(HOC)
1046.08	4.91	υ(CC)	β(HCN)	1445.53	18.18	β(HCH)	τ(HCCC)	1102.11	181.04	υ(OC)	β(HOC)
1027.09	6.73	υ(NC)	β(CNC)	1444.81	35.34	β(HCH)	τ(HCCC)	1074.17	69.53	υ(OC)	β(HCN)
744.48	56.45	τ(HCCC)	τ(CNCC)	1439.54	12.14	β(HCH)	τ(HCCC)	745.09	93.14	o(OCOC)	
730.88	45.01	τ(HCCC)	τ(CNCC)	1381.38	24.81	β(HCC)	β(CCC)	720.87	33.62	τ(CNCC)	τ(CCCN)
726.81	6.91	τ(HCCN)		823.66	13.46	υ(CC)	β(CCC)	620.36	69.44	β(OCO)	
645.27	10.12	β(CCC)		802.64	48.58	τ(HCCN)		611.02	73.83	β(OCO)	
599.47	4.75	β(CCN)		453.07	12.19	β(CCC)		603.91	133.08	τ(HOC)	
phn				**dmphn**				**dcphn**			
3138.16	45.44	υ(CH)		3126.2	45.38	υ(CH)		3649.77	86.6	υ(OH)	
3120.96	28.98	υ(CH)		3119.75	30.12	υ(CH)		3640.32	76.75	υ(OH)	

3110.93	15.51 υ(CH)		3106.11	14.2 υ(CH)		1767.58	231.66 υ(OC)	
3084.6	28.94 υ(CH)	υ(CH)	3036.88	21.24 υ(CH)		1722.58	365.47 υ(OC)	
3083.87	24.55 υ(CH)	υ(CH)	2975.23	29.21 υ(CH)		1538.22	29.18 υ(CC)	β(CCC)
1613.62	5.08 υ(CC)		2975.35	20.15 υ(CH)		1356.59	86.46 υ(OC)	β(HOC)
1605.92	8.72 υ(CC)	β(HCC)	1614.77	23.96 υ(CC)		1343.39	40.17 υ(CC)	
1590.9	9.33 υ(CC)		1611.46	46.86 υ(CC)		1306.66	99.84 υ(OC)	β(HOC)
1545.18	15.24 υ(CC)		1592.78	42.92 υ(CC)		1180.71	53.61 υ(CC)	β(HOC)
1496.34	33.73 υ(NC)	β(HCN)	1505.6	42.69 β(HCC)	β(CCN)	1159.87	56.72 β(HOC)	β(HCC)
1492.41	10.95 υ(CC)	β(HCC)	1488.26	59.39 υ(CC)	β(HCC)	1122.75	31.96 υ(CC)	β(HCC)
1412.18	34.45 β(HCN)		1438.53	17.5 β(HCH)	τ(HCCC)	1104.38	373.67 υ(OC)	υ(OC)
1309.5	4.02 υ(NC)	β(HCN)	1428.8	41.44 β(HCH)	τ(HCCC)	1100.11	143.12 υ(OC)	β(HCC)
1123.49	8.48 υ(CC)	β(HCC)	1408.6	27.37 β(HCC)		1059.25	83.8 υ(OC)	β(CCC)
1082.33	11.71 υ(CC)	β(HCC)	1329.45	16.21 υ(NC)		855.9	60.43 τ(HCCC)	
822.69	71.33 τ(HCCC)		1191.94	14.41 β(HCC)	β(HCC)	720.14	104.54 ο(OCO C)	
741.12	22 τ(HCCC)		1129.38	13.64 β(HCC)		682.65	35.9 υ(OC)	β(CCC)
726.96	30.06 τ(CCCC)	τ(CCCC)	986.59	11.92 β(HCH)	τ(HCCC)	614.04	109.4 τ(HOCC)	
606.94	6.66 β(CCC)		832.79	68.55 τ(HCCC)		583.83	36.97 β(OCO)	β(CCC)
94.16	5.41 τ(CCNC)		537.97	13.36 τ(CCCN)	τ(CCCN)	493.83	34.35 τ(CCNC)	

Greek letters υ, β, τ, ο denote stretching, bending, tortion and out of plane modes respectively

Table 4.33: The non-linear conductive properties of the ligands

	Dipole	<α>	Δα1	Δα2	Δα3	Γ	ß in esu	HOMO	LUMO	Gap in	Non-

							(1x10-30)			KJ/mol	Valence Lewis Orbitals
dcpz	3.55	92.52	-3.31	75.16	2819.12	-49.97	1.84	-0.3015	-0.0870	563.27	2.32%
phpz	2.49	124.37	-90.01	102.87	1240.26	-65.22	3.40	-0.2250	-0.0341	500.97	2.79%
bphpzm	3.21	273.88	-9.61	172.79	14881.42	-8.31	2.71	-0.2240	-0.0436	473.61	2.73%
bphpza	2.35	296.55	-48.38	133.87	7790.76	-11.62	4.19	-0.2273	-0.0569	447.56	2.84%
bpzpy	5.16	179.84	-78.73	143.88	7251.88	-6.22	7.91	-0.2412	-0.0564	485.39	2.76%
bmpzpy	5.19	233.64	-78.06	141.62	6981.98	-9.33	10.05	-0.2306	-0.0513	470.74	2.27%
bdcpzpy	4.66	267.46	-135.11	175.81	6327.24	-13.55	2.99	-0.2717	-0.0976	457.20	2.72%

Table 4.34: Assignment of the prominent IR picks of the ligands using the PED method

bpyr			**dmbpyr**			**dcbpyr**		
Freq	Int	Vibration	Freq	Int	Vibration	Freq	Int	Vibration
3143.43	5.05	υ(CH)	3118.65	41.42	υ(CH) υ(CH)	3647.4	86.05	υ(OH)
3142.75	30.16	υ(CH)	3116.37	14.03	υ(CH)	3645.65	85.75	υ(OH)
3134.79	13.82	υ(CH)	3088.13	29.71	υ(CH)	3096.08	29.02	υ(CH)
3132.07	17.5	υ(CH)	3087.84	19.95	υ(CH)	1744.04	334.41	υ(OC)
3119.95	5.07	υ(CH)	3070.06	13.34	υ(CH)	1741.81	245.55	υ(OC)
3090.23	28.13	υ(CH)	3070.44	13.05	υ(CH)	1572.05	70.3	υ(CC)
3090.62	24.68	υ(CH)	2978.88	24.74	υ(CH)	1392.35	91.63	υ(CC) β(CCC)
1587.35	73.62	υ(CC)	2978.41	23.91	υ(CH)	1380.49	67.75	β(HCC) β(CCC)
1565.85	28	β(HCC) υ(CC)	1595.18	107.12	υ(CC)	1338.5	77.81	υ(CC) υ(CC)
1451.68	23.93	υ(CC) β(HCN)	1593.63	53.65	υ(CC) β(HCC)	1329.35	96.32	β(HOC) β(HCC)
1417.84	46.82	β(HCC) β(HCN)	1566.58	39.07	υ(CC)	1326.49	61.18	υ(CC) β(HOC)
1406.33	5.39	υ(CC) β(HCC)	1557	22.82	υ(CC)	1161.06	137.93	υ(CC) β(HOC)
1098.16	7.81	υ(CC) β(HCC)	1465.43	13.55	υ(NC) β(HCC)	1155.19	237.45	υ(OC) β(HOC)
1046.08	4.91	υ(CC) β(HCN)	1445.53	18.18	β(HCH) τ(HCCC)	1102.11	181.04	υ(OC) β(HOC)
1027.09	6.73	υ(NC) β(CNC)	1444.81	35.34	β(HCH) τ(HCCC)	1074.17	69.53	υ(OC) β(HCN)
744.48	56.45	τ(HCCC) τ(CNCC)	1439.54	12.14	β(HCH) τ(HCCC)	745.09	93.14	ο(OCOC)
730.88	45.01	τ(HCCC) τ(CNCC)	1381.38	24.81	β(HCC) β(CCC)	720.87	33.62	τ(CNCC) τ(CCCN)
726.81	6.91	τ(HCCN)	823.66	13.46	υ(CC) β(CCC)	620.36	69.44	β(OCO

								)
645.27	10.12 β(CCC)		802.64	48.58 τ(HCCN)		611.02	73.83	β(OCO)
599.47	4.75 β(CCN)		453.07	12.19 β(CCC)		603.91	133.0 8	τ(HOC C)
	phn			**dmphn**			**dcphn**	
3138.16	45.44 υ(CH)		3126.2	45.38 υ(CH)		3649.77	86.6 υ(OH)	
3120.96	28.98 υ(CH)		3119.75	30.12 υ(CH)		3640.32	76.75 υ(OH)	
3110.93	15.51 υ(CH)		3106.11	14.2 υ(CH)		1767.58	231.66 υ(OC)	
3084.6	28.94 υ(CH)	υ(CH)	3036.88	21.24 υ(CH)		1722.58	365.4 7 υ(OC)	
3083.87	24.55 υ(CH)	υ(CH)	2975.23	29.21 υ(CH)		1538.22	29.18 υ(CC)	β(CCC)
1613.62	5.08 υ(CC)		2975.35	20.15 υ(CH)		1356.59	86.46 υ(OC)	β(HOC)
1605.92	8.72 υ(CC)	β(HCC)	1614.77	23.96 υ(CC)		1343.39	40.17 υ(CC)	
1590.9	9.33 υ(CC)		1611.46	46.86 υ(CC)		1306.66	99.84 υ(OC)	β(HOC)
1545.18	15.24 υ(CC)		1592.78	42.92 υ(CC)		1180.71	53.61 υ(CC)	β(HOC)
1496.34	33.73 υ(NC)	β(HCN)	1505.6	42.69 β(HCC)	β(CCN)	1159.87	β(HOC 56.72)	β(HCC)
1492.41	10.95 υ(CC)	β(HCC)	1488.26	59.39 υ(CC)	β(HCC)	1122.75	31.96 υ(CC)	β(HCC)
1412.18	34.45 β(HCN)		1438.53	17.5 β(HCH)	τ(HCCC)	1104.38	373.67 υ(OC)	υ(OC)
1309.5	4.02 υ(NC)	β(HCN)	1428.8	41.44 β(HCH)	τ(HCCC)	1100.11	143.12 υ(OC)	β(HCC)
1123.49	8.48 υ(CC)	β(HCC)	1408.6	27.37 β(HCC)		1059.25	83.8 υ(OC)	β(CCC)
1082.33	11.71 υ(CC)	β(HCC)	1329.45	16.21 υ(NC)		855.9	τ(HCC 60.43 C)	
822.69	71.33 τ(HCCC)		1191.94	14.41 β(HCC)	β(HCC)	720.14	104.5 4	o(OCO C)
741.12	22 τ(HCCC)		1129.38	13.64 β(HCC)		682.65	35.9 υ(OC)	β(CCC)
726.96	30.06 τ(CCCC)	τ(CCCC)	986.59	11.92 β(HCH)	τ(HCCC)	614.04	τ(HOC 109.4 C)	
606.94	6.66 β(CCC)		832.79	68.55 τ(HCCC)		583.83	β(OCO 36.97)	β(CCC)
94.16	5.41 τ(CCNC)		537.97	13.36 τ(CCCN)	τ(CCCN)	493.83	τ(CCN 34.35 C)	

Greek letters υ, β, τ, o denote stretching, bending, tortion and out of plane modes respectively

Table 4.35: The experimental ^{1}H-NMR shifts obtained in d-dmso

1H-NMR d-dmso	dmbpyr	phn	dmphn
CH_3	2.40 to 2.50		2.49 to 2.79
$C_{px\text{-}meta}$-H	7.27	7.77	7.62
C_{base}-H		7.99	7.86
$C_{px\text{-}para}$-H	8.22	8.50	8.34
$C_{px\text{-}ortho}$-H	8.52	9.10	

The subscript "px" represent the pyridine (pyr) in dmbpyr and phenanthroline (phn) in phn and dmphn.

Table 4.36: The computed ^{1}H-NMR shifts from the direct and fitting methods

bpyr			**dmbpyr**			**dcbpyr**			**phn**			**dmphn**			**dcphn**		
	Direct	Fitting		Direct	Fitting		Direct	Fitting		Direct	Fitting		Direct	Fitting		Direct	Fitting
H13	7.25	7.55	H15	7.14	7.45	H19	6.46	6.79	H15	7.80	8.09	H17	7.70	7.99	H21	7.96	8.25
H14	7.74	8.03	H16	8.84	9.10	H20	7.92	8.21	H16	7.80	8.09	H18	7.70	7.99	H22	7.96	8.24
H15	9.01	9.26	H17	7.41	7.71	H21	9.16	9.40	H17	8.15	8.42	H19	8.04	8.32	H23	8.28	8.56
H16	7.58	7.87	H18	7.40	7.70	H22	9.03	9.28	H18	8.15	8.42	H20	8.04	8.32	H24	8.29	8.56
H17	7.58	7.87	H19	8.84	9.10	H23	8.94	9.20	H19	7.64	7.93	H21	7.59	7.88	H25	8.90	9.16
H18	7.74	8.03	H20	7.16	7.47	H24	6.50	6.82	H20	9.31	9.55	H22	7.59	7.88	H26	8.71	8.97
H19	9.01	9.26	H21	2.45	2.90	H25	9.16	9.41	H21	7.64	7.93	H23	2.87	3.30	H27	6.64	6.96
H20	7.25	7.55	H22	2.61	3.05	H26	8.12	8.40	H22	9.31	9.55	H24	2.97	3.40	H28	6.52	6.85
			H23	2.02	2.49							H25	2.87	3.30			
			H24	2.57	3.02							H26	2.97	3.40			
			H25	2.56	3.01							H27	2.87	3.30			
			H26	1.96	2.42							H28	2.87	3.30			

Table 4.37: The computed ^{15}N-NMR shifts from the direct and fitting methods

bpyr	**dmbpyr**	**dcbpyr**	**phn**	**dmphn**	**dcphn**

	Direct	Fitting		Direct	Fitting		Direct	Fitting		Direct	Fitting		Direct	Fitting		Direct	Fitting
N5	-56.78	-83.71	N6	-64.74	-91.24	N8	-42.27	-69.99	N10	-61.81	-88.47	N10	-68.36	-94.67	N11	-55.77	-82.76
N9	-56.78	-83.71	N10	-64.86	-91.36	N12	-42.77	-70.46	N12	-61.81	-88.47	N12	-68.36	-94.67	N13	-47.70	-75.12

Table 4.38: The computed ^{13}C-NMR shifts from the direct and fitting methods

bpyr			**dmbpyr**			**dcbpyr**			**phn**			**dmphn**			**dcphn**		
	Direct	Fitting		Direct	Fitting		Direct	Fitting		Direct	Fitting		Direct	Fitting		Direct	Fitting
C1	117.92	105.21	C1	22.39	13.22	C2	163.99	149.58	C1	123.89	110.95	C1	122.60	109.72	C1	126.09	113.08
C2	131.38	118.17	C2	118.63	105.90	C4	118.69	105.95	C2	123.89	110.95	C2	122.60	109.72	C2	125.54	112.54
C3	148.55	134.71	C3	143.88	130.21	C5	133.40	120.12	C3	131.24	118.04	C3	131.45	118.24	C3	132.06	118.83
C4	118.75	106.00	C4	148.01	134.19	C6	149.71	135.83	C4	126.48	113.45	C4	124.55	111.59	C4	127.83	114.76
C6	158.36	144.16	C5	119.89	107.11	C7	117.92	105.21	C5	126.48	113.45	C5	124.55	111.59	C5	127.40	114.33
C7	158.37	144.16	C7	158.80	144.57	C9	154.65	140.58	C6	118.16	105.44	C6	117.89	105.18	C6	122.09	109.22
C8	118.75	106.01	C8	158.84	144.62	C10	154.31	140.25	C7	146.33	132.56	C7	145.13	131.41	C7	145.40	131.67
C10	131.38	118.17	C9	119.90	107.12	C11	116.51	103.85	C8	131.24	118.04	C8	131.45	118.24	C8	132.18	118.94
C11	148.55	134.71	C11	143.87	130.20	C14	133.65	120.35	C9	146.33	132.56	C9	145.13	131.41	C9	145.86	132.12
C12	117.92	105.21	C12	147.91	134.09	C15	149.74	135.85	C11	147.21	133.42	C11	157.20	143.04	C12	145.97	132.22
			C13	22.37	13.20	C16	163.59	149.19	C13	118.16	105.44	C13	117.89	105.18	C14	121.57	108.72
			C14	118.63	105.89	C17	120.76	107.94	C14	147.22	133.42	C14	26.60	17.27	C15	165.16	150.70
												C15	157.20	143.04	C16	145.38	131.66
												C16	26.60	17.27	C18	159.69	145.43

Table 4.39: The four Ramsey terms of the N-N bonds in the ligands

			bpyr		
	FC	SD	PSO	DSO	J
N5-C6		1.989	0.416	-3.589	0.087	-1.097
C7-N9		1.989	0.416	-3.589	0.087	-1.096
N5-N9		0.518	0.004	0.038	0.007	0.566
			dmbpyr		
N6-C7		1.982	0.421	-3.577	0.088	-1.087
C8-N10		2.008	0.424	-3.589	0.088	-1.069
N6-N10		0.532	0.003	0.035	0.007	0.578
			dcbpyr		
N8-C9		1.990	0.428	-3.608	0.089	-1.100
C10-N12		1.973	0.436	-3.624	0.089	-1.126
N8-N12		0.547	0.108	0.072	0.008	0.736
			phn		
C7-N10		-0.615	0.336	-3.197	0.092	-3.384
C9-N12		-0.615	0.336	-3.197	0.092	-3.385
N10-N12		0.379	0.101	0.069	0.008	0.557
			dmphn		
C7-N10		0.440	0.309	-3.081	0.096	-2.236
C9-N12		0.440	0.309	-3.081	0.096	-2.236
N10-N12		0.402	0.087	0.061	0.009	0.559
			dcphn		
C7-N11		2.208	0.373	-3.312	0.100	-0.631
C9-N13		1.880	0.382	-3.334	0.099	-0.973
N11-N13		0.262	0.117	0.070	0.010	0.458

Table 4.40: The selected bond properties of the ligands

Bonds	GBL_I (au)	BPL - GBL_I	ρ(r)	$\nabla^2\rho(r)$	ε	V	G	∇^2Ven	V/G
				bpyr					
N5 - C6	2.556	2.14E-03	0.337	-1.110	0.117	-0.768	0.245	27.266	3.132
C6 - C7	2.827	4.10E-05	0.269	-0.684	0.095	-0.289	0.059	15.819	4.909
C7 - N9	2.556	2.14E-03	0.337	-1.110	0.117	-0.768	0.245	27.266	3.132
				dmbpyr					
N6 - C7	2.554	2.02E-03	0.338	-1.116	0.117	-0.769	0.245	29.385	3.140
C7 - C8	2.827	3.50E-05	0.269	-0.684	0.093	-0.288	0.059	17.046	4.913
C8 - N10	2.554	2.02E-03	0.338	-1.116	0.118	-0.770	0.246	29.384	3.136
				dcbpyr					
N8 - C9	2.559	2.26E-03	0.337	-1.112	0.111	-0.763	0.242	32.328	3.148
C9 - C10	2.837	3.20E-05	0.265	-0.661	0.118	-0.282	0.058	18.332	4.825
C10 - N12	2.556	2.27E-03	0.338	-1.114	0.114	-0.768	0.245	32.379	3.137
				phn					
C7 - C9	2.764	1.05E-04	0.284	-0.737	0.163	-0.326	0.071	18.877	4.597
C7 - N10	2.569	2.24E-03	0.333	-1.115	0.105	-0.725	0.223	29.368	3.249
C9 - N12	2.569	2.24E-03	0.333	-1.115	0.105	-0.725	0.223	29.368	3.249
				dmphn					
C7 - C9	2.763	1.43E-04	0.284	-0.737	0.165	-0.327	0.072	20.278	4.577
C7 - N10	2.571	2.40E-03	0.332	-1.112	0.100	-0.719	0.220	31.585	3.261
C9 - N12	2.571	2.40E-03	0.332	-1.112	0.100	-0.719	0.220	31.585	3.262
				dcphn					
C7 - C9	2.770	9.90E-05	0.283	-0.732	0.159	-0.323	0.070	22.303	4.616
C7 - N11	2.557	2.52E-03	0.336	-1.095	0.110	-0.767	0.247	34.792	3.109
C9 - N13	2.555	2.58E-03	0.336	-1.093	0.110	-0.776	0.251	34.763	3.088

Table 4.41: The QTAIM and NBO properties of the nitrogen atoms that are available (N) for metal

coordination.

Atom	q(A)	$\|\mu_{intra}(A)\|$	$\|\mu_{bond}(A)\|$	$\|\mu(A)\|$	Vol(A),0.001	$\chi_{Intra\_Iso}(A)$	$\chi_{bond\_Iso}(A)$	$\chi_{Iso}(A)$	$\chi_{zz}(A)$	$\sigma_{Iso}(A,A)$	$\sigma_{Iso}(A',A)$	$\sigma_{Iso}(A)$	Anisotropy	Occ	Energy
bpyr															
N5	-1.152	0.087	1.009	1.045	117.974	-3.771	-4.810	-8.581	-16.867	-79.850	7.666	-72.185	533.9352	1.92104	-0.32918
N9	-1.152	0.087	1.009	1.045	117.956	-3.771	-4.808	-8.578	-16.865	-79.855	7.666	-72.189	533.9434	1.92103	-0.32916
Total	0.000	4.233	4.612	3.680	1395.438	-35.903	-58.631	-94.534	-161.803	-423.356	-181.763	-605.119	2758.7677		
dmbpyr															
N6	-1.154	0.086	1.015	1.060	118.506	-3.913	-4.723	-8.636	-16.614	-71.971	7.746	-64.225	525.9265	1.92045	-0.32604
N10	-1.154	0.084	1.016	1.060	118.520	-3.914	-4.717	-8.631	-16.552	-71.848	7.745	-64.103	525.8694	1.92043	-0.32605
Total	0.000	4.785	5.035	4.623	1714.945	-48.000	-69.318	-117.318	-181.736	-802.185	-255.862	-1058.047	2807.9105		
dcbpyr															
N8	-1.136	0.095	0.989	0.991	114.833	-3.457	-4.631	-8.088	-18.069	-94.084	7.390	-86.694	576.2422	1.92065	-0.34082
N12	-1.137	0.090	0.991	0.994	114.832	-3.465	-4.630	-8.095	-18.086	-93.595	7.399	-86.196	575.4809	1.92083	-0.33991
Total	-0.002	7.336	13.701	8.388	1867.198	-60.240	-66.529	-126.769	-217.134	-582.724	-219.813	-802.537	4369.5752		
phn															
N10	-1.152	0.142	1.012	1.021	116.808	-3.775	-5.244	-9.019	-19.675	-74.498	7.342	-67.156	543.2858	1.91856	-0.32582
N12	-1.152	0.142	1.012	1.021	116.808	-3.775	-5.241	-9.015	-19.669	-74.494	7.341	-67.153	543.2735	1.91855	-0.32582
Total	0.000	4.340	4.675	3.698	1537.415	-39.465	-80.758	-120.223	-237.732	-541.831	-216.257	-758.088	3083.1443		
dmphn															
N10	-1.158	0.129	1.004	1.026	115.371	-3.808	-5.056	-8.864	-19.169	-67.823	7.219	-60.604	498.0169	1.91709	-0.31824
N12	-1.158	0.129	1.004	1.026	115.406	-3.808	-5.055	-8.863	-19.166	-67.823	7.220	-60.603	498.0145	1.91706	-0.31821

Total	0.000	4.968	4.979	4.550	1857.125	-52.085	-90.320	-142.405	-256.319	928.169	288.464	1216.633	3107.6483	
						dcphn								
N11	-1.120	0.074	0.969	0.928	109.778	-3.401	-5.313	-8.714	-19.737	-80.713	7.516	-73.197	549.7021	1.91675	-0.33837
N13	-1.118	0.066	0.965	0.927	110.486	-3.320	-5.311	-8.631	-19.843	-88.772	7.507	-81.265	561.5419	1.91557	-0.33694
Total	0.000	7.287	13.117	8.275	2018.455	-64.306	-89.427	-153.733	-282.950	684.409	256.560	940.969	4655.9297		

Table 4.42: The electronic excitation of the ligands showing their triplet and singlet transitions

Ligang	**State**	**Wavelength**	***f***	**Transitions**
bpyr	Triplet-A	375.680		HOMO→LUMO (89%); HOMO→L+1 (11%); H-5→L+2 (4%); H-5→L+4 (5%)
	Triplet-A	330.040		H-2→L+2 (14%); H-1→LUMO (76%); H-1→L+1 (11%);
	Triplet-A	318.930		H-2→LUMO (66%); H-2→L+1 (11%); H-1→L+2 (28%);
	Singlet-A	313.990	0.0004	H-1→LUMO (87%);
	Singlet-A	292.280	0.0041	H-2→LUMO (86%); H-1→L+2 (2%);
	Singlet-A	288.920		H-2→L+2 (22%); H-1→L+1 (63%);
dmbpyr	Triplet-A	377.460		H-5→L+4 (10%); H-3→L+2 (10%); HOMO→LUMO (91%); H-4→LUMO (5%)
	Triplet-A	324.560		H-1→LUMO (71%); H-5→LUMO (6%); H-4→L+2 (6%); H-3→L+1 (4%)
	Triplet-A	316.390		H-5→LUMO (36%); H-4→L+2 (20%); H-3→L+1 (26%); H-1→LUMO (10%)
	Singlet-A	312.710	0.0005	H-1→LUMO (87%);
	Singlet-A	287.660	0.0044	H-2→LUMO (88%);
	Singlet-A	286.600	0.3159	HOMO→LUMO (68%); H-4→LUMO (6%); H-4→L+1 (2%); HOMO→L+1 (7%)
dcbpyr	Triplet-A	425.810		H-4→LUMO (13%); HOMO→LUMO (69%); HOMO→L+2 (35%); H-7→L+1 (7%)
	Triplet-A	407.320		H-2→L+1 (11%); H-1→LUMO (92%); H-1→L+6 (3%);
	Triplet-A	369.470		H-2→LUMO (59%); H-1→L+1 (43%); H-2→L+6 (3%);
	Singlet-A	360.690		H-1→LUMO (88%); H-2→L+1 (2%);
	Singlet-A	348.790	0.1497	HOMO→LUMO (76%); H-4→L+2 (4%); HOMO→L+2 (3%);
	Singlet-A	338.250	0.0028	H-2→LUMO (48%); H-1→L+1 (37%);
phn	Triplet-A'	450.900		H-2→L+1 (21%); HOMO→LUMO (103%); H-6→L+10 (2%); H-5→L+4 (3%)
	Triplet-A'	361.340		HOMO→L+1 (99%); H-4→LUMO (6%); H-4→L+4 (2%);5-→11

				(6)
	Triplet-A"	359.10	0	H-3→LUMO (13%); H-1→L+1 (86%); H-3→L+4 (3%); H-1→L+2 (5%)
	Singlet-A"	344.24	0	H-1→L+1 (83%); H-3→LUMO (2%);35-→11 (-24);35-→11 (-24)
	Singlet-A'	325.89	0.0003	H-2→LUMO (28%); HOMO→L+1 (66%);4-→9 (5);4-→9 (5)
	Singlet-A"	321.38	0.0013	H-1→LUMO (90%); H-3→L+1 (2%);35-→4 (-31);35-→4 (-31)
dmphn	Triplet-A	449.21	0	H-1→LUMO (22%); HOMO→L+1 (100%); H-5→L+4 (3%); H-4→LUMO (4%)
	Triplet-A	370.29	0	HOMO→LUMO (104%); H-4→L+1 (4%);5-→10 (5);5-→10 (5)
	Triplet-A	352.06	0	H-3→L+1 (10%); H-2→LUMO (87%); H-3→L+4 (3%); H-2→L+2 (6%)
	Singlet-A	349.04	0.0013	H-1→L+1 (22%); HOMO→LUMO (68%);4-→9 (5);4-→9 (5)
	Singlet-A	326.74	0	H-2→LUMO (89%);35-→10 (-25);35-→10 (-25);29-→80 (51)
	Singlet-A	317.39	0.0011	H-2→L+1 (89%);35-→4 (-31);35-→4 (-31);29-→92 (63)
dcphn	Triplet-A	489.24	0	HOMO→LUMO (108%); H-10→L+5 (3%); H-7→L+3 (2%); H-6→L+1 (5%)
	Triplet-A	392.59	0	H-3→L+1 (12%); H-1→LUMO (74%); H-1→L+1 (11%); H-3→L+2 (3%)
	Triplet-A	382.38	0	H-3→LUMO (37%); H-1→L+1 (48%); H-3→L+1 (9%); H-3→L+5 (2%)
	Singlet-A	371.54	0.0005	H-1→LUMO (87%);21-→5 (-16);38-→5 (-33);40-→90 (50)
	Singlet-A	358.76	0.1912	HOMO→LUMO (71%); H-2→L+1 (9%);4-→7 (3);3-→6 (3)
	Singlet-A	351.69	0.0002	H-3→LUMO (57%); H-1→L+1 (23%); H-1→L+2 (6%);38-→8 (-30)

Table 4.43: The molecular orbital (MO) contribution of the nitrogen atom(s) “N” available for metal coordination.

		bpyr		
	eV	N9	N5	others
L+5	0.14	-7	-7	116
L+4	0.03	-1	0	103
L+3	-0.12	-11	-11	124
L+2	-0.94	10	10	81
L+1	-1	5	5	90
LUMO	-1.6	10	10	80
HOMO	-6.81	2	2	96
H-1	-7.02	36	36	29
H-2	-7.22	34	34	32
H-3	-7.78	6	6	88
H-4	-7.97	16	15	69
H-5	-8.19	7	8	85
H-6	-9.98	5	5	90
H-7	-10.45	5	5	90
		dmbpyr		
	eV	N10	N6	others
L+5	0.19	-4	-4	111
L+4	0.03	1	1	99
L+3	-0.08	-11	-12	125
L+2	-0.74	10	8	83
L+1	-0.8	4	6	90
LUMO	-1.47	9	9	82
HOMO	-6.66	3	3	95
H-1	-6.9	35	36	29
H-2	-7.08	34	33	33
H-3	-7.54	10	11	79
H-4	-7.56	14	13	73
H-5	-7.8	2	2	96
H-6	-9.63	4	4	92
H-7	-10.1	3	3	93
		dcbpyr		
	eV	N8	N12	others
L+5	-0.25	-1	-3	106
L+4	-0.36	-8	-3	113
L+3	-0.42	2	2	96
L+2	-1.9	0	0	99
L+1	-2.21	5	7	87
LUMO	-2.7	12	10	77
HOMO	-7.13	2	2	95
H-1	-7.26	34	38	28
H-2	-7.79	35	31	34

H-3	-8.34	10	6	84
H-4	-8.36	10	17	72
H-5	-8.41	0	2	98
H-6	-8.48	2	0	97
H-7	-8.74	5	3	93

phn

	eV	N12	N10	others
L+5	0.13	-6	-6	114
L+4	0.03	4	4	91
L+3	-0.05	-6	-6	113
L+2	-0.64	4	4	92
L+1	-1.76	12	12	77
LUMO	-1.82	4	4	92
HOMO	-6.51	4	4	92
H-1	-6.84	35	35	30
H-2	-6.89	4	4	92
H-3	-7.31	34	34	33
H-4	-8.19	14	14	71
H-5	-8.39	2	2	95
H-6	-9.4	10	10	80
H-7	-9.86	4	4	92

dmphn

	eV	N12	N10	others
L+5	0.18	-12	-12	126
L+4	0.11	3	3	93
L+3	0.02	-7	-7	115
L+2	-0.47	5	5	90
L+1	-1.57	4	4	92
LUMO	-1.6	10	10	80
HOMO	-6.23	5	5	90
H-1	-6.65	2	2	95
H-2	-6.67	35	35	29
H-3	-7.14	34	34	33
H-4	-7.92	17	17	65
H-5	-8.14	1	1	97
H-6	-9.06	11	11	77
H-7	-9.64	4	4	92

dcphn

	eV	N13	N11	others
L+5	-0.19	5	5	90
L+4	-0.27	-6	-4	112
L+3	-0.53	1	1	98
L+2	-1.84	2	2	97
L+1	-2.17	15	16	69
LUMO	-2.76	5	5	90

HOMO	-6.99	4	3	93
H-1	-7.28	21	38	40
H-2	-7.34	4	5	91
H-3	-7.7	46	13	41
H-4	-7.93	2	0	98
H-5	-8.23	0	18	82
H-6	-8.6	13	13	74
H-7	-8.73	1	1	97

Table 4.44: The non-linear conductive properties of the ligands

	Dipole	<α>	Δα1	Δα2	Δα3	Γ	ß in esu (1x10-30)	HOMO	LUMO	Gap in KJ/mol	Non-Valence Lewis Orbitals
bpyr	3.24	136.67	-7.32	112.51	6302.94	-3.49	0.48	-0.2501	-0.0586	502.88	2.98%
dmbpyr	3.99	166.03	5.71	123.62	7624.68	-5.31	0.49	-0.2447	-0.0541	500.41	2.59%
dcbpyr	2.67	184.39	-129.75	165.79	5326.43	-7.13	1.61	-0.2622	-0.0990	428.47	2.67%
phn	3.43	165.31	-129.38	152.69	3287.10	-3.79	0.35	-0.2391	-0.0668	452.54	2.85%
dmphn	2.30	197.84	-134.72	168.35	5095.27	-5.96	2.94	-0.2289	-0.0588	446.54	2.49%
dcphn	6.06	218.27	-149.89	200.47	8861.17	-8.22	6.48	-0.2569	-0.1015	407.98	3.31%

Table 5.1: The synthesised complexes and their starting materials

	Starting Material	mmol	Solvent	Product	% yield
ST1	$RuCl_3 \cdot 3H_2O$	7.62	dmso	$RuCl_2(dmso)_4$	40.04
ST2	$RuCl_3 \cdot 3H_2O$	7.016	Ethanol	$[(cym)RuCl_2]_2$	60.20
ST3	$RuCl_3 \cdot 3H_2O$	11.2	Hcl	$Ru(bdmpzm)Cl_4$	47.50
ST4	$RuCl_3 \cdot 3H_2O$	1.2	Hcl	$Ru(bpzm)Cl_4$	62.86
C1	$RuCl_3 \cdot 3H_2O$	0.237	DMF	$[Ru(bpzm)_3]^{2+}$	20.06
C2	$RuCl_3 \cdot 3H_2O$	0.33	DMF	$[Ru(bpza)_3]^{2+}$	24.94
C3	$RuCl_3 \cdot 3H_2O$	0.702	EtOH	$[Ru(bdmpzm)_3]^{2+}$	18.45
C4	$RuCl_3 \cdot 3H_2O$	0.333	DMF	$[Ru(bdmpza)_3]^{2+}$	16.89
C5	$RuCl_3 \cdot 3H_2O$	0.622	EtOH	$Ru(bpzm)_2Cl_2$	23.69
C6	RuCl2(dmso)4	0.5	DMF	$Ru(bpza)_2Cl_2$	68.30
C7	$RuCl_3 \cdot 3H_2O$	2.85	EtOH	$Ru(bdmpzm)_2Cl_2$	60.79
C8	$RuCl_2(dmso)_4$	0.5	DMF	$Ru(bdmpza)_2Cl_2$	59.83
C9	$RuCl_2(dmso)_4$	0.5	DMF	$Ru(bpza)(bdmpza)Cl_2$	52.45

C10	$Ru(bdmpzm)Cl_4$	0.5 CH_2Cl_2	$Ru(bpza)(bdmpzm)Cl_2$	80.26
C11	$RuCl_2(dmso)_4$	0.4 DMF	$Ru(bpza)(bphpza)Cl_2$	30.77
C12	$RuCl_2(dmso)_4$	0.5 DMF	$Ru(bpza)(bpyr)Cl_2$	81.75
C13	$RuCl_2(dmso)_4$	0.5 DMF	$Ru(bpza)(dmbpyr)Cl_2$	67.76
C14	$RuCl_2(dmso)_4$	0.5 DMF	$Ru(bpza)(phn)Cl_2$	74.62
C15	$RuCl_2(dmso)_4$	0.5 DMF	$Ru(bpza)(dmphn)Cl_2$	37.77
C16	$Ru(bdmpzm)Cl_4$	0.4 THF	$Ru(bdmpzm)(bdmpza)Cl_2$	53.52
C17	$RuCl_2(dmso)_4$	0.4 DMF	$Ru(bdmpza)(bphpza)Cl_2$	28.22
C18	$RuCl_2(dmso)_4$	0.5 DMF	$Ru(bdmpza)(pyr)Cl_2$	15.15
C19	$RuCl_2(dmso)_4$	0.5 DMF	$Ru(bdmpza)(bmpyr)Cl_2$	24.12
C20	$RuCl_2(dmso)_4$	0.5 DMF	$Ru(bdmpza)(dmphn)Cl_2$	15.96
C21	$Ru(bdmpzm)Cl_4$	0.4 DMF	$Ru(bdmpzm)(bpzm)Cl_2$	50.68
C22	$Ru(bdmpzm)Cl_4$	0.4 DMF	$Ru(bdmpzm)(bphpza)Cl_2$	54.95
C23	$Ru(bdmpzm)Cl_4$	0.4 Toluene	$[Ru(bdmpzm)(bpzpy)Cl]^+$	27.44
C24	$Ru(bdmpzm)Cl_4$	0.4 THF	$[Ru(bdmpzm)(bdmpzpy)Cl]^+$	15.00
C25	$[(cym)RuCl_2]_2$	0.09 Methanol	$(cym)Ru(pz)Cl_2$	80.15
C26	$[(cym)RuCl_2]_2$	0.09 Methanol	$(cym)Ru(dmpz)Cl_2$	78.71
C27	$[(cym)RuCl_2]_2$	0.08 Methanol	$(cym)Ru(dcpz)Cl_2$	28.39
C28	$[(cym)RuCl_2]_2$	0.1633 Methanol	$[(cym)Ru(bpzm)Cl]^+$	92.31
C29	$[(cym)RuCl_2]_2$	0.1633 CH_3CN	$[(cym)Ru(bpza)Cl]^+$	20.58
C30	$[(cym)RuCl_2]_2$	0.1633 CH_3CN	$[(cym)Ru(bmpzm)Cl]^+$	24.87
C31	$[(cym)RuCl_2]_2$	0.088 CH_3CN	$[(cym)Ru(bmpza)Cl]^+$	44.50
C32	$[(cym)RuCl_2]_2$	0.1633 Methanol	$[(cym)Ru(bphpza)Cl]^+$	62.44
C33	$[(cym)RuCl_2]_2$	0.1633 Methanol	$[(cym)Ru(pyr)Cl]^+$	25.16
C34	$[(cym)RuCl_2]_2$	0.1633 Methanol	$[(cym)Ru(phn)Cl]^+$	97.62
C35	$[(cym)RuCl_2]_2$	0.1633 Methanol	$[(cym)Ru(bmpyr)Cl]^+$	90.33
C36	$[(cym)RuCl_2]_2$	0.1633 Methanol	$[(cym)Ru(dmphn)Cl]^+$	58.39
C37	$[(cym)RuCl_2]_2$	0.1633 Methanol	$[(cym)Ru(dcbpyr)Cl]^+$	36.65
C38	$[(cym)RuCl_2]_2$	0.1633 CH_3CN	$[(cym)Ru(dcphn)Cl]^+$	41.47
C39	$[(cym)RuCl_2]_2$	0.1633 Methanol	$[(cym)Ru(bpzpy)]^{2+}$	75.06
C40	$[(cym)RuCl_2]_2$	0.1633 Methanol	$[(cym)Ru(bdmpzpy)]^{2+}$	43.97

Table 5.2: The calculated and the found elemental analysis of the synthesised complexes (those in red is an indication of the presence of impurities).

	Calculat	Found

		ed					
		C	H	S	C	H	S
ST1	$RuCl_2(dmso)_4$	19.83	4.99	26.47	20.04	4.418	25.822
		C	H	N	C	H	N
ST2	$[(cym)RuCl_2]_2$	39.23	4.61	0	39.31	4.61	0
ST3	$Ru(bdmpzm)Cl_4$	29.55	3.61	12.53	30.06	4.14	12.32
ST4	$Ru(bpzm)Cl_4$	21.5	2.06	14.33	21.06	2.028	14.65
C1	$[Ru(bpzm)_3]^{2+}$	30.19	2.9	20.12	24.944	1.922	17.706
C2	$[Ru(bpza)_3]^{2+}$	29.79	2.5	17.37	30.28	2.743	18.92
C3	$[Ru(bdmpzm)_3]^{2+}$	39.49	4.82	16.74	39.514	4.665	16.093
C4	$[Ru(bdmpza)_3]^{2+}$	38.07	4.26	14.8	38.63	4.451	14.618
C5	$Ru(bpzm)_2Cl_2$	35.91	3.44	23.93	28.422	2.12	17.914
C6	$Ru(bpza)_2Cl_2$	34.54	2.9	20.14	34.581	3	20.186
C7	$Ru(bdmpzm)_2Cl_2$	45.52	5.56	19.3	35.438	3.881	15.263
C8	$Ru(bdmpza)_2Cl_2$	43.12	4.82	16.76	43.435	4.964	17.089
C9	$Ru(bpza)(bdmpza)Cl_2$	39.22	3.95	18.3	39.112	4.477	18.494
C10	$Ru(bpza)(bdmpzm)Cl_2$	40.15	4.26	19.71	40.21	4.685	19.76
C11	$Ru(bpza)(bphpza)Cl_2$	47.47	3.41	15.82	47.903	3.364	15.834
C12	$Ru(bpza)(bpyr)Cl_2$	41.55	3.1	16.15	41.87	3.9	16.77
C13	$Ru(bpza)(dmbpyr)Cl_2$	43.8	3.68	15.32	43.95	3.933	15.202
C14	$Ru(bpza)(phn)Cl_2$	44.13	2.96	15.44	41.34	4.138	15.3
C15	$Ru(bpza)(dmphn)Cl_2$	46.16	3.52	14.68	45.876	2.91	14.237
C16	$Ru(bdmpzm)(bdmpza)Cl_2$	44.23	5.16	17.94	37.639	2.909	14.467
C17	$Ru(bdmpza)(bphpza)Cl_2$	50.27	4.22	14.65	50.35	4.641	14.899
C18	$Ru(bdmpza)(pyr)Cl_2$	45.84	4.2	14.58	46.092	4.014	14.082
C19	$Ru(bdmpza)(dmbpyr)Cl_2$	47.69	4.67	13.9	47.17	4.23	13.43
C20	$Ru(bdmpza)(dmphn)Cl_2$	49.69	4.49	13.37	49.605	4.221	13.983
C21	$Ru(bdmpzm)(bpzm)Cl_2$	41.23	4.61	21.37	32.4	4.819	18.11
C22	$Ru(bdmpzm)(bphpza)Cl_2$	51.67	4.48	15.55	41.92	5.992	14.15
C23	$[Ru(bdmpzm)(bpzpy)Cl]^+$	37.91	3.62	18.09	30.914	2.455	12.897
C24	$[Ru(bdmpzm)(bdmpzpy)Cl]^+$	41.47	4.42	16.74			
C25	$(cym)Ru(pz)Cl_2$	41.72	4.85	7.48	41.9	4.587	7.52
C26	$(cym)Ru(dmpz)Cl_2$	44.78	5.51	6.96			
C27	$(cym)Ru(dcpz)Cl_2$	38.97	3.92	6.06	38.8	3.947	6.29
C28	$[(cym)Ru(bpzm)Cl]^+$	36.21	3.93	9.94	36.57	3.856	10.31
C29	$[(cym)Ru(bpza)Cl]^+$	35.57	3.65	9.22			
C30	$[(cym)Ru(bmpzm)Cl]^+$	40.68	4.88	9.04	40.45	4.785	8.82
C31	$[(cym)Ru(bmpza)Cl]^+$	39.8	4.55	8.44	39.59	4.258	7.91
C32	$[(cym)Ru(bphpza)Cl]^+$	47.41	3.98	7.37	47.93	3.971	7.46
C33	$[(cym)Ru(pyr)Cl]^+$	42	3.88	4.9			
C34	$[(cym)Ru(phn)Cl]^+$	44.34	3.72	4.7	44.11	3.796	4.77
C35	$[(cym)Ru(dmbpyr)Cl]^+$	44.04	4.37	4.67	44.14	4.593	4.71
C36	$[(cym)Ru(dmphn)Cl]^+$	46.2	4.2	4.49	46.23	4.264	4.52
C37	$[(cym)Ru(bcpyr)Cl]^+$	40.04	3.36	4.25	32.1	3.931	0.44
C38	$[(cym)Ru(dcphn)Cl]^+$	53.48	4.11	5.2	31.25	3.298	1.7

C39	$[(cym)Ru(bpzpy)]^{2+}$	42.64	3.92	11.84	34.19	3.035	6.45
C40	$[(cym)Ru(bdmpzpy)]^{2+}$	46.37	4.82	10.81	33.55	3.912	0.31

Table 5.3: The Assignment of the prominent IR binbrations of the complexes using PED

Freq.	Int.	Assignment	Freq.	Int.	Assignment	Freq.	Int.	Assignment	Freq.	Int.	Assignment
ST1=$RuCl_2(dmso)_4$			**ST2=$[(cym)RuCl_2]_2$**			**ST3=$Ru(bdmpzm)Cl_4$**			**ST4=$Ru(bpzm)Cl_4$**		
2990.83	31.92	υ(CH), υ(CH)	2977.67	48.48	υ(CH), υ(CH)	2981.45	31.04	υ(CH), υ(CH)	1431.77	46.62	β(CNN), υ(CC)
1297.12	37.04	β(HCH), β(HCH)	2970.37	51.44	υ(CH), υ(CH)	2948.76	63.82	υ(CH),	1430.68	35.89	υ(CC), β(CNN)
1073.25	205.33	υ(SO),	292.65	31.67	υ(RuCl),	1573.86	34.88	υ(CC), β(HCC)	1392.46	38.38	β(HCN), τ(HCNN)
1057.31	178.88	υ(SO), υ(SO)				1559.01	30.39	υ(CC), β(HCC)	1276.72	87.78	υ(NN), υ(NC)
1053.2	77.73	υ(SO), υ(SO)				1488.05	39.34	υ(CC),	1273.39	40.96	υ(NC),
1048.07	115.72	υ(SO),				1480.42	56.69	υ(CC),	1054.09	53.68	β(HCC), υ(CC)
1006.64	156.25	τ(HCSRu), τ(HCSRu)				1410.75	35.55	β(HCH), β(HCH)	724.46	56.88	τ(HCCC), τ(HCCN)
1005.51	33.81	τ(HCSRu), τ(HCSRu)				1400.26	57.88	β(HCH), β(HCH)	720.71	30.89	τ(HCCN), τ(HCCC)
396.76	35.95	β(CSO), β(OSC)				1283.49	76.79	υ(NC),	398.75	30.94	β(CNRu), τ(HCNN)
389.15	32.13	o(ORuCS), β(OSC)				1234.99	37.93	υ(CC), β(CNN)	329.21	70.52	υ(RuCl),
385.99	42.04	o(OCRuS), β(CSO)				349.5	38.95	υ(RuCl), υ(RuCl)	263.75	36.39	υ(RuCl),
						314.34	59.24	υ(RuCl),			
						304.36	31.9	υ(RuCl), υ(RuCl)			
C1=$[Ru(bpzm)_3]^{2+}$			**C2=$[Ru(bpza)_3]^{2+}$**			**C3=$[Ru(bdmpzm)_3]^{2+}$**			**C4=$[Ru(bdmpza)3]^{2+}$**		
1432.38	60.2	β(CNN),	3601.02	174.07	υ(OH),	1587.69	55.41	υ(CC), υ(CC)	3618.09	125.4	υ(OH),
1427.35	30.14	β(CNN), υ(NC)	1852.3	262.85	υ(OC),	1579.57	56.63	υ(CC),	3604.23	116.37	υ(OH),
1273.27	101.41	υ(NN), υ(NC)	1850.11	135.19	υ(OC),	1575.63	41.83	β(CCN), υ(CC)	3534.02	124.76	υ(OH),
1270.05	33.21	υ(NN), υ(NC)	1805.59	175.33	υ(OC),	1567.04	40.66	υ(CC), υ(CC)	2959.06	187	υ(CH),
1266.49	94.76	υ(NN), υ(NC)	1436.28	60.29	β(CNN),	1565.07	42.39	υ(CC), υ(CC)	1827.63	147.97	υ(OC),
1263.23	35.28	υ(NN),	1303.7	128.23	τ(HCCO), υ(NC)	1450.93	36.06	β(HCH), β(HCH)	1820.18	283.5	υ(OC),
1055.04	32.92	β(HCC), β(HCC)	1295.93	68.3	τ(HCCO), υ(NC)	1422.65	38.84	β(HCH),	1594.42	57.37	υ(CC),
739.93	79.43	τ(HCCN), τ(HCCC)	1293.39	115.31	τ(HCCO), υ(NC)	1419.67	56.42	β(HCH),	1588.7	52.01	υ(CC), υ(CC)
738.04	42.84	τ(HCCN), τ(HCCC)	1263.45	205.11	υ(OC), β(HOC)	1418.1	37.12	β(HCH), β(HCH)	1570.42	62.83	υ(CC), υ(CC)
736.92	63.29	τ(HCCN), τ(HCCC)	1259.28	211.91	υ(OC), β(HCC)	1403.46	58.45	υ(NC), β(CCN)	1421.03	51.69	β(HCH), β(HCH)
735.31	75.8	τ(HCCN), τ(HCCC)	1251.82	189.39	υ(OC), β(HCC)	1283.75	102.0	υ(NC),	1386.22	60.16	υ(NC),

						2					
730.87	47.33	τ(HCCN), τ(HCCC)	1187.99	58.39	β(HCC),	1281.33	32.83	β(CNC), υ(NC)	1380.67	65.5	υ(NC),
			1126.66	144.6	υ(OC), β(HOC)	1274.33	83.5	υ(NN),	1314.46	51.1	β(CNN), τ(HCCO)
			743.95	99.49	τ(HCCC), τ(HCCN)	1269.59	89.69	β(HCN), υ(NC)	1304.11	129.28	τ(HCCO), υ(NC)
			743	59.83	τ(HCCC), τ(HCCN)	1257.14	87.05	β(HCN),	1301.94	142.95	τ(HCCO), υ(NC)
			743.5	57.73	τ(HCCC), τ(HCCN)	1246.09	47.32	β(HCN), τ(HCNN)	1255.07	182.68	β(HOC), υ(OC)
			721.76	73.88	τ(HOCC),	1218.28	41.9	β(CNN), υ(NN)	1252.55	122.03	β(HCC), υ(NN)
			649.73	75.66	β(OCO),				1230.72	79.93	β(HCC),
			517	97.66	τ(HOCC),				1138.65	140.28	β(HOC), υ(OC)
			506.85	97.03	τ(HOCC),				676.27	93.93	τ(HOCC),
C5=Ru(bpzm)$_2$Cl$_2$			**C6=Ru(bpza)$_2$Cl$_2$**			**C7=Ru(bdmpzm)$_2$Cl$_2$**			**C8=(bdmpza)$_2$RuCl$_2$**		
2939.91	195.3	υ(CH), υ(CH)	3633.31	104.73	υ(OH),	3006.97	45.51	υ(CH), υ(CH)	3641.06	81.38	υ(OH),
1459.06	57.41	υ(NC),	3548.58	147.96	υ(OH),	2977.61	77.42	υ(CH), υ(CH)	3633.85	52.72	υ(OH),
1394.03	57.76	β(HCH), β(HCH)	2828.24	244.11	υ(CH),	2973.91	98.35	υ(CH), υ(CH)	2975.54	35.52	υ(CH), υ(CH)
1338.51	38.4	υ(CC), τ(HCNN)	2645.38	559.78	υ(CH),	2970.65	62.47	υ(CH), υ(CH)	2967.85	42.08	υ(CH), υ(CH)
1260.79	46.79	υ(CC), υ(NC)	1788.95	214.02	υ(OC),	2954.54	61.87	υ(CH), υ(CH)	2696.89	352.03	υ(CH),
1102.3	101.33	β(CNN),	1763.94	318.82	υ(OC),	1586.77	59.22	υ(CC),	1792.86	170.15	υ(OC),
1088.85	41.71	β(CNN), β(CCN)	1368.07	56.83	υ(CC), β(HCC)	1577.4	38.07	υ(CC),	1779.29	258.86	υ(OC),
695.39	126.68	τ(HCCC), τ(HCCC)	1307.09	68.47	τ(HCCO), υ(NC)	1431.28	51.32	β(HCH), β(HCH)	1597.25	36	υ(CC),
691.96	95.01	τ(HCCC), τ(HCCC)	1289.27	340.21	υ(OC), β(HOC)	1415.06	42.41	β(HCH), β(HCH)	1425.93	43.98	β(HCH),
			1128.27	214.94	υ(OC), β(HOC)	1305.68	119.29	υ(NN),	1314.64	108.02	τ(HCCO), β(HOC)
			1089.69	66.4	β(HCC), β(CNN)	1304.44	37.05	υ(NC),	1310.12	43.05	υ(NC),
			1085.94	54.79	β(HCC), β(CCN)	1190.34	86.62	β(CNN), υ(NN)	1171.17	63.47	υ(NN),
			717.54	60.28	τ(HCCN), τ(HCCC)				1147.71	53.72	β(HCC), β(HCC)
			714.29	62.9	τ(HCCN), τ(HCCC)				1142.9	146.74	υ(OC), β(HCC)
			712.85	70.28	τ(HCCC), τ(HCCN)				1120.64	84.96	υ(OC), β(HOC)
			696.84	46.35	τ(HCCC), τ(HCCN)				636.27	79.17	β(OCO), τ(HOCC)
			669.5	47.02	τ(HOCC), o(CNCN)				621.27	47.5	τ(CCNN),
			640.46	84.91	τ(HOCC), o(CNRuN)				612.69	35.3	β(OCO), τ(CCNN)

			633.36	48.7	o(CNRuN), β(OCO)				574.81	35.95	β(OCO), o(OCOC)
			604.32	62.13	τ(HOCC),				455.61	40.52	τ(HOCC),
C9=Ru(bpza)(bdmpza)Cl_2			**C10=Ru(bpza)(bdmpzm)Cl_2**			**C11=Ru(bpza)(bphpza)Cl_2**			**C12=Ru(bpza)(bpyr)Cl_2**		
3651.58	65.32	υ(OH),	3629.1	61.16	υ(OH),	3645.1	66.81	υ(OH),	3492.17	244.99	υ(OH),
3638.45	81.23	υ(OH),	2983.13	33.55	υ(CH), υ(CH)	3637.73	89.19	υ(OH),	2831.22	283.24	υ(CH),
2993.25	67.41	υ(CH), υ(CH)	2970.66	77.55	υ(CH), υ(CH)	3130.89	50.82	υ(CH), υ(CH)	1786.83	233.3	υ(OC),
2558.36	709.61	υ(CH),	1777.95	205.59	υ(OC),	3124.53	78.41	υ(CH), υ(CH)	1472.35	41.36	υ(CC), υ(CC)
1812.42	173.7	υ(OC),	1582.94	32.75	υ(CC), υ(CC)	3120.02	44.36	υ(CH), υ(CH)	1446.66	51.37	υ(CC), β(HCC)
1783.21	275.37	υ(OC),	1468.34	34.74	υ(NC), β(CNN)	2637.58	507.25	υ(CH),	1409.89	35.1	υ(NC), β(HCC)
1394.81	47.99	υ(NC), β(CNN)	1420.62	37.85	β(HCH), β(CNN)	1806.51	205.87	υ(OC),	1327.29	48.45	υ(NC), υ(NC)
1317.34	80.07	τ(HCCO),	1384.73	36.06	υ(NC), β(CNN)	1785.07	269.05	υ(OC),	1304.07	43	τ(HCCO), υ(CC)
1155.15	52.23	υ(OC), β(HCC)	1300.69	84.9	υ(NC), β(CNC)	1377.62	49.47	τ(HCCO), υ(NC)	1300.85	299.49	β(HOC),
1143.57	145.31	υ(OC), β(HCC)	1290.13	31.29	υ(NC),	1328.18	83.97	τ(HCCO), υ(NC)	1221.05	42.03	υ(NN),
1131.66	131.08	υ(OC), β(HOC)	1167.53	51.96	υ(CC),	1201.35	48.21	υ(NC), β(HCC)	1088.05	32.63	υ(NC), β(CCN)
1114.3	67.85	υ(NN), β(HOC)	1137.26	35.76	β(HCC),	1133.94	252.41	υ(OC), β(HOC)	1086.46	34.9	υ(NC), β(CNN)
1098.1	44.75	β(HCC), β(CNN)	1130.03	93.83	υ(OC), β(HOC)	1130.99	125.55	υ(OC), β(HOC)	1015.56	41.49	β(CCN), β(CCC)
685.54	50.89	τ(HCCN), τ(HCCC)	1096.98	51.17	υ(NC), β(HCC)	1096.86	65.2	β(HCC),	950.17	38.02	υ(NC), β(CNN)
674.19	118.19	τ(HOCC), β(OCO)	944.06	35.82	υ(NC), β(CCN)	730.67	68.35	τ(HCCC), τ(HCCN)	733.34	72.39	τ(HCCC), τ(HCCC)
654.08	42.18	τ(HOCC), o(CNRuN)	682.84	118.14	τ(HCCC), τ(HCCN)	684.72	50.89	o(NRuCN), β(CCC)	723.19	61.38	τ(HCCN), τ(HCCN)
642.8	58.71	τ(CNNC),	669.77	50.6	τ(HCCN), τ(HCCC)	683.48	46.45	τ(HCCN), τ(HCCC)	719.38	58.9	τ(HCCN), τ(HCCN)
632.32	43.18	τ(CCNN), β(OCO)	650.8	38.5	o(CNRuN),	671.51	92.99	τ(CCNN), β(OCO)	706.51	32.33	τ(CCNC), τ(CCCC)
566.74	66.35	τ(HOCC), β(OCO)	602.36	66.42	τ(HOCC), τ(CNNRu)	664.08	46.52	τ(HOCC), β(CCC)	615.17	45.19	o(OCOC), υ(NC)
			478.78	42.22	τ(HOCC), β(CNC)	647.38	91.73	β(OCO), τ(HOCC)			
C13=Ru(bpza)(dmbpyr)Cl_2			**C14=Ru(bpza)(phn)Cl_2**			**C15=Ru(bpza)(dmphn)Cl_2**			**C16=Ru(bdmpza)(bdmpzm)Cl_2**		
3477.54	275.9	υ(OH),	3491.17	258.43	υ(OH),	3335.07	514.78	υ(OH),	2982.61	31.8	υ(CH), υ(CH)
2979.88	50.03	υ(CH), υ(CH)	2834.08	297.79	υ(CH),	2897.62	286.03	υ(CH),	2976.56	33.25	υ(CH), υ(CH)
2979.73	36.01	υ(CH), υ(CH)	1786.95	241.28	υ(OC),	1782.08	287.3	υ(OC),	2974.21	62.74	υ(CH), υ(CH)

						3					
2832.28	287.7	υ(CH),	1505.81	34.21	υ(CC), υ(NC)	1458.91	30.49	β(HCH), β(HCH)	2946.37	1023.25	υ(OH),
1786.2	241.1	υ(OC),	1326.97	47.42	υ(NC), υ(OC)	1454.03	37.65	β(HCH), β(HCH)	1762.11	275.83	υ(OC), υ(OC)
1464.59	49.81	β(HCC), β(HCC)	1303.98	99.38	τ(HCCO), υ(NC)	1351.06	30.15	τ(HCCO), υ(NC)	1586.95	61.92	υ(CC),
1447.99	52.02	β(HCH), β(HCH)	1299.92	238.86	β(HOC),	1342.59	153.58	υ(OC), β(HOC)	1467.18	30.68	β(CNN), υ(CC)
1446.54	34.91	β(HCH), β(HCH)	1219.96	43.07	υ(NN),	1315.85	70.55	υ(NC), β(HOC)	1324.59	75.04	υ(OC), β(HCC)
1327.26	48.58	υ(NC), β(HOC)	1188.89	36.58	β(HCC), β(HCC)	1282.8	31.81	τ(HCCO), υ(NC)	1322.44	93.39	τ(HCCO), υ(OC)
1303.11	32.35	τ(HCCO), υ(CC)	1087.37	39.91	β(CNN),	1208.69	44.03	υ(NC), β(HCC)	1304.41	77.21	β(CNC), υ(NC)
1301.78	282.78	υ(OC), β(HOC)	1085.72	40.39	β(HCC), β(CNN)	1093.35	59.55	β(HCC), β(CNN)	1256.37	33.02	υ(OC), β(HCC)
1219.45	44.39	υ(NN),	950.1	39.87	β(CNN),	827.16	64.02	τ(HCCC), τ(HCCC)	1229.37	52.06	β(HCC),
1087.68	35.97	υ(NC), β(CCN)	817.35	61.33	τ(HCCC), τ(HCCC)	736.33	40.22	τ(HCCC), τ(HCCN)	1178.58	53.63	β(CNN),
1085.75	33.83	υ(NC), β(CNN)	723.28	55.05	τ(HCCC), τ(HCCN)	726.42	70.22	τ(HCCC), τ(HCCN)	1173.41	112.65	β(HOC),
1015.64	52.36	β(CCN), β(CCC)	718.21	62.77	τ(HCCC), τ(HCCN)	722.6	33.29	τ(HOCC),	808.69	31.69	τ(HOCC),
949.57	45.14	υ(NC), β(CNN)	701.97	40.76	τ(CCCC),	689.93	31.81	ο(CNRuN), β(OCO)			
800.09	44.71	τ(HCCN), τ(HCCC)	681.72	31.54	β(OCO),						
721.77	54.79	τ(HCCN), τ(HCCN)	615.16	44.95	υ(NC), τ(COOC)						
717.75	67.76	τ(HCCN), τ(HCCN)	with								
617.76	42.33	ο(OCOC), υ(NC)	IR								
C17=Ru(bdmpza)(bphpza)Cl2			**C18=Ru(bdmpza)(pyr)Cl_2**			**C19=Ru(bdmpza)(dmbpyr)Cl_2**			**C20=Ru(bdmpza)(dmphn)Cl_2**		
3649.66	65.36	υ(OH),	3253.9	578.32	υ(OH),	3188.99	737.68	υ(OH),	3239.32	624.12	υ(OH),
3458.99	248.2	υ(OH),	2982.88	49.68	υ(CH), υ(CH)	2979.19	48.65	υ(CH), υ(CH)	2841.16	300.27	υ(CH),
3186.79	58.24	υ(CH),	2819.62	328.3	υ(CH),	2977.92	55.05	υ(CH), υ(CH)	1805.94	323.83	υ(OC),
3046.21	95.09	υ(CH),	1808.14	323.11	υ(OC),	2976.49	32.74	υ(CH), υ(CH)	1574.04	37.31	υ(CC),
1800.67	177.95	υ(OC),	1572.24	30.11	υ(CC), β(HCC)	2816.97	342.12	υ(CH),	1451.35	44.56	υ(CC),
1785.54	119.13	υ(OC),	1569.79	30.79	υ(CC), β(CCN)	1782.56	379.48	υ(OC),	1409.81	58.03	υ(NC), β(HCH)
1499.11	46.21	υ(CC), β(HCC)	1475.94	34.86	υ(CC), υ(CC)	1564.68	32.61	υ(CC), β(HCC)	1394.86	42.24	β(CNN), υ(NC)
1336.81	59.69	υ(OC), β(HOC)	1413.44	34.81	υ(NC), β(HCC)	1471.08	32.03	υ(CC), υ(CC)	1352.05	201.81	υ(OC), β(HOC)
1271.98	48.68	υ(NN), υ(NC)	1406.58	72.78	υ(NC), β(HCH)	1447.7	41.01	β(HCH),	1327.57	30.92	υ(NC),

1219.7	162.72	υ(NC), β(HCC)
1183.48	125.5	υ(NC), β(HCC)
1136.59	87.51	υ(OC), β(HOC)
1129.09	155.49	υ(OC), β(HOC)
798.2	101.75	β(CCO), υ(NC)
763.65	70.55	τ(HCCC), τ(HCCC)
745.58	61.98	τ(HCCC), τ(HCCC)
736.02	96.91	τ(HCCN), τ(HCCC)
676.36	67.25	β(CCC), o(OCOC)
669.06	49.42	β(CCC), o(OCOC)
637.13	61.15	τ(HOCC), o(CCNN)

C21=Ru(bdmpzm)(bpzm)Cl$_2$

2972.94	93.03	υ(CH), υ(CH)
2965.16	96.03	υ(CH), υ(CH)
2942.81	189.07	υ(CH),
1568.44	49.38	υ(CC),
1452.64	45.25	υ(NC), β(HCN)
1450.45	33.79	β(CNN),
1448.6	31.93	υ(NC), β(CNN)
1392.97	33.56	β(HCH),
1273.37	42.12	υ(CC), υ(NC)
1269.05	50.26	τ(HCNN), β(HCN)
1096.38	49.57	β(CNN), β(CNN)
689.36	112.67	τ(HCCC), τ(HCCC)

1391.15	50.33	υ(NC), β(CNN)
1353.02	213.07	υ(OC), β(HOC)
1298.79	50.33	τ(HCCO), β(HCC)
1212.07	43.38	υ(CC), β(CNN)
1205.08	36.58	υ(OC), β(CNN)
1182.75	33.6	υ(OC),
1016.19	32.46	β(CCN), β(CCC)
736.03	68.94	τ(HCCC), τ(HCCC)
713.39	36.22	τ(HOCC),

C22=Ru(bdmpzm)(bphpza)Cl$_2$

3622.65	78.43	υ(OH),
3139.44	41.52	υ(CH), υ(CH)
3128.63	39.77	υ(CH), υ(CH)
3105.92	54.75	υ(CH),
2971.82	46.95	υ(CH), υ(CH)
2929.67	63.36	υ(CH),
1778.14	186.36	υ(OC),
1475.56	41.84	β(CNN), υ(NC)
1402.77	67.06	β(HCC), β(NNC)
1304.23	69.67	υ(NC),
1279.64	36.31	β(NNC),
1202.81	68.93	υ(NC), β(HCC)
1166.78	65.91	υ(NN), β(HCC)
1135.19	201.18	υ(OC), β(HOC)
740.14	68.06	τ(HCCC), τ(HCCN)
731.02	76.81	τ(HCCC), τ(HCCN)
722.56	50.81	τ(HOCC), o(OCOC)
691.91	38.16	τ(CCCC), τ(CCCC)

1446.11	30.65	β(HCH), β(HCH)
1445.24	39.56	β(CNN), β(HCH)
1397.89	78.99	υ(NC), β(HCH)
1387.19	44.9	β(CNN), υ(NC)
1344.45	167.34	υ(OC), β(HOC)
1297.28	53.6	τ(HCCO), β(HCC)
1205.09	37.1	υ(NC),
1172.34	47.15	υ(OC),
1014.26	51.59	β(CCN),
730.32	33.99	τ(HOCC),

C23=[Ru(bdmpzm)(bpzpy)Cl]$^+$

1569.48	45.54	υ(CC),
1477.9	100.83	υ(NC),
1464.04	38.21	υ(NC),
1462.23	94.79	υ(NC),
1423.85	56.38	υ(NC), β(CNN)
1414.85	59.42	β(HCH), β(HCH)
1379.19	39.48	υ(NC), β(CNN)
1269.05	130.72	υ(CC), υ(NN)
741.37	84.13	τ(HCCC), τ(CCCN)
710.32	60.86	τ(HCCN), τ(HCCC)
708.25	34.5	τ(HCCN), τ(HCCC)

1293.57	41.92	τ(HCCO), β(HCC)
1209.21	44.53	β(NNC), υ(NC)
1201.51	37.27	β(CNN), υ(OC)
1183.27	30.97	υ(OC),
825.03	49.61	τ(HCCC), τ(HCCC)
716.15	30.75	τ(HOCC),

C24=[Ru(bdmpzm)(bdmpzpy)Cl]$^+$

1593.19	73.48	υ(CC),
1461.05	137.28	υ(CC),
1456.31	32.78	β(HCH), υ(NC)
1451.32	33.48	β(HCH),
1442.23	37.55	β(HCH),
1421.36	33.48	β(HCH), τ(HCNN)
1414.87	36.18	υ(NC),
1413.42	35.47	υ(NC), β(HCH)
1389.5	32.08	υ(NC),
1385.63	33.23	β(CNN), υ(NC)
1269.17	72.54	β(HCN), υ(NC)
1267.86	39.81	β(HCC),
732.91	50.39	τ(HCCC), τ(HCCC)

			651.43	60.32	β(OCO),						
C25=(cym)Ru(pz)Cl_2			**C26=(cym)Ru(dmpz)Cl_2**			**C27=(cym)Ru(dcpz)Cl_2**			**C28=[(cym)Ru(bpzm)Cl]$^+$**		
3215.83	411.47	υ(NH),	3205.04	528.11	υ(NH),	3648.48	82.86	υ(OH),	1427.04	46.63	υ(CC), β(CNN)
3211.75	47.57	υ(CH), υ(CH)	3058.23	31.11	υ(CH), υ(CH)	3647.51	126.24	υ(OH),	1268.91	102.16	υ(CC), β(CNN)
3052.57	33.61	υ(CH), υ(CH)	3051.41	30.2	υ(CH), υ(CH)	3022.26	624.5	υ(NH),	1054.44	31.03	υ(NN), β(HCC)
2972.77	39.98	υ(CH), υ(CH)	2971.62	38.99	υ(CH), υ(CH)	2973.82	32.54	υ(CH), υ(CH)	725.2	75.49	τ(HCCN), τ(HCCC)
1268.55	48.94	β(HNC), β(HCC)	1568.37	55.99	υ(CC), β(HNC)	1752.45	222.96	υ(OC),	723.11	58.71	τ(HCCN), τ(HCCC)
1146.18	60.92	υ(CC), β(HNC)	1473.48	37.39	υ(CC), β(CNN)	1743.12	307.14	υ(OC),			
1052.3	43.69	υ(CC), β(HCC)	1413.81	35.74	υ(CC), β(HCH)	1544.48	36.73	υ(CC), β(HNC)			
745.25	64.64	τ(HNCC), τ(HCCC)	1287.25	81.15	υ(NC), β(HNC)	1445.7	73.08	β(CNN), β(CNN)			
			1212.62	48.54	υ(NN),	1397.03	270.41	υ(NC), υ(CC)			
			769.55	49.97	τ(HNCC), τ(HCCC)	1335.25	150.94	υ(NC), β(HOC)			
						1250.52	74.95	υ(NC), β(HNC)			
						1122.32	213.74	υ(OC), β(HOC)			
						1114.57	525.46	υ(OC), β(HOC)			
						1074.23	41.23	υ(OC), β(HCC)			
						990.41	96.91	β(CNN), β(CNN)			
						744.13	52.14	ο(OCOC), τ(HCCN)			
						704.98	54.74	υ(CC), β(OCO)			
						664.41	58.52	υ(OC), β(OCO)			
						630.5	55.47	τ(HOCC),			
						538.7	92.33	τ(HOCC),			
C29=[(cym)Ru(bpza)Cl]$^+$			**C30=[(cym)Ru(bdmpzm)Cl]$^+$**			**C31=[(cym)Ru(bdmpza)Cl]$^+$**			**C32=[(cym)Ru(bphpza)Cl]$^+$**		
3605.32	143.34	υ(OH),	1564.4	54.02	υ(CC),	3622.41	124.57	υ(OH),	3609.1	144.95	υ(OH),
1784.78	197.75	υ(OC),	1472.1	40.29	β(HCH), β(HCH)	2884.86	150.35	υ(CH),	1798.55	171.22	υ(OC),
1428.05	56.05	υ(NC), β(CNN)	1463.55	64.84	υ(NC), υ(NC)	1785.58	248.7	υ(OC),	1531.34	38.76	υ(CC), υ(NC)

1366.39	38.58	υ(OC), β(HCC)
1298.12	101.5	τ(HCCO), υ(NC)
1218.94	40.89	υ(NN), β(HCC)
1186.93	60.15	β(HOC), β(HCC)
1113.64	182.34	υ(OC), β(HOC)
1055.87	42.52	β(HCC), β(HCC)
732.67	65.49	τ(HCCN), τ(HCCC)
731.32	89.39	τ(HCCN), τ(HCCC)
702.21	81.28	τ(HOCC),
646.42	62.94	β(OCO),

C33=[(cym)Ru(pyr)Cl]$^{+}$

1451.2	47.12	β(HCH),
744.08	105.85	τ(HCCN), τ(HCCN)

C37=[(cym)Ru(dcbpyr)Cl]$^{+}$

3638.79	165.81	υ(OH),
3636.65	163.62	υ(OH),
1757.79	295.03	υ(OC),
1754.02	260.13	υ(OC),
1425.02	42.59	υ(CC),
1405.45	60.3	υ(CC), υ(CC)

1412.71	56.71	β(HCH),
1382.34	44.5	υ(NC), β(CNN)
1274.78	166.3	υ(NN), υ(NC)

C34=[(cym)Ru(phn)Cl]$^{+}$

828.92	69.56	τ(HCCC), τ(HCCC)
705.98	30.15	τ(CCCC), τ(CCCC)

C38=[(cym)Ru(dcphn)Cl]$^{+}$

3642	132.23	υ(OH),
3621.21	137.04	υ(OH),
1762.92	149.96	υ(OC),
1756.71	159.64	υ(OC),
1350.96	43.71	υ(CC),
1330.36	83.37	υ(OC), β(HOC)

1560.93	60.36	υ(CC),
1469.82	37.5	β(HCH), β(HCH)
1461.43	32.65	β(HCH), β(HCH)
1406.57	51.2	β(HCH),
1387.57	41.95	τ(HCCO), υ(NC)
1382.15	77.16	υ(NC), β(CNN)
1341.09	34.32	υ(CC), β(HOC)
1299.81	118.31	τ(HCCO),
1216.91	30.96	υ(CC), υ(NC)
1156.78	45.01	υ(NN), β(HCC)
1146.53	80.97	υ(NN), β(HCC)
1114.4	96.4	υ(OC), β(HOC)
1040.3	31.67	τ(HCCC), o(CCCC)
664.69	76.35	τ(HOCC),
639.79	52.65	τ(HCCN), o(CRuNN)
629.09	32.73	τ(CCNN), β(OCO)

C35=[(cym)Ru(dmbpyr)Cl]$^{+}$

1617.92	39.12	υ(CC), υ(CC)
1613.28	64.52	υ(CC),
1472.36	42.94	β(HCC), β(CCN)
1446.05	41.56	β(HCH), β(HCH)
803.72	52.32	τ(HCCN), τ(HCCC)

C39=[(cym)Ru(bpzpy)]$^{2+}$

3233.18	44.92	υ(CH), υ(CH)
1601.46	109.83	υ(CC),
1491.84	30.05	υ(CC), β(HCC)
1473.32	192.71	υ(NC), β(HCC)
1470.61	58.38	υ(NC), υ(NC)
1420.24	138.3	υ(NC), β(CNN)

1528.97	45.11	υ(CC), υ(CC)
1492.64	42.54	υ(CC),
1417.34	43.78	β(NNC),
1414.33	39.75	υ(NC), β(NNC)
1378.56	58.02	υ(OC), β(HOC)
1364.62	41.94	τ(HCCO), υ(NC)
1310.77	82.76	τ(HCCO), υ(NN)
1205.49	118.13	υ(NN), β(HCC)
1193.04	100.24	β(HCC), β(HOC)
1127.71	84.92	τ(HCCC), υ(OC)
1127.45	52.8	υ(OC),
1055.54	57.83	β(HCC), β(HCC)
761.15	38.85	τ(HCCN), τ(HCCC)
753.46	38.96	τ(HCCC), τ(CCCC)
749.49	62.31	τ(HCCC), τ(HCCC)
722.32	93	τ(HOCC),
646.76	72.85	β(OCO), o(CCRuC)

C36=[(cym)Ru(dmphn)Cl]$^{+}$

1470.29	36.23	β(HCH),
1433.68	33.54	β(HCH), β(HCH)
843.77	69.93	τ(HCCC), τ(HCCC)

C40=[(cym)Ru(bdmpzpy)]$^{2+}$

1599.35	197.54	υ(CC),
1555.03	46.23	υ(CC), υ(CC)
1479.77	222.05	υ(NC), υ(NC)
1439.6	183.78	β(CNN), β(HCH)
1418.46	55.5	β(HCH), β(HCH)
1406.86	103.47	υ(NC), β(HCH)

1338.23	190.5	υ(OC), β(HOC)	1314.51	93.4	υ(OC), β(HOC)	1350.7	32.78	υ(NC), β(HCC)	1385.66	30.49	β(HCC), β(HCC)
1338.93	166.04	υ(OC), β(HOC)	1171.42	56.28	υ(CC), β(HOC)	1041.15	60.65	β(HCC), β(HCC)	1375.42	44.74	υ(NC), υ(NC)
1158.53	136.2	β(HOC), β(HCC)	1164.2	57.15	υ(CC), β(HCC)	763.64	98.32	τ(HCCC), τ(HCCC)	1341.79	32.41	υ(NC), β(HCC)
1152.18	266.35	υ(CC), β(HOC)	1128.34	237.34	υ(OC), β(HOC)	735.16	78.82	τ(HCCC), τ(HCCN)	753.98	42.36	τ(HCCC), τ(HCCC)
1110.98	143.69	υ(OC),	1117.83	231.53	υ(OC), β(HOC)						
1091.3	131.81	υ(OC),	1068.98	192.57	υ(OC), β(CNC)						
750.13	87.33	τ(HCCN), o(OCOC)	854.91	68.38	τ(HCCC), τ(HCCC)						
702.56	49.37	τ(CCCN), o(OCOC)	709.12	35.5	o(OCOC),						
631.8	62.91	β(OCO),	677.52	50.27	β(OCO),						
622.26	40.75	β(OCO),	609.48	39.79	τ(HOCC), τ(HOCC)						
614.65	133.04	τ(HOCC),	582.12	36.73	τ(HOCC), β(CCC)						
			560.46	39.32	β(OCO), β(CCC)						

The symbols υ, β, τ, o denote stretching, bending, torsional and out of plane modes respectively

Table 5.4: The Assignment of the IR bibrations that are associated with the Ru atom in the complexes using PED

Freq.	**Int.**	**Assignment**	**Freq.**	**Int.**	**Assignment**	**Freq.**	**Int.**	**Assignment**	**Freq.**	**Int.**	**Assignment**
ST1=RuCl2(dmso)4			**ST2=[(cym)RuCl2]2**			**ST3=Ru(bdmpzm)Cl4**			**ST4=Ru(bpzm)Cl4**		
1030.68	24.87	τ(HCSRu), τ(HCSRu)	1015.28	11.92	τ(HCCRu), τ(HCCRu)	349.5	38.95	υ(RuCl), υ(RuCl)	631.93	6.06	o(RuCNN),
1006.64	156.25	τ(HCSRu), τ(HCSRu)	1013.62	16.43	τ(HCCRu), τ(HCCRu)	314.34	59.24	υ(RuCl),	398.75	30.94	β(CNRu), τ(HCNN)
1005.51	33.81	τ(HCSRu), τ(HCSRu)	842.24	16.85	τ(HCCRu), τ(HCCRu)	304.36	31.9	υ(RuCl), υ(RuCl)	359.96	17.61	υ(RuCl),
951.31	18.35	υ(SO), τ(HCSRu)	830.57	28.76	τ(HCCRu),	183.7	5.16	υ(RuN),	354.84	8.36	υ(RuCl), β(CNC)
389.15	32.13	o(ORuCS), β(OSC)	292.65	31.67	υ(RuCl),	139.14	2.5	β(ClRuCl),	329.21	70.52	υ(RuCl),
385.99	42.04	o(OCRuS), β(CSO)	283.21	13.24	υ(RuCl), υ(RuCl)	101.06	5.33	β(ClRuCl),	302.05	26.02	υ(RuCl),
356.92	18.31	o(OCRuS), β(CSO)	253.57	20.47	υ(RuCl), υ(RuCl)				263.75	36.39	υ(RuCl),
349.17	15.71	o(ORuCS), β(OSC)	244.83	8.14	υ(RuCl), β(ClRuCl)				239.02	5.19	υ(RuN),

284.2	17.88	υ(RuCl), β(CSRu)	239.06	21.45	υ(RuCl), β(ClRuCl)				221.32	4.24	β(CNRu), o(ClNNRu)
252.99	18.07	o(OCRuS), υ(RuCl)	199.49	13.23	τ(CCRuCl), υ(RuCl)						
C1=[Ru(bpzm)3]2+			**C2=[Ru(bpza)3]2+**			**C3=[Ru(bdmpzm)3]2+**			**C4=[Ru(bdmpza)3]2+**		
640.02	4.63	o(CRuNN),	638.02	21.36	o(CNRuN),	649.77	2.12	τ(NCNRu),	652.5	21.58	τ(CNNC), o(CRuNN)
634.98	6.65	τ(CNNC), o(CRuNN)	634.26	3.41	o(CNRuN),	647.7	2.31	τ(NCNRu),	649.78	5.42	o(CNRuN),
632.86	3.34	τ(CNNC), o(CRuNN)	630.38	15.01	τ(CNNC), o(CNRuN)				217.91	3.42	υ(RuN),
393.64	2.96	β(CNC), υ(RuN)	619.76	3.01	τ(CNNC), o(CNRuN)						
356.89	4.77	β(NRuN), υ(RuN)	362.55	3.2	υ(RuN),						
330.98	3.44	β(NRuN), υ(RuN)	300.92	3	υ(RuN),						
295.43	3.65	υ(RuN), υ(RuN)	198.86	2.41	υ(RuN),						
294.03	4.33	υ(RuN),	36.16	2.98	τ(CNNRu), τ(OCCN)						
203.6	3.01	o(NNNRu), β(NNRu)									
167.85	2.87	β(NRuN), υ(RuN)									
C5=Ru(bpzm)2Cl2			**C6=(bpza)2RuCl2**			**C7=Ru(bdmpzm)2Cl2**			**C8=(bdmpza)2RuCl2**		
391.35	14.65	υ(RuN), β(NRuN)	648.9	19.95	o(CNRuN),	650.39	4.73	τ(CNNC), o(CRuNN)	680.11	28.9	τ(HOCC), o(CRuNN)
335.63	14.26	υ(RuCl), υ(RuCl)	640.46	84.91	τ(HOCC), o(CNRuN)	284.02	2.53	β(CCC), o(ClNNRu)	651.9	17.75	o(CCNC), o(CRuNN)
291.85	18.93	υ(RuN), β(CNRu)	633.36	48.7	o(CNRuN), β(OCO)	282.68	18.99	β(CCC), υ(RuCl)	293.22	4.19	β(CCC), υ(RuCl)
221.02	5.19	τ(NNRuN), β(NRuN)	384.25	8.85	υ(RuN),	227.59	3.43	β(NNRu),	282.23	21.09	υ(RuCl),
203.64	12.29	υ(RuCl), β(CNRu)	377.61	5.98	β(NNRu),	223.16	3.45	o(CNRuN), o(CCNC)	178.91	3.23	τ(CNNRu),
176.44	3.98	υ(RuN), β(NRuN)	309.93	10.97	υ(RuCl),	198.96	2.83	τ(CNNRu), υ(RuN)	145.03	2.09	o(ClNNRu),
130.32	3.56	o(ClNClRu), β(ClRuN)	284.13	7.8	υ(RuN), υ(RuN)	161.9	4.43	υ(RuN), υ(RuN)	131.69	2.31	o(ClNNRu),
111.48	4.03	τ(NNRuN), τ(NNRuN)	216.41	10.26	β(NRuN), β(ClRuCl)	142.83	2.62	β(ClRuN), o(CCNC)	106.06	3.96	β(ClRuCl), τ(NNRuN)
63.53	4.47	o(ClNClRu), β(ClRuN)	203.48	7.63	υ(RuCl),	90.45	3.05	o(ClNClRu), o(CNRuN)	99.84	6.16	o(ClNClRu),
62.19	5.92	τ(CNNRu), τ(CNNRu)	175.84	10.05	o(ClNClRu), β(ClRuCl)	62.62	4.39	τ(CNNRu), o(NNNRu)			
C9=Ru(bpza)(bdmpza)Cl2			**C10=Ru(bpza)(bdmpzm)Cl2**			**C11=Ru(bpza)(bphpza)Cl2**			**C12=Ru(bpza)(bpyr)Cl2**		
654.08	42.18	τ(HOCC), o(CNRuN)	650.8	38.5	o(CNRuN),	684.72	50.89	o(NRuCN), β(CCC)	386.44	8.1	β(NNRu),
306.53	11.73	υ(RuCl),	640.59	10.78	τ(HCCN), o(CRuNN)	394.88	9	υ(RuN), υ(RuN)	320.63	12.32	υ(RuCl),
270.98	6.06	β(CCC), υ(RuCl)	602.36	66.42	τ(HOCC), τ(CNNRu)	383.81	3.2	β(NRuN),	312.31	13.98	υ(RuCl),
236.71	4.83	β(RuNC),	296.03	8.59	β(CCC), υ(RuCl)	308.32	10.46	υ(RuCl),	296.12	3.82	υ(RuN), υ(RuN)

211.8	9.06	τ(NRuNN), υ(RuCl)
188.47	4.26	β(NNRu), o(CCNC)
156.68	3.41	o(ClNClRu),
152.37	5.52	β(ClRuCl),
44.79	2.22	β(ClRuCl), o(CNNC)

C13=Ru(bpza)(dmbpyr)Cl2

391.4	7.27	υ(RuN),
293.75	20.93	υ(RuCl), β(CCC)
286.13	4.81	υ(RuN), υ(RuN)
280.95	12.79	υ(RuCl),
237.07	9.37	υ(RuCl),
189.03	4.39	υ(RuCl), β(NNRu)
177.31	5.4	τ(NNRuN), υ(RuN)
121.34	4.98	o(ClNClRu), β(CCN)
105.35	10.19	τ(NNRuN), β(ClRuCl)
52.84	11.47	o(CNNC), o(NNNRu)

C17=Ru(bdmpza)(bphpza)Cl2

658.67	9.81	o(CRuNN),
644.74	8.74	o(CRuNN), o(CRuNN)
341.4	3.43	υ(RuCl),
313.85	5.22	υ(RuCl),
302.85	15.95	υ(RuCl),
262.7	4.82	β(CCN), τ(CNNRu)
208.14	9.47	υ(RuN), υ(RuCl)
147.31	5.43	β(ClRuN), o(ClNClRu)
134.09	3.32	β(ClRuCl),
123.13	4.14	β(ClRuCl),

C21=Ru(bdmpzm)(bpzm)Cl2

648.12	3.55	o(CNRuN),
286.98	18.77	υ(RuCl),
223.82	5.79	υ(RuCl),
216.79	7.04	τ(CNNRu),
202.41	4.71	τ(CNNRu),
169.12	4.27	υ(RuN),
123.78	4.63	β(ClRuCl), o(ClNClRu)

C14=Ru(bpza)(phn)Cl2

392.36	5.01	υ(RuN), β(NRuN)
315.46	24.68	υ(RuCl),
264.69	11.13	υ(RuN), β(CNRu)
227.22	6.04	τ(CCNRu), τ(CCCN)
221.12	7.52	β(ClRuN),
202.69	2.73	υ(RuCl), β(NRuN)
176.3	4.49	τ(NNRuN), β(ClRuCl)
115.42	4.83	τ(RuClClN),
107.18	6.4	β(ClRuCl),
54.46	10.25	τ(CNRuN), τ(NRuCN)

C18=Ru(bdmpza)(pyr)Cl2

649.8	6.79	o(CNCC), o(CRuNN)
486	3.34	o(NNNRu),
332.36	6.91	υ(RuCl),
298.84	14.54	υ(RuCl),
223.83	7.31	β(NNRu),
189.25	5.44	υ(RuCl),
188.5	5.49	o(ClNNRu), o(NNNRu)
144.42	7.35	β(ClRuCl), o(ClNClRu)
116.5	3.67	υ(RuN),
66.82	4.05	τ(CNNRu),

C22=Ru(bdmpzm)(bphpza)Cl2

654.97	4.67	τ(HCCN), o(CNRuN)
285.78	3.65	υ(RuN),
237.77	6.99	υ(RuCl), β(CNRu)
213.12	7.41	τ(NNRuN), υ(RuCl)
192.03	6.45	β(CCN), o(ClNClRu)
148.28	7.87	β(ClRuCl),
145.76	3.45	β(ClRuCl), υ(RuN)

C15=Ru(bpza)(dmphn)Cl2

711.28	7.81	τ(CCCC), o(CRuCN)
689.93	31.81	o(CNRuN), β(OCO)
673.38	5.07	o(CNRuN), β(OCO)
321.41	3.87	o(CNCC), υ(RuCl)
309.11	14.42	υ(RuCl),
268.68	3.63	β(NRuN),
194.33	5.3	υ(RuCl),
123.62	5.76	o(ClNClRu), β(CCN)
112.51	10.5	β(ClRuCl),
99.37	6.5	o(CRuCN),

C19=Ru(bdmpza)(dmbpyr)Cl2

668.44	24	o(CNRuN), β(OCO)
412.5	6.06	β(OCC), β(NRuN)
348.68	2.79	o(CNRuN), o(CNCC)
296.78	4.44	υ(RuCl),
276.93	13.37	υ(RuCl),
224.67	10.73	υ(RuCl),
204.21	2.19	o(CNRuN),
189.86	5.15	o(ClNNRu), υ(RuN)
173.43	3.57	o(ClNNRu),
137.38	5.66	υ(RuN),

C23=[Ru(bdmpzm)(bpzpy)Cl]+

645.64	2.67	o(CNRuN), o(CNRuN)
228.88	11.6	υ(RuCl), β(NNRu)
199.08	6.49	υ(RuCl), β(ClRuCl)
175.53	3.87	τ(NNRuN), β(ClRuCl)
106.18	6.49	β(ClRuCl),
88.63	5.03	τ(CNCC), o(RuCCN)
57.1	11.99	τ(CNNRu), o(CNNC)

C16=Ru(bdmpza)(bdmpzm)Cl2

660.92	2.45	o(CRuNN),
283.63	16.82	υ(RuCl),
278.39	2.94	β(CCO), υ(RuCl)
241.64	2.89	β(ClRuCl), υ(RuN)
232.77	3.69	υ(RuCl),
192.36	10.17	β(ClRuCl), τ(CNNRu)
155.78	4.09	υ(RuN),
149.06	2.65	o(ClNClRu),
76.13	3.14	β(ClRuCl), o(ClNNRu)
67.91	4.67	τ(CNNRu),

C20=Ru(bdmpza)(dmphn)Cl2

653.05	3.26	o(CNRuN),
419.01	7.05	β(NRuN), o(CCNC)
349.09	7.3	β(NRuN), o(CCNC)
311.92	9.78	υ(RuCl),
287.2	8.04	β(CCC), υ(RuCl)
251.9	3.83	υ(RuN),
205.69	7.44	β(ClRuCl), υ(RuCl)
192.9	3.58	υ(RuCl),
149.93	13.65	β(ClRuCl),
129.55	3.88	β(ClRuN),

C24=[Ru(bdmpzm)(bdmpzpy)Cl]+

672.07	8.53	υ(RuN), β(CCC)

382.22	4.73	υ(RuN), β(CNRu)	286.78	16.84	υ(RuCl),	641.64	3.93	τ(HCCN), o(CNRuN)	647.84	2.27	o(CCNC), o(CNRuN)
335.39	6.15	υ(RuN), β(NRuN)	250.22	2.12	τ(CNNRu), υ(RuCl)	636.13	5.23	o(CNRuN), o(CNRuN)	646.76	2.18	o(CNRuN), o(CNRuN)
304.8	8.89	υ(RuCl),	240.94	3.87	τ(CNNRu), υ(RuCl)	635.35	4.52	τ(CCNN), o(CNRuN)	309.34	6.34	υ(RuCl),
259.7	10.85	υ(RuCl), β(NRuN)	235.85	2.95	υ(RuCl), β(NNRu)	349.26	3.88	υ(RuN), υ(RuCl)			
245.06	4.74	τ(CNNRu), o(CCNC)	234.3	2.34	υ(RuCl),	329.89	7.11	υ(RuN),			
212.28	12.16	υ(RuCl),	216.35	3.98	τ(CNNRu),	286.41	8.84	β(CCC), β(RuNC)			
151.17	4.94	υ(RuCl), β(NNRu)	160.11	2.67	τ(CNNRu),	235.65	4.22	τ(CCNC), υ(RuCl)			
118.62	3.32	β(ClRuN), o(CCNC)	101.58	2.25	β(ClRuCl), o(ClNClRu)	51.84	2.67	τ(NNRuN), τ(CNNRu)			
60.98	5.48	τ(CNNRu), τ(CNNRu)									
C25=(cym)Ru(pz)Cl2			**C26=(cym)Ru(dmpz)Cl2**			**C27=(cym)Ru(dcpz)Cl2**			**C28=[(cym)Ru(bpzm)Cl]+**		
1012.14	12.92	τ(HCCRu), τ(HCCRu)	1010.99	10.74	τ(HCCRu), τ(HCCRu)	1015.58	10.91	τ(HCCRu), τ(HCCRu)	1369.32	8.5	τ(HCCRu),
838.81	18.94	τ(HCCRu), τ(HCCRu)	848.45	4.62	τ(HCCRu), τ(HCCRu)	844.4	30.05	τ(HCCRu), τ(HCCRu)	1316.02	5.96	β(HCC), τ(HCCRu)
597.36	8.81	τ(CCNN), τ(CNNRu)	831.94	21.88	τ(HCCRu), τ(HCCRu)	654.47	15.05	o(CRuNN), τ(HOCC)	1005.54	16.15	τ(HCCRu), τ(HCCRu)
286.8	20.18	υ(RuCl),	638.19	3.77	o(CNRuN), o(CCRuC)	641.54	7.65	o(CRuCC),	848.3	16.45	τ(HCCRu), τ(HCCRu)
273.87	9.65	υ(RuCl),	291.41	5.23	υ(RuN), β(CCC)	544.18	10.41	o(CCRuC), β(CCC)	648.06	5.63	o(CCRuC), o(CRuCC)
232.08	14.37	υ(RuCl), o(NCCRu)	288.98	12.23	υ(RuCl), β(CCC)	286.84	19.17	υ(RuCl),	438.88	5.25	o(CRuCC), β(CCRu)
228.63	3.85	υ(RuN), o(CRuCC)	262.51	14.52	υ(RuCl), υ(RuCl)	267.19	7.65	υ(RuCl), β(CCO)	308.35	8.49	υ(RuC), υ(RuCl)
211.41	3.6	υ(RuN), β(CCC)	244.61	8.06	υ(RuCl), β(CCC)	241.46	14.73	υ(RuCl), β(CCO)	297.62	9.78	υ(RuCl), β(CCC)
182.45	6.73	o(ClCClRu),	219.11	8.29	τ(CNNRu), β(CCC)	213.18	9.12	o(CRuCC), τ(CRuNN)	252.47	7.61	υ(RuN), υ(RuN)
125.82	3.56	β(ClRuN), o(ClCNRu)	92.61	5.09	o(CCRuC), β(CCC)	196.82	5.29	o(ClCClRu), β(ClRuCl)	226.8	3.48	τ(CNNRu), υ(RuN)
C29=[(cym)Ru(bpza)Cl]+			**C30=[(cym)Ru(bdmpzm)Cl]+**			**C31=[(cym)Ru(bdmpza)Cl]+**			**C32=[(cym)Ru(bphpza)Cl]+**		
1006.82	15.14	τ(HCCRu), τ(HCCRu)	1364.32	5.84	τ(HCCRu), υ(CC)	1008.01	15.7	τ(HCCRu), τ(HCCRu)	1013.95	15.58	τ(HCCRu), τ(HCCRu)
848.28	15.5	τ(HCCRu), τ(HCCRu)	1006.88	16.18	τ(HCCRu), τ(HCCRu)	851.61	23.44	τ(HCCRu), τ(HCCRu)	890.22	4	τ(HCCRu), τ(HCCRu)
648.61	13.08	o(CCRuC), β(OCO)	876.52	12.52	τ(HCCRu), υ(CC)	649.16	9.12	o(CCRuC), o(CCRuC)	867.06	18.69	τ(HCCRu), τ(HCCRu)
628.22	22.52	o(CNRuN), ββ(OCO)	848.74	16.06	τ(HCCRu), τ(HCCRu)	639.79	52.65	τ(HCCN), o(CRuNN)	702.5	3.72	τ(HCCN), o(NCRuN)
438.8	5.53	υ(RuC), β(CCRu)	650.55	12.81	o(CCRuC),	633.88	14.14	τ(HCCN), o(CRuNN)	649.45	15.57	β(OCO), o(CCRuC)
376.33	6.24	υ(CC), β(NRuN)	541.18	5.96	o(CCRuC),	427.31	3.45	o(CCRuC), β(CCRu)	646.76	72.85	β(OCO), o(CCRuC)
304.91	7.65	υ(RuC), υ(RuCl)	377.2	4.68	β(CCC), υ(RuC)	396.79	3.25	β(NRuN),	293.41	11.9	υ(RuCl),
296.92	9.56	υ(RuCl), β(CCC)	310.53	7.83	υ(RuC),	295.16	11.24	υ(RuCl),	213.7	4.81	τ(HCCC), o(CRuCC)

249.56	3.44	υ(RuN),	294.48	11.25	υ(RuCl),	218.78	3.78	τ(CNNRu),	111.38	6.03	o(CCRuC),
219.53	6.88	o(CCRuC), τ(CNNRu)	234.89	8.69	β(NRuN), o(ClCNRu)	106.69	3.65	β(NNRu), o(CNNC)	109.34	5.47	τ(CCCRu), o(ClCNRu)
C33=[(cym)Ru(pyr)Cl]+			**C34=[(cym)Ru(phn)Cl]+**			**C35=[(cym)Ru(dmbpyr)Cl]+**			**C36=[(cym)Ru(dmphn)Cl]+**		
1013.91	17.24	β(HCH), τ(HCCRu)	1366.9	15.09	τ(HCCRu),	1009.61	14.54	τ(HCCRu), β(HCH)	1309.48	7.89	τ(HCCRu), β(HCC)
869.72	2.87	(HCCRu), τ(HCCRu)	1350.11	7.47	τ(HCCRu),	1007.33	7.84	τ(HCCRu), υ(NC)	1004.39	10.35	τ(HCCRu), τ(HCCRu)
841.74	16.35	τ(HCCRu), τ(HCCRu)	1309.54	8.6	τ(HCCRu), β(HCC)	868.19	3.56	τ(HCCRu), τ(HCCRu)	1002.51	22.44	τ(HCCRu), τ(HCCRu)
316.53	5.82	υ(RuCl), β(CCC)	1010.82	18.81	τ(HCCRu), τ(HCCRu)	844.53	16.07	τ(HCCRu), τ(HCCRu)	835.49	16.48	τ(HCCRu), τ(HCCRu)
299.23	11.86	υ(RuCl),	842.21	15.06	τ(HCCRu), τ(HCCRu)	642.63	2.51	o(CCRuC), β(CCRu)	642.95	6.42	o(CCRuC),
271.58	3.3	υ(RuN), β(CNRu)	378.96	3.66	o(CCRuC), o(CCRuC)	397.02	2.78	o(CCRuC), υ(RuC)	415.44	4.45	o(CCRuC), υ(RuC)
228.35	2.5	β(CCRu),	352.83	4.26	υ(RuC),	294.43	8.06	τ(CCNRu), υ(RuCl)	350.33	3.41	υ(RuCl), β(CCRu)
210.86	4.34	o(CCRuC), β(CCC)	315.28	7.05	υ(RuCl),	292.83	6.61	υ(RuCl),	313.28	4.76	o(CCCC), υ(RuCl)
150.16	2.1	β(ClRuN), τ(HCCRu)	288.2	10.16	υ(RuCl),	287.95	8.88	τ(CCNRu), υ(RuCl)	295.67	6.23	υ(RuCl),
92.18	4.41	o(CCRuN), o(CCNC)	96.42	5.64	τ(CCNRu), o(CCRuN)	172.77	2.72	o(CCRuC), β(CCC)	95.57	3.51	o(CCRuC), o(CCRuC)
C37=[(cym)Ru(dcbpyr)Cl]+			**C38=[(cym)Ru(dcphn)Cl]+**			**C39=[(cym)Ru(bpzpy)]2+**			**C40=[(cym)Ru(bdmpzpy)]2+**		
1011.23	22.05	τ(HCCRu), β(HCH)	1442.31	12.57	τ(HCCRu), β(HCH)	1001.57	25.94	τ(HCCRu), τ(HCCRu)	995.83	28.76	τ(HCCRu), τ(HCCRu)
876.47	6.74	τ(HCCRu), υ(CC)	1008.94	25.43	τ(HCCRu), τ(HCCRu)	947.26	6.15	τ(HCCRu), τ(HCCRu)	847.63	14.36	τ(HCCRu), τ(HCCRu)
846.87	13.24	τ(HCCRu), τ(HCCRu)	840.76	17.98	τ(HCCRu), τ(HCCRu)	941.51	24.36	τ(HCCRu), υ(NC)	664.54	2.15	υ(RuN), β(CNC)
552.13	6.28	o(CRuCC), β(CCO)	558.1	5.12	o(CCRuC),	854.88	11.58	τ(HCCRu), τ(HCCRu)	644.17	7.32	o(CCRuC), o(CRuCC)
473.71	12.75	o(CRuCN), o(CRuCN)	479.7	4.38	τ(CCCC), o(CRuCN)	649.2	13.61	o(CCRuC), o(CCRuC)	629.01	7.26	o(CNRuN),
425.98	11.08	o(CRuCC), β(CCN)	349.51	9.47	o(CCRuC), υ(RuC)	630.94	4.43	o(CNRuN), τ(NNCN)	427.75	8.14	β(CCC), o(CCRuC)
413.68	7.06	τ(CCCN), o(CRuCN)	316.12	5.78	υ(CC), υ(RuCl)	583.43	10.43	o(CNRuN),	385.63	2.3	o(CRuCC),
384.42	12.16	o(CRuCC),	310.25	4.48	υ(RuCl), β(OCC)	571.91	7.11	o(CNRuN),	382.18	2.34	o(CRuCC), υ(RuC)
291.45	11.93	υ(RuCl),	293.54	11.27	υ(RuCl),	373.7	6.51	υ(RuC), β(CCC)	340.45	2.86	β(CCC), υ(RuC)
270.92	10.62	τ(CCNRu), υ(RuCl)	215.29	6.45	o(CCRuC),	310.73	5.14	υ(RuN), β(CCC)	248.71	2.4	υ(RuN),

The symbols υ, β, τ, o denote stretching, bending, torsional and out of plane modes respectively

Table 5.5: The experimental and the theoretical ^{1}H-NMR chemical shift of the complexes

ST1=RuCl2(dmso)4			
	Direct	**Fitting**	**Exp.**
CH_3	2.1997 to 4.4991	2.65631 to 4.88673	
ST2=[(cym)RuCl$_2$]$_2$			
CH_3	0.6235 to 3.3231	1.12739 to 3.74601	0.085 to 2.6817
C_{cym}-H	2.9233, 4.0558	3.3582, 4.45673	3.2095 m
C_{others}-H	4.1213 to 5.6738	4.52026 to 6.02619	5.3889 to 5.7844
	0.6235 to 3.3231	1.12739 to 3.74601	0.085 to 2.6817
Ccy-H	2.9233, 4.0558	3.3582, 4.45673	3.2095 m
Cothers-H	4.1213 to 5.6738	4.52026 to 6.02619	5.3889 to 5.7844
ST3=Ru(bdmpzm)Cl$_4$ dmso-d6			
CH_3	1.343 to 2.3934	1.82531 to 2.8442	-3.493 to 2.5136
CH_3	3.2122 to 5.1828	3.63843 to 5.54992	
CH_2	4.7697, 10.6551	5.14921, 10.858	8.35, 15.3879
C4-H	6.0259, 6.425	6.36772, 6.75485	6.85
ST4=Ru(bpzm)Cl$_4$ dmso-d6			
C3-H	-1.8609 to 1.067	-1.28247 to 0.51239	1.4-2.60
C4-H	5.0695, 5.6906	5.44001, 6.04248	5.90, 6.10
C5-H	9.7245, 10.1933	9.95537, 10.4101	7.95, 8.25

C12=Ru(bpza)(bpyr)Cl$_2$ cd3od			
	Direct	**Fitting**	**Exp.**
C4-H	6.5058	6.83323	6.7
C_{both}-H	7.3994 to 9.6078	7.70002 to 9.84217	7.45 to 9.60
COOH	8.6863	8.94831	8.7
CHOO	11.6051	11.7795	10.15
C13=Ru(bpza)(bmpyr)Cl$_2$ cd3od			
	Direct	**Fitting**	**Exp.**
	2.161 to 2.7532	2.61877 to 3.1932	1.3 to 3.5, 4.65
C4-H	6.4838	6.81189	6.2
$C_{pyr\text{-}metal}$-H	7.285 to 8.0257	7.58905 to 8.30753	7.2 to 7.75
Cpz-H	8.2894 to 8.3592	8.56332 to 8.63102	8.25 to 8.50
COOH	8.7815	9.04066	8.65
C_{pyr}-H	9.4605	9.69929	9.25, 9.48
CHOO	11.6333	11.8069	9.8
C14=Ru(bpza)(phn)Cl$_2$ cd3od			
C4-H	6.3707, 6.3904	6.70218, 6.72129	6.30, 6.75
C_{both}-H	7.5782 to 9.9948	7.87345 to 10.2176	7.45-10.00
COOH	8.4649	8.73355	8.7
CHOO	12.0857	12.2457	10.5

C26=(cym)Ru(dmpz)Cl$_2$			
	Direct	**Fitting**	**Exp.**
CH_3	0.9433 to 3.0466	1.4376 to 3.4778	1.3256 to 2.8615
C_{cym}-H	3.4544	3.87337	3.3273
C4-H	5.9241	6.26898	6.0605
C_{others}-H	4.6375 to 5.1353	5.02098 to 5.50384	5.4900 to 6.2804
NH	12.3505	12.5026	6.1769
C27=(cym)Ru(dcpz)Cl$_2$			
CH_3	0.7938 to 2.9881	1.29259 to 3.42106	0.31 to 2.25
C_{cym}-H	3.4442	3.86347	3.5
COOH	6.0912, 6.3032	6.43106, 6.6367	6.49
C_{others}-H	5.1843 to 7.4766	5.55137 to 7.7749	5.25 to 8.10
NH	14.1274	14.2262	
C28=[(cym)Ru(bpzm)Cl]$^+$ cd3od			
CH_3	1.1682 to 2.8348	1.65575 to 3.27236	1.10250 to 2.8002
C_{cym}-H	3.7071	4.11849	2.9194
C_{others}-H	5.0375 to 8.0385	5.40898 to 8.31995	5.8779 to 8.2705
CH_2	5.4604, 6.163	5.81919, 6.50071	6.2793
C4-H	6.6671, 6.6916	6.98969, 7.01345	6.4228 m
C29=[(cym)Ru(bpza)Cl]$^+$			

CH_2	11.1008, 18.5331	11.2904, 18.4997	6.60, 8.65

C1=[Ru(bpzm)3]$^{2+}$ dmso-d6

C3-H & CH_2 close to Ru			1.9202 to 3.36128
CH_2	5.6819 to 6.2487	6.03404 to 6.58384	6.2825, 6.3981, 6.5036
C3-H	6.2753 to 7.8025	6.60964 to 8.09103	6.584, 7.3887 d
C4-H	6.8616 to 7.2786	7.17835 to 7.58284	7.1258, 8.3405
C5-H	8.1088 to 8.3001	8.38814 to 8.5737	8.9862 d

C2=[Ru(bpza)3]$^{2+}$ cd3od

CHOO	5.7556, 6.6172, 6.9762	6.10553, 6.94128, 7.28951	7.2
C3-H	6.0137-8.2067	6.35589-8.4831	3.3, 4.55, 6.62
C4-H	6.683-8.3555	7.00511-8.62744	8.3
COOH	6.6619, 6.9636, 7.7326	6.98464,7.27729, 8.02322	7.45
C5-H	8.2618 to 8.473	8.53655 to 8.74141	8.6

C3=[Ru(bdmpzm)3]$^{2+}$

CH_3	0.0444 to 0.7554	0.565668-1.25534	0.45 j=4.0645
CH_3	1.2721 to 2.7988	1.75654 to 3.23744	1.40 to 3.6
CH_2	4.9514 to 5.591	5.32546 to 5.94587	4.5-5.90
C4-H	6.0905 to 6.4874	6.43039 to 6.81538	6.10-7.50

C4=[Ru(bdmpza)3]$^{2+}$

CH3	-0.3125 to 3.3415	0.219475 to 3.76386	1.37 to 3.25

C15=Ru(bpza)(dmphn)Cl_2 cd3od

CH_3	2.4337 to 4.237	2.88329 to 4.63249	1.3-3.75
C4-H	6.2744 to 6.3412	6.60877 to 6.67356	6.75
C_{both}-H	7.531 to 9.5706	7.82767 to 9.80608	7.45 to 8.35
COOH	9.5706	9.80608	8.4
CHOO	12.2029	12.3594	8.75

C16=Ru(bdmpza)(bdmpzm)Cl_2

CH3	1.7417-3.0087	2.21205-3.44104	
CH2	5.1546	5.52256	
CHCOO	6.8879	7.20386	
C4-H	6.0986-6.3274	6.43824-6.66018	
OH	12.3233	12.4762	

C17=Ru(bdmpza)(bphpza)Cl_2

CH3	1.2658 to 4.7416	1.75043 to 5.12195	0.0005 to 4.5
C4-H	5.6465 to 6.6277	5.99971 to 6.95147	6.2 to 6.70
COOH	6.1607, 6.7229	6.49848, 7.04381	6
CHCOO	4.5957, 9.0467	4.98043, 9.2979	5.10, 8.45
Cothers-H	6.3964 to 11.204	6.72711 to 11.3905	6.30 to 8.30

C18=Ru(bdmpza)(pyr)Cl_2

CH_3	1.8435 to 4.4619	2.3108 to 4.85064	-1.25 to 4.5
CH_3	1.1805 to 2.883	1.66769 to 3.31911	1.25-1.89
C_{cym}-H	3.7585	4.16835	3.25 t
C_{others}-H	5.0384 to 8.076	5.40985 to 8.35632	4.5 to 8.47
C4-H	6.6248, 6.6443	6.94866, 6.96757	6.75
CHOO	7.0123	7.32453	7.45
COOH	7.558	7.85386	7.75

C30=[(cym)Ru(bdmpzm)Cl]$^{+}$ cd3od

CH_3	1.1465 to 3.4373	1.63471 to 3.85678	1.1911 to 2.5440
C_{cym}-H	3.5759	3.99122	3.3235
$C_{cym-others}$-H	5.1312 to 5.2828	5.49986 to 5.64692	4.5858 to 5.9934
CH_2	5.4869, 5.5524	5.84489, 5.90843	6.2284
C4-H	6.2582, 6.2691	6.59305, 6.60363	6.4599, 6.4984

C31=[(cym)Ru(bdmpza)Cl]$^{+}$ cd3od

CH_3	1.0621 to 3.481	1.55284 to 3.89917	1.25 to 2.80
C_{cym}-H	3.7142	4.12537	3.35
C_{others}-H	5.1197 to 6.3315	5.48871 to 6.66416	5.25 to 6.25
COOH	7.0006	7.31318	7.2
CHOO	8.1368	8.4153	7.35

C32=[(cym)Ru(bphpza)Cl]$^{+}$

CH_3	0.1214 to 2.6711	0.64035 8 to	0.8934 to

COOH	6.3312 to 7.1473	6.66386 to 7.45548	6.20 to 6.30
CHCOO	5.9573 to 8.4983	6.30118 to 8.76595	4.57 to 7.5
C4-H	6.1631 to 6.6569	6.50081 to 6.97979	5.85 to 6.75

C5=Ru(bpzm)2Cl$_2$ dmso-d6

CH_2 close to Ru			1.2475 to 2.6256
CH_2	5.0856	5.45563	5.45
C4-H	6.4822 to 6.4824	6.81033 to 6.81053	6.2832 to 6.398
C5-H	7.6729 to 7.6731	7.96531 to 7.96551	7.3900 d
C3-H	8.5384 to 8.5387	8.80485 to 8.80514	8.25
CH_2 close to Cl	9.9078 to 9.9087	10.1332 to 10.134	9.12

C6=(bpza)$_2$RuCl$_2$ cd3od

CH4-H	6.4986 to 6.5308	6.82624 to 6.85748	6.45 to 6.55
COOH	6.8246, 8.2115	7.14246, 8.48775	7.25
CH	8.0113 to 8.8952	8.29356 to 9.15094	7.75 to 8.25
CHCOO	11.4349, 12.0581	11.6145, 12.219	8.5

C7=Ru(bdmpzm)2Cl$_2$ dmso-d6

CH_3	1.7889 to 2.8282	2.25783 to 3.26595	0.5318 to 2.4231
CH_2	5.0994 to 7.3616	5.46902 to 7.66335	5.8128, 7.4897
C4-H	6.1307 to 6.1448	6.46938 to 6.48306	6.0301
C4-H	5.9843, 6.1466	6.32737, 6.4848	5.8
COOH	10.0172	10.2393	8.8
CHCOO	11.5059	11.6833	8.85
Cothers-H	7.2448 to 10.0188	7.55006 to 10.2408	7.25 to 8.75

C19=Ru(bdmpza)(bmpyr)Cl$_2$

CH_3	1.9143 to 4.2396	2.37947 to 4.63501	0.7 to 4.50
C4-H	6.0131, 6.1564	6.35531, 6.49431	5.75-6.2
C_{pyr}-H	7.1533 to 9.8071	7.4613 to 10.0355	7.00 to 8.25
COOH	10.3983	10.609	9.3
CHOO	11.5308	11.7075	9.8

C20=Ru(bdmpza)(dmphn)Cl$_2$

CH_3	1.8295 to 4.4504	2.29722 to 4.83949	0.0005 to 3.6
C4	5.9292, 6.0762	6.27392, 6.41651	4.5
COOH	10.4203	10.6303	7.9
CHCOO	11.8696	12.0361	8.62
Cothers	7.4764 to 8.0595	7.77471 to 8.34032	7.15 to 8.50

C21=Ru(bdmpzm)(bpzm)Cl$_2$

CH3	2.0064 to 4.6144	2.46881 to 4.99857	0.03 to 4.5
CH2	5.1876 to 10.0813	5.55457 to 10.3015	5.85
		3.11357	2.2399
C_{cym}-H	2.8585	3.29535	3.3232
CHOO	6.6128	6.93702	6.8836
COOH	7.3528	7.65482	7.7363
C4-H	6.4789, 6.5177	6.80713, 6.84477	6.7599 d
Cothers-H	3.9623 to 8.1705	4.36603 to 8.44798	3.8948 to 8.2431

C33=[(cym)Ru(bpyr)Cl]$^+$ cd3od

CH_3	0.18 to 3.6035	0.6972 to 4.01799	0.351 to 2.6466
C_{cym}-H	2.3908	2.84168	3.3236 m
C_{others}-H	5.092 to 9.1109	5.46184 to 9.36017	5.8573 to 9.4875

C34=[(cym)Ru(phn)Cl]$^+$ ch3od

CH_3	-0.1573 to 3.6117 ch3	0.37001 9 to 4.02595	0.992 to 2.6694
C_{cym}-H	2.4358	2.88533	3.3236 m
C_{others}-H	5.2484 to 9.3954	5.61355 to 9.63614	6.0115 to 9.8329

C35=[(cym)Ru(dmbpyr)Cl]$^+$ cd3od

CH_3	0.2371 to 3.6452	0.75258 7 to 4.05844	1.0543 to 2.6370
C_{cym}-H	2.3218	2.77475	3.3237 m
C_{others}-H	4.9021 to 8.9136	5.27764 to 9.16879	4.5896 to 9.2728

C36=[(cym)Ru(dmphn)Cl]$^+$ cd3od

CH_3	-0.6152 to 3.9726 ch3	-0.07414 4 to 4.37602	0.7511 to 4.5859

CH_2 close to Cl			12.2183

C8=(bdmpza)$_2$RuCl$_2$ cd3od

CH_3	1.5949 to 3.2835	2.06965 to 3.70759	1.3034 to 3.3233
OH	5.9067 to 6.0811	6.2521-6.42127	6.326
C4-H	5.9004 to 6.1089	6.24599 to 6.44823	
CHCOO	5.7043-10.395	6.05577-10.6058	

C9=Ru(bpza)(bdmpza)Cl$_2$ cd3od

CH_3	1.7475-3.4751	2.21767-3.89345	1.75-3.4
C4-H	5.9985-6.5453	6.34114-6.87154	6.6
COOH	6.4373, 6.5145	6.76678, 6.84166	7.4
CHCOO	6.1833, 12.8142	6.5204, 12.9524	8, 8.3

C10=Ru(bpza)(bdmpzm)Cl$_2$ cd3od

CH_3	1.8912, 3.3983	2.35706, 3.81895	1.37-3.38
CH_2	4.9934, 6.4977	5.3662, 6.82537	6.37
CHOO	6.1258	6.46463	7.6
COOH	6.2759	6.61022	7.9
C4-H	6.1501 to 6.5986	6.4882 to 6.92324	6.25, 7.45
Cmeta/auto-H	7.7382 to 8.573	8.02865 to 8.83841	7.12-9.38

C11=Ru(bpza)(bphpza)Cl2

C4-H	5.604 to 6.4217	5.95848 to 6.75165	6.1814-6.6143
	6.178 to 6.5853	6.51526 to 6.91034	6.2 to 6.60
$C_{meta/ortho}$	7.7364 to 8.6686	8.02691 to 8.93114	7.7 to 8.15

C22=Ru(bdmpzm)(bphpza)Cl$_2$

CH_3	1.3819 to 3.2435	1.86304 to 3.66879	0.5 to 3.00
CH_2	4.9123, 5.4407	5.28753, 5.80008	4.4
C4-H	5.3841 to 6.4622	5.74518 to 6.79093	5.65 to 6.50
COOH	6.5342	6.86077	6.5
CHOO	9.1972	9.44388	8.5
C_{others}-H	6.6881 to 9.7762	7.01006 to 10.0055	6.75 to 7.60

C23=[Ru(bdmpzm)(bpzpy)Cl]$^+$ dmso-d6

CH_3	1.235 to 3.5675	1.72055 to 3.98308	1.2433 to 2.90009
CH_2	5.4281, 6.083	5.78786, 6.42311	5.8132
C4-H	6.0487 to 6.92	6.38984 to 7.235	6.0305
C_{others}-H	7.2819 to 8.453	7.58604 to 8.72201	7.0168 to 8.52

C24=[Ru(bdmpzm)(bdmpzpy)Cl]$^+$

CH_3	1.1462 to 3.6205	1.63441 to 4.03449	0.004 to 3.3812
CH_2	5.2537, 5.6886	5.61869, 6.04054	4.4731
C4-H	5.8014 to 6.29	6.14996 to 6.6239	
C_{others}-H	7.1411 to 7.7839	7.44947 to 8.07298	

C25=(cym)Ru(pz)Cl$_2$

			ch3
C_{cym}-H	1.8429	2.31021	3.3234 m
C_{others}-H	5.0622 to 8.2611	5.43293 to 8.53587	5.9516 to 8.6379

C37=[(cym)Ru(dcbpyr)Cl]$^+$ cd3od

CH_3	0.1123 to 3.5295	0.63153 1 to 3.94622	1.3425 to 2.7960
C_{cym}-H	2.4061	2.85652	3.3238
C_{others}-H	5.1496 to 9.2194	5.51771 to 9.46542	5.5010 to 5.8967
COOH	7.1791, 7.2009	7.48633, 7.50747	?

C38=[(cym)Ru(dcphn)Cl]+

CH_3	-0.9366 to 3.5554	-0.38590 2 to 3.97134	1.3585 to 2.7951
C_{cym}-H	1.5631	2.03881	3.3231 m
C_{others}-H	4.7001 to 9.035	5.0817 to 9.28655	5.5746 to 5.8970
COOH	7.0155, 7.4272	7.32764, 7.72698	5.5014

C39=[(cym)Ru(bpzpy)]$^{2+}$ cd3od

CH3	-0.5245 to 2.8097 ch3	0.013835 to 3.24801	0.351 to 2.6204
Ccy-H	2.4369	2.88639	3.3235
Cothers-H	5.2069 to 8.6766	5.57329 to 8.9389	4.5856 to 8.9094
C4-H	7.3245, 7.3853	7.62737, 7.68634	7.0475 t

C40=[(cym)Ru(bdmpzpy)]$^{2+}$ cd3od

CH_3	0.3559 to 3.2041	0.867823 to 3.63058	0.85 to 2.7960
C_{cym}-H	2.0242	2.48607	3.3238 m

CHOO	5.8653, 12.6296	6.21194, 12.7733	6.1814	CH_3	0.8757	1.37203	0.9154 to 3.1464	C4-H	4.9929 to 8.4043	5.36571 to 8.67477	5.5016 to 5.8976
COOH	6.3765, 6.4681	6.70781, 6.79666	6.6471	C_{cym}-H	3.4953	3.91304	3.3234	C_{others}-H	6.7504, 6.9064	7.07049, 7.22181	5.7087, 5.7245
C_{other}-H	6.8428 to 9.6636	7.16012 to 9.89629	7.2158 to 8.0988	C_{others}-H	4.5919 to 7.5216	4.97674 to 7.81855	5.4703 to 8.0428				
				NH	12.5956	12.7403	8.2872				

Table 5.6: The theoretical ^{13}C-NMR chemical shift of the complexes

ST1=RuCl2(dmso)4			**C14=Ru(bpza)(phn)Cl_2**			**C28=[(cym)Ru(bpzm)Cl]$^+$**		
	Direct	**Fitting**		**Direct**	**Fitting**		**Direct**	**Fitting**
CH_3	47.3626 to 52.04	37.2616 to 41.766	CHCOOH	72.3495	61.324	CH_3	18.7789 to 26.512	9.73552 to 17.1825
ST2=[(cym)$RuCl_2$]$_2$			C4	104.598, 104.781	92.3792, 92.5556	C_{cym}-H	36.0267	26.3452
CH_3	18.3165 to 27.773	9.29023 to 18.3968	C_{others}	118.162 to 152.403	105.442 to 138.415	CH_2	62.6565	51.9896
C_{cym}-H	33.3454, 35.0746	23.7631, 25.4283	COOH	159.984	145.716	C_{arene}	79.0071 to 121.491	67.7353 to 108.647
Carene	69.7615 to 113.633	58.8318 to 101.08	**C15=Ru(bpza)(dmphn)Cl_2**			C4	107.453, 107.537	95.1291, 95.21
ST3=Ru(bdmpzm)Cl_4			CH_3	30.0523 to 30.2331	20.5918 to 20.7659	Cothers	129.475 to 147.91	116.335 to 134.089
CH_3	12.0589 to 27.3709	3.26416 to 18.0096	CHCOOH	70.4106	59.4568	**C29=[(cym)Ru(bpza)Cl]$^+$**		
CH_2	55.7778	45.3655	C4	104.07, 104.37	91.8708, 92.1595	CH_3	18.7987 to 26.2205	9.75459 to 16.9018
C4	107.921, 108.993	95.5792, 96.6112	COOH	162.12	147.773	C_{cym}-H	36.0429	26.3608
C_{others}	136.032, 172.764	122.65, 158.023	C_{others}	120.089 to 168.434	107.297 to 153.853	CHCOO	71.5687	60.5721
ST4=Ru(bpzm)Cl_4			**C16=Ru(bdmpza)(bdmpzm)Cl_2**			C_{arene}	79.2783 to 121.155	67.9964 to 108.324
CH_2	79.9513	68.6445	CH_3	13.3197 to 20.7833	4.47831 to 11.6658	C4	107.458, 107.572	95.1331, 95.2432
C4	95.5082, 96.9653	83.6258, 85.029	CHCOOH	60.2745 to 74.936	49.6958 to 63.8148	COOH	160.552	146.263
C_{others}	131.453 to	118.24 to	C4	107.241 to	94.9241 to	C_{others}	129.599 to	116.456 to

	135.939	122.561
C1=[Ru(bpzm)3]$^{2+}$		
CH_2	63.5237 to 63.9444	52.8248 to 53.2299
C4	109.026 to 109.907	96.6435 to 97.4917
C_{others}	133.046 to 146.798	119.775 to 133.018
C2=[Ru(bpza)3]$^{2+}$		
CHCOOH	71.8574 to 77.5718	60.8501 to 66.3531
C4	107.834 to 110.422	95.4951 to 97.9879
C_{others}	131.594 to 147.735	118.377 to 133.921
COOH	149.397 to 157.702	135.52 to 143.518
C3=[Ru(bdmpzm)$_3$]$^{2+}$		
CH_3	11.8745 to 18.0226	3.08658 to 9.0072
CH_2	56.2528 to 60.0261	45.8229 to 49.4566
C4	109.542 to 113.508	97.14 to 100.96
C_{others}	142.488 to 167.162	128.868 to 152.629
C4=[Ru(bdmpza)$_3$]$^{2+}$		
CH_3	12.2106 to 19.4121	3.41025 to 10.3453
CHCOO	70.0217 to 72.7851	59.0823 to 61.7435
COOH	155.401 to 156.647	141.303 to 142.502
C4	110.559 to 114.307	98.1199 to 101.729
Cothers	145.417 to 166.575	131.688 to 152.063
C5=Ru(bpzm)$_2$Cl$_2$		
CH_2	65.3462, 65.3487	54.5798, 54.5822
C4	103.088 to 103.09	90.9252 to 90.9271
C_{others}	126.328 to 144.377	113.305 to 130.686
C6=(bpza)$_2$RuCl$_2$		
	111.998	99.5058
COOH	160.593	146.302
C_{others}	137.258 to 169.654	123.831 to 155.028
C17=Ru(bdmpza)(bphpza)Cl$_2$		
CH3	13.7964 to 36.648	4.93737 to 26.9435
C4	115.879 to 118.399	103.243 to 105.669
COOH	157.57, 164.584	143.391, 150.146
CHCOO	74.8581, 77.9388	63.7398, 66.7065
Cothers	120.072 to 181.055	107.28 to 166.008
C18=Ru(bdmpza)(pyr)Cl$_2$		
CH3	14.0957 to 18.5064	5.2256 to 9.4731
C4	107.828, 108.928	95.4901, 96.5493
COOH	162.054	147.709
CHCOO	74.0061	62.9193
Cothers	116.682 to 157.968	104.017 to 143.775
C19=Ru(bdmpza)(bmpyr)Cl$_2$		
CH_3	14.3045 to 22.2162	5.42667 to 13.0456
CHCOOH	73.9388	62.8545
C4	108.002 to 109.163	95.6571 to 96.7759
C_{others}	118.276 to 157.95	105.551 to 143.757
COOH	162.358	148.003
C20=Ru(bdmpza)(dmphn)Cl$_2$		
CH3	14.1904 to 26.9404	5.3168 to 17.595
C4	107.877, 108.065	95.5369, 95.7176
COOH	162.363	148.007
CHCOO	74.6515	63.5408
	148.559	134.714
C30=[(cym)Ru(bdmpzm)Cl]$^{+}$		
CH_3	12.657 to 27.073	3.84013 to 17.7227
C_{cym}-H	37.1282	27.4059
CH_2	56.1486	45.7225
C_{arene}	73.5806 to 130.166	62.5096 to 117.001
C4	109.509, 109.657	97.1087, 97.2507
C_{others}	141.036 to 157.607	127.469 to 143.427
C31=[(cym)Ru(bdmpza)Cl]$^{+}$		
CH_3	15.5562 to 26.8291	6.63206 to 17.4879
C_{cym}-H	36.7463	27.0381
CHCOO	73.5519	62.4819
C_{arene}	73.8723 to 130.694	62.7905 to 117.51
C4	110.787, 112.756	98.3396, 100.236
C_{others}	142.338 to 159.196	128.723 to 144.958
COOH	159.875	145.611
C32=[(cym)Ru(bphpza)Cl]$^{+}$		
CH_3	18.7785 to 26.2859	9.73514 to 16.9648
C_{cym}-H	35.3002	25.6455
CHCOO	72.2393	61.2179
C_{arene}	73.5694 to 127.554	62.4988 to 114.486
C4	109.993 to 110.92	97.5747 to 98.4673
COOH	158.471	144.259
C_{others}	123.334 to 164.701	110.422 to 150.259
C33=[(cym)Ru(bpyr)Cl]$^{+}$		
CH_3	19.1232 to 27.0098	10.0671 to 17.6619

CHCOOH	72.1369, 74.386	61.1193, 63.2852
C4	104.04 to 104.713	91.8415 to 92.4899
C_{others}	126.704 to 145.995	113.667 to 132.244
COOH	161.287 to 163.813	146.971 to 149.404

C7=Ru(bdmpzm)$_2$Cl$_2$

CH_3	13.3833 to 21.1533	4.53956 to 12.0221
CH_2	60.0465, 60.0466	49.4762, 49.4763
C4	107.205 to 110.517	94.8901 to 98.0791
C_{others}	136.267 to 166.561	122.877 to 152.049

C8=Ru(bdmpza)$_2$Cl$_2$

CH_3	13.0639 to 21.9522	4.23198 to 12.7914
CHCOOH	70.9543 to 75.2078	59.9804 to 64.0766
C4	108.44 to 111.769	96.0794 to 99.2849
COOH	160.161 to 161.017	145.887 to 146.71
C_{others}	135.815 to 173.386	122.441 to 158.622

C9=Ru(bpza)(bdmpza)Cl$_2$

CH_3	15.5098 to 18.9948	6.58738 to 9.94343
CHCOOH	73.82, 75.4064	62.7401, 64.2678
C4	103.767, 108.817	91.5787, 96.4426
C_{others}	128.885 to 157.716	115.767 to 143.532
COOH	162.388, 163.275	148.031, 148.885

C10=Ru(bpza)(bdmpzm)Cl$_2$

CH_3	13.2915 to 22.1584	4.45115 to 12.99
CH_2	61.2872	50.671
CHCOOH	76.4295	65.253
Cothers	118.888 to 168.237	106.141 to 153.663

C21=Ru(bdmpzm)(bpzm)Cl$_2$

CH_3	13.4804 to 18.6111	4.63307 to 9.57393
CH_2	59.0564 to 64.6519	48.5228 to 53.9112
C4	103.728 to 107.549	91.5415 to 95.2214
C_{others}	127.706 to 157.332	114.633 to 143.162

C22=Ru(bdmpzm)(bphpza)Cl$_2$

CH_3	12.8977 to 23.1103	4.07193 to 13.9067
CHCOOH	61.9346 to 72.5808	51.2945 to 61.5468
C4	108.846 to 112.139	96.47 to 99.6411
COOH	163.992	149.576
C_{others}	121.102 to 172.733	108.272 to 157.994

C23=[Ru(bdmpzm)(bpzpy)Cl]$^+$

CH_3	12.5549 to 18.8141	3.74181 to 9.76942
CH_2	55.8971	45.4803
$C_{pyr\text{-}meta}$	102.3, 104.445	90.1667, 92.2315
C4	108.984, 109.543	96.6032, 97.1411
Cothers	126.207 to 158.756	113.188 to 144.533

C24=[Ru(bdmpzm)(bdmpzpy)Cl]$^+$

CH_3	11.907, 18.3856	3.11788, 9.35677
CH_2	56.1542	45.7279
$C_{pyr\text{-}meta}$	100.451, 102.543	88.3857, 90.4004
C4	108.089 to 109.407	95.7413 to 97.0107
C_{others}	133.53 to 159.222	120.241 to 144.983

C25=(cym)Ru(pz)Cl2

C_{cym}-H	35.8508	26.1758
C_{arene}	85.0657 to 111.04	73.5697 to 98.5827
C_{others}	119.835 to 151.834	107.053 to 137.868

C34=[(cym)Ru(phn)Cl]$^+$

CH_3	18.7032 to 26.9675	9.66262 to 17.6211
C_{cym}-H	35.7585	26.0869
C_{arene}	84.4084 to 110.293	72.9367 to 97.8634
C_{others}	122.069 to 150.257	109.204 to 136.349

C35=[(cym)Ru(bmpyr)Cl]$^+$

CH_3	19.3161 to 27.2417	10.2528 to 17.8852
C_{cym}-H	36.101	26.4167
C_{arene}	84.4764 to 116.693	73.0022 to 104.027
C_{others}	120.585 to 151.507	107.775 to 137.553

C36=[(cym)Ru(dmphn)Cl]$^+$

CH_3	18.9445 to 28.653	9.89499 to 19.2443
C_{cym}-H	35.2764	25.6226
C_{arene}	80.3863 to 120.244	69.0634 to 107.447
C_{others}	123.3 to 163.651	110.39 to 149.248

C37=[(cym)Ru(dcbpyr)Cl]$^+$

CH_3	19.0201 to 27.1085	9.9678 to 17.7569
C_{cym}-H	35.9646	26.2853
C_{arene}	85.8985 to 112.987	74.3717 to 100.458
C_{others}	120.263 to 152.049	107.464 to 138.075
COOH	159.41 to 159.976	145.163 to 145.708

C38=[(cym)Ru(dcphn)Cl]$^+$

C4	104.57 to 111.54	92.3521 to 99.0647
COOH	162.81	148.437
C_{others}	128.089 to 166.493	115.001 to 151.984

C11=Ru(bpza)(bphpza)Cl_2

CHCOOH	73.9941, 75.3019	62.9078, 64.1672
C4	103.105 to 107.7	90.9412 to 95.3662
C_{others}	121.575 to 161.444	108.728 to 147.122
COOH	160.185 to 162.003	145.91 to 147.66

C12=Ru(bpza)(bpyr)Cl_2

CHCOOH	71.8354	60.8289
C4	104.52	92.3043
C_{others}	117.342 to 156.954	104.652 to 142.798
COOH	161.254	146.939

C13=Ru(bpza)(dmbpyr)Cl_2

CH_3	22.2139	13.0434
CHCOOH	71.8527	60.8456
C4	104.425	92.2132
C_{others}	118.415 to 156.586	105.685 to 142.444
COOH	161.36	147.041
CH_3	19.2194 to 26.5616	10.1597 to 17.2303
C_{cym}-H	34.6488	25.0182
C4	102.958	90.7997
C_{arene}	76.6877 to 108.219	65.5017 to 95.8662
C_{others}	122.235, 135.042	109.363, 121.697

C26=(cym)Ru(dmpz)Cl_2

CH_3	11.7005 to 26.7558	2.91902 to 17.4173
C_{cym}-H	34.8921	25.2525
C4	105.316	93.0707
C_{arene}	80.5659 to 107.099	69.2364 to 94.7875
C_{others}	137.421, 150.238	123.988, 136.33

C27=(cym)Ru(dcpz)Cl_2

CH_3	18.91 to 26.4946	9.86177 to 17.1657
C_{cym}-H	35.169	25.5192
C_{arene}	76.3656 to 114.84	65.1915 to 102.242
C4	114.258	101.682
C_{others}	129.729, 139.425	116.58, 125.918
COOH	154.51, 159.353	140.444, 145.108
CH_3	18.5994 to 28.6687	9.56266 to 19.2594
C_{cym}-H	36.6414	26.9371
C_{arene}	85.3531 to 118.217	73.8465 to 105.494
C_{others}	125.413 to 155.32	112.424 to 141.224
COOH	160.975 to 164.542	146.67 to 150.105

C39=$[(cym)Ru(bpzpy)]^{2+}$

CH_3	17.5248, 27.4515	8.52782, 18.0872
C_{cym}-H	37.4655	27.7307
$C_{pyr-meta}$	107.246 to 107.524	94.929 to 95.1972
C_{arene}	77.3561 to 127.122	66.1454 to 114.07
C4	113.882 to 114.335	101.32 to 101.756
Cothers	130.487 to 151.771	117.31 to 137.807

C40=$[(cym)Ru(bdmpzpy)]^{2+}$

CH_3	15.2042 to 27.3715	6.29308 to 18.0102
C_{cym}-H	35.6869	26.0179
$C_{pyr-meta}$	105.05 to 106.165	92.8141 to 93.8887
C_{arene}	80.0787 to 114.876	68.7672 to 102.277
C4	113.327, 114.411	100.786, 101.829
C_{others}	143.64 to 165.472	129.977 to 151.001

Table 5.7: The theoretical ^{15}N-NMR chemical shift of the complexes

	Direct	Fitting
ST3=Ru(bdmpzm)Cl_4		
N13	-181.495, -181.049	-201.692, -201.271
*N15	-156.809, -144.702	-178.34, -166.887
ST4=Ru(bpzm)Cl_4		
N6	-157.105 to -148.771	-178.62 to -170.736
*N9	-142.573 to -116.768	-164.873 to -140.461
C1=[Ru(bpzm)3]$^{2+}$		
N11	-176.048 to -171.199	-196.54 to -191.952
*N15	-130.373 to -123.828	-153.331 to -147.139
C2=[Ru(bpza)3]$^{2+}$		
N20	-176.97 to -173.766	-197.412 to -194.381
*N24	-134.993 to -121.229	-157.702 to -144.681
C3=[Ru(bdmpzm)3]$^{2+}$		
N10	-183.353 to -176.566	-203.45 to -197.03
*N29	-141.777 to -128.006	-164.119 to -151.092
C4=[Ru(bdmpza)3]$^{2+}$		
N	-187.441 to -175.14	-207.318 to -195.68
*N	-148.996 to -127.453	-170.948 to -150.569
C5=Ru(bpzm)2Cl_2		
N20	-165.549 to -165.544	-186.607 to -186.603
*N12	-96.7244 to -96.7137	-121.5 to -121.489
C6=(bpza)$_2$RuCl$_2$		
N11	-168.083 to -165.971	-189.004 to -187.007
*N25	-99.8158 to -95.1468	-124.424 to -120.007
C7=Ru(bdmpzm)2Cl_2		
N21	-166.733, -166.733	-187.728, -187.728
*N22	-92.9174, -92.9148	-117.898, -117.896
**N15	-80.3983, -80.3983	-106.055, -106.055
C14=Ru(bpza)(phn)Cl_2		
N26	-167.658, -167.039	-188.603, -188.017
*N25	-97.1494, -95.5598	-121.902, -120.398
**N14	-75.3446, -75.2441	-101.274, -101.179
C15=Ru(bpza)(dmphn)Cl_2		
N19	-165.185, -161.526	-186.264, -182.802
*N21	-92.9129, -92.7386	-117.894, -117.729
**N13	-89.8653, -89.6946	-115.011, -114.849
C16=Ru(bdmpza)(bdmpzm)Cl_2		
N19	-181.222 to -176.065	-201.435 to -196.556
*N11	-121.603 to -85.4027	-145.035 to -110.789
C17=Ru(bdmpza)(bphpza)Cl_2		
N	-181.563 to -167.398	-201.757 to -188.356
*N	-148.271 to -78.279	-170.263 to -104.05
C18=Ru(bdmpza)(bpyr)Cl_2		
N	-173.395, -171.84	-194.03, -192.558
*N	-105.426, -104.475	-129.731, -128.831
**N	-71.0856, -68.9597	-97.2452, -95.2341
C19=Ru(bdmpza)(bmpyr)Cl_2		
N21	-172.97, -171.239	-193.628, -191.99
*N22	-102.059,	-126.546,
C25=(cym)Ru(pz)Cl_2		
N6	-175.844	-196.347
*N7	-136.851	-159.459
C26=(cym)Ru(dmpz)Cl_2		
N14	-179.772	-200.062
*N10	-144.371	-166.573
C27=(cym)Ru(dcpz)Cl_2		
N6	-149.63	-171.549
*N8	-103.087	-127.518
C28=[(cym)Ru(bpzm)Cl]$^+$		
N7	-177.922, -177.858	-198.312, -198.252
*N6	-138.632, -137.807	-161.144, -160.363
C29=[(cym)Ru(bpza)Cl]$^+$		
N7	-177.432, -176.844	-197.849, -197.293
*N6	-138.416, -137.287	-160.94, -159.871
C30=[(cym)Ru(bdmpzm)Cl]$^+$		
N21	-182.473, -182.278	-202.618, -202.433
*N10	-153.084, -152.365	-174.816, -174.136
C31=[(cym)Ru(bdmpza)Cl]$^+$		
N14	-181.13, -176.366	-201.347, -196.841
*N13	-148.759, -142.106	-170.724, -164.431
C32=[(cym)Ru(bphpza)Cl]$^+$		
N12	-178.776, -178.136	-199.121, -198.515
*N18	-143.577, -139.581	-165.822, -162.041
C33=[(cym)Ru(bpyr)Cl]$^+$		

N12	-175.653 to -172.202	-196.166 to -192.902
*N14	-109.383 to -82.5676	-133.474 to -108.107

C8=(bdmpza)$_2$RuCl$_2$

N22	-182.799 to -174.672	-202.926 to -195.238
*N26	-108.623 to -75.8315	-132.756 to -101.735

C9=Ru(bpza)(bdmpza)Cl$_2$

N12	-173.823 to -170.386	-194.435 to -191.184
*N11	-105.216 to -95.5199	-129.533 to -120.36

C10=Ru(bpza)(bdmpzm)Cl$_2$

N21	-181.444 to -173.345	-201.645 to -193.983
*N13	-109.567 to -71.3737	-133.649 to -97.5178

C11=Ru(bpza)(bphpza)Cl$_2$

N35	-177.488 to -167.536	-197.902 to -188.488
*N20	-111.161 to -102.287	-135.156 to -126.762

C12=Ru(bpza)(bpyr)Cl$_2$

N19	-167.14, -167.14	-188.112, -188.113
*N21	-94.6212, -94.6204	-119.51, -119.509
**N11	-71.0549, -71.0546	-97.2162, -97.2159
	101.685	126.192
**N17	-79.6672, -77.6318	-105.363, -103.438

C20=Ru(bdmpza)(dmphn)Cl$_2$

N	-175.591, -172.745	-196.107, -193.415
*N	-104.192, -103.005	-128.564, -127.441
**N	-82.9872, -80.2264	-108.504, -105.892

C21=Ru(bdmpzm)(bpzm)Cl$_2$

N17	-171.251 to -169.201	-192.002 to -190.062
*N12	-106.409 to -91.2202	-130.662 to -116.293

C22=Ru(bdmpzm)(bphpza)Cl$_2$

N32	-179.023 to -171.119	-199.354 to -191.877
*N35	-117.541 to -80.3074	-141.192 to -105.969

C23=[Ru(bdmpzm)(bpzpy)Cl]$^+$

N8	-181.61, -146.035	-201.801, -168.147
*N21	-135.611, -93.6459	-158.287, -118.587
**N22	-120.774	-144.251

C24=[Ru(bdmpzm)(bdmpzpy)Cl]$^+$

N23	-183.436, -150.135	-203.529, -172.026
*N31	-133.077, -100.797	-155.889, -125.353
**N18	-120.52	-144.01
	-117.649, -117.001	-141.294, -140.681

C34=[(cym)Ru(phn)Cl]$^+$

N20	-122.033, -121.999	-145.442, -145.409

C35=[(cym)Ru(dmbpyr)Cl]$^+$

N16	-127.587, -126.295	-150.696, -149.473

C36=[(cym)Ru(dmphn)Cl]$^+$

N16	-127.805, -127.479	-150.902, -150.593

C37=[(cym)Ru(dcbpyr)Cl]$^+$

N18	-107.593, -106.867	-131.781, -131.094

C38=[(cym)Ru(dcphn)Cl]$^+$

N17	-113.457, -108.732	-137.328, -132.858

C39=[(cym)Ru(bpzpy)]$^{2+}$

N14	-152.866, -152.189	-174.609, -173.969
*N10	-132.773, -129.918	-155.602, -152.9
**N20	-180.978	-201.204

C40=[(cym)Ru(bdmpzpy)]$^{2+}$

N21	-157.459, -157.311	-178.955, -178.815
*N8	-142.11, -137.12	-164.434, -159.713
**N23	-184.133	-204.188

Table 5.8: The theoretical ^{99}Ru-NMR chemical shift of the complexes

ST1=$RuCl_2(dmso)_4$	3377.96	**C19=Ru(bdmpza)(bmpyr)Cl_2**	6333.7
ST2=$[(cym)RuCl_2]_2$	2654.78, 2452.7	**C20=Ru(bdmpza)(dmphn)Cl_2**	7265.29
ST3=Ru(bdmpzm)Cl_4	-13438.4	**C21=Ru(bdmpzm)(bpzm)Cl_2**	7914.36
ST4=Ru(bpzm)Cl_4	-40545.6	**C22=Ru(bdmpzm)(bphpza)Cl_2**	9855.22
C1=$[Ru(bpzm)_3]^{2+}$	5526.45	**C23=$[Ru(bdmpzm)(bpzpy)Cl]^+$**	5787.75
C2=$[Ru(bpza)_3]^{2+}$	5530.61	**C24=$[Ru(bdmpzm)(bdmpzpy)Cl]^+$**	5841.54
C3=$[Ru(bdmpzm)_3]^{2+}$	7790.17	**C25=(cym)Ru(pz)Cl_2**	1679.79
C4=$[Ru(bdmpza)_3]^{2+}$	9015.25	**C26=(cym)Ru(dmpz)Cl_2**	1936.47
C5=$Ru(bpzm)_2Cl_2$	6862.85	**C27=(cym)Ru(dcpz)Cl_2**	2137.24
C6=$(bpza)_2RuCl_2$	6442.06	**C28=$[(cym)Ru(bpzm)Cl]^+$**	1947.45
C7=Ru(bdmpzm)2Cl_2	9268.49	**C29=$[(cym)Ru(bpza)Cl]^+$**	1988.9
C8=$(bdmpza)_2RuCl_2$	9816.82	**C30=$[(cym)Ru(bdmpzm)Cl]^+$**	2236.22
C9=Ru(bpza)(bdmpza)Cl_2	6676.96	**C31=$[(cym)Ru(bdmpza)Cl]^+$**	2347.68
C10=Ru(bpza)(bdmpzm)Cl_2	7639.57	**C32=$[(cym)Ru(bphpza)Cl]^+$**	2515.19
C11=Ru(bpza)(bphpza)Cl_2	7248.84	**C33=$[(cym)Ru(bpyr)Cl]^+$**	1616.12
C12=Ru(bpza)(bpyr)Cl_2	5450.3	**C34=$[(cym)Ru(phn)Cl]^+$**	1606.05
C13=Ru(bpza)(bmpyr)Cl_2	5561.2	**C35=$[(cym)Ru(dmbpyr)Cl]^+$**	1570.07
C14=Ru(bpza)(phn)Cl_2	5831.23	**C36=$[(cym)Ru(dmphn)Cl]^+$**	2118.21
C15=Ru(bpza)(dmphn)Cl_2	8247.75	**C37=$[(cym)Ru(dcbpyr)Cl]^+$**	1589.16
C16=Ru(bdmpza)(bdmpzm)Cl_2	9547.58	**C38=$[(cym)Ru(dcphn)Cl]^+$**	2274.08
C17=Ru(bdmpza)(bphpza)Cl_2	7679.13	**C39=$[(cym)Ru(bpzpy)]^{2+}$**	2628.34
C18=Ru(bdmpza)(bpyr)Cl_2	6293.47	**C40=$[(cym)Ru(bdmpzpy)]^{2+}$**	2556.3